

Empowering Local Industry with Energy Efficiency and Clean Energy Services

Manipal University Jaipur is utilizing its expertise and resources to establish collaborations with local industries, aiming to promote a more seamless transition to sustainable energy practices. A key service offered by the university to these industries is the conduct of energy efficiency assessments. These assessments entail comprehensive analyses of a company's energy usage patterns, equipment, and operational processes. By leveraging its research capabilities, Manipal University Jaipur identifies potential areas for enhancing energy efficiency. This analytical approach empowers industries to make well-informed decisions regarding energy conservation strategies.

Manipal University Jaipur organizes workshops, seminars, and training sessions specifically designed to meet the needs of local industries. These educational programs encompass a variety of subjects, such as energy-efficient technologies, sustainable practices, and the adoption of renewable energy sources. Through these initiatives, industries acquire practical knowledge and skills necessary for implementing energy-saving strategies. The university collaborates with local industries to investigate and develop renewable energy solutions tailored to their unique requirements. This research not only supports the participating industries but also contributes to the broader advancement of clean energy technologies. Manipal University Jaipur also offers guidance and insights into energy-related policies and regulations, assisting industries in navigating the intricate landscape of incentives, rebates, and compliance obligations associated with energy efficiency and the adoption of clean energy solutions.



**MANIPAL UNIVERSITY
JAIPUR**

DIRECTORATE OF STUDENTS' WELFARE

Tech & Future 2.0

Technical Event

**International Society of Automation (ISA) MUJ,
Autonomous Initiative
&
AIC MUJ**

OFFLINE EVENT

Date of Event (15th – 19th March 2023)

(10:00 AM - 04:00 PM)

Index

S. No.	Activity Heads	Page no.
1.	Introduction of the Event	1
2.	The objective of the Event	1
3.	Beneficiaries of the Event	1
4.	Brief Description of the event	1
5.	Photographs	2 - 3
6.	Brochure or creative of the event	4
7.	Schedule of the Event	4
8.	Attendance of the Event	5-11
9.	Link to MUJ website	12

1. Introduction of the Event

A five-day workshop event organized by the International Society of Automation (ISA MUJ Student Chapter) in collaboration with AIC MUJ & Autonomous Initiative. Workshop on Days 1 & 2 i.e., on 15th & 16th March 2023, was conducted by the Co-founder of SmarDen Technologies, Mr. Shrey Sharma, and an Alumni of MUJ, Mr. Arsh Dhingra in AB1 105 on basics of IoT and automation mainly targeted towards students who are just getting into automation. On days 3, 4, and 5 i.e., on 17th, 18th, and 19th March 2023, a workshop was again conducted by the Co-founder of SmarDen Technologies, in AB2 025, where advanced topics of automation and IoT were covered.

SmarDen Technologies Pvt. Ltd. is an IoT-based Home Automation solution-providing company, focused on converting conventional electrical equipment into smart equipment.

2. Objectives of the Event

The Event was aimed to:

- a. Encourage and enhance knowledge about Smart Automation and IoT.
- b. Solve and implement the solution to real-world problems in various domains with the help of IoT and Automation.

3. Beneficiaries of the Event

- a. MUJ and Non-MUJ students.
- b. ISA Members.
- c. Autonomous Initiative Members
- d. Faculty Members of MUJ.

4. Brief Description of the event

The International Society of Automation (ISA MUJ Student Chapter) organized a five-day workshop event in collaboration with AIC MUJ & Autonomous Initiative. The first two days of the workshop, on 15th & 16th March 2023, were conducted by Mr. Shrey Sharma, Co-founder of SmarDen Technologies, and Mr. Arsh Dhingra, an alumnus of MUJ. The focus of these sessions, held in AB1 105, was on the basics of IoT and automation, specifically for students who are new to automation. The remaining three days of the workshop, on 17th, 18th, and 19th March 2023, were held by the Co-founder of SmarDen Technologies in AB2 025. These sessions covered advanced topics of automation and IoT.

5. Photographs



Image 1: Mr. Shrey Sharma explaining the process of interfacing sensors with Microcontrollers.

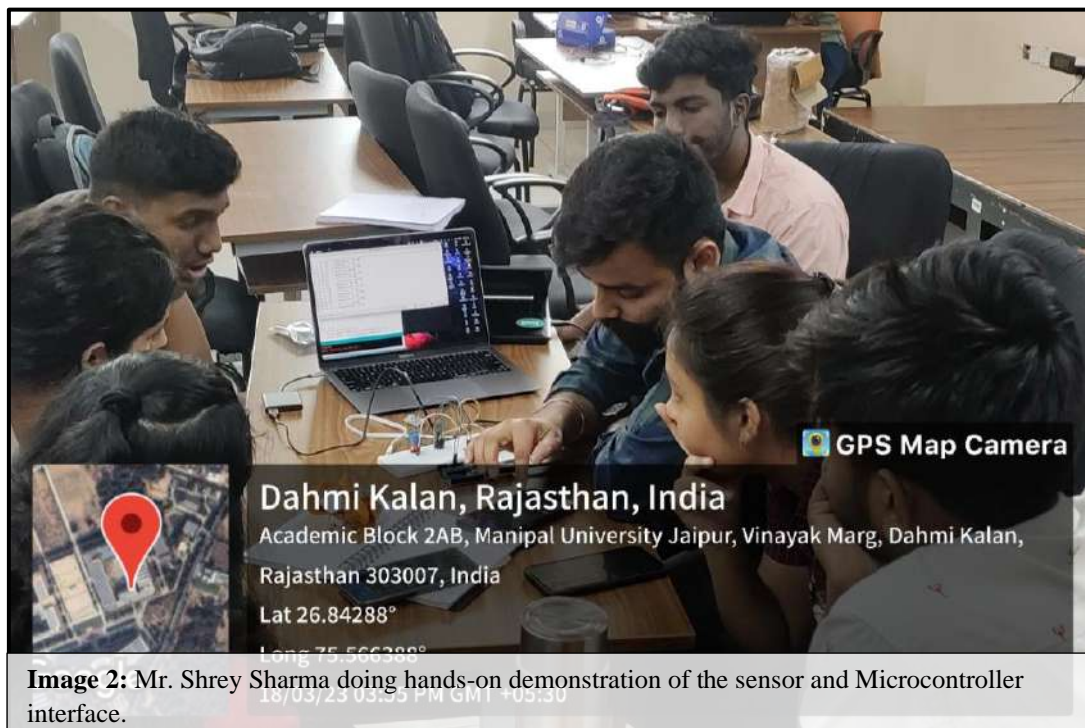


Image 2: Mr. Shrey Sharma doing hands-on demonstration of the sensor and Microcontroller interface.



Image 3: Mr. Arsh Dhingra teaching Python Basics.



Image 4: Group Photo along with the Director of SAMM and Club Coordinators.

6. Brochure or Creative of the Event



Department of Mechatronics Engineering
In Association with
International Society of Automation, Autonomous Initiative & AIC MUJ

TECH & FUTURE 2.0

SHREY SHARMA
Co Founder SmarDen Automations Pvt Ltd

ARSH DHINGRA
Faculty at Manav Rachna (MUJ Alumni)

5 day Workshop on IoT
(Basic to Advance)
&
Startup Opportunities in IoT

Open to Students
&
Faculty

REGISTER NOW

Date : 15 March - 19 March 2023
Venue : AB 1 105
Time: 10 am - 4 pm
(Lunch break: 12pm - 2pm)

For more information
Mohaneesh Pradhan: 8092122462
Kanad Nemade: 9127266933

ISA MUJ CHAPTER | isa_muj_chapter

7. Schedule of the event

The event was from 15th of March 2023 to 19th of March 2023, 10:00 PM- 04:00 PM

8. Attendance of the event:

Total attendees: 50

18/3/23 Session 1 : 10:00am - 12:00pm

Sr. No.	Name	Registration No.	Signature
1	New Sangrvi	209403036	By
2	New Jain	209403011	New
3	Yatin Kohli	209403007	Yatin
4	Pulkit Gupta	209403046	Pulkit
5	Rohitagan Sengha	209403034	Rohit
6	Annamaya Rosalkar	209403065	Anam
7	Hansu Padmalwar	209403047	Hansu
8	Bhavya Shah	209403024	Bhavya
9	Soham Mukherjee	209403022	Soham
10	Susmit Gosh	209403013	Susmit
11	Sanyam Dices	209403004	Sanyam
12	Shukanya Singh	219302025	Shukanya
13	Ashwinhat's	209403052	Ashwinhat
14	PRIYANSHU PARIKH	209403023	Priyanshu
15	Nalith Bhaskaran	209403038	Nalith
16	Rahul Acharya	209403032	Rahul
17	MARVI GARG	209403055	Marvi
18	Priyadarshi Lajee	219310341	Priyadarshi
19	Nivesh Kumar Aggarwal	209403066	Nivesh
20	Vanshit Aggarwal	209403061	Vanshit
21	Anjan Bhatia	209403011	Anjan
22	Shivam Kamekar	209403071	Shivam
23	Neel Saradkar	209403052	Neel
24	Mounalini Ahadje	209403045	Mounalini
25	Raj Shah	209403037	Raj
26	Soubrav Sancheti	209403044	Soubrav
27	Bahul Hason Anthony	209403057	Bahul
28	Seridodhi Bahul	209403048	Seridodhi
29	Bomma Aarthik	209403012	Bomma
30	Shrivooraa Katagari	209403020	Shrivooraa
31	Vedant Mishra	209403041	Vedant
32	Aadhya Dia	219311107	Aadhya
33	Riddhima Saha	219311058	Riddhima
34	Mohit Goyal	219311133	Mohit
35	TSHA	219311102	TSHA
36	Avaneesh Kulbarni	219402016	Avaneesh
37	Devashish Singh	219303161	Devashish
38	Aarjun. S. Umekar	219407003	Aarjun
39	Chintora Naga Brundha Reddy	209403069	Chintora
40	Suraj Rohit Venkat	209403043	Suraj
41	K. Lalith Sai Kishore	209403028	K. Lalith
42	SUSANT RAO	209403035	Susant
43	Sai Naga Karthik	209403030	Sai Naga
44	UTKASH RAO	209202168	Utkash
45	Sanyash Subhawal	209202206	Sanyash
46	Dhisham Kapoor	209403016	Dhisham
47	Bithu Kumar	209303223	Bithu
48	Sunjay Mahendra	219311219	Sunjay
49	Vidhi Garg	219311154	Vidhi
50	Sansh Butaney	209403064	Sansh

15/3/23

Session 2: 2 pm - 4 pm

Sr. No.	Name	Registration No.	Signature
1	Shukanya Singh	219302025	[Signature]
2	Sayush Lakshawat	209707206	[Signature]
3	Dharam Kapse	209403016	[Signature]
4	Abhishek Deep	209202169	[Signature]
5	Utkarsh Ras	209202168	[Signature]
6	Priyadarshi Rajeev	219310341	[Signature]
7	Avaneesh Kulkarni	219402016	[Signature]
8	Aarjun S. Vmikas	219407003	[Signature]
9	Kalith Blankaran	209403038	[Signature]
10	Amrutha Agarwal	219301541	[Signature]
11	Dhar Desai	209403068	[Signature]
12	Rahul Acharya	209403032	[Signature]
13	Sekil Singh	209403059	[Signature]
14	Rivam Kamarkar	209403071	[Signature]
15	Maan Gang	209403055	[Signature]
16	Priyanshu Parik	209403023	[Signature]
17	Nishu Kumar Agarwal	209403066	[Signature]
18	Darashish Singh	219303101	[Signature]
19	Mohit Goyal	219311133	[Signature]
20	ISHA	219311102	[Signature]
21	Sanjay	219311215	[Signature]
22	Chely Fernandes	209303150	[Signature]
23	Surat Rohit Venkat	209403043	[Signature]
24	Chintha Naga Bramhadevi	209403059	[Signature]
25	Vidhi Gang	219311154	[Signature]
26			
27			
28			
29			
30			
31			
32			
33			
34			
35			
36			
37			
38			
39			
40			
41			
42			
43			
44			
45			
46			
47			
48			
49			
50			

15/3/23 Session 2 : 2pm - 4pm

Sr. No.	Name	Registration No.	Signature
1	Bonima Arthik	209403072	
2	Shubopanna Katayari	209403020	
3	Rahul Sejadoddi	209403045	
4	Dhruvil Shah	219403008	
5	Ritik kumar	219403022	
6	Adarsh Baulhadra	219403036	
7	Deepak Kumar Lilari	219311038	
8	Ishita Singh	219311036	
9	Sohaj gem	219311023	
10	Anushi Anboma	219311005	
11	Dhruv Sharma	219311026	
12	Riddhansa Saha	219311058	
13	Aadhya via	219311007	
14	Harsh Padmaluar	209403047	
15	Shravya Saha	209403014	
16	Anannaya Rasalkar	209403065	
17	Mohit Goyal	219311133	
18	ISHA	219311102	
19	Sanjay	219311215	
20	Ashwini K Singhal	209403025	
21	Nivish Kumar Aggarwal	209403066	
22	Pulkit Gupta	209403056	
23	Sarah Butaney	209403064	
24			
25			
26			
27			
28			
29			
30			
31			
32			
33			
34			
35			
36			
37			
38			
39			
40			
41			
42			
43			
44			
45			
46			
47			
48			
49			
50			

16/3/23

Session 1: 10 am -> 12 pm

Sr. No.	Name	Registration No.	Signature
1	Rishi kumar	219403022	Rishi
2	Abhishek Bhaskaran	209403038	Abhishek
3	Rahul Acharya	209403032	Rahul
4	Neel Sasudkar	209403053	Neel
5	Manuajini Ghadge	209403045	Manuajini
6	Aarjun S. Umrikar	219407003	Aarjun
7	Parashikhi Singh	219303111	Parashikhi
8	Dhrum Derai	209403006	Dhrum
9	Sami Singh	209403051	Sami
10	Manan Singh	209403022	Manan
11	Pulkit Gupta	209403046	Pulkit
12	Somya Lalchand	209202206	Somya
13	Bhishik Kumar	209302223	Bhishik
14	Darshan Kapoor	209403018	Darshan
15	Vidhi Gang	219311154	Vidhi
16	Chely Fernando	209203150	Chely
17	Mohit Goyal	219311133	Mohit
18	Shubanya Singh	219302085	Shubanya
19	Saahil Butaney	209403064	Saahil
20	Anannaya Rasalkar	209403065	Anannaya
21			
22			
23			
24			
25			
26			
27			
28			
29			
30			
31			
32			
33			
34			
35			
36			
37			
38			
39			
40			
41			
42			
43			
44			
45			
46			
47			
48			
49			
50			

16/3/23

Session 2: 2pm - 4pm.

Sr. No.	Name	Registration No.	Signature
1	Dhruv Desai	209403061	
2	Pulkit Gupta	209403046	
3	Rahul Acharya	209403032	
4	Lalit Bhutani	209402038	
5	Maan Garg	209401055	
6	Sayush Lakshani	209202206	
7	Pravesh Kapoor	209403016	
8	Ashwin Singh	209403025	
9	Vidhi Garg	219311154	
10	Suhag	219311115	
11	Mohit Goyal	219311133	
12	Ashwin Deep	209202161	
13	Shukanya Singh	219302025	
14	Karan Nene	219402006	
15	Sanchi Butaney	209403064	
16			
17			
18			
19			
20			
21			
22			
23			
24			
25			
26			
27			
28			
29			
30			
31			
32			
33			
34			
35			
36			
37			
38			
39			
40			
41			
42			
43			
44			
45			
46			
47			
48			
49			
50			

17/3/21

Session 1: 10 am - 12 pm

Sr. No.	Name	Registration No.	Signature
1	Akshay K. Singh	209403025	[Signature]
2	Pulkit Gupta	209403046	Pulkit
3	Nirpendra Prasad	209202026	N Prasad
4	Sayush Lakshmi	209202206	[Signature]
5	Abhishek Deep	209202169	Abhishek
6	Dhruv Desai	209403068	[Signature]
7	Sahil Singh	209403059	Sxx
8	Shivam Kametkar	209403071	[Signature]
9	Priyadarshi Rajeev	219310341	Priyadarshi
10	Rahul Anandya	209402777	[Signature]
11	Mohan Garg	209402055	[Signature]
12	Lalita Bhaskaran	209402078	[Signature]
13	Krishnamurthy K	209202297	[Signature]
14	Devsham Kapoor	209403016	[Signature]
15	Love	219311046	[Signature]
16	Shubham	219311319	[Signature]
17	Vidhi Garg	219311154	[Signature]
18	Mohit Goyal	219311335	[Signature]
19	Devarshi Singh	219303161	[Signature]
20	KANAD NEMADE	219408006	kanad
21	Sanchi Buleeny	209403064	Sanchi
22	Anamaya Rasolkar	209403065	[Signature]
23			
24			
25			
26			
27			
28			
29			
30			
31			
32			
33			
34			
35			
36			
37			
38			
39			
40			
41			
42			
43			
44			
45			
46			
47			
48			
49			
50			

17/3/23

Session 2: 2pm - 4pm

Sr. No.	Name	Registration No.	Signature
1	Ananmaya Rosalkar	209403065	Anan
2	Savit Singh	209403059	Savit
3	Pallavi Gupta	209403096	Pallavi
4	Dhruv Desai	209403068	Dhruv
5	Prashant K. Singh	209403025	Prashant
6	Maan Gang	209403055	Maan
7	Swam Kamrun	209403070	Swam
8	Lalita Anandaram	209403038	Lalita
9	Krishnashanti K	209202237	Krishna
10	Nirpendra	209202026	Nirpendra
11	Rahul Ananya	209403033	Rahul
12	JUVYAN	219311219	Juvyan
13	Paryadarsi Rajeev	219310341	Paryadarsi
14	Devashish Singh	219303101	Devashish
15	Mohit Goyal	219311133	Mohit
16	Ashish K. Desai	209202169	Ashish
17	Sayush Salunkhe	209202206	Sayush
18	KANAD NEMADE	219408006	Kanad
19	Sande Butaney	209403064	Sande
20	Darshan Kapoor	209403016	Darshan
21			
22			
23			
24			
25			
26			
27			
28			
29			
30			
31			
32			
33			
34			
35			
36			
37			
38			
39			
40			
41			
42			
43			
44			
45			
46			
47			
48			
49			
50			

9. Post-event link:

<https://jaipur.manipal.edu/muj/life-at-muj/Student-CLUBS.html>



Sarah Butaney

(3rd Year, 209403064, Department of Mechatronics)

Student Coordinator

Contact Number
9558164250



Dr. Princy Randhawa

(Department of Mechatronics)

Faculty Coordinator

Contact Number
9521099223



Darshan Kapoor

(3rd Year, 209403016, Department of Mechatronics)

Student Coordinator

Contact Number
8839593813



Dr. Shambo Roy Choudhury

(Department of Mechatronics)

Faculty Coordinator

Contact Number
7888379160



**MANIPAL UNIVERSITY
JAIPUR**



**MANIPAL UNIVERSITY
JAIPUR**

FACULTY OF ENGINEERING

School of Electrical, Electronics and Communication (SEEC)

ELECTRICAL ENGINEERING

AICTE recognized ICT Mode FDP

on

“Smart Grid and Integration of Distributed Generation”

Date of Event: 28th August-1st September 2023



Content of Report

1. Introduction of the Event
2. Objective of the Event
3. Beneficiaries of the Event
4. Details of the Speaker
5. Brief Description of the event
6. Flyer of the FDP
7. Photographs
8. Schedule of the Event
9. Attendance of the Event

1. Introduction of the Event

Department of Electrical Engineering, SEEC organised a AICTE recognized ICT Mode faculty development program on “Smart Grid and Integration of Distributed Generation” in association with MUJ-TECH & NITTTR Chandigarh, from 28th August – 1st September 2023 at Manipal University Jaipur.

2. Objective of the Event

Objectives of Course:

1. The participants apprised about the latest trends in Smart Grid and Distributed Generation such as Power Electronic Interfaces in DC and AC Micro-grid, Distributed Generation Integration and Pricing, Energy Storage and Battery Management and Hardware in Loop.
2. The participants provided with relevant study material and were evaluated at the end of the course.

3. Beneficiaries of the Event

This FDP was organized for students, PhD research scholars, faculty members for host institute as well as for other institutes.

4. Details of the Speaker

- a. Dr. C.K. Chanda, Professor, EED, IEST, Shibpur
- b. Dr. A.V.Ravi Teja, Assistant Professor, IIT, Ropar
- c. Dr. Moumita Das, Assistant Professor, IIT, Mandi
- d. Dr. Poonam Saini, Assistant Professor, PEC, Chandigarh
- e. Dr. Ajay Sheoran, Associate Professor, EED, PEC, Chandigarh
- f. Dr. Poonam Syal, Professor, EED, NITTTR Chandigarh
- g. Dr. Shimi.S.L, Associate Professor, EED, PEC, Chandigarh
- h. Dr. Ritula Thakur, Associate Professor, EED, NITTTR Chandigarh
- i. Er. Mohini Gunjal, Research Scholar, NITTTR Chandigarh
- j. Er. M. Soujanya, Research Scholar, NITTTR Chandigarh
- k. Dr Lini Mathew, Professor, EED, NITTTR Chandigarh

5. Brief Description of the event

A five-days' Faculty Development Programme (FDP) on topic "Smart Grid and Integration of Distributed Generation" was organised by department of Electrical Engineering on 28th August-1st September 2023 in association with MUJ-TECH & NITTTR Chandigarh. The program was conducted in online mode using Google Meet. Eminent experts from industry and academia engaged the sessions, other than the NITTTR faculty. The aim of this FDP was to understand the concept of smart grid, hybrid renewable energy systems, distributed generation integration, and its pricing. Smart micro grid operation with Integration of renewable energy sources and electric vehicles were also explained. Different islanding detection techniques on micro grid and power quality issues of DG Integration with grid were also elaborated to participants. Some advance topics were explained such as cyber security in smart grid, advanced metering infrastructure, energy storage systems in smart grid. A hands-on session was also conducted for participants to understand Hardware in Loop and Real Time Simulation.

The FDP served to bring communities together to share knowledge, learn from one another and develop understanding for future energy sector.

The Course contents were:

1. Concept of Smart Grid, Hybrid Renewable Energy Systems
2. Distributed Generation Integration and Pricing
3. Smart Micro Grid Operation with Integration of RES and EV
4. Islanding Detection Techniques on Micro Grid
5. Power Quality Issues of DG Integration with Grid
6. Cyber Security in Smart Grid
7. Advanced Metering Infrastructure
8. Energy Storage Systems in Smart Grid
9. Concept of Hardware in Loop and modelling and Simulation of Micro-Grid

6. Flyer of the FDP



**MANIPAL UNIVERSITY
JAIPUR**

**Department of Electrical Engineering
School of Electrical, Electronics and Communication Engineering
(SEECE)**

is organizing

**Five-Days Faculty Development Program
on
Smart Grid and Integration of
Distributed Generation
(ICT Mode)**

in association with

**National Institute of Technical Teachers Training and Research (NITTTR)
- Chandigarh and MUJ-TEC**

August 28 to September 01, 2023 | Lab 113, First Floor, 1AB, MUJ

Chief Patron

Patron

Co-Patrons

Organizers

Conveners

Mr S. Vaitheeswaran
Chairperson, MUJ

Dr G K Prabhu
President, MUJ

Dr Thammaiah CS
Pro-President, MUJ

Dr Nitu Bhatnagar
Registrar, MUJ

Dr Arun Shanbhag
Dean, FoE, MUJ

Dr Amit Soni
Director SEECE

Dr Devi Prasad Sharma
Director MUJ-TEC

Dr Amit Saraswat
HoD- Electrical Engineering

Dr Neeraj Kanwar
Convener

Mr Samarendra Pratap Singh
Co-Convener

Scan the QR Code
Registration Link



Looking forward to your active participation
in the sessions related to Smart Grid and Integration of
Distributed Generation

<https://fdp.nitttrchd.ac.in/backingup/>



7. Photographs

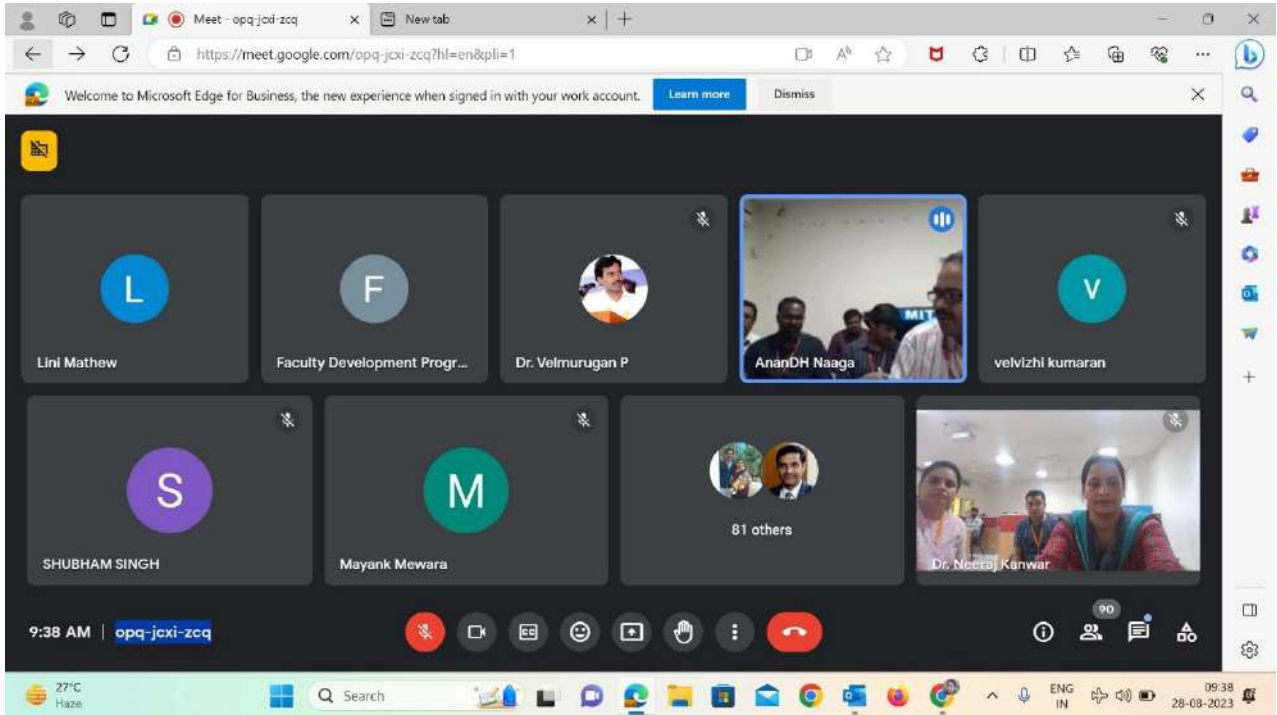


Fig.1 Starting of FDP

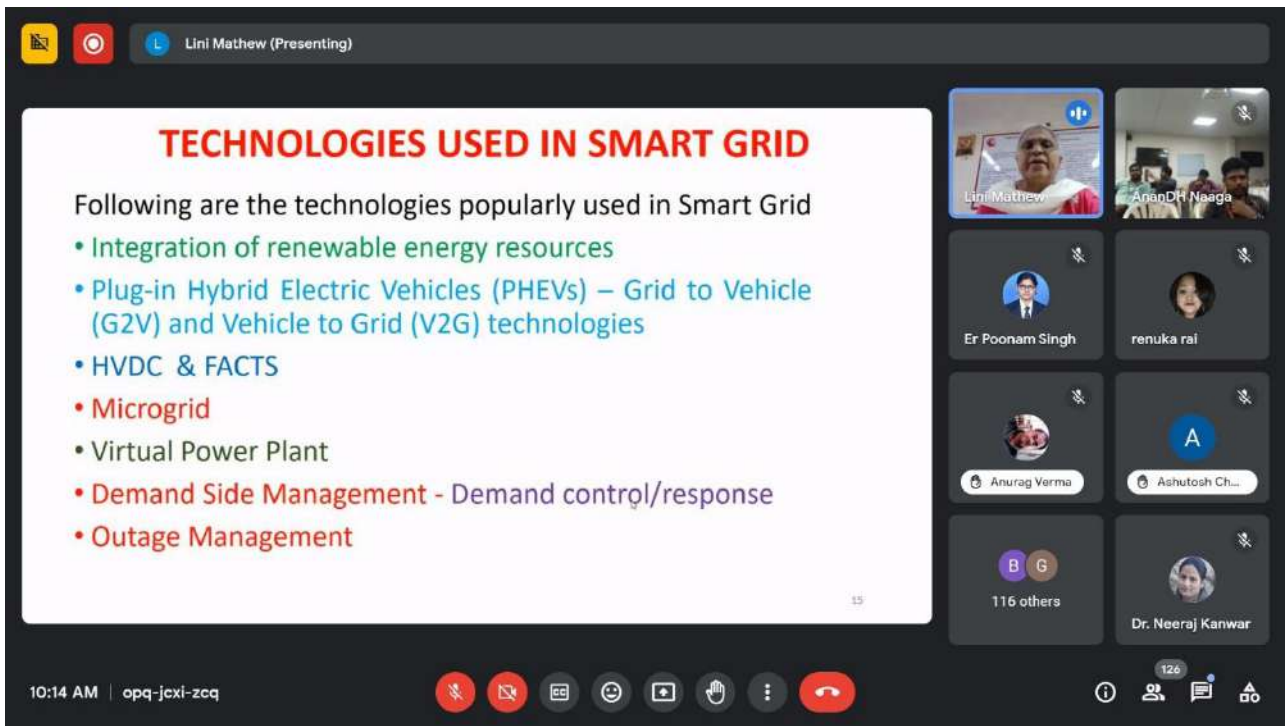


Fig.2 Introduction about Smart Grid

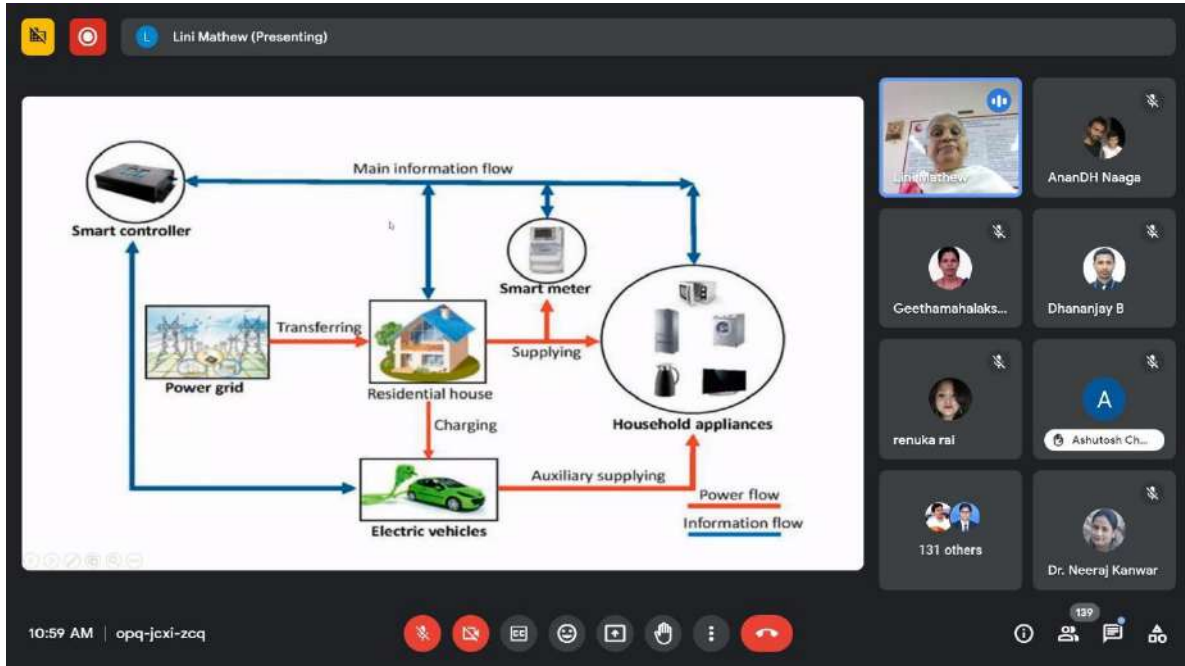


Fig. 3 Discussion about Smart meters

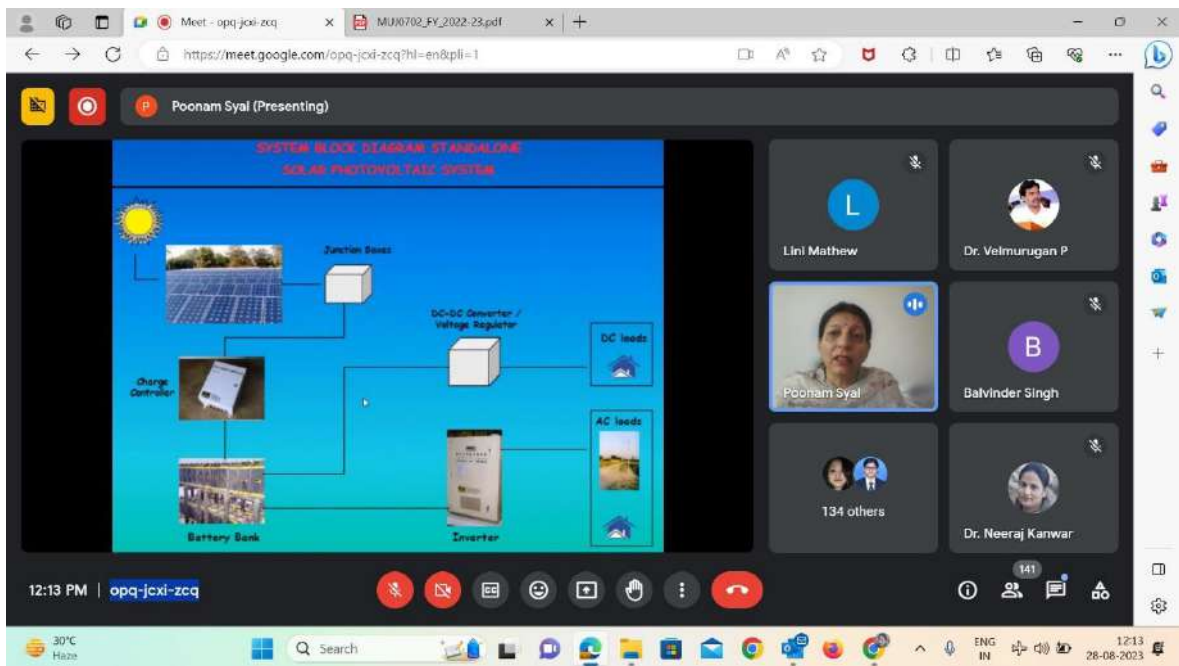


Fig.4 Introduction for SPV systems

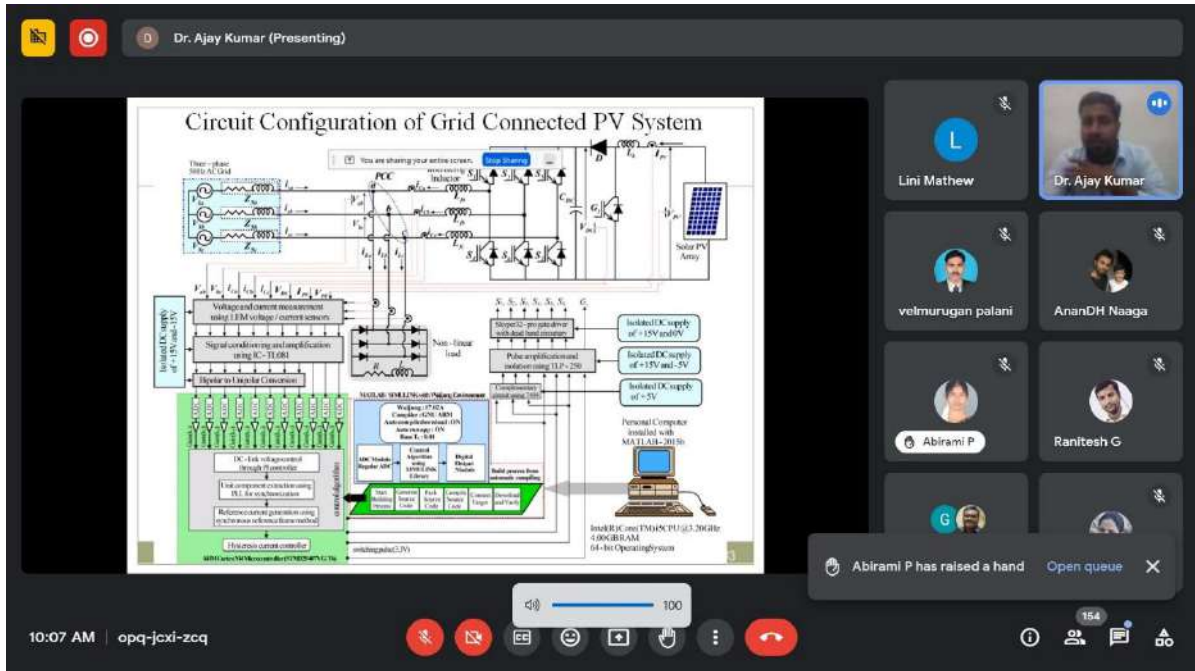


Fig.5 Grid-connected PV system

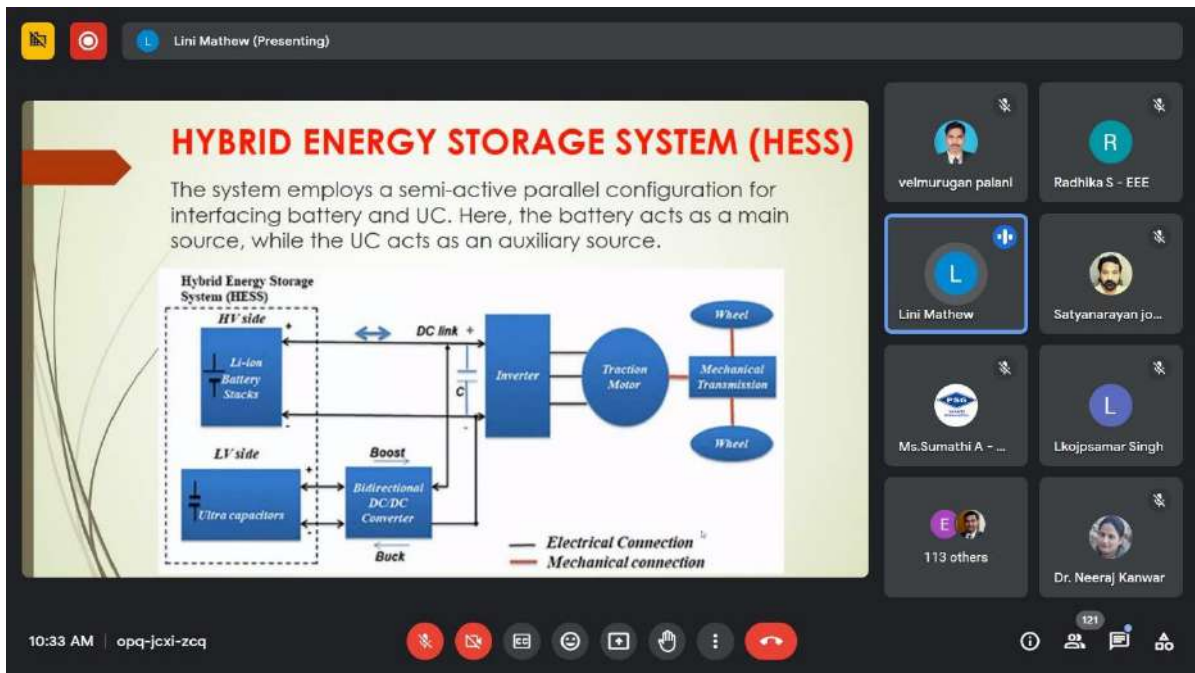


Fig.6 Explanation for hybrid energy storage system

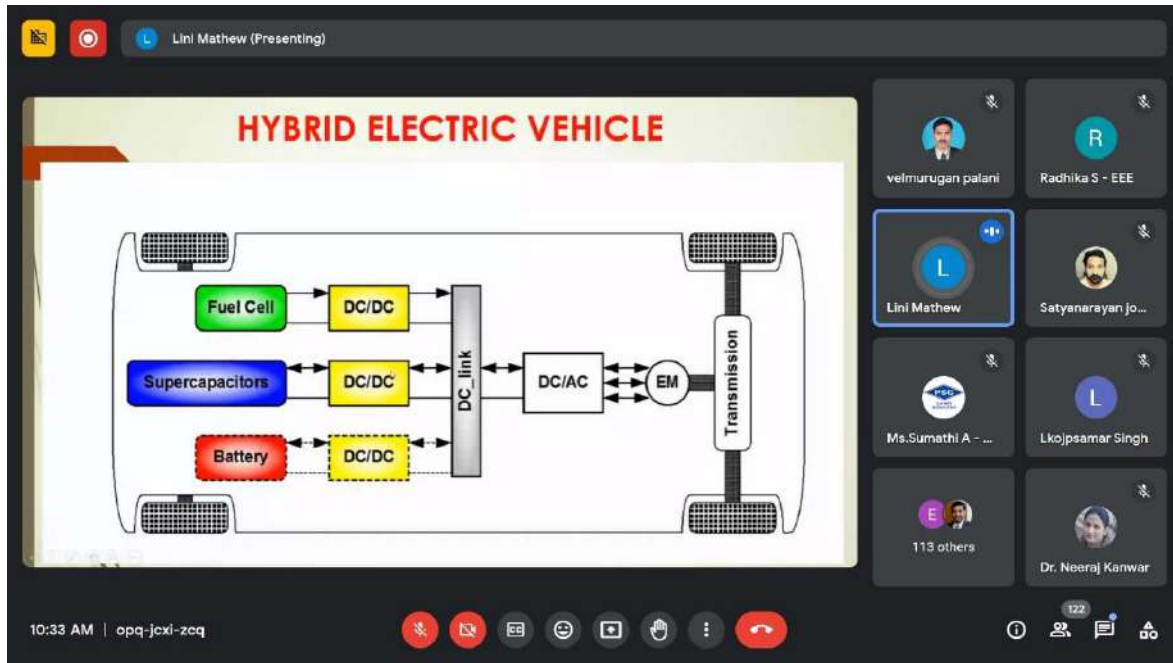


Fig.7 Hybrid electric vehicles



Fig.8 Cybersecurity in smart grids



Fig.9 Power quality issues in smart grid



Fig. 11 High speed railway traction application

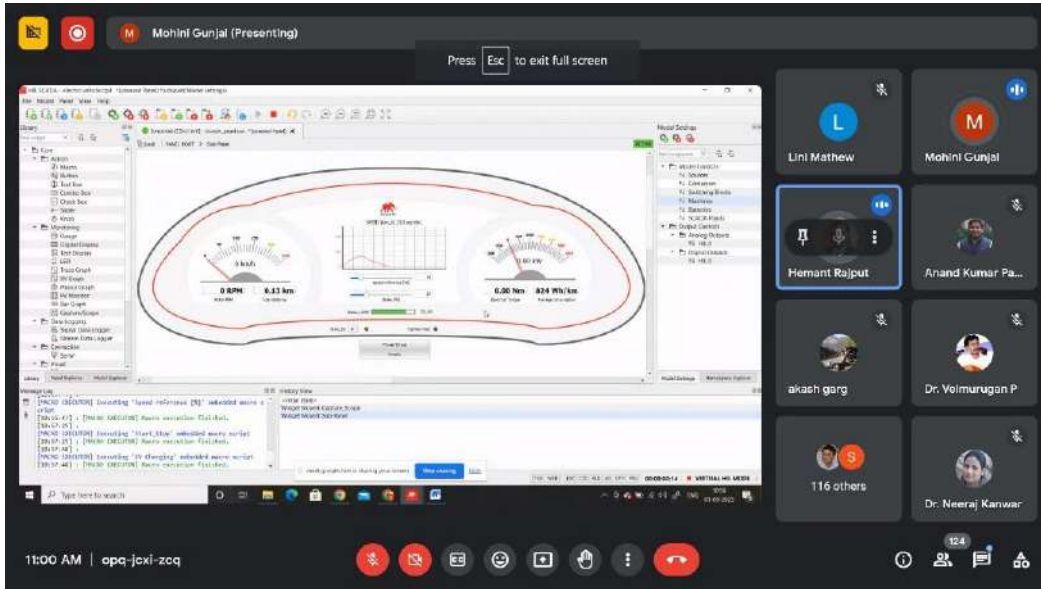


Fig. 10 Hands-on for Real time simulator

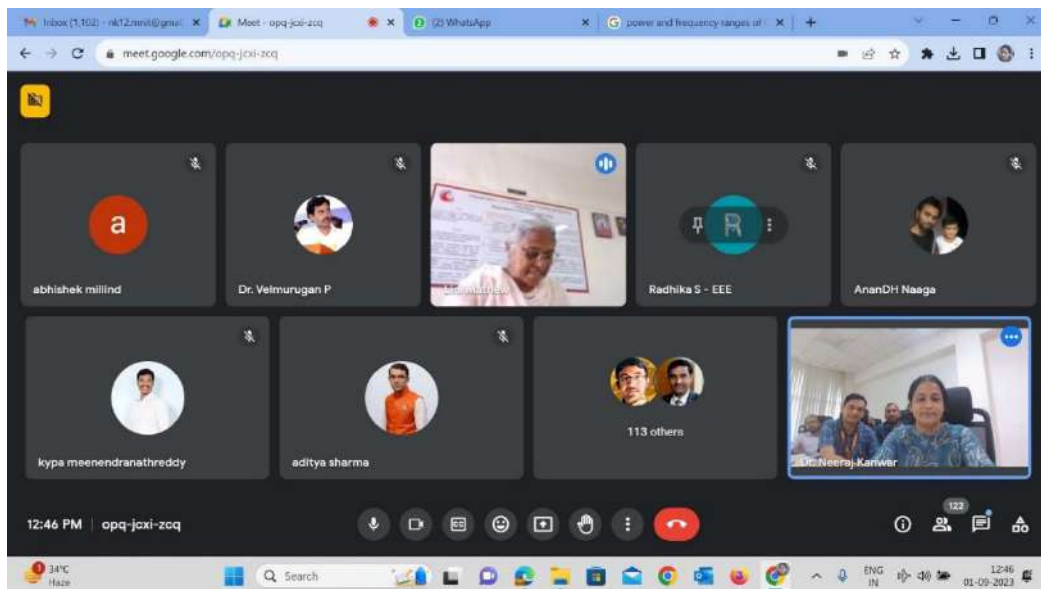


Fig. 12 Vote of thanks

8. Schedule of the event

Date: 28th August – 1st September 2023

Mode: Online through Google Meet

Topic: Smart Grid and Integration of Distributed Generation

The schedule for each session of FDP was as follows:

DAY & DATE	Live Session - 1 9.30 AM to 11.00 AM	Live Session - 2 11.30 AM to 1.00 PM	Live Session - 3 2.30 PM to 4.00 PM
Monday 28/08/2023	Modern Era Energy Grid (LM)	Renewable Energy Sources (PS)	Microgrid – Types, Topologies and Control (MS)
Tuesday 29/08/2023	Design, Development and Implementation of Grid Connected Solar PV System (AS)		Challenges in Smart Grid Implementation (CKC)
Wednesday 30/08/2023	Smart Grid – Architecture, Standards and Technologies (LM)	Cyber Security in Smart Grid with some Practical Examples (PS)	Measurement based Power Quality Study of EV & DG Integration into the Grid (SSL)
Thursday 31/08/2023	Grid Connected EVs and their related Power Quality Issues (RT)	Wind Power Extraction and Grid Connection Techniques (AVR)	Power Electronic Traction for High Speed Trains (MD)
Friday 01/09/2023	Real Time Simulation of various DG systems and Microgrid using Typhoon HIL (MG)		FDP Valediction

CKC: Dr. C.K. Chanda, Professor, EED, IEST, Shibpur

AVR: Dr. A.V.Ravi Teja, Assistant Professor, IIT, Ropar

MD: Dr. Moumita Das, Assistant Professor, IIT, Mandi

PS: Dr. Poonam Saini, Assistant Professor, PEC, Chandigarh

AS: Dr. Ajay Sheoran, Associate Professor, EED, PEC, Chandigarh

PS: Dr. Poonam Syal, Professor, EED, NITTTR Chandigarh

SSL: Dr. Shimi.S.L, Associate Professor, EED, PEC, Chandigarh

RT: Dr. Ritula Thakur, Associate Professor, EED, NITTTR Chandigarh

MG: Er. Mohini Gunjal, Research Scholar, NITTTR Chandigarh

MS: Er. M. Soujanya, Research Scholar, NITTTR Chandigarh

LM: Dr Lini Mathew, Professor, EED, NITTTR Chandigarh

9. Attendance of the Event Total attendee-22

Sr. No.	Name of the Participant	Name of the Institute
1	DR. AMIT SARASWAT	MANIPAL UNIVERSITY JAIPUR
2	BHUWAN PRATAP SINGH	MANIPAL UNIVERSITY JAIPUR
3	DR. CHANDRA PRAKASH GUPTA	MANIPAL UNIVERSITY JAIPUR
4	DR. DIVYA RISHI SHRIVASTAVA	MANIPAL UNIVERSITY JAIPUR
5	DR. SUMAN SHARMA	SWAMI KESHVANAND INSTITUTE OF TECHNOLOGY, MANAGEMENT & GRAMOTHAN, JAIPUR
6	DR. MANISH KUMAR THUKRAL	MANIPAL UNIVERSITY JAIPUR
7	GAURAV GANGIL	MANIPAL UNIVERSITY JAIPUR
8	MOHIT JAMBU	GULZAR GROUP OF INSTITUTIONS
9	MOHIT KUMAR SHARMA	MANIPAL UNIVERSITY JAIPUR
10	MUKESH KUMAR KUMAWAT	MANIPAL UNIVERSITY JAIPUR
11	DR. NEERAJ KANWAR	MANIPAL UNIVERSITY JAIPUR
12	DR. NEHA JANU	MANIPAL UNIVERSITY JAIPUR
13	NIDHI CHOUDHARY	MANIPAL UNIVERSITY JAIPUR
14	RAJESH KUMAR	MANIPAL UNIVERSITY JAIPUR
15	RISHI RATAN SINHA	MANIPAL UNIVERSITY JAIPUR
16	SAMARENDRA PRATAP SINGH	MANIPAL UNIVERSITY JAIPUR
17	SATYA NARAYAN AGARWAL	MANIPAL UNIVERSITY JAIPUR
18	SMRITI JAIN	SWAMI KESHVANAND INSTITUTE OF TECHNOLOGY, MANAGEMENT & GRAMOTHAN, JAIPUR
19	DR. SUNIL KUMAR GOYAL	MANIPAL UNIVERSITY JAIPUR
20	VIKAS KUMAR BORADAK	MANIPAL UNIVERSITY JAIPUR
21	DR. VINAY GUPTA	MANIPAL UNIVERSITY JAIPUR
22	DR. VISHAL DAS	MANIPAL UNIVERSITY JAIPUR



MANIPAL UNIVERSITY JAIPUR



Dr. Neeraj Kanwar, Centre Coordinator (Local Coordinator)

Neeraj
05/09/2023

Mr. Samarendra Pratap Singh, Supporting Faculty (Co-coordinator)

S.P. Singh
05/09/2023

Conveners

HOD
Department of Electrical Engineering
School of Electrical,
Electronics & Communication (SEEC)
Manipal University Jaipur

Dr. Amit Saraswat


05/09/2023

Seal and Signature of Head with date



सत्यमेव जयते

INDIA NON JUDICIAL Government of Rajasthan

e-Stamp

Certificate No. : IN-RJ39965195867844S
Certificate Issued Date : 14-Dec-2020 03:56 PM
Account Reference : NONACC (SV)/ rj3119204/ JAIPUR/ RJ-JP
Unique Doc. Reference : SUBIN-RJRJ311920470892870480170S
Purchased by : E GREEN
Description of Document : Article 4 Affidavit
Property Description : MAHIMA DESIRE, JAISINGHPURA, JAIPUR, RAJASTHAN
Consideration Price (Rs.) : 0
(Zero)
First Party : E GREEN
Second Party : NA
Stamp Duty Paid By : E GREEN
Stamp Duty Payable (Rs.) : 100
(One Hundred only)
Surcharge for Infrastructure Development (Rs.) : 10
(Ten only)
Surcharge for Propagation and Conservation of Cow (Rs.) : 20
(Twenty only)
Stamp Duty Amount (Rs.) : 130
(One Hundred And Thirty only)

HOPE GREEN
[Signature]
Proprietor

[Signature]
Dinesh Pruthi
ATC - MULTITASKING



RS 0003759237

Statutory Alert:

1. The authenticity of this Stamp certificate should be verified at 'www.shcliestamp.com' or using e-Stamp Mobile App of Stock Holding. Any discrepancy in the details on this Certificate and as available on the website / Mobile App renders it invalid.
2. The onus of checking the legitimacy is on the users of the certificate.
3. In case of any discrepancy please inform the Competent Authority.

Memorandum of Understanding

This **Memorandum of Understanding** Agreement ("**Agreement**") is entered into on this the 15 December 2020 by and amongst:

1. **AIC – MUJ Incubation Foundation (U93090RJ2018NPL061558)**, registered under the provisions of the Companies Act 2013 and having its registered office at C/O Manipal University Jaipur, Dehmi kalan, Jaipur Ajmer Expressway, Rajasthan - 303007 (herein after referred to as the "**Incubator**" which expression shall, unless it be repugnant to the subject or context thereof, include its successors and permitted assigns)
2. The persons set out in Schedule I hereto (hereinafter referred to as individually as a "**Founder**" and collectively as the "**Founders**", which expression shall, unless repugnant to the context or meaning thereof, include their respective heirs, executors, administrators and permitted assigns);

AND

3. **E GREEN <(CIN) Number>**, a company incorporated under the laws of India and having its registered office at MAHIMA DESIRE, JAISINGHPURA, JAIPUR , RAJASTHAN(hereinafter referred to as the "**Company**", which expression shall unless repugnant to the context or meaning thereof, include its successors and permitted assigns).

Each of the Founders, the Incubator and the Company shall hereinafter be referred to individually as a "**Party**" and collectively as the "**Parties**".

WHEREAS the Company, is seeking professional and infrastructural support and guidance more specifically enumerated in Schedule II (the "**Incubator Facilities**"). The Incubator has hereby committed to support and mentor the Company and the Founders for a period of twelve months<Incubation Period> from the **Effective Date**.

NOW THEREFORE, in consideration of the foregoing and other good and valuable consideration, the receipt and adequacy of which are hereby expressly acknowledged, the Parties, intending to be legally bound, hereby agree as follows:


E GREEN
Proprietor


Dinya Pritwani


1. Definitions & Interpretation:

1.1 Definitions:

Act shall mean the Companies Act, 1956 and the Companies Act, 2013, as may be applicable, together with the rules and regulations hereunder, as may be amended, modified, supplemented or re-enacted from time to time;

Board shall mean the board of directors of the Company;

Business shall mean the Egreen is into manufacturing of recycled utility & gifting products such as handmade paper.

Direct Competitor shall mean any Person engaged in the same or similar business as the Business;

Effective Date shall mean the date on which the Parties mutually agree on the Machine List and Timelines;

Equity Shares or **Shares** shall mean equity shares of the Company having face value INR 10;

Fair Market Value shall mean the value of the Company and the pro rata value of Shares as determined by an independent valuer appointed by the Company for this purpose;

Law shall mean any statute, law, regulation, ordinance, rule, judgment, notification, rule of common law, order, decree, bye-law, Governmental Approval, directive, guideline, requirement or other governmental restriction, or any similar form of decision of, or determination by, or any interpretation, policy or administration, having the force of law of any of the foregoing, by any Governmental Authority having jurisdiction over the matter in question, whether in effect as of the date of this Agreement or thereafter;

Success Fee shall mean a claim by Incubator for a success fee or incentive fee calculated at the rate of 5% of total business or funds generated via connections or programs executed or facilitated by incubator. The funds could be generated by Sales, Paid Contracts, Grants received, Investor Capital Raised, etc.

1.2 Interpretation: Any capitalized term used but not defined herein shall have the meaning ascribed thereto in the Investment Agreement.

2. Consideration.

Further for business or funds generated via connections or programs executed or facilitated by AIC a success fees would be charged by the incubator and the same shall be payable within 30 (thirty) days of the contract.

3. Relationship: The Incubator shall be an independent contractor and nothing in this Agreement shall render the Incubator an employee, worker, agent or partner of the Company.

EGREEN
Proprietor


Dinaya Prithwani
FOUNDATION • AIC - MUMBAI

4. Term & Termination:

- 4.1 This Agreement shall come into effect on the Execution Date and shall remain valid and binding on the Parties until such time that it is terminated in accordance with Clause 4.2 below
- 4.2 Termination:
- (i) This Agreement may be terminated at the option of the Incubator if the Success Fee is not transferred in accordance with Clause 2.
- (ii) This Agreement may be terminated at the option of the Incubator in the following circumstances:
(a) use of the Incubator Facilities by the Company for purposes other than for furtherance of its business;
(b) causing damage to the Incubator's property;
(c) Breach by the Company of the covenants set out in Schedule III hereto.
- (iii) This Agreement may be terminated at the option of the Company or the Founders if (a) the Effective Date has not occurred within 3 months of the Execution Date or (b) there is a material deviation in the Machine List and Timelines.
- (iv) This Agreement may be terminated at the option of the Company or the Founders in the event the Incubator fails to comply with its responsibilities under this Agreement or materially breaches the terms of this Agreement.
- (v) This Agreement may be terminated at any time by the mutual agreement of the Founders and the Incubator.
- 4.3 In the event of termination by the Incubator for the reasons set out in (ii) above, the Incubator may require the Company to vacate the premises with 7 days' notice, subject to the Dispute Resolution procedure set out herein.
- 4.4 In the event of termination by the Company or the Founders for the reasons set out in (iii)(b) or (iv) above, 50% of the Success Fee must be transferred back to the respective Founders by the Incubator as soon as commercially possible, subject to the Dispute Resolution procedure set out herein.
- 4.5 The termination of this Agreement shall not relieve any Party of any obligation or liability accrued prior to the date of termination.
- 4.6 The clauses of this Agreement which by their nature should survive termination shall survive such termination.

5. Exit: [Not Applicable]

- 5.1 Buyback Option: At any time after a period of three years from the Execution Date, the Incubator shall, subject to applicable Law, have the right to request the Company to buyback its all of the Incubation Shares at a price per Share equal to the fair market value of the Shares determined by an independent third party appraising firm mutually agreed by the Incubator and the Company.
- 5.2 Founders' Right to Repurchase: At any time after a period of three years from the Execution Date, the Founders, shall, subject to applicable Law, have the right to repurchase their portion of the Incubation Shares from the Incubator at a price per Share equal to the fair market value of the Shares determined by an independent third party appraising firm mutually agreed by the Incubator and the Company.
- 5.3 Incubator's Tag Along Right: In the event the Founders finalize an agreement for the sale of all (and not less than all) their shares in the Company at any time (subject to the terms of the Investment Agreement) to a Buyer at an agreed upon price per share, the Incubator shall have the right,

FOLEGREEN
Incubator



Diya Birtwani


exercisable at its sole option, to exit the Company and require the Founders to cause the Buyer to purchase all (but not less than all) of the Incubation shares at the same price per share.

6. Limitation of Liability:

6.1 In no event shall the Party be liable to any other Parties for any special, incidental, indirect or consequential damages arising out of or in connection with this Agreement.

6.2 In no event shall a Party or any of its partners, officers, employees, representatives or agents be liable for any liability whatsoever for any losses or expenses of any nature suffered by another Party arising directly or indirectly from any act or omission of such Party or its employees, agents or representatives hereunder.

7. **Tax Liability:** Any and all tax liability that may be incurred by a Party as a consequence of operation of Applicable Law shall be borne by the respective Party.

8. **Costs and Expenses:** Each Party will bear its own expenses incurred in connection with the preparation, negotiation and execution of this Agreement. In addition, all costs and expenses in relation to payment of any stamp duty, registration duty and service taxes on the Definitive Documents under applicable Law shall be borne equally by the Company and the Incubator.

9. **Indemnity:** Each Party hereby agree to protect, defend, indemnify and hold harmless the other Parties, their employees, officers, partners, agents or representatives from and against any and all liabilities, damages, fines, penalties and costs (including legal costs and disbursements), arising from or relating to any third party claims, demands, fines, penalties and other sanctions imposed by any authority for non-compliance with any applicable law pursuant to and by virtue of this Agreement; and/ or any losses, liabilities, expenses, damages and / or claims suffered or incurred by the Incubator (including reasonable legal fees) as a result of such Party's negligence, fraud or wilful default in relation to this Agreement.

Each Party shall also indemnify and keep indemnified the other Parties for any breach of the terms and conditions of this Agreement.

10. Intellectual Property:

10.1 "**Intellectual Property**" includes patents, inventions, know how, trade secrets, trademarks, service marks, designs, tools, devices, models, methods, procedures, processes, systems, principles, algorithms, works of authorship, flowcharts, drawings, and other confidential and proprietary information, data, documents, instruction manuals, records, memoranda, notes, user guides, ideas, concepts, information, materials, discoveries, developments, and other copyrightable works, and techniques in either printed or machine-readable form, whether or not copyrightable or patentable

10.2 "**Intellectual Property Rights**" include: (i) all right, title, and interest under any statute or under common law including patent rights; copyrights including moral rights; and any similar rights in respect of Intellectual Property, anywhere in the world, whether negotiable or not; (ii) any licenses, permissions and grants in connection therewith; (iii) applications for any of the foregoing and the right to apply for them in any part of the world; (iv) right to obtain and hold appropriate registrations in Intellectual Property; (v) all extensions and renewals thereof; and (vi) causes of action in the past, present or future, related thereto including the rights to damages and profits, due or accrued, arising out of past, present or future infringements or violations thereof and the right to sue for and recover the same.

10.3 Except as set out in this Clause 11, each Party agrees that all Intellectual Property Rights, which are held by the other Party, shall remain in the sole and exclusive ownership of such other Party.

10.4 Any Intellectual Property and Intellectual Property Rights developed or conceived by the Company while receiving guidance or support as described in Schedule II shall vest absolutely and irrevocably with the Company.

FOREGREEN
PROMOTERS
[Signature]

[Signature]
AIC - MUMBAI
ASSOCIATION

11. Non-Disclosure:

- 11.1 All information and data belonging to the Company of confidential and proprietary nature be it specifically documented or not, shall be termed as confidential information ("**Confidential Information**"). This includes but is not limited to:
- a. creative information, including symbols, photographs, animations, videos, models, techniques, experimental methods, designs, concepts, research, insights and other creations;
 - b. technical information, including research programs and methods, product development plans, functional and technical specifications, technology, inventions, ideas, concepts, drawings, designs, analysis, research, methods, techniques, processes, computer software, data, databases, flowcharts, patent applications, and other technical know-how and materials;
 - c. business information, including business plans, business strategies and/or data arising thereof, sales and marketing research, materials and plans, accounting and financial information, projections, performance results, cost data, customer information, personnel records and the like;
 - d. all proprietary information related to the Company; and
 - e. any other valuable information of the Company designated as confidential by the circumstances in which it is provided.
- 11.2 Confidential Information does not include such information or data that: (a) is or becomes generally known to the public without restriction through no fault of the Incubator, or (b) that the Incubator knew without restriction prior to its disclosure by Company.
- 11.3 The Incubator shall hold in confidence and not disclose or use any Confidential Information, except in connection with this Agreement or with the prior written permission of the Company. This Clause shall survive the termination of this Agreement.
- 11.4 Upon termination of this Agreement or as otherwise requested by the Company, the Incubator will promptly return to the Company all items and copies containing or embodying Confidential Information without retaining any copies (soft or hard copies) with himself

12. Dispute Resolution:

- 12.1 The Parties agree to negotiate in good faith to resolve any dispute between them regarding this Agreement. If the negotiations do not resolve the dispute to the reasonable satisfaction of the Parties, then the dispute shall be submitted to final and binding arbitration at the request the disputing Parties upon written notice to that effect to the other disputing Parties. In the event of such arbitration:
- 12.1.1 The arbitration shall be conducted in accordance with the Indian Arbitration and Conciliation Act, 1996 (the "**Arbitration Act**") in force at the relevant time (which is deemed to be incorporated into this Agreement by reference);
- 12.1.2 All proceedings of the arbitration shall be in the English language. The venue and seat of arbitration shall be at Jaipur, India;
- 12.1.3 All proceedings shall be conducted before a panel of 3 (three) arbitrators wherein, one arbitrator will be appointed by the claimants, the second arbitrator will be appointed by the respondents and the third arbitrator will be appointed jointly by the other two arbitrators; and
- 12.1.4 Arbitration awards rendered shall be final, binding and shall not be subject to any form of appeal.
- 12.2 Nothing shall preclude a Party from seeking interim equitable or injunctive relief, or both. The pursuit of equitable or injunctive relief shall not be a waiver of the right of the Parties to pursue any other remedy or relief through the arbitration described in this Clause 12.

FOR EGREEN
Proprietor

Divya Pritwani
FOUNDER & AIC - MUMBAI

13. Miscellaneous:

- 13.1 The Parties agree that the Incubator shall sign a "Deed of Adherence" to the Investment Agreement in a format as mutually agreed between the Parties.
- 13.2 This Agreement may be modified, amended or supplemented only by the mutual written agreement of the Parties. A waiver or any failure or delay by the Incubator to require the enforcement of the obligations, agreements, undertakings or covenants in this Agreement shall not be construed as a waiver by the Incubator of any of its rights, unless made in writing referring specifically to the relevant provisions of this Agreement and signed by a duly authorized representative of the Incubator. Any such waiver shall not affect in any way the validity of this Agreement or the right to enforce such obligation, agreement, undertaking or covenant at any other time. All rights and remedies existing under this Agreement, except as otherwise provided herein are cumulative to, and not exclusive of any rights or remedies otherwise available.
- 13.3 If for any reason whatsoever, any provision of this Agreement is or becomes, or is declared by a court of competent jurisdiction to be, invalid, illegal or unenforceable, then the Parties shall negotiate in good faith to agree on such provision to be substituted, which provisions shall, as nearly as practicable, leave the Parties in the same or nearly similar position to that which prevailed prior to such invalidity, illegality or unenforceability.
- 13.4 Except as may be otherwise provided herein, all notices, requests, waivers and other communications made pursuant to this Agreement shall be in writing and signed by or on behalf of the Party giving it. Such notice shall be served by delivering by hand, registered post, electronic mail or courier to the address set forth below. In each case it shall be marked for the attention of the relevant Party set forth below. Any notice so served shall be deemed to have been duly given (i) in case of delivery by hand, when hand delivered to the other Party; or (ii) when sent by registered post, where 7 (seven) Business Days have elapsed after deposit in the mail with certified mail receipt requested postage prepaid; or (iii) when delivered by courier on the 2nd (second) Business Day after deposit with an overnight delivery service, postage prepaid, with next Business Day delivery guaranteed, provided that the Party issuing the notice receives a confirmation of delivery from the delivery service provider; or (iv) for electronic mail notification, upon confirmation of such notification by any of the means as aforesaid.
- To the Founders:**
Attention : Ashutosh Sharma
Address : MAHIMA DESIRE, JAISINGHPURA, JAIPUR, RAJASTHAN
Email : go.egreen@gmail.com
- To the Company:**
Attention : EGREEN
Address : MAHIMA DESIRE, JAISINGHPURA, JAIPUR, RAJASTHAN
Email : go.egreen@gmail.com
- To the Incubator:**
Attention : CEO
Address : C/o Manipal University Jaipur, Dehmikalan, Bagru, Jaipur, Pin- 303007
Email : divya.pritwani@jaipur.manipal.edu
- 13.5 No Party shall assign this Agreement or any of its rights or obligations hereunder without the prior written consent of the other Parties.
- 13.6 This Agreement supersedes all earlier agreements, arrangements, letters, correspondence, understandings etc. with respect to the subject matter of this Agreement. For the avoidance of doubt, it is clarified that this Agreement does not supersede the Investment Agreement.
- 13.7 The Agreement may be executed and delivered in counterparts, each of which shall be deemed an original.
- 13.8 Save and except as otherwise stated in this Agreement, in the event that a Party commits a

FOR EGREEN
Ashutosh
Proprietor

Divya Pritwani
FOUNDACTION • AIC - MUI INCUBATION

default of the terms of this Agreement then, the non-defaulting Parties shall, in addition to any other rights and remedies available under this Agreement, be entitled to seek specific performance of this Agreement and such other remedies as may be permitted to it under applicable Law.

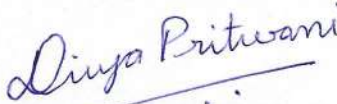
- 13.9 Each Party shall act in good faith in the performance of its respective responsibilities under this Agreement and will not unreasonably delay, condition or withhold the giving of any consent, decision or approval that is either requested or reasonably required by any other Party in order to perform its responsibilities.

IN WITNESS, WHEREOF the Parties have put their respective hands on the day and year first herein above written.

Signed and delivered by

For and on behalf of

1. AIC – MUJ Incubation Foundation




Chief Executive Officer

2. Founders



Ashutosh Sharma

3. Startup Name



Ashutosh Sharma
Director – E Green

SCHEDULE I

LIST OF FOUNDERS

1. Ashutosh Sharma

Ashutosh
Proprietor

Diya Prithvi



SCHEDULE II

INCUBATOR FACILITIES

1. The Incubator shall provide the Incubator Facilities as listed below for a period of twelve months from the Effective Date ("**Incubation Period**"):

A. Physical Infrastructure:

- Developed office space approximately admeasuring <No. of seats>. with furniture and air-conditioning machines to occupy and use for Business Incubator activities.
- 24x7 high speed Internet Connectivity
- Access to Maker Space/Fab Lab.

Notwithstanding anything contained in this Agreement, AIC – MUJ Incubation Foundation shall have absolute right and ownership of the office space provided to locate the Company (the company to be promoted by the Promoters). The Estate Officer of the AIC – MUJ Incubation Foundation shall be deemed to be a competent authority under the Public Premises (Eviction of Unauthorised Occupants) Act, 1971 for necessary actions in connection with the office space so occupied by the Company.

B. Common Infrastructure:

The Incubator will provide following facilities to the Company, which will be shared by all Companies located in the Incubator:

- Laser Printer
- Photocopier
- Scanner
- Meeting/Conference room with projection equipment

The ownership of all assets so provided as a part of Incubator supports and services rests with Incubator AIC – MUJ Incubation Foundation as the case may be.

The support and services described in clauses A and B herein above shall be herein after referred to as "Incubator facilities".

C. Network of Mentors and Experts:

Incubator will facilitate liaison with mentors, professionals and experts in technology, legal, financial and related matters on such terms and conditions as may be stipulated by them.

D. Event and Meetings:

Incubator will organise events to facilitate the companies located in the BI in networking and to showcase their technologies. Incubator will also facilitate meetings with visitors of AIC – MUJ Incubation Foundation and its constituent Institutions such as alumni, venture capitalists, industry professionals.

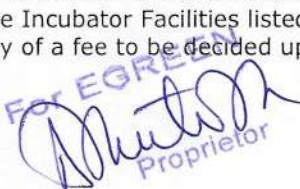
E. Information Pool:

Incubator will maintain access to information and knowledge pool generally useful new enterprises. The Incubator will also facilitate access to departmental laboratories of AIC – MUJ Incubation Foundation Institutions by the Company (Promoters) for their product development purposes with approval of the concerned department.

F. Access to Markets & Talent

Incubator will provide help to incubatee, by providing assistance in marketing, get access to markets and access to desired talent.

2. In the event of a material deviation/delay in the Machine List and Timelines, the Company and the Founders shall have the right to demand that the Incubator extends the incubation period in accordance with such deviation/delay.
3. Further, at the end of the Incubation Period, the Incubator shall, at the Company's request, continue to make the Incubator Facilities listed in A and B above available to the Company upon payment by the Company of a fee to be decided upon by the incubator and the founder.

For AGREED

Proprietor


Director


For EGREEN
Muthiah
Proprietor

Diya Prithwan


SCHEDULE III

COVENANTS OF THE COMPANY

1. The Company shall keep Incubator facilities extended for their usage in good condition and shall not cause damage thereto.
2. The Company shall not cause any nuisance or annoyance to other companies or units working in the AIC – MUJ Incubation Foundation.
3. The Company shall not engage in any unlawful activities during its stay in the AIC – MUJ Incubation Foundation. The Company shall comply with provisions of the relevant Rules, Regulations and Acts applicable to it. The Company shall also ensure that its Promoters and its employees do not engage in any unlawful activities during their stay in the AIC – MUJ Incubation Foundation.
4. The Company shall comply with the terms of the AIC – MUJ Incubation Foundation Policy during its stay in the AIC – MUJ Incubation Foundation. Amendments or changes, from time to time, in the Policy shall be binding on the Company unless Incubator decides otherwise. The Company shall be responsible to update itself from time to time on amendments in the Policy. Incubator shall not be held liable for lack of communication and intimation to the Company on specific amendment in the Policy.
5. The Company shall submit information to Incubator about all material changes or development taken place in their companies from time to time such as (but not limited to) change in name of the company, change in project or product profile, change in directors, promoters or shareholders, acquisition of a new office, additional equity or debt investments. Prior concurrence of Incubator shall be obtained for effecting such changes and Incubator shall have a right to stipulate such additional conditions as Incubator in its absolute discretion deem fit for effecting any change as stated herein above.
6. The Company undertakes and agrees that the information to be submitted by it will be correct and Incubator shall not be responsible for verifying the correctness of the information to be submitted by the Company. In the event that any information submitted by the Company is found to be incorrect, Incubator will proceed to take appropriate actions for breach of the provision of this Agreement.
7. The Company shall disclose to Incubator, information on executive involvements of their promoters in other companies or Business Incubator entities. The Company shall also ensure that its promoters, employees or any other person connected to the Company or its promoters shall avoid all conflicting situations and that they shall not use their positions in multiple capacities to the benefit of the other roles. The Company shall disclose to Incubator, information or situation of conflict of interests involving its promoters, employees or any other person connected to the company or its promoters.
8. The performance of the Company shall be subject to the periodical assessment by Incubator. The Company will work with the Incubator to set mile stones for the period of incubation. The Company shall submit with Incubator information on quarterly basis in a format as reasonably required by the Incubator. The Company will have to submit their annual reports within a period of 7 days from the date of its approval.


ROHIT
Proprietor


Divya Poutwani




**MANIPAL UNIVERSITY
JAIPUR**

(University under Section 2(f) of the UGC Act)

**Department of Electrical Engineering
School of Electrical, Electronics and Communication Engineering**

Report on Collaborative activities

Name of Partnering Organizations:

- 1 MNIT Jaipur, India

Name of Participants:

- 1 Dr Divya Rishi Shrivastava, Department of Electrical Engineering, Manipal University Jaipur, India
- 2 Prof Shahbaz Ahmed Siddiqui, Department of Mechatronics Engineering, Manipal University Jaipur, India
- 3 Dr Kusum Verma, Department of Electrical Engineering, MNIT Jaipur

Name of the Activity:

Research Work on ‘Synchronized Data-driven Composite Scheme for Augmenting Power Grid Stability’
(Journal Publication)


HOD
Department of Electrical Engineering
School of Electrical,
Electronics & Communication (SEEC)
Manipal University Jaipur



Synchronized Data-driven Composite Scheme for Augmenting Power Grid Stability

Divya Rishi Shrivastava¹ · Shahbaz Ahmed Siddiqui² · Kusum Verma³

Received: 9 March 2022 / Accepted: 30 October 2023
© King Fahd University of Petroleum & Minerals 2023

Abstract

This paper proposes a synchrophasor measurement-assisted integrated scheme to enhance power grid stability via transient stability assessment and emergency control of power systems in real-time. The synchrophasor measurements are time-stamped network information available from Phasor Measurement Units (PMUs). The Transient Stability Assessment (TSA) is based on measured generator bus angles obtained directly by PMUs at the control center. These synchronized angle measurements are utilized to construct features, and a Random Forest classifier is implemented to infer the TSA in real-time. The TSA results are determined within the first three cycles following the fault clearance. For operating scenarios that are unstable, an effective emergency control scheme is developed to avoid system degradation. The control strategy utilizes wide-area measurements to formulate a proportional sharing principle-based methodology in real-time. The composite scheme estimates the location and magnitude of the emergency measures to enhance grid stability. The performance of the proposed composite scheme is tested on an IEEE 39-bus test system. The results highlight that the scheme is computationally efficient and robust to topological changes.

Keywords Emergency control · Power flow tracing · Transient stability enhancement · Wide-area measurements

1 Introduction

The increasing demand for electrical energy and the deregulated competitive environment is forcing the utilities to operate closer to their extreme settings. These stressed operating conditions make the system more vulnerable to wide-area disturbances, leading to cascading outages and

finally to system blackouts. With large disturbances, the generator's mechanical and electrical power imbalance results in large rotor angle excursions. In situations where these deviations are larger than the steady-state values, the system tends toward unstable settings. Therefore, it is important to detect abnormal scenarios as early as possible so that emergency control strategies can be implemented in advance and avoid systems leading to a transiently unstable state [1, 2]. To detect abnormal situations, real-time power system monitoring is solicited. The Phasor Measurement Units (PMU) with synchrophasor technology provide real-time power network data [3]. The PMU communicates time-synchronized voltage magnitude and angle, line currents, and frequency of vital nodes from remote locations to the centralized control center [4]. The presence of PMU on the high side of the generator bus infers the rotor angle measurements in real time, as typically the rotor angles are proportional to these bus phase angles [5]. In the literature [5–9], these PMU measurements have been effectively utilized in assessing the system's Transient Stability State (TSA) earlier than the system actually becomes unstable. The investigations in [3–9] utilize post fault network data of varying length, evaluate decision variables, and predict the future system stability status.

✉ Shahbaz Ahmed Siddiqui
shajju77@gmail.com;
shahbazahmed.siddiqui@jaipur.manipal.edu

Divya Rishi Shrivastava
divyarishi.shrivastava@jaipur.manipal.edu

Kusum Verma
kverma.ee@mnit.ac.in

¹ Department of Electrical Engineering, Manipal University Jaipur, Dehmi Kalan, Jaipur-Ajmer Expressway, Jaipur 303007, India

² Department of Mechatronics Engineering, Manipal University Jaipur, Dehmi Kalan, Jaipur-Ajmer Expressway, Jaipur 303007, India

³ Department of Electrical Engineering, Malaviya National Institute of Technology Jaipur, Jawahar Lal Nehru Marg, Jhalana Gram, Malviya Nager, Jaipur 302017, India



Notably, the complexity of the method tends to increase as the number of decision variables increases. As a post-fault scenario in the power network may lead the system toward unstable settings, corrective actions for false estimations of future transient instability may degrade the system. Therefore, a methodology to assess TSA should (1) construct the predictors with a small, synchronized data window and (2) timely predict the future system state with high accuracy. In general, it is unlikely to protect the power network against all exigencies that otherwise may lead the system to collapse. Unplanned disturbances can lead to power system emergencies. These exigencies can have significant impacts on the stability and reliability of the power system. As such, it is important to understand the causes and effects of these disturbances in order to develop effective strategies for mitigating their impact. The disturbances may exhibit a wide range of magnitudes, spanning from minor perturbations to significant disruptions. Small perturbations in an interconnected power network may lead to low-frequency oscillations. The reliability of power systems is susceptible to failure as a result of inadequately damped oscillations [10, 11]. The implementation of a power system stabilizer (PSS) has been identified as a potential solution to controlling oscillations in large power systems. The initiation of major network faults may cause network parameters to exceed extreme levels. The presence of large faults in a power system can potentially compromise its overall functionality and reliability if not addressed in a timely manner. Wide-area protection and control systems give crucial statistics about the impending state of the system and offer better coordinated actions to preserve the integrity of the system against large disturbances [12, 13]. The remedial actions against wide-area disturbances are labeled as Special Protection Systems (SPS) or Remedial Action Schemes (RAS) and include generator rejection, load rejection, underfrequency or undervoltage load shedding, etc. [14].

The emergency load shedding is an intentional interruption of the minimum consumers to balance generation-load power, thus preventing the entire system from collapsing. In this regard, the literature [15–26] proposes various strategies to enhance the system's performance. These reported schemes mainly focus on either underfrequency or undervoltage or the rate of change of frequency/voltage. Based on system necessity, the strategies are activated if the decision criteria exceed a predefined threshold [15–19]. Moreover, these control actions are derived based on post-disturbance frequency or voltage variations. Various other schemes [20–24] have also been reported, utilizing the combination of underfrequency and undervoltage immediately after the disturbance to determine the location and amount of load to be shed. However, the majority of the methods available are successful in improving voltage or frequency stability,

and little research effort is reported to improve transient stability. Zare et al. [25] propose an adaptive tripping index and splitting strategy for unstable oscillating areas. In [26], preventive control through generator rescheduling, generator tripping, and/or load shedding-based emergency control is proposed for improving transient stability in real time. For real-time emergency control, the majority of literature adopts load shedding and generator tripping options to avoid system degradation. Interestingly, the identification of the candidate generator to be tripped, location, and amount of load to be shed in real time are more critical. Post-TSA assessment, improper estimation, and implementation of emergency control actions may otherwise lead the system to blackout.

Therefore, based on the literature review, it is evident that to enhance system transient stability, a more robust wide area composite scheme is solicited. The besought composite scheme should utilize synchronized measurements to predict the future state of the power system, and if necessary, the scheme identifies and implement emergency control actions in real time. The emergency control strategy should also suggest the location, magnitude of control actions, and time instant at which the strategy to be initiated. This paper proposes a composite scheme to augment grid stability that utilizes generator bus angles, performs TSA by predicting the future system state within three cycles after Fault Clearing Time (FCT), and suggests the appropriate RAS type: generator tripping and/or load shedding, location and amount of emergency control action, and time instant for implementation. The main highlights of the proposed integrated approach for transient stability enhancement are:

- (i) A new transient stability assessment method is proposed with less computational burden and a three-cycle PMU data window. The developed TSA encompasses a Random Forest (RF) classifier-based approach to predict future system transient instability in three cycles post-FCT.
- (ii) To sustain the system against forthcoming transient instability, post-TSA assessment, the proposed composite scheme decides the location, type, and magnitude of emergency control actions to be initiated in real time. The location of control action is determined using the proportional sharing principle (power flow tracing method) [27].
- (iii) The projected composite scheme is PMU data driven, and therefore, has enhanced generalizing capability in enhancing system stability in real-time.
- (iv) The overall time requirements from TSA to the implementation of emergency control is 150 ms, which makes it appropriate for real-time applications to enhance system security.

The proposed approach is investigated on the IEEE 39-bus New England system with topological variations. The effectiveness of the proposed scheme is assessed through a comparative assessment with the available literature [7, 9,

[16], and [23]. The outline of the proposed composite scheme is illustrated in Fig. 1.

2 Problem Formulation

Wide-area monitoring and control aims to determine the transient instability state of the system by analyzing post-disturbance rotor angles. The basic equation governing the dynamics of the i th machine in the n -machine system is given as [28]:

$$\frac{d\delta_i}{dt} = \Delta\omega_i \text{ for } i = 1, 2, \dots, n \tag{1}$$

$$\frac{d\Delta\omega_i}{dt} = \frac{1}{M_i} (P_{mi} - P_{ei} - D_i \Delta\omega_i) \text{ for } i = 1, 2, \dots, n \tag{2}$$

where

$$P_{ei} = G_{ii} E_i^2 + \sum_{\substack{j=1 \\ j \neq i}}^n E_i E_j \{G_{ij} \cos(\delta_i - \delta_j) + B_{ij} \sin(\delta_i - \delta_j)\} \tag{3}$$

where, δ_i represents generator rotor angle and $\Delta\omega_i$ is rotor speed deviation, P_{mi} is input mechanical power, and P_{ei} is the electrical power output. M_i is the moment of inertia, D_i is the damping coefficient, $G_{ii} + j B_{ij}$ is the transfer admittance between the i th and j th generator.

For a multi-machine network, it is suitable to analyze the post-disturbance generator’s performance with respect to the system [29]. Therefore, in this work, rotor angle relative to the system Center of Angles (COA) is utilized as:

$$\delta_{COA} = \frac{\sum_{i=1}^n \delta_i H_i}{\sum_{i=1}^n H_i} \tag{4}$$

where for i th machine, δ_i is generator rotor angle and H_i is its inertia constant. However, for real-time applications, it is appropriate to replace the inertia constant H_i with the high-side active power injection P_i . Thus, a modified formula for finding COA in real-time using synchrophasors can be given as:

$$\delta_{COA} = \frac{\sum_{i=1}^n \delta_i P_i}{\sum_{i=1}^n P_i} \tag{5}$$

For the i th machine, the rotor angle $\delta_{i,COA}$ referred to COA is obtained as

$$\delta_{i,COA}(t) = \delta_i(t) - \delta_{COA}(t) \tag{6}$$

where t is the instant of time. Equation (6) represents i th generator rotor angle with respect to all other generators for any given time instant. Therefore, the $\delta_{i,COA}(t)$ represents the increase or decrease in rotor angle for i th generator with respect to the system COA. In this work, the generator bus phase angles are utilized, as these angles are characteristically proportional to the generator rotor angles [5].

3 Proposed Composite Scheme to Enhance Grid Stability

The abnormal system state is mainly due to faults, sudden increase or decrease in load/generation, etc., which makes the generator’s rotor angle to change from its pre-disturbance position. The large excursion of the rotor angles from the pre-disturbance state is an indicator of the system’s unstable state. Post-FCT, increased deviations without bounds indicate that the respective generator(s) are accelerating and diverging from the rest of the machines; similarly, a monotonous decrease indicates that the corresponding generator(s) are decelerating with respect to other machines.

3.1 Real-Time TSA of the System

Post-disturbance system dynamics vary rapidly; this makes real-time TSA a challenging task. To enhance the system’s transient stability, the development of a robust control scheme that evaluates the future system state within a few cycles is solicited. In the development and implementation of emergency control actions, real-time TSA is the foremost step. Power system transient stability can be assessed through time-domain simulations [9]. Post-fault clearance, the network scenario may lead the system toward stable or unstable settings. For assessment, these stable and unstable settings are labeled as 0 and 1, respectively. Therefore, the machine learning models for available features, classify the target TSA as a binary ($\{0,1\}$) classification. To perform TSA as a binary classification, frequently used models are support vector classifier (SVC), decision tree classifier (DT), random forest (RF), multilayer perceptron (MLP), k-nearest neighbor (k-NN), etc. In this paper, future system stability/instability is predicted through a random forest (RF) classifier [35]. Random Forest is an ensemble of multiple decision trees. RF performs efficiently for high-dimensional and unbalanced data. The performance of classifier tools is measured in terms of correct predictions, labeled as accuracy.

After fault clearance, the rotor angle’s initial swing can be utilized for assessing and enhancing transient stability. A thorough examination of the trajectories indicates that for the unstable operating scenarios, trajectories deviate sharply from COA immediately after FCT as compared to the stable cases. With detailed observation of all the operating states

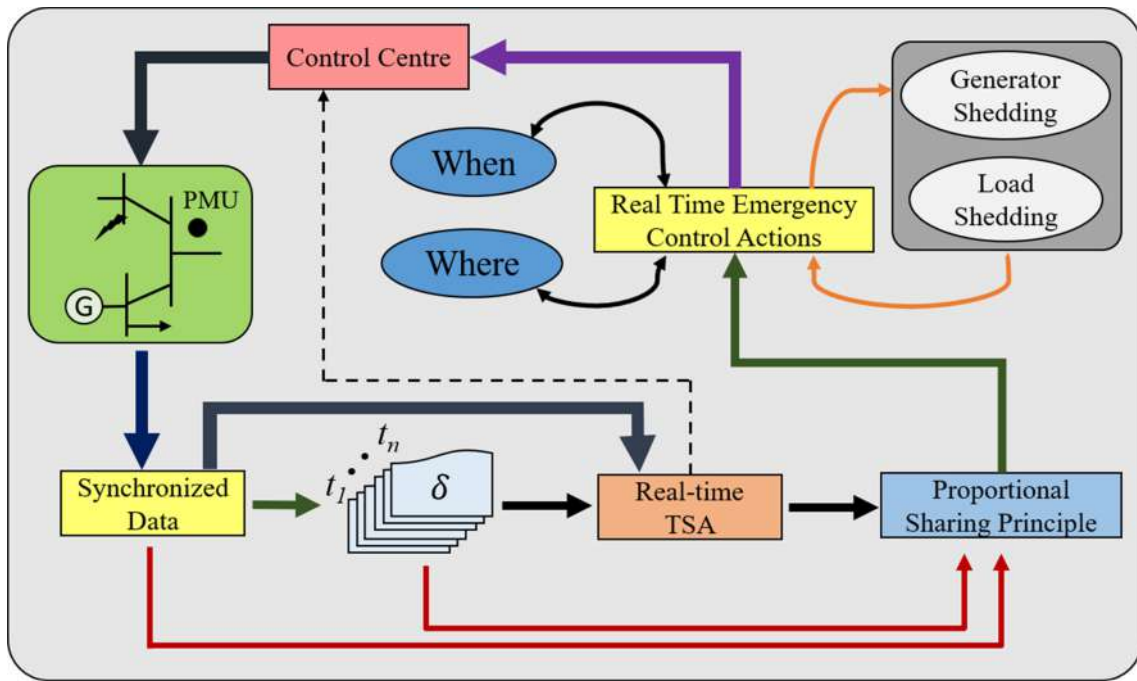


Fig. 1 Outline of proposed composite scheme

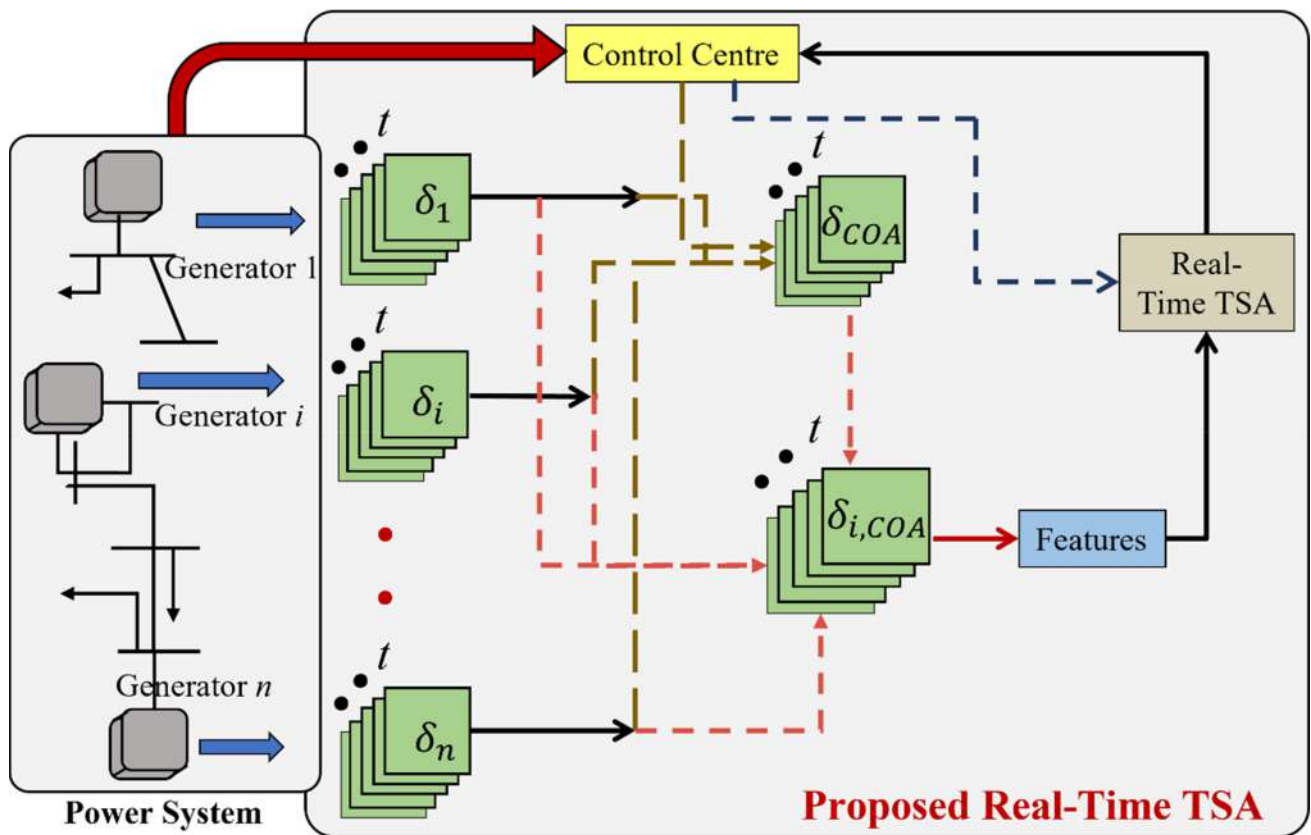


Fig. 2 Summary of proposed real-time TSA

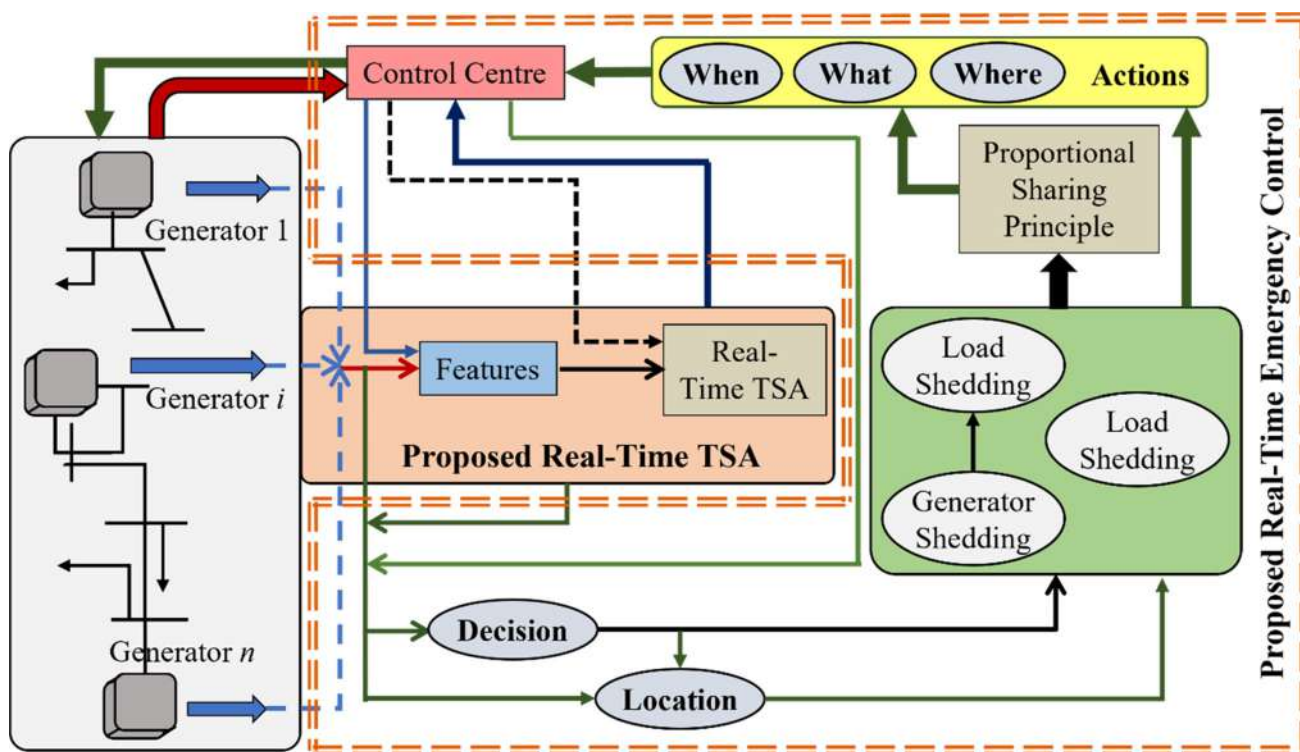


Fig. 3 Summary of proposed real-time emergency control

under various disturbances, it is found that the stability status of the system can be determined within the first few cycles after FCT. Therefore, in the present study, we have taken 3 cycles post-FCT for evaluating the TSA of the system, and rotor trajectories are calculated with respect to COA as:

$$\Delta\delta_i(t') = \delta_{i,COA}(t') - \delta_{i,COA}(FCT) \tag{7}$$

where, FCT = fault clearing time, $t' = FCT + 3$ cycles for present study, $\delta_{i,COA}(t')$ and $\delta_{i,COA}(FCT)$ are determined by (6). For i th generator and t' time instant, $\Delta\delta_i(t')$ is change in rotor angle from the fault clearing time with respect to COA. For all generators, following the FCT, the change in rotor angle from the fault clearing time with respect to the system COA is calculated. Absolute values of rotor trajectories calculated in (7) are utilized as features for machine learning models to classify the future system state, shown as:

$$Features = |\Delta\delta_i(t')| \tag{8}$$

The developed RF model utilizes the features calculated in (8) and distinguishes the power system’s future stable (0) and unstable (1) states. The real-time TSA assessment is then shared with the control center for required emergency control actions. The summary for real-time stability assessments through synchronized measurements is illustrated in Fig. 2.

3.2 Proposed Wide-Area Emergency Control Actions

The tendency of rotor angle excursion can provide vital information to frame emergency control: generation reduction/load shedding. Depending on the post-FCT system state, $\Delta\delta_i(t')$ may be positive or negative. Positive changes represent the generator(s) acceleration relative to the rest of the system. In such a scenario, tripping of candidate generator(s) can be a possible remedial action. Similarly, a negative $\Delta\delta_i(t')$ indicates the generator(s) are decelerating, and to enhance the system transient stability state, load shedding may be an appropriate remedial action. Therefore, the generator(s) speeding away are to be tripped before the entire system is transient unstable. The tripping of these candidate generators may, however, result in a system power imbalance. Unavailability of the spinning reserve will root the other generators to decelerate. Thus, it is necessary to shed the load proportional to the tripped generator. Similarly, when the disturbance slows down the generators, the system will be overloaded, and hence load shedding can be a probable solution. The necessity of emergency control is initiated in the control center with a predicted TSA assessment, and the power flow tracing method [27] is utilized to calculate the amount and location for load shedding.

3.3 Proportional Sharing Principle for Load Shedding

The proportional sharing principle (power flow tracing method) calculates the proportional power usage of lines and generators by consumers and is hence used for charging in various electricity markets [27]. In recent years, the power flow tracing method has been extensively applied to the power network dynamic problem as load shedding, control islanding, etc. [23, 30–32]. By utilizing the proportional sharing principle, the contribution of the candidate generator and line to each load can be calculated. The proportional sharing principle is categorized as an upstream and downstream process with equal computational effort. The comprehensive investigation of the upstream and downstream approaches is discussed in [27]. For any node, incoming and outgoing power are equal, and for an arbitrary bus a , it is calculated as [33]:

$$P_a = \sum_{b \in F_a} |P_{a-b}| + P_{La} + \sum_{b \in F_a} |P_{loss(a-b)}| \text{ for } a = 1, 2, \dots, n \tag{9}$$

where, F_a is the set of nodes directly supplied by node a , $|P_{a-b}|$ is the real power flow in line $a-b$, P_{La} is the active power demand at node a , and $P_{loss(a-b)}$ is the loss in line $a-b$. Equation (9) is rewritten as,

$$P_a - \sum_{b \in F_a} c_{ba} P_b = P_{La} \text{ or, AdP} = \text{PL} \tag{10}$$

where A_d represents $(n \times n)$ downstream matrix shown in (11) and P_L is load demand vector for all the nodes.

$$[A_d]_{ab} = \begin{cases} 1, & \text{for } a = b \\ c_{ba} = \frac{-|P_{b-a}|}{P_b}, & \text{for } b \in F \\ 0, & \text{otherwise} \end{cases} \tag{11}$$

The next step is to calculate the contribution of real power from generator at bus a in load demand at node c , which is determined as,

$$P_{Ga}^{LC} = \frac{P_{Ga} P_{Lc}}{P_a} [A_d^{-1}]_{ac}, \text{ for } c = 1, 2, \dots, n \tag{12}$$

where P_{Ga}^{LC} is portion of the active load demand at bus c provided by generator at node a , P_{Ga} is the power contributed by generator connected to bus a , P_{Lc} is the load demand at bus c , and P_a is bus a nodal power. Moreover, the proportion of the power P_{a-b} to the load at bus c as P_{a-b}^{LC} is,

$$P_{a-b}^{LC} = \frac{|P_{a-b}| P_{Lc}}{P_a} [A_d^{-1}]_{ac}, \text{ for } c = 1, 2, \dots, n \tag{13}$$

Thus, to calculate the contribution of power from the generator connected to bus a to various loads, (12) is used. Similarly, the proportion of power from line $a-b$ to various loads is calculated using (13). Following the fault clearance, the control centre upon receiving the transient stability assessment, activates the proposed emergency control scheme. Subsequently, Generator tripping is initiated at FCT + 6 cycles if the rotor angle trajectory swings in a positive direction. Likewise, load shedding is introduced if the angle swings in the negative direction. However, if generation tripping is activated, proportionate load shedding is triggered for candidate load buses at FCT + 9 cycles. The proposed real-time emergency control is summarized in Fig. 3. The figure also illustrates the post-TSA step-by-step proposal for the control actions. The time-instant for activating the emergency control methodology is TSA time instant (FCT + 3 cycle), + 3 cycle, and + 6 cycle for generator shedding and load shedding, respectively. The 3 cycle and 6 cycle delays are intentionally used, considering the various delays associated with implementing response-based corrective actions [13]. Thus, post-FCT, the transient instability detection and actions for its enhancements are carried out within 150 ms. The generator(s) rotor angle trajectory that exceeds the positive threshold is first to be shed and the part of the loads fed by the tripped generator is shed using (12). Similarly, if generator angle exceeds threshold in the negative direction, load shedding is initiated. The location and amount of load to be shed are determined using (12) or (13) and depend on the generator outage or line outage.

4 Proposed Composite Scheme: Results and Discussion

The proposed scheme is tested on a standard IEEE 39-bus test system [34]. The three-phase faults are considered as disturbance at various locations with different fault durations and varying operating conditions. For all the scenarios, the fault application time (FAT) is 1 s, and the fault clearing time (FCT) is 6–12 cycles from the FAT. The considered test system is modeled using the DIgSILENT Power Factory software [36]. By utilizing the time-stamped measurements feature in it, synchronized data of the test system at 60 Hz sampling frequency is generated. The proposed algorithm is tested under different disturbances using this synchronized data of voltage and frequency. These synchronized measurements are almost similar to the data normally received from PMUs. The rotor trajectories are obtained from FCT once in every cycle from all the generating buses, and simultaneously, the voltage magnitudes and phase angles are observed for each cycle after FCT from all the buses.

4.1 Test Results of Real-Time Transient Instability Assessment

In the test system, three-phase faults are created on all the buses with varying operating conditions. The loads are randomly varied from 90 to 110% of the base load in steps of 1%. The total number of cases obtained is 885, with 359 stable and 526 unstable cases. Out of the available 885 cases, 80% are utilized to train the classifier model, and new 20% of the total cases are utilized to predict the future system instability/stability state, as illustrated in Fig. 4. The Random Forest classifier is developed and trained to classify



Fig. 4 Summary of cases for real-time TSA

Table 1 Details of data from PMU, features and target for TSA

Synchronized data from PMU	Features	Target
Generator bus angle, voltage magnitude at FCT and FCT + 3 cycle	10	1

transient stability status based on features from synchronized measurements. Table 1 shows the details of input data from PMU measurements to construct features, the dimensions of features, and the target TSA for the RF classifier model.

To assess the effectiveness of the RF model, we compared its performance with that of other commonly used classifier models, including the Support Vector Classifier (SVC), Decision Tree (DT), K-Nearest Neighbor (K-NN), and Multi-Layer Perceptron (MLP). The result of the comparative performance is detailed in Fig. 5. The figure shows the overall assessment accuracy, percentage missed, and false alarms for different classifier models. As illustrated, the overall prediction accuracy for RF is higher than other models. Moreover, the number of stable cases classified as unstable (False Alarm) is maximum for the DT model and 0 for the RF model, while the number of unstable cases classified as stable (Missed Alarm) is fewer for the RF model. Therefore, with maximum prediction accuracy, zero false alarms, and limited missed alarms, the RF model is more suitable for real-time TSA assessments.

4.2 Test Results of Proposed Wide-Area Emergency Control

The proposed methodology for wide-area emergency control is initiated for all simulated unstable settings, and the application results are shown here for the three different disturbances. The results obtained show that the proposed

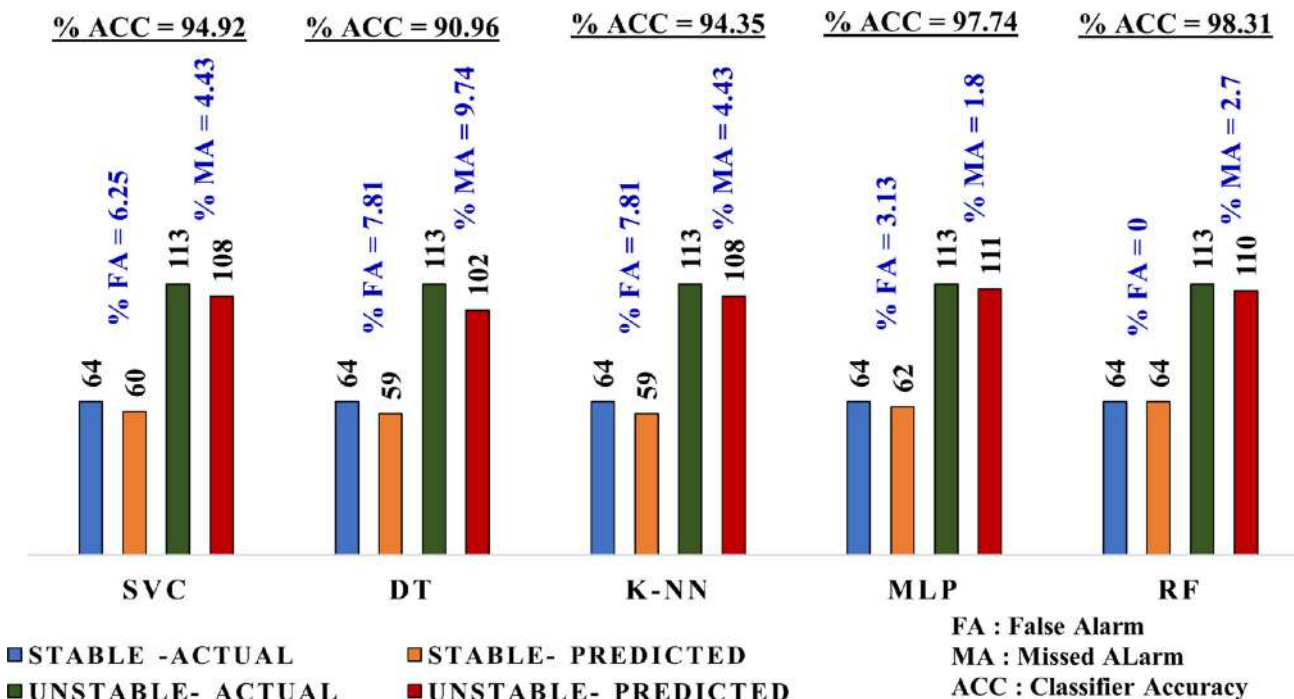


Fig. 5 Performance of different classifier models

scheme can enhance transient stability for the maximum number of unstable cases.

4.3 Disturbance-I: 3-Phase Fault: Line 26–28

In disturbance I, a 3-phase fault is applied at 1 s and cleared by opening breakers on lines 26–28. Following the fault, the generator’s rotor angle is shown in Fig. 6 (a). Post-FCT, features are calculated using (8), and the proposed real-time TSA assess system to be unstable in FCT + 3 cycles. Post-TSA, on assessing the tendency of all rotor angles, generator G9

diverges more than the rest of the generators. As illustrated, generator G9 rotor angle increases monotonically from the rest of the system. Alternatively, the rotor angles of the remaining generators decrease from their pre-fault values. Subsequently, the proposed emergency control strategy suggests that at FCT + 6 cycles, generator G9 is to be tripped, and at FCT + 9 cycles, a proportionate load is to be shed from all the critical loads contributed by it. Prior to fault application, real power contributed by generator G9 to various load bus is obtained through the proposed scheme, and these buses are marked as candidate buses for load shedding. Applying the

Fig. 6 a Pre-emergency control Generators rotor angle
b Post-emergency control remaining Generators rotor angle

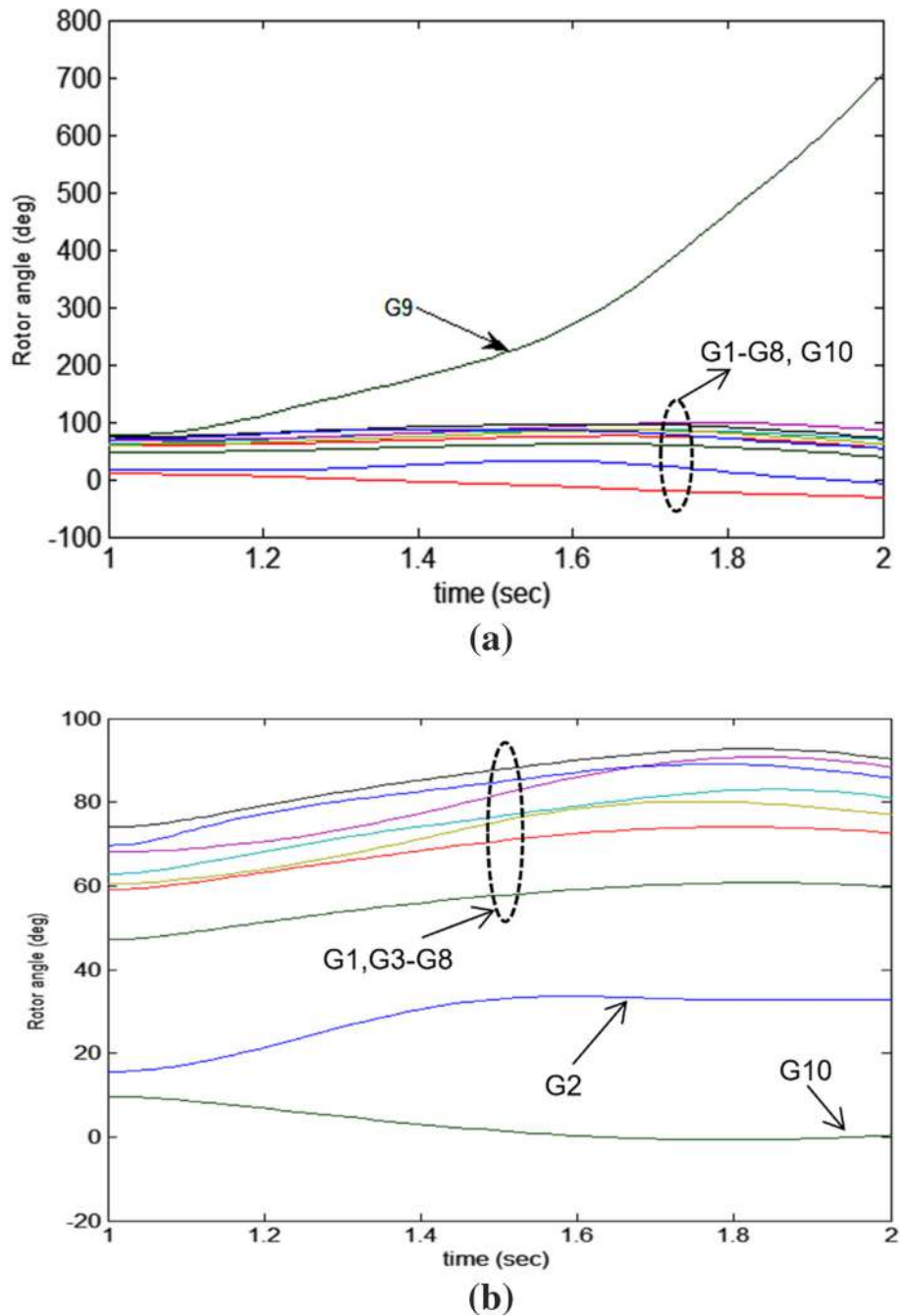


Fig. 7 Proposed scheme-based distribution of load shedding (MW) for disturbance-I

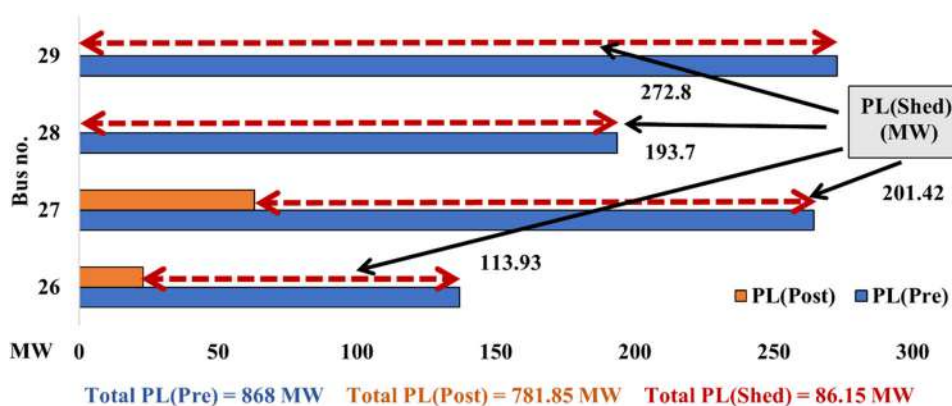
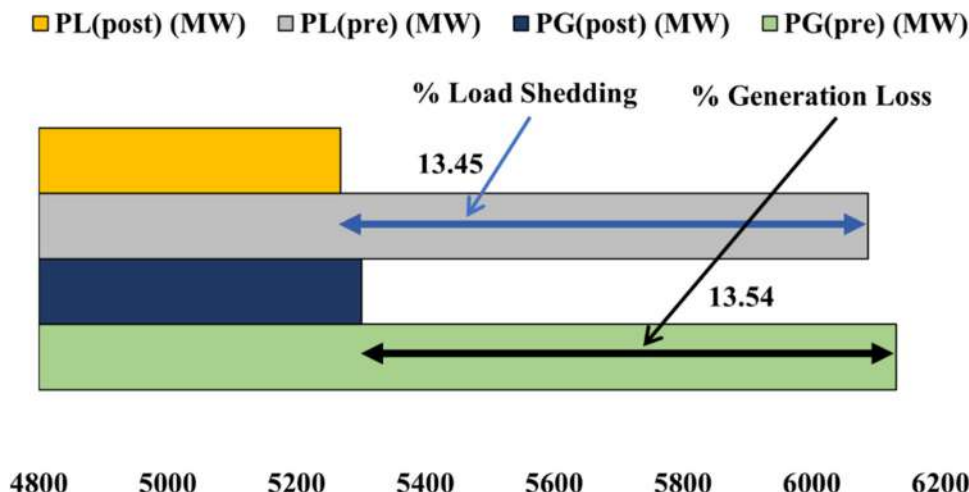


Fig. 8 Post-emergency control percentage generation and load loss for disturbance-I



load shedding to the identified critical buses, Fig. 6b shows the generator rotor angles of the other 9 generators.

As seen, the angles of all other generators were exceeding in the negative direction before the execution of the emergency control action, recovers transient stability settings. The details of the pre-fault load, power contributed by tripped generator G9, and post-shedding load are shown in Fig. 7. The total power generation PG and load PL and their percentage reduction for pre- and post-emergency control action execution are shown in Fig. 8.

4.4 Disturbance -II: An Unintentional Islanding Case: 3 Phase Fault on Line 16–19

This representative disturbance discusses an unintentional islanding scenario, wherein it is formed by applying a 3-phase fault on lines 16–19 at 1 s, cleared by opening the line, and can be visualized through the single-line diagram in Fig. 9. The island-I comprises 35 buses and 8 generators, and island-II has 4 buses and 2 generators. The pre-fault total power generation and load demand in island-I are 4990.14 MW and 5459.9 MW, respectively, and similarly in island-II,

1140 MW and 628 MW, respectively. Thus, the pre-fault operating condition comprises a power imbalance on both islands. This power imbalance in island-I causes the generators to slow down, and as island-II has more power generation than load demand, the generators accelerate. The generator’s response to unintentional islanding is shown in Fig. 10a. Post-FCT TSA assessment, generators G4 (bus 33) and G5 (bus 34) diverge simultaneously from the rest of the machines. Out of G4 and G5, the tendency of G4 rotor angle to diverge is more than G5. The proposed scheme thus suggests its shedding. In this case, line 16–19, transmitting 502.6 MW from bus 19 to bus 16 in island-I, is tripped.

Moreover, in pre-fault system operation, the generator G4 supplies active power to lines 16–19 and 19–20. Therefore, a total of 632 MW must be shed from generator G4. Post-application of the proposed emergency control scheme, the stable settings of generator rotor angle for two islands are shown in Fig. 10b and Fig. 10c. The generator shedding is initiated at FCT + 6 cycles via tripping generator G4, and to balance out the power, load shedding is executed at FCT + 9 cycles at candidate load buses. The distribution of total load shed (625.59 MW) among identified load buses is shown in

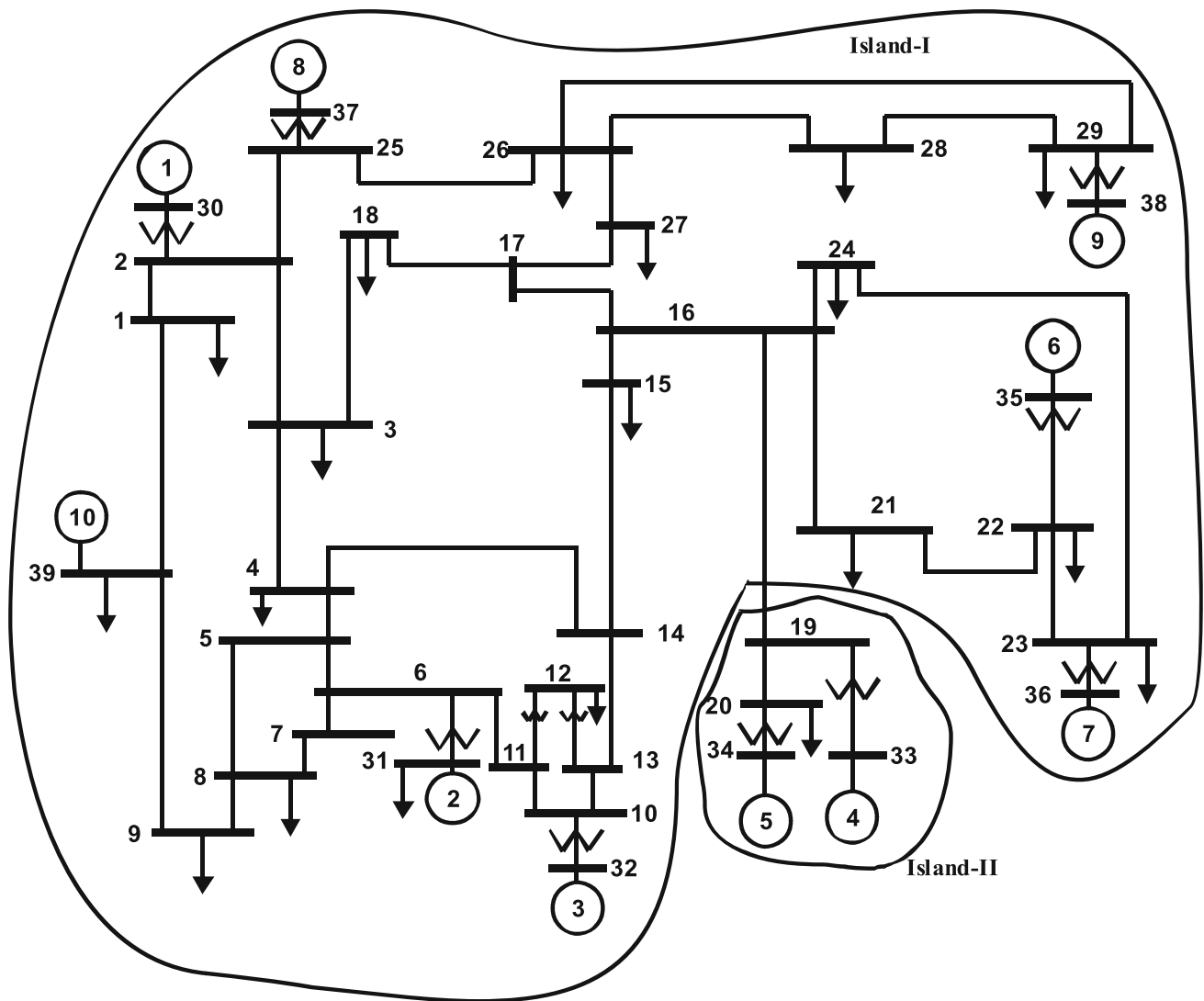


Fig. 9 IEEE 39-bus test system single line diagram including islands formed for Disturbance-II

Fig. 11. The figure reflects that the fraction of load shed for bus 15, bus 16, and bus 18 is higher. As these buses are closer to line 16–19, the % load shed for these buses is greater. In Fig. 10c, post FCT, the generator G5 rotor angle in island-II was increasing monotonically. Notably, post emergency control actions, the generator G5 attains stable settings within 1 s. As in island-II generator G5 is the only generator; its dynamics is shown separately. Moreover, percentage reductions in generation and load power for two islands, pre-and post-composite schemes, are shown in Fig. 12.

4.5 Disturbance-III-3: 3-Phase Fault: Bus 28 Cascaded with 3 Phase Fault: Line 4–5

Disturbance-III considers a more severe fault, wherein a 3-phase fault on bus 28 at 1 s is cleared by opening line 28–29 at (FAT + 9 cycle = FCT-I). Instantly at FCT-I + 1 cycle, a

3-phase fault on line 4–5 is applied and cleared by opening it after 9 cycles (FCT-II). Since the power generated from generator G9 is delivered through tripped line 28–29 and bus 29 is close to this generator, at FCT-I + 3 cycles, the G9 rotor angle advances more. The post-fault dynamics for this disturbance are shown in Fig. 13a. Prior to the application of fault-1, the active power output of generator G9 was 830 MW. Therefore, equivalent load needs to be shed from the candidate loads through an integrated scheme to bring the system back to a stable state. The projected scheme suggests trip generator G9 at (FCT-I) + 6 cycles. An equivalent load power is shed for identified loads at (FCT-I) + 9 cycles. Moreover, the cascading fault applied on line 4–5 causes generator G10 to decelerate faster. The trajectory for generator G10 is shown in Fig. 13a. Prior to fault-2, the real power in line 4–5 was 150.86 MW (from bus 5 to 4).

Fig. 10 a Pre-emergency control Generator rotor angles. **b** Post-emergency control Generator rotor angle in Island-I (8 Generators). **c** Post-emergency control Generator G5 rotor angle in island-II

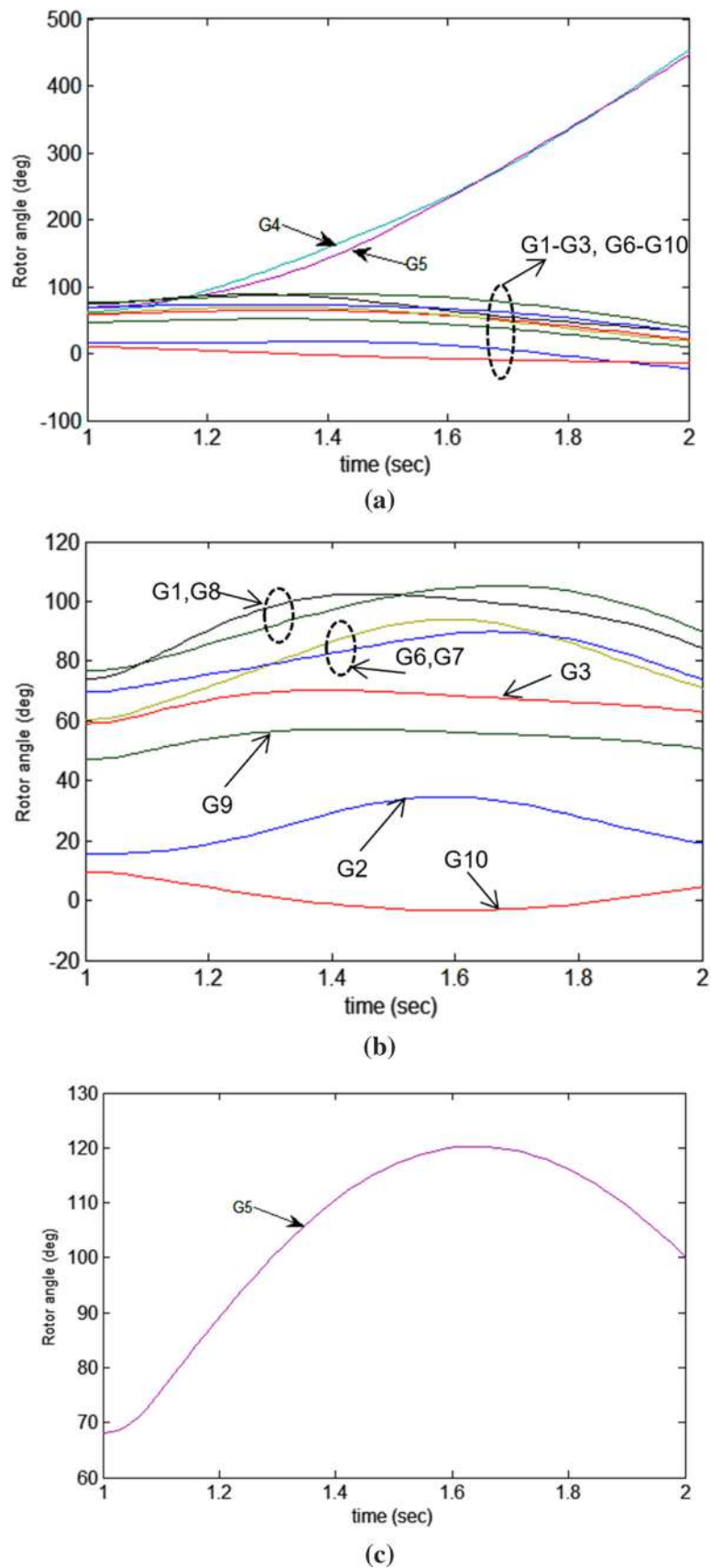


Fig. 11 Distribution of load shedding (MW) for unintentional islanding case

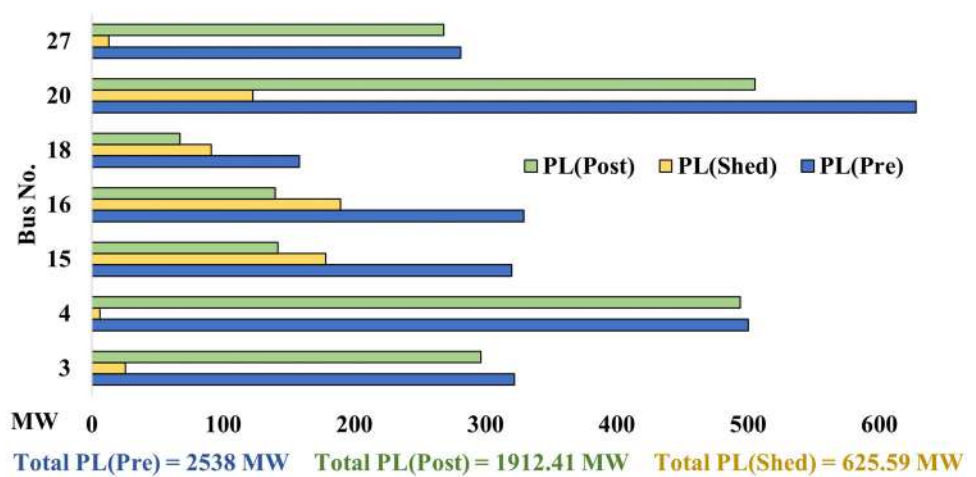
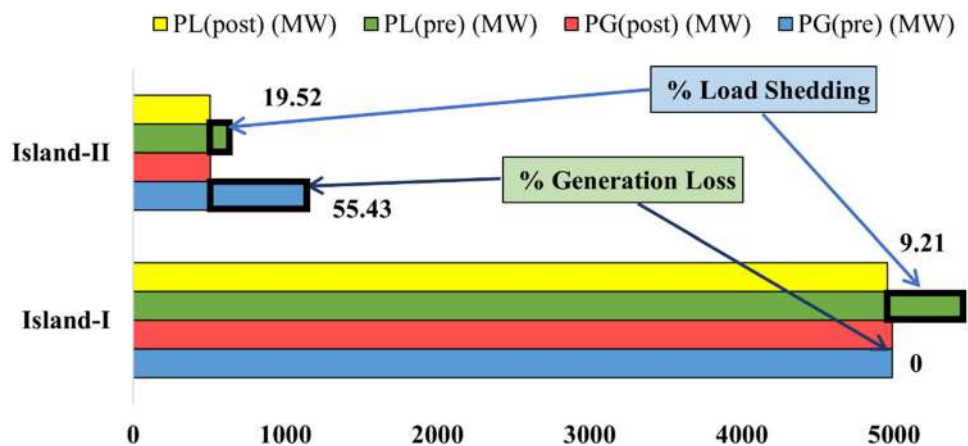


Fig. 12 Post-emergency control percentage generation and load loss for disturbance-II



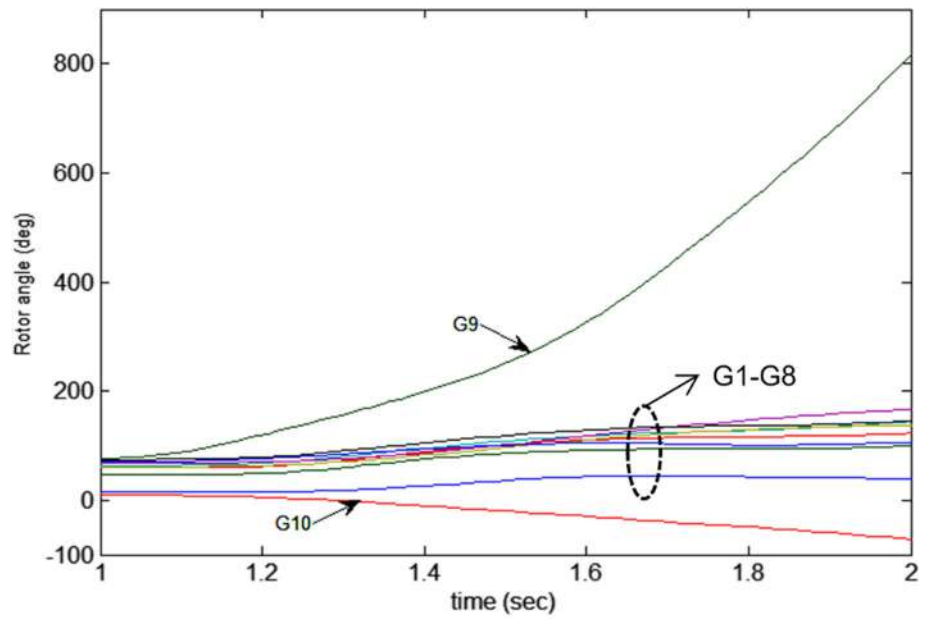
The proportional load is therefore essential to be shed from the identified loads. Corresponding to the pre-fault power of line 4–5, load shedding is applied at FCT-II + 6 cycles. Figure 13b illustrates that the remaining generators are bounded, and post-implementation of the composite scheme, the system advances back to stable settings. Post FCT-II, the generator G10 was decreasing monotonously, attains bounded operation after the application of proposed composite scheme. The scheme is applied; the active power of tripped generator G9 and line 4–5 is distributed among candidate loads at FCT-I + 9 cycles and FCT-II + 6 cycles, respectively, as shown in Fig. 14. The available power generation PG and load power PL and their proportional reduction for pre- and post-emergency control execution are detailed in Fig. 15. The overall timeline of the proposed composite scheme can be visualized in Fig. 16. The illustration shows different characteristics starting from fault application time, fault clearing time, time for TSA assessment, time to initiate emergency control actions, and overall response time of the composite scheme, viz., 150 ms. Noticeably, the proposed

integrated real-time approach timely assesses TSA and evaluates the location and type of emergency control action in real time.

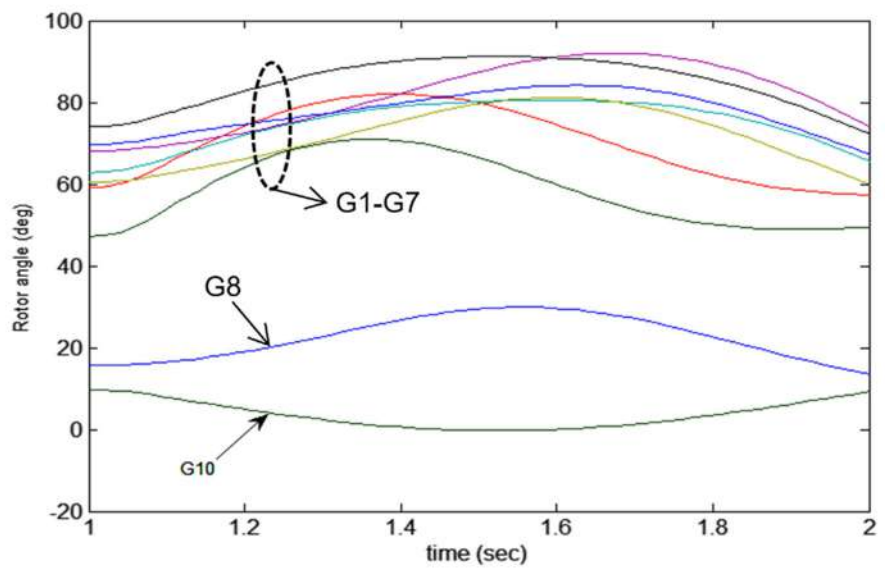
4.6 Comparative Assessment of the Proposed Scheme

The performance of the proposed composite scheme with the available literature is detailed in Table 2. The different characteristics considered for comparison are: (1) type of instability; (2) real-time TSA assessment; (3) PMU data length; (4) feature dimensions for TSA; (5) real-time emergency control recommended and implemented; (6) location, magnitude, and type of emergency control action instigated; (7) computational burden; and (8) overall assessment time from FCT to control action implementation. As shown, the composite scheme detects future transient instability, identifies location, determines type and amount of control actions, and initiates them within 150 ms from the FCT.

Fig. 13 a Rotor angle of generators pre-emergency control application. **b** Rotor angles post-emergency control application (With G9 tripped)



(a)



(b)

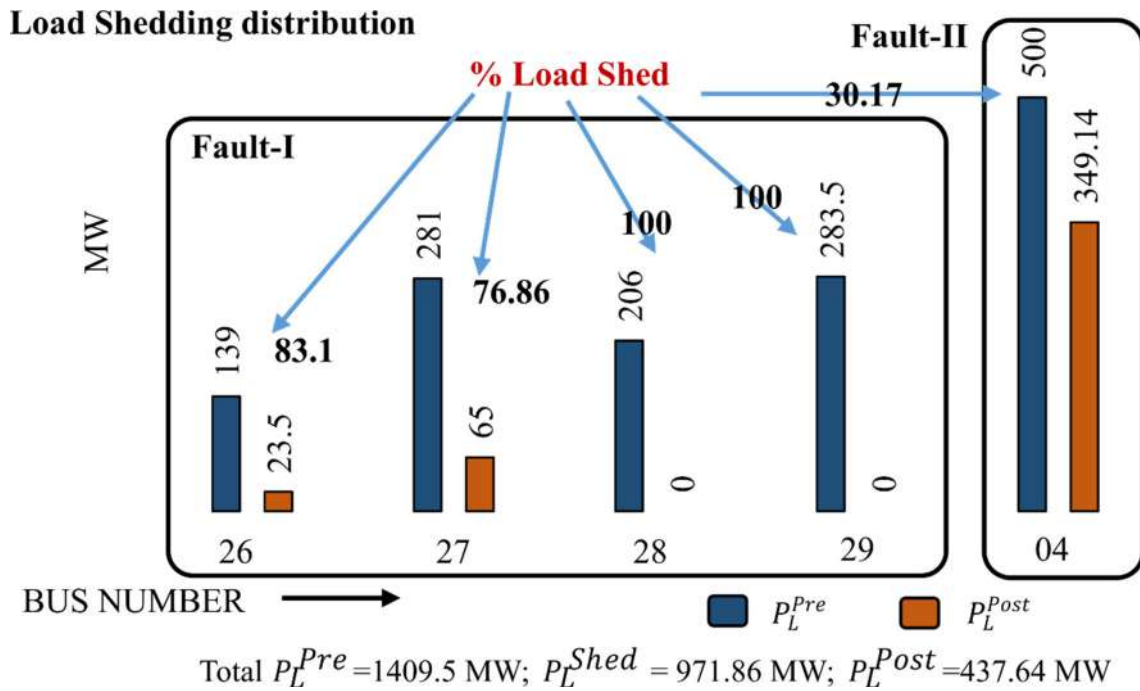


Fig. 14 Distribution of load shedding based on proposed scheme for Disturbance-III

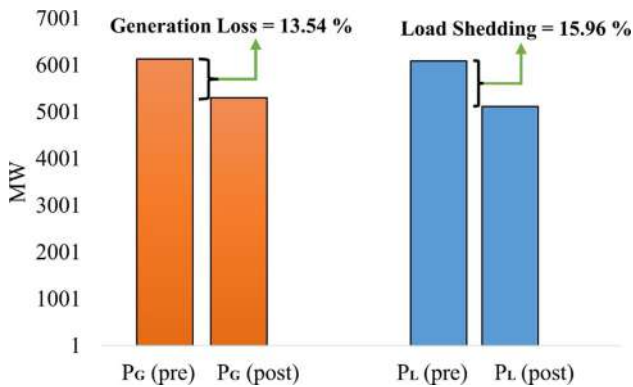


Fig. 15 Post-emergency control generation and load loss for Disturbance-III

5 Conclusions

Modern power systems are highly interconnected and operate with less spinning reserves. Unattended wide-area disturbances may therefore lead the system toward extreme settings. Hence, early prediction of an emerging transient instability state and effective emergency control schemes are required to mitigate the impending system degradation. The

proposed composite scheme first predicts the system stability state in three cycles after fault clearing time. Based on the nature of the emerging swing, the scheme then suggests a suitable emergency control action and augments sustainability. Depending on the deficit and surplus generation, the proposed scheme also determines the location where generator and/or load shedding to be initiated. To assess the amount of load shedding, a scheme utilizing the proportional sharing principle is tested successfully. With this integrated approach, it is found that load shedding at only a few candidate load buses that are being supplied by a lost generator or line is sufficient for system transient stability improvement. A comparative assessment of the proposed scheme with available literature is also showcased. The test results indicate the suitability of the proposed strategy to improve power grid stability in real-time. The present work controls the modern power system and hence enhance its transient stability without renewable energy integrations. However, for future studies similar framework can be developed for the power system integrated with renewable energy sources like wind energy, low inertia based solar energy, etc.

Fig. 16 Overall timeline of proposed integrated approach

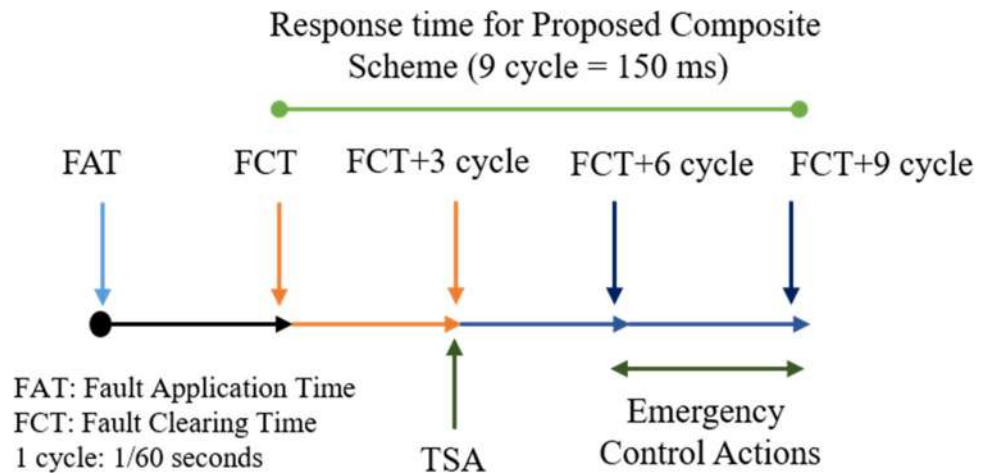


Table 2 Performance comparison of proposed scheme with available literature

Method	Type of Instability	Real-time TSA	Synchronized data length for TSA	Features dimensions for TSA	Real-time Emergency Control	Location, amount, and type	Computational burden	Overall time (s)
Shrivastava et al. [7]	Angle	Yes	6 cycles	10	No	No	Minimum	–
Soni et al. [9]	Angle	Yes	6 cycles	50	No	No	Minimum	–
Kabir et al. [16]	Voltage	No	–	–	No	Yes	Minimum	–
Tang et al. [23]	Frequency and voltage	No	–	–	No	Yes	Minimum	–
Proposed	Angle	Yes	3 cycles	10	Yes	Yes	Minimum	0.15

Author contributions All authors contributed to the study conception and design. Material preparation, data collection and analysis were performed by [Divya Rishi Shrivastava], [Shahbaz Ahmed Siddiqui], and [Kusum Verma]. The first draft of the manuscript was written by [Shahbaz Ahmed Siddiqui] and all authors commented on previous versions of the manuscript. The contribution of [Divya Rishi Shrivastava] and [Shahbaz Ahmed Siddiqui] is equal and therefore should be considered as first authors. All authors read and approved the final manuscript.

Funding The authors did not receive support from any organization for the submitted work.

Declarations

Conflict of interest The authors have no relevant financial or non-financial interests to disclose.

References

- Begovic, M.; Novosel, D.; Karlsson, D.; Henville, C.; Michel, G.: Wide-area protection and emergency control. *Proc. IEEE* **93**(5), 876–891 (2005). <https://doi.org/10.1109/JPROC.2005.847258>
- Kundur, P., et al.: Definition and classification of power system stability IEEE/CIGRE joint task force on stability terms and definitions. *IEEE Trans. Power Syst.* **19**(3), 1387–1401 (2004)
- Subbouhi, A.R.; Vahedi, A.: Transient stability prediction of power system; a review on methods, classification and considerations. *Electr. Power Syst. Res.* **190**, 106853 (2021). <https://doi.org/10.1016/j.epsr.2020.106853>
- IEEE standard for synchrophasor measurements for Power Systems. *IEEE Std C37.118.1–2011* (Revision of IEEE Std C37.118–2005), 1–61 (2011). <https://doi.org/10.1109/IEEESTD.2011.6111219>.
- Huang, D.; Yang, X.; Chen, S.; Meng, T.: Wide-area measurement system-based model-free approach of post-fault rotor angle trajectory prediction for on-line transient instability detection. *IET Gener. Transm. Distrib.* **12**(10), 2425–2435 (2018). <https://doi.org/10.1049/iet-gtd.2017.1523>
- Siddiqui, S.A.; Verma, K.; Niazi, K.R.; Fozdar, M.: Real-time monitoring of post-fault scenario for determining generator coherency and transient stability through ANN. *IEEE Trans. Ind. Appl.* **54**(1), 685–692 (2018). <https://doi.org/10.1109/TIA.2017.2753176>
- Shrivastava, D.R.; Siddiqui, S.A.; Verma, K.: Model free robust real-time severity analyser using PMU measurements. *Int. J. Electr. Power Energy Syst.* **133**, 107333 (2021). <https://doi.org/10.1016/j.ijepes.2021.107333>

8. Mazhari, S.M.; Khorramdel, B.; Chung, C.Y.; Kamwa, I.; Novosel, D.: A simulation-based classification approach for online prediction of generator dynamic behavior under multiple large disturbances. *IEEE Trans. Power Syst.* **36**(2), 1217–1228 (2021). <https://doi.org/10.1109/TPWRS.2020.3021137>
9. Soni, B.P.; Saxena, A.; Gupta, V.; Surana, S.L.: Identification of generator criticality and transient instability by supervising real-time rotor angle trajectories employing RBFNN. *ISA Trans.* **83**, 66–88 (2018). <https://doi.org/10.1016/j.isatra.2018.08.008>
10. Ekinci, S.; Izci, D.; Zeynelgil, H. L.; Orenc, S.: An Application of Slime Mould Algorithm for Optimizing Parameters of Power System Stabilizer. *2020 4th International Symposium on Multidisciplinary Studies and Innovative Technologies (ISMSIT)*, Istanbul, Turkey (2020). <https://doi.org/10.1109/ISMSIT50672.2020.9254597>
11. Izci, D.: A novel improved atom search optimization algorithm for designing power system stabilizer. *Evol. Intel.* **15**, 2089–2103 (2022). <https://doi.org/10.1007/s12065-021-00615-9>
12. Liu, Z.; Chen, Z.; Sun, H.; Hu, Y.: Multiagent system-based wide-area protection and control scheme against cascading events. *IEEE Trans. Power Deliv.* **30**(4), 1651–1662 (2015). <https://doi.org/10.1109/TPWRD.2014.2371337>
13. Bhui, P.; Senroy, N.: Real-time prediction and control of transient stability using transient energy function. *IEEE Trans. Power Syst.* **32**(2), 923–934 (2017). <https://doi.org/10.1109/TPWRS.2016.2564444>
14. Remedial Action Scheme, Definition Development, Project 2020–05.2 – Special Protection Systems. https://www.nerc.com/pa/Stand/Prjct201005_2SpclPrct_nSstmPhs2/FAQ_RAS_Definition_0604_final.pdf (2014). Assessed 01 January 2022.
15. Samet, H.; Rashidi, M.: Coordinated under frequency load and capacitor shedding for bulk power systems. *IET Gener. Transm. Distrib.* **7**(8), 719–812 (2013). <https://doi.org/10.1049/iet-gtd.2012.0194>
16. Kabir, M.A.; Chowdhury, A.H.; Masood, N.A.: A dynamic-adaptive load shedding methodology to improve frequency resilience of power systems. *Int. J. Electr. Power Energy Syst.* **122**, 106169 (2020). <https://doi.org/10.1016/j.ijepes.2020.106169>
17. Voropai, N.I.; Efimov, D.N.; Etingov, P.V.; Panasetzky, D.A.: Smart emergency control in electric power systems. *IFAC Proc. Volumes* **44**(1), 1658–1664 (2011). <https://doi.org/10.3182/20110828-6-IT-1002.00449>
18. Otomega, B.; Cutsem, T.V.: Undervoltage load shedding using distributed controllers. *IEEE Trans. Power Syst.* **22**(4), 1898–1907 (2007). <https://doi.org/10.1109/TPWRS.2007.907354>
19. Ahsan, M.Q.; Chowdhury, A.H.; Ahmed, S.S.; Bhuyan, I.H.; Haque, M.A.; Rahman, H.: Technique to develop auto load shedding and islanding scheme to prevent power system blackout. *IEEE Trans. Power Syst.* **27**(1), 198–205 (2012). <https://doi.org/10.1109/TPWRS.2011.2158594>
20. Prasetijo, D.; Lachs, W.R.; Sutanto, D.: A new load shedding scheme for limiting underfrequency. *IEEE Trans. Power Syst.* **9**(3), 1371–1378 (1994). <https://doi.org/10.1109/59.336128>
21. Ghaleh, A.P.; Pasand, S.; Saffarian, A.: Power system stability enhancement using a new combinational load-shedding algorithm. *IET Gener. Transm. Distrib.* **5**(5), 551–560 (2011). <https://doi.org/10.1049/iet-gtd.2010.0626>
22. Girgis, A.A.; Marthure, S.: Application of active power sensitivity to frequency and voltage variations on load shedding. *Electr. Power Syst. Res* **80**, 306–310 (2010). <https://doi.org/10.1016/j.epsr.2009.09.013>
23. Tang, J.; Liu, J.; Ponci, F.; Monti, A.: Adaptive load shedding based on combined frequency and voltage stability assessment using synchrophasor measurements. *IEEE Trans. Power Syst.* **28**(2), 2035–2047 (2013)
24. Novosel, D.; King, R.L.: Using artificial neural networks for load shedding to alleviate overloaded lines. *IEEE Trans. Power Deliv.* **9**(1), 425–433 (1994). <https://doi.org/10.1109/61.277714>
25. Zare, H.; Yaghobi, H.; Alinejad-Beromi, Y.: Adaptive concept of controlled islanding in power systems for wide-area out-of-step prediction of synchronous generators based on adaptive tripping index. *IET Gener. Transm. Distrib.* **12**(6), 3829–3836 (2018). <https://doi.org/10.1049/iet-gtd.2018.0319>
26. Siddiqui, S.A.; Verma, K.; Niazi, K.R.; Fozdar, M.: A unified control scheme for power system transient stability enhancement through preventive and emergency control. *Int. Trans. Electr. Energ. Syst.* **26**(2), 365–383 (2016). <https://doi.org/10.1002/etep.2086>
27. Bialek, J.: Tracing the flow of electricity. *IEE Proc. Gen. Transm. Distrib.* **143**(4), 313–320 (1996). <https://doi.org/10.1049/ip-gtd:19960461>
28. Verma, K.; Niazi, K.R.: A coherency based generator rescheduling for preventive control of transient stability in power systems. *Int. J. Electr. Power Energy Syst.* **45**(1), 10–18 (2013). <https://doi.org/10.1016/j.ijepes.2012.08.072>
29. Kundur, P.: *Power system stability and control*. McGraw Hill Education (2006).
30. Hamid, Z.A.; Musirin, I.: Optimal fuzzy inference system incorporated with stability index tracing: an application for effective load shedding. *Expert Syst. Appl.* **41**(4), 1095–10103 (2014). <https://doi.org/10.1016/j.eswa.2013.07.105>
31. Norris S.: Preventing wide area blackouts in transmission systems: A new approach for intentional controlled islanding using power flow tracing. PhD Thesis, Durham University. <http://etheses.dur.ac.uk/10713/> [Assessed 10 January 2022].
32. Norris, S.; Guo, S.; Bialek, J.: Tracing of power flows applied to islanding. 2012 IEEE Power and Energy Society General Meeting (2012). <https://doi.org/10.1109/PESGM.2012.6345343>.
33. Bialek, J.: Topological generation and load distribution factors for supplement charge allocation in transmission open access. *IEEE Trans. Power Syst.* **12**(3), 1185–1193 (1997). <https://doi.org/10.1109/59.630460>
34. Pai, M.A.: *Energy function analysis for power system stability*. Kluwer Academic Publishers, Springer, US (1989)
35. Shrivastava, D.R.; Siddiqui, S.A.; Verma, K.: A new synchronized data-driven-based comprehensive approach to enhance real-time situational awareness of power system. *Int. Trans. Electr. Energ. Syst.* **31**(5), e12887 (2021). <https://doi.org/10.1002/2050-7038.12887>
36. DlgSIELNT Power Factory 2020 software.

Springer Nature or its licensor (e.g. a society or other partner) holds exclusive rights to this article under a publishing agreement with the author(s) or other rightsholder(s); author self-archiving of the accepted manuscript version of this article is solely governed by the terms of such publishing agreement and applicable law.



Computational study of heat transfer enhancement using porous foams with phase change materials: A comparative review

E. Hamidi^a, P.B. Ganesan^{a b}  , R.K. Sharma^c, K.W. Yong^a

^a Department of Mechanical Engineering, Faculty of Engineering, Universiti Malaya, 50603, Kuala Lumpur, Malaysia

^b Centre for Research in Biotechnology for Agriculture (CEBAR), Level 3, Research Management & Innovation Complex, Universiti Malaya, 50603, Kuala Lumpur, Malaysia

^c Department of Mechanical Engineering, Manipal University Jaipur, 303007, Jaipur, India

Received 30 July 2022, Revised 9 January 2023, Accepted 24 January 2023, Available online 8 February 2023, Version of Record 8 February 2023.

 What do these dates mean?



Show less 

 Share  Cite

<https://doi.org/10.1016/j.rser.2023.113196> 

[Get rights and content](#) 

Highlights

- Phase Change Materials' basic concepts, constraints, and solutions, are discussed.

- Foam fillers to boost thermal conductivity of phase change materials are reviewed.
- Numerical simulation techniques for thermal energy storage systems are evaluated.
- Computational modelling of metal foams in different applications is contrasted.
- The Lattice Boltzmann method was found to be capable of making the most precise predictions.

Abstract

Phase change materials (PCMs) in thermal energy storage can improve energy efficiency and sustainability, which notably makes them a potential solution to the problems of energy and the environment. Numerical simulations, along with experimental research, contribute significantly to the development of PCM applications. Among many different methods used to improve the thermal conductivity of PCMs, the inclusion of metal foams with high thermal conductivity and a solid structure is largely preferred. The purpose of this review is the investigation of the challenges and the recent developments in computational methods for simulating the heat transfer in latent heat thermal energy storage systems that use metal foams to enhance the thermal conductivity of PCMs. Computational strategies including different software, geometry implementation methods, dimensions and scales of models, boundary conditions, porosity and pore density of foam samples as well as their materials are reviewed, evaluated and compared with applications of metal foams in heat exchangers. This review demonstrates that even though the Lattice Boltzmann method accounts for 30% of the numerical studies in this area—which can be due to the need for more costly equipment and the lack of reliable commercial software—it yields more accurate predictions since in this method the complex geometry of foams can be implemented with much greater accuracy.

Graphical abstract



[Download: Download high-res image \(310KB\)](#)

[Download: Download full-size image](#)

Computational study of heat transfer enhancement using porous foams with phase change materials: A comparative review

Introduction

A thermal energy system needs an efficient and economical heat storage. Sensible heat storage, latent heat storage, or a combination of the two or three different types of thermal energy storage (TES) systems. Latent heat storage uses stored energy when a material transitions from one phase to another, whereas sensible heat storage raises the temperature of storage materials as energy is stored [1]. The ability to produce high energy storage densities and the properties for heat storage at a constant temperature in accordance with the phase change temperature of the heat storage material makes latent heat thermal energy storage (LHTES) one of the more alluring heat storage techniques [2]. This feature can help with one of the practical issues with solar thermal systems, which need a reliable way to store and release extra heat produced during times of sunlight for use at night [3,4]. Heat storage can be applied to most types of buildings where heating is necessary and the relatively high electricity pricing allows heat storage to be economical compared with other forms of heating [[5], [6], [7]]. This property can also improve the efficiency of solar distillation systems, which are strongly recommended for seawater desalination over those powered by fossil fuels to reduce greenhouse gas emissions. With minimal adverse environmental impacts, this solution has the potential to prevent impending water shortage crises due to population growth and the rapid expansion of industries [[8], [9], [10], [11], [12]].

The use of metal foam as a porous medium is of utmost importance due to its capacity to hold molten phase change material (PCM) and the enhancement of its thermal conductivity. The metal foams are highly conductive when mixed with organic or

inorganic PCMs, which significantly improves their thermal conductivity. There has been substantial work reported in the literature in this area, and it has also been presented in the form of review papers [[13], [14], [15], [16], [17], [18]]. The majority of these review articles highlight experimental studies. However, there are a lot of excellent works on numerical modeling that also need to be compiled for a ready source of information for upcoming scientists and researchers. To the best of the authors' knowledge, a review comparing methods and associated numerical techniques for simulating thermal conductivity enhancement of PCM/metal foam composites is still lacking. Different types of PCMs, associated thermal conductivity enhancement methods, and the technical details regarding numerical simulation of heat transfer inside metal foams as PCM thermal conductivity enhancers are reviewed and evaluated in this work.

The current section serves as the introduction to the five sections that make up this review. The fundamental idea behind PCMs, as well as their classification, drawbacks, and methods for improvement, are covered in the second section. The third section discusses improving the thermal conductivity of PCMs using foam additives, and the fourth section discusses and analyzes the computational methods used in numerically simulating thermal energy storage systems. The review is concluded in the final section, which also discusses the future scope and outlines the challenges in the numerical simulation techniques for thermal energy storage systems.

An extensive effort has been made in this review to take into account the majority of the studies that have been published in this field from 2010 through 2021. The criteria for selecting the articles were based on the utilization of foams as enhancer additives in the improvement of PCMs' thermal conductivity, whether numerically or experimentally. In addition, for comparison, studies from the same time period regarding heat exchangers in which metal foams are investigated numerically have been collected. In order to provide a broader perspective, these data have been provided to the reader in the form of statistical information via various charts in the corresponding sections. The challenges and new developments in computational simulation of PCM/foam composites are discussed in this review, which will make it easier for readers to select the best strategy for numerical modeling of PCM thermal conductivity enhancement using foams based on their requirements and available options.

Access through your organization

Check access to the full text by signing in through your organization.

Access through **your organization**

Phase change materials

When energy is available, it can be stored and used later with the aid of energy storage systems, which fall into three major categories: thermochemical, chemical, and thermal energy storage systems. Thermochemical systems are not a preferred option for energy storage due to their high cost and commercial unavailability. On the contrary, thermal energy storage systems are quite popular as sensible and latent heat energy storage [19]. A latent heat thermal energy storage system, which uses phase ...

PCM-impregnated foam supports

Here, the application of foams with four different materials, i.e., copper, aluminum, nickel, and graphite, is reviewed from both an experimental and numerical standpoint. The number of studies on foam/PCM composites between 2010 and 2021 is illustrated in Fig. 5. The information compares the quantity of numerical and experimental studies for the three different configurations, i.e., rectangular, cylindrical, and tube-in-shell.

In a rectangular configuration, a rectangular or cubic ...

Computational strategies

Here, different approaches and specifics of computational modeling of heat and mass transfer through metal foams are reviewed. In addition to discussing features such as geometry, porosity, and meshing, their applications in the fields of PCMs and heat exchangers are contrasted. Fig. 13 presents the number of publications since 2016 on numerical simulation of heat transfer and fluid flow through metal foams in distinctive applications of PCM and heat exchanger. It is evident from the data that ...

Conclusions

Significance and necessity of latent heat thermal energy storage devices have been demonstrated by extensive research over the last four decades. Incorporating highly conductive fillers, such as graphite or metal foams, is a prevalent technique for increasing the thermal conductivity of PCMs. This review addresses challenges and discusses significant developments in enhancing computational methods for numerical simulation of PCM/foam composites, yielding the following findings:

Graphite and ...

Declaration of competing interest

The authors declare that they have no known competing financial interests or personal relationships that could have appeared to influence the work reported in this paper. ...

Acknowledgement

This study was funded by Universiti Malaya Impact-oriented Interdisciplinary Research Grant (IIRG005A-2020IISS) and Universiti Malaya Research Grant Programme (No: RP031C-15AFR). ...

[Recommended articles](#)

References (351)

W. Cui

[Heat transfer enhancement of phase change materials embedded with metal foam for thermal energy storage: a review](#)

Renew Sustain Energy Rev (2022)

M. Naghavi *et al.*

[A critical assessment on synergistic improvement in PCM based thermal batteries](#)

Renew Sustain Energy Rev (2021)

T. Ma *et al.*

[Photovoltaic panel integrated with phase change materials \(PV-PCM\): technology overview and materials selection](#)

Renew Sustain Energy Rev (2019)

A. Waqas *et al.*

[Phase change material \(PCM\) storage for free cooling of buildings—a review](#)

Renew Sustain Energy Rev (2013)

S. Mousavi *et al.*

[PCM embedded radiant chilled ceiling: a state-of-the-art review](#)

Renew Sustain Energy Rev (2021)

A. Buonomano *et al.*

[The impact of thermophysical properties and hysteresis effects on the energy performance simulation of PCM wallboards: experimental studies, modelling, and validation](#)

Renew Sustain Energy Rev (2020)

A. Kabeel *et al.*

[Experimental study on tubular solar still using Graphene Oxide Nano particles in Phase Change Material \(NPCM's\) for fresh water production](#)

J Energy Storage (2020)

A. Bamasag

[Machine learning-based prediction and augmentation of dish solar distiller performance using an innovative convex stepped absorber and phase change material with nanoadditives](#)

Process Saf Environ Protect (2022)

E.B. Moustafa *et al.*

[A new optimized artificial neural network model to predict thermal efficiency and water yield of tubular solar still](#)

Case Stud Therm Eng (2022)

A.H. Elsheikh *et al.*

[Productivity forecasting of solar distiller integrated with evacuated tubes and external condenser using artificial intelligence model and moth-flame optimizer](#)

Case Stud Therm Eng (2021)



[View more references](#)

Cited by (39)

[Hybrid battery thermal management systems based on phase transition processes: A comprehensive review](#)

2024, Journal of Energy Storage

[Show abstract](#)

[Review of enhancing boiling and condensation heat transfer: Surface modification](#)

2024, Renewable and Sustainable Energy Reviews

[Show abstract](#)

Advancements in foam-based phase change materials: Unveiling leakage control, enhanced thermal conductivity, and promising applications

2023, Journal of Energy Storage

[Show abstract](#) ✓

Evaluation of different methods to ameliorate the performance of PV/T systems using hybrid nanofluids and PCM in a spiral tube with different cross sections

2023, Results in Engineering

[Show abstract](#) ✓

Experimental and numerical investigations on the thermal performance enhancement of a latent heat thermal energy storage unit with several novel snowflake fins

2023, Renewable Energy

[Show abstract](#) ✓

Thermal heat transfer and energy modeling through incorporation of phase change materials (PCMs) into polyurethane foam

2023, Renewable and Sustainable Energy Reviews

[Show abstract](#) ✓



[View all citing articles on Scopus](#) ↗

[View full text](#)

© 2023 Elsevier Ltd. All rights reserved.



All content on this site: Copyright © 2024 Elsevier B.V., its licensors, and contributors. All rights are reserved, including those for text and data mining, AI training, and similar technologies. For all open access content, the Creative Commons licensing terms apply.





**MANIPAL UNIVERSITY
JAIPUR**

(University under Section 2(f) of the UGC Act)

Department of Electrical Engineering
School of Electrical, Electronics and Communication Engineering

Report on Collaborative activities

Name of Partnering Organizations:


1. MNIT Jaipur, India
2. BSDU-Jaipur, India
3. College of Engineering-Kong Saud University, Saudi Arabia
4. Faculty of Electrical Engineering, Universiti Teknologi Malaysia
5. Universidad Castilla-La Mancha, Spain

Name of Participants:

1. Dr Divya Rishi Shrivastava, Department of Electrical Engineering, Manipal University Jaipur, India
2. Prof Shahbaz Ahmed Siddiqui, Department of Mechatronics Engineering, Manipal University Jaipur, India
3. Dr Kusum Verma, Department of Electrical Engineering, MNIT Jaipur
4. S. Singh, BSDU-Jaipur, India
5. Majid A. Alotaibi, College of Engineering-Kong Saud University, Saudi Arabia
6. Hasmat Malik, Faculty of Electrical Engineering, Universiti Teknologi Malaysia
7. Fausto P. G. Marquez, Universidad Castilla-La Mancha, Spain

Name of the Activity:

Research Work on 'Data-Driven Unified Scheme to Enhance the Stability of Solar Energy Integrated Power System in Real-Time'
(Journal Publication)


HOD
Department of Electrical Engineering
School of Electrical,
Electronics & Communication (SEEC)
Manipal University Jaipur

RESEARCH ARTICLE

Data-Driven Unified Scheme to Enhance the Stability of Solar Energy Integrated Power System in Real-Time

DIVYA RISHI SHRIVASTAVA¹, SHAHBAZ AHMED SIDDIQUI²,
KUSUM VERMA³, (Senior Member, IEEE), SATYENDRA SINGH⁴, MAJED A. ALOTAIBI⁵,
HASMAT MALIK^{6,7}, (Senior Member, IEEE), AND FAUSTO PEDRO GARCÍA MÁRQUEZ⁸

¹Department of Electrical Engineering, Manipal University Jaipur, Jaipur 303007, India

²Department of Mechatronics Engineering, Manipal University Jaipur, Jaipur 303007, India

³Department of Electrical Engineering, Malaviya National Institute of Technology Jaipur, Jaipur 302017, India

⁴Faculty of Electrical Skills Education, Bhartiya Skill Development University, Jaipur 302037, India

⁵Department of Electrical Engineering, College of Engineering, King Saud University, Riyadh 11421, Saudi Arabia

⁶Department of Electrical Power Engineering, Faculty of Electrical Engineering, University Teknologi Malaysia (UTM), Johor Bahru 81310, Malaysia

⁷Department of Electrical Engineering, Graphic Era (Deemed to be University), Dehradun 248002, India

⁸Ingenium Research Group, Universidad Castilla-La Mancha, 13071 Ciudad Real, Spain

Corresponding authors: Hasmat Malik (hasmat.malik@gmail.com) and Majed A. Alotaibi (MajedAlotaibi@ksu.edu.sa)

This research was supported by the Researchers Supporting Project at King Saud University, Riyadh, Saudi Arabia, for funding this research work through the Project number RSP2023R278.

ABSTRACT Solar energy penetration in power grids helps to maintain power balance between generation and demand, thus enhances power grid performance. However, these integrations reduce grids' time margin to respond against sudden frequency changes and re-establishing generation-demand equivalency. Thereby, it poses challenges to the performance and stability of the power system. It therefore becomes increasingly important to comprehend the real-time system data, identify and initiate necessary remedies to sustain the healthy system's operation. This article presents a data-driven unified methodology for enhancing grid stability in solar energy-penetrated power network. The proposed method is a two-stage unified framework that incorporates Prompt Instability Evaluation (PIE) to evaluate impending system transient instability in first stage. In the second stage for a system unstable operation a Decision Assisted Adaptive Control (DAAC) is developed and implemented for corrective emergency control. A novel PIE is presented to perform a post-disturbance transient stability assessment using short-synchronized moving data. The PIE assesses the upcoming transient instability within the first few cycles following fault inception. Next, a novel DAAC is proposed to design an emergency remedial scheme for identifying location (where), magnitude, and type in real-time for unstable operations. The DAAC utilizes a novel Decision Rule Based Inference (DRBI) to evaluate suitable action sets that may be deployed by the DAAC to sustain system stability. The simulation results demonstrate the suitability of the proposed study on the system's performance in the absence/presence of solar energy with topological variations.

INDEX TERMS Decision assisted adaptive control, exponentially weighted moving average, solar energy, transient stability assessment.

I. INTRODUCTION

Globally, electricity demand is expanding at an unprecedented rate, and power networks have adapted by utilizing a mix of various energy sources to meet this growing demand.

The associate editor coordinating the review of this manuscript and approving it for publication was Nagesh Prabhu¹.

Renewable Energy Penetration (REP) to the existing power grids has achieved enormous attention of utility engineers, system operators and researchers in recent years. The REP at the key and critical locations enhances the performance of the power grid. Yet, integrating renewable sources to the system pose severe challenges to the real-time system monitoring, operation, and control of the systems. The capability

to self-heal from emergencies, greater grid resiliency, and operating ease are critical characteristics for ensuring the reliability and continuity of electric power in REP integrated power systems [1]. This necessitates real-time network information, effective situational awareness, and an appropriate strategy for dealing with the emergent abnormal settings. Synchrophasor technology [2] transfers time-stamped synchronized wide-area network data. A suitable cluster of Phasor Measurement Units (PMU) is used in the technology to calculate the synchronized voltage and current phasor measurements.

The appropriate analysis and assessment of this synchronized data exhibits grid integrity and is becoming increasingly crucial for Renewable Energy Penetration (REP). REP not only diversifies the fuel utility but also contributes to the conservation of natural resources and improves energy security. Increased renewable penetration, on the other hand, pose challenges in grid operation due to a variation in system inertia. Any disturbance in the power network upsets the generation-demand equilibrium and, subsequently, changes the system frequency. The system inertia impacts the synchronous operation of the machines and assists the time-margin of power grids to respond to these arising imbalances [3]; however, integration of REP with no inertia such as solar energy with conventional grids decreases the system inertia. In the scenario of hybrid power generation, the synchronous generator's response to system disturbances in terms of rotor angles and speed deviations may degrade further. Under such circumstances, a large disturbance may drive the generator angles to advance more rapidly against the rest of the system. The fast advancement of the generator may lead its rotor to achieve an out-of-step state more rapidly. This state is generally described as transient instability. Therefore, post-disturbance power system Transient Stability Assessment (TSA), particularly incorporating solar energy integration, is critical for grid smooth operation.

In conventional power grids, machine-learning models in unison with wide area measurements are utilized to predict the generator's online dynamic behaviour [4]. The online dynamic analysis is more important for post-fault online system investigations and less feasible towards the real-time framework. Reference [5] proposes the Wide Area Transient Instability Severity Analyzer (WATISA) to early predict the severity imposed by an ensuing event. Although the assessment is timely, accurate, and model free, its suitability is limited to only conventional power systems. The transient potential and kinetic energy coupled with parametric space estimate the transient stability margins [6]. These estimates evaluate the region of attraction (ROA) encompassing the equilibrium solution set. The ROA is inversely proportional to system loading; therefore, it is not a suitable instability indicator. To approximate the transient stability boundary, literature also investigates critical clearing time (CCT) estimates, which signify the maximum allowable time to clear a fault. The mahalanobis-kernel regression [7]

and generator-based threshold computation [8] are a few state-of-the-art methods to compute CCT for the generators. Cui et al. [9] present a combinational transfer learning strategy to improve TS prediction using convolutional neural networks.

A spatial distribution time adaptive methodology for predicting the transient stability status of the system is proposed in [10]. The time-adaptive framework is developed using several cycles of long-term memory classifiers, and a trust score is proposed for the reliability index. A time-delay neural network and bidirectional long short-term memory network-based data-driven TSA methodology is presented in [11]. Reference [12] proposes an active transfer learning-based approach that employs deep belief network maximum mean discrepancy. An improved deep belief network-based methodology incorporating structural characteristics of the network is proposed in [13]. To interpret the transient stability predictor outcomes, local linear interpreter model is also presented. A probabilistic transient stability assessment for wind energy integrated power grid is proposed in [14]. The scheme estimates the transient stability criterion using extreme learning machine and Gauss-Hermite integral based point estimation.

The early transient instability estimates, calculation of CCT/stability boundaries, and real-time stability assessments augment the situational awareness and determines the time instant to execute the emergency remedial strategy, if the system tends to approach unstable settings. In this regard, [15] presents an islanding and auto load shedding technique to stabilize the system and prevent blackout. Methodology utilizing voltage stability Index and load bus ranking [16] presents dynamic adaptive load shedding to ensure frequency resiliency in the power network. A unified approach to first assess the transient stability status and subsequently, implement preventive and emergency control strategy is proposed in [17]. The strategy utilizes synchronized voltage and angle measurements to predict the system instability and formulate the emergency actions: generator tripping and/or load shedding. The adaptive load shedding scheme based on voltage stability assessment [18], [19], combined frequency stability assessment and power flow tracing methodology [20] are utilized to enhance grid stability.

Unlike other power sources, solar energy integration has no effect on frequency-power equivalency but however reduces time margins and stability boundaries. Such power additions adversely impact grids' stability and therefore, the post-disturbance stability assessments are becoming more significant in these grids [20]. Adetokun et al. [21] explores P-V and Q-V based indices to improve voltage stability and enhance grid resiliency of large solar energy integrated power grid. The Quasi-Differential Search based SVC is investigated in [22] to improve transient instability. The approach enhances the oscillation damping, thereby decreasing the steady state settling time. However, it does not suggest the requisite strategy to augment the transient instability of

the system if post-disturbance, the network is tending to exceed the extreme settings. Wandhare et al. [23] show-cases energy function assisted scheme to damp out low frequency power swings. The low frequency oscillations are system response to small or less severe disturbances. The power imbalance due to small disturbances are effectively damped out by power system stabilizers and other control schemes. These control schemes do not significantly damp out power swings arisen due to large or severe disturbance(s) and requires real-time remedial action schemes to preserve grid stability. To augment transit stability in renewable energy integrated power networks, fault current limiters are also utilized to suppress the fault current and subsequently, improves of fault ride through capability [24]. Jawad et al. [25] proposes Battery Energy Storage System (BESS) assisted frequency stability enhancement of solar energy penetrated grid. Post-disturbance, BESS augments the power generation and provide a brief-support in maintaining system power balance. However, both the PV system and the BESS do not provide frequency support or system inertia, that otherwise further advances the already advanced generator from the rest of the network and eventually leads to out-of-step. Chandra et al. [26] recently presented synchronized measurements and a voltage stability index-assisted adaptive load shedding technique to maintain the steady-state frequency of a power network with solar park.

From the review of the literature, it can be concluded that the available methods and techniques for solar PV energy and conventional synchronous generator-based hybrid power generation either regain frequency stability through an emergency strategy or validate the integration of solar energy to the grid. To the author's best of knowledge, literature on improvement of power grid steadiness in terms of real-time TSA and, subsequently, deploying the emergency remedial strategy in real-time with solar energy penetration has not been reported. Thus, the investigation in this paper focuses on the effective monitoring, assessment and control of solar energy integrated power grid. First, Real-time prognosis of impending transient instability following the disturbance is investigated. Next, if necessary, the methodology ensures the transient stability of the PV integrated power system by framing and deploying corrective actions in real-time. The major contributions of this paper are summarized as:

1. First, Prompt Instability Evaluation (PIE) is developed to accomplish early transient stability assessment of the grid having high solar energy penetrations. The highlight of PIE is its ability to identify time-instant of the emergency strategy initiation (if required). The PIE utilize short moving window of real power generated (including power from solar PV) by the power sources as input.
2. Next, subsequent to the PIE assessments, a novel Decision Assisted Adaptive Control (DAAC) is triggered to assess the type, location (where), and magnitude of actions for unstable operating scenarios of grid. The

proposed DAAC encompasses Decision Rule Based Inference (DRBI) to identify and initiate set-of-actions at a suitable location.

3. To maintain transient stability of solar integrated power system and prevent the major portion of the system from collapse, the proposed composite scheme is an essentially response-based framework. Moreover, all the actions are implemented in real-time using synchrophasor measurements. Therefore, the proposed scheme has a generalization capability which finds application to any system (with or without solar energy sources) in a wide range of operational scenarios.

The proposed composite methodology is evaluated using a modified New England 39 Bus test system that incorporates solar energy. Fig. 1 illustrates an overall summary of the unified framework. The remainder of the paper is organized as: Section II describes the Prompt Instability Evaluation of impending transient system instability in presence/absence of solar energy. Section III describes the Decision Assisted Adaptive Control (DACC) strategy to control system stability and enhance grid performance. The results and discussion on the test system with/without solar energy penetration are discussed in Section IV. The conclusions of the investigations are presented in Section V. Fig. 2 illustrates the section wise structure of the paper.

II. REAL-TIME POWER SYSTEM STABILITY ASSESSMENT

The post-disturbance power system severity can be assessed by timely monitoring any one or more of bus voltage, frequency, and angles. This section presents a novel real-time transient stability assessment (TSA) of power systems with/without solar energy penetration. First, the mathematical formulation of power system dynamics with/without solar energy is detailed. Subsequently, the proposed methodology of prompt instability evaluation for imminent transient instability is presented.

A. POWER SYSTEM DYNAMICS

The electric power delivered by synchronous machine is [19]:

$$P_{ej} = P_{mj} - \left(\frac{2H_j S_j}{f_n} \right) \frac{df_{Gj}}{dt} \quad (1)$$

where, f_n is nominal frequency, P_{ej} (MW) is electric power generated, P_{mj} (MW) is mechanical power, H_j (MW.s/MVA) is inertia constant, S_j (MVA) is machine rating, and f_{Gj} is frequency of j^{th} machine. During equilibrium condition, electrical power equals the mechanical power and Eq (1) is thus modified as:

$$\frac{df_{Gj}}{dt} = 0 \rightarrow P_{ej} = P_{mj} \quad (2)$$

In steady state condition, rate of change of frequency equals zero. If the equilibrium is disturbed during transient conditions, the rate of change in frequency can be either positive, indicating a decrease in electrical output, or negative, suggesting an increase in real power output and is given

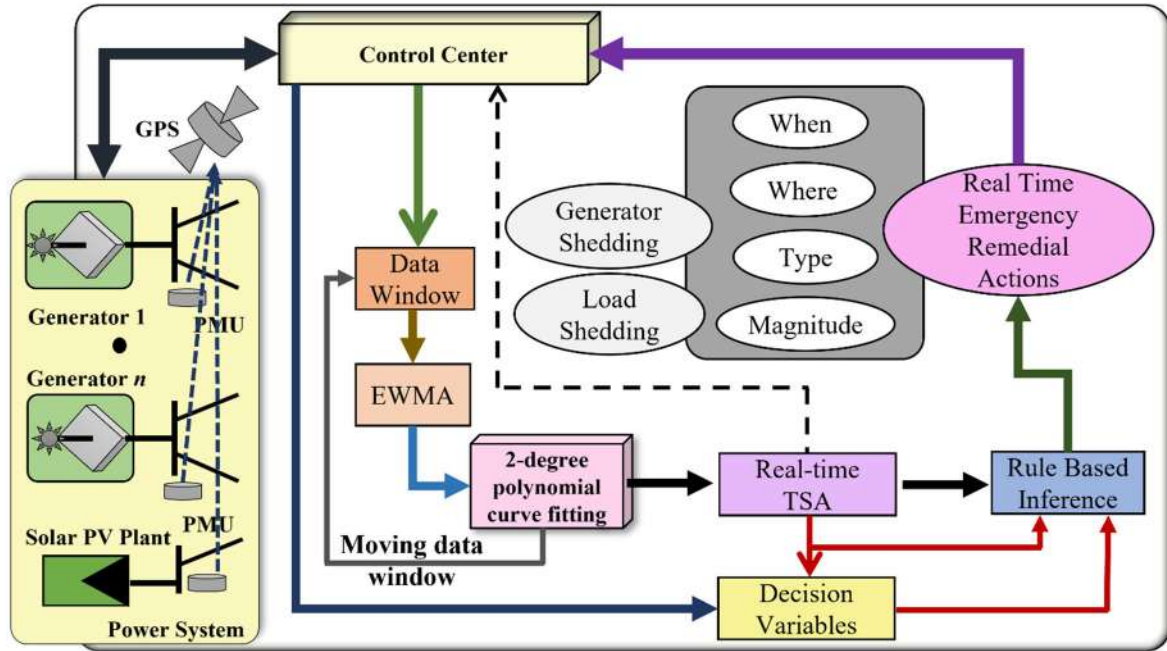


FIGURE 1. Overall summary of the proposed unified scheme.

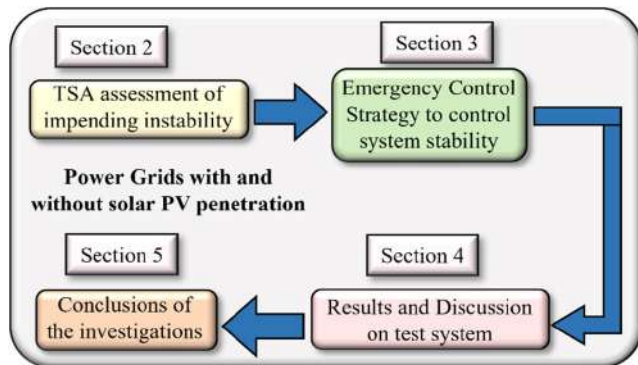


FIGURE 2. The section wise structure of the paper.

as:

$$\begin{aligned} \frac{df_{Gj}}{dt} > 0 &\Rightarrow Pe_j \downarrow \\ \frac{df_{Gj}}{dt} < 0 &\Rightarrow Pe_j \uparrow \end{aligned} \quad (3)$$

The combined generated power (Pe) delivered by n machines is:

$$Pe = \sum_{j=1}^n Pe_j \quad (4)$$

The total system inertia based on the individual generator inertia constant and rated MVA power is calculated as:

$$H = \frac{\sum_{i=1}^n H_i S_i}{\sum_{i=1}^n S_i} \quad (5)$$

The PV system does not use a spinning mechanism to generate electricity. Thus, the solar farm’s power does not have power-frequency equivalency. Furthermore, this integration adds no inertia to the system; rather, total inertia in the network reduces [3]. The decreased inertia lowers the critical clearing time for machines, causing them to get out of synchronism. Solar energy penetration can be incorporated into the grid either by replacing conventional synchronous machine plants or into the areas without conventional generators. In the first scenario, Eq. (6) with $n'=n$, can be used to determine the total power supplied. In contrast, in the second case, the total power is calculated using Eq. (6) with $n' = n - PV$, where PV is the number of solar plants in the grid. The power delivered by a power system with n' power generating sources is:

$$Pe = \sum_{j=1}^{n'} Pe_j + P_{PV} \quad (6)$$

where, P_{PV} is power generated by the solar parks. The overall system inertia is reduced with SE and a decreased SG-based generation mix, and is computed as:

$$H' = \frac{\sum_{i=1}^{n'} H_i S_i}{\sum_{i=1}^{n'} S_i + S_{PV}} \quad (7)$$

where, S_{PV} is solar plants MVA from and H' reduced inertia.

B. PROMPT INSTABILITY EVALUATION (PIE)

One of the consequences of the ensuing event in the network is an angular separation of rotor angles amongst the

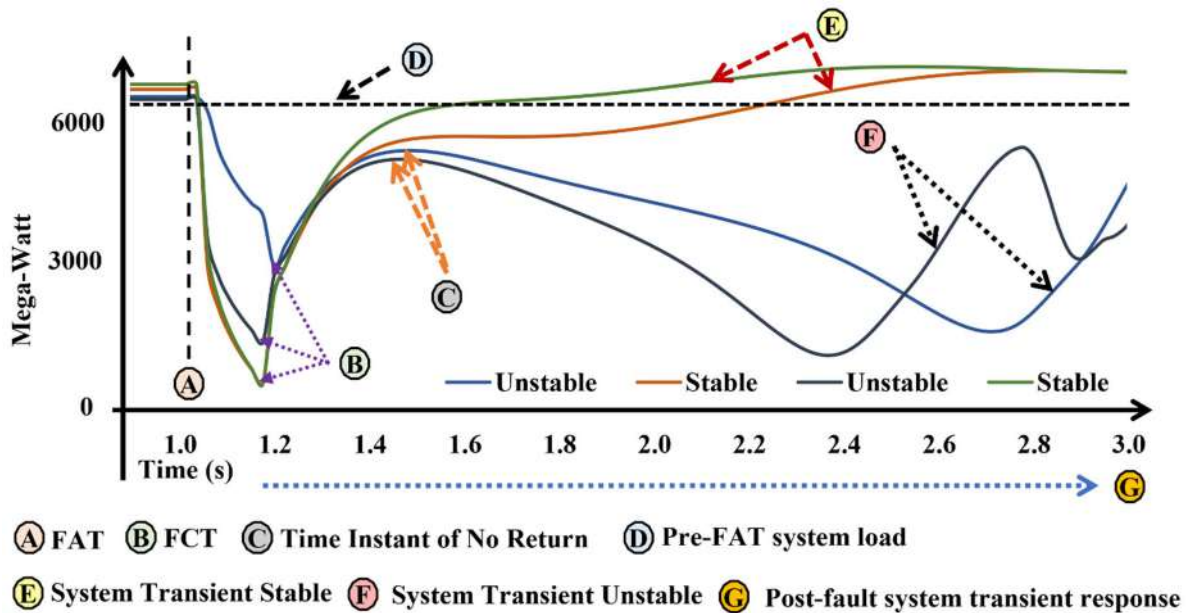


FIGURE 3. System power time series for transient stable and unstable operating scenario.

synchronous machines. In accordance with post-event system dynamics, an increase in power produced by an advanced generator tends to decrease the separation in rotor angles. At a specific time-instant, the increase in rotor angle of the accelerated generator decreases power supply, which may further lead the generator to fall out-of-step. The information of rotor angle separation is crucial for power system secure operation and is known as transient stability. Transient Stability is the rotor angle stability of the system to regain synchronism when subjected to large disturbance(s). Following the disturbance, prompt TSA assessment ensures sufficient time margin to formulate and deploy emergency control and augment grid sustainability. In this regard, timely, effective interpretation and valuation of short-synchronized data window is besought to estimate early TSA before the system actually exceeds the transient stability limits. Fig. 3 illustrates the variation of the total system active power for ensuing transient stable and unstable operating scenarios. This figure reflects that the variation in electric power is different for stable and unstable operating scenarios. Initially, the system is operating in equilibrium state such that rate of change of frequency is zero. At FAT, a severe fault (short circuit) occurs, resulting in disturbance of equilibrium and decreased generated power output from sources. Next, post-FCT, all the power sources tend to recover from the fault. Situations where the system power recovers and re-establishes equipoise, results in transient stable system. Few scenarios where at certain instant of time, the total system power starts decreasing, the system will be moving to transiently unstable operations.

Thus, the total system power variations possess crucial information of transient stability of the system and therefore power variations can be utilized for identifying state of the system. Henceforth, continuous investigation of total gener-

ated power short-data window can be utilized to assess the estimations of awaiting instability. The short data window ensures fast response of system’s instability status. However, long data window may provide more better estimation but have a large response time; such that, the system will already advance towards extreme settings leading to complete collapse. Thus, there is a trade-off between accuracy and response time, present short data length successfully appraises TSA in adequate response time for real-time applications. Fig. 4 displays the procedure utilizing a time series of generator rotor angle and total active power. The figure exhibit’s fault initiation, clearance, three-cycle moving average of power data window, time-instant of no return T , early transient instability detection, time of detection (t_d), and available time margin to assess and deploy remedial measures. The mathematical formulation of the proposed PIE is detailed below. Let, Pe_{DW} be three-cycle window of generated power in the power system through Eq (6) as:

$$Pe_{DW} = [Pe(t_i)Pe(t_{i+1})Pe(t_{i+2})] \quad \forall t \in [FCT + 1cycle, t_d] \quad (8)$$

The moving data window of generated total power is employed to acclimatize the power system dynamics in real-time. Exponentially Weighted Moving Average (EWMA) is used for this purpose. EWMA [27], [28] is a statistical approach to remove noise (random fluctuations) and prioritizing recent measurements. Such that, recent measurements are weighted substantially higher than the preceding data to determine real-time system dynamics. For i^{th} time sample, the filtered data points can be calculated through Eq (9) and

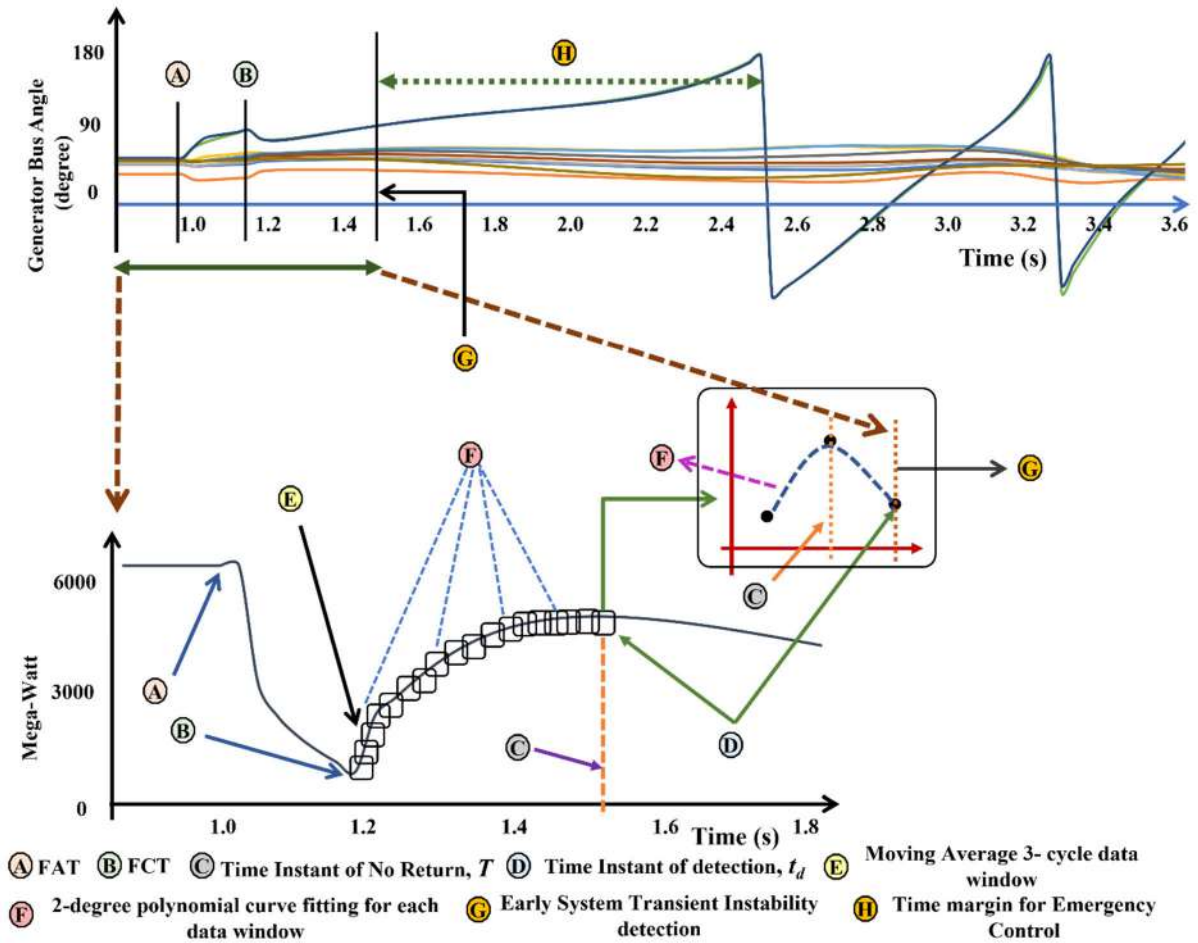


FIGURE 4. Proposed power system transient instability assessment.

weighing factor α is calculated through Eq (10) as:

$$Pe'[t] = \alpha Pe[t] + (1 - \alpha) Pe'[t - 1] \quad (9)$$

$$\alpha = \frac{2}{span + 1} \quad (10)$$

In this work, span equals two data samples. The processed three cycle data available from Eq (9) is applied to 2-Degree polynomial fitting by minimizing the least squared error:

$$\min(E) = \min \sum_{m=1}^3 |p(x_m) - Pe'_m|^2 \quad (11)$$

The Eq (12) is utilized to validate the maxima within 2-degree polynomial of the form:

$$p(x) = c_0 + c_1x + c_2x^2 \quad (12)$$

The maxima ensure the time of no return, that is, post-fault, the system does not tend towards recovery mode. Alternatively, within next few cycles, it will exceed transient unstable settings. Hence, at this step we are able to identify viz. (a) system is in-advance predicted to be transient stable or unstable, (2) time of initiation of emergency control actions, as shown

in Fig. 5. The immediate detection of unstable operating state of the system ensures sufficient time margin to assess and deploy the wide area emergency remedial actions in real time.

III. REAL-TIME WIDE AREA EMERGENCY REMEDIAL STRATEGY

This section details the proposed real-time emergency action strategy appropriate for power systems with /without solar farm. The approach incorporates Decision Assisted Adaptive Control (DAAC) that leverages network real-time data to develop appropriate procedures. To sustain system stability, DAAC identifies action type (what), location (where), and magnitude based on a set of inference rules.

A. DECISION ASSISTED ADAPTIVE CONTROL (DAAC)

The real-time instability detection in the last section by PIE triggers the Decision Assisted Adaptive Control (DAAC). The DAAC computes the decision variables utilized by inference rules to identify the action type, location, and magnitude in the proposed strategy. These decision variables estimate the individual generator and system power imbalance and are based on real-time network information. As the DAAC

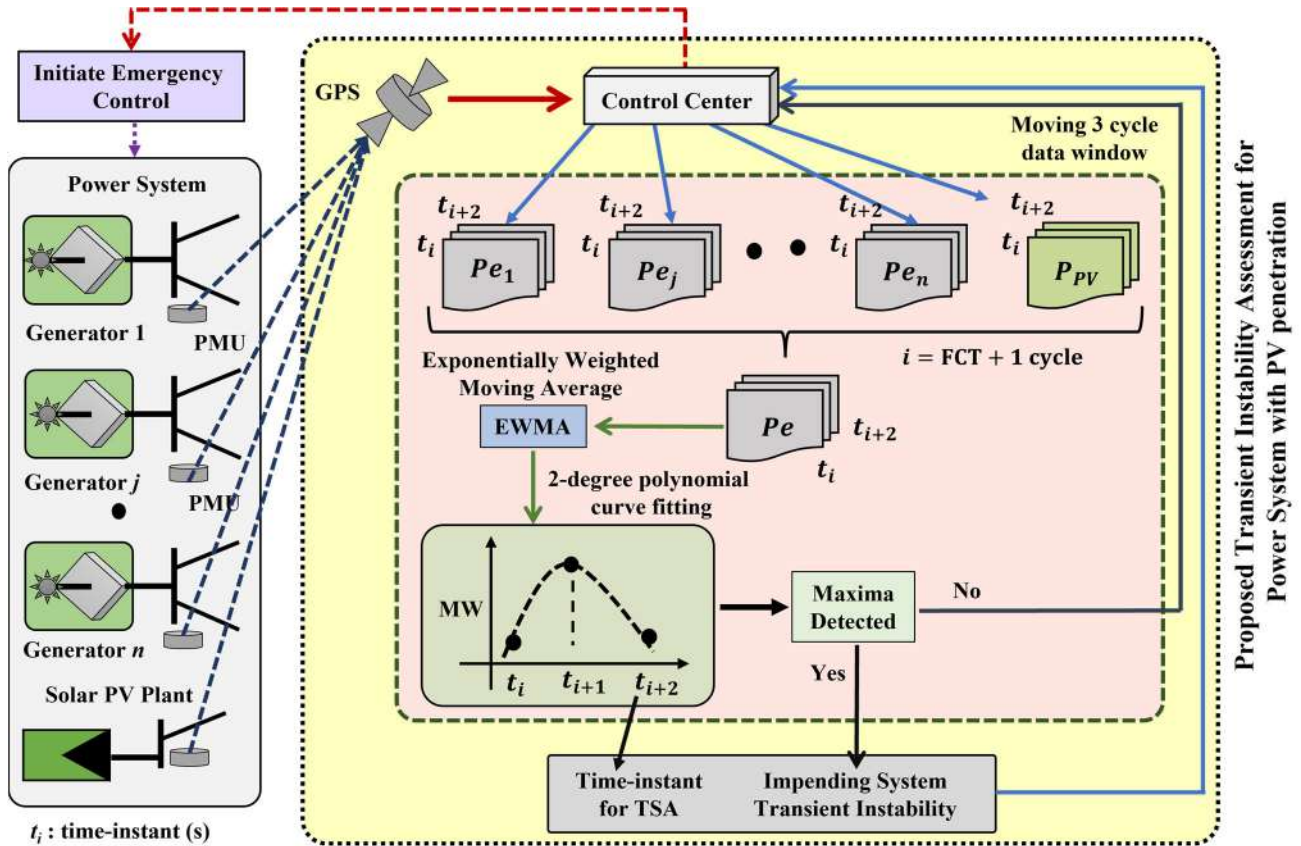


FIGURE 5. Overall summary of prompt instability evaluation.

is network data-driven, it is adaptive to system’s topological and functional variations. Subsequent to PIE assessment, for j^{th} machine and at the time instant of PIE assessment, synchronized generator frequency along with MVA rating (S) and generator inertia (H), estimates the generator power imbalance dPg_j as:

$$dPg_j = \left(\frac{2H_j S_j}{f_n} \right) \frac{df_{Gj}}{dt} \forall j \in n \quad (13)$$

Summation of Eq (13) for all the n machines (n' in case of solar energy penetration) in power grid, estimates the total system power imbalance $delP$ as:

$$delP = \frac{2}{f_n} \sum_{j=1}^n H_j S_j \frac{df_{Gj}}{dt} \quad (14)$$

Although the generator frequency is qualitatively identical to the frequency of the node to which it is connected, the effect of interconnected nodes and local loads results in a small numerical difference. These trivial differences are utilized to estimate individual machine power imbalance. Thus, for j^{th} machine, estimated power imbalance due to frequency of the node connected to the machine is:

$$dPg_j^F = \left(\frac{2H_j S_j}{f_n} \right) \frac{df_{Gj}^F}{dt} \quad (15)$$

where, f_{Gj}^F is frequency of generator node and dPg_j^F is estimated power imbalance due to node frequency for j^{th}

machine. The calculation of Eq (13) – (15) performed for single time instant, not only facilitates the fast identification of remedial solutions, but also decreases memory utilization for the power data processors located at centralized control centres. These power imbalances are taken as input to Decision Rule Based Inference (DRBI) to find the appropriate “type, location and magnitude” of the actions. The overall implementation of DAAC is summarized in Fig. 6.

B. DECISION RULE BASED INFERENCE

To endure system synchronism under abnormal scenarios a novel strategy Decision Rule Based Inference (DRBI) is proposed. DRBI, in its initial step, determines the type of action (What) to be employed. At time instant T , if any generator in the network is supplying excess power such that it is accelerating against the rest of the system, it is necessary to reject that generator from the system. The rejection of generation may cause other machines to share the power imbalance in proportion to their respective inertias. However, generator rejection has to be supplemented by load shedding, as it may still give rise to a power imbalance in the system. Therefore, relative load shedding is to be initiated to balance the generation-load imbalance. In contrast, load shedding is proposed if the load demand exceeds the power output from generators, affecting one of the machines to slow down in comparison to the rest of the system. The power imbalance

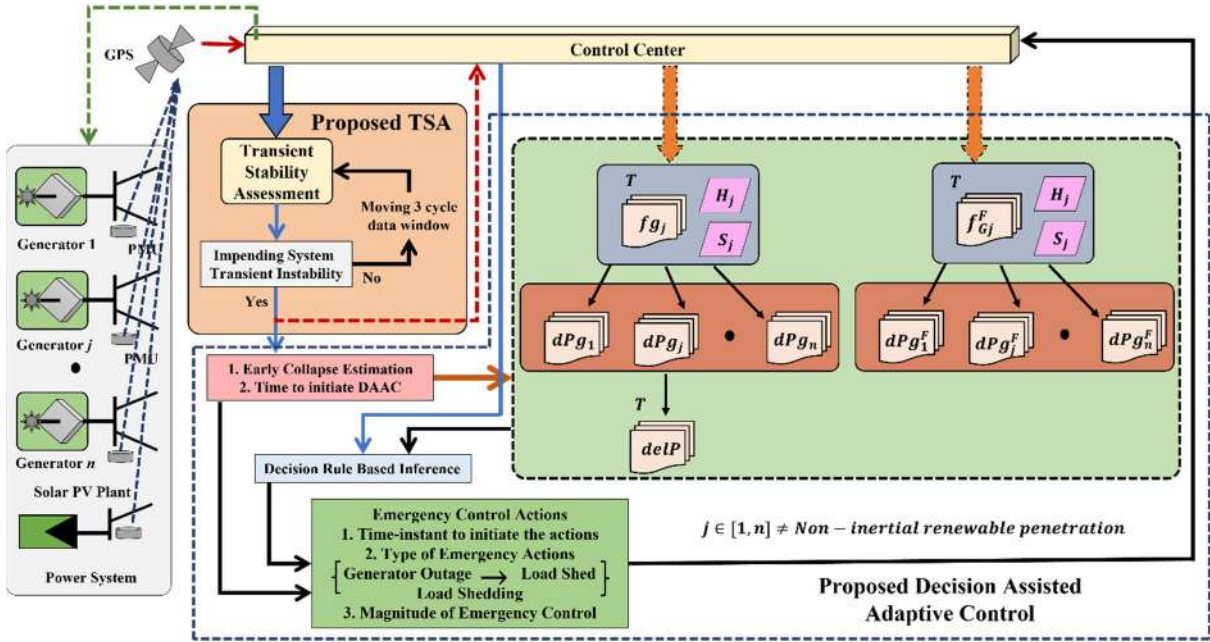


FIGURE 6. Proposed real-time emergency control strategy.

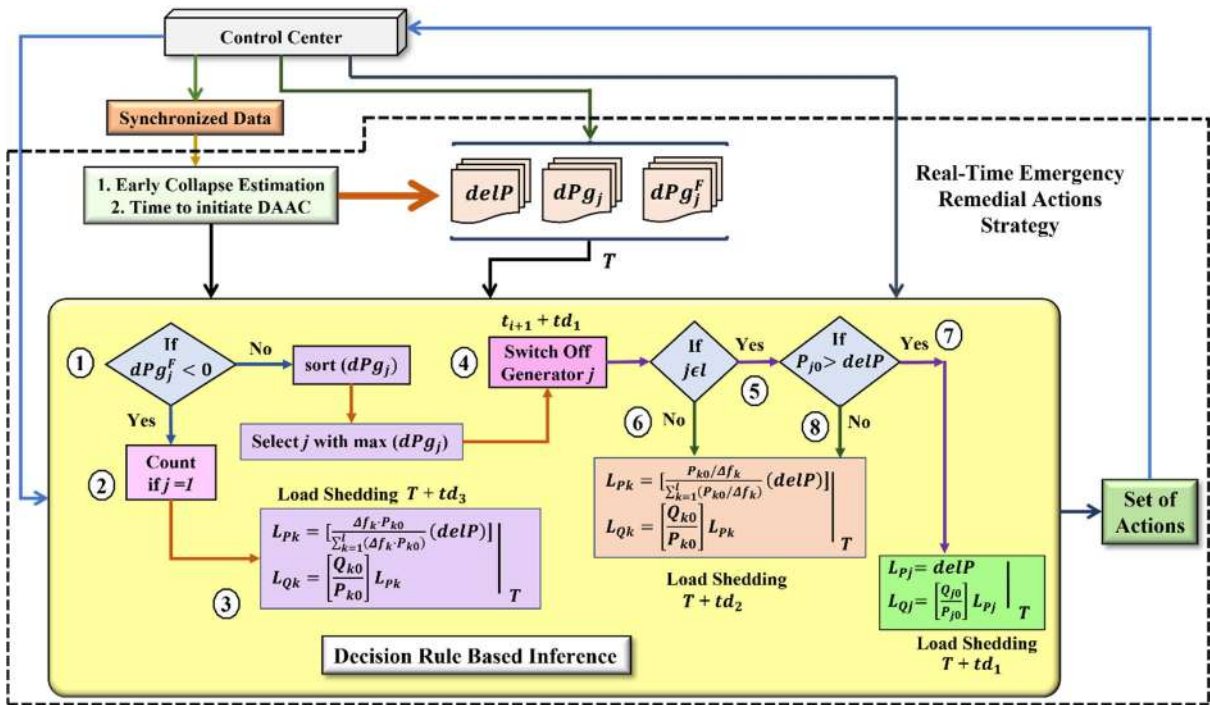


FIGURE 7. Proposed decision rule based inference (DRBI).

estimate computed through Eq (15) serves the decision variables for deciding the control action type: generator tripping and/or load shedding as:

$$dPg_{jT}^F \rightarrow \left\{ \begin{array}{l} < 0 \rightarrow \text{LoadShedding} \\ > 0 \rightarrow \text{GeneratorRejection} \end{array} \right\} \quad (16)$$

The negative estimates of dPg_{jT}^F for any generator infer the increased load demand. The set of actions corresponding to load curtailment is necessary to sustain stability. Alternately,

positive estimates for all generators indicate excess power generation and it necessitates generation rejection followed by proportional load shedding. Fig. 7 highlights the suitable action type (What), location (Where), and magnitude (How) following the calculation of Eq (16). In the proposed DRBI, the set of actions as a stepwise approach are labelled as Action Set (AS) and are highlighted in Table 1. These Action Sets indicate the step-by-step approach to be adopted among each action type, the appropriate location and magnitude for

TABLE 1. Action set in proposed DRBI.

Action Type	Action type in Proposed DRBI	Stepwise approach (Action Set)
Generator Rejection	Generator Tripping followed by Load curtailment [AS ⁽¹⁾ → AS ⁽⁴⁾]	AS ⁽¹⁾ → AS ⁽⁴⁾ → AS ⁽⁵⁾ → AS ⁽⁷⁾ AS ⁽¹⁾ → AS ⁽⁴⁾ → AS ⁽⁵⁾ → AS ⁽⁸⁾
Load Shedding	Load Shedding [AS ⁽¹⁾ → AS ⁽²⁾]	AS ⁽¹⁾ → AS ⁽²⁾ → AS ⁽³⁾

AS⁽¹⁾: Identification of action type; AS⁽²⁾: Decision of load shedding; AS⁽³⁾: Calculation of magnitude for load shedding; AS⁽⁴⁾: Detection of location for generator rejection; AS⁽⁵⁾: Post generator rejection, detection of location of load shedding ; AS⁽⁶⁾: Calculation of magnitude for load shedding ; AS⁽⁷⁾: calculation of magnitude for load shedding; AS⁽⁸⁾: Post generator rejection, calculation of magnitude for load shedding.

necessary remedial measures. Each of these action set is detailed in the following sub-sections.

1) GENERATOR TRIPPING: ACTION TYPE AS⁽¹⁾ → AS⁽⁴⁾

a: LOCATION IDENTIFICATION

As the generator rejection decision is indicated, the location of the generator to be tripped is assessed. Since generation rejection is the consequence of increased generation in the system, the generator with excessive power generation among *n* machines is the candidate generator to be tripped. Apparently, the machine with the maximum imbalance contributes most to surplus generation. Its rejection will suitably ease the imbalance in the system. Thus, at time instant *T*, Eq (17) is sorted in descending order to identify the individual generator maximum power imbalance. The candidate generator with maximum imbalance (say *j*th generator) is to be rejected. The process of identifying the candidate generator to be tripped, is represented as,

$$sort(dPg_{j|T}) \Rightarrow \max \left[\left(\frac{2H_j S_j}{f_n} \right) \frac{df_{Gj}}{dt} \Big|_T \right] \forall j \in n \quad (17)$$

b: MAGNITUDE AND LOCATION OF LOAD CURTAILMENT

The surplus power generation prior to generator rejection indicates a low power demand at load sites at time-instant of instability detection. Following the generator rejection, curtailment of large load buses may manifest an increased power demand from the system. Thus, it is imperative to identify the buses with light loads and curtail the adequate magnitude in real-time. Considering this fact, a new Load Sharing Index (*LSI*) has been developed in this work to identify the percentage share of total system load being shared by individual load bus. It basically calculates the share of individual load based on frequency deviation against nominal frequency at *T*. The deviation is then normalized by the cumulative deviation for all the load sites to obtain the percentage share. After tripping the identified generator, for the system with *l* loads, *LSI* for *k*th load is calculated as,

$$LSI_k = \frac{f_k|T - f_n}{\sum_{k=1}^l (f_k|T - f_n)} \times 100 \forall k \in l \quad (18)$$

where, *f_k|_T* is *k*th load bus frequency at time *T* and *f_n* is nominal frequency. Following the generator trip, the numerical

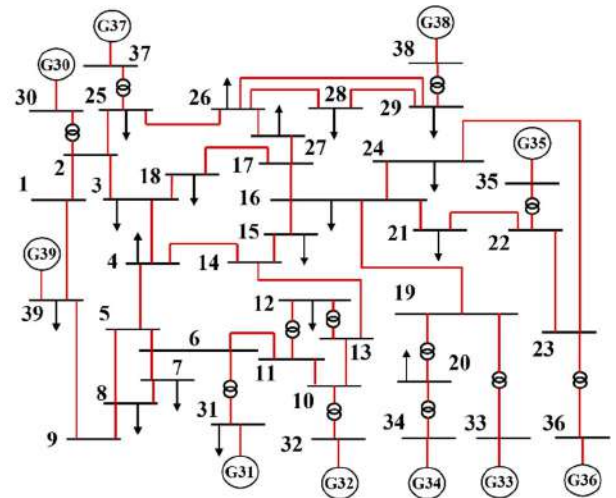


FIGURE 8. IEEE 39 bus test system.

TABLE 2. Detailed data generation.

Event Category	Stable Cases	Unstable Cases	Total Cases
N-2 contingency leading to bus isolation	78	50	128
Short circuit cleared with line outage	29	4	33
Cascaded faults	25	8	33
Total Cases	132	62	194

N: Number of lines.

valuations from *LSI* are then utilized to estimate the location of load sites for load curtailment.

c: ACTION SET AS⁽¹⁾ → AS⁽⁴⁾ → AS⁽⁵⁾ → AS⁽⁷⁾

The *LSI* for all the loads is sorted to identify the least load sharing node.

If the load bus is same as that of the tripped generator and that the load pre-disturbance magnitude exceeds estimated imbalance *delP* at *T* time-instant, the equivalent magnitude *L_{Pj}* from this candidate load bus is curtailed. The electrical loads are in general characterized into two components: real and reactive. It is impractical to consider only real component for load shedding. Therefore, it is essential to shed the adequate quadrature component of the load. The reactive component *L_{Qj}* to be shed is calculated in proportion to the ratio of pre-disturbance reactive and real power component and *L_{Pj}*. Overall, the set-of-actions for this strategy is labelled as AS⁽¹⁾ → AS⁽⁴⁾ → AS⁽⁵⁾ → AS⁽⁷⁾. Thus, the necessary magnitude of candidate load to be shed is calculated as,

$$\left. \begin{matrix} L_{Pj} \\ L_{Qj} \end{matrix} \right\} \Rightarrow \left\{ \frac{|delP|_T}{[Q_{j0}/P_{j0}] L_{Pj}} \right\} \forall j \in l \quad (19)$$

where, for *j*th location, *L_{Pj}* is active power and *L_{Qj}* is reactive power of the candidate load to be shed, *P_{j0}* is pre-disturbance active power, *Q_{j0}* is pre-disturbance reactive power for *j*th load.

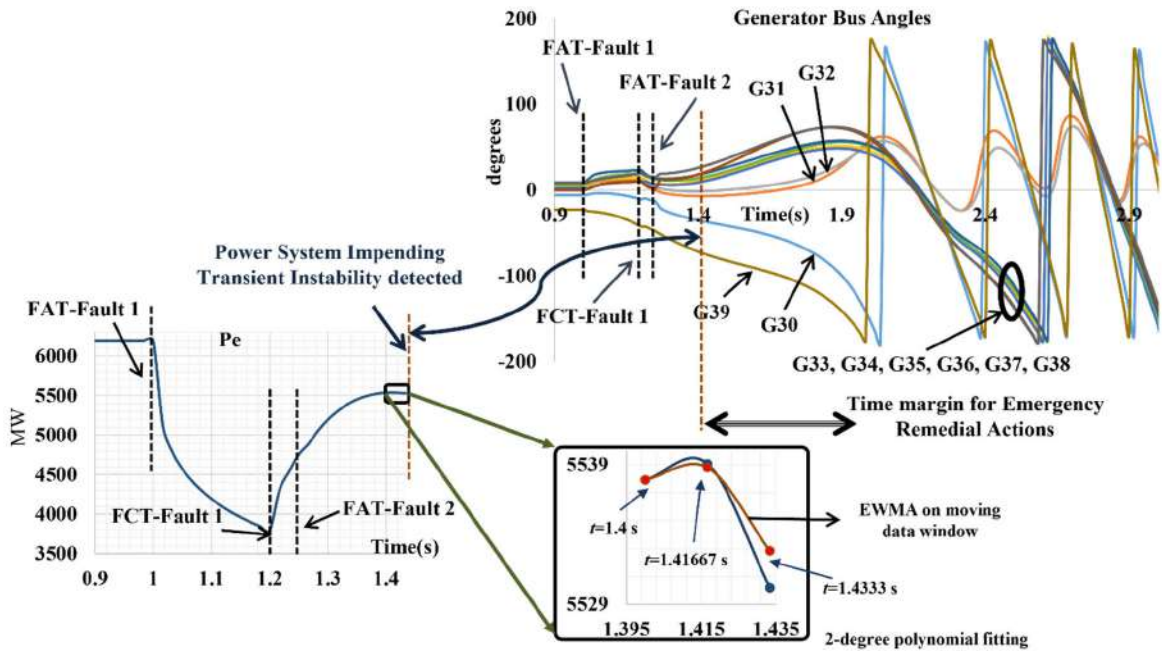


FIGURE 9. Proposed TSA for illustrative example I.

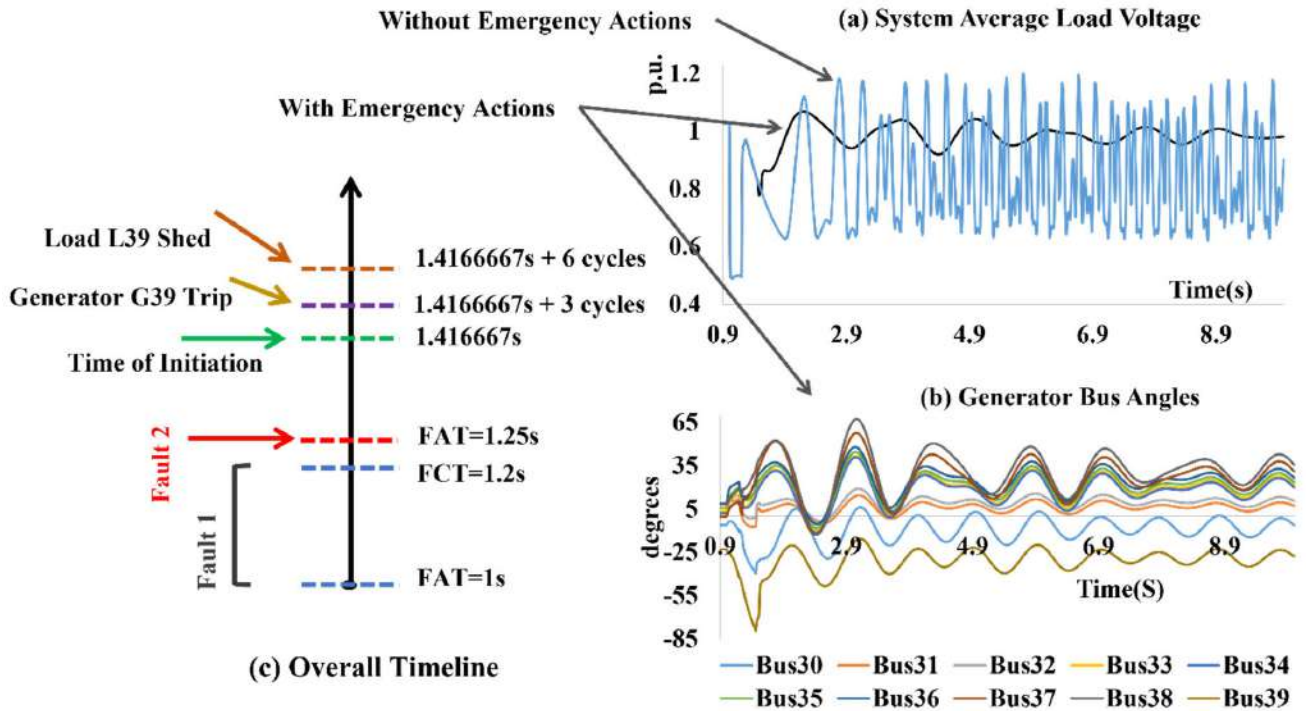


FIGURE 10. Outcome of three cycle delayed emergency remedial strategy for illustrative example I.

d : ACTION SET $AS(1) \rightarrow AS(4) \rightarrow AS(5) \rightarrow AS(8)$ AND ACTION SET $AS(1) \rightarrow AS(4) \rightarrow AS(6)$

Alternatively, if the identified LSI calculation suggest the load bus that is not the same as of tripped generator ($j \notin I$) or, if the pre-disturbance magnitude load at j^{th} location is less than that of the estimated power imbalance ($P_{j0} < delP$); each load in the network is considered as a candidate load for load shedding. The magnitude L_{Pk} of the load to be curtailed

is decided based on frequency deviation of the candidate load bus at T time-instant, pre-disturbance load amount, and power imbalance. The load with smaller frequency deviation from nominal frequency and a less pre-disturbance loading shares the major component of load shedding. Similarly, the reactive component L_{Qk} to be shed is calculated in proportion to ratio of pre-disturbance reactive and real power component, and L_{Pk} . Overall, the set-of-actions for the

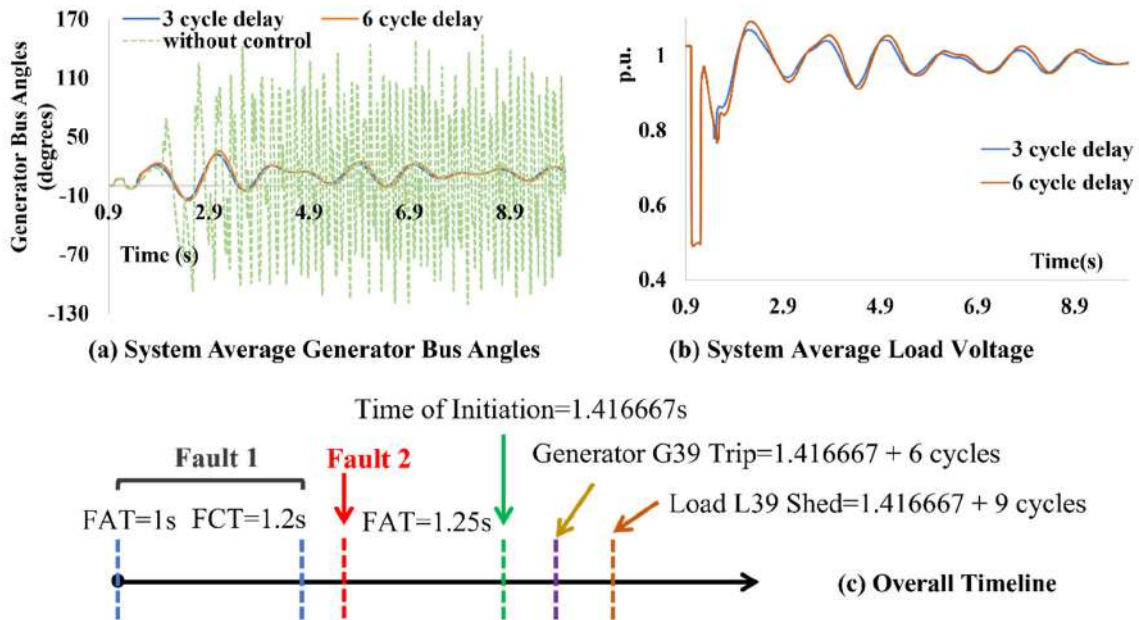


FIGURE 11. Impact of additional three cycle delayed Emergency Remedial Strategy for illustrative example 1.

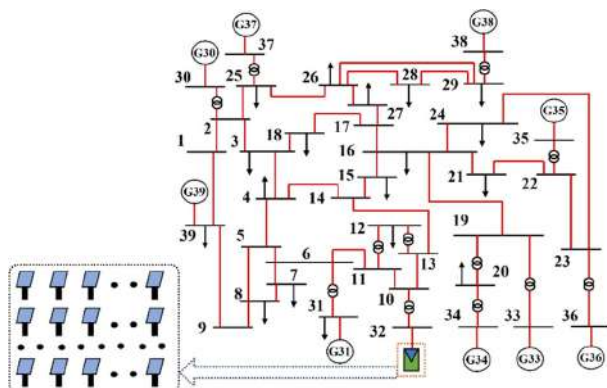


FIGURE 12. Modified new england 39 bus system with conventional generator replaced by solar farm at Bus 32.

situation ($j \notin l$) is labelled as $AS^{(1)} \rightarrow AS^{(4)} \rightarrow AS^{(6)}$, while the action strategy for the situation ($P_{j0} < delP$) is labelled as $AS^{(1)} \rightarrow AS^{(4)} \rightarrow AS^{(5)} \rightarrow AS^{(8)}$. In both instances, the magnitude of load to be shed from all the load in the system is calculated as,

$$\left. \begin{matrix} L_{Pk} \\ L_{Qk} \end{matrix} \right\} \Rightarrow \left[\left[\left(\frac{P_{k0}}{\Delta f_k} \right) delP \right] / \sum_{k=1}^n \left(\frac{P_{k0}}{\Delta f_k} \right) \right] \Bigg|_{T} \forall k \in l \quad (20)$$

where, for k^{th} load, L_{Pk} is active power and L_{Qk} is reactive power to be curtailed, P_{k0} and Q_{k0} is pre-disturbance active and reactive power, and Δf_k is the frequency deviation against nominal frequency.

2) LOAD SHEDDING: ACTION TYPE $AS^{(1)} \rightarrow AS^{(2)}$

α : ACTION SET $AS^{(1)} \rightarrow AS^{(2)} \rightarrow AS^{(3)}$

At the instant of instability detection, the negative power imbalance depicted by Eq (16) showcases the excess power

demand. This additional power demand is numerically equivalent to the estimated power imbalance. Under this scenario, one or more generators may slow down. In the operational scenario of a single generator being slow down, all loads in the network are labelled as candidate loads. In proposed *DRBI*, these adopted set-of-actions are labelled as $AS^{(1)} \rightarrow AS^{(2)} \rightarrow AS^{(3)}$. To distribute the imbalance among the loads, frequency change methodology [19] is utilized to calculate the magnitude of load shedding and is calculated by:

$$\left. \begin{matrix} L_{Pk} \\ L_{Qk} \end{matrix} \right\} \Rightarrow \left[\left[\frac{(P_{k0} \cdot \Delta f_k \cdot delP) / \sum_{k=1}^n P_{k0} \cdot \Delta f_k}{\left[\frac{Q_{k0}}{P_{k0}} \right] L_{Pk}} \right] \right]_{T} \forall k \in l \quad (21)$$

where, at k^{th} location, Δf_k is the frequency deviation against nominal frequency, L_{Pk} is active power, L_{Qk} is reactive power to be shed. The frequency dependent strategy for load shedding distribution among the candidate loads, depends on individual load pre-disturbance numeric value and load bus frequency. Such that, a load with greater frequency deviation from nominal frequency and more pre-disturbance loading, shares the larger component of load shedding.

C. ACTUAL TIME OF ACTION DEPLOYMENT

Although the instigation of emergency actions is signaled at the time of instability detection, the actual initiation of actions is delayed. The delay in deployment is due to various associated delays for executing corrective actions [29] including latency in communication to central logic, substations, power plants, delays due to circuit breaker operating time, and computer processing time. Thus, post T time instant,

TABLE 3. Comparative evaluation of the proposed PIE with state-of-art learning techniques.

S.no.	Technique	Number of Test Cases	Overall Accuracy Actual/ Estimated	False Alarm Actual/ Estimated	Missed Alarm Actual/ Estimated	Impending Instability (Y/N)	When to Initiate ECA (Y/N)	Time-instant of Action Quantity Calculation (Y/N)
1	Random Forest	39	39/38	24/24	15/14	Y	N	N
2	Multilayer Perceptron	39	39/37	31/30	8/7	Y	N	N
3	k-NN	39	39/38	28/27	11/11	Y	N	N
4	DT	39	39/38	28/28	11/10	Y	N	N
5	AdaBoost	39	39/38	25/24	14/14	Y	N	N
6	Proposed PIE	194	194/189	132/127	62/62	Y	Y	Y

TABLE 4. Emergency remedial scheme for illustrative example I.

Action Type and Location	Time (s)	Action Magnitude
TSA detection	1.417	$delP=627.808$ MW
Trip G 39	$1.417 + td_1$	Shed 1000 MW Power Generation
Load Shed L39	$1.417 + td_3$	Shed 36.76% Load of 1707.925 MW and 383.5 MVAr

td_1 , td_2 , and td_3 are time delays in the actual initiation of control actions such that this delay corresponds to a specific Action Set.

IV. RESULTS AND DISCUSSION

This section validates the implementation of the proposed unified scheme on the IEEE 39 Bus test system with and without solar energy integration. The DIGSILENT Power Factory is utilized to perform the simulation of the test system. The test system conventionally has 39 nodes, 34 lines, 12 transformers, 19 loads, and 10 synchronous generator-based power sources with a base 6266.82 MVA generation and load of 6257.77 MVA and, as shown in Fig. 8 [5]. In this paper, real-time data is available with 1 sample/cycle (60 Hz sampling frequency). The performance of the proposed composite scheme is tested on generated database consisting of different faults with different system loading. The disturbances simulated are considered individually and in cascaded scenario and are categorized in stable/unstable scenarios. Table 2 illustrates the generated dataset comprising event category, unstable/stable cases and total cases. In the subsequent sections, first the performance scores of the proposed PIE and DAAC implementation are discussed. Next, execution of proposed strategy on test system in absence of solar farm is showcased through illustrative example I. Subsequently, to test suitability of the proposed scheme to enhance stability and avoid grid collapse on SE penetrated power system, one representative example with single SE penetration (illustrative example II) and illustrative example III with multiple bus SE penetration are employed. Finally, a comparative assessment of the presented work against available state-of-art is showcased. The proposed strategy is realized on a PC with Intel i5 CPU 2.4 GHz processor and 16 GB RAM.

TABLE 5. Emergency remedial scheme for illustrative example II.

Action Type and Location	Time (s)	Action Magnitude
TSA detection	1.4167	$delP=600.334$ MW
Shed All Loads	$1.4167+td_2$ (0.05 s)	Shed proportionate % load illustrated in Figure 17(a) with total load shed equal to $delP$

A. PERFORMANCE EVALUATION OF PROPOSED PIE AND DAAC

A comparative evaluation of the proposed PIE scheme with the data-mining techniques available in literature is accomplished and is detailed in Table 3. The Table presents statistics regarding the count of cases that were incorrectly classified as stable (referred to as ‘‘Missed Alarm’’) and the count of cases that were incorrectly classified as unstable (referred to as ‘‘False Alarm’’) for each type of event. As is apparent, the proposed PIE for TSA provides multiple objectives, including predicting future instability, reducing the occurrence of false and missing alarms, and evaluating the time required to execute emergency actions. A comparative analysis has been performed to assess the effectiveness of machine learning approaches available in literature and the proposed PIE methodology for different cases.

The data mining techniques, in comparison to the proposed PIE, require training using 80% of the available data, while the remaining 20% is utilized for testing the models. However contrary to these techniques, the PIE approach does not employ learning models; instead, all the generated data is subjected to testing. The results indicate that the performance of the suggested PIE method in assessing the likelihood of impending system transient instability is superior. Upon identification of impending instability for the unstable cases in Table 3, DAAC is deployed to sustain system stability and augment power grid operation. The proposed control action strategy successfully augments grid performance and stability.

In the subsequent sub-sections, the performance of DAAC is displayed by two illustrative examples in the absence/presence of solar plant. Moreover, the performance of the composite scheme is also showcased on solar plant integration at multiple locations with an illustrative example.

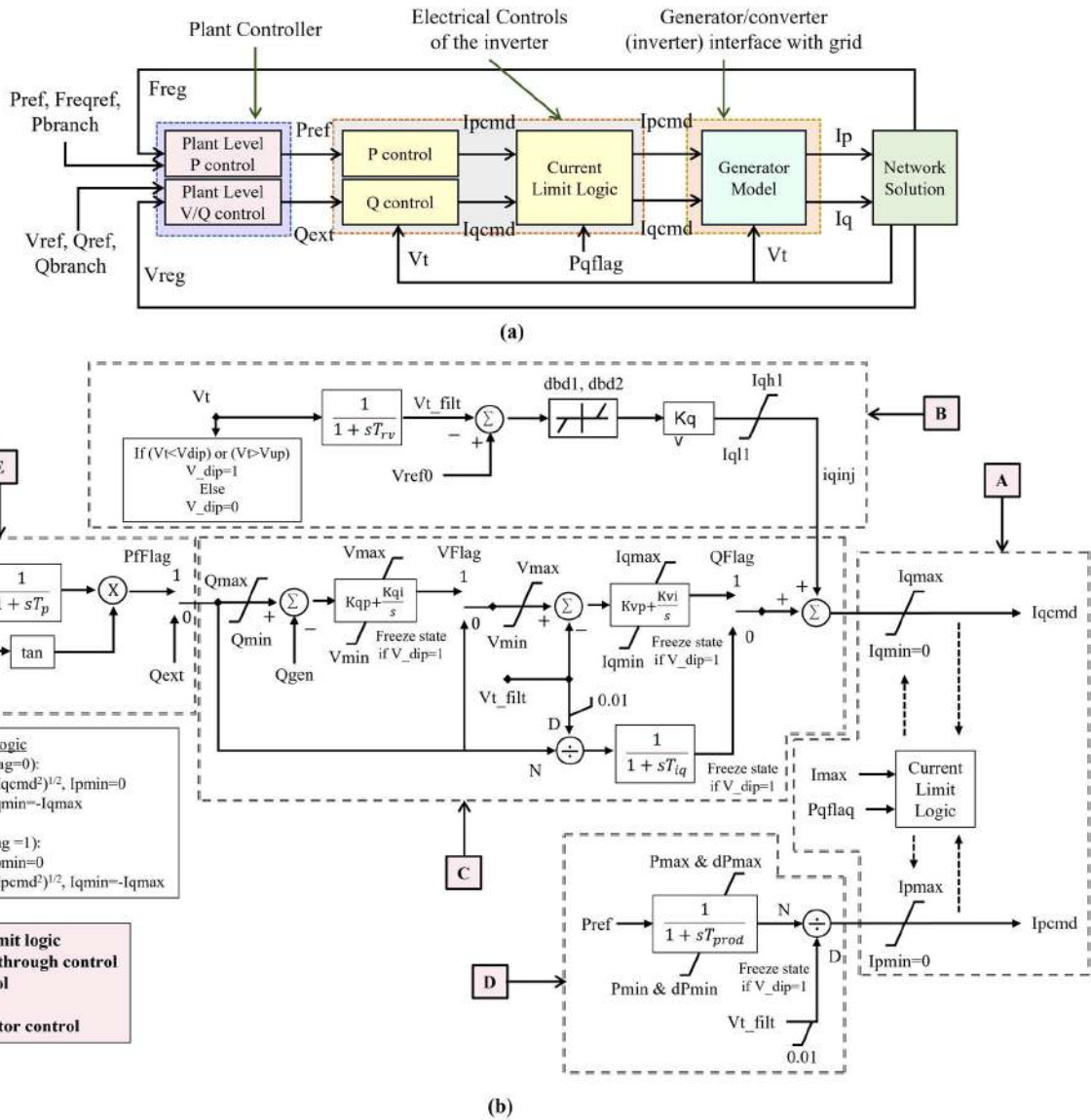


FIGURE 13. (a) The dynamic model of PV plant; (b) Electrical control model block diagram.

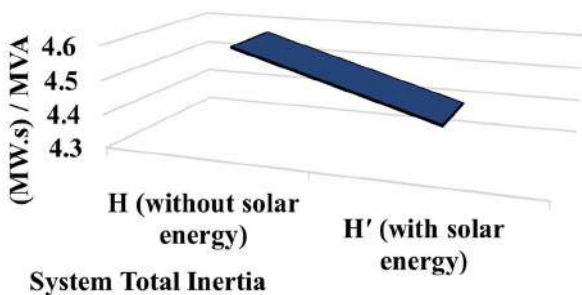


FIGURE 14. System inertia in presence and absence of solar energy penetration.

B. TEST RESULTS OF THE PROPOSED FRAMEWORK ON TEST POWER SYSTEM IN ABSENCE OF SE PENETRATION

In this section, the proposed scheme is employed on test system in absence of solar energy integrations. For this purpose, stepwise assessment on illustrative example I is showcased.

1) ILLUSTRATIVE EXAMPLE I: CASCADING EVENT SCENARIO

System loading: 101% of base case

Fault 1: Short Circuit near Bus 03

Fault 1 FAT=1s

Fault1 Cleared: FCT=1.2s by opening Line 03-18, and subsequently,

Fault 2: Line 02-25 Outage

Fault 2 FAT=1.25s

Example I is an illustration of cascaded events intended to comprehend the system response with and without the suggested unified methodology. Fig. 9 represents the generator(s) bus angles response to the consecutive faults. At 2 seconds, Generators G30 and G39 are clearly out-of-phase with the event 1 post-fault clearance and the simultaneous onset of event 2. This transient instability spreads to the remaining generators, and G33-G38 are out of synchronization during the following few cycles (about 2.6 seconds), the system

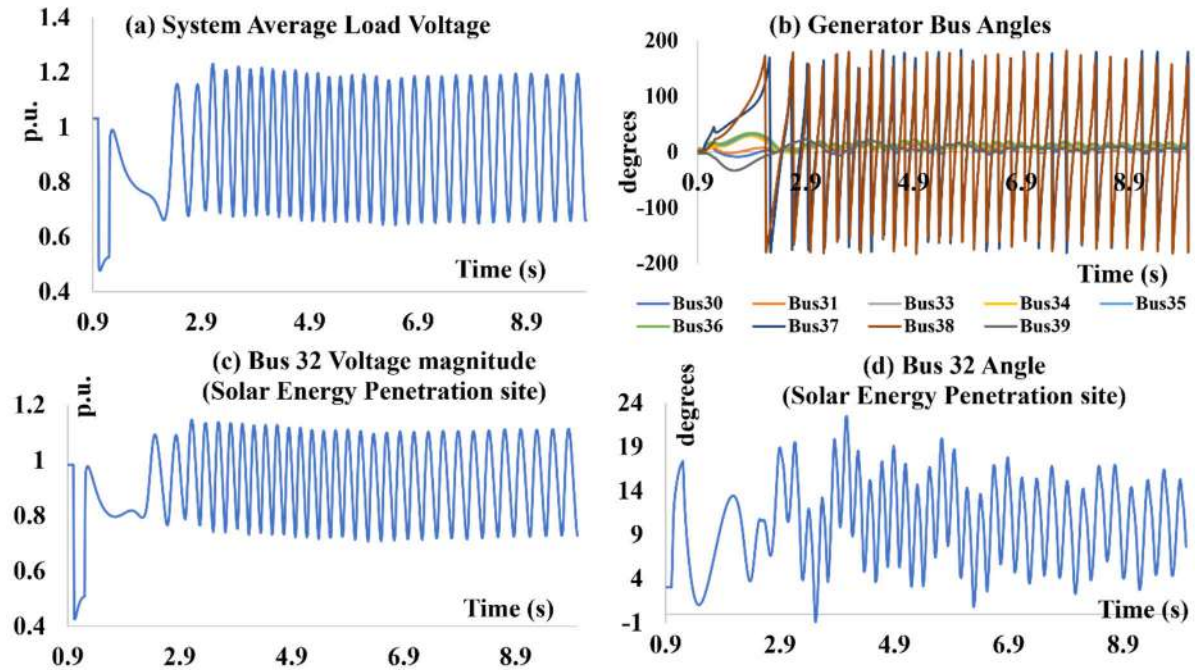


FIGURE 15. Illustrative Example II: without emergency remedial strategy.

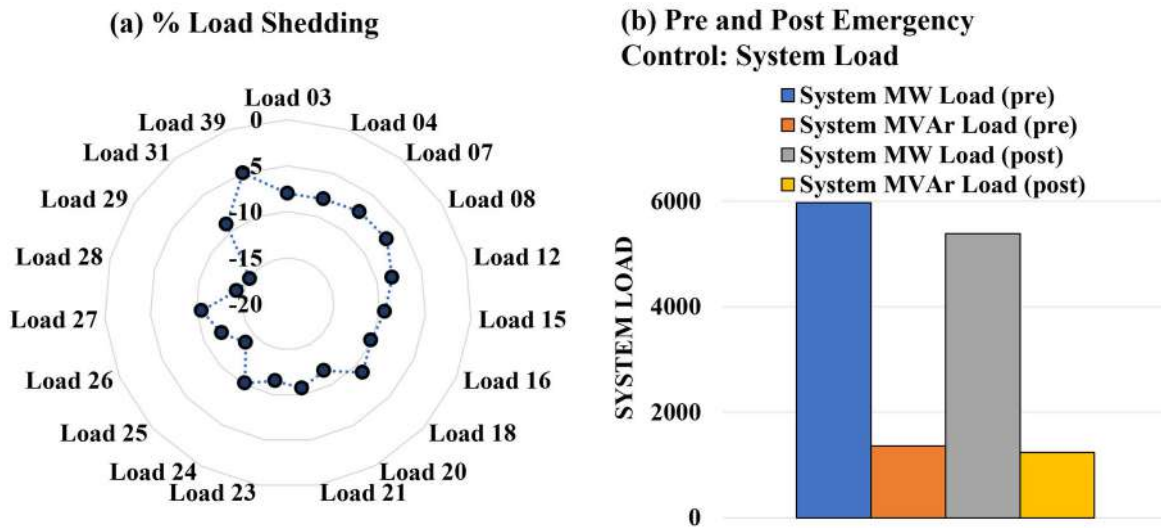


FIGURE 16. Illustrative Example II: load shedding.

collapses. To avert a blackout, it is critical to detect the instability early, formulate, and execute emergency steps. The PIE module is initiated to estimate the forthcoming instability scenario. The PIE module identifies the impending transient instability settings at 1.417 seconds, allowing approximately 0.6 seconds to schedule and deploy an emergency control strategy. The proposed TSA indicate that (1) the system is transiently unstable; (2) the time of control initiation; and (3) DAAC implementation is flagged. The proposed Emergency control strategy computes the action type, location, and magnitude tabulated in Table 4. The action type $AS^{(1)} \rightarrow AS^{(4)}$ that is generator rejection followed by load shedding is suggested with an appropriate magnitude of respective action. Due to

different delays associated with deploying the remedial control strategy, the actual time of initiating emergency control is delayed.

The emergency control strategy effectively avoids grid collapse even with a 3-cycle (0.05 s) time delay, as evident from Fig. 10. The figure showcases the system average load voltage profile, generator bus angles, and overall timeline of the complete procedure. At times, due to network congestion, the delay in deployment may be more. In this regard, the remedial solution is deployed with an additional delay of 3 cycles (a total of 6 cycle delay) as shown in Fig. 11. The figure elaborates: effect of delays in deployment for system average load voltage, generator bus angle against no control

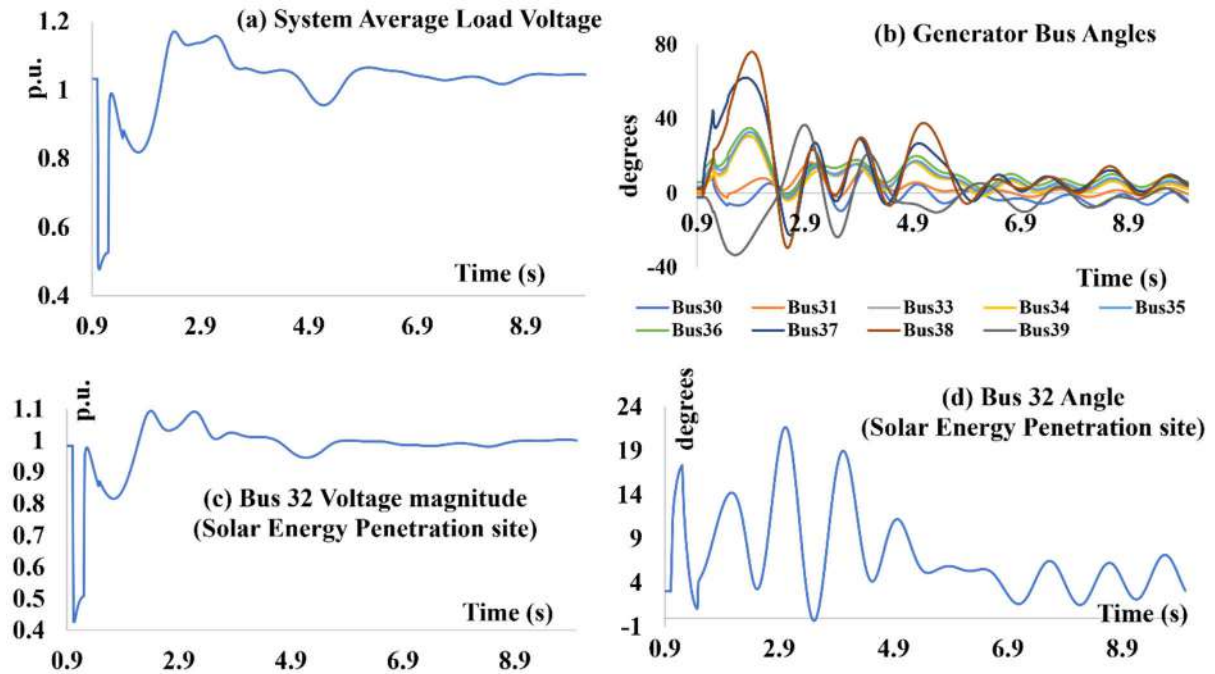


FIGURE 17. Illustrative Example II: with emergency remedial strategy.

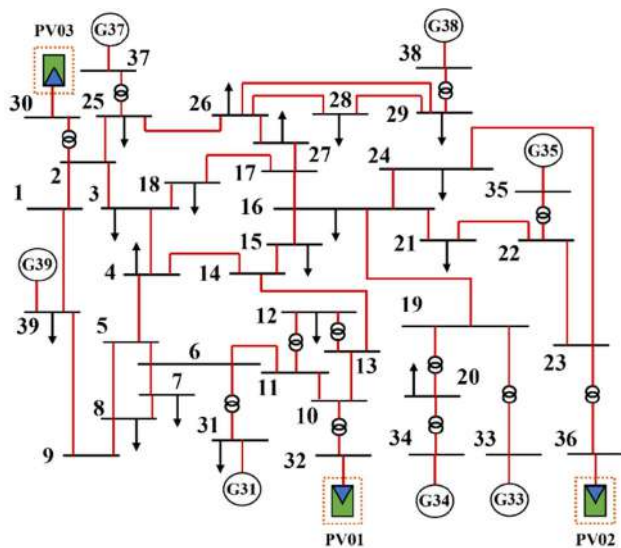


FIGURE 18. Modified new england 39 bus system with conventional generator replaced by solar farm at bus 30, bus 32, and bus 36.

application, and overall timeline for the proposed composite scheme for 6-cycle delayed deployment. The results highlight that there is no significant variation in system voltage profile and generator angle for an additional time delay. Evidently, the results validate the applicability of the proposed unified strategy to mitigate transient instability and avoid grid collapse even under a series of faults.

C. TEST RESULTS FOR SOLAR ENERGY INTEGRATED POWER SYSTEM (SINGLE LOCATION)

This section examines the applicability of the proposed method on the test system that has been modified by solar

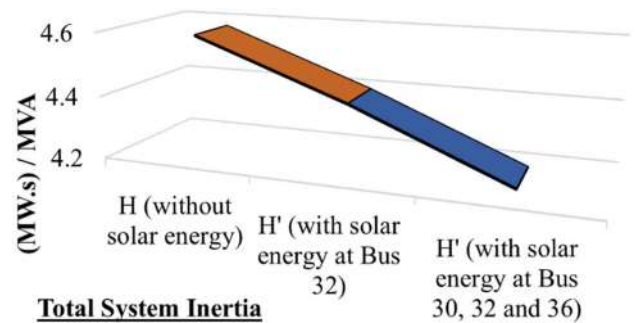


FIGURE 19. System inertia in absence and presence of solar energy penetration at single and multiple locations.

energy integration. Fig. 12 demonstrates the modified test system with a solar PV farm replacing a conventional generator at Bus 32. The 650 MW solar PV farm with 50 columns and 20 rows, adding 1000 PV units; each unit has a 720 kVA 0.9 pf inverter that generates 650 kW of electricity. The dynamic model of a solar PV plant utilized in the study consists of (a) a plant controller, (b) electrical controls, and (c) a grid interface module [30]. The Plant Controller utilizes voltage and reactive power output to imitate var/volt control and frequency and active power output to follow active power control at the plant level. The power output acts as a reference to the electric control model to give real and reactive current as output and terminal voltage and generated power as feedback. The real/reactive currents are utilized by the grid interface module to process and inject real/reactive current into the grid. The overall layout of the dynamic model is outlined in Fig. 13 (a). The faster active power recovery (fault ride through capability) of PV inverters indicates the response of PV inverter against voltage sags due to grid disturbances.

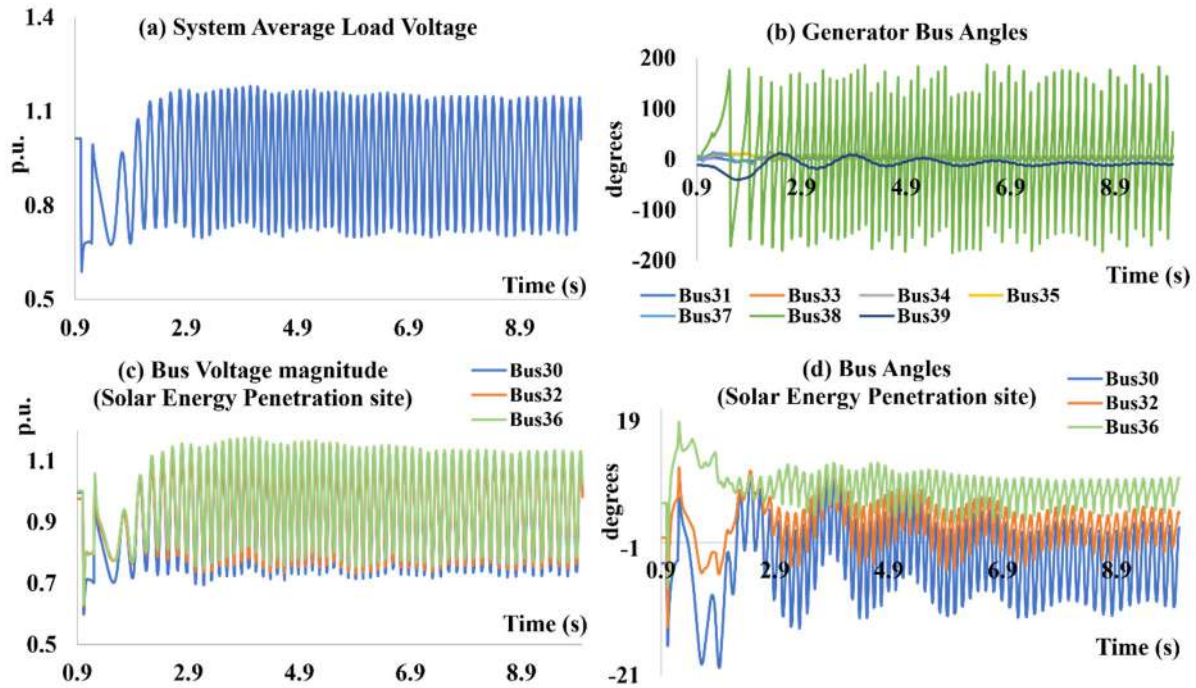


FIGURE 20. Illustrative Example III: without emergency remedial strategy.

TABLE 6. Emergency remedial scheme for illustrative example III.

Action Type and Location	Time (s)	Action Magnitude
TSA detection	1.3167	$\Delta P=682.049$ MW
Trip G 38	1.3667	Shed 830 MW Power Generation
Shed All Loads	1.4167	Shed proportionate % load illustrated in Figure 22(a) with total load shed equal to ΔP

In this condition, the inverter remains connected to the power grid and delivers the requisite amount of reactive current during the time of grid faults with zero real current injection. The control model as shown in Fig. 13 (b), which is considered in this work, enhances the active power recovery capability and other essential parameters, thus improving the fault ride through capability.

Following the solar energy integration, the system operates within permissible frequency settings of about 60 Hz nominal frequency ($f_{low}(norm) = 59.9$ Hz, $f_{high}(norm) = 60.1$ Hz) [26]. However, with solar energy penetration, the system inertia decreases, and it is highlighted in Fig. 14. The decreased inertia indicates a reduced time-margin to sustain system frequency within operating limits until control settings are initiated. The performance of the proposed strategy enabling real-time emergency control of modified test system is demonstrated with the following illustrative example.

1) ILLUSTRATIVE EXAMPLE II

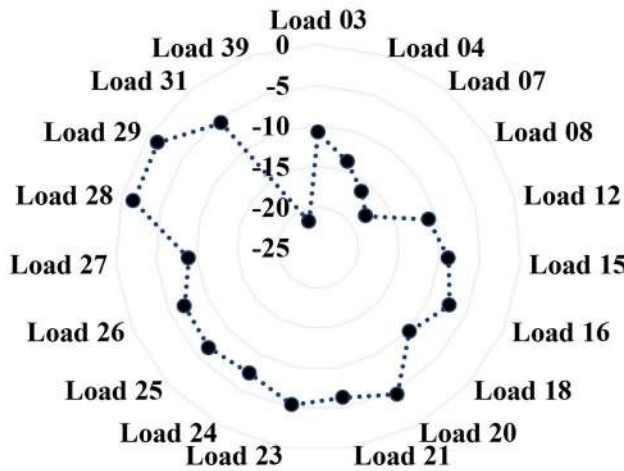
At System Loading 98% of base case and 10.72% solar energy penetration, Short Circuit fault occurred

near Bus 02, FAT=1s; Cleared by opening Line 02-25, FCT=1.2s.=

This scenario reflects a response of the SE penetrated test system when subjected to a disturbance as shown in Fig. 15. The figure also displays the Bus 32 (solar energy source) voltage magnitude and angle response for the considered disturbance. Subsequent to the fault clearance, within one second, G37 and G38 generators are out-of-step. The arisen instability is then propagated in whole system and can be visualized via the system load voltage profile. The proposed PIE assess the system to be unstable and time to initiate remedial strategy. The application of DAAC suggests load shedding equal to the estimated power imbalance in the system, viz. 600.334 MW. The recommendations of the strategy are tabulated in Table 5. The distribution of % load shedding among different loads is calculated and illustrated in Fig. 16 (a). Moreover, Fig. 16 (b) displays the total system load for pre and post deployment of strategy with active (MW) and quadrature (MVar) components. The application results in Fig. 17 showcase the successful implementation of the proposed method in controlling system stability and enhancing grid performance even in the presence of SE penetration. The post-emergency control system performance is shown via the average load profile, generator node angles, and solar penetration site voltage profile.

D. TEST RESULTS OF THE MULTIPLE LOCATIONS SOLAR ENERGY INTEGRATED POWER SYSTEM

The capability of the proposed composite scheme is further tested on the New England 39 bus test system modified with multiple solar plants replacing conventional generators at



(b) Pre and Post Emergency Control: System Load

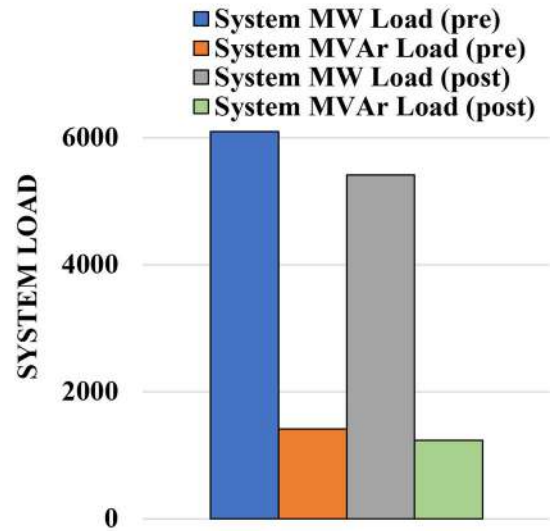


FIGURE 21. Illustrative Example III: load shedding post generation.

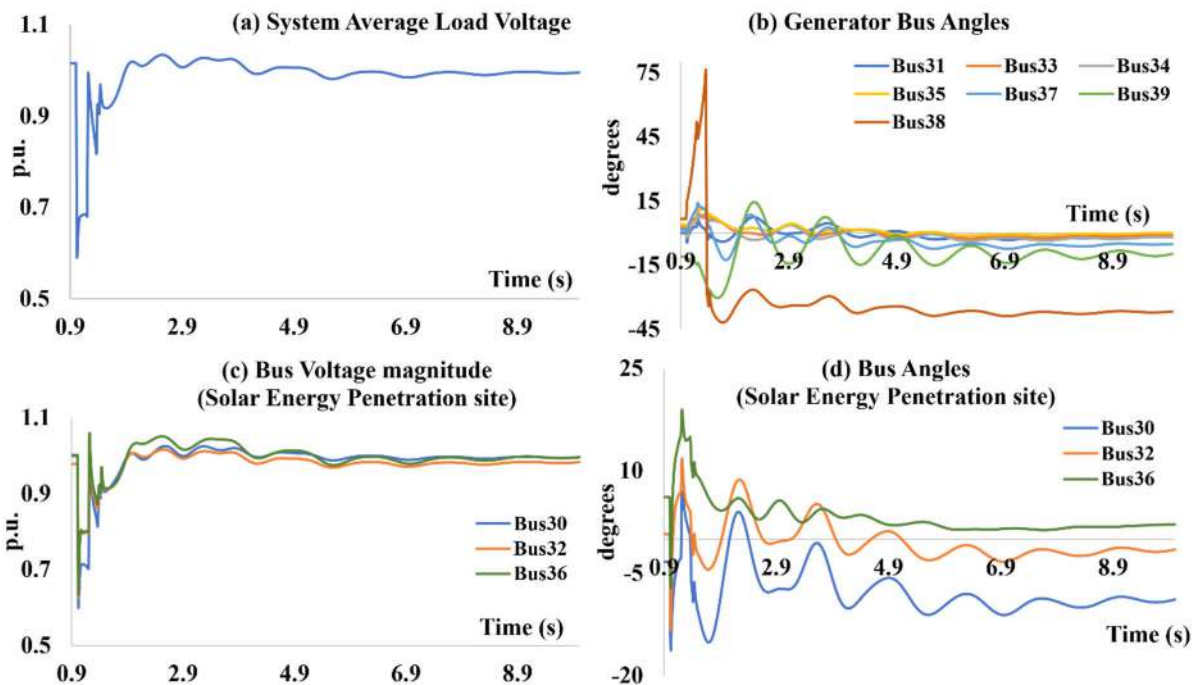


FIGURE 22. Illustrative Example III: with emergency remedial strategy.

Bus 30, Bus 32, and Bus 36, as shown in Fig. 18. A solar PV farm rated at 330 MVA is located at Bus 30, 660 MVA is located at Bus 32, and 550 MVA is located at Bus 36. However, the multiple solar energy penetration decreases system inertia further than that of single site penetration, as shown in Fig. 19. The proposed strategy enabling real-time emergency control of the modified test system with SE penetration at multiple buses is demonstrated with Illustrative Example III.

1) ILLUSTRATIVE EXAMPLE III

At 100% System Loading and 22.795 % solar energy penetration, Short Circuit fault occurred at Line 26-28, FAT=1s, Location= 50%; Cleared by opening Line 26-28, FCT=1.2s.

The example III demonstrates another effective application of the proposed scheme on increased solar energy integrated test system when subjected to a disturbance. The network response for ensuing event is shown in Fig. 20. Post-fault

TABLE 7. Performance comparison of proposed work.

Scheme	Solar Energy Penetration	Prompt Stability Evaluation		Type of Emergency Measures			Nature of Enhanced Grid Operation	Type of Execution
		%FA	%MA	GR	LSPGR	LS		
[17]	No	2.467	1.405	Generator Out	$\geq delP$	$\geq delP$	Transient Stability	Real-Time
[26]	~2.5 % (Single bus: 147 MW)	NA	NA	NA	NA	$delP$ (stepwise)	Frequency Stability	Online
[31]	No	NA	NA	Generator Out	NA	NA	Transient Stability	Real-Time
Proposed	~22.8% (Multiple bus: 1400 MW)	3.78	0	Generator Out	$delP$ (DRBI)	$delP$ (DRBI)	Transient Stability	Real-Time

FA: False alarm; MA: Missed alarm; GR: Generator rejection; LSPGR: load shedding post-generator rejection; LS: Load shedding; NA: Not available/applicable

clearance, with course of time, initially, generator G38 is most advanced against the rest of the system and is out-of-step by around 1.55 seconds. Subsequently, this instability is propagated to the rest of the system, and the grid collapses. It is therefore important to assess the impending instability state and apply remedial solutions to avert the grid failure. The prompt TSA assessment, post-assessment action type judgement, time of initiation, and action magnitude are tabulated in Table 6. As generator G38 is accelerating more than other generators and driving other machines to slow down more, it is appropriate to trip the generator. As G38 tripping adds to the power imbalance, load shedding corresponding to the estimated imbalance is necessary. Load Sharing Index estimates suggest an adequate magnitude of load shedding from all the loads essentially in proportion to the 682.049 MW power imbalance. The distribution of % load shedding among different loads is calculated and illustrated in Fig. 21 (a).

Moreover, Fig. 21 (b) displays the total system load for pre and post deployment of a strategy with active (MW) and quadrature (MVar) components. A delay of 3 cycle in generator trip and 3 cycle delay (total 6 cycle) in subsequent load shedding are considered to allow different associated delays. The application results in Fig. 22 showcase the successful implementation of the proposed methodology in controlling system stability and enhancing the grid performance even in the presence of SE penetration at multiple locations. The post-emergency control system performance is shown via the average load profile, generator node angles, and solar penetration site voltage profile.

E. COMPARATIVE ASSESSMENT OF THE PROPOSED FRAMEWORK

The performance of the proposed method has been further validated through a comparison with the present state of the art. Investigations on the transient stability assessment and effective deployment of emergency control mechanisms for these solar energy integrated systems is relatively rare. Therefore, we have considered following references [17], [26] and [31] for the comparisons which empirically contributes similar to that of this article. Table 7 showcases the superiority of the proposed scheme with respect to consid-

ered references. The attributes considered for the evaluation are: (1) solar energy penetration in the grid, (2) false and missed alarms of real-time stability assessment, (3) types of emergency measures and their magnitude, (4) nature of enhanced grid operation and (5) type of execution. Evidently, the proposed scheme flags prompt TSA assessment with zero missed alarms, very few false alarms, computes the action type, location, and magnitude of emergency strategy in real time with minimum computation burden. Additionally, the presented method is suitable for both the power systems: conventional grids and grids with solar energy penetration at single and multiple buses.

V. CONCLUSION

In the scenario of increased power demand, the grid operators are poised to increase renewable energy penetration. The increased generation combination impels the centralized control centers to effectively monitor and perform vulnerability assessment. Grid control centers are required to identify and implement the intended emergency control measures and improve grid sustainability based on the assessments. Essentially, these measures are required to be insensitive to renewable energy generation in the grid. In view of it following contributions has been accomplished in this article:

1. A unified approach that ensures system synchronism in a solar integrated power network by first assessing the imminent susceptibility, then preparing and deploying the emergency scheme is presented effectively.
2. To determine when corrective action should be taken and to evaluate the impending transient instability of the system in the presence of SE, the EWMA treated short-moving synchronized data window of power generated from the sources is employed.
3. A DAAC based emergency corrective technique is implemented to maintain the system’s transient stability and improve grid performance in real-time. The DAAC utilizes DRBI to assess the action set comprising of action type, location, and magnitude of actions.

The scheme is tested on New England 39 Bus test system in the absence and presence of SE. The expediency of the unified strategy in enhancing grid performance even in the presence of single and multiple solar energy farms

is highlighted. A comparative performance of the proposed work with the available state-of-art establishes the utility of the projected scheme.

ACKNOWLEDGMENT

The authors extend their appreciation to the Researchers Supporting Project at King Saud University, Riyadh, Saudi Arabia, for funding this research work through the project number RSP2023R278. The authors would like to acknowledge the technical support from Intelligent Prognostic Private Ltd., Delhi, India, researcher's supporting Project for this research work. The authors would like to acknowledge the technical support from Ingenium Research Group, Universidad Castilla-La Mancha, Ciudad Real, Spain. They would also like to thank the Power System Laboratory, Electrical Engineering Department, Manipal University, Jaipur, for giving them the opportunity to utilize the software facility.

REFERENCES

- [1] M. Kezunovic, J. D. McCalley, and T. J. Overbye, "Smart grids and beyond: Achieving the full potential of electricity systems," *Proc. IEEE*, vol. 100, no. Special Centennial Issue, pp. 1329–1341, May 2012, doi: [10.1109/JPROC.2012.2187131](https://doi.org/10.1109/JPROC.2012.2187131).
- [2] M. Begovic, D. Novosel, D. Karlsson, C. Henville, and G. Michel, "Wide-area protection and emergency control," *Proc. IEEE*, vol. 93, no. 5, pp. 876–891, May 2005, doi: [10.1109/JPROC.2005.847258](https://doi.org/10.1109/JPROC.2005.847258).
- [3] P. Tielens and D. Van Hertem, "The relevance of inertia in power systems," *Renew. Sustain. Energy Rev.*, vol. 55, pp. 999–1009, Mar. 2016, doi: [10.1016/j.rser.2015.11.016](https://doi.org/10.1016/j.rser.2015.11.016).
- [4] S. M. Mazhari, B. Khorramdel, C. Y. Chung, I. Kamwa, and D. Novosel, "A simulation-based classification approach for online prediction of generator dynamic behavior under multiple large disturbances," *IEEE Trans. Power Syst.*, vol. 36, no. 2, pp. 1217–1228, Mar. 2021, doi: [10.1109/TPWRS.2020.3021137](https://doi.org/10.1109/TPWRS.2020.3021137).
- [5] D. R. Shrivastava, S. A. Siddiqui, and K. Verma, "Model free robust real-time severity analyser using PMU measurements," *Int. J. Electr. Power Energy Syst.*, vol. 133, Dec. 2021, Art. no. 107333, doi: [10.1016/j.ijepes.2021.107333](https://doi.org/10.1016/j.ijepes.2021.107333).
- [6] A. Sajadi, R. Preece, and J. Milanovic, "Identification of transient stability boundaries for power systems with multidimensional uncertainties using index-specific parametric space," *Int. J. Electr. Power Energy Syst.*, vol. 123, Dec. 2020, Art. no. 106152, doi: [10.1016/j.ijepes.2020.106152](https://doi.org/10.1016/j.ijepes.2020.106152).
- [7] X. Liu, Y. Min, L. Chen, X. Zhang, and C. Feng, "Data-driven transient stability assessment based on kernel regression and distance metric learning," *J. Modern Power Syst. Clean Energy*, vol. 9, no. 1, pp. 27–36, Jan. 2021, doi: [10.35833/MPCE.2019.000581](https://doi.org/10.35833/MPCE.2019.000581).
- [8] Y. J. Isbeih, M. S. El Moursi, W. Xiao, and E. El-Saadany, "Generator-based threshold for transient stability assessment," *IET Smart Grid*, vol. 2, no. 3, pp. 407–419, Sep. 2019, doi: [10.1049/iet-stg.2018.0292](https://doi.org/10.1049/iet-stg.2018.0292).
- [9] H. Cui, Q. Wang, Y. Ye, Y. Tang, and Z. Lin, "A combinatorial transfer learning framework for online transient stability prediction," *Sustain. Energy, Grids Netw.*, vol. 30, Jun. 2022, Art. no. 100674, doi: [10.1016/j.segan.2022.100674](https://doi.org/10.1016/j.segan.2022.100674).
- [10] H. Wang and S. Wu, "Transient stability assessment with time-adaptive method based on spatial distribution," *Int. J. Electr. Power Energy Syst.*, vol. 143, Dec. 2022, Art. no. 108464, doi: [10.1016/j.ijepes.2022.108464](https://doi.org/10.1016/j.ijepes.2022.108464).
- [11] G. Wang, J. Guo, S. Ma, X. Zhang, Q. Guo, S. Fan, and H. Xu, "Data-driven transient stability assessment with sparse PMU sampling and online self-check function," *CSEE J. Power Energy Syst.*, vol. 9, no. 3, pp. 910–920, May 2022, doi: [10.17775/CSEEJPES.2021.05890](https://doi.org/10.17775/CSEEJPES.2021.05890).
- [12] B. Li and J. Wu, "Adaptive assessment of power system transient stability based on active transfer learning with deep belief network," *IEEE Trans. Autom. Sci. Eng.*, vol. 20, no. 2, pp. 1047–1058, Apr. 2023, doi: [10.1109/TASE.2022.3181029](https://doi.org/10.1109/TASE.2022.3181029).
- [13] S. Wu, L. Zheng, W. Hu, R. Yu, and B. Liu, "Improved deep belief network and model interpretation method for power system transient stability assessment," *J. Modern Power Syst. Clean Energy*, vol. 8, no. 1, pp. 27–37, Jan. 2020, doi: [10.35833/MPCE.2019.000058](https://doi.org/10.35833/MPCE.2019.000058).
- [14] Y. Liu, J. Wang, and Z. Yue, "Improved multi-point estimation method based probabilistic transient stability assessment for power system with wind power," *Int. J. Electr. Power Energy Syst.*, vol. 142, Nov. 2022, Art. no. 108283, doi: [10.1016/j.ijepes.2022.108283](https://doi.org/10.1016/j.ijepes.2022.108283).
- [15] M. Q. Ahsan, A. H. Chowdhury, S. S. Ahmed, I. H. Bhuyan, M. A. Haque, and H. Rahman, "Technique to develop auto load shedding and islanding scheme to prevent power system blackout," *IEEE Trans. Power Syst.*, vol. 27, no. 1, pp. 198–205, Feb. 2012, doi: [10.1109/TPWRS.2011.2158594](https://doi.org/10.1109/TPWRS.2011.2158594).
- [16] M. A. Kabir, A. H. Chowdhury, and N. A. Masood, "A dynamic-adaptive load shedding methodology to improve frequency resilience of power systems," *Int. J. Electr. Power Energy Syst.*, vol. 122, Nov. 2020, Art. no. 106169, doi: [10.1016/j.ijepes.2020.106169](https://doi.org/10.1016/j.ijepes.2020.106169).
- [17] S. A. Siddiqui, K. Verma, K. R. Niazi, and M. Fozdar, "A unified control scheme for power system transient stability enhancement through preventive and emergency control," *Int. Trans. Electr. Energy Syst.*, vol. 26, no. 2, pp. 365–383, Feb. 2016, doi: [10.1002/etep.2086](https://doi.org/10.1002/etep.2086).
- [18] T. Shekari, A. Gholami, F. Aminifar, and M. Sanaye-Pasand, "An adaptive wide-area load shedding scheme incorporating power system real-time limitations," *IEEE Syst. J.*, vol. 12, no. 1, pp. 759–767, Mar. 2018, doi: [10.1109/JSYST.2016.2535170](https://doi.org/10.1109/JSYST.2016.2535170).
- [19] J. Tang, J. Liu, F. Ponci, and A. Monti, "Adaptive load shedding based on combined frequency and voltage stability assessment using synchrophasor measurements," *IEEE Trans. Power Syst.*, vol. 28, no. 2, pp. 2035–2047, May 2013, doi: [10.1109/TPWRS.2013.2241794](https://doi.org/10.1109/TPWRS.2013.2241794).
- [20] D. S. Kumar, A. Sharma, D. Srinivasan, and T. Reindl, "Stability implications of bulk power networks with large scale PVs," *Energy*, vol. 187, Nov. 2019, Art. no. 115927, doi: [10.1016/j.energy.2019.115927](https://doi.org/10.1016/j.energy.2019.115927).
- [21] B. B. Adetokun, J. O. Ojo, and C. M. Muriithi, "Application of large-scale grid-connected solar photovoltaic system for voltage stability improvement of weak national grids," *Sci. Rep.*, vol. 11, no. 1, Dec. 2021, Art. no. 24526, doi: [10.1038/s41598-021-04300-w](https://doi.org/10.1038/s41598-021-04300-w).
- [22] S. R. Paital, P. K. Ray, A. Mohanty, and S. Dash, "Stability improvement in solar PV integrated power system using quasi-differential search optimized SVC controller," *Optik*, vol. 170, pp. 420–430, Oct. 2018, doi: [10.1016/j.ijleo.2018.05.097](https://doi.org/10.1016/j.ijleo.2018.05.097).
- [23] R. G. Wandhare and V. Agarwal, "Novel stability enhancing control strategy for centralized PV-grid systems for smart grid applications," *IEEE Trans. Smart Grid*, vol. 5, no. 3, pp. 1389–1396, May 2014, doi: [10.1109/TSG.2013.2279605](https://doi.org/10.1109/TSG.2013.2279605).
- [24] M. K. Hossain and M. H. Ali, "Transient stability augmentation of PV/DFIG/SG-based hybrid power system by parallel-resonance bridge fault current limiter," *Electr. Power Syst. Res.*, vol. 130, pp. 89–102, Jan. 2016, doi: [10.1016/j.epr.2015.08.016](https://doi.org/10.1016/j.epr.2015.08.016).
- [25] A. Jawad, S. A. Naim, C. Saha, and N.-A. Masood, "Frequency stability enhancement of a large-scale PV integrated grid," in *Proc. 11th Int. Conf. Electr. Comput. Eng. (ICECE)*, Dec. 2020, pp. 290–293.
- [26] A. Chandra and A. K. Pradhan, "An adaptive underfrequency load shedding scheme in the presence of solar photovoltaic plants," *IEEE Syst. J.*, vol. 15, no. 1, pp. 1235–1244, Mar. 2021, doi: [10.1109/JSYST.2020.2995050](https://doi.org/10.1109/JSYST.2020.2995050).
- [27] S.-Y. Kuo and Y.-H. Chou, "Building intelligent moving average-based stock trading system using metaheuristic algorithms," *IEEE Access*, vol. 9, pp. 140383–140396, 2021, doi: [10.1109/ACCESS.2021.3119041](https://doi.org/10.1109/ACCESS.2021.3119041).
- [28] M. B. Perry, "The exponentially weighted moving average," in *Wiley Encyclopedia of Operations Research and Management Science*. Hoboken, NJ, USA: Wiley, 2011, doi: [10.1002/9780470400531.eorms0314](https://doi.org/10.1002/9780470400531.eorms0314).
- [29] P. Bhui and N. Senroy, "Real-time prediction and control of transient stability using transient energy function," *IEEE Trans. Power Syst.*, vol. 32, no. 2, pp. 923–934, Mar. 2017, doi: [10.1109/TPWRS.2016.2564444](https://doi.org/10.1109/TPWRS.2016.2564444).
- [30] G. Lammert, L. D. P. Ospina, P. Pourbeik, D. Fetzer, and M. Braun, "Implementation and validation of WECC generic photovoltaic system models in DlgSILENT PowerFactory," in *Proc. IEEE Power Energy Soc. Gen. Meeting (PESGM)*, Jul. 2016, pp. 1–5.
- [31] Y. Zhang, M. Pavella, and L. Wehenkel, "A method for real-time transient stability emergency control," *IFAC Proc. Volumes*, vol. vol., 30, no. 17, pp. 633–638, 1997, doi: [10.1016/S1474-6670\(17\)46476-7](https://doi.org/10.1016/S1474-6670(17)46476-7).

•••

Significance of Chemical Reaction Under the Influence of Joule Heating for Walters' B Fluid Flow towards an Extending Sheet

Original Paper Published: 02 December 2023

Volume 9, article number 154, (2023) Cite this article



International Journal of Applied and Computational Mathematics

[Aims and scope](#)

[Submit manuscript](#)


[Pooja Soni](#), [Kalpna Sharma](#) , [Hamza Berrehal](#) & [Kavita Jat](#)

 83 Accesses  1 Citation [Explore all metrics](#) →

Abstract

In this present work, the flow of hydromagnetic viscous Walters' B fluid towards a vertical extending sheet under the consequence of joule heating, chemical reaction, and convective boundary condition is investigated. Initially, the mathematical modeling is constructed, and then the PDEs are changed into the non-linear ODEs with the use of appropriate similarity transformation, and then by using the Optimal-Auxiliary-Functions-Method (OAFM), the system of non-linear ODEs has been solved. By using graphs and tables the behaviors of all the different parameters are described. The graphs show that by increasing Eckart number and Biot number, the temperature profile also increases. On the other hand, by increasing the Soret number, we see that the

concentration profile increases, while the opposite impact is shown for higher values of the chemical reaction parameter. The local Sherwood number, Nusselt number, and coefficient of skin friction are identified. Higher thermal buoyancy effect values indicate more serious cooling problems, which are typically encountered in engineering fields and in the manufacturing sector for the cooling of systems or electronic parts. The problem investigated here is important and frequently occurs in a variety of real-world contexts, including the polymer extrusion process. Additionally, it is used in processes such as tinning of copper wires, annealing, drawing, heat-treated materials moving on conveyer belts, manufacture of plastic films, artificial fibers, paper production, crystal growth, and other similar ones.

i This is a preview of subscription content, [log in via an institution](#)  to check access.

Access this article

Log in via an institution

Buy article PDF 39,95 €

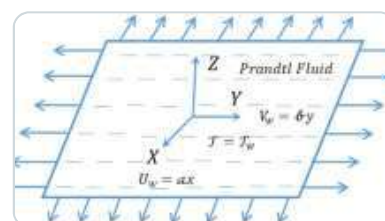
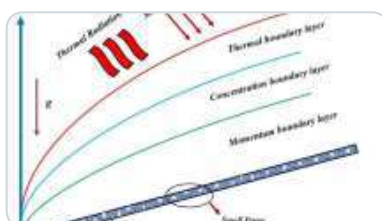
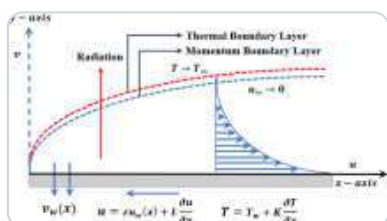
Price includes VAT (India)

Instant access to the full article PDF.

Rent this article via [DeepDyve](#) 

[Institutional subscriptions](#) →

Similar content being viewed by others



Cattaneo-Christov and Darcy-Forchheimer heat flux on Reiner-Philippoff fluid with...

Article | 23 August 2024

Energy transfer through third-grade fluid flow across an inclined stretching sheet subje...

Article | Open access
10 November 2023

Investigation of heat generation and radiation effects on boundary layer flow o...

Article | Open access
24 October 2024

Availability of Data and Material

The data that support the findings of this study are available from the corresponding author upon request.

Code Availability

OAFM by using the Maple software.

Abbreviations

u, v : Velocity components (m s^{-1})

x, y : Space coordinats (m)

(ϑ) : Kinematic viscosity ($\text{m}^2 \text{s}^{-1}$)

k_0 : Elastic parameter

(σ) : Electrical conductivity (s m^{-1})

K : Permeability of porous medium (m^2)

g : Acceleration due to gravity (m s^{-2})

T: Fluid temperature (K)

C: Fluid concentration (m kg^{-3})

β_T : Thermal expansion coefficient ($1/\text{K}$)

β_c : Concentration expansion coefficient ($\text{m}^3 \text{kg}^{-1}$)

k: Thermal conductivity ($\text{W m}^{-1} \text{K}^{-1}$)

α : Thermal diffusivity ($\text{m}^2 \text{s}^{-1}$)

C_p: Specific heat capacity at constant pressure ($\text{J kg}^{-1} \text{K}^{-1}$)

Q₀: Volumetric heat generation/absorption rate (J)

D_m: Mass diffusivity ($\text{m}^2 \text{s}^{-1}$)

T_m: Mean fluid temperature (K)

k_c: Reaction rate coefficient (mol/s m^3)

K_T: Thermal diffusion ratio

h₁: Heat transfer coefficient (W K/m^2)

ρ : Density (Kg m^{-3})

Mn: Magnetic Field parameter

Ps: Porosity parameter

A: Ratio rate

We: Weissenberg number

λ_T : Thermal Buoyancy parameter

λ_m : Mass Buoyancy parameter

Gr_x : Thermal Grashof number

Gc_x : Solutal Grashof number

Re_x : Reynolds number

Pr : Prandtl number

Sc : Schmidt number

Sr : Soret number

Ra : Radiation parameter

Q : Internal heat generation/absorption (W/m^3)

Ec : Eckart number

Bi : Biot number

q_r : Radiation heat flux (W/m^2)

$(\{\sigma\}^{\{*\}})$: Stefan-Boltzmann constant ($W m^{-2} K^{-4}$)

R : Chemical reaction parameter

References

1. Forrest, G., Wilkinson, W.L.: Laminar heat transfer to temperature-dependent Bingham fluids in tubes. *Int. J. Heat Mass Transf.* **16**(12), 2377–2391 (1973)

[Article](#) [Google Scholar](#)

2. Mahapatra, T.R., Gupta, A.S.: Magnetohydrodynamic stagnation-point flow towards a stretching sheet. *Acta Mech.* **152**(1), 191–196 (2001)

[Article](#) [Google Scholar](#)

3. Bhattacharyya, S., Pal, A., Gupta, A.S.: Heat transfer in the flow of a viscoelastic fluid over a stretching surface. *Heat Mass Transf.* **34**(1), 41–45 (1998)

[Article](#) [Google Scholar](#)

4. Gholinia, M., Hoseini, M.E., Gholinia, S.: A numerical investigation of free convection MHD flow of Walters-B nanofluid over an inclined stretching sheet under the impact of Joule heating. *Therm. Sci. Eng. Prog.* **11**, 272–282 (2019)

[Article](#) [Google Scholar](#)

5. Akinbo, B.J., Olajuwon, B.I.: Impact of radiation and chemical reaction on stagnation-point flow of Hydromagnetic Walters' B fluid with Newtonian heating. *Int. Commun. Heat Mass Transfer* **121**, 105115 (2021)

[Article](#) [Google Scholar](#)

6. Qaiser, D., Zheng, Z., Khan, M.R.: Numerical assessment of mixed convection flow of Walters-B nanofluid over a stretching surface with Newtonian heating and mass transfer. *Therm. Sci. Eng. Prog.* **22**, 100801 (2021)

[Article](#) [Google Scholar](#)

7. Akinbo, B.J., Olajuwon, B.I.: Stagnation-point flow of a Walters' B fluid towards a vertical stretching surface embedded in a porous medium with elastic-deformation and chemical reaction. *J. Heat Mass Transf. Res.* **9**(1), 27–38 (2022)

[Google Scholar](#)

8. Mahapatra, T., Gupta, A.S.: Heat transfer in stagnation-point flow towards a stretching sheet. *Heat Mass Transf.* **38**(6), 517–521 (2002)

[Article](#) [Google Scholar](#)

9. Hayat, T., Asad, S., Mustafa, M., Alsulami, H.H.: Heat transfer analysis in the flow of Walters' B fluid with a convective boundary condition. *Chin. Phys. B* **23**(8), 084701 (2014)

[Article](#) [Google Scholar](#)

10. Gautam, A.K., Rajput, S., Bhattacharyya, K., Verma, A.K., Arif, M.G., Chamkha, A.J.: Existence of multiple solutions for magnetohydrodynamic flows of second-grade and Walter's B fluids due continuously contracting flat sheet with partial slip. *Partial Differ. Equ. Appl. Math.* **6**, 100434 (2022)

[Article](#) [Google Scholar](#)

11. Mahat, R., Saqib, M., Khan, I., Shafie, S., Noor, N.A.M.: Thermal radiation effect on Viscoelastic Walters'-B nanofluid flow through a circular cylinder in convective and constant heat flux. *Case Stud. Therm. Eng.* **39**, 102394 (2022)

[Article](#) [Google Scholar](#)

12. Khan, M.I., Qayyum, S., Hayat, T., Khan, M.I., Alsaedi, A.: Entropy optimization in flow of Williamson nanofluid in the presence of chemical reaction and Joule heating. *Int. J. Heat Mass Transf.* **133**, 959–967 (2019)

13. Swain, K., Animasaun, I.L., Ibrahim, S.M.: Influence of exponential space-based heat source and Joule heating on nanofluid flow over an elongating/shrinking sheet with an inclined magnetic field. *Int. J. Ambient Energy* **43**(1), 4045–4057 (2022)

14. Hafeez, A., Khan, M., Ahmed, A., Ahmed, J.: Features of Cattaneo–Christov double diffusion theory on the flow of non-Newtonian Oldroyd–B nanofluid with Joule heating. *Appl. Nanosci.* **12**(3), 265–272 (2022)

15. Reddy, M. G., Krishnamurthy, M. R., Praveena, M. M., Naik, L. S., Prakasha, D. G., & Ganesh Kumar, K. (2022). Unsteady absorption flow and dissipation heat transfer over a non-Newtonian fluid. *Waves in Random and Complex Media*, 1–15.

16. Rehman, K.U., Khan, A.A., Malik, M.Y., Pradhan, R.K.: Combined effects of Joule heating and chemical reaction on non-Newtonian fluid in double stratified medium: a numerical study. *Results Phys.* **7**, 3487–3496 (2017)

17. Shafiq, A., Hammouch, Z., Turab, A.: Impact of radiation in a stagnation point flow of Walters' B fluid towards a Riga plate. *Therm. Sci. Eng. Prog.* **6**, 27–33 (2018)

18. Waqas, H., Alghamdi, M., Muhammad, T., Khan, M.A.: Bioconvection transport of magnetized Walter's B nanofluid across a cylindrical disk with nonlinear radiative heat transfer. *Case Stud. Therm. Eng.* **26**, 101097 (2021)

19. Nadeem, S., Mehmood, R., Motsa, S.S.: Numerical investigation on MHD oblique flow of Walter's B type nano fluid over a convective surface. *Int. J. Therm. Sci.* **92**, 162–172 (2015)

20. Shah, I.A., Bilal, S., Akgül, A., Tekin, M.T., Botmart, T., Zahran, H.Y., Yahia, I.S.: On analysis of magnetized viscous fluid flow in permeable channel with single wall carbon nano tubes dispersion by executing nano-layer approach. *Alex. Eng. J.* **61**(12), 11737–11751 (2022)

21. Jat, K., Sharma, K.: Unsteady MHD flow of tangent hyperbolic nanofluid over an inclined stretching sheet and heat transfer analysis. *NanoWorld J* **8**(S1), S104–S110 (2022)

22. Bilal, S., Ullah, A., Shah, I.A., Asjad, M.I., Almusawa, M.Y., Eldin, S.M.: Analysis of free and forced convections in the flow of radiative viscous fluid with oxytactic microorganisms. *Front. Mater.* **10**, 1138313 (2023)

23. Bilal, S., Shah, I.A.: A comprehensive physical insight about thermo physical aspects of Carreau fluid flow over a rotated disk of variable thickness by implementing finite difference approach. *Propuls. Power Res.* **11**(1), 143–153 (2022)

24. Akinbo, B.J., Olajuwon, B.I.: Radiation and thermal-diffusion interaction on stagnation-point flow of Walters' B fluid toward a vertical stretching sheet. *Int. Commun. Heat Mass Transfer* **126**, 105471 (2021)

[Article](#) [Google Scholar](#)

25. Akinbo, B.J.: Influence of convective boundary condition on heat and mass transfer in a Walters' B fluid over a vertical stretching surface with thermal-diffusion effect. *J. Therm. Eng.* **7**(7), 1784–1796 (2021)

[Google Scholar](#)

26. Marinca, V., Herisanu, N.: Optimal auxiliary functions method for a pendulum wrapping on two cylinders. *Mathematics* **8**(8), 1364 (2020)

[Article](#) [Google Scholar](#)

27. Herisanu, N., Marinca, V.: An efficient analytical approach to investigate the dynamics of a misaligned multirotor system. *Mathematics* **8**(7), 1083 (2020)

[Article](#) [Google Scholar](#)

28. Bilal, S., Shah, I.A., Akgül, A., Tekin, M.T., Botmart, T., Yahia, I.S.: A comprehensive mathematical structuring of magnetically effected Sutterby fluid flow immersed in dually stratified medium under boundary layer approximations over a linearly stretched surface. *Alex. Eng. J.* **61**(12), 11889–11898 (2022)

[Article](#) [Google Scholar](#)

29. Bilal, S., Shah, I.A., Ramzan, M., Nisar, K.S., Elfasakhany, A., Eed, E.M., Ghazwani, H.A.S.: Significance of induced hybridized metallic and non-metallic nanoparticles in single-phase nano liquid flow between permeable disks by analyzing shape factor. *Sci. Rep.* **12**(1), 3342 (2022)

Funding

There is no financial support for this work.

Author information

Authors and Affiliations

Department of Mathematics & Statistics, Manipal University Jaipur, Jaipur, Rajasthan, India

Pooja Soni, Kalpna Sharma & Kavita Jat

Department of Physics, Exact Sciences Faculty, Constantine 1 University, 25000, Constantine, Algeria

Hamza Berrehal

Contributions

Conceptualization, PS; KS; Methodology, KS; PS and HB; Formal analysis, HB; Investigation, KJ and KS; Resources, KS; Data curation, PS and HB; Writing—original draft, PS; Writing—review and editing, KS and PS; Supervision, HB; KS. All authors have read and agreed to the published version of the manuscript.

Corresponding author

Correspondence to [Kalpna Sharma](#).

Ethics declarations

Conflict of interest

The authors have no conflicts to disclose.

Additional information

Publisher's Note

Springer Nature remains neutral with regard to jurisdictional claims in published maps and institutional affiliations.

Rights and permissions

Springer Nature or its licensor (e.g. a society or other partner) holds exclusive rights to this article under a publishing agreement with the author(s) or other rightsholder(s); author self-archiving of the accepted manuscript version of this article is solely governed by the terms of such publishing agreement and applicable law.

[Reprints and permissions](#)

About this article

Cite this article

Soni, P., Sharma, K., Berrehal, H. *et al.* Significance of Chemical Reaction Under the Influence of Joule Heating for Walters' B Fluid Flow towards an Extending Sheet. *Int. J. Appl. Comput. Math* **9**, 154 (2023). <https://doi.org/10.1007/s40819-023-01633-0>

Accepted

26 October 2023

Published

02 December 2023

DOI

<https://doi.org/10.1007/s40819-023-01633-0>

Keywords

[Joule heating](#)

[Weissenberg number](#)

[Similarity variables](#)

[Convection](#)

[Chemical reaction](#)

[OAFM](#)

Gronwall type inequality on generalized fractional conformable integral operators

Vandana Palsaniya , Ekta Mittal , Sunil Joshi  and D. L. Suthar  

From the journal [Analysis](#)

<https://doi.org/10.1515/anly-2022-1105>

Abstract

In 2015, Abdeljawad defined the conformable fractional derivative (Grunwald–Letnikov technique) to iterate the conformable fractional integral of order $0 < \alpha \leq 1$ (Riemann approach), yielding Hadamard fractional integrals when $\alpha = 0$. The Gronwall type inequality for generalized operators unifying Riemann–Liouville and Hadamard fractional operators is obtained in this study. We use this inequality to show how the order and initial conditions affect the solution of differential equations with generalized fractional derivatives. More features for generalized fractional operators are established, as well as solutions to initial value problems in several new weighted spaces of functions.

Keywords: [Generalized conformable integral operator](#); [conformable derivative](#); [Gronwall inequality](#); [Cauchy problem](#)

MSC 2020: [34A08](#); [26A33](#); [47D09](#)

References

- [1] Y. Adjabi, F. Jarad and T. Abdeljawad, On generalized fractional operators and a Gronwall type inequality with applications, *Filomat* 31 (2017), no. 17, 5457–5473. [10.2298/FIL1717457A](https://doi.org/10.2298/FIL1717457A) (<https://doi.org/10.2298/FIL1717457A>)
- [2] Y. Adjabi, F. Jarad, D. Baleanu and T. Abdeljawad, On Cauchy problems with Caputo Hadamard fractional derivatives, *J. Comput. Anal. Appl.* 21 (2016), no. 4, 661–681.
- [3] C. Corduneanu, *Principles of Differential and Integral Equations*, Allyn and Bacon, Boston, 1971.
- [4] T. H. Gronwall, Note on the derivatives with respect to a parameter of the solutions of a system of differential equations, *Ann. of Math. (2)* 20 (1919), no. 4, 292–296. [10.2307/1967124](https://doi.org/10.2307/1967124) (<https://doi.org/10.2307/1967124>)

- [5] F. Jarad, T. Abdeljawad and D. Baleanu, On the generalized fractional derivatives and their Caputo modification, *J. Nonlinear Sci. Appl.* 10 (2017), no. 5, 2607–2619.
[10.22436/jnsa.010.05.27](https://doi.org/10.22436/jnsa.010.05.27) (<https://doi.org/10.22436/jnsa.010.05.27>)
- [6] U. N. Katugampola, New approach to a generalized fractional integral, *Appl. Math. Comput.* 218 (2011), no. 3, 860–865.
[10.1016/j.amc.2011.03.062](https://doi.org/10.1016/j.amc.2011.03.062) (<https://doi.org/10.1016/j.amc.2011.03.062>)
- [7] T. U. Khan and M. A. Khan, Generalized conformable fractional operators, *J. Comput. Appl. Math.* 346 (2019), 378–389.
[10.1016/j.cam.2018.07.018](https://doi.org/10.1016/j.cam.2018.07.018) (<https://doi.org/10.1016/j.cam.2018.07.018>)
- [8] A. A. Kilbas, Hadamard-type fractional calculus, *J. Korean Math. Soc.* 38 (2001), no. 6, 1191–1204.
- [9] A. A. Kilbas, H. M. Srivastava and J. J. Trujillo, *Theory and Applications of Fractional Differential Equations*, North-Holland Math. Stud. 204, Elsevier Science, Amsterdam, 2006.
- [10] V. Kiryakova, *Generalized Fractional Calculus and Applications*, Pitman Res. Notes in Math. Ser. 301, Longman Scientific & Technical, Harlow, 1994.
- [11] K. S. Miller and B. Ross, *An Introduction to the Fractional Calculus and Fractional Differential Equations*, John Wiley & Sons, New York, 1993.
- [12] K. S. Nisar, G. Rahman, J. Choi, S. Mubeen and S. Arshad, Certain Gronwall inequality associated with Riemann–Liouville K - and Hadamard k -fractional derivative and their applications, *East Asian Math. J.* 34 (2018), no. 3, 249–263.
- [13] K. S. Nisar, G. Rahman and A. Khan, Some new inequalities for generalized fractional conformable integral operators, *Adv. Difference Equ.* 2019 (2019), Paper No. 427.
[10.1186/s13662-019-2362-3](https://doi.org/10.1186/s13662-019-2362-3) (<https://doi.org/10.1186/s13662-019-2362-3>)
- [14] K. S. Nisar, A. Tassaddiq, G. Rahman and A. Khan, Some inequalities via fractional conformable integral operators, *J. Inequal. Appl.* 2019 (2019), Paper No. 217.
[10.1186/s13660-019-2170-z](https://doi.org/10.1186/s13660-019-2170-z) (<https://doi.org/10.1186/s13660-019-2170-z>)
- [15] D. Qian, Z. Gong and C. Li, A generalised Gronwall inequality and its application to a fractional differential equations with Hadamard derivatives, 3rd Conference on Nonlinear Science and Complexity NSC10, Cankaya University, Ankara (2010), 1–6.
- [16] G. Rahman, A. Khan, T. Abdeljawad and K. S. Nisar, The Minkowski inequalities via generalized proportional fractional integral operators, *Adv. Difference Equ.* 2019 (2019), Paper No. 287.
[10.1186/s13662-019-2229-7](https://doi.org/10.1186/s13662-019-2229-7) (<https://doi.org/10.1186/s13662-019-2229-7>)
- [17] G. Rahman, K. S. Nisar and F. Qi, Some new inequalities of the Grüss type for conformable fractional integrals, *AIMS Math.* 3 (2018), no. 4, 575–583.
[10.3934/Math.2018.4.575](https://doi.org/10.3934/Math.2018.4.575) (<https://doi.org/10.3934/Math.2018.4.575>)

[18] G. Rahman, K. S. Nisar, S. Mubeen and J. Choi, Certain inequalities involving the (k, ρ) – fractional integral operator, Far East J. Math. Sci. 103 (2018), no. 11, 1879–1888.
[10.17654/MS103111879](https://doi.org/10.17654/MS103111879) (<https://doi.org/10.17654/MS103111879>)

[19] G. Rahman, Z. Ullah and A. Khan, Certain Chebyshev-type inequalities involving fractional conformable integral operators, Mathematics 7 (2019), no. 4, Paper No. 364.
[10.3390/math7040364](https://doi.org/10.3390/math7040364) (<https://doi.org/10.3390/math7040364>)

[20] H. Ye, J. Gao and Y. Ding, A generalized Gronwall inequality and its application to a fractional differential equation, J. Math. Anal. Appl. 328 (2007), no. 2, 1075–1081.
[10.1016/j.jmaa.2006.05.061](https://doi.org/10.1016/j.jmaa.2006.05.061) (<https://doi.org/10.1016/j.jmaa.2006.05.061>)

Received: 2022-09-18

Accepted: 2023-10-02

Published Online: 2023-11-30

Published in Print: 2024-08-01

© 2023 Walter de Gruyter GmbH, Berlin/Boston

— or —

From the journal



Analysis
Volume 44 Issue 3

Articles in the same Issue

Frontmatter

Gronwall type inequality on generalized fractional conformable integral operators

Asymptotic modelling of viscoelastic von Kármán membrane shells

Global sharp gradient estimates for a nonlinear parabolic equation on Riemannian manifolds

Scattering of an inhomogeneous coupled Schrödinger system in the conformal space

Existence of non-negative periodic solutions for a degenerate anisotropic parabolic equation with strongly nonlinear source

Fractional integral inequalities for the s - (κ, H) -convex function

Some properties of Ψ -gamma, Ψ -beta and Ψ -hypergeometric matrix functions

On the fractional q -integral operators involving q -analogue of Mittag-Leffler function

Downloaded on 29.10.2024 from

<https://www.degruyter.com/document/doi/10.1515/anly-2022-1105/html>



MANIPAL UNIVERSITY JAIPUR

(University under Section 2(f) of the UGC Act)

Department of Electrical Engineering **School of Electrical, Electronics and Communication Engineering**

Report on Collaborative activities

Name of Partnering Organizations:


1. MNIT Jaipur, India
2. BSDU-Jaipur, India
3. College of Engineering-Kong Saud University, Saudi Arabia
4. Faculty of Electrical Engineering, Universiti Teknologi Malaysia
5. University of Waterloo, Waterloo

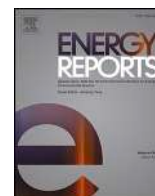
Name of Participants:

1. Dr Divya Rishi Shrivastava, Department of Electrical Engineering, Manipal University Jaipur, India
2. Prof Shahbaz Ahmed Siddiqui, Department of Mechatronics Engineering, Manipal University Jaipur, India
3. Dr Kusum Verma, Department of Electrical Engineering, MNIT Jaipur
4. S. Singh, BSDU-Jaipur, India
5. Majid A. Alotaibi, College of Engineering-Kong Saud University, Saudi Arabia
6. Hasmat Malik, Faculty of Electrical Engineering, Universiti Teknologi Malaysia
7. Mohammed E. Nasser, University of Waterloo, Waterloo

Name of the Activity:

Research Work on ‘A novel synchronized data-driven composite scheme to enhance photovoltaic (pv) integrated power system grid stability’
(Journal Publication)


HOD
Department of Electrical Engineering
School of Electrical,
Electronics & Communication (SEEC)
Manipal University Jaipur



A novel synchronized data-driven composite scheme to enhance photovoltaic (pv) integrated power system grid stability

Divya Rishi Shrivastava^a, Shahbaz Ahmed Siddiqui^{b,*}, Kusum Verma^c, S. Singh^d, Majed A. Alotaibi^{e,*}, Hasmat Malik^{f,g,**}, Mohammed E. Nassar^h

^a Department of Electrical Engineering, Manipal University Jaipur, Jaipur, India

^b Department of Mechatronics Engineering, Manipal University Jaipur, Jaipur, India

^c Department of Electrical Engineering, Malaviya National Institute of Technology Jaipur, Jaipur, India

^d Faculty of Electrical Skills Education, Bhartiya Skill Development University, Jaipur 302037, India

^e Department of Electrical Engineering, College of Engineering, King Saud University, Saudi Arabia

^f Department of Electrical Power Engineering, Faculty of Electrical Engineering, Universiti Teknologi Malaysia (UTM), Johor Bahru 81310, Malaysia

^g Department of Electrical Engineering, Graphic Era (Deemed to be University), Dehradun 248002, India

^h Department of Electrical and Computer Engineering, University of Waterloo, Waterloo, ON N2L 3G1, Canada

ARTICLE INFO

Keywords:

Decision boundary based control
Decision assisted inference
Moving average
Solar PV energy
Early transient stability assessment (TSA)

ABSTRACT

The performance of power networks is enhanced by the penetration of solar energy, which helps to equate continuously the generation and demand power imbalance. However, the time margin that grids must adapt to unforeseen frequency fluctuations and restore generation-demand equivalency is reduced by these linkages. Consequently, it exerts the stability and performance of the power grid at risk. Thus, it becomes vital to assess real-time system data and to recognize and implement suitable remedies to maintain a healthy system performance. In order to improve grid stability in power networks that have solar energy penetration, this manuscript suggests a data driven integrated framework. The proposed approach is a two-step framework wherein the first stage assesses impending transient instability in the system through novel Instability Evaluation (IE). Step two involves creating and deploying a Decision Boundary based Control (DBC) to stabilize an unstable system following an emergency control strategy. An IE module employing short-synchronized movement data is presented for evaluating post-disturbance transient stability (TS). In the initial cycles following the fault initiation, the IE projects the impending transient instability. Next, an innovative DBC creates an emergency remedial system for unstable processes that determines the nature, magnitude and location of the remedial action. The DBC assesses pertinent action sets that it implements to sustain system stability using a proposed Decision Assisted Inference (DAI) technique. The simulation investigations validate the aptness of suggested analysis on the performance of power system with and without PV and topological variations.

1. Introduction

Worldwide, the electric power demand is growing at an unprecedented rate. To keep up with the surging demand, power grids have integrated various renewable energy sources. Researchers, utility

engineers, and system operators have recently shown an increased interest in the prospect of sustainable Renewable Energy Penetration (REP) to the power grids. The efficiency of the electricity grid is enhanced by the REP at strategic and vital sites. However, real-time monitoring, assessment of the status, and its control are significantly

Abbreviation: CCT, critical clearing time; DBC, Decision Boundary based Control; DAI, Decision Assisted Inference; EWMA, Exponentially Weighted Moving average; FA, False Alarm; FAT, Fault Application Time; FCT, Fault Clearing Time; IE, Instability Evaluation; LSI, Load Severity Index; MA, Missed Alarm; MW, Megawatt; MVA, Mega voltampere; MVAR, Mega voltampere reactive; PMU, Phasor Measurement Units; PV, Photovoltaic; SE, Solar Energy; SG, Synchronous Generation; TS, Transient Stability; TSA, Transient Stability Assessment.

* Corresponding authors.

** Corresponding author at: Department of Electrical Power Engineering, Faculty of Electrical Engineering, Universiti Teknologi Malaysia (UTM), Johor Bahru 81310, Malaysia

E-mail addresses: shahbazahmed.siddiqui@jaipur.manipal.edu (S.A. Siddiqui), MajedAlotaibi@ksu.edu.sa (M.A. Alotaibi), hasmat@utm.my (H. Malik).

<https://doi.org/10.1016/j.egy.2023.12.029>

Received 10 August 2023; Received in revised form 23 November 2023; Accepted 9 December 2023

Available online 28 December 2023

2352-4847/© 2023 The Authors. Published by Elsevier Ltd. This is an open access article under the CC BY-NC-ND license (<http://creativecommons.org/licenses/by-nc-nd/4.0/>).

challenged by the incorporation of renewable energy sources. REP integrated power systems (Kezunovic and Overbye, 2018) have self-healing capabilities in the event of an emergency, increased grid resilience, and user-friendly interfaces to guarantee the reliability of electric power. Handling these unexpected aberrant setups requires real-time power data, situational awareness, and a suitable response strategy. Wide-area network data is transferred in sync using synchrophasor technology (Dragomir and Iliescu, 2015). The technique employs a group of Phasor Measurement Units (PMUs) to keep track of the system's health in terms of the synchronized voltage and current phasor readings. In the context of Renewable Energy Penetration (REP), it is becoming increasingly important to verify and analyse this synchronized data in order to establish the grid's integrity. REP also helps conserve natural resources and increase energy independence by providing fuel diversity. However, rising renewable penetration creates issues to grid operation because to decreasing system inertia.

In the event of a power outage, the frequency of the system will shift when the balance between supply and demand is disturbed. System inertia, which impacts synchronous operation of machinery, gives power grids a buffer of time to adapt to these emerging imbalances (Li et al., 2023). System inertia is decreased when REP with zero inertia, like solar energy, is integrated with traditional grids. In regard to hybrid mode of the power generation, the ability of synchronous generator to respond promptly to the disturbances of system (i.e., specifically fluctuations in speed deviations, rotor angles etc.), may be significantly hindered. The generator angles may progress ahead of the rest of the system in response to a large disturbance. A faster rate of generator progress may hasten the rotor's fall into an out-of-phase condition. This state is often referred to as "transitional instability." Therefore, TSA of the power system after a disturbance is crucial for the grid's continued smooth functioning, particularly in the case of solar energy integration. Wide-area observations and machine-learning models are utilized in conventional power infrastructures to predict the online dynamic behavior of generators (Xie et al., 2023). Online dynamic analysis is a vital component of post-fault examinations of online systems; however, its practicality reduces in the setting of real-time frameworks. In order to foresee the severity of an oncoming incident, the Wide Area Transient Instability Severity Analyzer is recommended (Shrivastava et al., 2021). The evaluation is fast, accurate, and model-independent; however, it can only be used with traditional power grids.

Phase plane trajectories (Latiki et al., 2022) approximates the transient stability margin based on CCT estimations, which represent the maximum time margin to clear a fault, are being investigated in the literature. Examples of state-of-the-art methods used in the computation of CCT for generators include Mahalanobis-kernel regression (Liu et al., 2020) and parametric sensitivity analysis (Shrestha and González-Longatt, 2021). Zhan et al. (2023) propose a conditional generative adversarial network and hybrid transfer learning approach in order to enhance the prediction of TS. In anticipation of the transient stability status of the system, an adaptive spatial-temporal methodology in conjugation with long short-term memory ensemble is suggested in Reference (Tang et al., 2020). A convolutional neural network-based TSA, oscillatory and non-oscillatory instability mode is presented in (Shi et al., 2020). In reference (Li et al., 2022), a technique is proposed that makes use of the internal feature transmission of deep forest and is based on active transfer learning. By incorporating pre-trained InageNet, (Kim et al., 2023) suggests a deep belief network-based method. A local linear interpreter model is also used to make sense of the results of the transient stability predictors. For power systems that incorporate renewable energy, (Mochamad et al., 2022) suggests multi-stability boundary analysis. The methodology is tested over varied power electronic device penetration considering small and large disturbances rotor angle stability, voltage and frequency stability. Reference (Abrar and Masood, 2023; Mehrabi et al., 2019) offers an automatic load reduction strategy that serves to stabilize the system and avert blackouts in this regard.

In (Paital et al., 2018), an SVC based on quasi-differential search is examined in an effort to mitigate transient instability. By increasing the damping of oscillations, the method reduces the time required for the stable state to settle. Nevertheless, it does not propose the necessary approach to enhance the system's transient instability in the event that, following the disruption, the network begins to approach the maximum configurations. Kucuktezcan et al (Kucuktezcan and Istemihan Genc, 2015). proposes Big Bang-Bang based optimization algorithm to enhance dynamic security of the power system by minimizing the operational cost of corrective-preventive control actions. The computational burden and search space reduction is decreased by decision trees and correlation coefficients to formulate load shedding and generator rescheduling and enhance the transient stability of the system. Chandra et al (Chandra and Pradhan, 2021). introduced a load reduction technique via voltage stability index to stabilize the frequency of a SE based power network. The evolving transient instability may be repressed by employing recurrent corrective control (Babu and Sarkar, 2021). The control strategy is decentralized scheme to first identify coherent generator in real-time and subsequently, the scheme is deployed in zone-wise distributed manner. Grid stability is improved through the deployment of an adaptive load shedding strategy that is based upon assessment of the power flow tracing (Kumar et al., 2019) and stability (Kumar et al., 2019; Bekhradian et al., 2023). In contrast to alternative power sources, the integration of solar energy does not impact frequency-power equivalence. However, it does impair time margins and stability bounds. As these power sources pose a risk to the stability of the grid, timely stability assessments are gaining importance in these systems (Kumar et al., 2019). Reference (Siddiqui et al., 2016) proposes a unified method for assessing the status of transient stability before implementing preventive and emergency control strategies. By employing synchronized voltage and angle measurements, the strategy is capable of forecasting system instability and devising emergency measures such as load reduction and generator tripping. Voltage stability can also be improved through the deployment of an adaptive load shedding strategy (Tang et al., 2013).

Post angle/voltage instability, a nonlinear programming based corrective action scheme is proposed to improve the dynamic security of the power system (Tuglie et al., 2000). The methodology enhances security in the online time frame by minimizing objecting function-based load shedding. A novel approach to mitigate transient instability and short-term voltage fluctuations is proposed by employing emergency demand response (Kang et al., 2018). The trajectory sensitivity ranking based load shedding, load recovery and multi-objective evolutionary algorithms based coordinated preventive control-corrective actions are recommended to enhance the grid performance. A unique approach for corrective load shedding and preventive generation rescheduling is proposed to sustain wind energy penetrated power system transient stability (Yuan and Xu, 2020). The approach encompasses bi-level optimization model with risk coordination parameter. The load shedding and generation rescheduling cost optimization through golden section search and stability constraints is performed. A sudden generation loss that triggers power flow redistribution and power imbalance may eventually lead the system to instability. A two-loop integrated algorithm based coordinated optimization scheme initiates load shedding and corrective line switching (Shi et al., 2019). The frequency or voltage security is achieved by linearized sensitivity based iterative optimization and coordination within action type is achieved through neighbor search to optimize magnitude of loads to be shed. A macrolevel dynamic assessment methodology and microlevel static coherency assessment (Babu and Sarkar, 2020) are employed upon real-time network data to identify coherent generators, deploy generator rejection, and load curtailment.

Existing approaches and strategies for hybrid power generation utilizing conventional synchronous generators and solar PV energy and either devise schemes for solar PV integration or implement an emergency remedy to restore frequency stability, according to the literature

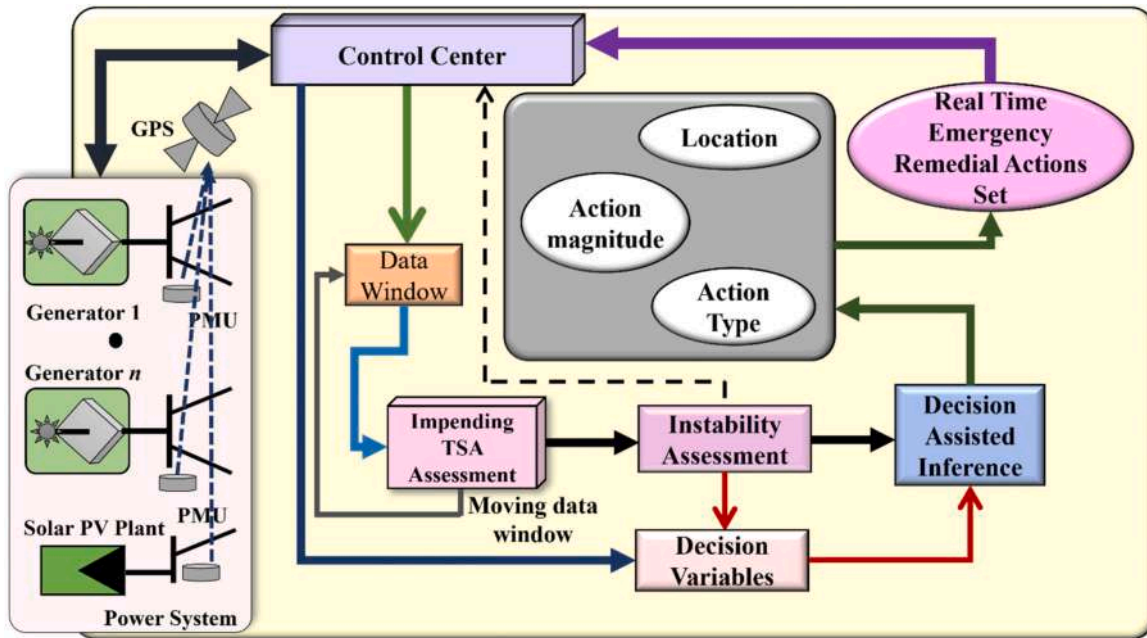


Fig. 1. A general outline of the proposed composite scheme.

review. The effectiveness of monitoring, evaluating, and controlling a solar-powered electricity grid is the subject of this study. An investigation is commenced into the current estimation of forthcoming transient instability subsequent to the disruption. Furthermore, should the need arise, the methodology can be utilized to establish and implement real-time corrective actions in order to guarantee the transient stability of the power system that has been penetrated by solar energy. The key contributions of the investigations are potted as:

1. First, IE is developed to carry out an early evaluation of a power grid's transient stability when a significant amount of solar energy is integrated. The ability of IE to determine the precise instant at which an emergency strategy can be implemented is its main advantage. The IE leverages the real power' short moving window of the power sources including solar PV power.
2. Following the evaluation of the IE scenarios, a unique Decision Boundary-based Control (DBC) is initiated to determine the magnitude, type, and location (where) of actions required for preventing unstable grid operating conditions. A novel Decision Assisted Inference (DAI) is incorporated into the proposed DBC in order to identify and initiate action sets at an appropriate location.
3. In order to safeguard the solar integrated power system against significant component failure and ensure transient stability, the proposed composite scheme functions as a response-oriented framework. In addition, realization of each action-set occurs in real-time through the application of synchrophasor measurements. Due to this, the proposed scheme is applicable to a vast array of operational scenarios and can be implemented in any system.

The proposed methodology is tested with a solar-powered adaptation of the New England 39 Bus evaluation system. A high-level overview of the unified framework is illustrated in Fig. 1.

2. Early assessment of impending instability

Bus frequency, voltage, and angle monitoring can be used to assess the state of the electrical grid following a disturbance. In this section, we present a novel approach to performing transient stability assessments (TSAs) in real time, comparing power systems with and without significant penetration of solar energy. The synchronous machine's electric

power output with j^{th} machine frequency f_{Gj} is (Tang et al., 2013):

$$Pe_j = Pm_j - \left(\frac{2H_j S_j}{f_n} \right) \frac{df_{Gj}}{dt} \quad (1)$$

When mechanical and electrical powers are equivalent in an equilibrium state, Eq. (1) is changed to read as follows:

$$\frac{df_{Gj}}{dt} = 0 \Rightarrow Pe_j = Pm_j \quad (2)$$

In a state of equilibrium, the rate of change of frequency is equal to zero. The rate of change in frequency, can be positive or negative depending on whether the equilibrium is disturbed during transient conditions, implying a decreased electrical output or increased actual power output, respectively as follows:

$$\begin{aligned} \frac{df_{Gj}}{dt} > 0 &\Rightarrow Pe_j \downarrow \\ \frac{df_{Gj}}{dt} < 0 &\Rightarrow Pe_j \uparrow \end{aligned} \quad (3)$$

For n machines, the total generated electrical power (Pe) is:

$$Pe = \sum_{j=1}^n Pe_j \quad (4)$$

For i^{th} generator inertia and MVA rating, the system inertia is calculated as:

$$H = \frac{\sum_{i=1}^n H_i S_i}{\sum_{i=1}^n S_i} \quad (5)$$

The PV system produces power without the need of a spinning gear. Power-frequency equivalence does not exist for the power produced by the solar farm. Moreover, the system's overall inertia decreases as a result of this integration rather than increasing it (Li et al., 2023). Machines lose synchronism when their critical clearance time is lowered due to the decreased inertia. The solar energy penetration into the grid can occur through either by replacing the conventional plants by solar PV or by injecting SE at strategic locations. First, the total power Pe can be found through Eq. (6). In contrast with PV as number of solar farms

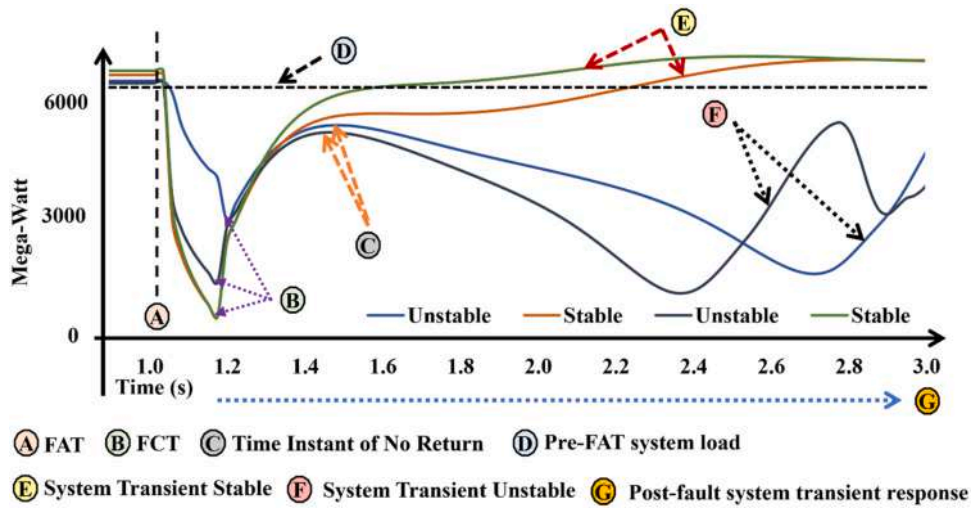


Fig. 2. Typical templates for transient unstable and stable scenario.

delivering P_{PV} power, Eq. (6) is used in the second situation to determine the total power with $n' = n - PV$. Together, the total power delivered in either situation is:

$$P_e = \sum_{j=1}^{n'} P_{e_j} + P_{PV} \quad (6)$$

With SE and a lower SG-based generation, the reduced system inertia is:

$$H' = \frac{\sum_{i=1}^{n'} H_i S_i}{\sum_{i=1}^{n'} S_i + S_{PV}} \quad (7)$$

2.1. Instability evaluation (IE)

One consequence of the subsequent event in the power network is a variation in rotor angles among the synchronous machines. According to the dynamics of the system following an event, a more advanced

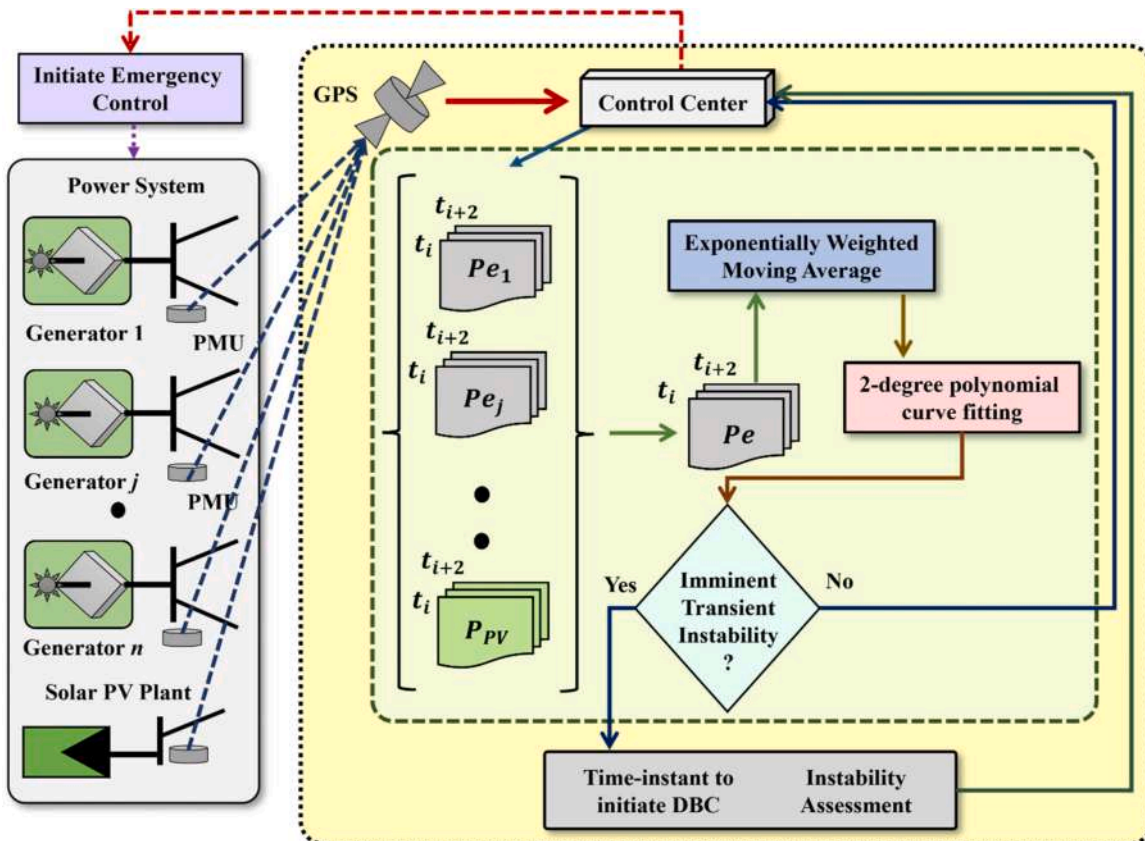


Fig. 3. Proposed Instability Assessment.

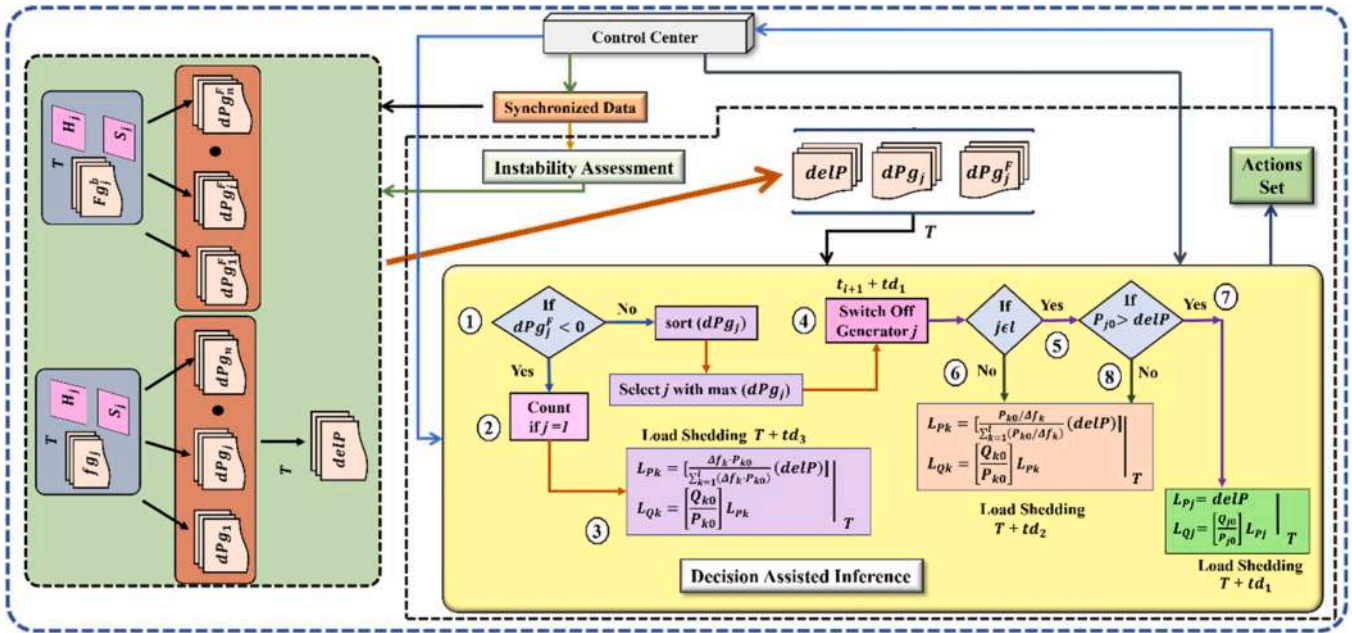


Fig. 4. Proposed Decision Boundary based Control (DBC).

machine tends to decrease the disparity between the angles. Because the accelerated generator’s rotor angle is greater at that instant in time, less power is delivered, which could throw the generator out-of-step. This capacity of the system to restore synchronization following a substantial disruption is denoted as Transient Stability, also known as rotor angle stability. Early TSA evaluation after the disturbance allows adequate time to establish and apply emergency control and increase grid sustainability. Predicting TSA status of the system before it exceeds the stability bounds requires quick and effective analysis, and evaluation of the limited synchronized data window. Fig. 2 illustrates the variations in total active power of the system in the subsequent transient stable and unstable operating circumstances.

The figure illustrates how the fluctuation in electric power varies depending on whether operational conditions are stable or unstable. At first, the system is in an equilibrium condition where there is no rate of change in frequency. A major fault (short circuit) happens at FAT, disrupting equilibrium and lowering source-generated power output. All of the power sources then typically recover from the interruption following FCT. Situations in which the power of the system recovers, and equilibrium is restored are indicative of a transient stable system. In a few instances where the total power of the system begins to decrease at a specific instant, the system will be advancing towards transiently unstable operation. Therefore, power variations can be employed to determine the state of the system, as they contain vital information regarding the transient stability of the system. The ongoing analysis of the brief time frame of data pertaining to the overall power generation can thus be employed to assess predictions regarding imminent instability. The short data window assures rapid response to the instability status of the system. Even though the potential for more accurate estimations, extended data windows have an extended processing time and can compel the system to approach extreme configurations, ultimately resulting in its complete failure. Therefore, a trade-off is achieved between response time and accuracy; currently, the short length of the data adequately evaluates the TSA for real-time applications. Let, Pe_{DW} be generated power three-cycle window and represented through Eq. (6) as:

$$Pe_{DW} = [Pe(t_i)Pe(t_{i+1})Pe(t_{i+2})] \quad (8)$$

$\forall t \in [FCT + 1cycle, t_d]$

The dynamics of the power system are continuously modified in real

time based on an evolving data window of the generated total power. In order to do this, we employ the Exponentially Weighted Moving Average (EWMA). In order to prioritize current measurements and eliminate noise (irregularities), EWMA is used (Kuo and Chou, 2021). As a result, in order to determine the dynamics of a system in real time, the most recent observations are given a far heavier weight than older data. Eq. (9) can be used to find the filtered data for the t^{th} time sample, and Eq. (10) can be used to find the weighted factor:

$$Pe'_t = \alpha Pe_t + (1 - \alpha)Pe'_{t-1} \quad (9)$$

$$\alpha = 2(span + 1)^{-1} \quad (10)$$

Two data points are considered a span in this work. The least-squares regression is utilized to fit a 2-degree polynomial to the three-cycle data in Eq. (9).

$$\min(E) = \min \sum_{m=1}^3 |p(x_m) - Pe'_m|^2 \quad (11)$$

Eq. (12) is employed to verify the validity of the maxima in the form of a two-degree polynomial:

$$p(x) = c_0 + c_1x + c_2x^2 \quad (12)$$

Maximas ensures the point at which the system will no longer attempt to recover following an event. Alternatively, it will exceed transitory unstable settings within the future cycles. This leads to the following conclusions: Fig. 3 demonstrates that (1) the time at which emergency control operations must be started depends on whether the system is predicted to be transiently stable or unstable. Timely detection of an unstable system allows for adequate evaluation and implementation of corrective steps for real-time, wide-area emergency control.

3. Decision boundary based control (DBC)

This section elucidates the proposed Decision Boundary-based Control (DBC). DBC determines what, where, and how much of an activity occurs based on a predetermined set of inference rules in order to maintain system stability. The decision boundaries are estimated by the Decision Assisted Inference (DAI) to determine the type of action, its location and magnitude are computed by the DBC. These decision var-

ables, which are derived from real-time network data, estimate the power variations among individual generator and the system as a whole. Due to its reliance on network data, the DBC exhibits adaptability towards variations in system topology and functionality. Subsequent to the IE assessment, for j^{th} machine, the generator power imbalance dPg_j is estimated as:

$$dPg_j = \left(\frac{2H_j S_j}{f_n} \right) \frac{df_{Gj}}{dt} \forall j \in n \quad (13)$$

The total power imbalance $delP$ is the overall estimated imbalance for all the n (equivalent to n' for solar energy) machines as:

$$delP = (2/f_n) \sum_{j=1}^n S_j H_j (df_{Gj}/dt) \quad (14)$$

While the generator frequency and the generator bus frequency (f_{Gj}^F for j^{th} machine) are qualitatively identical, a minor numerical discrepancy arises due to the influence of local loads and the interconnected nodes. These minor variations are employed to approximate power imbalances in individual machines. Thus, for j^{th} machine, the $delP$ due to frequency of the node is:

$$dPg_j^F = \left(\frac{2H_j S_j}{f_n} \right) \frac{df_{Gj}^F}{dt} \quad (15)$$

As input to Decision Assisted Inference (DAI), these power imbalances determine the most suitable action set. Fig. 4 demonstrates the proposed DBC and DAI.

3.1. Decision assisted inference (DAI)

In order to ensure system synchronization in atypical circumstances, a novel approach labeled Decision Assisted Inference (DAI) is proposed. DAI initially ascertains the nature of the action (What) that is to be implemented. It is imperative to eliminate a generator from the system at time instant T if its power supply is excessive and causing it to accelerate in opposition to the remainder of the system. Other machines may be compelled to distribute the power imbalance proportionally to their inertias in the event that generation is rejected. However, load curtailment must be implemented in conjunction with generator rejection, as the latter may still result in an imbalance of power within the system. Relative load reduction must therefore be implemented in order to rectify the generation-load imbalance. On the other hand, load shedding is a proposed solution in which one machine in the system experiences a reduction in speed compared to the others when the power output from generators fails to meet the load demand. The estimation of power imbalance dPg_{jr}^F derived from Eq. (15) is utilized as a criterion for determining whether to implement load shedding or generator failure as the control action.

$$dPg_{jr}^F \rightarrow \left\{ \begin{array}{l} < 0 \rightarrow \text{Load Shedding} \\ > 0 \rightarrow \text{Generator Rejection} \end{array} \right\} \quad (16)$$

The higher load demand is implied by the negative estimates of dPg_{jr}^F for any given generator. Load reduction procedures must be followed to ensure the system remains stable. When all estimations are positive, it means there is too much power being produced, which requires rejecting some of the generators' output and then reducing the load proportionally. As seen in Fig. 4, after computing Eq. (16), appropriate action type, location, and magnitude are highlighted. The suggested DAI also shows the sequence of steps to be taken. These Action Sets detail the order in which each type of action should be taken, as well as the best place to take corrective measures and their ideal scale. In the sections that follow, we'll go into greater depth about each of these action packs.

3.1.1. Generator tripping

3.1.1.1. Location identification. The assessment of the generator to be tripped initiates as soon as the decision of the generator's rejection is identified. Given that generation rejection occurs as a result of increased generation, the machine generating the largest amount of electricity is likely the generator to be taken out of the system. Evidently, the generator exhibiting the largest imbalance is the primary contributor to the generation of surplus. Its rejection will effectively rectify the systemic imbalance. Therefore, Eq. (17) is arranged in descending order at time instant T in order to determine the maximal power imbalance of each generator. The generator candidate with the greatest imbalance (j^{th} generator, for example) must be rejected. The procedure for determining the generator to be removed is:

$$\text{sort}(dPg_j|_T) \Rightarrow \max \left[\left(\frac{2H_j S_j}{f_n} \right) \frac{df_{Gj}}{dt} \right]_{|_T} \forall j \in n \quad (17)$$

3.1.1.2. Location and magnitude of subsequent load shedding. At the moment of detecting instability, the presence of excessive power prior to curtailing the generator suggests a low demand for power. In the event that the generator rejects a load, the system may experience an increase in power demand due to the restriction of large load buses. Therefore, it is critical to promptly recognize the nodes representing light loads and reduce their magnitude accordingly. This work thus proposes a novel Load Sharing Index (LSI) to determine the proportion of the overall system load that is being distributed among individual load buses. In essence, it computes the portion of individual load by comparing the deviation in frequency to the nominal frequency f_n . The percentage share is then calculated by normalizing the frequency deviation by the cumulative deviation of all load sites. Subsequent to the generator trip, for the load shedding, the location of load sites is estimated using the numerical valuations obtained from LSI . The LSI for the k^{th} load in a system with l loads is computed as follows:

$$LSI_k = \frac{f_k|_T - f_n}{\sum_{k=1}^l (f_k|_T - f_n)} \times 100 \quad \forall k \in l \quad (18)$$

where, nominal frequency f_n and k^{th} load bus frequency $f_k|_T$ is computed at time T . The least load sharing node is determined by sorting the LSI for each load. The magnitude L_{pj} from the load bus is reduced if the estimated imbalance $delP$ is less than the load pre-disturbance magnitude at time-instant T and that the load bus is identical to the one that triggered the generator. In general, electrical burdens are divided into two categories: reactive and real. Strictly considering the real component of load shedding is unrealistic. Consequently, it is critical to eliminate the appropriate reactive component of the load. The amount of the quadrature power L_{Qj} that is to be shed is determined by dividing the ratio of the real power component and L_{pj} prior to the disturbance. The steps (1) \rightarrow (4) \rightarrow (5) \rightarrow (7) constitute the full action set for this strategy.

In contrast, if, the LSI estimates load bus that differs from the one of the tripped generators location such that $j \neq l$, or if the estimated power imbalance ($P_{j0} < delP$) is greater than load at the j^{th} location prior to the disturbance, every load in the power network is regarded as intransigent for load curtailment. The determination of L_{pk} to be shed, relies upon its frequency deviation at T , the quantity of load prior to the disturbance, and power imbalance. The load exhibiting a reduced pre-disturbance loading and a lesser frequency deviation from nominal frequency collectively endures the majority of the load shedding implications. The quadrature component L_{Qk} , which is intended to be curtailed, is similarly computed in terms of the fraction of the real power (pre-disturbance) over the reactive component, and L_{pk} . In its entirety, the sequence of events is designated as steps (1) \rightarrow (4) \rightarrow (6) and steps (1) \rightarrow (4) \rightarrow (5) \rightarrow (8), respectively.

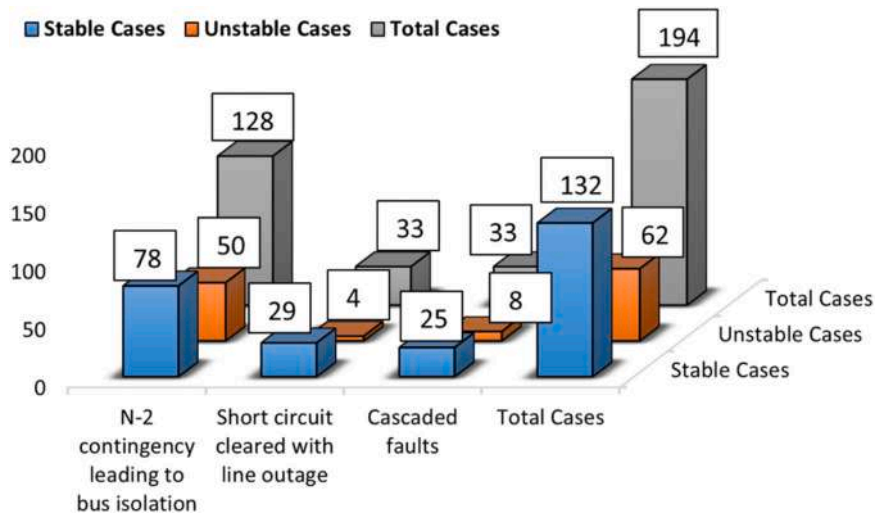


Fig. 5. Detailed data generation.

3.1.2. Load shedding

The excess power demand is illustrated by the negative $delP$ represented by Eq. (16). The estimated $delP$ is numerically equivalent to this additional power demand. In the event of such a scenario, one or more generators might experience a deceleration. When a single generator experiences a slowdown in operation, every load within the power network is designated as a candidate load. The proposed DAI assesses these implemented steps of action as (1) → (2) → (3). In order to even out the imbalance among the loads, the percentage load shedding is computed using frequency change methodology (Tang et al., 2013). The allocation of load shedding magnitude among potential loads is determined by the frequency-dependent technique, which takes into account the frequency of the load bus and the pre-disturbance numerical value of each individual load. Thus, the higher load shedding component is shared by loads with both larger pre-disturbance loading and larger frequency deviations from nominal frequency.

3.2. Actual time of action deployment

Even while emergency measures are recommended during the assessment of instability, they are not often implemented right once. Delays in deployment are induced by factors such as communication to substations, central logic, power plants, operating time for circuit breakers, and processor time (Bhui and Senroy, 2017). The delays td_1 , td_2 , and td_3 after time instant T refer to delays that correspond to a particular set of actions.

4. Results and discussions

In this section, the suggested integrated strategy is tested using the New England 39 Bus test system (NE39BTS), with/without solar PV farms. The test system simulation is carried out using the DigSILENT

Power Factory. The test system (Shrivastava et al., 2021) typically consists of 34 lines, 39 nodes, 19 loads, 12 transformers, and 10 synchronous generator-based power sources. In this work, one sample per cycle (60 Hz) of synchronized data is utilized. A database comprised of various faults with varying system loadings is used to test the performance of the suggested composite scheme. The simulated disturbances are classified as stable or unstable scenarios and are taken into account both singly and in cascaded scenarios. The resulting dataset displayed in Fig. 5 comprises of the total cases investigated, event-based categorization and stability status-based categorization. Additionally, the sub-sections provide a detailed explanation of the performance scores achieved by the suggested implementation of IE and DBC. Following this, in order to evaluate the efficacy of the proposal in improving stability and preventing grid collapse on a power system penetrable by SE, two representative examples: with multiple bus SE penetrations and without solar PV farms, is utilized. An analysis of the presented work in comparison to the current state of the art is presented as a final step.

4.1. Performance evaluation of proposed IE and DBC

The IE based early assessment is validated over the generated dataset to early assess forthcoming first swing transient instability. In each case, IE has implemented the imminent stable/unstable settings. The results of a comparative analysis between the proposed IE scheme and existing machine learning techniques in the literature are presented in Table 1. A comparison of the methods was carried out to assess the veracity of the proposed IE methodology with respect to the different test cases that were taken into consideration. In contrast to the proposed IE, data mining techniques incorporate 80% of the data into their training sets, while the remaining 20% is allocated for model evaluation. However, the proposed IE scheme does not utilize the machine learning models and instead performs testing on every generated database. It is found

Table 1
Evaluation of the proposed IE.

S. no.	Method	Test Cases	Overall Accuracy (%)	False Alarm (%)	Missed Alarm (%)	Impending Instability (Yes/No)	When to Initiate DBC (Yes/No)	Time-instant of Action Quantity Calculation (Yes/No)
1	Random Forest	39	97.43	100	93.3	Yes	No	No
2	Multilayer Perceptron	39	94.9	96.7	87.5	Yes	No	No
3	k-NN	39	97.43	96.4	100	Yes	No	No
4	DT	39	97.43	100	90.9	Yes	No	No
5	AdaBoost	39	97.43	96	100	Yes	No	No
6	Proposed IE	194	97.43	96.2	100	Yes	Yes	Yes

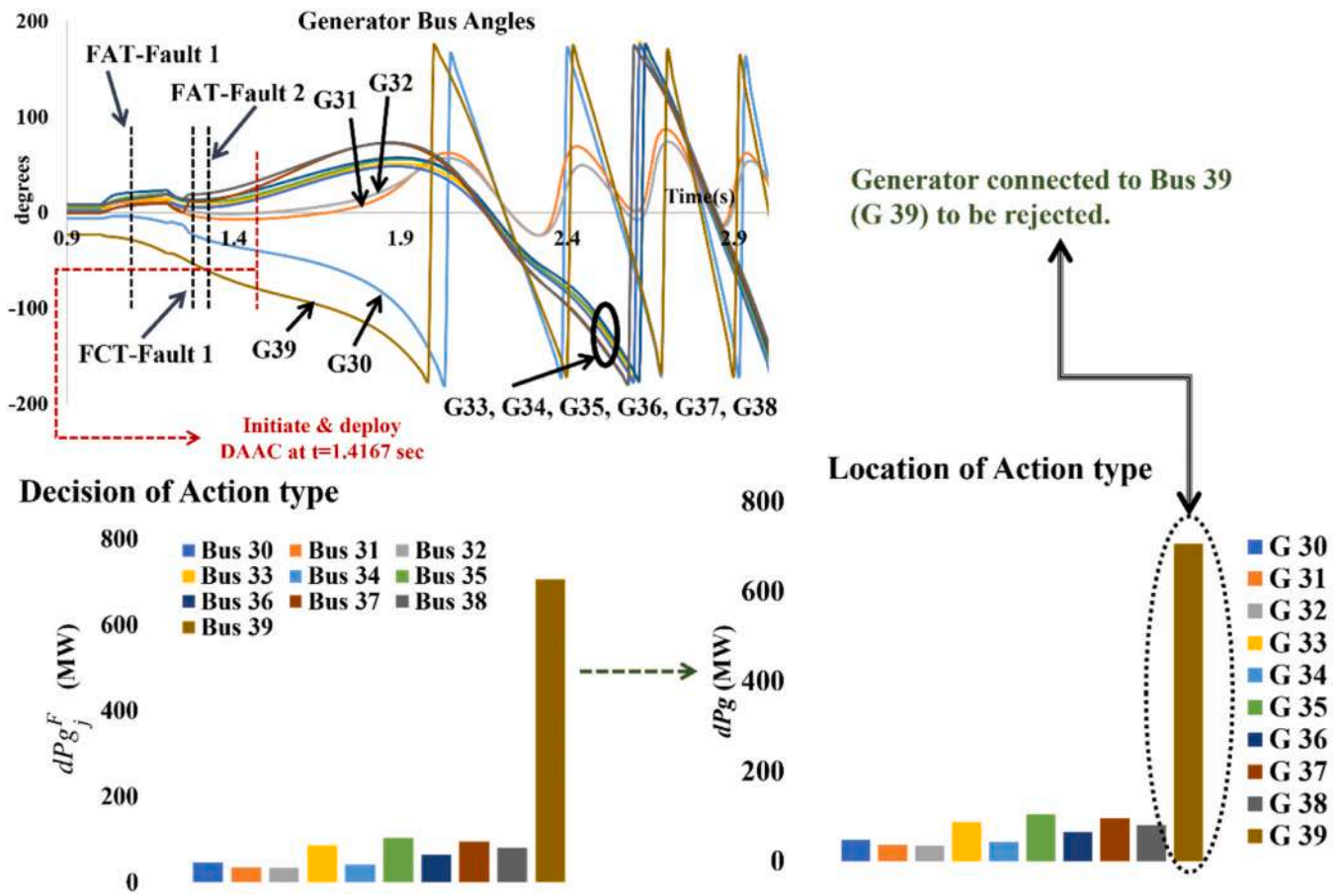


Fig. 6. Proposed IE and DBC: Example I.

that the performance of the proposed IE in predicting upcoming transient instability of a system is superior. For each event type, the table additionally provides information regarding the count of stable cases misidentified as unstable cases (Missed Alarm) and stable cases misidentified as unstable cases (False Alarm). Apparently, the proposed IE for TSA evaluates time to initiate emergency actions, mitigates false and missed alarms, and predicts impending instability. When impending instability is detected for the unstable circumstances, DBC is initiated to maintain system stability and performance. In the next subsections, the performance of IE and DBC based scheme is demonstrated using two

cases: absence and presence of the solar plant, respectively.

4.2. Illustrative example I with conventional generation

With 101% of base case system load, Short Circuit fault near Bus 03 applied at 1 s and cleared at 1.2 s by opening breakers of Line 03–18, subsequently, breakers of Line 02–25 opened at 1.25 s.

The Example entails to demonstrate the implications of the suggested composite procedure on the system’s response to a series of events. Fig. 6 depicts the response to the multiple faults through the generator bus

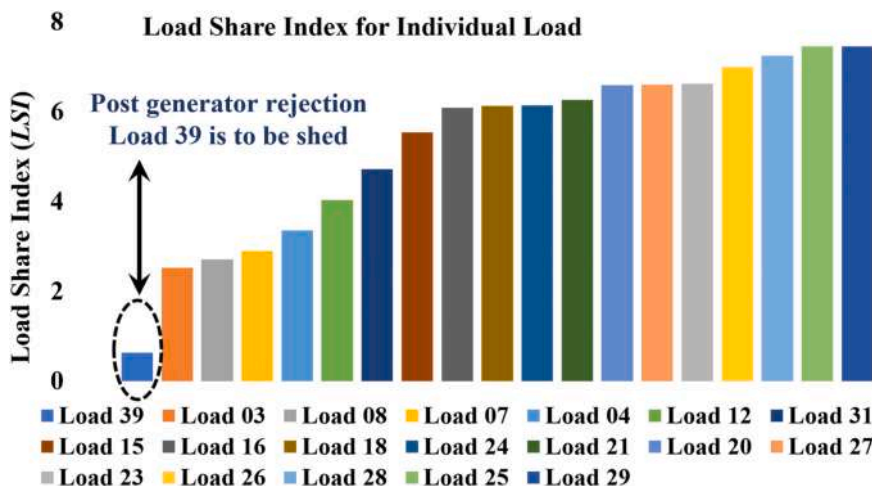


Fig. 7. Innovative load share index (LSI) post generator rejection.

Table 2

Example I: Initiation of proposed strategy.

Action Type	Actions location	Action magnitude	Time (s)
TSA assessment	All Machines	Power imbalance $delP$	1.417
Generator Trip	G 39	Shed 1000 MW	$1.417 + td_1$
Load Shedding	L 39	Shed 627.8 MW and 149.97 MVA _r	$1.417 + td_3$

angle variations. Generators G39 and G30 are out of sync when fault 2 begins at the same time as the post-fault clearance of event 1 at 2 s. After the transient instability has caused G33–G38 to be out of sync ~ 2.6 s, leading the grid to collapse. Avoiding a complete system shutdown requires prompt detection of instability, development of contingency plans, and implementation of those plans. The IE module is activated to make a best-guess prediction of the impending instability. An emergency control strategy can be prepared and put into action after the IE module detects the imminent transient instability at 1.417 s. The proposed TSA emphasizes three crucial aspects: (1) the system’s transient instability; (2) the control initiation time; and (3) the implementation of DBC. Fig. 6 depicts the decision-making process for deciding which action to take and where to do it. After the generator is rejected, however, a load reduction equal to the estimated power imbalance is requested to prevent the imbalance from worsening. Since G 39 was rejected at the same time, LSI calculations indicate that Load L39 was reduced by 627.808 MW, as shown in Fig. 7. As a percentage, it equates to 36.76% of the total starting MW demand being reduced. Table 2 tabulates the action type, location, and magnitude as estimated by the suggested emergency control technique. DBC is implemented when there is a risk of instability so as to safeguard the system from instability and boost the power grid’s performance. The recommended control action plan improves the grid’s stability and performance.

The DAI suggests generator rejection followed by load shedding through steps (1) – step (4) with an appropriate amplitude of

corresponding action. Delays in applying the emergency control technique delays the initiation of emergency actions. The emergency control method successfully prevents grid failure even with delayed actions. The response of the system with proposed strategy is illustrated in Fig. 8. At times, deployment times may increase at certain periods due to network congestion. Fig. 8 depicts the application of the corrective strategy, which includes a three-cycle (6-cycle) and nine-cycle (12-cycle) delay, respectively. The picture elaborates on the effects of 6- and 12-cycle delayed deployment on the average load voltage and the generator bus angle in the absence of control application.

The outcomes show that the voltage profile of the system and the generator angle are unaffected by an additional delay in time. The findings prove beyond a reasonable doubt that the proposed composite technique is successful in reducing transient instability and avoiding grid jeopardize, even with application of cascaded faults.

4.3. Results for the solar PV integrations

In order to further evaluate the performance of the proposed composite scheme, the NE39BTS is modified so that conventional generators are replaced at Nodes 30, 32, and 36 with multiple solar plants with a rated output of 330 MVA, 660 MVA, and 550 MVA, respectively, as depicted in Fig. 9.

An electrical controls module, a plant controller, and a grid interface module for solar PV plant is utilized from the research (Tang et al., 2013). At the plant level, the Plant Controller emulates var/volt control through the utilization of voltage and reactive power output, while active power control is followed by frequency and active power output. For the electric control model to provide feedback in the form of generated power and terminal voltage, the power output serves as a reference for actual and reactive current. The grid interface module processes and infuses actual and reactive current into the grid through the utilization of these currents. PV inverters’ response to voltage drops caused by grid disturbances is manifested by their fault ride through capability, which enables them to recover active power more quickly.

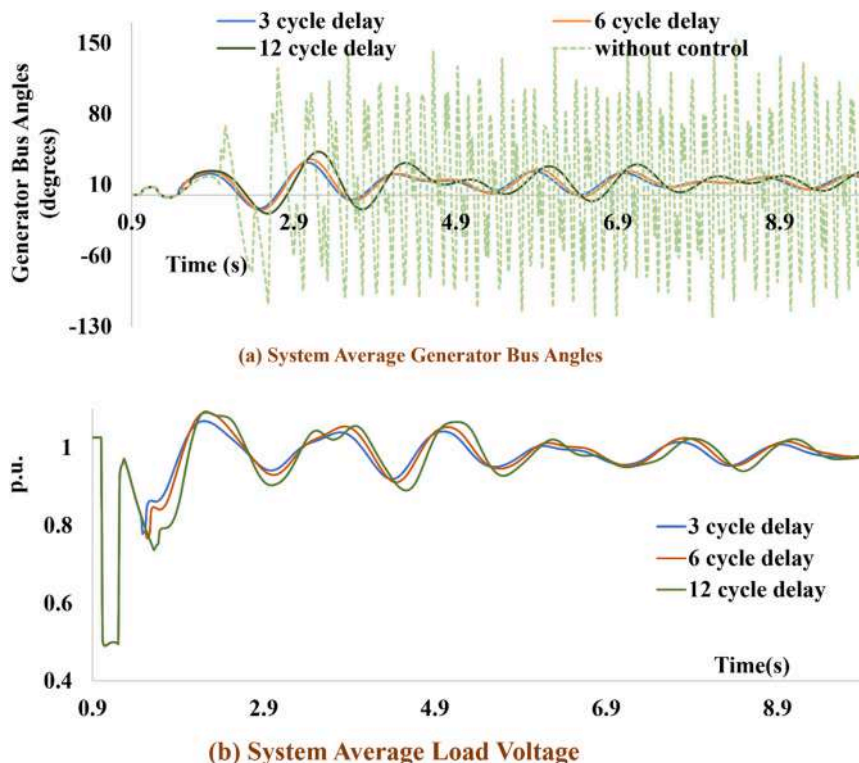


Fig. 8. Impact of additional delay: Illustrative Example I.

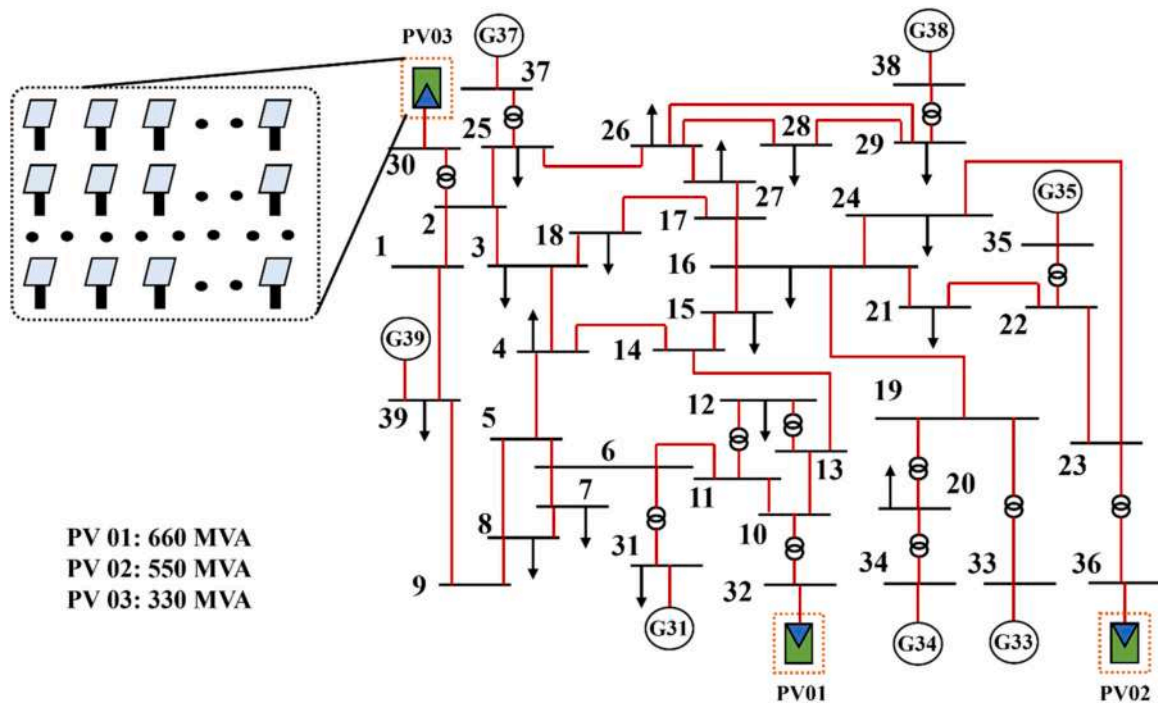


Fig. 9. NE39BTS with PV penetration.

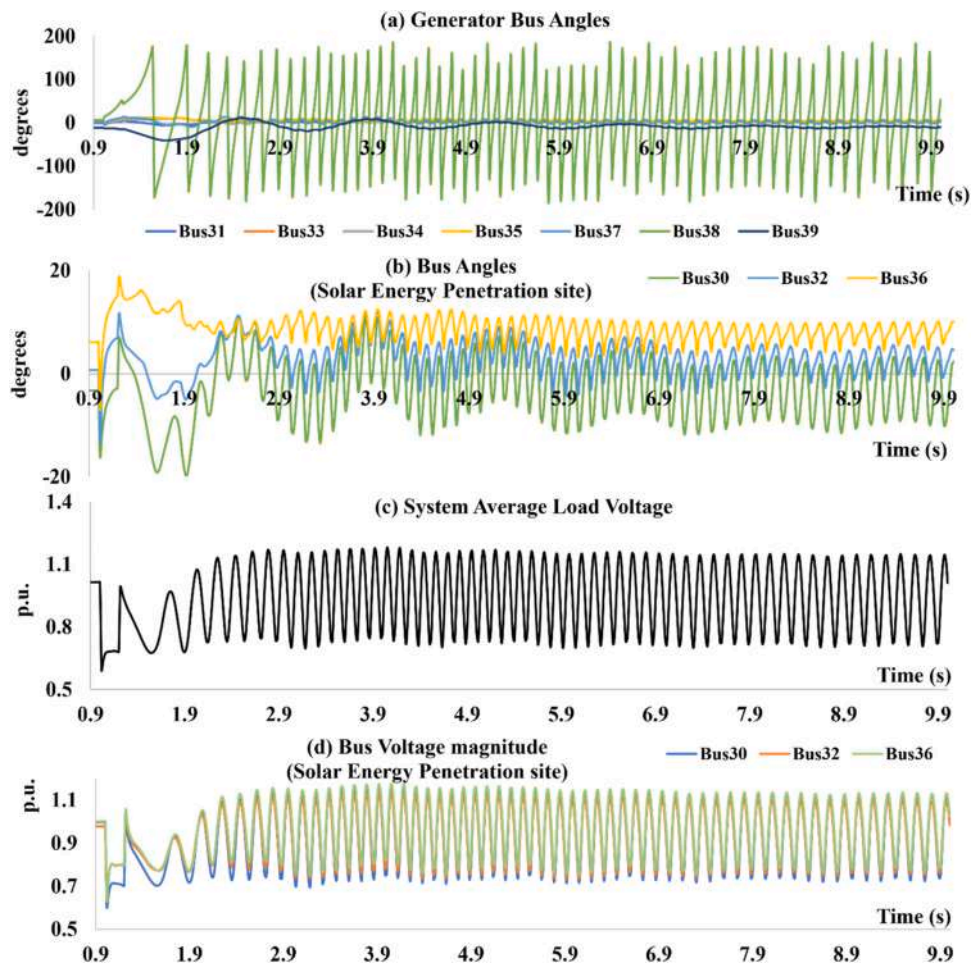


Fig. 10. Response of system without composite scheme: Example II.

Table 3
Illustrative Example II: Emergency Remedial Scheme.

Action Type	Actions location	Action magnitude	Time (s)
TSA detection	All Machines	Power Imbalance <i>delP</i>	1.3167
Trip Generator	G 38	830 MW	1.3667
Load Shedding	All Loads	Shed % load with total load shed equal to <i>delP</i>	1.4167

The inverter maintains its connection and keeps supplying the required amount of reactive current while injecting zero real current in the event of a power grid interruption. This study’s control model increases active power recovery capability and other important characteristics, which enhances fault ride through capability. Once solar energy is integrated, the system operates at nominal frequencies of 60 Hz (Chandra and Pradhan, 2021). When integrated by SE at many sites, the updated test system’s emergency control can be facilitated in real-time, as demonstrated in Illustrative Example II.

4.3.1. Example II

With the base case of system Load and SE Penetration: 22.795%, Short Circuit fault at 50% of Line 26–28 applied at time: 1 s, Fault clearing time: 1.2 s by opening Line 26–28.

Example. II demonstrates a successful use of the indicated approach on a SE penetrated test system following a disruption. Fig. 10 depicts the network’s response post-event. Following fault clearance, G38 generator is the more advanced machine compared to other machines; for approximately 1.55 s, it exceeds transient stability limits. The instability is further transmitted to the other machines, resulting in the grid’s collapse. As a result, it is necessary to assess the impending state of instability and implement corrective measures to prevent the system from collapsing. Table 3 summarizes the IE evaluation, post-assessment action type evaluation, action start time, and action amount. It is appropriate to trigger the generator given that generator G38 causes other machines to decelerate more while accelerating more than other generators.

As G38 tripping worsens the power imbalance, a reduction in the load proportional to the imbalance is solicited. The LSI estimates a sufficient amount of load reduction from all loads, based on the power imbalance. Fig. 11 (a) depicts the computed % load shedding distribution across various loads. Additionally, Fig. 11 (b) shows the overall system load before and after a strategy involving active and reactive

components. A 3-cycle delayed generator trip and a 3-cycle (total of six-cycle) delayed load shedding are taken into consideration to account for varying associated delays. The application results shown in Fig. 12 show how the proposed approach may be used successfully to safeguard system stability and enhance grid performance even when SE penetration increases at various locations in the system. The efficacy of the post-emergency control system can be assessed through various indicators, such as voltage magnitude and angles at the conventional machines and solar PV penetration sites.

4.4. Performance assessment of the proposed scheme with available literature

To evaluate the proposal, Table 4 demonstrates its comparison with to state-of-the-art. Solar energy grid penetration, early stability assessment, emergency response scheme, enhanced grid stability characteristics, execution mode, and deployment burden are considered as important attributes. As shown, the proposed approach provides an early evaluation and assesses the action plan for the emergency remedy in real time with computational ease. Furthermore, the approach can be implemented in both conventional and solar-powered grids.

5. Conclusion

In response to rising electricity demand, power grids are preparing to augment the renewable energy integrations in their operations. The higher generation combination compels centralized control centers to monitor and assess vulnerabilities more efficiently. The contributions of the paper for solar PV integrated power grids can be concluded as:

1. Effectively presents a unified technique that first assesses the upcoming instability and then prepares and executes the emergency scheme to maintain system synchronism.
2. The moving average-treated short electrical power data window from the sources is used to assess the probable of system transient instability in the presence of SE and to predict the time of initiation for corrective actions.
3. Depending on the evaluation, a DBC-based remedial scheme is used to sustain transient system stability of SE penetrated power system and improve its grid. The DBC use DAI to evaluate the set of actions including, action location, its type, and its magnitude.

The importance of a coordinated strategy in increasing grid performance even when multiple solar energy farms are present is successfully

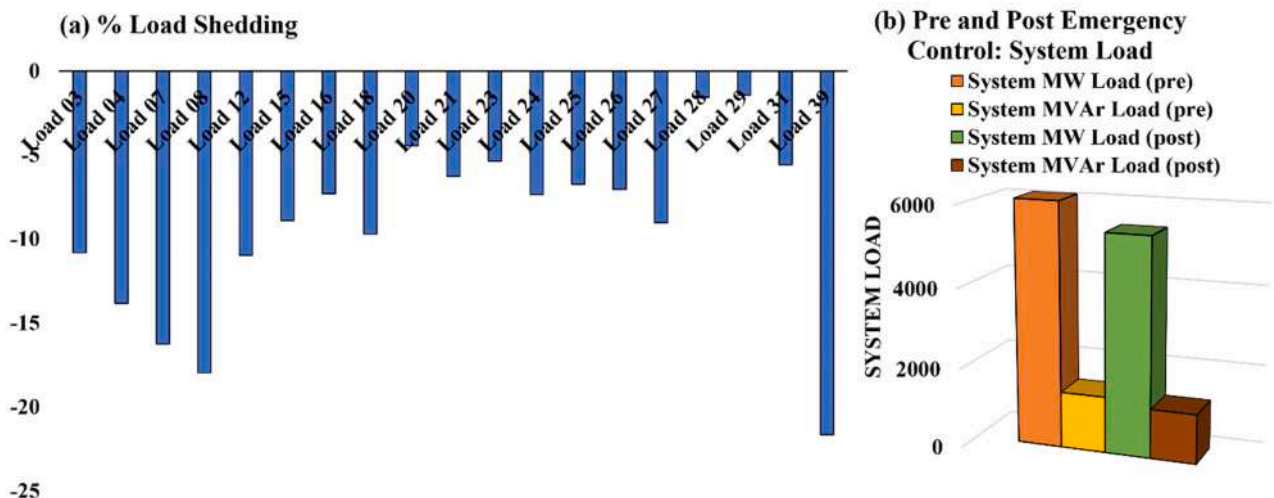


Fig. 11. Load shedding post generation rejection: Example II.

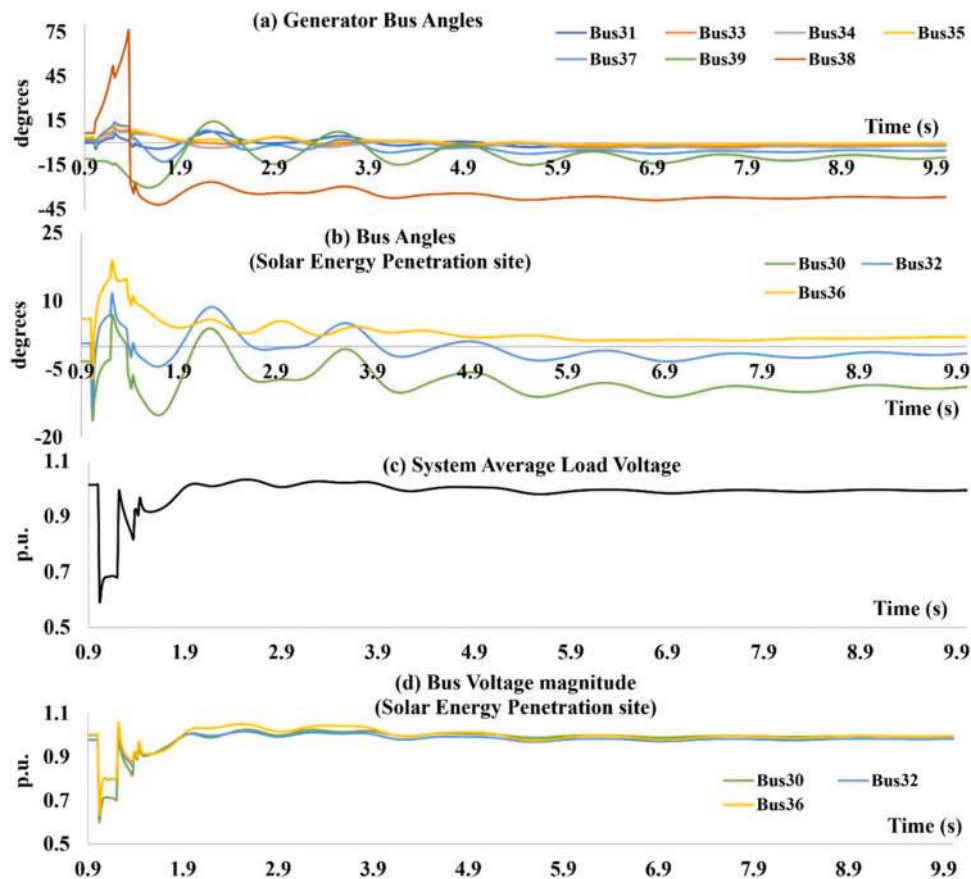


Fig. 12. Proposed DBC implementation: Example II.

Table 4
Performance comparison of proposed work.

Scheme	Solar Energy Penetration	Early Stability Assessment	Type of Emergency Measures	Nature of Enhanced Grid Stability	Type of Execution	Deployment Burden
(Paital et al., 2018)	Yes	No	Not available	Tuned SVC controller based steady state stability enhancement	Offline	Minimum
(Chandra and Pradhan, 2021)	Yes	No	Step wide Load Shedding	Steady State Frequency	Real-Time	Minimum
(Siddiqui et al., 2016)	No	Yes	Generation Shedding and/or Load Shedding	Transient Stability Based	Real-Time	Minimum
Proposed	Yes	Yes	Generation rejection and/or Load Shedding	Transient Stability Based	Real-Time	Minimum

demonstrated by comparing its performance to the available state-of-the-art.

Funding

This research is funded by researchers supporting project at King Saud University, Riyadh, Saudi Arabia, through the project number RSP2023R278.

CRedit authorship contribution statement

Satyendra Singh: Conceptualization, Data curation, Formal analysis, Investigation, Methodology, Resources, Validation, Visualization, Writing – original draft, Writing – review & editing. **Majed A Alotaibi:** Conceptualization, Data curation, Formal analysis, Funding acquisition, Investigation, Methodology, Project administration, Resources, Software, Supervision, Validation, Visualization, Writing – original draft, Writing – review & editing. **Mohammed E. Nassar:** Conceptualization,

Data curation, Formal analysis, Resources, Software, Supervision, Visualization, Writing – original draft, Writing – review & editing. **Hasmat Malik:** Conceptualization, Data curation, Formal analysis, Funding acquisition, Investigation, Methodology, Project administration, Resources, Software, Supervision, Validation, Visualization, Writing – original draft, Writing – review & editing. **Divya Rishi Shrivastava:** Conceptualization, Data curation, Formal analysis, Investigation, Methodology, Validation, Visualization, Writing – original draft, Writing – review & editing. **Shahbaz Ahmed Siddiqui:** Conceptualization, Data curation, Formal analysis, Investigation, Methodology, Software, Validation, Visualization, Writing – original draft, Writing – review & editing. **Kusum Verma:** Conceptualization, Data curation, Formal analysis, Investigation, Methodology, Software, Validation, Visualization, Writing – original draft, Writing – review & editing.

Declaration of Competing Interest

The authors declare that they have no known competing financial interests or personal relationships that could have appeared to influence the work reported in this paper.

Data availability

Data will be made available on request.

Acknowledgements

The authors extend their appreciation to the Researchers Supporting Project at King Saud University, Riyadh, Saudi Arabia, for funding this research work through the project number RSP2023R278 to perform this research. The authors extend their appreciation to the Researchers Supporting Project at Manipal University Jaipur, India, MNIT Jaipur India, Bhartiya Skill Development University Jaipur, India, Universiti Teknologi Malaysia (UTM), Malaysia (UTMFR: Q.J130000.3823.23H05 and UTMER: Q.J130000.3823.31J06), University of Waterloo Canada and Graphic Era (Deemed to be University), India. The authors extend their appreciation to Intelligent Prognostic Private Limited Delhi, India for providing technical support in this research work.

References

- Abbar S.F. and N.-A. Masood, 2023. "An Adaptive Load-Shedding Method for Renewable Integrated Power Systems," International Conference on Power, Instrumentation, Control and Computing (PICC), Thrissur, India, pp. 1–6, DOI: (10.1109/PICC57976.2023.10142566).
- Babu, G.V.N.Y., Sarkar, V., 2020. Transient instability mitigation via repetitive corrective actions based upon the real-time macrocoherency evaluation. *IEEE Syst. J.* 14 (4), 5084–5095.
- Babu, G.V.N.Y., Sarkar, V., 2021. Application of recurrent corrective control for the transient instability mitigation in a synchronous interconnection with multiple control areas. *Electr. Power Syst. Res.* 201, 107520.
- Bekhradian, R., Sanaye-Pasand, M., Mahari, A., 2023. Adaptive wide-area load shedding scheme based on the sink and source concept to preserve power system stability. *IEEE Syst. J.* 17 (1), 503–512. <https://doi.org/10.1109/JSYST.2022.3168541>.
- Bhui, P., Senroy, N., 2017. Real-time prediction and control of transient stability using transient energy function. *IEEE Trans. Power Syst.* 32 (2), 923–934. <https://doi.org/10.1109/TPWRS.2016.2564444>.
- Chandra, A., Pradhan, A.K., 2021. An adaptive underfrequency load shedding scheme in the presence of solar photovoltaic plants. *IEEE Syst. J.* 15 (1), 1235–1244. <https://doi.org/10.1109/JSYST.2020.2995050>.
- Dragomir I.-M. and S.S. Iliescu 2015. "Synchronphasors Applications in Power System Monitoring, Protection and Control," 20th International Conference on Control Systems and Computer Science, Bucharest, Romania, pp. 978–983, DOI: (10.1109/CSCS.2015.66).
- Kang, R., Xu, Y., Dong, Z.Y., et al., 2018. Preventive-corrective demand response to improve short-term voltage stability and transient stability in power systems. *Power Syst. Comput. Conf.* 2018, 1–7.
- Kezunovic, M., Overbye, T.J., 2018. Off the beaten path: resiliency and associated risk. *IEEE Power Energy Mag.* 16 (2), 26–35. <https://doi.org/10.1109/MPE.2017.2780961>.
- Kim, J., Lee, H., et al., 2023. Transient stability assessment using deep transfer learning. *IEEE Access* 11, 116622–116637. <https://doi.org/10.1109/ACCESS.2023.3320051>.
- Kucuktezcan, C.F., Istemihan Genc, V.M., 2015. Preventive and corrective control applications in power systems via Big Bang–Big Crunch optimization. *Int. J. Electr. Power Energy Syst.* 67, 114–124.
- Kumar, D.S., Sharms, A., et al., 2019. Stability implications of bulk power networks with large scale PVs. *Energy* 187. <https://doi.org/10.1016/j.energy.2019.115927>.
- Kuo, S.Y., Chou, Y.H., 2021. Building intelligent moving average-based stock trading system using metaheuristic algorithms. *IEEE Access* 9, 140383–140396. <https://doi.org/10.1109/ACCESS.2021.3119041>.
- Latiki, L., Medjdoub, A., Taib, N., 2022. Critical clearing time, angle for power systems postfault stability assessment. *Period. Polytech. Electr. Eng. Comput. Sci.* 66 (3), 277–285. <https://doi.org/10.3311/PEe.19858>.
- Li, L., Zhu, D., et al., 2023. Review of frequency regulation requirements for wind power plants in international grid codes. *Renew. Sust. Energ. Rev.* 187, 113731 <https://doi.org/10.1016/j.rser.2023.113731>.
- Li, X., Liu, C., et al., 2022. Deep learning-based transient stability assessment framework for large-scale modern power system. *Int. J. Electr. Power Energy Syst.* 139, 108010 <https://doi.org/10.1016/j.ijepes.2022.108010>.
- Liu, X., Zhang, X., et al., 2020. Data-driven transient stability assessment model considering network topology changes via mahalanobis kernel regression and ensemble learning. *J. Mod. Power Syst. Clean. Energy* 8 (6), 1080–1091. <https://doi.org/10.35833/MPCE.2020.000341>.
- Mehrabi, K., Golshannavaz, S., Afsharnia, S., 2019. An improved adaptive wide-area load shedding scheme for voltage and frequency stability of power systems. *Energy Syst.* 10, 821–842. <https://doi.org/10.1007/s12667-018-0293-9>.
- Mochamad, R.F., Preece, R., Hasan, K.N., 2022. Probabilistic multi-stability operational boundaries in power systems with high penetration of power electronics. *Int. J. Electr. Power Energy Syst.* 135, 107382 <https://doi.org/10.1016/j.ijepes.2021.107382>.
- Paital, S.R., Ray, P.K., et al., 2018. Stability improvement in solar PV integrated power system using quasi-differential search optimized SVC controller. *Optik* 170, 420–430. <https://doi.org/10.1016/j.ijleo.2018.05.097>.
- Shi, F., Zhang, H., Cao, Y., et al., 2019. Enhancing event-driven load shedding by corrective switching with transient security and overload constraints. *IEEE Access* 7, 101355–101365.
- Shi, Z., Yao, W., et al., 2020. Convolutional neural network-based power system transient stability assessment and instability mode prediction. *Appl. Energy* 263, 114586. <https://doi.org/10.1016/j.apenergy.2020.114586>.
- Shrestha, A., González-Longatt, F., 2021. Parametric sensitivity analysis of rotor angle stability indicators. *Energies* 14 (16), 5023. <https://doi.org/10.3390/en14165023>.
- Shrivastava, D.R., Siddiqui, S.A., Verma, K., 2021. Model free robust real-time severity analyser using PMU measurements. *Int. J. Electr. Power Energy Syst.* 133 <https://doi.org/10.1016/j.ijepes.2021.107333>.
- Siddiqui, S.A., Verma, K., et al., 2016. A unified control scheme for power system transient stability enhancement through preventive and emergency control. *Int. Trans. Electr. Eng. Syst.* 26 (2), 365–383. <https://doi.org/10.1002/etep.2086>.
- Tang, B., Yang, J., et al., 2020. Spatial-temporal adaptive transient stability assessment for power system under missing data. *Int. J. Electr. Power Energy Syst.* 123, 106237 <https://doi.org/10.1016/j.ijepes.2020.106237>.
- Tang, J., Liu, J., et al., 2013. Adaptive load shedding based on combined frequency and voltage stability assessment using synchrophasor measurements. *IEEE Trans. Power Syst.* 28 (2), 2035–2047. <https://doi.org/10.1109/TPWRS.2013.2241794>.
- Tuglie, E.D., Dicorato, M., Scala, M.L., et al., 2000. A corrective control for angle and voltage stability enhancement on the transient time-scale. *IEEE Trans. Power Syst.* 15 (4), 1345–1353.
- Xie, L., Zheng, X., et al., 2023. Massively digitized power grid: opportunities and challenges of use-inspired AI. *Proc. IEEE* 111 (7), 762–787. <https://doi.org/10.1109/JPROC.2022.3175070>.
- Yuan, H., Xu, Y., 2020. Preventive-corrective coordinated transient stability dispatch of power systems with uncertain wind power. *IEEE Trans. Power Syst.* 35 (5), 3616–3626.
- Zhan, X., Han, S., Rong, N., Cao, Y., 2023. A hybrid transfer learning method for transient stability prediction considering sample imbalance. *Appl. Energy* 333, 120573. <https://doi.org/10.1016/j.apenergy.2022.120573>.



Applications of the Laplace variational iteration method to fractional heat like equations

Alok Bhargava ^a✉, Deepika Jain ^b✉, D.L. Suthar ^c ✉

[Show more](#) ▾

Outline | Share Cite

<https://doi.org/10.1016/j.padiff.2023.100540> ↗

[Get rights and content](#) ↗

Under a Creative Commons [license](#) ↗

open access

Abstract

The importance of differential equations of integer order and fractional order can be seen in many areas of engineering and applied sciences. The present work involves fractional order heat equations that arise in numerous applications of engineering and aims to find series solutions by the Laplace variational iteration method (LVIM). The method combines the Laplace transform and the variational iteration method. To show the efficiency and validity of LVIM, we have exemplarily considered 1-D, 2-D, and 3-D fractional heat equations and solve them by LVIM. Exact solutions are gained in expressions of the Mittag-Leffler function. The results are also explored through graphs and charts.

Previous

Next

Keywords

1. Introduction

Fractional calculus can be used to present facts and deeper aspects in different fields such as Physics, Chemistry, Engineering, and other fields of applied science and applied mathematics. From a theoretical and practical point of view, the region presents several fundamental problems¹ and the recent developments as well as its applications.[2], [3], [4] Like the parental importance, the fractional differential equations have many applications in different streams of engineering and applied sciences. The significance of these equations can demonstrate non-linear oscillation of earthquake, electromagnetism, electrochemistry, acoustics, signal processing, diffusion processes[5], [6], [7] and many other areas. Some very recent work presented by Mastoi et al.,⁸ Ghanbari⁹ and Djilali and Ghanbari,¹⁰ Yadav et al.,¹¹ Ramani et al.¹² can be referred for the latest update in the field.

The heat equation is a significant partial differential equation, which was developed by Joseph Fourier in 1822. These equation expresses the distribution of heat (or variation of temperature) in a section over time. These equations have reputation in various scientific grounds. It is an ideal parabolic partial differential equation in mathematics and related to the 'Brownian motion' via the Fokker–Planck equation.^{13,14} The diffusion equation is the generalized version of the heat equation, emerges in relation with the learning of chemical diffusion and other processes respectively. The heat equation tells that if a warm body is put in a container of cold water, the body temperature will reduce, and ultimately (after a particular period, and on a condition of no external heat provided) the temperature will reach the state of equilibrium. Authors like Jafari et al.,¹ Yang and Machado,¹⁵ Mastoi et al.,⁸ Rüländ and Salo,¹⁶ and Mamun et al.¹⁷ are in the list those have contributed their concerned work in the field.

For the current issue, we take into consideration the following fractional heat equations with variable coefficients:

$$D_{\tau}^{\vartheta} u = F(\alpha, \beta, \gamma) \frac{\partial^2 u}{\partial \alpha^2} + G(\alpha, \beta, \gamma) \frac{\partial^2 u}{\partial \beta^2} + H(\alpha, \beta, \gamma) \frac{\partial^2 u}{\partial \gamma^2} \quad , \quad (1.1)$$
$$0 < \vartheta \leq 1$$

with the initial conditions

$$u(\alpha, \beta, \gamma, 0) = h(\alpha, \beta, \gamma), \quad u_t(\alpha, \beta, \gamma, 0) = m(\alpha, \beta, \gamma). \quad (1.2)$$

An analytical approach that is more powerful than the traditional variational technique is named as "Variational iteration method" (VIM), which was initially recommended by

He.¹⁸ The “Laplace variational iteration method” (LVIM) is a combination of the “Laplace transform” and “variational iteration method”. Applications of VIM to fractional differential equations are slow to converge, mainly because they directly use the Lagrange multipliers of ordinary differential equations (ODEs).¹⁹ Wu and Baleanu²⁰ pointed out that it can be difficult to apply integrals by parts of the Riemann–Liouville (RL) integral resulting from the constructed correction function. Zada et al.²¹ established new iterative approach for the solutions of fractional order inhomogeneous partial differential equations. To overcome this shortcoming, they proposed to identify generalized Lagrange multipliers via the Laplace transform. Without the need for linearization, discretization, or perturbation, the LVIM is a form of semi-analytical methodology that can be used with both linear and non-linear equations. This method is better than Finite Difference Method and the Finite Element Method. It is not a time-consuming procedure and provides an accurate and error-free solution quickly. This method has been utilized by many authors to solve several problems.[22], [23], [24] Applying the LVIM to solve heat equations is what makes this study novel, and its approach has also been found to converge rapidly to the exact solution of the fractional heat-like equations.

This approach of the LVIM demonstrates the effectiveness of the method to get the precise and more accurate solution of the exemplary problems considered here. For the future prospects, it may be assumed that observing the solution of the problems discussed here, the LVIM may be used to solve more sensitive problems of science containing ODEs and Fractional differential equations[25], [26], [27] with more precision.

Preliminaries

Definition 1.1

The Caputo derivative²⁸ of random order of the function $u(\alpha, \tau)$ is well-defined as

$$D_{\tau}^{\vartheta} u(\alpha, \tau) = \frac{1}{\Gamma(m-\vartheta)} \int_0^{\tau} (\tau - \delta)^{m-\vartheta-1} u^{(m)}(\alpha, \delta) d\delta = J_{\tau}^{m-\vartheta} D^m u(\alpha, \tau), \quad (1.3)$$

$$(m - 1 < \vartheta \leq m, m \in \mathbb{N}),$$

where $D^{\vartheta} = \frac{d^{\vartheta}}{d\tau^{\vartheta}}$ and $J_{\tau}^{\vartheta}(\cdot)$ displays the Riemann–Liouville integral operator of fractional order,²⁹ $\vartheta > 0$.

$$J_{\tau}^{\vartheta} u(\alpha, \tau) = \frac{1}{\Gamma(\vartheta)} \int_0^{\tau} (\tau - \delta)^{\vartheta-1} u(\alpha, \delta) d\delta, \quad (1.4)$$

$$(\delta > 0, m - 1 < \vartheta \leq m, m \in \mathbb{N}).$$

Definition 1.2

The Laplace Transform³⁰ of $f(\tau)$, $\tau > 0$ is well-defined as

$$\mathcal{L}[f(\tau)] = F(s) = \int_0^{\infty} e^{-s\tau} f(\tau) d\tau. \quad (1.5)$$

Definition 1.3

The Laplace transform of $D_t^\vartheta u(x', t)$ is defined as

$$\begin{aligned} \mathcal{L}[D_\tau^\vartheta u(\alpha, \tau)] &= \mathcal{L}[u(\alpha, \tau)] \\ &- \sum_{n=0}^{m-1} u^n(\alpha, 0) s^{\vartheta-n-1}, (m-1 < \vartheta \leq m, m \in \mathbb{N}). \end{aligned} \quad (1.6)$$

Definition 1.4

The Mittag-Leffler function³¹ is described as

$$E_\vartheta(\tau) = \sum_{n=0}^{\infty} \frac{\tau^n}{\Gamma(\vartheta n + 1)}, \quad (\vartheta \in \mathbb{C}, \Re(\vartheta) > 0). \quad (1.7)$$

$$E_{\vartheta, \theta}(\tau) = \sum_{n=0}^{\infty} \frac{\tau^n}{\Gamma(\vartheta n + \theta)}, \quad (\vartheta, \theta \in \mathbb{C}, \Re(\vartheta) > 0, \Re(\theta) > 0).$$

Variational Iteration Method (VIM)

The VIM recognized by He¹⁸ and it has wide applications to analyse either accurate or aggregate solutions of linear and nonlinear difficulties.[32], [33], [34], [35] The VIM gives the solution in an infinite rapidly convergent series. We deliberate the succeeding equation to demonstrate the perception of VIM:

$$\mathbf{L}u(\alpha, \tau) + \mathbf{N}u(\alpha, \tau) = \mathbf{f}(\alpha, \tau) \quad (1.8)$$

where 'u' is the unknown function, **L** and **N** are linear and nonlinear operators, and **f** is the source term. The correction functional for Eq.(1.8) is given as:

$$u_{n+1}(\alpha, \tau) = u_n(\alpha, \tau) + \int_0^\tau \lambda [Lu_n(\xi, \tau) + Nu_n(\xi, \tau) - f(\xi, \tau)] d\xi \quad (1.9)$$

here ' λ ' is a general Lagrange multiplier that can be found by the variation theory and \check{u}_n is measured as a restricted variation $\delta u_n = 0$.

Laplace Variational Iteration Method (LVIM)

'Laplace Variational Iteration Method' (LVIM) is the mixture of 'Laplace transform' and 'Variational Iteration Method' (VIM). The VIM has recently focused heavily on solving a broad variety of problems, including algebraic, differential, partial-differential, functional-delay, and integral-differential ones. The key component of this method is the construction of a correction functional employing a general Lagrange multiplier that has been carefully chosen so that its adjustment solution is superior to the initial assessment function. The purpose of this work is to broaden the applicability of LVIM to provide convergent answers for fractional differential equations. It is applied by several authors for solving many kinds of difficulties of applied mathematics. For instance, we can see the works of Abassy et al.,²² Hammouch and Mekkaoui,²³ Arife and Yildirim³⁶ etc. Here, in this work, a new approach of Laplace Variational Iteration Method (LVIM) has been

taken under consideration to find the solutions of problems of fractional heat like equations one, two and three dimensions.

We consider the following, a general fractional non-linear non-homogeneous partial differential equation with the initial situations of the system to illustrate the basic terminology of this method,

$$D_{\tau}^{\vartheta} u(\alpha, \tau) + Lu(\alpha, \tau) + Nu(\alpha, \tau) = f(\alpha, \tau), \quad (1.10)$$

$$m - 1 < \vartheta \leq m, m \in \mathbb{N},$$

$$u^n(\alpha, 0) = h_k(\alpha), \quad n = 0, 1, 2, 3, \dots, m - 1, \quad (1.11)$$

where D_{τ}^{ϑ} is the ϑ order fractional Caputo derivative. L, N and f are same as acknowledged with (1.8).

Using Laplace transform¹⁷ on (1.10), we get

$$\mathcal{L}[u(\alpha, \tau)] = \frac{1}{s^{\vartheta}} \sum_{n=0}^{m-1} s^{\vartheta-1-n} u^n(\alpha, 0) + \frac{1}{s^{\vartheta}} \mathcal{L}[f(\alpha, \tau)] \quad (1.12)$$

$$- \frac{1}{s^{\vartheta}} \mathcal{L}[Lu(\alpha, \tau) + Nu(\alpha, \tau)],$$

taking inverse Laplace transform, we have

$$u(\alpha, \tau) = \mathcal{L}^{-1} \left[\frac{1}{s^{\vartheta}} \sum_{n=0}^{m-1} s^{\vartheta-1-n} u^n(\alpha, 0) + \frac{1}{s^{\vartheta}} \mathcal{L}[f(\alpha, \tau)] \right] \quad (1.13)$$

$$- \mathcal{L}^{-1} \left[\frac{1}{s^{\vartheta}} \mathcal{L}[Lu(\alpha, \tau) + Nu(\alpha, \tau)] \right],$$

by differentiating (1.13), concerning τ , we get

$$\frac{\partial u(\alpha, \tau)}{\partial \tau} = \frac{\partial}{\partial t} \left\{ \mathcal{L}^{-1} \left[\frac{1}{s^{\vartheta}} \sum_{n=0}^{m-1} s^{\vartheta-1-n} u^n(\alpha, 0) + \frac{1}{s^{\vartheta}} \mathcal{L}[f(\alpha, \tau)] \right] \right. \quad (1.14)$$

$$\left. - \mathcal{L}^{-1} \left[\frac{1}{s^{\vartheta}} \mathcal{L}[Lu(\alpha, \tau) + Nu(\alpha, \tau)] \right] \right\},$$

the above way has been adopted to be able to design the correction functional for (1.14) as

$$u_{n+1}(\alpha, \tau) = u_n(\alpha, \tau) \quad (1.15)$$

$$+ \int_0^{\tau} \lambda \left[\frac{\partial u_n(\alpha, \varepsilon)}{\partial \varepsilon} - \frac{\partial}{\partial \varepsilon} \left\{ \mathcal{L}^{-1} \left[\frac{1}{s^{\vartheta}} \sum_{n=0}^{m-1} s^{\vartheta-1-n} u^n(\alpha, 0) + \frac{1}{s^{\vartheta}} \mathcal{L}[f(\alpha, \tau)] \right] \right. \right.$$

$$\left. \left. - \mathcal{L}^{-1} \left[\frac{1}{s^{\vartheta}} \mathcal{L}[Lu(\alpha, \varepsilon) + Nu(\alpha, \varepsilon)] \right] \right\} \right] d\varepsilon.$$

By variation theory, λ for (1.15) can be obtained as

$$1 + \lambda|_{\varepsilon=\tau} = 0,$$

So,

$$\lambda = -1.$$

From (1.15), we get

$$\begin{aligned} u_{n+1}(\alpha, \tau) &= u_n(\alpha, \tau) \\ &- \int_0^\tau \left[\frac{\partial u_n(\alpha, \varepsilon)}{\partial \varepsilon} - \frac{\partial}{\partial \varepsilon} \left\{ \mathcal{L}^{-1} \left[\frac{1}{s^\vartheta} \sum_{n=0}^{m-1} s^{\vartheta-1-n} u^n(\alpha, 0) + \frac{1}{s^\vartheta} \mathcal{L}[f(\alpha, \tau)] \right] \right. \right. \\ &\left. \left. - \mathcal{L}^{-1} \left[\frac{1}{s^\vartheta} \mathcal{L}[Lu(\alpha, \varepsilon) + Nu(\alpha, \varepsilon)] \right] \right\} \right] d\varepsilon \quad ; n = 0, 1, 2, \dots \end{aligned}$$

start with the preliminary iteration

$$u_0(\alpha, \tau) = u(\alpha, 0) + \tau u_\tau(\alpha, 0).$$

The exact solution will be given as

$$u(\alpha, \tau) = \lim_{n \rightarrow \infty} u_n(\alpha, \tau) \quad .$$

2. Main results

Applications of LVIM for Solving fractional heat-like equations

In this section, we consider three fractional heat like equations of one dimension (1-D), two dimensions (2-D) and three dimensions (3-D) respectively and find their solutions with the approach of LVIM. These exemplary problems are of high importance in Thermal engineering, Mechanical engineering, Chemical engineering, and various fields of Thermal Physics and Chemistry.

Further, the numerical and graphical discussion of the obtained results are also presented to highlight the behaviour of the solutions of the differential equations.

Problem 1

Let us examine the given one-dimensional fractional heat-like equation

$$D_t^\vartheta u(\alpha, \tau) = \frac{1}{2} \alpha^2 \frac{\partial^2 u}{\partial \alpha^2} \quad ; 0 < \vartheta \leq 1, \quad (2.1)$$

with the initial condition

$$u(\alpha, 0) = \alpha^2. \quad (2.2)$$

Solution: Taking the Laplace transform of (2.1) and using the condition (2.2), we obtain

$$\mathcal{L}[u(\alpha, \tau)] = \frac{\alpha^2}{s} + \frac{1}{2s^\vartheta} x'^2 \mathcal{L} \left[\frac{\partial^2 u}{\partial \alpha^2} \right], \quad (2.3)$$

applying inverse Laplace transform to (2.3), we get

$$u(\alpha, \tau) = \alpha^2 + \mathcal{L}^{-1} \left[\frac{1}{2s^\vartheta} x^2 \mathcal{L} \left[\frac{\partial^2 u}{\partial \alpha^2} \right] \right], \quad (2.4)$$

differentiating (2.4) concerning t , we have

$$\frac{\partial u}{\partial \tau} = \frac{\partial}{\partial \tau} \mathcal{L}^{-1} \left[\frac{1}{2s^\vartheta} \alpha^2 \mathcal{L} \left[\frac{\partial^2 u}{\partial \alpha^2} \right] \right], \quad (2.5)$$

the correction functional for (2.5) with $\lambda = -1$ is given by

$$u_{n+1}(\alpha, \tau) = u_n(\alpha, \tau) - \int_0^\tau \left[\frac{\partial u_n(\alpha, \varepsilon)}{\partial \varepsilon} - \frac{\partial}{\partial \varepsilon} \mathcal{L}^{-1} \left\{ \frac{1}{2s^\vartheta} \alpha^2 \mathcal{L} \left(\frac{\partial^2 u_n}{\partial \alpha^2} \right) \right\} \right] d\varepsilon.$$

The initial iteration is

$$u_0(\alpha, \tau) = u_0(\alpha, 0) = \alpha^2, \quad (2.6)$$

then, we have

$$u_1(\alpha, \tau) = u_0(\alpha, \tau) - \int_0^\tau \left[\frac{\partial u_0(\alpha, \varepsilon)}{\partial \varepsilon} - \frac{\partial}{\partial \varepsilon} \mathcal{L}^{-1} \left\{ \frac{1}{2s^\vartheta} \alpha^2 \mathcal{L} \left(\frac{\partial^2 u_0}{\partial \alpha^2} \right) \right\} \right] d\varepsilon, \quad (2.7)$$

$$u_1(\alpha, \tau) = \alpha^2 + \alpha^2 \frac{\tau^\vartheta}{\Gamma(\vartheta+1)}, \quad (2.8)$$

$$u_2(\alpha, \tau) = u_1(\alpha, \tau) - \int_0^\tau \left[\frac{\partial u_1(\alpha, \varepsilon)}{\partial \varepsilon} - \frac{\partial}{\partial \varepsilon} \mathcal{L}^{-1} \left\{ \frac{1}{2s^\vartheta} \alpha^2 \mathcal{L} \left(\frac{\partial^2 u_1}{\partial \alpha^2} \right) \right\} \right] d\varepsilon \quad (2.9)$$

$$u_2(\alpha, \tau) = \alpha^2 + \alpha^2 \frac{\tau^\vartheta}{\Gamma(\vartheta+1)} + \alpha^2 \frac{\tau^{2\vartheta}}{\Gamma(2\vartheta+1)}, \quad (2.10)$$

then the term given below in the successive approximation is

$$u_n(\alpha, \tau) = \alpha^2 \left[1 + \frac{\tau^\vartheta}{\Gamma(\vartheta+1)} + \frac{\tau^{2\vartheta}}{\Gamma(2\vartheta+1)} + \frac{\tau^{3\vartheta}}{\Gamma(3\vartheta+1)} \cdots \right]. \quad (2.11)$$

Therefore, the solution is given by

$$u(\alpha, \tau) = \lim_{n \rightarrow \infty} u_n(\alpha, \tau) = \alpha^2 E_\vartheta(\tau^\vartheta), \quad (2.12)$$

where $E_\vartheta(\cdot)$, is the well-known Mittag-Leffler function,²⁷ defined in (1.7).

Special Case

Letting $\vartheta = 1$, then

$$u(\alpha, \tau) = \alpha^2 E_1(\tau^1) = \alpha^2 e^\tau.$$

Numerical and Graphical discussion for Problem 1.

In this part we found a record for numerical explanation of Eq.(2.11) and plot some graphs for different values of $\vartheta = 0.25, 0.5, 0.75, 1$ (see Table 1, Table 2, Table 3, Table 4).

Figs. 1, 2, 3, and 4 show the estimated solution of Eq.(2.1) for different fix standards of ϑ and shows the exponential behaviour of the solution.

Table 1. For fix $\vartheta = 0.25$.

τ	$\alpha = 1$	$\alpha = 3$	$\alpha = 5$	$\alpha = 7$	$\alpha = 9$
0	1	9	25	49	81
2	5.737677	51.639095	143.441931	281.146185	464.751857
4	7.894520	71.050685	197.363015	386.831509	639.456169
6	9.661923	86.957309	241.548082	473.434241	782.615787
8	11.222737	101.004635	280.568430	549.914123	909.041714
10	12.648798	113.839182	316.219951	619.791104	1024.552642

Table 2. For fix $\vartheta = 0.5$.

τ	$\alpha = 1$	$\alpha = 3$	$\alpha = 5$	$\alpha = 7$	$\alpha = 9$
0	1	9	25	49	81
2	26.893845	60.511151	168.086532	329.449602	544.600364
4	53.099122	119.473025	331.869514	650.464247	1075.257225
6	83.279063	187.377893	520.494149	1020.16853	1686.401044
8	116.852302	262.917679	730.326888	1431.440702	2366.259119
10	153.426279	345.209128	958.914244	1879.471919	3106.882153

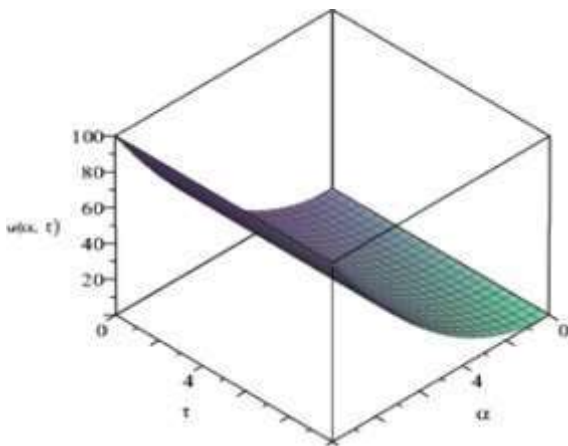
Table 3. For fix $\vartheta = 0.75$.

	1	3	5	7	9
0	1	9	25	49	81
2	27.294236	61.412032	170.588978	334.354398	552.708290
4	75.8864748	170.744568	474.290468	929.609317	1536.701116

τ	$\alpha = 1$	$\alpha = 3$	$\alpha = 5$	$\alpha = 7$	$\alpha = 9$
6	153.315341	344.959518	958.220884	1878.112934	3104.635665
8	261.677129	588.773541	1635.482059	3205.544836	5298.961871
10	402.654942	905.973621	2516.593392	4932.523048	8153.762590

Table 4. For fix $\vartheta = 1$.

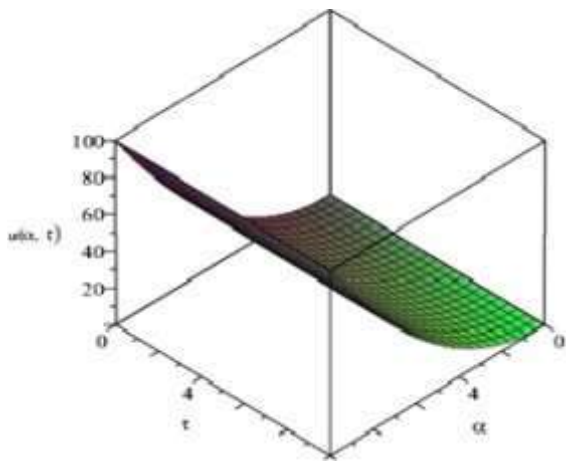
τ	$\alpha = 1$	$\alpha = 3$	$\alpha = 5$	$\alpha = 7$	$\alpha = 9$
0	1	9	25	49	81
2	25.33	57	158.33	310.33	513
4	94.66	213	591.66	1159.66	1917
6	244	549	1525	2989	4941
8	504.33	1137	3158.33	6190.33	10233
10	910.66	2049	5691.66	11155.66	18441



[Download: Download high-res image \(166KB\)](#)

[Download: Download full-size image](#)

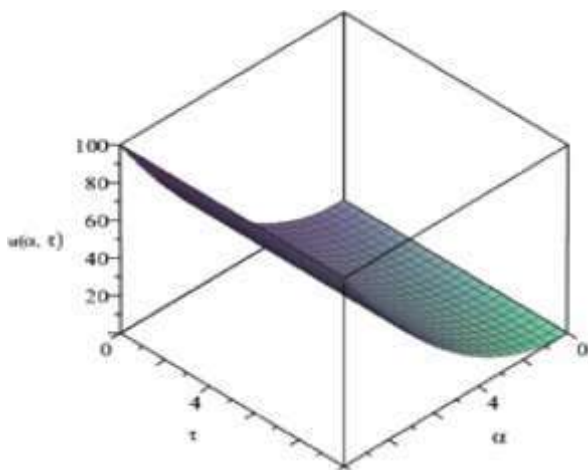
Fig. 1. $\vartheta = 0.25$.



[Download: Download high-res image \(174KB\)](#)

[Download: Download full-size image](#)

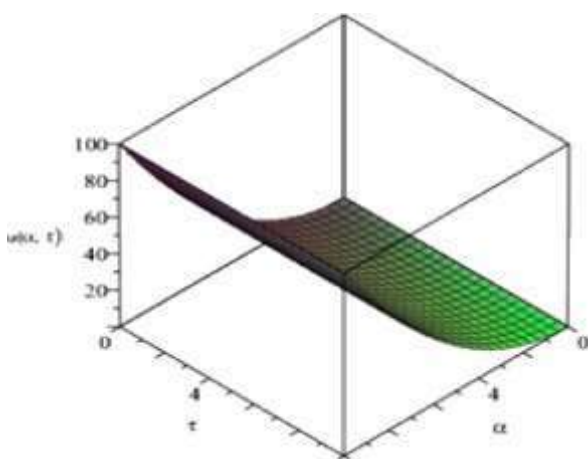
Fig. 2. $\vartheta = 0.5$.



[Download: Download high-res image \(170KB\)](#)

[Download: Download full-size image](#)

Fig. 3. $\vartheta = 0.75$.



[Download: Download high-res image \(175KB\)](#)

[Download: Download full-size image](#)

Fig. 4. $\vartheta = 1$.

Problem 2

Let us examine the given two-dimensional fractional heat-like equation

$$D_{\tau}^{\vartheta} u(\alpha, \beta, \tau) = \frac{\partial^2 u}{\partial \alpha^2} + \frac{\partial^2 u}{\partial \beta^2}, \quad 0 < \vartheta \leq 1, \quad (2.13)$$

with initial condition

$$u(\alpha, \beta, 0) = \sin \alpha \sin \beta. \quad (2.14)$$

Solution: Taking the Laplace transform of (2.13) and using the condition specified by (2.14), we find,

$$\mathcal{L}[u(\alpha, \beta, \tau)] = \frac{\sin \alpha \sin \beta}{s} + \frac{1}{s^{\vartheta}} \mathcal{L} \left[\frac{\partial^2 u}{\partial \alpha^2} + \frac{\partial^2 u}{\partial \beta^2} \right], \quad (2.15)$$

applying inverse Laplace transform, we have

$$u(\alpha, \beta, \tau) = \sin \alpha \sin \beta + \mathcal{L}^{-1} \left[\frac{1}{s^{\vartheta}} \mathcal{L} \left[\frac{\partial^2 u}{\partial \alpha^2} + \frac{\partial^2 u}{\partial \beta^2} \right] \right], \quad (2.16)$$

differentiating (2.16) concerning τ , we have

$$\frac{\partial u}{\partial \tau} = \frac{\partial}{\partial \tau} \mathcal{L}^{-1} \left[\frac{1}{s^{\vartheta}} \mathcal{L} \left[\frac{\partial^2 u}{\partial \alpha^2} + \frac{\partial^2 u}{\partial \beta^2} \right] \right]. \quad (2.17)$$

The correction functional for (2.17) with $\lambda = -1$ is given by

$$u_{n+1}(\alpha, \beta, \tau) = u_n(x', y', \tau) - \int_0^{\tau} \left[\frac{\partial u_n(\alpha, \beta, \epsilon)}{\partial \epsilon} - \frac{\partial}{\partial \epsilon} \mathcal{L}^{-1} \left\{ \frac{1}{s^{\vartheta}} \mathcal{L} \left(\frac{\partial^2 u_n}{\partial \alpha^2} + \frac{\partial^2 u_n}{\partial \beta^2} \right) \right\} \right] d\epsilon. \quad (2.18)$$

The initial iteration

$$u_0(\alpha, \beta, \tau) = u_0(\alpha, \beta, 0) = \sin \alpha \sin \beta, \quad (2.19)$$

then, we have

$$u_1(\alpha, \beta, \tau) = u_0(\alpha, \beta, \tau) - \int_0^{\tau} \left[\frac{\partial u_0(\alpha, \beta, \epsilon)}{\partial \epsilon} - \frac{\partial}{\partial \epsilon} \mathcal{L}^{-1} \left\{ \frac{1}{s^{\vartheta}} \mathcal{L} \left(\frac{\partial^2 u_0}{\partial \alpha^2} + \frac{\partial^2 u_0}{\partial \beta^2} \right) \right\} \right] d\epsilon \quad (2.20)$$

$$u_1(\alpha, \beta, \tau) = \sin \alpha \sin \beta - 2 \sin \alpha \sin \beta \frac{\tau^{\vartheta}}{\Gamma(\vartheta+1)}, \quad (2.21)$$

$$u_2(\alpha, \beta, \tau) = u_1(\alpha, \beta, \tau) - \int_0^{\tau} \left[\frac{\partial u_1(\alpha, \beta, \epsilon)}{\partial \epsilon} - \frac{\partial}{\partial \epsilon} \mathcal{L}^{-1} \left\{ \frac{1}{s^{\vartheta}} \mathcal{L} \left(\frac{\partial^2 u_1}{\partial \alpha^2} + \frac{\partial^2 u_1}{\partial \beta^2} \right) \right\} \right] d\epsilon \quad (2.22)$$

$$u_2(\alpha, \beta, \tau) = \sin\alpha \sin\beta - 2\sin\alpha \sin\beta \frac{\tau^\vartheta}{\Gamma(\vartheta+1)} + 4\sin\alpha \sin\beta \frac{\tau^{2\vartheta}}{\Gamma(2\vartheta+1)}, \quad (2.23)$$

then the term given below in the successive approximation is

$$u_n(\alpha, \beta, \tau) = \sin\alpha \sin\beta \left[1 + \frac{(-2\tau^\vartheta)}{\Gamma(\vartheta+1)} + \frac{(-2\tau^\vartheta)^2}{\Gamma(2\vartheta+1)} + \frac{(-2\tau^\vartheta)^3}{\Gamma(3\vartheta+1)} \dots \right]. \quad (2.24)$$

Therefore, the solution is given by

$$u(\alpha, \beta, \tau) = \lim_{n \rightarrow \infty} u_n(\alpha, \beta, \tau) = \sin\alpha \sin\beta E_\vartheta(-2\tau^\vartheta), \quad (2.25)$$

where $E_\vartheta(\cdot)$, is the well-known Mittag-Leffler function.

Special Case

letting $\vartheta = 1$, then

$$u(\alpha, \beta, \tau) = \sin\alpha \sin\beta E_1(-2\tau^1) = e^{-2\tau} \sin\alpha \sin\beta.$$

Numerical and Graphical discussion for Problem 2.

In this part we found a record for numerical explanation of Eq.(2.24) and plot some graphs for different values of $\vartheta = 0.25, 0.5, 0.75, 1$ (see Table 5, Table 6, Table 7, Table 8).

Figs. 5, 6, 7, and 8 show the estimated solution of (2.24) for different standards of ϑ and shows the sine and cosine wave behaviour of the solution.

Table 5. For fix $\vartheta = 0.25$.

τ	$\alpha = 1$	$\alpha = 3$	$\alpha = 5$	$\alpha = 7$	$\alpha = 9$
0	0.174524	0.052335	0.871557	0.121869	0.156434
2	-0.172432	-0.517153	-0.861221	-1.204240	-1.545793
4	-0.309144	-0.927056	-1.543839	-2.158741	-2.771012
6	-0.432256	-1.296243	-2.158651	-3.018429	-3.874529
8	-0.547144	-1.640767	-2.732392	-3.820687	-4.904327
10	-0.656209	-1.967829	-3.277051	-4.582281	-5.881928

Table 6. For fix $\vartheta = 0.5$.

τ	$\alpha = 1$	$\alpha = 3$	$\alpha = 5$	$\alpha = 7$	$\alpha = 9$
0	0.174524	0.052335	0.871557	0.121869	0.156434
2	-0.195695	0.586847	-0.977283	-1.366530	-1.754111
4	-0.622312	-1.866179	-3.107772	-4.345579	-5.578092
6	-1.203769	-3.609841	-6.011515	-8.405865	-10.789974
8	-1.912004	-5.733685	-9.548379	-13.351441	-17.138236
10	-2.730308	-8.187597	-13.634911	-19.06561	-24.47308

Table 7. For fix $\vartheta = 0.75$.

τ	$\alpha = 1$	$\alpha = 3$	$\alpha = 5$	$\alpha = 7$	$\alpha = 9$
0	0.174524	0.052335	0.871557	0.121869	0.156434
2	-0.158411	-0.475041	-0.791092	-1.106179	-1.419918
4	-0.909123	-2.726263	-4.540082	-6.348369	-8.148922
6	-2.442173	-7.323544	-12.195993	-17.053583	-21.89039
8	-4.869943	-14.603897	-24.320058	-34.006588	-43.651687
10	-8.274852	-24.814475	-41.323865	-57.782909	-74.171553

Table 8. For fix $\vartheta = 1$.

τ	$\alpha = 1$	$\alpha = 3$	$\alpha = 5$	$\alpha = 7$	$\alpha = 9$
0	0.174524	0.052335	0.871557	0.121869	0.156434
2	-0.098896	-0.296570	-0.493882	-0.690592	-0.886461
4	-1.052961	-3.157602	-5.258396	-7.352783	-9.438212
6	-3.909339	-11.723254	-19.522886	-27.298732	-35.041320
8	-9.942054	-29.814049	-49.649721	-69.424902	-89.115500
10	-20.110989	-60.308466	-100.432467	-140.434106	-180.264648

Table 9. For fix $\vartheta = 0.25$.

τ	$\alpha = 1$	$\alpha = 3$	$\alpha = 5$	$\alpha = 7$	$\alpha = 9$
0	1	81	625	2401	6561
2	5.737677	464.751857	3586.048285	13776.16309	37644.90047
4	7.8945206	639.456169	4934.075381	18954.74399	51795.94972
6	9.661923	782.615787	6038.702061	23198.27783	63391.87874
8	11.2227372	909.0417147	7014.210761	26945.79205	73632.37889
10	12.648798	1024.552642	7905.498778	30369.76411	82988.76398

Table 10. For fix $\vartheta = 0.5$.

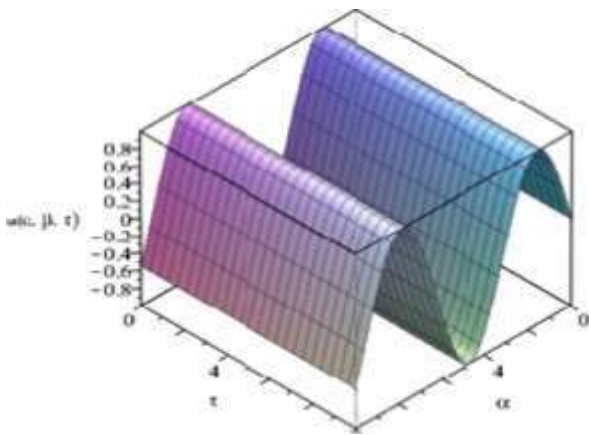
τ	$\alpha = 1$	$\alpha = 3$	$\alpha = 5$	$\alpha = 7$	$\alpha = 9$
0	1	81	625	2401	6561
2	6.723461	544.600364	4202.163303	16143.03054	44112.62948
4	13.274780	1075.257225	8296.737850	31872.74812	87095.83525
6	20.819765	1686.401044	13012.35374	49988.25812	1.365984846 10^5
8	29.213075	2366.259119	18258.17221	70140.59438	1.916669886 10^5
10	38.356569	3106.882153	23972.85612	92094.12405	2.516574544 10^5

Table 11. For fix $\vartheta = 0.75$.

τ	$\alpha = 1$	$\alpha = 3$	$\alpha = 5$	$\alpha = 7$	$\alpha = 9$
0	1	81	625	2401	6561
2	6.885719	557.743276	4303.57466	16532.61242	45177.20538
4	19.0761595	1545.168919	11922.59969	45801.85896	1.251586825 10^5
6	38.4705302	3116.112951	24044.08142	92367.74317	2.504051490 10^5
8	65.5950983	5313.202962	40996.93643	1.574938311 10^5	4.303694400 10^5
10	100.871581	8170.598080	63044.73826	2.421926665 10^5	6.618184444 10^5

Table 12. For fix $\vartheta = 1$.

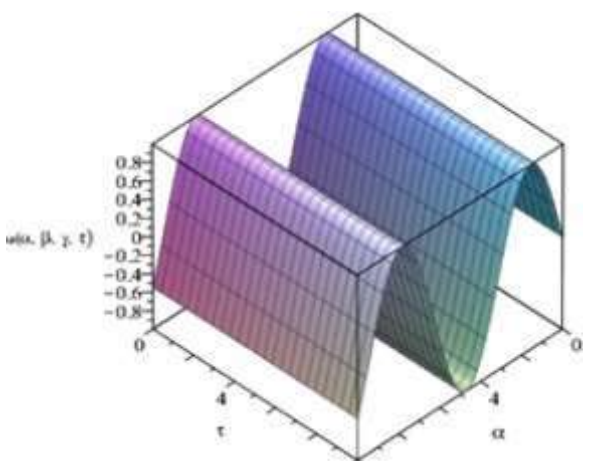
τ	$\alpha = 1$	$\alpha = 3$	$\alpha = 5$	$\alpha = 7$	$\alpha = 9$
0	1	81	625	2401	6561
2	6.3333	513	3958.3333	15206.3333	41553
4	23.6666	1917	14791.6666	56,823.6666	155277
6	61	4941	38125	146461	400221
8	126.3333	10233	78958.3333	303326.3333	828873
10	227.6666	18441	142291.66	546627.66	1493721



[Download: Download high-res image \(233KB\)](#)

[Download: Download full-size image](#)

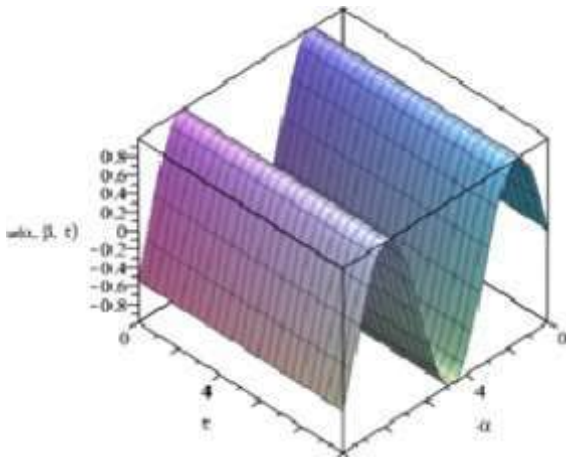
Fig. 5. $\vartheta = 0.25$.



[Download: Download high-res image \(240KB\)](#)

[Download: Download full-size image](#)

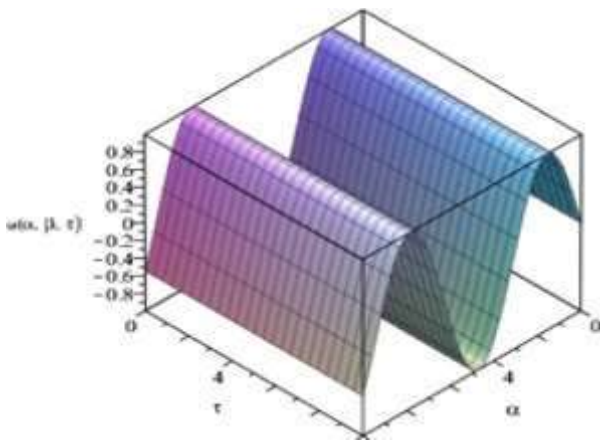
Fig. 6. $\vartheta = 0.5$.



[Download: Download high-res image \(236KB\)](#)

[Download: Download full-size image](#)

Fig. 7. $\vartheta = 0.75$.



[Download: Download high-res image \(239KB\)](#)

[Download: Download full-size image](#)

Fig. 8. $\vartheta = 1$.

Problem 3

Let us examine the given three-dimensional fractional heat-like equation

$$D_{\tau}^{\vartheta} u(\alpha, \beta, \gamma, \tau) = \alpha^4 \beta^4 \gamma^4 + \frac{1}{36} \left[\alpha^2 \frac{\partial^2 u}{\partial \alpha^2} + \beta^2 \frac{\partial^2 u}{\partial \beta^2} + \gamma^2 \frac{\partial^2 u}{\partial \gamma^2} \right], \quad (2.26)$$

$$0 < \vartheta \leq 1,$$

with the initial condition

$$u(\alpha, \beta, \gamma, 0) = 0. \quad (2.27)$$

Solution: Taking the Laplace transform of (2.26) and using the condition specified by (2.27), we find,

$$\mathcal{L}[u(\alpha, \beta, \gamma, \tau)] = \frac{1}{s^\vartheta} \mathcal{L}(\alpha^4 \beta^4 \gamma^4) \quad (2.28)$$

$$+ \frac{1}{36s^\vartheta} \mathcal{L} \left[\alpha^2 \frac{\partial^2 u}{\partial \alpha^2} + \beta^2 \frac{\partial^2 u}{\partial \beta^2} + \gamma^2 \frac{\partial^2 u}{\partial \gamma^2} \right],$$

applying inverse Laplace transform, we get

$$u(\alpha, \beta, \gamma, \tau) = \left[(\alpha^4 \beta^4 \gamma^4) \frac{\tau^\vartheta}{\Gamma(\vartheta+1)} \right] \quad (2.29)$$

$$+ \mathcal{L}^{-1} \left[\frac{1}{36s^\vartheta} \mathcal{L} \left[\alpha^2 \frac{\partial^2 u}{\partial \alpha^2} + \beta^2 \frac{\partial^2 u}{\partial \beta^2} + \gamma^2 \frac{\partial^2 u}{\partial \gamma^2} \right] \right],$$

differentiating (2.29) concerning τ , we have

$$\frac{\partial u}{\partial \tau} = (\alpha^4 \beta^4 \gamma^4) \frac{\vartheta \tau^{\vartheta-1}}{\Gamma(\vartheta+1)} \quad (2.30)$$

$$+ \frac{\partial}{\partial t} \left\{ \mathcal{L}^{-1} \left[\frac{1}{36s^\vartheta} L \left[\alpha^2 \frac{\partial^2 u}{\partial \alpha^2} + \beta^2 \frac{\partial^2 u}{\partial \beta^2} + \gamma^2 \frac{\partial^2 u}{\partial \gamma^2} \right] \right] \right\}.$$

The correction functional for (2.30) with $\lambda = -1$ is given by

$$u_{n+1}(\alpha, \beta, \gamma, \tau) = u_n(\alpha, \beta, \gamma, \tau) - \int_0^\tau \left[\frac{\partial u_n(\alpha, \beta, \gamma, \varepsilon)}{\partial \varepsilon} - (\alpha^2 \beta^2 \gamma^2) \frac{\vartheta \tau^{\vartheta-1}}{\Gamma(\vartheta+1)} \right] \quad (2.31)$$

$$- \frac{\partial}{\partial \varepsilon} \left\{ \mathcal{L}^{-1} \left[\frac{1}{36s^\vartheta} L \left[\alpha^2 \frac{\partial^2 u_n}{\partial \alpha^2} + \beta^2 \frac{\partial^2 u_n}{\partial \beta^2} + \gamma^2 \frac{\partial^2 u_n}{\partial \gamma^2} \right] \right] \right\} d\varepsilon$$

and the initial iteration

$$u_0(\alpha, \beta, \gamma, \tau) = (\alpha^4 \beta^4 \gamma^4) \frac{\tau^\vartheta}{\Gamma(\vartheta+1)}, \quad (2.32)$$

then, we have

$$u_1(\alpha, \beta, \gamma, \tau) = u_0(\alpha, \beta, \gamma, \tau) - \int_0^\tau \left[\frac{\partial u_0(\alpha, \beta, \gamma, \varepsilon)}{\partial \varepsilon} - (\alpha^2 \beta^2 \gamma^2) \frac{\vartheta \tau^{\vartheta-1}}{\Gamma(\vartheta+1)} \right] \quad (2.33)$$

$$- \frac{\partial}{\partial \varepsilon} \left\{ \mathcal{L}^{-1} \left[\frac{1}{36s^\vartheta} \mathcal{L} \left[\alpha^2 \frac{\partial^2 u_0}{\partial \alpha^2} + \beta^2 \frac{\partial^2 u_0}{\partial \beta^2} + \gamma^2 \frac{\partial^2 u_0}{\partial \gamma^2} \right] \right] \right\} d\varepsilon$$

$$u_1(\alpha, \beta, \gamma, \tau) = (\alpha^4 \beta^4 \gamma^4) \frac{\tau^\vartheta}{\Gamma(\vartheta+1)} + (\alpha^4 \beta^4 \gamma^4) \frac{\tau^{2\vartheta}}{\Gamma(2\vartheta+1)}, \quad (2.34)$$

$$u_2(\alpha, \beta, \gamma, \tau) = u_1(\alpha, \beta, \gamma, \tau) - \int_0^\tau \left[\frac{\partial u_1(\alpha, \beta, \gamma, \varepsilon)}{\partial \varepsilon} - (\alpha^2 \beta^2 \gamma^2) \frac{\alpha \tau^{\alpha-1}}{\Gamma(\alpha+1)} \right] \quad (2.35)$$

$$- \frac{\partial}{\partial \varepsilon} \left\{ \mathcal{L}^{-1} \left[\frac{1}{36s^\vartheta} \mathcal{L} \left[\alpha^2 \frac{\partial^2 u_1}{\partial \alpha^2} + \beta^2 \frac{\partial^2 u_1}{\partial \beta^2} + \gamma^2 \frac{\partial^2 u_1}{\partial \gamma^2} \right] \right] \right\} d\varepsilon$$

$$u_2(\alpha, \beta, \gamma, \tau) = (\alpha^4 \beta^4 \gamma^4) \frac{\tau^\vartheta}{\Gamma(\vartheta+1)} + (\alpha^4 \beta^4 \gamma^4) \frac{\tau^{2\vartheta}}{\Gamma(2\vartheta+1)} \quad (2.36)$$

$$+ (\alpha^4 \beta^4 \gamma^4) \frac{\tau^{3\vartheta}}{\Gamma(3\vartheta+1)},$$

then the term given below in the successive approximation is

$$u_n(\alpha, \beta, \gamma, \tau) = (\alpha^4 \beta^4 \gamma^4) \left[\frac{(\tau^\vartheta)}{\Gamma(\vartheta+1)} + \frac{(\tau^\vartheta)^2}{\Gamma(2\vartheta+1)} + \frac{(\tau^\vartheta)^3}{\Gamma(3\vartheta+1)} \dots \right]. \quad (2.37)$$

Therefore, the solution is given by

$$u(\alpha, \beta, \gamma, \tau) = \lim_{n \rightarrow \infty} u_n(\alpha, \beta, \gamma, \tau) = (\alpha^4 \beta^4 \gamma^4) [E_{\vartheta}(\tau^{\vartheta}) - 1], \quad (2.38)$$

here $E_{\vartheta}(\cdot)$, is the well-known Mittag-Leffler function.

Special Case

Letting $\vartheta = 1$, then

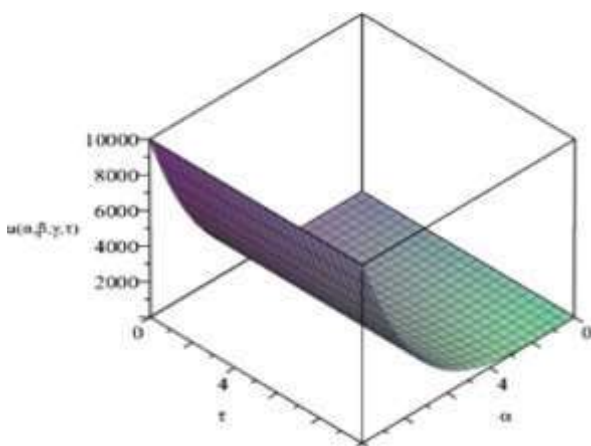
$$u(\alpha, \beta, \gamma, \tau) = (\alpha^4 \beta^4 \gamma^4) [E_1(\tau^1) - 1] = (\alpha^4 \beta^4 \gamma^4)(e^{\tau} - 1). \quad (2.39)$$

Numerical and Graphical discussion for Problem 3.

In this part we found a record for numerical explanation of Eq.(2.37) and plot some graphs for different values of $\vartheta = 0.25, 0.5, 0.75, 1$ (see Table 9, Table 10, Table 11, Table 12).

Figs. 9, 10, 11, and 12 show the estimated solution of Eq.(2.37) for different standards of ϑ and shows the specific exponential behaviour of the solution.

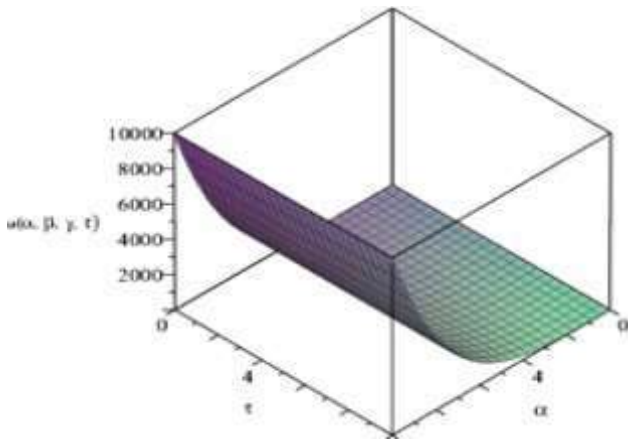
The results obtained in (2.12), (2.25), (2.38) are comparable with the results obtained by Natural transform decomposition method³⁷ and Optimal Homotopy Analysis method³⁸ and are more refined in view of the linearization, discretization, and perturbation, which are not needed in LVIM. Although, due to lack of space, we are not presenting the comparison in this manuscript but for the purpose one may refer.^{37,38}



Download: [Download high-res image \(185KB\)](#)

Download: [Download full-size image](#)

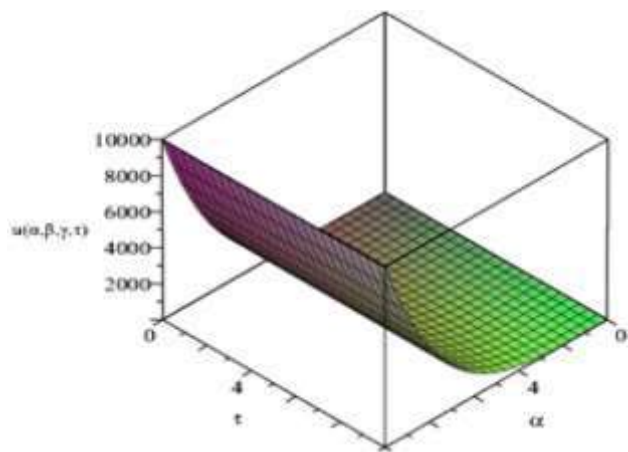
Fig. 9. $\vartheta = 0.25$.



[Download: Download high-res image \(186KB\)](#)

[Download: Download full-size image](#)

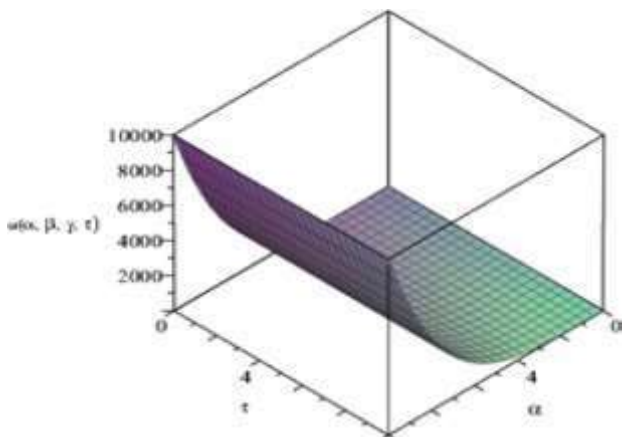
Fig. 10. $\vartheta = 0.5$.



[Download: Download high-res image \(211KB\)](#)

[Download: Download full-size image](#)

Fig. 11. $\vartheta = 0.75$.



[Download: Download high-res image \(188KB\)](#)

[Download: Download full-size image](#)

3. Conclusion

In the presented manuscript, the ‘Laplace variational iteration method’ is effectively implemented for the 1-D, 2-D, and 3-D fractional heat like differential equations, wherever we apply the fractional Caputo derivative. The analytical results in particular have generated in terminologies of a power series that converges to the exact solutions. The graphical consequences of the analysis are also acknowledged. [Fig. 1](#), [Fig. 2](#), [Fig. 3](#), [Fig. 4](#), [Fig. 5](#), [Fig. 6](#), [Fig. 7](#), [Fig. 8](#), [Fig. 9](#), [Fig. 10](#), [Fig. 11](#), [Fig. 12](#) show the behaviour of the estimated solution of the [Problems 1](#), [2](#), and [3](#) respectively with suitable parametric values. The exemplary problems considered here are very popular and important in the domains of Mechanical, Thermal and Chemical engineering, Thermal Physics and chemical reactions. Hence, it is assumed that the results obtained here may be very useful for research and industrial use.

CRedit authorship contribution statement

Alok Bhargava: Creation of the work, Design of the work, Handled the analysis. **Deepika Jain:** Design of the work, Handled the analysis, Conceptualized, Doublechecked the Analysis part. **D.L. Suthar:** Manuscript’s drafting or critical revision for important intellectual content.

Declaration of competing interest

The authors declare that they have no known competing financial interests or personal relationships that could have appeared to influence the work reported in this paper.

Acknowledgements

The authors express their sincere thanks to the reviewers for their careful reading and suggestions that helped to improve this paper. All authors read and approved the final version of manuscript

Funding

No funding was received for conducting this study.

[Special issue articles](#) [Recommended articles](#)


Data availability

No data was used for the research described in the article.

References

- [1] Jafari H., Kadem A., Baleanu D., Yilmaz T.
Solutions of the fractional Davey–Stewartson equations with variational iteration method
Romanian Rep Phys, 64 (2) (2012), pp. 337-346
[View in Scopus ↗](#) [Google Scholar ↗](#)

- [2] Baleanu D., Jajarmi A., Mohammadi H., Rezapour S.
A new study on the mathematical modelling of human liver with Caputo–Fabrizio fractional derivative
Chaos Solitons Fractals, 134 (2020), Article 109705
 [View PDF](#) [View article](#) [View in Scopus ↗](#) [Google Scholar ↗](#)

- [3] Jajarmi A., Baleanu D., Sajjadi S.S., Nieto J.J.
Analysis and some applications of a regularized Ψ –Hilfer fractional derivative
J Comput Appl Math, 415 (2022), Article 114476
 [View PDF](#) [View article](#) [View in Scopus ↗](#) [Google Scholar ↗](#)




- [4] Defterli O., Baleanu D., Jajarmi A., Sajjadi S.S., Alshaikh N., Asad J.H.
Fractional treatment: An accelerated mass–spring system
Romanian Rep Phys, 74 (4) (2022), p. 122
[View in Scopus ↗](#) [Google Scholar ↗](#)

- [5] Debnath L.
Recent applications of fractional calculus to science and engineering
Int J Math Math Sci, 54 (2003), pp. 3413-3442
[View in Scopus ↗](#) [Google Scholar ↗](#)

- [6] Alaria A., Khan A.M., Suthar D.L., Kumar D.
Application of fractional operators in modelling for charge carrier transport in amorphous semiconductor with multiple trapping
Int J Appl Comput Math, 5 (6) (2019), p. 167
[View in Scopus ↗](#) [Google Scholar ↗](#)

- [7] **Advances in Fractional Calculus: Theoretical Developments and Applications in Physics and Engineering**
Springer, Dordrecht (2007)
[Google Scholar ↗](#)

- [8] Mastoi S., Ganie A.H., Saeed A.M., Ali U., Rajput U.A., Othman W.A.M.
Numerical solution for two-dimensional partial differential equations using SM's method
Open Phys, 20 (1) (2022), pp. 142-154
[Crossref ↗](#) [View in Scopus ↗](#) [Google Scholar ↗](#)
- [9] Ghanbari B.
A fractional system of delay differential equation with nonsingular kernels in modeling hand-foot-mouth disease
Adv Differential Equations, 2020 (1) (2020), p. 536
[View in Scopus ↗](#) [Google Scholar ↗](#)
- [10] Djilali S., Ghanbari B.
The influence of an infectious disease on a prey-predator model equipped with a fractional-order derivative
Adv Differential Equations, 2021 (2021), p. 20
[View in Scopus ↗](#) [Google Scholar ↗](#)
- [11] Yadav L.K., Agarwal G., Suthar D.L., Purohit S.D.
Time-fractional partial differential equations: A novel technique for analytical and numerical solutions
Arab J Basic Appl Sci, 29 (1) (2022), pp. 86-98
[Crossref ↗](#) [View in Scopus ↗](#) [Google Scholar ↗](#)
- [12] Ramani P., Khan A.M., Suthar D.L., Kumar D.
Approximate analytical solution for non-linear Fitzhugh–Nagumo equation of time fractional order through fractional reduced differential transform method
J Comput Appl Math, 8 (2) (2022), p. 61
[View in Scopus ↗](#) [Google Scholar ↗](#)
- [13] Welty J., Rorrer G.L., Foster D.G.
Fundamentals of Momentum, Heat, and Mass Transfer
(7th ed.), John Wiley & Sons, New York, NY (2019)
[Google Scholar ↗](#)
- [14] Habenom H., Suthar D.L.
Numerical solution for the time-fractional Fokker–Planck equation via shifted Chebyshev polynomials of the fourth kind
Adv Differential Equations, 2020 (2020), p. 315
[View in Scopus ↗](#) [Google Scholar ↗](#)

- [15] Yang X.J., Machado J.T.
A new fractional operator of variable order: Application in the description of anomalous diffusion
Phys A, 481 (2017), pp. 276-283
 [View PDF](#) [View article](#) [Google Scholar ↗](#)
- [16] Rüländ A., Salo M.
Quantitative approximation properties for the fractional heat equation
Math Control Relat Fields, 10 (1) (2020), pp. 1-26
[Crossref ↗](#) [View in Scopus ↗](#) [Google Scholar ↗](#)
- [17] Mamun A.A., Ali M.S., Miah M.M.
A study on an analytic solution 1D heat equation of a parabolic partial differential equation and implement in computer programming
Int J Sci Eng Res, 9 (9) (2018), pp. 913-921
[Google Scholar ↗](#)
- [18] He J.H.
Variational iteration method-A kind of non-linear analytical technique: Some examples
Int J Non Linear Mech, 34 (4) (1999), pp. 699-708
 [View PDF](#) [View article](#) [View in Scopus ↗](#) [Google Scholar ↗](#)
- [19] He J.H.
Approximate analytical solution for seepage flow with fractional derivatives in porous media
Comput Methods Appl Mech Engrg, 167 (1-2) (1998), pp. 57-68
 [View PDF](#) [View article](#) [View in Scopus ↗](#) [Google Scholar ↗](#)
- [20] Wu G.C., Baleanu D.
Variational iteration method for fractional calculus-a universal approach by Laplace transform
Adv Differential Equations, 2013 (2013), p. 18
[View in Scopus ↗](#) [Google Scholar ↗](#)
- [21] Zada L., Nawaz R., Ahsan S., Nisar K.S., Baleanu D.
New iterative approach for the solutions of fractional order inhomogeneous partial differential equations
AIMS Math, 6 (2) (2021), pp. 1348-1365
[Crossref ↗](#) [View in Scopus ↗](#) [Google Scholar ↗](#)
- [22] Abassy T.A., El-Tawil M.A., El-Zoheiry H.

Exact solutions of some nonlinear partial differential equations using the variational iteration method linked with Laplace transforms and the Padé technique

Comput Math Appl, 54 (7–8) (2007), pp. 940-954

 [View PDF](#) [View article](#) [View in Scopus ↗](#) [Google Scholar ↗](#)

[23] Hammouch Z., Mekkaoui T.

A Laplace-variational iteration method for solving the homogeneous Smoluchowski coagulation equation

Appl Math Sci, 6 (17) (2012), pp. 879-886

[View in Scopus ↗](#) [Google Scholar ↗](#)

[24] Pareek N., Gupta A., Agarwal G., Suthar D.L.

Natural transform along with HPM technique for solving fractional ADE

Adv Math Phys, 2021 (2021), Article 9915183

[View in Scopus ↗](#) [Google Scholar ↗](#)

[25] Baleanu D., Hasanabadi M., Vaziri A.M., Jajarmi A.

A new intervention strategy for an HIV/AIDS transmission by a general fractional modeling and an optimal control approach

Chaos Solitons Fractals, 167 (2023), Article 113078

 [View PDF](#) [View article](#) [View in Scopus ↗](#) [Google Scholar ↗](#)

[26] Baleanu D., Jassim H.K., Khan H.

A modification fractional variational iteration method for solving non-linear gas dynamic and coupled Kdv equations involving local fractional operators

Therm Sci, 22 (Suppl 1) (2018), pp. 165-175

[Crossref ↗](#) [Google Scholar ↗](#)

[27] Jan R., Qureshi S., Boulaaras S., Pham V.T., Hincal E., Guefaifia R.

Optimization of the fractional-order parameter with the error analysis for human immunodeficiency virus under Caputo operator

Discrete Contin Dyn Syst Ser S, 16 (2023)

[Google Scholar ↗](#)

[28] Caputo M.

Elasticità e Dissipazione

Zanichelli, Bologna, Italy (1969)

[Google Scholar ↗](#)

[29] Podlubny I.

Fractional Differential Equations

(1st ed.), Academic Press, San Diego, CA (1998)

[Google Scholar ↗](#)

[30] Schiff J.L.

The Laplace Transform. Theory and Applications

Springer-Verlag, New York, NY (1999)

[Google Scholar ↗](#)

[31] Mittag-Leffler G.M.

On the new function $E_\alpha(x)$

C R Acad Sci Paris, 137 (2) (1903), pp. 554-558

[Google Scholar ↗](#)

[32] He J.H.

An approximation to solution of space and time fractional telegraph equations by the variational iteration method

Math Probl Eng, 2012 (2012), Article 394212

[View in Scopus ↗](#) [Google Scholar ↗](#)

[33] He J.H., Wu X.H.

Variational iteration method: New development and applications

Comput Math Appl, 54 (7–8) (2007), pp. 881-894



[View PDF](#)

[View article](#)

[View in Scopus ↗](#)

[Google Scholar ↗](#)

[34] Khuri S.A., Sayfy A.

A Laplace variational iteration strategy for the solution of differential equations

Appl Math Lett, 25 (12) (2012), pp. 2298-2305



[View PDF](#)

[View article](#)

[View in Scopus ↗](#)

[Google Scholar ↗](#)

[35] Wazwaz A.M.

Partial Differential Equations and Solitary Waves Theory

Springer, Higher Education Press, Berlin, Beijing (2009)

[Google Scholar ↗](#)

[36] Arife A.S., Yildirim A.

New modified variational iteration transform method for solving eighth-order boundary value problems in one step

World Appl Sci J, 13 (10) (2011), pp. 2186-2190

[Google Scholar ↗](#)

[37] Khan H., Shah R., Kumam P., Arif M.

Analytical solutions of fractional-order heat and wave equations by the natural transform decomposition method

Entropy, 21 (6) (2019), p. 597

[Crossref ↗](#) [View in Scopus ↗](#) [Google Scholar ↗](#)

[38] Sarwar S., Alkhalaf S., Iqbal S., Zahid M.A.

A note on optimal homotopy asymptotic method for the solutions of fractional order heat-and wave-like partial differential equations

Comput Math Appl, 70 (5) (2015), pp. 942-953



[View PDF](#)

[View article](#)

[View in Scopus ↗](#)

[Google Scholar ↗](#)

Cited by (4)

[A new solution approach to proportion delayed and heat like fractional partial differential equations](#)

2024, Partial Differential Equations in Applied Mathematics

[Show abstract](#) ✓

[Local fractional Laplace transform method to analyze fractional heat equation](#)

2024, Partial Differential Equations in Applied Mathematics

[Show abstract](#) ✓

[An examination of the flow of magnetohydrodynamic viscous fluid and heat transfer between penetrable disks using the variation iteration method and finite element method](#)

2024, International Journal of Thermofluids

[Show abstract](#) ✓

[Local Fuzzy Fractional Partial Differential Equations in the Realm of Fractal Calculus with Local Fractional Derivatives ↗](#)

2023, Fractal and Fractional



ELSEVIER

All content on this site: Copyright © 2024 Elsevier B.V., its licensors, and contributors. All rights are reserved, including those for text and data mining, AI training, and similar technologies. For all open access content, the Creative Commons licensing terms apply.

 RELX™

A new mobile data collection and mobile charging (MDCMC) algorithm based on reinforcement learning in rechargeable wireless sensor network

Santosh Soni^a, Pankaj Chandra^a, Devendra Kumar Singh^b, Prakash Chandra Sharma^{c,*} and Dinesh Saini^d

^aDepartment of Information Technology, Guru Ghasidas Vishwavidyalaya (Central University), Bilaspur, India

^bDepartment of Computer Science & Engineering, Guru Ghasidas Vishwavidyalaya (Central University), Bilaspur, India

^cDepartment of Information Technology, Manipal University Jaipur, Jaipur, India

^dDepartment of Computer Communication Engineering, Manipal University Jaipur, Jaipur, India

Abstract. Recent research emphasized the utilization of rechargeable wireless sensor networks (RWSNs) in a variety of cutting-edge fields like drones, unmanned aerial vehicle (UAV), healthcare, and defense. Previous studies have shown mobile data collection and mobile charging should be separately. In our paper, we created an novel algorithm for mobile data collection and mobile charging (MDCMC) that can collect data as well as achieves higher charging efficiency rate based upon reinforcement learning in RWSN. In first phase of algorithm, reinforcement learning technique used to create clusters among sensor nodes, whereas, in second phase of algorithm, mobile van is used to visit cluster heads to collect data along with mobile charging. The path of mobile van is based upon the request received from cluster heads. Lastly, we made the comparison of our proposed new MDCMC algorithm with the well-known existing algorithms RLLO [32] & RL-CRC [33]. Finally, we found that, the proposed algorithm (MDCMC) is effectively better collecting data as well as charging cluster heads.

Keywords: Mobile sink, mobile charger, charging efficiency, reinforcement learning, rechargeable wireless sensor node, mobile data collection and mobile charging

1. Introduction

The Rechargeable Wireless Sensor Network (RWSN) is a mixture of multiple sensors used for monitoring purpose along with sensed data collection in mesh environment. Generally, sensors sense the data and route to sink/end user through direct or

in hop manner. The RWSNs uses rechargeable battery when compared to traditional WSN. Now it is possible to charge these batteries in remote location also. The data collection model along with mobile charging is really needed of the time. The data collection model used to work traditionally (single hop & multi-hop) along with newly deployed techniques like mobile data collection based upon mobile sink whenever the distance from the sink to base station is too long. The mobile sink follows the dynamic path

*Corresponding author. Prakash Chandra Sharma, Department of Information Technology, Manipal University Jaipur, Jaipur, India. E-mail: prakashsharma12@gmail.com.

Availability optimization of power generating units used in sewage treatment plants using metaheuristic techniques

Monika Saini, Ashish Kumar, Dinesh Kumar Saini, Punit Gupta

Published: May 4, 2023 • <https://doi.org/10.1371/journal.pone.0284848>

Abstract

Metaheuristic techniques have been utilized extensively to predict industrial systems' optimum availability. This prediction phenomenon is known as the NP-hard problem. Though, most of the existing methods fail to attain the optimal solution due to several limitations like slow rate of convergence, weak computational speed, stuck in local optima, etc. Consequently, in the present study, an effort has been made to develop a novel mathematical model for power generating units assembled in sewage treatment plants. Markov birth-death process is adopted for model development and generation of Chapman-Kolmogorov differential-difference equations. The global solution is discovered using metaheuristic techniques, namely genetic algorithm and particle swarm optimization. All time-dependent random variables associated with failure rates are considered exponentially distributed, while repair rates follow the arbitrary distribution. The repair and switch devices are perfect and random variables are independent. The numerical results of system availability have been derived for different values of crossover, mutation, several generations, damping ratio, and population size to attain optimum value. The results were also shared with plant personnel. Statistical investigation of availability results justifies that particle swarm optimization outdoes genetic algorithm in predicting the availability of power-generating systems. In present study a Markov model is proposed and optimized for performance evaluation of sewage treatment plant. The developed model is one that can be useful for sewage treatment plant designers in establishing new plants and purposing maintenance policies. The same procedure of performance optimization can be adopted in other process industries too.

Citation: Saini M, Kumar A, Saini DK, Gupta P (2023) Availability optimization of power generating units used in sewage treatment plants using metaheuristic techniques. PLoS ONE 18(5): e0284848. <https://doi.org/10.1371/journal.pone.0284848>

Editor: Nebojsa Bacanin, Univerzitet Singidunum, SERBIA

Received: January 20, 2023; **Accepted:** April 10, 2023; **Published:** May 4, 2023

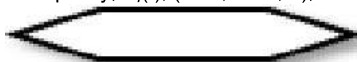
Copyright: © 2023 Saini et al. This is an open access article distributed under the terms of the [Creative Commons Attribution License](#), which permits unrestricted use, distribution, and reproduction in any medium, provided the original author and source are credited.

Data Availability: All relevant data are within the paper.

Funding: The author(s) received no specific funding for this work.

Competing interests: The authors have declared that no competing interests exist.

Abbreviations: $P_0(t)$, Probability that system is working with full capacity; $\Psi_i(1 \leq i \leq 6)$, Respectively failure rates in subsystems H, I, J, K, L, M ; $\Omega_i(1 \leq i \leq 6)$, Respectively repair rate in subsystems H, I, J, K, L, M ; h, i, j, k, l, m , Subsystem has failed; H, I, J, K, L, M , All subsystems are working with full capacity; $P_i(t)$, ($i = 1, \dots, 6$), Probability of subsystem on i^{th} state at time t ; S_i , ($i = 0, 1, 2, \dots, 6$), State of the subsystem;



, System is working with full capacity;



, System is in failure state

1. Introduction

Water is the precious commodity on earth for the survival of living creatures. It is as important as air, and no one can imagine life on earth without water. On the earth, 71% surface is covered by water, among which 96.5% is stored in oceans. Till now, instead of technological advancements, human being is not in a position to use ocean water for drinking and agriculture purposes. Only a limited amount of water is available which can be used for drinking and agriculture. Water resources are very limited, and many areas in various countries depend on rain and rivers' water supply. Countries like India, which accommodate 16% of the world population while only 4% of water resources, face challenges in providing drinking water for their citizens as ground water level is very low in some areas below 600 feet. In this challenging scenario, it becomes important to use water resources with great care, and simultaneously such techniques will be developed through which used wastewater can be recycled.

Many researchers are consistently working in this direction, and significant growth has been observed in the field of wastewater treatment by establishing sewage treatment plants. Sewage treatment is the procedure of removing pollutants from wastewater produced by households and industries. Sewage treatment is a three-stage procedure having physical, chemical, and biological stages. The water treated through sewage treatment is safe for the environment and can be utilized for agriculture, while semi-solid sludge can be decomposed either in land or used for energy generation in the form of methane gas. Sewage treatment plant has a very complex design, and it is assembled using many subsystems/components. The sewage treatment plant's complexity influences the system's operational performance, and it becomes necessary to operate these plants with utmost care. This can be

achieved by the reliability and availability of the plants. As the sewage treatment plants for other industries like process industries, mechanical systems, production lines, transport industries and network systems, reliability and availability are key performance measures for successful operation.

Keeping in mind all the above facts, the present study is designed to research the provision of strength-producing units in sewage remedy plants. In the existing study, an attempt has been made to provide a unique mathematical version for strength-producing unit assembled in sewage remedy plants. Markov birth-death of life technique is followed for version improvement and technology of Chapman-Kolmogorov differential-difference equations. The worldwide answer is found in the use of metaheuristic strategies particularly genetic algorithm (GA) and particle swarm optimization (PSO). All time-established random variables related to failure charges are taken into consideration and exponentially dispensed even as restore charges comply with the arbitrary distribution. The restore and transfer gadgets are best and random variables are unbiased to every other. The numerical consequences of gadget availability had been derived for exclusive values of crossover, mutation, several generations, damping ratio, and population size to attain optimum value. The results were also shared with plant personnel. Statistical investigation of availability results justifies that PSO outdoes GA in predicting the availability of power-generating systems. The findings of the present study will be very useful for sewage treatment plant designers in establishing new plants and purposing maintenance policies. The proposed methodology and algorithms can be utilized in other production and process industries like Paper and Pulp, Shoe Manufacturing, Sugar Industry, Sewage Treatment Plant, etc., to optimize the performance of the systems. In short, the main contributions of present study are as follows:

- › Development of mathematical model for power generating unit of sewage treatment plant
- › Elimination the best values of failure and repair rates using GA and PSO
- › Optimization of mathematical model using GA and PSO and prediction of optimal availability

This complete study is divided into eight sections, including an introduction and detailed literature review presented in section 2. Section 3 discusses the system description. Section 4 material and methods in which some relevant definitions are appended. The proposed mathematical model is presented in Section 5. Experimental results and optimization strategies and their implementation are appended in Sections 6 and 7, respectively. Concluding remarks and future directions are discussed in Section 8.

2. Literature review

Several studies have been conducted on design perspectives and the establishment of sewage treatment plants. Olsson (1976) [1] presented the state-of-the-art design of sewage treatment plants to control their failures and enhance operationality. Berthouex et al. [2] (1978) investigated some quality aspects of monitoring the sewage treatment plants. Boger [3] (1992) explored the applicability of neural networks in the operation of wastewater treatment plants. Wang and Pham [4] (1999) proposed various maintenance models for production industries using the concept of imperfect maintenance. Li and Pham [5] (2005) discussed the effect of random shock and multi-component failure on degraded systems reliability. Amari et al. [6] (2006) used the Markov process to develop an industry's cost-effective maintenance schedule. Pham [7] (2006) described the important concepts used in reliability modelling.

Ling and Isa [8] (2006) suggested bioremediation of oil sludge contaminated soil by using sewage sludge in the fields. Mjalli et al. [9] (2007) used an artificial neural network and black-box modelling to predict wastewater treatment plants' performance. Yang et al. [10] (2010) developed the assessment system for measuring operational energy performance in wastewater treatment plants. Manzini et al. [11] (2010) suggested various maintenance policies for industrial systems. Wang and Pham [12] (2011) modelled dependent competing risks having multiple degradations and random shock using copulas. Amari et al. [13] (2012) used warm standby redundancy in k-out-of-n systems. Malhotra and Negi [14] (2013) used particle swarm optimization (PSO) in reliability investigation. You and Pham [15] (2016) conducted the reliability evaluation of a CNC system using the field data. Mannina et al. [16] (2016) presented a detailed review of the tools for measuring greenhouse gases from wastewater treatment plants.

Pham [17] (2016) suggested applications of computing in reliability management. Duan et al. [18] (2017) discussed a model for recovering thermal energy from small-scale sewage treatment plants situated in northern Canada. Gautam et al. [19] (2017) developed a cost-effective treatment technology for small sewage treatment plants in different parts of India. Zhu and Pham [20] (2018) used the martingale process with Gamma distributed environmental factors in software reliability evaluation. Xie et al. [21] (2018) proposed an efficient stochastic model for hybrid-electric buses predicting energy management with reference to the state-of-charge advisory. Olyaei et al. [22] (2018) developed a system for assessing flood reliability due to wastewater treatment plants. Mlynski et al. [23] (2019) investigated the applications of mathematical simulation methods for assessing the operational reliability of wastewater treatment plants. Boyd et al. [24] (2019) discussed the flowing in forecasting for wastewater treatment plants. Pham and Pham [25] (2019) proposed a general reliability model using a stochastic fault-detection rate. Lin et al. [26] (2019) performed a reliability evaluation of a multi-state air transport network system using the concept of multiple demands. Gu et al. [27] (2019) used copula methodology for reliability calculations of mechanical systems under dependent failure mechanism. Chang [28] (2019) used a simulation approach for the reliability estimation of a stochastic production system. Lin and Chen [29] (2020) used the flow data mining technique in the reliability evaluation of multistate networks. Huang et al. [30] (2020) discussed the impact of multiple terminals under stocks for the reliability investigation of multi-state distribution networks. Zhu and Pham [31] (2020) used stochastic modelling in the development of software reliability model. Lee et al. [32] (2020) discussed the concept of dependent failure and SPRT in software reliability. Mesquita et al. [33] (2021) developed reliable technologies for assessing the feasibility of biogas use in sewage treatment plants. Al Abdali et al. [34] (2021) carried out a reliability analysis of blowers used in sewage treatment plants. Niu et al. [35] (2021) studied a multi-state system's reliability under the concept of cost and spoilage. Zhu [36] (2021) proposed a new model of complex systems' reliability evaluation under an imperfect maintenance strategy. Ostadi and Hamedankhah [37] (2021) suggested a two-phase reliability optimization methodology for series-parallel systems. Piri et al. [38] (2021) analyzed pumping stations' reliability for sewage networks using a hybrid neural network and genetic algorithm. The applicability of metaheuristic approaches observed in various files like environment [39–42], energy [43,44], and business [45–47].

Sinwar et al. [48] (2021) used GA and PSO for the availability and performance investigation of physical processing units in the sewage treatment plant. Kumar et al. [49] (2022) used metaheuristic approaches in the optimization of operational availability of cooling towers of STTPs. Saini et al. [50,51] optimized the availability of condenser of STTPs, and biological and chemical units of treatment plants using evolutionary and swarm-based algorithms. It is observed that many researchers carried out studies related to the design of sewage treatment plant, but the reliability aspects of plants as well as the power generating unit is not so extensively discussed so far in the literature.

3. System description

Two factors, domestic uses and industrialization, are mainly responsible for polluting water bodies. Solid waste and chemicals from industries are drained from industries into water bodies. The wastewater generated through domestic use can also be recycled. The power generating unit is studied out of the four main units, physical processing unit, biological and chemical processing unit, power generation processing unit, and sludge digestion processing units. The power generation processing unit is used to generate energy by treating the remaining sludge in the finalized stage of this treatment. For this, it incorporates in six subsystems as sludge digesting units, which lessen the quantity of sludge and shape biogas like methane and carbon dioxide, fueloline maintaining tank saved gases and stability the fluctuation withinside the manufacturing of biogases in digester and burner disposed extra and undesirable gases from the system. Gas scrubber eliminates hydrogen sulfide, neutralize dangerous components, and soak up pollutant from this, and fueloline engine runs on gaseous gasoline and a heated digester. In the last level electricity is generated with the assist of fueloline engine, and all STP units function. Sludge digesters, in addition to the electricity era, include a unit configured as 2-out-of-2: G, at the same time as fueloline maintaining tank, fueloline burner, fueloline scrubber and fueloline engine are composed of unmarried units.

4. Statistical analysis

4.1 Mann-Whitney U-test

Mann-Whitney U-test is used to test the equality of two population means when sample size is small and normality is not attained. Suppose x_1, x_2, \dots, x_m a sample taken from a population having cumulative density function (c.d.f) $F_x(x)$ and another sample z_1, z_2, \dots, z_n has been taken from another population with c.d.f. $F_z(z)$. The populations do not follow the normal distributions. If we want to test the significance $H_0: F_x(x) = F_z(z)$ against an alternative hypothesis, $H_1: F_x(x) \leq F_z(z)$ then Mann-Whitney U-test is the most appropriate test for it. Here, U-statistic is a measure of the difference between the ranked observations of the two samples. For comparison, the global output of metaheuristic approaches to non-parametric tests is always recommended as parametric test assumptions are not satisfied.

4.2. Stochastic differential difference equations using markov process

A stochastic process is called the Markov process if its dynamic behaviour is such that the probability distribution for reaching the next state only depends on the present state, not on how it arrives at the present state. In formulating a Markov model, it is necessary to define all the states of the model. If the hazard rate between two states is constant, the model is homogenous; otherwise, it is nonhomogeneous.

4.3 Assumptions

1. Sufficient repair facility is available in the plant immediately.
2. Distribution for the failure rate and repair rates are considered exponentially distributed.
3. System performs as new with full capacity after the repair.
4. Switch devices are perfect.
5. No occurrence of simultaneous failures.

4.4 Simulating environment

For simulating the experiments, we used MATLAB R2019a on the Windows 10 64-bit operating system with 8 GB of RAM and an Intel Core i5 8th generation CPU. Initially, random samples are generated using exponential distribution and then GA and PSO algorithms applied to obtain the optimal solution.

4.5 State transition diagram

In this section, a state transition diagram of power generating unit is designed by considering exponentially distributed failure and repair rates based on the configuration of system as given in Fig_1.



Fig 1. Configuration diagram of power generating unit.
<https://doi.org/10.1371/journal.pone.0284848.g001>

4.6 Failure and repair rates

The failure of the system or a component is the inability of the system to deliver its intended function satisfactorily. Hazard rate is the instantaneous speed of failures. It is expressed as the ratio of the number of failures in a small interval of time to the product of number of surviving items. Repairs are the process of restoration work of any failed system. The ability of an item, under stated conditions of use, to be retained in, or restored to, a state in which it can perform its required functions.

5. Mathematical modelling of the power generation processing unit

The mathematical model of the power generating unit is developed using the Markov birth-death process based on the state changeover diagram (Fig_2) where all repair rates are exponentially distributed. This model is described below:

$$P_0(t + \Delta t) = [(1 - 2\Psi_1 - \Psi_2 - \Psi_3 - \Psi_4 - \Psi_5 - 2\Psi_6)P_0(t) + \Omega_1 P_1(t) + \Omega_2 P_2(t) + \Omega_3 P_3(t) + \Omega_4 P_4(t) + \Omega_5 P_5(t) + \Omega_6 P_6(t)] \Delta t$$

$$P_0(t + \Delta t) - P_0(t) = [(-2\Psi_1 - \Psi_2 - \Psi_3 - \Psi_4 - \Psi_5 - 2\Psi_6)P_0(t) + \Omega_1 P_1(t) + \Omega_2 P_2(t) + \Omega_3 P_3(t) + \Omega_4 P_4(t) + \Omega_5 P_5(t) + \Omega_6 P_6(t)] \Delta t \quad (2)$$

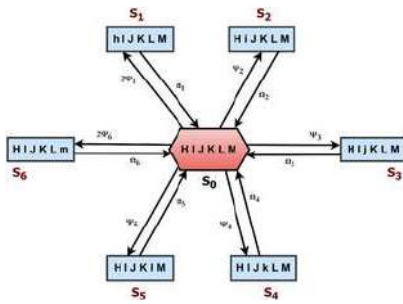


Fig 2. State changeover of the power generation processing system.
<https://doi.org/10.1371/journal.pone.0284848.g002>

Dividing both sides by Δt and limit $\Delta t \rightarrow \infty$

$$\lim_{\Delta t \rightarrow 0} \frac{P_0(t + \Delta t) - P_0(t)}{\Delta t} = \lim_{\Delta t \rightarrow 0} [(-2\Psi_1 - \Psi_2 - \Psi_3 - \Psi_4 - \Psi_5 - 2\Psi_6)P_0(t) + \Omega_1 P_1(t) + \Omega_2 P_2(t) + \Omega_3 P_3(t) + \Omega_4 P_4(t) + \Omega_5 P_5(t) + \Omega_6 P_6(t)]$$

$$\left[\frac{dP_0(t)}{dt} \right] + (2\Psi_1 + \Psi_2 + \Psi_3 + \Psi_4 + \Psi_5 + 2\Psi_6)P_0(t) = \Omega_1 P_1(t) + \Omega_2 P_2(t) + \Omega_3 P_3(t) + \Omega_4 P_4(t) + \Omega_5 P_5(t) + \Omega_6 P_6(t) \quad (3)$$

$$\left[\frac{d}{dt} + \Omega_1 \right] P_1(t) = 2\Psi_1 P_0(t) \quad (4)$$

$$\left[\frac{d}{dt} + \Omega_2 \right] P_2(t) = \Psi_2 P_0(t) \quad (5)$$

$$\left[\frac{d}{dt} + \Omega_3 \right] P_3(t) = \Psi_3 P_0(t) \quad (6)$$

$$\left[\frac{d}{dt} + \Omega_4 \right] P_4(t) = \Psi_4 P_0(t) \quad (7)$$

$$\left[\frac{d}{dt} + \Omega_5 \right] P_5(t) = \Psi_5 P_0(t) \quad (8)$$

$$\left[\frac{d}{dt} + \Omega_6 \right] P_6(t) = 2\Psi_6 P_0(t) \quad (9)$$

Initial Conditions:

$$P_0(0) = 1$$

$$P_i(0) = 0, \quad i = 1 \text{ to } 7, \quad (10)$$

To calculate long-run availability, we can take $\frac{d}{dt} = 0$ as $t \rightarrow \infty$ and $P_i(t) = P_i$

From Eqs (1–9), steady-state probabilities are:

$$P_1 = \frac{2\Psi_1}{\Omega_1} P_0 \quad P_2 = \frac{\Psi_2}{\Omega_2} P_0 \quad P_3 = \frac{\Psi_3}{\Omega_3} P_0$$

$$P_4 = \frac{\Psi_4}{\Omega_4} P_0 \quad P_5 = \frac{\Psi_5}{\Omega_5} P_0 \quad P_6 = \frac{2\Psi_6}{\Omega_6} P_0$$

Using normalized condition $\sum P_i = 1$

$$P_0 = \left(1 + \frac{2\Psi_1}{\Omega_1} + \frac{\Psi_2}{\Omega_2} + \frac{\Psi_3}{\Omega_3} + \frac{\Psi_4}{\Omega_4} + \frac{\Psi_5}{\Omega_5} + \frac{2\Psi_6}{\Omega_6} \right)^{-1}$$

long run availability (A_v)

$$A_v = P_0 = \left(1 + \frac{2\Psi_1}{\Omega_1} + \frac{\Psi_2}{\Omega_2} + \frac{\Psi_3}{\Omega_3} + \frac{\Psi_4}{\Omega_4} + \frac{\Psi_5}{\Omega_5} + \frac{2\Psi_6}{\Omega_6} \right)^{-1}$$

(11)

6. Optimization strategies

In current age scientists consistently trying to develop new designs for existing systems so that maximum output may be extracted with the minimum cost investment. It is also tried those existing systems optimally used for a long duration. The designing and operationality generally involve the tuning of models for physical structures. Optimization can be used to manage the assignments of design, operation, and tuning models systemically. It is a technique used to select the best solution from a set of feasible solutions. In a more elaborated way, it is explained as a technique that finds the set of variables known as decision variables. It provides the optimum objective function value in a search space bounded by constraints and non-negativity conditions. Several statistical techniques exist in the literature, viz. maximum likelihood estimation, method of moments, least-square estimation, Bayes estimation etc., for parameter estimation and optimization, various linear and non-linear programming techniques exist. Linear programming, integer programming, and dynamic programming are a few techniques to find the optimum value of the objective function, but these only provide the local solution. Metaheuristic and evolutionary algorithms are recently developed techniques which show high efficiency in providing the optimal solution to complex real-world problems and are free from the nature of the problem. Recently, these techniques became popular for finding the optimum solution for complex problems. Metaheuristic approaches are classified into three categories: nature, population, and memory. Recently, several metaheuristic approaches (Ant Colony Optimization, Neural Networks, Grey Wolf Optimization, Whale Optimization) proposed by researcher to optimize the performance of process industries and showed the applications in their reliability prediction. Though, no work is reported in availability optimization of power generating unit of sewage treatment plants. To fill this research gap in the present analysis an effort is made to optimize the availability of power generating units by using two well-known nature-based algorithms, genetic algorithm (GA) and particle swarm optimization (PSO). These algorithms are not affected by the nonlinearity and problem size. Here, a population is randomly generated and assigned to each particle. The best solution is attained corresponding to the Pbest and Gbest. The efficiency of the algorithms is statistically tested using the methodology proposed by Derrac et al. [52] (2011). Mathematically, the optimization problem of the proposed model is formulated using availability function (11) as objective function as follows:

Objective function: Max. A_v

$$\text{Subject to : } \begin{cases} \Psi_i \geq 0 \\ \Omega_i \geq 0 \end{cases}$$

(12)

Where $i = 1,2,3,4,5,6$.

6.1 Genetic algorithm

A genetic algorithm (GA) works on the Darwinian theory of survival of the fittest between organisms in danger of extinction by environmental factors and hunters. Goldberg and Holland [53] (1988) developed a genetic algorithm for the first time and used it to find optimal solutions to complex engineering problems. It is based on genetic and natural selection and falls under evolutionary computation. A large population of possible solutions exists in a genetic algorithm, and these solutions undergo crossover and mutation for reproduction. Each possible solution has an assigned fitness value, and better-fitted candidates are chosen for mutation and producing a new generation of solutions. It is observed that the fittest member can easily adopt the changes and have the highest chances of survival. The same characteristics are also followed by their offspring as inherent traits. It resulted in the fittest generations' production. Moreover, genomic mutations happen randomly among the members of the population, and these also improve the long-term persistence of fit members and their evolutionary progenies. The individual generated through genetic algorithms are known as chromosomes and are treated as a solution to the optimization problem. The chromosome is the combination of genes those stands for decision variables in the optimization problem, and the ability to survive is termed the fitness value of the individual. The surviving individuals of the previous generation and their offspring made the population of each generation. The offspring are generated using genetic operators, namely mutation and crossover. To generate a new generation of solutions, parents are selected, and the probability of selection is proportional to the fitness value of parent. Higher the fitness value resulted in a higher chance of survive. The higher fitness value candidates always get priority over the others. The process goes on until the stopping criteria are satisfied. The flowchart of genetic algorithm is shown in Fig.3. The working pattern of traditional GA is as follows:

- Step 1: Generate a random population of possible solutions
- Step 2: Calculate the fitness value of each member and select a few as parents based on their fitness value to produce new offspring
- Step 3: A new generation of individuals (possible solutions) produced by applying genetic operators' crossover and mutation.
- Step 4: Iteratively, the old individuals are replaced by new individuals, and the process repeatedly continues until the stopping criteria are satisfied.
- Step 5: Go to step 2 if the stopping criteria are not satisfied

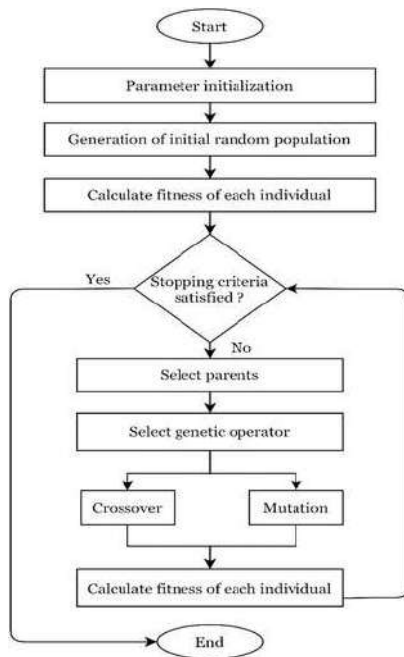


Fig 3. Flowchart of genetic algorithm.
<https://doi.org/10.1371/journal.pone.0284848.g003>

6.1.1. Crossover.

It is one of the essential operators among genetic operators. The new offspring is generated by crossover through the exchange of genes between parents. It is applied to two solutions/parents. Under crossover operation, few decision variables of both solutions are exchanged, i.e., in newly developed solutions, few decision variables come from the first solution, and the rest comes from the second. There are three types of crossover patterns observed: one-point crossover, two-point crossover and uniform crossover. A random crossover point is used in a one-point crossover, and a child is reproduced having some genes of the parent located on one side of the crossover point and rest comes from the parent on the other side. In the two-point crossover, two points are considered, and solutions are generated by the crossover of the parents located outside the crossover points. All the parent solution within crossover points is protected. In uniform, crossover points are randomly generated. In the present analysis, uniform crossover generates the new population.

6.1.2. Mutation.

It provides new genetic material for the population. It generally changes some genes of the offspring. It replaces some decision variable of the new solution with any random number while other decision variables remain unchanged. Mutations are of two kinds, viz. uniform and non-uniform. Uniform mutation replaces the gene with another gene from the feasible solution space. Non-uniform mutation introduces a localized search space for an optimal solution where sets of decision variables/genes are based on the boundaries. These boundaries shrink with the increasing number of iterations of GA.

6.2 Particle Swarm Optimization (PSO)

Computational intelligence techniques based on swarm behaviour gained popularity during the last few decades. The methods based on animals' social and biological behaviour collectively and individually when interacting with each other or with the environment are termed swarm-based, and it is termed swarm intelligence. In swarm intelligence, a group of individuals/solutions handles real-world systems by ordinating themselves by self-discipline and decentralization. Particle swarm optimization (PSO) is a well-known example of swarm-based computational intelligence technique. It is worked on the social behaviour of birds and replicates the behaviour of the herds. In this technique, initially, it is assumed that a herd of birds is looking for food, and no information is available for the food. As an effective strategy, the herd follow the bird, which knows the nearest food source. The PSO works on the same approach and utilizes an initial numerical solution from the search space to optimize the problem's solution. Each solution is termed a bird in an optimization problem and a particle. The set of particles is known as swarm. The particles have a fitness value derived using an objective function and a velocity with which particles move in the problem's search space. A chief guides all the particles in the search space. The particles change their position based on their personal best position as well as group best position. The flowchart of particle swarm optimization is shown in Fig 4.

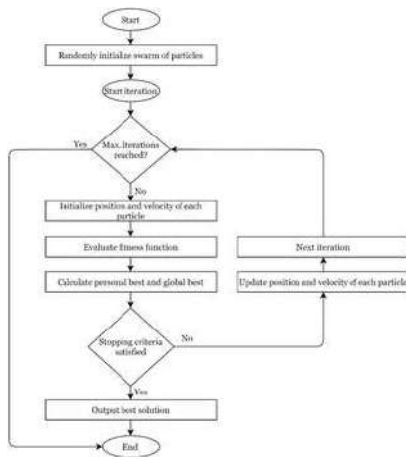


Fig 4. Flowchart of particle swarm optimization algorithm.
<https://doi.org/10.1371/journal.pone.0284848.g004>

The implementation criteria of PSO are described as follows:

Step 1: Input the initial numerical velocity and acceleration values of all the particles from the solution search space.

Step 2: Calculate the fitness value using the objective function of the problem for all the particles. These derived values are the best personal position and fitness values achieved. The best position among all the particles is termed as global best position.

Step 3: The new solutions are generated by updating the position and velocity based on personal and global best.

Step 4: The next iteration is started; fitness values are recalculated, and personal and global best positions are updated.

Step 5: If convergence criteria are met, stop; otherwise, go back to step 3.

7. Implementation of optimization strategies

In complex industrial systems like sewage treatment plants, many components are involved, and their global solution is impossible to achieve. So, here in this situation use of metaheuristic approaches is recommended. The performance of the sewage treatment plant is highly influenced by its subsystems' failure and repair rate. The failure and repair rate parameter constraints for the power generation processing unit are as follows: (Ψ_1, Ω_1) , (Ψ_2, Ω_2) , (Ψ_3, Ω_3) , (Ψ_4, Ω_4) , (Ψ_5, Ω_5) , (Ψ_6, Ω_6) .

The range of parameter constraints are: $\Psi_1 \in [0.001, 0.02]$, $\Psi_2 \in [0.0003, 0.006]$, $\Psi_3 \in [0.0002, 0.04]$, $\Psi_4 \in [0.0005, 0.07]$, $\Psi_5 \in [0.0001, 0.009]$, $\Psi_6 \in [0.0023, 0.075]$, $\Omega_1 \in [0.89, 2.35]$, $\Omega_2 \in [0.02, 1.34]$, $\Omega_3 \in [0.0032, 3.45]$, $\Omega_4 \in [0.56, 2.33]$, $\Omega_5 \in [0.063, 1.89]$, $\Omega_6 \in [2.77, 4.98]$. The range of failure and repair rates is taken arbitrarily after investigating various studies.

In the present study, the long-run availability of the power generation processing unit is optimized by applying genetic algorithm and Particle swarm optimization on the optimization model appended in Eq.(12).

In implementing GA, five steps are mainly involved, namely encoding, fitness function, selection, mutation, and crossover. Here, value encoding is used to encode the chromosome values; a random selection technique is used to select the parent population to operate crossover. Here, uniform crossover and mutation are used to generate new offspring. As an illustration, all the five steps are explained below:

(i) Encoding

Encoding is an operator in GA used for mapping chromosomes, a set of different values. It is highly dependent on the objective function of the study. A sample chromosome value is given as below:

Power generation processing unit

$\Psi_1 = 0.0006$, $\Psi_2 = 0.0014$, $\Psi_3 = 0.0033$, $\Psi_4 = 0.0089$, $\Psi_5 = 0.0004$, $\Psi_6 = 0.0015$, $\Omega_1 = 1.78$, $\Omega_2 = 0.75$, $\Omega_3 = 2.45$, $\Omega_4 = 1.89$, $\Omega_5 = 0.075$, $\Omega_6 = 3.25$

(ii) Fitness Function

Fitness function is described as the obtained solution quality near the prescribed set of values. A sample chromosome with a fitness value is given as below:

Power generation processing unit

$\Psi_1 = 0.006$, $\Psi_2 = 0.0014$, $\Psi_3 = 0.0033$, $\Psi_4 = 0.0089$, $\Psi_5 = 0.0004$, $\Psi_6 = 0.015$, $\Omega_1 = 1.78$, $\Omega_2 = 0.75$, $\Omega_3 = 2.45$, $\Omega_4 = 1.89$, $\Omega_5 = 0.075$, $\Omega_6 = 3.25$

The fitness value of availability for power generating units is 0.9977.

(iii) Selection: Here, the parent population are selected randomly to generate an offspring population.

(iv) Crossover: Cross-over operator is a technique in which the child population is generated from the paired parent population. Here the uniform method of crossover is applied.

Power generation processing unit

$\Psi_1 = 0.0034, \Psi_2 = 0.0016, \Psi_3 = 0.0009, \Psi_4 = 0.0027, \Psi_5 = 0.0004, \Psi_6 = 0.0154, \Omega_1 = 5.0452, \Omega_2 = 0.5375, \Omega_3 = 3.6653, \Omega_4 = 0.4712, \Omega_5 = 0.1761, \Omega_6 = 3.9891$

(v) Mutation: The mutation operator is useful to maintain the diversity from one generated population to the next.

Power generation processing unit

$\Psi_1 = 0.0130, \Psi_2 = 0.0004, \Psi_3 = 0.0018, \Psi_4 = 0.0005, \Psi_5 = 0.0000, \Psi_6 = 0.0047, \Omega_1 = 2.2237, \Omega_2 = 0.9349, \Omega_3 = 0.7339, \Omega_4 = 0.8068, \Omega_5 = 0.2604, \Omega_6 = 5.6486$

The results of genetic algorithm appended in Tables 1–4. From Table 1, it is revealed that at mutation probability 0.55, crossover probability 0.62, number of evaluations 200, the maximum availability of power generating unit is 0.9980, corresponding to population size 10. The estimated parameters values given against the population size 10.

Pop Size	EV	CR	MT	AV	SE	AV	SE	AV	SE
Availability	0.9980	0.9970	0.9970	0.9980	0.9980	0.9980	0.9980	0.9980	0.9980
Ψ_1	0.0034	0.0016	0.0009	0.0027	0.0004	0.0154	5.0452	0.5375	3.6653
Ψ_2	0.0034	0.0016	0.0009	0.0027	0.0004	0.0154	5.0452	0.5375	3.6653
Ψ_3	0.0034	0.0016	0.0009	0.0027	0.0004	0.0154	5.0452	0.5375	3.6653
Ψ_4	0.0034	0.0016	0.0009	0.0027	0.0004	0.0154	5.0452	0.5375	3.6653
Ψ_5	0.0034	0.0016	0.0009	0.0027	0.0004	0.0154	5.0452	0.5375	3.6653
Ψ_6	0.0034	0.0016	0.0009	0.0027	0.0004	0.0154	5.0452	0.5375	3.6653
Ω_1	5.0452	0.5375	3.6653	0.4712	0.1761	3.9891			
Ω_2	5.0452	0.5375	3.6653	0.4712	0.1761	3.9891			
Ω_3	5.0452	0.5375	3.6653	0.4712	0.1761	3.9891			
Ω_4	5.0452	0.5375	3.6653	0.4712	0.1761	3.9891			
Ω_5	5.0452	0.5375	3.6653	0.4712	0.1761	3.9891			
Ω_6	5.0452	0.5375	3.6653	0.4712	0.1761	3.9891			

Table 1. Effect of population size on availability of power generation processing unit by using Genetic Algorithm (Evolution = 200, Mutation = 0.55, Crossover = 0.62).

<https://doi.org/10.1371/journal.pone.0284848.t001>

Evolution	EV	CR	MT	AV	SE	AV	SE	AV	SE
Availability	0.9972	0.9970	0.9970	0.9972	0.9972	0.9972	0.9972	0.9972	0.9972
Ψ_1	0.0034	0.0016	0.0009	0.0027	0.0004	0.0154	5.0452	0.5375	3.6653
Ψ_2	0.0034	0.0016	0.0009	0.0027	0.0004	0.0154	5.0452	0.5375	3.6653
Ψ_3	0.0034	0.0016	0.0009	0.0027	0.0004	0.0154	5.0452	0.5375	3.6653
Ψ_4	0.0034	0.0016	0.0009	0.0027	0.0004	0.0154	5.0452	0.5375	3.6653
Ψ_5	0.0034	0.0016	0.0009	0.0027	0.0004	0.0154	5.0452	0.5375	3.6653
Ψ_6	0.0034	0.0016	0.0009	0.0027	0.0004	0.0154	5.0452	0.5375	3.6653
Ω_1	5.0452	0.5375	3.6653	0.4712	0.1761	3.9891			
Ω_2	5.0452	0.5375	3.6653	0.4712	0.1761	3.9891			
Ω_3	5.0452	0.5375	3.6653	0.4712	0.1761	3.9891			
Ω_4	5.0452	0.5375	3.6653	0.4712	0.1761	3.9891			
Ω_5	5.0452	0.5375	3.6653	0.4712	0.1761	3.9891			
Ω_6	5.0452	0.5375	3.6653	0.4712	0.1761	3.9891			

Table 2. Effect of evolution on availability of power generation processing unit by using Genetic Algorithm (Population size = 60, Mutation = 0.55, Crossover = 0.62).

<https://doi.org/10.1371/journal.pone.0284848.t002>

Crossover	CR	CR	CR	CR	CR	CR	CR	CR
Availability	0.9982	0.9982	0.9982	0.9982	0.9982	0.9982	0.9982	0.9982
Ψ_1	0.0034	0.0016	0.0009	0.0027	0.0004	0.0154	5.0452	0.5375
Ψ_2	0.0034	0.0016	0.0009	0.0027	0.0004	0.0154	5.0452	0.5375
Ψ_3	0.0034	0.0016	0.0009	0.0027	0.0004	0.0154	5.0452	0.5375
Ψ_4	0.0034	0.0016	0.0009	0.0027	0.0004	0.0154	5.0452	0.5375
Ψ_5	0.0034	0.0016	0.0009	0.0027	0.0004	0.0154	5.0452	0.5375
Ψ_6	0.0034	0.0016	0.0009	0.0027	0.0004	0.0154	5.0452	0.5375
Ω_1	5.0452	0.5375	3.6653	0.4712	0.1761	3.9891		
Ω_2	5.0452	0.5375	3.6653	0.4712	0.1761	3.9891		
Ω_3	5.0452	0.5375	3.6653	0.4712	0.1761	3.9891		
Ω_4	5.0452	0.5375	3.6653	0.4712	0.1761	3.9891		
Ω_5	5.0452	0.5375	3.6653	0.4712	0.1761	3.9891		
Ω_6	5.0452	0.5375	3.6653	0.4712	0.1761	3.9891		

Table 3. Effect of crossover on availability of power generation processing unit by using Genetic Algorithm (Population size = 60, Evolution = 200, Mutation = 0.55).

<https://doi.org/10.1371/journal.pone.0284848.t003>

Mutation	MT	MT	MT	MT	MT	MT	MT	MT
Availability	0.9977	0.9977	0.9977	0.9977	0.9977	0.9977	0.9977	0.9977
Ψ_1	0.0034	0.0016	0.0009	0.0027	0.0004	0.0154	5.0452	0.5375
Ψ_2	0.0034	0.0016	0.0009	0.0027	0.0004	0.0154	5.0452	0.5375
Ψ_3	0.0034	0.0016	0.0009	0.0027	0.0004	0.0154	5.0452	0.5375
Ψ_4	0.0034	0.0016	0.0009	0.0027	0.0004	0.0154	5.0452	0.5375
Ψ_5	0.0034	0.0016	0.0009	0.0027	0.0004	0.0154	5.0452	0.5375
Ψ_6	0.0034	0.0016	0.0009	0.0027	0.0004	0.0154	5.0452	0.5375
Ω_1	5.0452	0.5375	3.6653	0.4712	0.1761	3.9891		
Ω_2	5.0452	0.5375	3.6653	0.4712	0.1761	3.9891		
Ω_3	5.0452	0.5375	3.6653	0.4712	0.1761	3.9891		
Ω_4	5.0452	0.5375	3.6653	0.4712	0.1761	3.9891		
Ω_5	5.0452	0.5375	3.6653	0.4712	0.1761	3.9891		
Ω_6	5.0452	0.5375	3.6653	0.4712	0.1761	3.9891		

Table 4. Effect of mutation on availability of power generation processing unit by using Genetic Algorithm (Population size = 60, Evolution = 200, Crossover = 0.62).

<https://doi.org/10.1371/journal.pone.0284848.t004>

From Table 2, it is revealed that at mutation probability 0.55, crossover probability 0.62, and population size 60, the maximum availability of power generating unit is 0.9972 after 25 evolutions. Table 3 revealed that at mutation probability 0.55, population size 60, and the number of evaluations 200, the maximum availability of power generating unit is 0.9982, corresponding to crossover probability 0.8.

Table 4 revealed that at crossover probability 0.62, population size 60, and the number of evaluations 200, the maximum availability of power generating unit is 0.9977, corresponding to mutation probability 0.3.

It is observed that optimum availability using a genetic algorithm can be achieved at a crossover probability of 0.8, a population size of 60, mutation probability of 0.55, and a number of evaluations of 200. The implementation of particle swarm optimization generated numerical results in various situations. The numerical results with respect to number of generations, number of iterations

From Table 7, it is revealed that at weight damping ratio 0.95, availability got optimized corresponding to population size 15, inertia weight 1, maximum iteration 25, p-best 1.7 and g-best 2.3. Fig 7 showed the pattern of availability along with the damping ratio. Figs 8 and 9 revealed the convergence pattern of the availability function using GA and PSO.

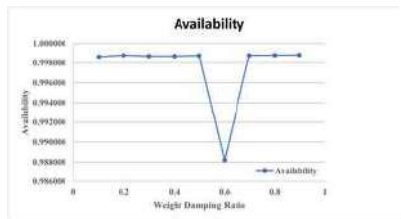


Fig 7. Damping ratio vs. availability.
<https://doi.org/10.1371/journal.pone.0284848.g007>

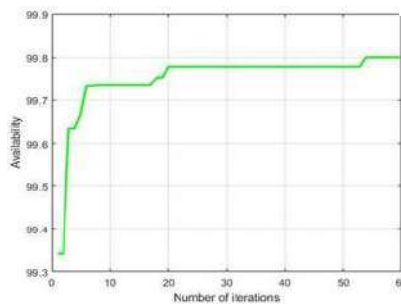


Fig 8. Convergence of availability using GA.
<https://doi.org/10.1371/journal.pone.0284848.g008>

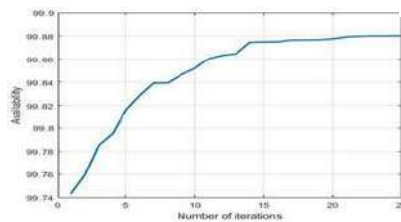


Fig 9. Convergence of availability using PSO.
<https://doi.org/10.1371/journal.pone.0284848.g009>

After applying Mann-Whitney U-test on the availability of GA and PSO, the following statistics were obtained: z-value = 3.363 and U statistics = 0.0001. At 5% level of significance, our z critical value is 1.96. Herewith, z calculated is greater than z critical value, so we reject the null hypothesis that the performance of both algorithms is equal. It is concluded that Particle Swarm Optimization algorithm outperforms on Genetic algorithm in the prediction of optimal availability of power generating unit of sewage treatment plant.

8. Conclusion

In present study, an effort is made to predict the optimal availability of power generating unit of sewage treatment plant using genetic algorithm and particle swarm optimization. For this purpose, a stochastic model of power generating unit is proposed. The numerical result for the proposed model is derived and optimized. For the power generation processing unit, simulation is done for the population size, which varies from 10 to 80. The maximum availability value is 0.9980, corresponding to the population size of 10 in the considered range of population size. The evaluation varies from 25 to 225 maximum availability value is 0.9972, corresponding to the evaluation value equal to 25. The maximum availability achieved corresponding to crossover and mutation is 0.9982 at 0.8 and 0.9977, corresponding to the mutation value 0.3. Finally, after observing all the derived results, it is revealed that genetic algorithm predicts the maximum availability of power generation processing unit 0.9982 at population size 60, evolution 200, mutation probability 0.55 and crossover probability 0.8. The best-fitted parameter values of failure and repair rates are also derived. After observing particle swarm optimization results, it is identified that the predicted optimum availability value is 0.998833, corresponding to the maximum number of iterations 25, population size 15, inertia weight 1, damping ratio 0.95, p-best 1.7 and g-best 2.3. The statistical investigation of GA and PSO results justified that PSO outperforms than GA. The proposed model and result will be helpful to system developers in designing the subsystems of the sewage treatment plant and establishing new plants. The proposed methodology and algorithms can be utilized in other production and process industries like Paper and Pulp, Shoe Manufacturing, Sugar Industry, Sewage Treatment Plant, etc., to optimize the performance of the systems. Some new optimization algorithms like Differential evolution [54] Ant colony optimization [55], Grey wolf optimizer [56]; Elephant herding optimization [57]; Moth search algorithm [58], Earthworm optimization algorithm [59], Monarch butterfly optimization [60], Harris hawks optimization [61], and Slime mould algorithm [62] as future work to investigate more accurately the performance of the availability of power generating unit. The present model is proposed under the assumptions that failure and repair are constantly distributed, no simultaneous failures and availability of sufficient repair facilities. These can be observed as the limitations of the present work and

system performs better under these conditions. Though the present study is conducted on a medium size sewage treatment plant it can not be established in the entities like small industries, residential societies etc. So, there is a need to explore the possibility of establishment of large size and more complex sewage treatment plants and their performance evaluation. The analysis of large size and more complex sewage treatment plants can be done in future work.

References

1. Olsson, G. (1976). State of the art in sewage treatment plant control.
2. Berthouex P. M., Hunter W. G., & Pallesen L. (1978). Monitoring sewage treatment plants: some quality control aspects. *Journal of Quality Technology*, 10(4), 139–149.
[View Article](#) • [Google Scholar](#)
3. Boger Z. (1992). Application of neural networks to water and wastewater treatment plant operation. *ISA transactions*, 31(1), 25–33.
[View Article](#) • [Google Scholar](#)
4. Wang H., & Pham H. (1999). Some maintenance models and availability withimperfect maintenance in production systems. *Annals of Operations Research*, 91, 305–318.
[View Article](#) • [Google Scholar](#)
5. Li W., & Pham H. (2005). Reliability modeling of multi-state degraded systems with multi-competing failures and random shocks. *IEEE transactions on reliability*, 54(2), 297–303.
[View Article](#) • [Google Scholar](#)
6. Amari, S. V., McLaughlin, L., & Pham, H. (2006, January). Cost-effective condition-based maintenance using Markov decision processes. In *RAMS'06. Annual Reliability and Maintainability Symposium, 2006.* (pp. 464–469). IEEE.
7. Pham H. (2006). System reliability concepts. In *System software reliability* (pp. 9–75). Springer, London.
8. Ling C. C., & Isa M. H. (2006). Bioremediation of oil sludge contaminated soil by co-composting with sewage sludge. *JSIR*.
[View Article](#) • [Google Scholar](#)
9. Mjalli F. S., Al-Asheh S., & Alfadala H. E. (2007). Use of artificial neural network black-box modeling for the prediction of wastewater treatment plants performance. *Journal of Environmental Management*, 83(3), 329–338. pmid:16806660
[View Article](#) • [PubMed/NCBI](#) • [Google Scholar](#)
10. Yang L., Zeng S., Chen J., He M., & Yang W. (2010). Operational energy performance assessment system of municipal wastewater treatment plants. *Water Science and Technology*, 62(6), 1361–1370. pmid:20861551
[View Article](#) • [PubMed/NCBI](#) • [Google Scholar](#)
11. Manzini R., Regattieri A., Pham H., & Ferrari E. (2010). *Maintenance for industrial systems* (pp. 409–432). London: Springer.
12. Wang Y., & Pham H. (2011). Modeling the dependent competing risks with multiple degradation processes and random shock using time-varying copulas. *IEEE Transactions on Reliability*, 61(1), 13–22.
[View Article](#) • [Google Scholar](#)
13. Amari S. V., Pham H., & Misra R. B. (2012). Reliability characteristics of k-out-of-n warm standby systems. *IEEE Transactions on Reliability*, 61(4), 1007–1018.
[View Article](#) • [Google Scholar](#)
14. Malhotra R., & Negi A. (2013). Reliability modeling using particle swarm optimization. *International Journal of System Assurance Engineering and Management*, 4(3), 275–283.
[View Article](#) • [Google Scholar](#)
15. You D., & Pham H. (2016). Reliability analysis of the CNC system based on field failure data in operating environments. *Quality and Reliability Engineering International*, 32(5), 1955–1963.
[View Article](#) • [Google Scholar](#)
16. Mannina G., Ekama G., Caniani D., Cosenza A., Esposito G., Gori R., et al. (2016). Greenhouse gases from wastewater treatment—A review of modelling tools. *Science of the Total Environment*, 551, 254–270. pmid:26878638
[View Article](#) • [PubMed/NCBI](#) • [Google Scholar](#)
17. Pham H. (2016). Reliability management and computing. *Annals of Operations Research*, 244(1), 1–2.
[View Article](#) • [Google Scholar](#)
18. Duan, X., Haque, I. R., & Ducey, A. (2017, November). Thermal Energy Recovery From Small Sewage Treatment Plants in Northern Canadian Communities. In *ASME International Mechanical Engineering Congress and Exposition* (Vol. 58417, p. V006T08A064). American Society of Mechanical Engineers.
19. Gautam S., Ahmed S., Dhingra A., & Fatima Z. (2017). Cost-effective treatment technology for small size sewage treatment plants in India. *JSIR*.
[View Article](#) • [Google Scholar](#)
20. Zhu M., & Pham H. (2018). A software reliability model incorporating martingale process with gamma-distributed environmental factors. *Annals of Operations Research*, 1–22.

[View Article](#) • [Google Scholar](#)

21. Xie S., Hu X., Xin Z., & Li L. (2018). Time-efficient stochastic model predictive energy management for a plug-in hybrid electric bus with an adaptive reference state-of-charge advisory. *IEEE Transactions on Vehicular Technology*, 67(7), 5671–5682.
[View Article](#) • [Google Scholar](#)
22. Olyaei M. A., Karamouz M., & Farmani R. (2018). Framework for assessing flood reliability and resilience of wastewater treatment plants. *Journal of Environmental Engineering*, 144(9), 04018081.
[View Article](#) • [Google Scholar](#)
23. Młyński D., Bugajski P., & Młyńska A. (2019). Application of the mathematical simulation methods for the assessment of the wastewater treatment plant operation work reliability. *Water*, 11(5), 873.
[View Article](#) • [Google Scholar](#)
24. Boyd G., Na D., Li Z., Snowling S., Zhang Q., & Zhou P. (2019). Influent forecasting for wastewater treatment plants in North America. *Sustainability*, 11(6), 1764.
[View Article](#) • [Google Scholar](#)
25. Pham T., & Pham H. (2019). A generalized software reliability model with stochastic fault-detection rate. *Annals of Operations Research*, 277(1), 83–93.
[View Article](#) • [Google Scholar](#)
26. Lin Y. K., Nguyen T. P., & Yeng L. C. L. (2019). Reliability evaluation of a multi-state air transportation network meeting multiple travel demands. *Annals of Operations Research*, 277(1), 63–82.
[View Article](#) • [Google Scholar](#)
27. Gu Y. K., Fan C. J., Liang L. Q., & Zhang J. (2019). Reliability calculation method based on the Copula function for mechanical systems with dependent failure. *Annals of Operations Research*, 1–18.
[View Article](#) • [Google Scholar](#)
28. Chang P. C. (2019). Reliability estimation for a stochastic production system with finite buffer storage by a simulation approach. *Annals of Operations Research*, 277(1), 119–133.
[View Article](#) • [Google Scholar](#)
29. Lin Y. K., & Chen S. G. (2020). Reliability evaluation in terms of flow data mining for multistate networks. *Annals of Operations Research*, 1–13.
[View Article](#) • [Google Scholar](#)
30. Huang C. F. (2020). System reliability for a multi-state distribution network with multiple terminals under stocks. *Annals of Operations Research*, 1–14.
[View Article](#) • [Google Scholar](#)
31. Zhu M., & Pham H. (2020). A generalized multiple environmental factors software reliability model with stochastic fault detection process. *Annals of Operations Research*, 1–22.
[View Article](#) • [Google Scholar](#)
32. Lee D. H., Chang I. H., & Pham H. (2020). Software reliability model with dependent failures and SPRT. *Mathematics*, 8(8), 1366.
[View Article](#) • [Google Scholar](#)
33. Mesquita T., Sousa I., Fernanda M., & Rosa A. P. (2021). A simple and reliable proposal to determine the technical feasibility of biogas use and the energetic self-sustainability in UASB-based sewage treatment plants. *Water Science and Technology*.
[View Article](#) • [Google Scholar](#)
34. Al Abdali Z., Al Alwai S., Al Hosni A., Al Sinani M., & Padmavathi N. (2021). Reliability Analysis of blowers of a Wastewater Treatment Plant. *Advances in Dynamical Systems and Applications (ADSA)*, 16(2), 739–754.
[View Article](#) • [Google Scholar](#)
35. Niu Y. F., He C., & Fu D. Q. (2021). Reliability assessment of a multi-state distribution network under cost and spoilage considerations. *Annals of Operations Research*, 1–20.
[View Article](#) • [Google Scholar](#)
36. Zhu M. (2021). A new framework of complex system reliability with imperfect maintenance policy. *Annals of Operations Research*, 1–27.
[View Article](#) • [Google Scholar](#)
37. Ostadi B., & Hamedankhah R. (2021). A two-stage reliability optimization approach for solving series–parallel redundancy allocation problem considering the sale of worn-out parts. *Annals of Operations Research*, 304(1), 381–396.
[View Article](#) • [Google Scholar](#)
38. Piri J., Pirzadeh B., Keshtegar B., & Givehchi M. (2021). Reliability analysis of pumping station for sewage network using hybrid neural networks-genetic algorithm and method of moment. *Process Safety and Environmental Protection*, 145, 39–51.
[View Article](#) • [Google Scholar](#)
39. Jovanovic L., Jovanovic G., Perisic M., Alimpic F., Stanisic S., Bacanin N., et al. (2023). The Explainable Potential of Coupling Metaheuristics-Optimized-XGBoost and SHAP in Revealing VOCs' Environmental Fate. *Atmosphere*, 14(1), 109.

[View Article](#) • [Google Scholar](#)

40. Al-Janabi S., Mohammad M., & Al-Sultan A. (2020). A new method for prediction of air pollution based on intelligent computation. *Soft Computing*, 24(1), 661–680.
[View Article](#) • [Google Scholar](#)
41. Nayak D. R., Pady N., Mallick P. K., Bagal D. K., & Kumar S. (2022). Brain tumour classification using noble deep learning approach with parametric optimization through metaheuristics approaches. *Computers*, 11(1), 10.
[View Article](#) • [Google Scholar](#)
42. Zivkovic M., Bacanin N., Antonijevic M., Nikolic B., Kvascev G., Marjanovic M., et al. (2022). Hybrid CNN and XGBoost Model Tuned by Modified Arithmetic Optimization Algorithm for COVID-19 Early Diagnostics from X-ray Images. *Electronics*, 11(22), 3798.
[View Article](#) • [Google Scholar](#)
43. Bacanin N., Stoean C., Zivkovic M., Rakic M., Strulak-Wójcikiewicz R., & Stoean R. (2023). On the Benefits of Using Metaheuristics in the Hyperparameter Tuning of Deep Learning Models for Energy Load Forecasting. *Energies*, 16(3), 1434.
[View Article](#) • [Google Scholar](#)
44. Makhadmeh S. N., Al-Betar M. A., Alyasseri Z. A. A., Abasi A. K., Khader A. T., Damaševićius R., et al. (2021). Smart home battery for the multi-objective power scheduling problem in a smart home using grey wolf optimizer. *Electronics*, 10(4), 447.
[View Article](#) • [Google Scholar](#)
45. Stankovic, M., Antonijevic, M., Bacanin, N., Zivkovic, M., Tanaskovic, M., & Jovanovic, D. (2022, October). Feature Selection by Hybrid Artificial Bee Colony Algorithm for Intrusion Detection. In *2022 International Conference on Edge Computing and Applications (ICECAA)* (pp. 500–505). IEEE.
46. Jouhari H., Lei D., Al-qaness M. A., Elaziz M. A., Damaševićius R., Korytkowski M., et al. (2020). Modified Harris Hawks optimizer for solving machine scheduling problems. *Symmetry*, 12(9), 1460.
[View Article](#) • [Google Scholar](#)
47. Makhadmeh S. N., Al-Betar M. A., Awadallah M. A., Abasi A. K., Alyasseri Z. A. A., Doush I. A., et al. (2022). A modified coronavirus herd immunity optimizer for the power scheduling problem. *Mathematics*, 10(3), 315.
[View Article](#) • [Google Scholar](#)
48. Sinwar D., Saini M., Singh D., Goyal D., & Kumar A. (2021). Availability and performance optimization of physical processing unit in sewage treatment plant using genetic algorithm and particle swarm optimization. *International Journal of System Assurance Engineering and Management*, 1–12.
[View Article](#) • [Google Scholar](#)
49. Kumar A., Saini M., Gupta N., Sinwar D., Singh D., Kaur M., et al. (2022). Efficient stochastic model for operational availability optimization of cooling tower using metaheuristic algorithms. *IEEE Access*, 10, 24659–24677.
[View Article](#) • [Google Scholar](#)
50. Saini M., Goyal D., Kumar A., & Patil R. B. (2022). Availability optimization of biological and chemical processing unit using genetic algorithm and particle swarm optimization. *International Journal of Quality & Reliability Management*.
[View Article](#) • [Google Scholar](#)
51. Saini M., Gupta N., Shankar V. G., & Kumar A. Stochastic modeling and availability optimization of condenser used in steam turbine power plants using GA and PSO. *Quality and Reliability Engineering International*. 2022.
[View Article](#) • [Google Scholar](#)
52. Derrac J., García S., Molina D., & Herrera F. (2011). A practical tutorial on the use of nonparametric statistical tests as a methodology for comparing evolutionary and swarm intelligence algorithms. *Swarm and Evolutionary Computation*, 1(1), 3–18.
[View Article](#) • [Google Scholar](#)
53. Goldberg D. E., & Holland J. H. (1988). Genetic algorithms and machine learning.
[View Article](#) • [Google Scholar](#)
54. Storn R., & Price K. (1997). Differential evolution—a simple and efficient heuristic for global optimization over continuous spaces. *Journal of global optimization*, 11(4), 341–359.
[View Article](#) • [Google Scholar](#)
55. Dorigo M., Birattari M., & Stutzle T. (2006). Ant colony optimization. *IEEE computational intelligence magazine*, 1(4), 28–39.
[View Article](#) • [Google Scholar](#)
56. Mirjalili S., Mirjalili S. M., & Lewis A. (2014). Grey wolf optimizer. *Advances in engineering software*, 69, 46–61.
[View Article](#) • [Google Scholar](#)
57. Wang G. G., Deb S., & Coelho L. D. S. (2018). Earthworm optimization algorithm: a bio-inspired metaheuristic algorithm for global optimization problems. *International journal of bio-inspired computation*, 12(1), 1–22.
[View Article](#) • [Google Scholar](#)
58. Wang G. G. (2018). Moth search algorithm: a bio-inspired metaheuristic algorithm for global optimization problems. *Memetic Computing*, 10(2), 151–164.

[View Article](#) • [Google Scholar](#)

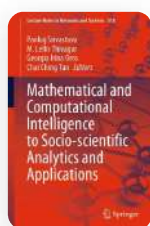
59. Wang, G. G., Deb, S., & Coelho, L. D. S. (2015, December). Elephant herding optimization. In 2015 3rd International Symposium on Computational and Business Intelligence (ISCB) (pp. 1–5). IEEE.
60. Wang G. G., Deb S., & Cui Z. (2019). Monarch butterfly optimization. *Neural computing and applications*, 31(7), 1995–2014.
[View Article](#) • [Google Scholar](#)
61. Heidari A. A., Mirjalili S., Faris H., Aljarah I., Mafarja M., & Chen H. (2019). Harris hawks optimization: Algorithm and applications. *Future generation computer systems*, 97, 849–872.
[View Article](#) • [Google Scholar](#)
62. Li S., Chen H., Wang M., Heidari A. A., & Mirjalili S. (2020). Slime mould algorithm: A new method for stochastic optimization. *Future Generation Computer Systems*, 111, 300–323.
[View Article](#) • [Google Scholar](#)

[Home](#) > [Mathematical and Computational Intelligence to Socio-scientific Analytics and Applications](#) > Chapter

Sufficient Conditions of q -Starlikeness and q -Convexity Associated with Basic Hypergeometric Function

| Chapter | First Online: 03 January 2023

| pp 131–142 | [Cite this chapter](#)



Mathematical and Computational Intelligence to Socio-scientific Analytics and Applications

[Murli M. Gour](#), [Sunil Joshi](#)  & [Sunil D. Purohit](#)

 Part of the book series: [Lecture Notes in Networks and Systems](#) ((LNNS, volume 518))

Abstract

In this paper, we determine certain coefficient inequalities for the classes of q -starlike and q -convex function and find the sufficient conditions for normalized basic hypergeometric function to belonging in these classes. The technique developed in this present investigations can be used with other functions.

i This is a preview of subscription content, [log in via an institution](#) to check access.

Access this chapter

Log in via an institution

^ Chapter

EUR 29.95

Price includes VAT (India)

Available as PDF

Read on any device

Instant download

Own it forever

Buy Chapter

v eBook

EUR 106.99

v Softcover Book

EUR 129.99

Tax calculation will be finalised at checkout

Purchases are for personal use only

[Institutional subscriptions](#) →

Similar content being viewed by others



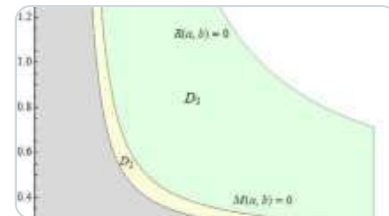
Higher-order q -derivatives and their applications to subclasses of...

Article | Open access
07 October 2021



Some geometric properties of a class of functions related to the Fox–Wright functions

Article | 18 February 2020



Monotonicity and concavity properties of the Gaussian hypergeometric...

Article | 12 September
2022

References

1. Agarwal R, Paliwal GS, Parihar HS (2017) Geometric properties and neighborhood results for a subclass of analytic functions involving Komatu integral. Stud Univ Babeş–Bolyai Math 62(3):377–394

[Article](#) [MathSciNet](#) [MATH](#) [Google Scholar](#)

2. Agarwal R, Paliwal GS (2020) Ruscheweyh–Goyal derivative of fractional order, its properties pertaining to pre-starlike type functions and applications. Appl Appl Math Special issue 6:103–121

[MathSciNet](#) [MATH](#) [Google Scholar](#)

3. Agrawal S, Sahoo SK (2017) A generalization of starlike functions of order alpha. Hokkaido Math J 46(1):15–27

[Article](#) [MathSciNet](#) [MATH](#) [Google Scholar](#)

4. Duren PL (1983) Univalent functions. Grundlehren der Mathematischen Wissenschaften [Fundamental Principles of Mathematical Sciences], vol 259. Springer, New York

[Google Scholar](#)

5. Gasper G, Rahman M (1990) Basic hypergeometric series. With a foreword by Richard Askey. Encyclopedia of Mathematics and its Applications, vol 35. Cambridge University Press, Cambridge

[Google Scholar](#)

6. Gour MM, Joshi S, Goswami P (2020) Sufficient condition for (q) -starlike and (q) -convex functions associated with generalized confluent hypergeometric functions. Adv Theory Non-linear Anal Appl (ATNAA) 4(4):421–431

[Google Scholar](#)

7. Goyal SP, Goyal R (2007) Sufficient conditions for starlikeness of multivalent functions of order (δ) . J Indian Acad Math 29(1):115–124

[MathSciNet](#) [MATH](#) [Google Scholar](#)

8. Ismail MEH, Merkes E, Styer D (1990) A generalization of starlike functions. Complex Variables Theory Appl 14(1–4):77–84

[Article](#) [MathSciNet](#) [MATH](#) [Google Scholar](#)

9. Janowski W (1973) Some extremal problems for certain families of analytic functions. I Ann Polon Math 28:297–326

[Article](#) [MathSciNet](#) [MATH](#) [Google Scholar](#)

10. Seoudy TM, Aouf MK (2016) Coefficient estimates of new classes of (q) -starlike and (q) -convex functions of complex order. J Math Inequal 10(1):135–145

[Article](#) [MathSciNet](#) [MATH](#) [Google Scholar](#)

11. Slater L (1966) Generalized hypergeometric functions. Cambridge University Press, Cambridge

[MATH](#) [Google Scholar](#)

12. Srivastava HM, Bansal D (2017) Close-to-convexity of a certain family of (q) -Mittag-Leffler functions. J Nonlinear Var Anal 1(1):61–69

[MATH](#) [Google Scholar](#)

13. Srivastava HM, Khan B, Khan N, Ahmed QZ (2019) Coefficient inequalities for (q) -starlike functions associated with the Janowski functions. Hokkaido Math J 48(2):407–425

[Article](#) [MathSciNet](#) [MATH](#) [Google Scholar](#)

14. Srivastava HM (2020) Operators of basic (or (q) -) calculus and fractional (q) -calculus and their applications in geometric function theory of complex analysis. Iran J Sci Technol Trans A Sci 44(1):327–344

[Article](#) [MathSciNet](#) [Google Scholar](#)

15. Srivastava HM, Aouf MK, Mostafa AO (2019) Some properties of analytic functions associated with fractional (q) -calculus operators. Miskolc Math Notes 20(2):1245–1260

[Article](#) [MathSciNet](#) [MATH](#) [Google Scholar](#)

Acknowledgements

The authors are thankful to the referees for their valuable remarks and comments for the improvement of the paper.

Author information

Authors and Affiliations

Department of Mathematics and Statistics, Manipal University Jaipur, Jaipur, India

Murli M. Gour & Sunil Joshi

Department of Mathematics, Rajasthan Technical University Kota, Kota, India

Sunil D. Purohit

Corresponding author

Correspondence to [Sunil Joshi](#).

Editor information

Editors and Affiliations

Department of Mathematics, MNNIT Allahabad, FATER Academy of India, Prayagraj, India

Pankaj Srivastava

School of Mathematics, Madurai Kamaraj University, Madurai, India

M. Lellis Thivagar

Department of Mathematics and Computer Science, University of Oradea, Oradea, Romania

Georgia Irina Oros

Rattanakosin International College of Creative Entrepreneurship, Rajamangala University of Technology, Nakhon Pathom, Thailand

Chai Ching Tan

Rights and permissions

[Reprints and permissions](#)

Copyright information

© 2022 The Author(s), under exclusive license to Springer Nature Singapore Pte Ltd.

About this chapter

Cite this chapter

Gour, M.M., Joshi, S., Purohit, S.D. (2022). Sufficient Conditions of q -Starlikeness and q -Convexity Associated with Basic Hypergeometric Function. In: Srivastava, P., Thivagar, M.L., Oros, G.I., Tan, C.C. (eds) Mathematical and Computational Intelligence to Socio-scientific Analytics and Applications. Lecture Notes in Networks and Systems, vol 518. Springer, Singapore. https://doi.org/10.1007/978-981-19-5181-7_9

[.RIS](#) [.ENW](#) [.BIB](#)

DOI

https://doi.org/10.1007/978-981-19-5181-7_9

Published

03 January 2023

Publisher Name

Springer, Singapore

Print ISBN

978-981-19-5180-0

Online ISBN

978-981-19-5181-7

eBook Packages

[Mathematics and Statistics](#)

[Mathematics and Statistics](#)

[\(R0\)](#)

Publish with us

[Policies and ethics](#) [↗](#)

Stochastic modeling and parameter estimation of turbogenerator unit of a thermal power plant under classical and Bayesian inferential framework

Ashish Kumar, Ravi Chaudhary, Kapil Kumar, Monika Saini, Dinesh Kumar Saini, Punit Gupta

Published: October 20, 2023 • <https://doi.org/10.1371/journal.pone.0292154>

Abstract

The work reported in present study deals with the development of a novel stochastic model and estimation of parameters to assess reliability characteristics for a turbogenerator unit of thermal power plant under classical and Bayesian frameworks. Turbogenerator unit consists of five components namely turbine lubrication, turbine governing, generator oil system, generator gas system and generator excitation system. The concepts of cold standby redundancy and Weibull distributed random variables are used in development of stochastic model. The shape parameter for all the random variables is same while scale parameter is different. Regenerative point technique and semi-Markov approach are used for evaluation of reliability characteristics. Sufficient repair facility always remains available in plant as well as repair done by the repairman is considered perfect. As the life testing experiments are time consuming, so to highlight the importance of proposed model Monte Carlo simulation study is carried out. A comparative analysis is done between true, classical and Bayesian results of MTSF, availability and profit function.

Citation: Kumar A, Chaudhary R, Kumar K, Saini M, Saini DK, Gupta P (2023) Stochastic modeling and parameter estimation of turbogenerator unit of a thermal power plant under classical and Bayesian inferential framework. PLoS ONE 18(10): e0292154. <https://doi.org/10.1371/journal.pone.0292154>

Editor: Bhisham Sharma, Chitkara University, INDIA

Received: May 31, 2023; **Accepted:** September 13, 2023; **Published:** October 20, 2023

Copyright: © 2023 Kumar et al. This is an open access article distributed under the terms of the [Creative Commons Attribution License](#), which permits unrestricted use, distribution, and reproduction in any medium, provided the original author and source are credited.

Data Availability: All relevant data are within the paper.

Competing interests: The authors have declared that no competing interests exist.

1. Introduction

The increasing demand and technological advancements inclined the complexity of industrial and mechanical systems. The products generated by these industries are extensively used in day-to-day life of human being. The thermal power plant is also a such system which is prominently contribute to energy generation sector in most of the countries. Availability, mean time to system failure and performance of the thermal power plants attract the attention of system designers to assess the effectiveness of plants during last few decades. Various subsystems of these plants critically influence the performance. Turbogenerator is a prominent component of thermal power plant that influences the performance of whole plant. So, reliability characteristics evolution of these components become necessary to evaluate performance of the plant. Several methodologies like fault tree analysis, failure mode effect analysis, Markovian approach and reliability block diagram approach are used in previous studies under various kind of failure distributions. Such a distribution to investigate reliability of industrial systems is proposed by Weibull [1]. Weibull distribution have wide applicability in life testing, reliability modeling and estimation due to its flexible shapes of the failure rate functions.

Provision of spare component is also a reliability enhancement technique that can be used in such systems. Masters et al. [2] developed a model for confidence interval estimation of availability function for Weibull distributed operating system. Dhillon and Anuda [3] developed a stochastic model under arbitrary failure rates and common cause failures. Coit [4] optimized the redundancy of components in non-repairable systems. Yadavalli et al. [5] used concept of preparation time to develop asymptotic confidence limits for availability function of parallel systems. Lim et al. [6] developed bootstrap confidence interval for steady state availability of systems. Yadavalli et al. [7] conducted a Bayesian study for two-unit system under impact of common cause shock failures. Chien et al. [8] developed asymptotic confidence limits for a repairable system having imperfect service facility. Ke et al. [9] performed the Bayesian estimation of standby system under imperfect coverage. Hsu et al. [10] done Bayesian and asymptotic estimation under reboot and imperfect coverage for repairable system. Gupta et al. [11] done the cost analysis of non-identical unit's system considering Weibull distribution for failure and repair rates. Singh et al. [12] drawn some statistical inferences for a time dependent dynamical system. Chaturvedi et al. [13] developed a robust model for Weibull distribution under Bayesian framework.

Kishan and Jain [14] conducted the parameter estimation for a parallel unit system to evaluate the reliability measures. It is considered that all time dependent random variables are Weibull distributed having common shape parameter. Kumar and Saini [14] proposed a stochastic model for single unit system to assess the impact of preventive maintenance under Weibull distribution. Liu et al. [15] conducted the reliability evaluation of a system of non-identical units under fuzzy environment. Kumar et al. [16] studied the effect of hot and cold standby redundancy on availability of thermal power plants. Kumar and Garg [17] estimated parameters of generalized inverted Rayleigh distribution under random censoring. Pariaman et al. [18] discussed several methodologies for availability enhancement of thermal power plants. Dongliang et al. [19] used phase time distribution for reliability estimation of non-identical unit systems. Kumar et al. [20–22] investigated the impact of various kind of priorities and preventive maintenance on systems of Weibull distributed random variables. Chopra and Ram [23] proposed a stochastic model for parallel

system with waiting time. Dey et al. [24] provided an extension of generalized exponential distribution having application in Ozone data. Gupta and Singh [25] conducted classical and Bayesian analysis of Weibull distribution under outliers. Han et al. [26] explored the needs of Bayesian statistics in various studies.

Pundir et al. [27] developed a stochastic framework for parallel system of non-identical units having priority in repair disciplines. Kumar and Kadyan [28, 29] proposed reliability models for performance evaluation of industrial system using supplementary variable technique. Kumar and Kumar [30] estimate various statistical properties of inverse Weibull distribution under random censoring. Saini and Kumar [31] developed a stochastic model for single unit system under abnormal environmental conditions to assess impact of inspection and degradation. Saini et al. [32] proposed a stochastic model to evaluate the profit of redundant system under priority. Pundir et al. [33] analysed the impact of presence of prior on reliability estimation of standby system. Patawa et al. [34] drawn various inferences for reliability measures of non-identical system with standby redundancy and waiting time in Bayesian framework. Rathi et al. [35] developed a model for reliability improvement using redundancies and Markov process.

Though, a lot of work has been carried out in the direction of reliability evaluation of industrial system, but it is focused only on modelling, MTSF, steady state availability and performance evaluation by considering constant failure and repair rates of components. The estimation of the parameters is still not extensively explored for industrial system specially in field of thermal power plants. The reliability modelling and classical & Bayesian estimation of reliability measures of turbogenerator unit yet not discussed in literature so far. So, in the present work a novel stochastic model for turbogenerator system comprises with five components of thermal power plant is proposed by considering Weibull distribution for failure and repair rates having different scale parameter and common shape parameter. As Weibull distribution is the most popular in reliability modeling and estimation due to its flexible shapes of the failure rate functions. To extract concrete findings from stochastic model simulation study is conducted. The following system reliability measures, which are useful for plant designers and maintenance managers, are derived using semi-Markovian approach and regenerative point technique:

- › Steady state transition probabilities associated with various states of turbogenerator system
- › Mean sojourn times associated with various regenerative states of turbogenerator system
- › True and estimated values of mean time to system failure (MTSF) of turbogenerator system
- › True and estimated values of steady state availability of turbogenerator system
- › True and estimated values of profit of turbogenerator system

Due to random behaviour of lifetime of the components of turbogenerator the parameter of associated distribution is estimated in classical and Bayesian framework. The posterior densities are not easy to simulate directly so Metropolis-Hastings algorithm of the MCMC procedure is utilized to generate the random samples from this posterior density. The Monte Carlo simulation technique is employed to derive the numerical values of reliability measures in classical and Bayesian framework. The mean square error (MSE), confidence interval length along with MTSF, availability and profit are evaluated in classical framework while under Bayesian framework posterior mean square error, width of highest posterior density are computed. To highlight the importance of study, a comparative analysis is also made through numerical results and graphs. The whole manuscript is organized into five sections including the current introduction section. Section 2 includes the notations and system description. All the reliability measures obtained in section 3 while section 4 devoted to the estimation of parameters in classical and Bayesian framework. Concluding remarks are made in section 5.

2. Notations and system description

In this section the system description of turbogenerator and notation used for model development are appended.

2.1 Notations

S_i : i^{th} state of the turbogenerator

θ_i/β_i ($i = 1, 2, 3, 4, 5$): Scale parameter of failure/repair time distribution for i^{th} unit

η : Shape parameter of failure/repair time distribution of each unit

$f_i(t)$: Failure rate of i^{th} unit where $f_i(t) = \theta_i \eta t^{\eta-1} e^{-\theta_i t^\eta}$, $\theta_i > 0, t > 0$

$g_i(t)$: Repair rate of i^{th} unit where $g_i(t) = \beta_i \eta t^{\eta-1} e^{-\beta_i t^\eta}$, $\beta_i > 0, t > 0$

$q_{ij}(t)/Q_{ij}(t)$: Pdf and c.d.f. of one step or direct transition time from $S_i \in E$ to $S_j \in E$

$p_{ij}(t)$: Steady state transition probability from state S_i to S_j such that, $p_{ij} = \lim_{t \rightarrow \infty} Q_{ij}(t)$

$p_{ij}^{(k)}(t)$: steady state transition probability from state S_i to S_j via S_k such that, $p_{ij}^{(k)} = \lim_{t \rightarrow \infty} Q_{ij}^{(k)}(t)$

$Z_i(t)$: Probability that system sojourns in state S_i up to time t

μ_i : Mean sojourn time in state S_i i.e., $\mu_i = \int_0^\infty P(T_i > t) dt$

$R_i(t)$: Reliability of the system at time t when system starts from $S_i \in E$

$A_i(t)$: Probability that the system will be operative in state $S_i \in E$ at epoch t

$B_i(t)$: Probability that the repairman will be busy in state $S_i \in E$ at epoch t

$P_i(t)$: Profit incurred by the system during interval $(0, t)$

** : Symbol for Laplace Transform of a function i.e., $Q_{ij}^{**}(s) = \int_0^\infty q_{ij}(t) e^{-st} dt$

• : Regenerative point

X: Non-regenerative point

A_0 : Turbine governing unit (A) is operative

B_0 : Turbine lubrication unit (B) is operative

C_0 : generator oil system (C) is operative

D_0 : generator gas system (D) is operative

E_0 : generator extinction system € is in normal mode and operative

E_s Unit-E is in standby mode

a_r/a_{wr} : Turbine governing unit (A) is either in repair/waiting for repair

b_r/b_{wr} : Turbine lubrication unit (B) is either in repair/waiting for repair

c_r/c_{wr} : generator oil system (C) is either in repair/waiting for repair

d_r/d_{wr} : generator gas system (D) is either in repair/waiting for repair

e_{wr} : Unit-E is in non-operative mode and under waiting for repair

e_r : Unit-E is in non-operative mode and under repair

2.2 System description

The turbogenerator is a critical component of thermal power plant and its availability influence the performance of whole plant in production of electricity. The considered turbogenerator [36] in present study is installed in a thermal power plant in India that produce 500 MW electricity. It consists of five subsystems (i) turbine governing "A" (ii) turbine lubrication "B", (iii) generator oil system "C" (iv) generator gas system "D" and (v) generator extinction system "E". There is no provision of standby component for turbine governing, turbine lubrication, generator oil system, and generator gas system while provision of one cold standby component is made for generator extinction system. The failure of single unit subsystems immediately resulted as the complete system failure. The flow chart of system is shown in Fig.1. The system works under a set of assumptions like failure and repair rates are statistically independent to each other, no multiple failures, standby units worked in full capacity and after repair unit worked as new one. Under this assumption, here the reliability characteristics of turbogenerator is assessed using regenerative point technique and semi-Markovian approach. A stochastic model is proposed and expressions for various reliability measures are derived. The failure and repair rates are obtained from time to failure and time to repair data. Further, the parameter estimation is done under classical and Bayesian inferential frameworks. The state transition diagram of the proposed stochastic model is shown in Fig.2.

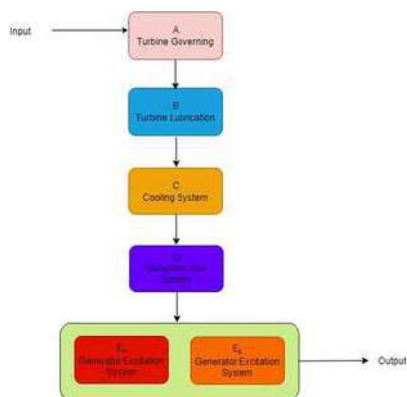


Fig 1. Flowchart of turbogenerator system.

<https://doi.org/10.1371/journal.pone.0292154.g001>

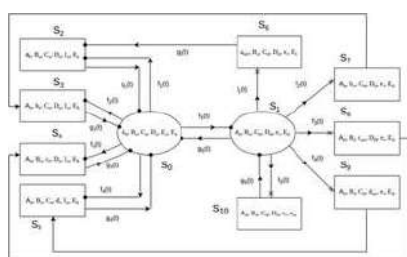


Fig 2. State transition diagram of turbogenerator system.

3. Reliability measures of turbogenerator system

3.1 Transition probabilities

The state space of the turbogenerator system is discrete in nature having states $\{S_0, S_1, S_2, S_3, S_4, S_5, S_6, S_7, S_8, S_9, S_{10}\}$. The probability of movement among these states is known as transition probability. Here, p_{ij} represent the transition from state 'i' to 'j'. By simple probabilistic considerations value of p_{ij} is obtained by following expression for the non-zero elements of transition probability matrix (TPM):

$$p_{ij} = \lim_{t \rightarrow \infty} Q_{ij}(t) = \int_0^{\infty} q_{ij}(t) dt \tag{1}$$

The associated transition probability matrix of present system is defined as:

$$X = \begin{bmatrix} p_{00} & \dots & p_{0,10} \\ \vdots & \ddots & \vdots \\ p_{10,0} & \dots & p_{10,10} \end{bmatrix}$$

So, Eq (1) gives the values of all the entries of TPM (X) as the probability of transition from state S_0 to state S_1 with transition rate $f_5(t)$ without any transition to other states. The detailed procedure is presented in [1]. Mathematically,

$$Q_{01}(t) = \int_0^{\infty} f_5(t) F_1(t) F_2(t) F_3(t) F_4(t) dt$$

taking Laplace transform from both side

$$Q_{01}^{**}(s) = \int_0^{\infty} \theta_5 \eta t^{\eta-1} e^{-(\theta_1+\theta_2+\theta_3+\theta_4+\theta_5+s)t} dt = \lim_{s \rightarrow 0} \frac{\theta_5}{(\theta_1 + \theta_2 + \theta_3 + \theta_4 + \theta_5 + s)}$$

$$\Rightarrow p_{01} = \lim_{s \rightarrow 0} Q_{01}^{**}(s) = \frac{\theta_5}{(\theta_1 + \theta_2 + \theta_3 + \theta_4 + \theta_5)}$$

Similarly, $p_{02} = \frac{\theta_1}{(\theta_1 + \theta_2 + \theta_3 + \theta_4 + \theta_5)}$, $p_{03} = \frac{\theta_2}{(\theta_1 + \theta_2 + \theta_3 + \theta_4 + \theta_5)}$, $p_{04} = \frac{\theta_3}{(\theta_1 + \theta_2 + \theta_3 + \theta_4 + \theta_5)}$,

$$p_{05} = \frac{\theta_4}{(\theta_1 + \theta_2 + \theta_3 + \theta_4 + \theta_5)}$$
, $p_{16} = \frac{\theta_1}{(\theta_1 + \theta_2 + \theta_3 + \theta_4 + \theta_5 + \beta_5)}$, $p_{17} = \frac{\theta_2}{(\theta_1 + \theta_2 + \theta_3 + \theta_4 + \theta_5 + \beta_5)}$,

$$p_{18} = \frac{\theta_3}{(\theta_1 + \theta_2 + \theta_3 + \theta_4 + \theta_5 + \beta_5)}$$
, $p_{19} = \frac{\theta_4}{(\theta_1 + \theta_2 + \theta_3 + \theta_4 + \theta_5 + \beta_5)}$, $p_{1,10} = \frac{\theta_5}{(\theta_1 + \theta_2 + \theta_3 + \theta_4 + \theta_5 + \beta_5)}$, $p_{10} = \frac{\beta_5}{(\theta_1 + \theta_2 + \theta_3 + \theta_4 + \theta_5 + \beta_5)}$, $p_{20} = \lim_{s \rightarrow 0} Q_{20}^{**}(s) = 1$, $p_{30} = \lim_{s \rightarrow 0} Q_{30}^{**}(s) = 1$, $p_{40} = \lim_{s \rightarrow 0} Q_{40}^{**}(s) = 1$, $p_{50} = \lim_{s \rightarrow 0} Q_{50}^{**}(s) = 1$, $p_{62} = \lim_{s \rightarrow 0} Q_{62}^{**}(s) = 1$, $p_{73} = \lim_{s \rightarrow 0} Q_{73}^{**}(s) = 1$, $p_{84} = \lim_{s \rightarrow 0} Q_{84}^{**}(s) = 1$, $p_{95} = \lim_{s \rightarrow 0} Q_{95}^{**}(s) = 1$, $p_{10,1} = \lim_{s \rightarrow 0} Q_{10,1}^{**}(s) = 1$.

It is easily verified that sum of all entries of each row is unity.

3.2 Mean sojourn times

The average time spent by a system is known as mean sojourn time. The detailed procedure is presented in [1]. If T_i represent the average sojourn/survival time of turbogenerator at a particular state S_i , then the mean sojourn time in the state S_i is evaluated using mathematical expressions:

$$\mu_i = \int_0^{\infty} P_r(T_i > t) = \sum_j m_{ij} \tag{2}$$

where $m_{ij} = -\frac{d}{ds} [Q_{ij}^{**}(s)]_{s=0}$.

Using Eq (2), mean sojourn time at state S_0 is evaluated as follows:

$$\mu_0 = \int_0^{\infty} F_1(t) F_2(t) F_3(t) F_4(t) F_5(t) dt \tag{3}$$

Taking Laplace transform on Eq (3) both side, we get

$$\mu_0^{**}(s) = \int_0^{\infty} e^{-\theta_1 t} e^{-\theta_2 t} e^{-\theta_3 t} e^{-\theta_4 t} e^{-\theta_5 t} e^{-st} dt$$

After solving it, we get

$$\mu_0^{**}(s) = \lim_{s \rightarrow 0} \frac{\Gamma(1+1/\eta)}{(\theta_1 + \theta_2 + \theta_3 + \theta_4 + \theta_5 + s)^{1/\eta}} \Rightarrow \mu_0 = \frac{\Gamma(1+1/\eta)}{(\theta_1 + \theta_2 + \theta_3 + \theta_4 + \theta_5)^{1/\eta}}$$

Similarly

$$\mu_1 = \frac{\Gamma(1+1/\eta)}{(\theta_1 + \theta_2 + \theta_3 + \theta_4 + \theta_5 + \beta_5)^{1/\eta}}, \mu_2 = \frac{\Gamma(1+1/\eta)}{(\beta_1)^{1/\eta}}, \mu_3 = \frac{\Gamma(1+1/\eta)}{(\beta_2)^{1/\eta}}, \mu_4 = \frac{\Gamma(1+1/\eta)}{(\beta_3)^{1/\eta}}, \mu_5 = \frac{\Gamma(1+1/\eta)}{(\beta_4)^{1/\eta}}$$

3.3 Mean time to system failure

To evaluate turbogenerator reliability $R_i(t)$ at time "t" starting from regenerative state S_i to a failed state S_j , it represents the c.d.f of first passage time. The detailed methodology of mean time of system failure evaluation is presented in [37]. By considering failed states as absorbing state and using probabilistic arguments, following recursive relations for $R_i(t)$ are derived based on state transition diagram given in Fig 2:

$$R_0(t) = Q_{01}(t)1R_1(t) + Z_0(t) \quad (4)$$

$$R_1(t) = Q_{10}(t)1R_0(t) + Z_1(t) \quad (5)$$

Where,

$$Z_0(t) = Q_{02}(t) + Q_{03}(t) + Q_{04}(t) + Q_{05}(t) \quad (6)$$

$$Z_1(t) = Q_{16}(t) + Q_{17}(t) + Q_{18}(t) + Q_{19}(t) + Q_{1,10}(t) \quad (7)$$

By taking Laplace transformation of Eqs (4–5) and solving for $R_0^{**}(s)$, we get

$$R_0^{**}(s) = \frac{N_0}{D_0} = \frac{Z_0^{**}(s) + Q_{01}^{**}(s)Z_1^{**}(s)}{1 - Q_{01}^{**}(s)Q_{10}^{**}(s)} \quad (8)$$

The inverse Laplace transformation of Eq (8) gives the reliability of turbogenerator. the mean time to system failure is derived as follows:

$$\begin{aligned} MTSF &= \lim_{s \rightarrow 0} \frac{1 - R_0^{**}(s)}{s} = \lim_{s \rightarrow 0} \frac{1 - Q_{01}^{**}(s)Q_{10}^{**}(s) - Z_0^{**}(s) - Q_{01}^{**}(s)Z_1^{**}(s)}{s(1 - Q_{01}^{**}(s)Q_{10}^{**}(s))} = \frac{\mu_0 + P_{01}\mu_1}{1 - P_{01}P_{10}} \\ &= \frac{a[(\sum \theta_i + \theta_5)(\sum \theta_i + \theta_5 + \beta_5) + \theta_5(\sum \theta_i + \theta_5)^{1/\eta}(\sum \theta_i + \theta_5 + \beta_5)^{1-1/\eta}]}{[(\sum \theta_i + \theta_5)^{1+1/\eta}(\sum \theta_i + \theta_5 + \beta_5) - \theta_5\beta_5(\sum \theta_i + \theta_5)^{1/\eta}]} \end{aligned} \quad (9)$$

where $a = \Gamma(1+1/\eta)$

3.4 Availability analysis

Let $A_i(t)$ be the probability of turbogenerator that it is in up-state at instant 't' given that the system entered regenerative state S_i at t = 0. The recursive relations for $A_i(t)$ are derived based on state transition diagram given in Fig 2:

$$A_0(t) = Z_0(t) + Q_{01}(t)1A_1(t) + Q_{02}(t)1A_2(t) + Q_{03}(t)1A_3(t) + Q_{04}(t)1A_4(t) + Q_{05}(t)1A_5(t) \quad (10)$$

$$A_1(t) = Z_1(t) + Q_{10}(t)1A_0(t) + Q_{12}^6(t)1A_2(t) + Q_{13}^7(t)1A_3(t) + Q_{14}^8(t)1A_4(t) + Q_{15}^9(t)1A_5(t) + Q_{11}^{10}(t)1A_1(t) \quad (11)$$

$$A_2(t) = Q_{20}(t)1A_0(t) \quad (12)$$

$$A_3(t) = Q_{30}(t)1A_0(t) \quad (13)$$

$$A_4(t) = Q_{40}(t)1A_0(t) \quad (14)$$

$$A_5(t) = Q_{50}(t)1A_0(t) \quad (15)$$

Taking Laplace transformation on Eqs (10–15) and solving for $A_0^{**}(s)$ we get

$$A_0^{**}(s) = \frac{N_1(s)}{D_1(s)}$$

Where,

$$D_1 = [1 - Q_{1,10}^{**}(s)][A + CQ_{02}^{**}(s) + DQ_{03}^{**}(s) + EQ_{04}^{**}(s) + FQ_{05}^{**}(s)] + Q_{01}^{**}(s)[B + CQ_{16}^{**}(s) + DQ_{17}^{**}(s) + EQ_{18}^{**}(s) + FQ_{19}^{**}(s)]$$

$$N_1 = Z_0^{**}(s)[1 - Q_{1,10}^{**}(s)] + Q_{01}^{**}(s)Z_1^{**}(s)$$

$$A = 1 - Q_{01}^{**}(s) - Q_{02}^{**}(s) - Q_{03}^{**}(s) - Q_{04}^{**}(s) - Q_{05}^{**}(s)$$

$$B = 1 - Q_{11}^{10**}(s) - Q_{12}^{6**}(s) - Q_{13}^{7**}(s) - Q_{14}^{8**}(s) - Q_{15}^{9**}(s) - Q_{10}^{**}(s)$$

$$C = 1 - Q_{20}^{**}(s)$$

$$D = 1 - Q_{30}^{**}(s)$$

$$E = 1 - Q_{40}^{**}(s)$$

$$F = 1 - Q_{50}^{**}(s)$$

After taking inverse Laplace transformation Eq (16), we get

$$\begin{aligned} \text{Availability} &= \lim_{s \rightarrow 0} A_0^{**}(s) = \lim_{s \rightarrow 0} \frac{N_1 + sN_1}{D_1} \\ &= \frac{\mu_0(1 - P_{1,10}) + P_{01}\mu_1}{[1 - P_{1,10}][\mu_0 + P_{02}m_{20} + P_{03}m_{30} + P_{04}m_{40} + P_{05}m_{50}] + P_{01}[\mu_1 + P_{16}m_{20} + P_{17}m_{30} + P_{18}m_{40} + P_{19}m_{50}]} \end{aligned} \quad (17)$$

3.5 Busy period of server

Let $B_i(t)$ be the probability that repairman is busy in repairing the failed unit at epoch "t" given that the turbogenerator system entered state S_i at $t = 0$. The recursive relations for $B_i(t)$ are derived based on state transition diagram given in Fig.2:

$$B_0(t) = Q_{01}(t)1B_1(t) + Q_{02}(t)1B_2(t) + Q_{03}(t)1B_3(t) \quad (18)$$

$$B_1(t) = Q_{10}(t)1B_0(t) + Q_{12}^6(t)1B_2(t) + Q_{13}^7(t)1B_3(t) + Q_{14}^8(t)1B_4(t) + Q_{15}^9(t)1B_5(t) + Q_{11}^{10}(t)1B_1(t) \quad (19)$$

$$B_2(t) = Z_2(t) + Q_{20}(t)1B_0(t) \quad (20)$$

$$B_3(t) = Z_3(t) + Q_{30}(t)1B_0(t) \quad (21)$$

$$B_4(t) = Z_4(t) + Q_{40}(t)1B_0(t) \quad (22)$$

$$B_5(t) = Z_5(t) + Q_{50}(t)1B_0(t) \quad (23)$$

Taking Laplace transformation on both sides of Eqs (18–23) and solving for $B_0^{**}(s)$, we get

$$B_0^{**}(s) = \frac{N_2(s)}{D_1(s)}$$

Where,

$$\begin{aligned} N_2 &= [1 - Q_{1,10}^{**}(s)][Z_2^{**}(s)Q_{02}^{**}(s) + Z_3^{**}(s)Q_{03}^{**}(s) + Z_4^{**}(s)Q_{04}^{**}(s) + Z_5^{**}(s)Q_{05}^{**}(s)] + Q_{01}^{**}(s)[Z_2^{**}(s)Q_{16}^{**}(s) + Z_3^{**}(s)Q_{17}^{**}(s) \\ &\quad + Z_4^{**}(s)Q_{18}^{**}(s) + Z_5^{**}(s)Q_{19}^{**}(s)] \end{aligned}$$

The busy period in steady state is given by as follows:

$$\begin{aligned} \text{Busy Period of server} &= \lim_{s \rightarrow 0} B_0^{**}(s) = \lim_{s \rightarrow 0} \frac{N_2 + sN_2}{D_1} \\ &= \frac{[1 - P_{1,10}][P_{02}\mu_2 + P_{03}\mu_3 + P_{04}\mu_4 + P_{05}\mu_5] + P_{01}[P_{16}\mu_2 + P_{17}\mu_3 + P_{18}\mu_4 + P_{19}\mu_5]}{[1 - P_{1,10}][\mu_0 + P_{02}m_{20} + P_{03}m_{30} + P_{04}m_{40} + P_{05}m_{50}] + P_{01}[\mu_1 + P_{16}m_{20} + P_{17}m_{30} + P_{18}m_{40} + P_{19}m_{50}]} \end{aligned} \quad (24)$$

3.6 Profit function

The expected profit P incurred by the system in long run is

$$P = k_0 \text{Availability} - k_1 \text{Busy period of server}$$

Where k_0 : revenue per unit time; k_1 : cost per unit time

4. Estimation of reliability measures under classical and Bayesian setups

4.1 Classical estimation

Let us assume that the failure ($f_i(\cdot)$; $i = 1, 2, 3, 4, 5, 6$) and repair ($g_i(\cdot)$; $i = 1, 2, 3, 4, 5, 6$) rates of various components of turbogenerator followed Weibull distribution having common shape and different scale parameters. Where:

$$f_i(t) = \theta_i \eta t^{\eta-1}; \quad i = 1, 2, 3, 4, 5, 6$$

$$g_i(t) = \beta_i \eta t^{\eta-1}; \quad i = 1, 2, 3, 4, 5, 6$$

Here, θ_i, β_i are scale parameters while common scale parameter is η . All these random variables are statistically independent. As the main aim of present study is to estimate the parameters and reliability measures of turbogenerator in classical and Bayesian inferential setups. So, here maximum likelihood (ML) estimation method is employed as a powerful tool of classical estimation. The maximum likelihood estimators (MLE) of all the parameters are estimated for all the parameters of random variables.

Suppose ten independent random samples of size n_i ($i = 1, 2, 3, \dots, 10$) are drawn from Weibull distribution with failure rates ($f_i(\cdot)$; $i = 1, 2, 3, 4, 5, 6$) and repair rates ($g_i(\cdot)$; $i = 1, 2, 3, 4, 5, 6$) respectively.

$$\begin{aligned} \hat{Y}_1 &= (y_{11}, y_{12}, \dots, y_{1n_1}) \hat{Y}_2 = (y_{21}, y_{22}, \dots, y_{2n_2}) \\ \hat{Y}_3 &= (y_{31}, y_{32}, \dots, y_{3n_3}) \hat{Y}_4 = (y_{41}, y_{42}, \dots, y_{4n_4}) \\ \hat{Y}_5 &= (y_{51}, y_{52}, \dots, y_{5n_5}) \hat{Y}_6 = (y_{61}, y_{62}, \dots, y_{6n_6}) \\ \hat{Y}_7 &= (y_{71}, y_{72}, \dots, y_{7n_7}) \hat{Y}_8 = (y_{81}, y_{82}, \dots, y_{8n_8}) \\ \hat{Y}_9 &= (y_{91}, y_{92}, \dots, y_{9n_9}) \hat{Y}_{10} = (y_{10,1}, y_{10,2}, \dots, y_{10,n_{10}}) \end{aligned}$$

The joint likelihood function based on above ten samples is given by

$$L = L(\hat{Y}_1, \hat{Y}_2, \hat{Y}_3, \hat{Y}_4, \hat{Y}_5, \hat{Y}_6, \hat{Y}_7, \hat{Y}_8, \hat{Y}_9, \hat{Y}_{10} | \theta_1, \theta_2, \theta_3, \theta_4, \theta_5, \beta_1, \beta_2, \beta_3, \beta_4, \beta_5) \\ \prod_{i=1}^{n_1} \theta_1^{\eta} \theta_2^{\eta} \theta_3^{\eta} \theta_4^{\eta} \theta_5^{\eta} \beta_1^{\eta} \beta_2^{\eta} \beta_3^{\eta} \beta_4^{\eta} \beta_5^{\eta} \eta^{n_1+n_2+n_3+n_4+n_5+n_6+n_7+n_8+n_9+n_{10}} S_1 S_2 S_3 S_4 S_5 S_6 S_7 S_8 S_9 S_{10} \cdot e^{-(\theta_1 T_1 + \theta_2 T_2 + \theta_3 T_3 + \theta_4 T_4 + \theta_5 T_5 + \beta_1 T_6 + \beta_2 T_7 + \beta_3 T_8 + \beta_4 T_9 + \beta_5 T_{10})} \quad (26)$$

where

$$S_i = \prod_{j=1}^{n_i} y_{ij}^{\eta-1} \quad \text{and} \quad T_i = \sum_{j=1}^{n_i} y_{ij}^{\eta} \quad i = 1, 2, \dots, 10$$

Taking log on both side of Eq (26), we get

$$\log L = n_1 \log \theta_1 + \dots + n_{10} \log \beta_5 + \sum n_i \log \eta + \log S_1 + \dots + \log S_{10} - (\theta_1 T_1 + \dots + \beta_5 T_{10}) \quad (27)$$

The ML estimates (say $\hat{\theta}_1, \hat{\theta}_2, \hat{\theta}_3, \hat{\theta}_4, \hat{\theta}_5, \hat{\beta}_1, \hat{\beta}_2, \hat{\beta}_3, \hat{\beta}_4, \hat{\beta}_5$) of the shape and scale parameters $\theta_1, \theta_2, \theta_3, \theta_4, \theta_5, \beta_1, \beta_2, \beta_3, \beta_4, \beta_5$.

$$\begin{aligned} \hat{\theta}_1 &= \frac{n_1}{\sum_{j=1}^{n_1} y_{1j}^{\eta}}; \hat{\theta}_2 = \frac{n_2}{\sum_{j=1}^{n_2} y_{2j}^{\eta}}; \hat{\theta}_3 = \frac{n_3}{\sum_{j=1}^{n_3} y_{3j}^{\eta}}; \hat{\theta}_4 = \frac{n_4}{\sum_{j=1}^{n_4} y_{4j}^{\eta}}; \hat{\theta}_5 = \frac{n_5}{\sum_{j=1}^{n_5} y_{5j}^{\eta}}; \hat{\beta}_1 = \frac{n_6}{\sum_{j=1}^{n_6} y_{6j}^{\eta}}; \hat{\beta}_2 = \frac{n_7}{\sum_{j=1}^{n_7} y_{7j}^{\eta}}; \\ \hat{\beta}_3 &= \frac{n_8}{\sum_{j=1}^{n_8} y_{8j}^{\eta}}; \hat{\beta}_4 = \frac{n_9}{\sum_{j=1}^{n_9} y_{9j}^{\eta}}; \hat{\beta}_5 = \frac{n_{10}}{\sum_{j=1}^{n_{10}} y_{10,j}^{\eta}} \end{aligned} \quad (28)$$

By using invariance property of invariance property of MLE, the expressions for MLE of MTSF, availability and profit function can be easily derived. Here $\hat{M}TSF$, $\hat{A}v$ and \hat{P} represented the MLE of MTSF, availability and profit function respectively. The asymptotic distribution of

$$(\hat{\theta}_1 - \theta_1, \hat{\theta}_2 - \theta_2, \hat{\theta}_3 - \theta_3, \hat{\theta}_4 - \theta_4, \dots, \hat{\beta}_5 - \beta_5)' \sim N_{10}(0, I^{-1})$$

Here, I^{-1} represented the Fisher information matrix having diagonal elements

$$I_{11} = \frac{n_1}{\theta_1^2}, I_{22} = \frac{n_2}{\theta_2^2}, I_{33} = \frac{n_3}{\theta_3^2}, I_{44} = \frac{n_4}{\theta_4^2}, I_{55} = \frac{n_5}{\theta_5^2}, I_{66} = \frac{n_6}{\beta_1^2}, I_{77} = \frac{n_7}{\beta_2^2}, I_{88} = \frac{n_8}{\beta_3^2}, I_{99} = \frac{n_9}{\beta_4^2}, I_{10,10} = \frac{n_{10}}{\beta_5^2}$$

And rest of the elements are equal to zero.

The asymptotic distribution of MTSF, availability and profit are as follows:

$$(\hat{M}TSF - MTSF) \sim N_{10}(0, A^{I^{-1}} A); (\hat{A}v - Av) \sim N_{10}(0, B^{I^{-1}} B); (\hat{P} - P) \sim N_{10}(0, C^{I^{-1}} C)$$

Where, $A' = \left(\frac{\partial MTSF}{\partial \theta_1}, \frac{\partial MTSF}{\partial \theta_2}, \frac{\partial MTSF}{\partial \theta_3}, \frac{\partial MTSF}{\partial \theta_4}, \frac{\partial MTSF}{\partial \theta_5}, \frac{\partial MTSF}{\partial \beta_1}, \frac{\partial MTSF}{\partial \beta_2}, \frac{\partial MTSF}{\partial \beta_3}, \frac{\partial MTSF}{\partial \beta_4}, \frac{\partial MTSF}{\partial \beta_5} \right)'$

$$B' = \left(\frac{\partial AV}{\partial \theta_1}, \frac{\partial AV}{\partial \theta_2}, \frac{\partial AV}{\partial \theta_3}, \frac{\partial AV}{\partial \theta_4}, \frac{\partial AV}{\partial \theta_5}, \frac{\partial AV}{\partial \beta_1}, \frac{\partial AV}{\partial \beta_2}, \frac{\partial AV}{\partial \beta_3}, \frac{\partial AV}{\partial \beta_4}, \frac{\partial AV}{\partial \beta_5} \right)'$$

$$C' = \left(\frac{\partial P}{\partial \theta_1}, \frac{\partial P}{\partial \theta_2}, \frac{\partial P}{\partial \theta_3}, \frac{\partial P}{\partial \theta_4}, \frac{\partial P}{\partial \theta_5}, \frac{\partial P}{\partial \beta_1}, \frac{\partial P}{\partial \beta_2}, \frac{\partial P}{\partial \beta_3}, \frac{\partial P}{\partial \beta_4}, \frac{\partial P}{\partial \beta_5} \right)'$$

Few of the expressions are shown in Appendix A ([S1 Appendix](#)).

4.2 Bayesian estimation

Bayesian estimation of parameters as well as reliability measures of turbogenerator is performed as it is considered that all parameters associated with failure and repair rates followed some distribution. In present study, all random variables followed two parameter Weibull distribution having known shape parameter (η). The family of gamma distributions is amply flexible as it can model a variety of prior information. Moreso, non-informative priors are particular cases of gamma priors. Also, the parameters of the gamma priors can be merged with model parameters, so that mathematical computations become easy. The scale parameter ($\theta_1, \theta_2, \theta_3, \theta_4, \theta_5, \beta_1, \beta_2, \beta_3, \beta_4, \beta_5$) of distribution associate with random variables followed the Gamma distribution having parameters (termed as hyper parameters) ($\alpha_i, \delta_i; i = 1, 2, 3, \dots, 10$) and described as given below:

$$\theta_1 \sim \text{GAMMA}(\alpha_1, \delta_1)$$

$$\theta_2 \sim \text{GAMMA}(\alpha_2, \delta_2)$$

$$\theta_3 \sim \text{GAMMA}(\alpha_3, \delta_3)$$

$$\theta_4 \sim \text{GAMMA}(\alpha_4, \delta_4)$$

$$\theta_5 \sim \text{GAMMA}(\alpha_5, \delta_5)$$

$$\beta_1 \sim \text{GAMMA}(\alpha_6, \delta_6)$$

$$\beta_2 \sim \text{GAMMA}(\alpha_7, \delta_7)$$

$$\beta_3 \sim \text{GAMMA}(\alpha_8, \delta_8)$$

$$\beta_4 \sim \text{GAMMA}(\alpha_9, \delta_9)$$

$$\beta_5 \sim \text{GAMMA}(\alpha_{10}, \delta_{10})$$

The values of hyperparameters in the case of informative priors are taken in such a way that the mean of the prior distribution comes out equal to the true value of the parameter. The posterior distributions are derived using likelihood function (26) and prior distributions of $\theta_1, \theta_2, \theta_3, \theta_4, \theta_5, \beta_1, \beta_2, \beta_3, \beta_4, \beta_5$ as follows:

$$\theta_1 | Y_{-1} \sim \text{GAMMA}(n_1 + \alpha_1, \delta_1 + \sum_{j=1}^{n_1} Y_{1j}^{\eta}) \quad (29)$$

$$\theta_2 | Y_{-2} \sim \text{GAMMA}(n_2 + \alpha_2, \delta_2 + \sum_{j=1}^{n_2} Y_{2j}^{\eta}) \quad (30)$$

$$\theta_3 | Y_{-3} \sim \text{GAMMA}(n_3 + \alpha_3, \delta_3 + \sum_{j=1}^{n_3} Y_{3j}^{\eta}) \quad (31)$$

$$\theta_4 | Y_{-4} \sim \text{GAMMA}(n_4 + \alpha_4, \delta_4 + \sum_{j=1}^{n_4} Y_{4j}^{\eta}) \quad (32)$$

$$\theta_5 | Y_{-5} \sim \text{GAMMA}(n_5 + \alpha_5, \delta_5 + \sum_{j=1}^{n_5} Y_{5j}^{\eta}) \quad (33)$$

$$\beta_1 | Y_{-6} \sim \text{GAMMA}(n_6 + \alpha_6, \delta_6 + \sum_{j=1}^{n_6} Y_{6j}^{\eta}) \quad (34)$$

$$\beta_2 | Y_{-7} \sim \text{GAMMA}(n_7 + \alpha_7, \delta_7 + \sum_{j=1}^{n_7} Y_{7j}^{\eta}) \quad (35)$$

$$\beta_3 | Y_{-8} \sim \text{GAMMA}(n_8 + \alpha_8, \delta_8 + \sum_{j=1}^{n_8} Y_{8j}^{\eta}) \quad (36)$$

$$\beta_4 | Y_{-9} \sim \text{GAMMA}(n_9 + \alpha_9, \delta_9 + \sum_{j=1}^{n_9} Y_{9j}^{\eta}) \quad (37)$$

$$\beta_{10} | Y_{-10} \sim \text{GAMMA}(n_{10} + \alpha_{10}, \delta_{10} + \sum_{j=1}^{n_{10}} Y_{10j}^{\eta})$$

The Bayes estimator of the scale parameters $\theta_1, \theta_2, \theta_3, \theta_4, \theta_5, \beta_1, \beta_2, \beta_3, \beta_4, \beta_5$ under squared error loss function are the means of posterior distribution given in Eqs (29)–(38) and as follows:

$$\hat{\theta}_1 = \frac{\delta_1 + \sum_{j=1}^{n_1} y_{1j}^\eta}{n_1 + \theta_1}, \hat{\theta}_2 = \frac{\delta_2 + \sum_{j=1}^{n_2} y_{2j}^\eta}{n_2 + \theta_2}, \hat{\theta}_3 = \frac{\delta_3 + \sum_{j=1}^{n_3} y_{3j}^\eta}{n_3 + \theta_3}$$

$$\hat{\theta}_4 = \frac{\delta_4 + \sum_{j=1}^{n_4} y_{4j}^\eta}{n_4 + \theta_4}, \hat{\theta}_5 = \frac{\delta_5 + \sum_{j=1}^{n_5} y_{5j}^\eta}{n_5 + \theta_5}, \hat{\beta}_1 = \frac{\delta_6 + \sum_{j=1}^{n_6} y_{6j}^\eta}{n_6 + \beta_1}$$

$$\hat{\beta}_2 = \frac{\delta_7 + \sum_{j=1}^{n_7} y_{7j}^\eta}{n_7 + \beta_2}, \hat{\beta}_3 = \frac{\delta_8 + \sum_{j=1}^{n_8} y_{8j}^\eta}{n_8 + \beta_3}, \hat{\beta}_5 = \frac{\delta_{10} + \sum_{j=1}^{n_{10}} y_{10j}^\eta}{n_{10} + \beta_5}, \hat{\beta}_4 = \frac{\delta_9 + \sum_{j=1}^{n_9} y_{9j}^\eta}{n_9 + \beta_4}$$

5. Simulation study

In this section, MLE and Bayes estimates for parameters of Weibull distribution associated with failure and repair rates of turbogenerator are obtained. The MLE and Bayes estimates of scale parameters $\theta_1, \theta_2, \theta_3, \theta_4, \theta_5, \beta_1, \beta_2, \beta_3, \beta_4, \beta_5$ and hence, by invariance property, for MTSF, availability and profit function are estimated under the assumption of known scale parameter. The theoretical results are validated through a simulation study. The comparison is made by using mean square error of estimates and width of confidence intervals. As the hazard rate of Weibull distribution is increasing, decreasing and constant according to the shape value of the parameter so investigation is also made for different values of shape parameters. Random sample of size 50 has been generated from Weibull distribution having various values of the parameters. The samples are generated for following set of values:

For $\eta = 0.50, 1, \text{ and } 2$

- $n = 50, \theta_1 = 0.01, \theta_2 = 0.05, \theta_3 = 0.06, \theta_4 = 0.065, \theta_5 = 0.045, \beta_1 = 0.3, \beta_2 = 0.4, \beta_3 = 0.5, \beta_4 = 0.6, \beta_5 = 0.7$
- $n = 50, \theta_1 = 0.02, \theta_2 = 0.05, \theta_3 = 0.06, \theta_4 = 0.065, \theta_5 = 0.045, \beta_1 = 0.3, \beta_2 = 0.4, \beta_3 = 0.5, \beta_4 = 0.6, \beta_5 = 0.7$
- $n = 50, \theta_1 = 0.03, \theta_2 = 0.05, \theta_3 = 0.06, \theta_4 = 0.065, \theta_5 = 0.045, \beta_1 = 0.3, \beta_2 = 0.4, \beta_3 = 0.5, \beta_4 = 0.6, \beta_5 = 0.7$
- $n = 50, \theta_1 = 0.04, \theta_2 = 0.05, \theta_3 = 0.06, \theta_4 = 0.065, \theta_5 = 0.045, \beta_1 = 0.3, \beta_2 = 0.4, \beta_3 = 0.5, \beta_4 = 0.6, \beta_5 = 0.7$
- $n = 50, \theta_1 = 0.05, \theta_2 = 0.05, \theta_3 = 0.06, \theta_4 = 0.065, \theta_5 = 0.045, \beta_1 = 0.3, \beta_2 = 0.4, \beta_3 = 0.5, \beta_4 = 0.6, \beta_5 = 0.7$
- $n = 50, \theta_1 = 0.06, \theta_2 = 0.05, \theta_3 = 0.06, \theta_4 = 0.065, \theta_5 = 0.045, \beta_1 = 0.3, \beta_2 = 0.4, \beta_3 = 0.5, \beta_4 = 0.6, \beta_5 = 0.7$
- $n = 50, \theta_1 = 0.07, \theta_2 = 0.05, \theta_3 = 0.06, \theta_4 = 0.065, \theta_5 = 0.045, \beta_1 = 0.3, \beta_2 = 0.4, \beta_3 = 0.5, \beta_4 = 0.6, \beta_5 = 0.7$
- $n = 50, \theta_1 = 0.08, \theta_2 = 0.05, \theta_3 = 0.06, \theta_4 = 0.065, \theta_5 = 0.045, \beta_1 = 0.3, \beta_2 = 0.4, \beta_3 = 0.5, \beta_4 = 0.6, \beta_5 = 0.7$
- $n = 50, \theta_1 = 0.09, \theta_2 = 0.05, \theta_3 = 0.06, \theta_4 = 0.065, \theta_5 = 0.045, \beta_1 = 0.3, \beta_2 = 0.4, \beta_3 = 0.5, \beta_4 = 0.6, \beta_5 = 0.7$
- $n = 50, \theta_1 = 0.1, \theta_2 = 0.05, \theta_3 = 0.06, \theta_4 = 0.065, \theta_5 = 0.045, \beta_1 = 0.3, \beta_2 = 0.4, \beta_3 = 0.5, \beta_4 = 0.6, \beta_5 = 0.7$

By using above values of parameters fifty random samples generated and MLE and Bayes estimated (for non-informative prior) of parameters, MTSF, availability and profit function is obtained. For Bayesian investigation 10000 realization by using non-informative prior and posterior densities. The values of the Gamma hyper parameters are obtained by setting $\alpha/\beta_i = \frac{b_i}{a_i}$. All the estimates along with true value, mean square errors, and length of intervals/HPD are summarized in Tables 1–7 and shown graphically in Figs 3–11. The profit function is evaluated by taking 5000 and 600, respectively. For all the numerical computations, the programs are developed in R-environment.

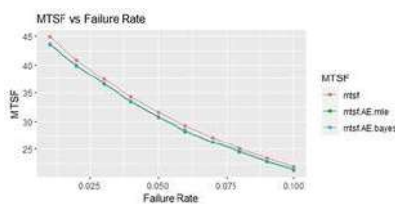


Fig 3. Behaviour of MTSF with varying failure rate (θ_1) for $\eta = 0.5$.

<https://doi.org/10.1371/journal.pone.0292154.g003>

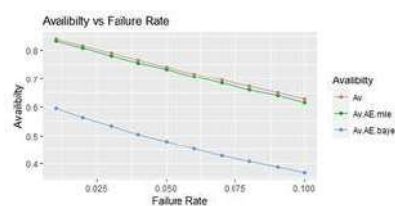


Fig 4. Behaviour of availability with varying failure rate (θ_1) for $\eta = 0.5$.

<https://doi.org/10.1371/journal.pone.0292154.g004>

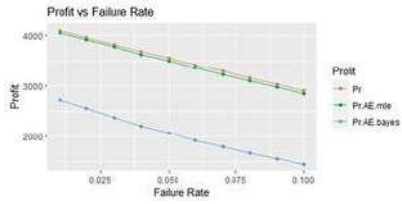


Fig 5. Behaviour of profit with varying failure rate (Θ_1) for $\eta = 0.5$.
<https://doi.org/10.1371/journal.pone.0292154.g005>

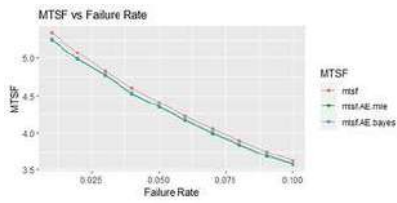


Fig 6. Behaviour of MTSF with varying failure rate (Θ_1) for $\eta = 1$.
<https://doi.org/10.1371/journal.pone.0292154.g006>

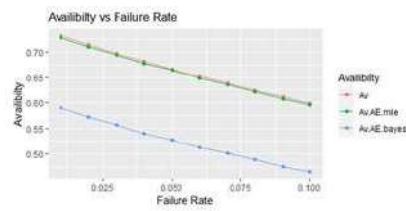


Fig 7. Behaviour of availability with varying failure rate (Θ_1) for $\eta = 1$.
<https://doi.org/10.1371/journal.pone.0292154.g007>

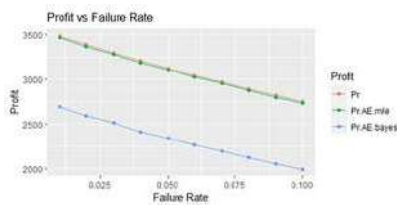


Fig 8. Behaviour of profit with varying failure rate (Θ_1) for $\eta = 1$.
<https://doi.org/10.1371/journal.pone.0292154.g008>

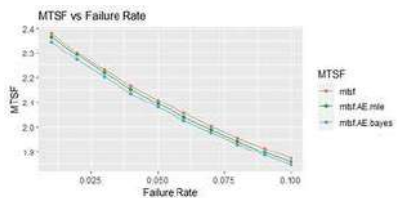


Fig 9. Behaviour of MTSF with varying failure rate (Θ_1) for $\eta = 2$.
<https://doi.org/10.1371/journal.pone.0292154.g009>

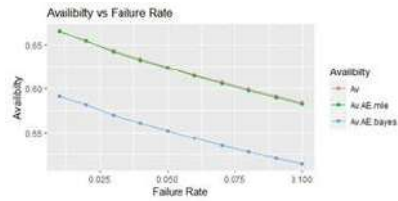


Fig 10. Behaviour of availability with varying failure rate (Θ_1) for $\eta = 2$.
<https://doi.org/10.1371/journal.pone.0292154.g010>

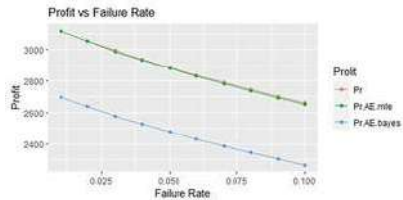


Fig 11. Behaviour of profit with varying failure rate (Θ_1) for $\eta = 2$.
<https://doi.org/10.1371/journal.pone.0292154.g011>

Estimate θ_1	0.1	0.2	0.3	0.4	0.5	0.6	0.7	0.8	0.9
True MTSF	44.9493	46.9493	47.9113	48.8397	49.7361	50.6052	51.4513	52.2784	53.0914
MTSF_MLE	42.2394	45.9513	46.6116	48.3013	47.1121	47.2012	47.4111	48.2213	49.1011
MTSF_AE	42.9191	46.9191	46.9191	48.9191	48.9191	49.2012	49.2012	49.2012	49.2012
MTSF_Bayes	43.0211	46.9493	46.6116	48.3013	48.0711	48.4711	48.4711	48.4711	48.4711
MTSF_Profit_MLE	33.8891	33.7114	33.7114	33.7114	33.7114	33.7114	33.7114	33.7114	33.7114
MTSF_Profit_AE	33.8891	33.7114	33.7114	33.7114	33.7114	33.7114	33.7114	33.7114	33.7114
MTSF_Profit_Bayes	33.8891	33.7114	33.7114	33.7114	33.7114	33.7114	33.7114	33.7114	33.7114

Table 1. Values of MTSF for fixed $\eta = 0.5$ and varying Θ_1 .
<https://doi.org/10.1371/journal.pone.0292154.t001>

Estimate θ_1	0.1	0.2	0.3	0.4	0.5	0.6	0.7	0.8	0.9
True Availability	0.6094	0.6142	0.6191	0.6241	0.6291	0.6341	0.6391	0.6441	0.6491
Avail_MLE	0.6094	0.6142	0.6191	0.6241	0.6291	0.6341	0.6391	0.6441	0.6491
Avail_AE	0.6111	0.6161	0.6211	0.6261	0.6311	0.6361	0.6411	0.6461	0.6511
Avail_Bayes	0.6111	0.6161	0.6211	0.6261	0.6311	0.6361	0.6411	0.6461	0.6511
Avail_Profit_MLE	0.6111	0.6161	0.6211	0.6261	0.6311	0.6361	0.6411	0.6461	0.6511
Avail_Profit_AE	0.6111	0.6161	0.6211	0.6261	0.6311	0.6361	0.6411	0.6461	0.6511
Avail_Profit_Bayes	0.6111	0.6161	0.6211	0.6261	0.6311	0.6361	0.6411	0.6461	0.6511

Table 2. Values of availability for fixed $\eta = 0.5$ and varying Θ_1 .
<https://doi.org/10.1371/journal.pone.0292154.t002>

Estimate θ_1	0.1	0.2	0.3	0.4	0.5	0.6	0.7	0.8	0.9
True Profit	2891.74	2891.74	2891.74	2891.74	2891.74	2891.74	2891.74	2891.74	2891.74
Profit_MLE	2891.74	2891.74	2891.74	2891.74	2891.74	2891.74	2891.74	2891.74	2891.74
Profit_AE	2891.74	2891.74	2891.74	2891.74	2891.74	2891.74	2891.74	2891.74	2891.74
Profit_Bayes	2891.74	2891.74	2891.74	2891.74	2891.74	2891.74	2891.74	2891.74	2891.74
Profit_Profit_MLE	2891.74	2891.74	2891.74	2891.74	2891.74	2891.74	2891.74	2891.74	2891.74
Profit_Profit_AE	2891.74	2891.74	2891.74	2891.74	2891.74	2891.74	2891.74	2891.74	2891.74
Profit_Profit_Bayes	2891.74	2891.74	2891.74	2891.74	2891.74	2891.74	2891.74	2891.74	2891.74

Table 3. Values of profit for fixed $\eta = 0.5$ and varying Θ_1 .
<https://doi.org/10.1371/journal.pone.0292154.t003>

Estimate θ_1	0.1	0.2	0.3	0.4	0.5	0.6	0.7	0.8	0.9
True MTSF	5.5174	5.5174	5.5174	5.5174	5.5174	5.5174	5.5174	5.5174	5.5174
MTSF_MLE	5.5174	5.5174	5.5174	5.5174	5.5174	5.5174	5.5174	5.5174	5.5174
MTSF_AE	5.5174	5.5174	5.5174	5.5174	5.5174	5.5174	5.5174	5.5174	5.5174
MTSF_Bayes	5.5174	5.5174	5.5174	5.5174	5.5174	5.5174	5.5174	5.5174	5.5174
MTSF_Profit_MLE	5.5174	5.5174	5.5174	5.5174	5.5174	5.5174	5.5174	5.5174	5.5174
MTSF_Profit_AE	5.5174	5.5174	5.5174	5.5174	5.5174	5.5174	5.5174	5.5174	5.5174
MTSF_Profit_Bayes	5.5174	5.5174	5.5174	5.5174	5.5174	5.5174	5.5174	5.5174	5.5174

Table 4. Values of MTSF for fixed $\eta = 1$ and varying Θ_1 .
<https://doi.org/10.1371/journal.pone.0292154.t004>

Estimate θ_1	0.1	0.2	0.3	0.4	0.5	0.6	0.7	0.8	0.9
True Availability	0.7111	0.7111	0.7111	0.7111	0.7111	0.7111	0.7111	0.7111	0.7111
Avail_MLE	0.7111	0.7111	0.7111	0.7111	0.7111	0.7111	0.7111	0.7111	0.7111
Avail_AE	0.7111	0.7111	0.7111	0.7111	0.7111	0.7111	0.7111	0.7111	0.7111
Avail_Bayes	0.7111	0.7111	0.7111	0.7111	0.7111	0.7111	0.7111	0.7111	0.7111
Avail_Profit_MLE	0.7111	0.7111	0.7111	0.7111	0.7111	0.7111	0.7111	0.7111	0.7111
Avail_Profit_AE	0.7111	0.7111	0.7111	0.7111	0.7111	0.7111	0.7111	0.7111	0.7111
Avail_Profit_Bayes	0.7111	0.7111	0.7111	0.7111	0.7111	0.7111	0.7111	0.7111	0.7111

Table 5. Values of availability for fixed $\eta = 1$ and varying Θ_1 .
<https://doi.org/10.1371/journal.pone.0292154.t005>

Estimator θ_1	0.1	0.2	0.3	0.4	0.5	0.6	0.7	0.8	0.9
True Profit	5486.11	4380.12	3796.83	3297.26	2873.99	2522.21	2241.1	1999.07	1793.89
Profit_MLE_MSD	27880.02	40866.62	49222.70	57136.26	64812.66	72334.80	80000.00	88000.00	96333.33
Profit_Bayes	5889.54	4780.84	4192.43	3688.42	3263.93	2913.21	2625.81	2378.54	2174.09
Profit_Bayes_MSD	488812.84	448112.81	415871.01	388461.04	363881.62	342452.26	323888.50	308434.80	298881.07
ProfitLength_MSD	117.23	93.22	81.96	73.89	67.72	63.22	59.14	56.11	53.19
ProfitLength_Bayes	475.82	475.82	475.82	475.82	475.82	475.82	475.82	475.82	475.82

Table 6. Values of profit for fixed $\eta = 1$ and varying θ_1 .
<https://doi.org/10.1371/journal.pone.0292154.t006>

Estimator θ_1	0.1	0.2	0.3	0.4	0.5	0.6	0.7	0.8	0.9
True MTSF	5.3454	5.2575	5.2629	5.2629	5.2629	5.2629	5.2629	5.2629	5.2629
MTSF_MLE_MSD	0.011	0.012	0.010	0.010	0.010	0.010	0.010	0.010	0.010
MTSF_Bayes	2.3658	2.3658	2.3658	2.3658	2.3658	2.3658	2.3658	2.3658	2.3658
MTSF_Bayes_MSD	0.011	0.012	0.010	0.010	0.010	0.010	0.010	0.010	0.010
MTSFLength_MSD	0.011	0.012	0.010	0.010	0.010	0.010	0.010	0.010	0.010
MTSFLength_Bayes	0.011	0.012	0.010	0.010	0.010	0.010	0.010	0.010	0.010

Table 7. Values of MTSF for fixed $\eta = 2$ and varying θ_1 .
<https://doi.org/10.1371/journal.pone.0292154.t007>

It is observed from numerical values given in Tables 1–3 that mean time to system failure, availability and profit incurred by turbogenerator decreases with the increase of failure rate θ_1 . The MLE and Bayes estimates of MTSF, availability and profit of turbogenerator also exhibit the same pattern with respect to failure rate θ_1 . The mean square error of MLE and Bayes estimators derived and found that it is less in maximum likelihood estimation along with confidence intervals length at $\eta = 0.5$. The same pattern is also shown graphically as mean time to system failure (Fig. 3), availability (Fig. 6) and profit (Fig. 9).

For the shape parameter $\eta = 1$, it is revealed from numerical values given in Tables 4–6 that mean time to system failure, availability and profit incurred by turbogenerator decreases with the increase of failure rate θ_1 . It is observed that true value, MLE and Bayes estimates of MTSF at $\theta_1 = 0.1$ attained the values 5.3454, 5.2575 and 5.2629 respectively. The MLE and Bayes estimates of availability and profit of turbogenerator also exhibit the same pattern with respect to failure rate θ_1 . The mean square error of MLE and Bayes estimators derived and found that it is less in maximum likelihood estimation along with confidence intervals length for $\eta = 1$. The same pattern is also shown graphically as mean time to system failure (Fig. 4), availability (Fig. 8) and profit (Fig. 10).

For the shape parameter $\eta = 2$, it is revealed from numerical values given in Tables 7–9 that mean time to system failure, availability and profit incurred by turbogenerator decreases with the increase of failure rate θ_1 . It is observed that true value, MLE and Bayes estimates of MTSF at $\theta_1 = 0.1$ attained the values 2.3779, 2.3658 and 2.3461 respectively. The MLE and Bayes estimates of availability and profit of turbogenerator also exhibit the same pattern with respect to failure rate θ_1 . The mean square error of MLE and Bayes estimators derived and found that it is less in maximum likelihood estimation along with confidence intervals length for $\eta = 2$. The same pattern is also shown graphically as mean time to system failure (Fig. 5), availability (Fig. 8) and profit (Fig. 11). The numerical results exhibit that the numerical values of estimators declined with respect to the increase in shape parameter $\eta = 0.5, 1$ & 2 respectively.

Estimator θ_1	0.1	0.2	0.3	0.4	0.5	0.6	0.7	0.8	0.9
True Availability	0.9977	0.994	0.9899	0.9856	0.9813	0.9770	0.9727	0.9684	0.9641
Avail_MLE_MSD	0.0000	0.0000	0.0000	0.0000	0.0000	0.0000	0.0000	0.0000	0.0000
Avail_Bayes	0.9977	0.994	0.9899	0.9856	0.9813	0.9770	0.9727	0.9684	0.9641
Avail_Bayes_MSD	0.0000	0.0000	0.0000	0.0000	0.0000	0.0000	0.0000	0.0000	0.0000
AvailLength_MSD	0.0000	0.0000	0.0000	0.0000	0.0000	0.0000	0.0000	0.0000	0.0000
AvailLength_Bayes	0.0000	0.0000	0.0000	0.0000	0.0000	0.0000	0.0000	0.0000	0.0000

Table 8. Values of availability for fixed $\eta = 2$ and varying θ_1 .
<https://doi.org/10.1371/journal.pone.0292154.t008>

Estimator θ_1	0.1	0.2	0.3	0.4	0.5	0.6	0.7	0.8	0.9
True Profit	5486.11	4380.12	3796.83	3297.26	2873.99	2522.21	2241.1	1999.07	1793.89
Profit_MLE_MSD	27880.02	40866.62	49222.70	57136.26	64812.66	72334.80	80000.00	88000.00	96333.33
Profit_Bayes	5889.54	4780.84	4192.43	3688.42	3263.93	2913.21	2625.81	2378.54	2174.09
Profit_Bayes_MSD	488812.84	448112.81	415871.01	388461.04	363881.62	342452.26	323888.50	308434.80	298881.07
ProfitLength_MSD	117.23	93.22	81.96	73.89	67.72	63.22	59.14	56.11	53.19
ProfitLength_Bayes	475.82	475.82	475.82	475.82	475.82	475.82	475.82	475.82	475.82

Table 9. Values of profit for fixed $\eta = 2$ and varying θ_1 .
<https://doi.org/10.1371/journal.pone.0292154.t009>

6. Conclusion

In present study, the classical and Bayesian estimation of the reliability characteristics is performed of a turbogenerator system. For a particular set of parametric values true MTSF, steady state availability and profit function are evaluated. Tables 1–9 reflected that MTSF, availability and profit decrease with the failure rate (θ_1) of turbine governing unit. The values of mean time to system failure, availability and profit sharply declined with the increase of the shape parameter $\eta = 0.5, 1$ and 2. From the simulation results as shown in Tables 1–9, it is observed that for the shape parameter $\eta = 0.5, 1$ and 2 the true value of MTSF, availability, profit, MLE and Bayes estimates of MTSF, MLE and Bayes estimates of availability and MLE and Bayes estimates of profit decreases with respect to failure rate (θ_1) of turbine governing unit. The mean square error (MSE) of maximum likelihood estimators and width of confidence intervals of MTSF, availability and profit are less in comparison of the Bayes MSE and HPD for $\eta = 0.5, 1$ and 2. Hence, it is recommended that to use ML estimated over Bayes estimation for estimation of reliability characteristics of turbogenerator. The work may be further extended by considering other informative priors for the distribution. Further, the proposed methodology may be opted for the reliability evaluation of other similar kind of mechanical systems as well as in process industries.

Supporting information

S1 Appendix.

<https://doi.org/10.1371/journal.pone.0292154.s001>

(DOCX)

References

1. Weibull W. (1951). A statistical distribution function of wide applicability. *Journal of Applied Mechanics*, 18, 293–297.
[View Article](#) • [Google Scholar](#)
2. Masters B. N., Lewis T. O., & Kolarik W. J. (1992). A confidence interval for the availability ratio for systems with Weibull operating time and lognormal repair time. *Microelectronics Reliability*, 32(1–2), 89–99.
[View Article](#) • [Google Scholar](#)
3. Dhillon B. S., & Anuda O. C. (1993a). Common cause failure analysis of a non-identical unit parallel system with arbitrarily distributed repair times. *Microelectronics Reliability*, 33(1), 87–103.
[View Article](#) • [Google Scholar](#)
4. Coit D. W. (2001). Cold-standby redundancy optimization for non-repairable systems. *IIE Transactions*, 33(6), 471–478.
[View Article](#) • [Google Scholar](#)
5. Yadavalli V. S. S., Botha M., & Bekker A. (2002). Asymptotic confidence limits for the steady state availability of a two-unit parallel system with 'preparation time' for the repair facility. *Asia-Pacific Journal of Operational Research*, 19(2), 249.
[View Article](#) • [Google Scholar](#)
6. Lim J. H., Shin S. W., Kim D. K., & Park D. H. (2004). Bootstrap confidence intervals for steady-state availability. *Asia-Pacific Journal of Operational Research*, 21(03), 407–419.
[View Article](#) • [Google Scholar](#)
7. Yadavalli V. S. S., Bekker A., & Pauw J. (2005). Bayesian study of a two-component system with common-cause shock failures. *Asia-Pacific Journal of Operational Research*, 22(01), 105–119.
[View Article](#) • [Google Scholar](#)
8. Chien Y. H., Ke J. C., & Lee S. L. (2006). Asymptotic confidence limits for performance measures of a repairable system with imperfect service station. *Communications in Statistics—Simulation and Computation*, 35(3), 813–830.
[View Article](#) • [Google Scholar](#)
9. Ke J. C., Lee S. L., & Hsu Y. L. (2008). Bayesian analysis for a redundant repairable system with imperfect coverage. *Communications in Statistics—Simulation and Computation*, 37(5), 993–1004
[View Article](#) • [Google Scholar](#)
10. Hsu Y. L., Lee S. L., & Ke J. C. (2009). A repairable system with imperfect coverage and reboot: Bayesian and asymptotic estimation. *Mathematics and Computers in Simulation*, 79(7), 2227–2239
[View Article](#) • [Google Scholar](#)
11. Gupta R., Kumar P., & Gupta A. (2013). Cost benefit analysis of a two dissimilar unit cold standby system with Weibull failure and repair laws. *International Journal of System Assurance Engineering and Management*, 4(4), 327–334
[View Article](#) • [Google Scholar](#)
12. Singh B., Rathi S., & Kumar S. (2013). Inferential statistics on the dynamic system model with time-dependent failure rate. *Journal of Statistical Computation and Simulation*, 83(1), 1–24.
[View Article](#) • [Google Scholar](#)
13. Chaturvedi A., Pati M., & Tomer S. K. (2014). Robust Bayesian analysis of Weibull failure model. *Metron*, 72(1), 77–95.
[View Article](#) • [Google Scholar](#)
14. Kishan R., & Jain D. (2014). Classical and Bayesian analysis of reliability characteristics of a two-unit parallel system with Weibull failure and repair laws. *International Journal of System Assurance Engineering and Management*, 5(3), 252–261
[View Article](#) • [Google Scholar](#)
15. Liu Y., Li X., & Du Z. (2014). Reliability analysis of a random fuzzy repairable parallel system with two non-identical components. *Journal of Intelligent & Fuzzy Systems*, 27(6), 2775–2784
[View Article](#) • [Google Scholar](#)
16. Kumar R., Sharma A. K., & Tewari P. C. (2014). Effect of various pump hot-cold redundancy on availability of thermal power plant subsystems. *International Journal of Intelligent Enterprise*, 2(4), 311–324
[View Article](#) • [Google Scholar](#)
17. Kumar K., & Garg R. (2014). Estimation of the parameters of randomly censored generalized inverted Rayleigh distribution. *International Journal of Agricultural and Statistical Sciences*, 10(1), 147–55.
[View Article](#) • [Google Scholar](#)
18. Pariaman H., Garniwa I., Surjandari I., & Sugiarto B. (2015). Availability improvement methodology in thermal power plant. *Scientific Journal of PPI-UKM*, 2(1), 43–52.

[View Article](#) • [Google Scholar](#)

19. Dongliang Y., Fang L., & Tong C. (2016, May). Analysis of parallel system reliability model with two dissimilar units based on phase-type distribution. *In 2016 Chinese Control and Decision Conference (CCDC)* (pp. 2290–2295).
[View Article](#) • [Google Scholar](#)
20. Kumar A., Saini M., & Devi K. (2016). Analysis of a redundant system with priority and Weibull distribution for failure and repair. *Cogent Mathematics*, 3(1), 1135721
[View Article](#) • [Google Scholar](#)
21. Kumar A., Barak M. S., & Devi K. (2016). Performance analysis of a redundant system with Weibull failure and repair laws. *Investigación Operacional*, 37(3), 247–257
[View Article](#) • [Google Scholar](#)
22. Kumar A., Saini M., & Devi K. (2018). Stochastic modeling of non-identical redundant systems with priority, preventive maintenance, and Weibull failure and repair distributions. *Life Cycle Reliability and Safety Engineering*, 7(2), 61–70
[View Article](#) • [Google Scholar](#)
23. Chopra G., & Ram M. (2017). Stochastic analysis of two non-identical unit parallel system incorporating waiting time. *International Journal of Quality & Reliability Management*, 34(6).
[View Article](#) • [Google Scholar](#)
24. Dey S., Alzaatreh A., Zhang C., & Kumar D. (2017). A new extension of generalized exponential distribution with application to Ozone data. *Ozone: Science & Engineering*, 39(4), 273–285.
[View Article](#) • [Google Scholar](#)
25. Gupta P. K., & Singh A. K. (2017). Classical and Bayesian estimation of Weibull distribution in presence of outliers. *Cogent Mathematics*, 4, 1300975.
[View Article](#) • [Google Scholar](#)
26. Han H., Park J., & Thoma S. J. (2018). Why do we need to employ Bayesian statistics and how can we employ it in studies of moral education?: With practical guidelines to use JASP for educators and researchers. *Journal of Moral Education*, 47(4), 1–537.
[View Article](#) • [Google Scholar](#)
27. Pundir P. S., Patawa R., & Gupta P. K. (2018). Stochastic outlook of two non-identical unit parallel system with priority in repair. *Cogent Mathematics & Statistics*, 5(1), 1467208
[View Article](#) • [Google Scholar](#)
28. Kumar R., & Kadyan M. S. (2018). Performance analysis and maintenance planning of evaporation system in the sugar industry by using supplementary variable technique. *Journal of Industrial Integration and Management*, 3(01), 1850004
[View Article](#) • [Google Scholar](#)
29. Kumar R., & Kadyan M. S. (2019). Improving industrial systems reliability—An application in sugar industry. *Journal of Industrial Integration and Management*, 4(04), 195001
[View Article](#) • [Google Scholar](#)
30. Kumar K., & Kumar I. (2019). Estimation in inverse Weibull distribution based on randomly censored data. *Statistica*, 79(1), 47–74.
[View Article](#) • [Google Scholar](#)
31. Saini M., & Kumar A. (2020). Stochastic modeling of a single-unit system operating under different environmental conditions subject to inspection and degradation. *Proceedings of the National Academy of Sciences, India Section A: Physical Sciences*, 90(2), 319–326
[View Article](#) • [Google Scholar](#)
32. Saini M., Devi K., & Kumar A. (2020, May). Stochastic Modeling and Profit Evaluation of a Redundant System with Priority Subject to Weibull Densities for Failure and Repair. *In International Conference on Information and Communication Technology for Intelligent Systems* (pp. 11–20). Springer, Singapore
33. Pundir P. S., Patawa R., & Gupta P. K. (2020). Analysis of Two Non-Identical Unit Cold Standby System in Presence of Prior Information. *American Journal of Mathematical and Management Sciences*, 1–16.
[View Article](#) • [Google Scholar](#)
34. Patawa R., Pundir P.S., Singh A.K. et al. Some inferences on reliability measures of two-non-identical units cold standby system waiting for repair. *Int J Syst Assur Eng Manag* (2021).
[View Article](#) • [Google Scholar](#)
35. Rathil P., Kumar G., Asjad M., & Sonil U. (2022). Reliability Improvement of a Multistage Reciprocating Compressor with Redundancies Using Markov Approach. *Journal of Industrial Integration and Management*, 1–19.
[View Article](#) • [Google Scholar](#)
36. Jagtap H. P., Bewoor A. K., Kumar R., Ahmadi M. H., & Chen L. (2020). Performance analysis and availability optimization to improve maintenance schedule for the turbo-generator subsystem of a thermal power plant using particle swarm optimization. *Reliability Engineering & System Safety*, 204, 107130.
[View Article](#) • [Google Scholar](#)

37. Kumar A., & Saini M. (2014). Cost-benefit analysis of a single-unit system with preventive maintenance and Weibull distribution for failure and repair activities. *Journal of Applied Mathematics, Statistics and Informatics*, 10(2), 5–19
[View Article](#) • [Google Scholar](#)



Thermodynamical study of chemically-reactive and thermal-radiative magnetized oscillatory Couette flow in a porous medium filled channel

Tarun Sharma ^a✉, Pooja Sharma ^b✉, A.H. Seikh ^c✉, Amjad Iqbal ^d✉, Navin Kumar ^e✉

Show more ▾

☰ Outline | 🔗 Share 🗣️ Cite

<https://doi.org/10.1016/j.csite.2023.103136> ↗

[Get rights and content](#) ↗

Under a Creative Commons [license](#) ↗

open access

Abstract

The thermodynamical study of a mathematical model of unsteady natural convective MHD oscillatory flow through a porous medium-filled channel of infinite plates with chemical reaction and thermal radiation effect is taken into account in this respective research. The time-dependent flow governing equations (PDEs); comprises momentum, energy and concentration equations are derived for the concerned physical model and converted into dimensionless second-order ordinary differential equations (ODEs) for fluctuation of small amplitude. Further, the set of ODEs is solved by MATLAB's built-in dsolve function. The graphical analysis of fluid velocity, temperature and concentration profiles has been explicated for flow parameters. According to the results, the transient velocity and concentration profiles expand when the chemical reaction parameter and Schmidt number increase, whereas a strong magnetic field retards the transient velocity profile. In addition, the velocity, temperature, and concentration profiles decline whenever the frequency of oscillation is increased. The elucidated flow model and mathematical results are significant to be used in real-life applications, including packed bed reactors, chemical reactors, cooling the towers and rocket engines, designing of heat

exchangers, sewage and wastewater treatment, chemical and magnetic filtration, and separation etc.

[< Previous](#)

[Next >](#)

Keywords

Chemical reaction; MHD; Oscillatory flow; Thermal radiation

Nomenclature

T_1^*

temperature of moving wall/plate

C_1^*

concentration of moving wall/plate

h^*

dimensional width of the channel

C^*

dimensional concentration

T^*

dimensional temperature

K^*

dimensional permeability of a porous medium

u^*

dimensional velocity

u_p^*

dimensional velocity of moving wall/plate

ω^*

dimensional oscillation frequency

K_R

Chemical reaction parameter

Gc

Grashoff number of mass transfer concentration

Gr

Grashoff number of heat transfer

K

permeability of the porous medium

D_M

Mass/molecular diffusivity

U_0

constant velocity/free stream velocity

$K_{\lambda w}$

absorption coefficient

Sc

Schmidt number

M

magnetic field parameter

Pr

Prandtl number

R

thermal radiation parameter

g

acceleration due to gravity

ρ

density (kg/m^3)

σ

electrical conductivi

C_P

specific heat

μ

dynamic viscosity (kg/ms)

t

time (s)

ν

kinematic viscosity (m^2/s)

K

thermal conductivity ($\text{W}/\text{m K}$)

u

fluid velocity component in x direction. (m/s)

T

fluid temperature (K)

C

solute concentration (kg/m^3)

B_0

magnetic field strength (N/mA^2)

1. Introduction

In the last half-century, MHD flows through porous media have been considered a topic of great interest, due to the use of a variety of industrial applications such as cooling or heating of equipment, design of heat exchangers, cooling of the power plant and nuclear reactor. The other significant applications are MHD flow meters, MHD pumps, MHD generators, and magnetic filtration in metallurgical fields and other subfields [1].

The applications of MHD flows are also used in the biomedical field (hemodynamic), where blood flow mechanisms through blood vessels and drug delivery processes in the human body are studied [2]. In the last few years, it is found that magnetic field is predominantly used in biomedical fields such as drug delivery, treatment of cancer (chemotherapy) and arterial blood flow [3] etc.

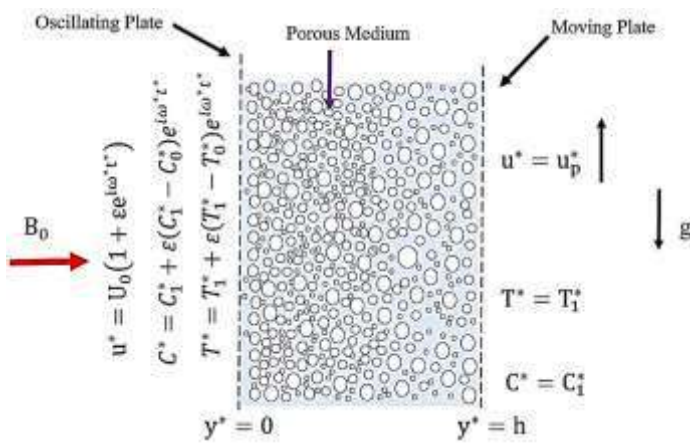
There are various fields, where heat and mass transfer effects are studied together with or without magnetic field, due to industrial use and practical purposes [4] like the dying process in garment industries, transpiring cooling (new and advanced technique of cooling, where the temperature is maintained by moving liquid or gas through walls) in space vehicles, evaporation of water and chemical from their mixtures, separation of toxic and hazardous chemicals and other substance in chemical industries during several chemical processes, heat insulation, chemical catalyst reactors, recovery of oil and gas from their reservoirs, sewage and wastewater treatment plants, food processing and preserving industries, production of polymers and manufacturing of glassware and ceramic products etc., are few significant areas of practical interest [[5], [6], [7], [8], [9], [10], [11], [12], [13], [14], [15]].

In continuation, the study of oscillatory flow cannot be ignored whenever heat and mass transfer enhancement is taken into consideration. The heat transfer rate is slow when fluid is at rest condition (heat transfer occurs due to molecular conduction), but whenever fluid motion is set due to oscillatory flow then the heat transfer rate is comparatively high, and this phenomenon is used in several biomedical and engineering fields [10,[16], [17], [18]]. The literature survey conferred that a variety of research work related to MHD oscillatory flows has been done in applied sciences and core engineering domains and these studies also confirm the progress in this field. It is observed that Makinde and Mhone [19] have discussed the electrically conducting oscillatory flow through the porous channel and studied the combined effect of external magnetic field and thermal radiation. Anwar Beg et al. [20] have presented their mathematical model for MHD oscillatory flow through a rotating channel and explained the magnetic field effect at different angles and found that such kind of flow has a significant role in various chemical and material processing industries as well as in biomedical fields. Later Singh and Kumar [21] studied the hall current effect for MHD oscillatory flow in a rotating channel, and this study is found suitable for the engineering fields, where oscillatory flow with hall current effects is considered such as the design of hall MHD generator and so on. Makinde et al. [22,23] have extended the earlier work of Makinde and Mhone [19] and analysed the combined effect of external magnetic field and thermal radiation with buoyancy force. In these analyses [19,22,23], they have found that an external magnetic field is considered as the resistive force which helps to retard the fluid velocity, whether it is clear fluid or dusty fluid. It also noticed that this result is useful in practical fields such as crude oil extraction from the reservoirs, sewage and wastewater treatment plants and other subfields whenever parameters like porosity and permeability of medium are taken into action. In the continuation, researchers like Sasikumar et al. [24], Goyal and Kumari [25], Sharma et al. [10,26,27], Deb [28], Sharma et al. [29] and others have explored the MHD oscillatory flow through channel pertaining to real-world practical applications.

In the present analysis, we have attempted to bridge the gap with the aforesaid literature work and explored the chemical reactive and thermal radiative MHD oscillatory Couette flow through the vertical porous channel, where one wall/plate of the channel oscillates in its own plan and other plate moves toward the flow direction. In the present work, we have used MATLAB's built-in dsolve function for the solution of the second-order BVP, which has not been done yet. It is useful to handle complex non-linear differential equations and helpful for the solution of the system of ODEs and PDEs [[30], [31], [32]], and as per the knowledge, this method has not been used yet for the solution of the present flow scheme. The finding of this work may be used in real-life applications, including chemical reactors, cooling the towers and rocket engines, designing of heat exchangers, chemical and magnetic filtration, and separation etc.

2. Mathematical model

Chemically reactive, MHD natural convective, viscous incompressible and electrically conducting oscillatory flow through a vertical channel, which is saturated with porous medium and bounded between two infinite thin plates in the influence of the magnetic field, and thermal radiation effects have been explained. For a schematic view of the flow scheme and geometry, the first plate at position $y^* = 0$ is awaked by velocity $u^* = U_0 (1 + \varepsilon e^{i\omega^* t^*})$ and oscillates in its own plane with oscillation frequency ω^* , and the other plate at the distance $y^* = h$ is moving vertically (x^* -axis) towards the flow direction with some fixed velocity u_p^* , and the magnetic field is applied along the y^* axis, i.e. perpendicular to flow direction. Since, both the walls/plates of the channel are considered infinite in length, therefore edge effects of plates are neglected, and this is the reason that existing flow model equations are in y^* and t^* only (Fig. 1).



[Download: Download high-res image \(371KB\)](#)

[Download: Download full-size image](#)

Fig. 1. Flow model.

The set of equations that defines the flow model is given as [10,33]

Conservation of mass:

$$\frac{\partial u^*}{\partial x^*} = 0, \quad (1)$$

Conservation of momentum/motion:

$$\frac{\partial u^*}{\partial t^*} - \nu \frac{\partial^2 u^*}{\partial y^{*2}} + \frac{\nu}{K^*} u^* - g\beta (T^* - T_0^*) - g\beta (C^* - C_0^*) + \frac{\sigma B_0^2}{\rho} u^* = 0, \quad (2)$$

Conservation of energy/Heat:

$$\frac{\partial T^*}{\partial t^*} - \frac{\kappa}{\rho C_p} \left(\frac{\partial^2 T^*}{\partial y^{*2}} \right) + \frac{1}{\rho C_p} \left(\frac{\partial q_r^*}{\partial y^*} \right) = 0, \quad (3)$$

Conservation of species/Concentration:

$$\frac{\partial C^*}{\partial t^*} - D_m \frac{\partial^2 C^*}{\partial y^{*2}} - k_c (C^* - C_0) = 0. \quad (4)$$

The boundary constraints are:

$$\left. \begin{aligned} y^* = 0; \quad u^* &= U_0 (1 + \varepsilon e^{i\omega^* t^*}), \quad C^* = C_1^* + \varepsilon (C_1^* - C_0^*) e^{i\omega^* t^*} \\ T^* &= T_1^* + \varepsilon (T_1^* - T_0^*) e^{i\omega^* t^*}; \\ y^* = h; \quad u^* &= u_p^*, \quad C^* = C_1^*, \quad T^* = T_1^*; \end{aligned} \right\}, \quad (5)$$

Cogley et al. [[21], [34]] model is used for heat flux, and presented as:

$$\frac{\partial q_w^*}{\partial y^*} = 4 (T^* - T_0^*) \int_0^\infty K_{\lambda w} \left(\frac{\partial e_{b\lambda}}{\partial T} \right)_w d\lambda = 4\alpha^2 (T^* - T_1^*). \quad (6)$$

Where all the quantities are mentioned in the nomenclature.

3. Mathematical solution

To solve the model equations, we have used the following non-dimensional quantities and physical parameters:

$$\begin{aligned} y &= \frac{y^*}{h}, \quad u = \frac{u^*}{U_0}, \quad t = \frac{t^* v}{h^2}, \quad \omega = \frac{h^2 \omega^*}{v}, \quad T = \frac{T^* - T_0^*}{T_1^* - T_0^*}, \quad u_p = \frac{u_p^*}{U_0}, \quad M = \frac{\sigma B_0^2 h^2}{\rho v}, \quad R \\ &= \frac{4\alpha^2 h^2}{\kappa}, \\ v &= \frac{\mu}{\rho}, \quad Gr = \frac{g\beta h^2 (T_1^* - T_0^*)}{v U_0}, \quad Gc = \frac{g\beta h^2 (C_1^* - C_0^*)}{v U_0}, \quad K_R = \frac{k_c h^2}{v}, \quad Pr = \frac{\mu C_p}{\kappa}, \\ K &= \frac{h^2}{K^*}, \quad C = \frac{C^* - C_0^*}{C_1^* - C_0^*}, \quad Sc = \frac{v}{D_m}. \end{aligned} \quad (7)$$

Now, putting (6) in (3), and after using (7) into (2), (3), (4), we have the dimensionless form of equations (2), (3), (4) as:

$$\frac{\partial^2 u}{\partial y^2} - \frac{\partial u}{\partial t} - (K + M) u + Gr T + Gc C = 0; \quad (8)$$

$$\frac{\partial^2 T}{\partial y^2} - Pr \frac{\partial T}{\partial t} - R T = 0; \quad (9)$$

$$\frac{\partial^2 C}{\partial y^2} - Sc \frac{\partial C}{\partial t} + (K_R Sc) C = 0; \quad (10)$$

Also, the boundary conditions are changed in dimensionless form as:

$$\left. \begin{aligned} \text{Oscillating plate } y = 0 : \quad u &= (1 + \varepsilon e^{i\omega t}); \quad T = (1 + \varepsilon e^{i\omega t}); \\ C &= (1 + \varepsilon e^{i\omega t}); \\ \text{Moving plate } y = 1 : \quad u &= u_p; \quad T = 1; \quad C = 1; \end{aligned} \right\}. \quad (11)$$

Since, equations (8), (9), (10) are second-order partial differential equations in two independent variables y and t , and due to this reason, the solution of these equations is not possible at this stage. To reduce these PDE into ODE, we used the following scheme for small amplitudes:

$$\eta(y, t) = \eta_0(y) + \varepsilon e^{i\omega t} \eta_1(y) + O(\varepsilon^2). \quad (12)$$

here η is a symbolic representation of velocity u , temperature T and concentration C . Now, using (12), (8), (9), (10), (11) and discarding the higher order term ε , we have:

$$\frac{d^2 u_0}{dy^2} - (K + M) u_0 + Gr T_0 + Gc C_0 = 0, \quad (13)$$

$$\frac{d^2 T_0}{dy^2} - R T_0 = 0, \quad (14)$$

$$\frac{d^2 C_0}{dy^2} + (K_R Sc) C_0 = 0, \quad (15)$$

$$\frac{d^2 u_1}{dy^2} - (K + M + i\omega) u_1 + Gr T_1 + Gc C_1 = 0, \quad (16)$$

$$\frac{d^2 T_1}{dy^2} - (R + i\omega Pr) T_1 = 0, \quad (17)$$

$$\frac{d^2 C_1}{dy^2} + Sc (K_R - i\omega) C_1 = 0, \quad (18)$$

with boundary conditions:

$$\left. \begin{array}{l} \text{Oscillating plate } y = 0 : u_0 = 1, u_1 = 1, T_0 = 1, T_1 = 1, C_0 = 1, \\ C_1 = 1, \\ \text{Moving plate } y = 1 : u_0 = u_p, u_1 = 0, T_0 = 1, T_1 = 0, C_0 = 1, \\ C_1 = 0 \end{array} \right\}. \quad (19)$$

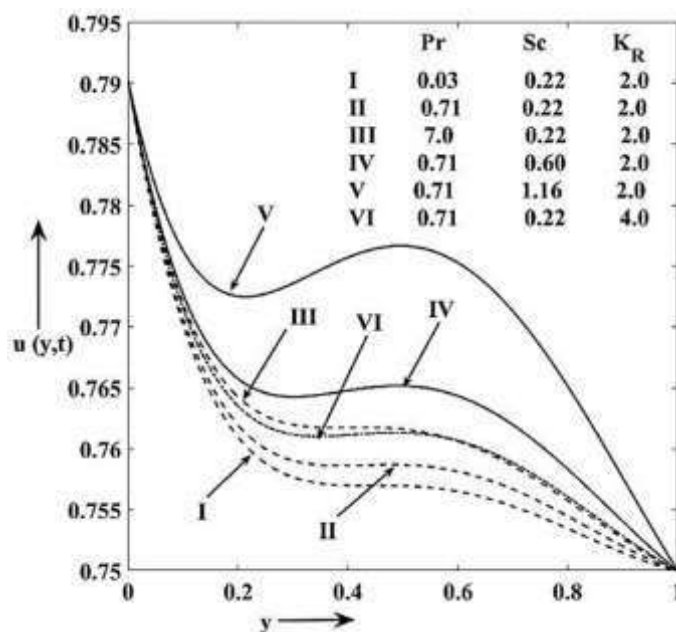
In MATLAB dsolve command, one can find the symbolic solution of ODEs and PDEs with the associated boundary conditions. It is important to note that the dsolve command may solve a closed-form (implicit) solution also whenever an explicit solution is not possible. Nowadays MATLAB's built-in functions (dsolve, ode23 and ode45 etc.) are being used to solve complex or lengthy ODE and PDE, because these methods provide immediate solutions (in a fraction of time) with maximum accuracy that is not possible sometimes by traditional method [[30], [31], [32], [35]]. Here equations (13), (14), (15), (16), (17), (18) are second-order ODE, and these are solved for boundary conditions (19) by using MATLAB dsolve function, and with the help of (12) we get the complete solution that is not given here due to sake of conciseness.

4. Result and discussion

In order to find the physical importance of chemically reactive and thermal radiative MHD oscillatory couette flow through a vertical (one plate is oscillating, and the second plate is moving in flow direction) porous channel, we obtained the numerical/symbolic solution as well as graphical solution by MATLAB's built-in function dsolve for flow governing equations such as the equation of momentum, heat and mass transfer with leading flow parameters like Schmidt number (**Sc**), Hartman number or magnetic field parameter (**M**), parameter of buoyancy force (**Gr**) and (**Gr**), Prandtl number (**Pr**), parameter of thermal radiation (**R**), flow medium permeability (**K**), chemical reaction parameter (**K_R**), and frequency of oscillation (ω). In this analysis, standard numerical values of flow parameters are taken into the consideration, like **Sc** value 0.22 for hydrogen (**H**), 0.60 for water (**H₂O**) and 1.16 for acetic acid (**CH₃COOH**) are chosen due to use in several industrial applications [29], and the numerical value of **Pr** is taken as 0.03 for mercury (**Hg**), 0.71 for air (Nobel gases), and 7.0 fixed for water (**H₂O**) at 20°C, whereas random values of other parameters except $u_p = 0.75$ (velocity of moving plate), scalar quantity $\varepsilon = 0.25$ ($\varepsilon \ll 1$) are considered.

4.1. Transient velocity profile

Fig. 2 explains the physical relevance of the Prandtl number (**Pr**), Schmidt number (**Sc**) and



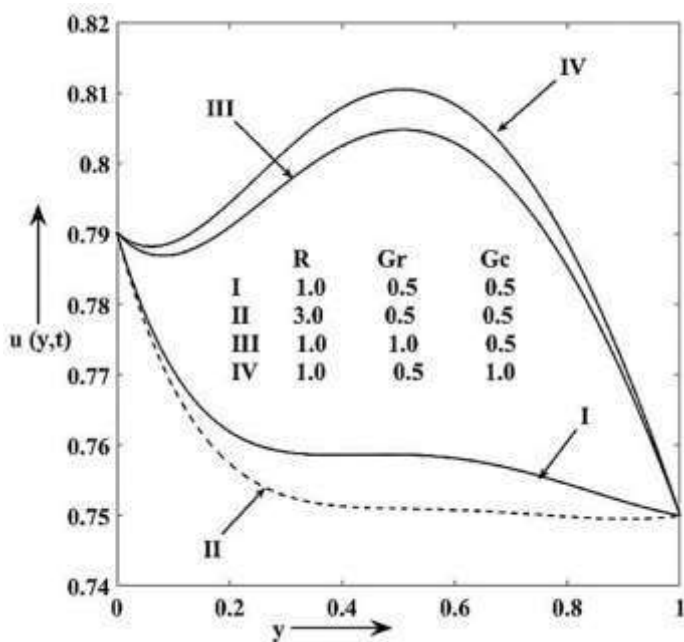
[Download: Download high-res image \(311KB\)](#)

[Download: Download full-size image](#)

Fig. 2. Velocity Profile against y when $Gr = 0.5, R = 1.0, K = 0.5, \omega = Gc = 0.5, 10, M = 1.0,$

chemical reaction (**K_R**) with velocity profile. It depicts that the fluid velocity enhances in the middle part of the channel for different species, hydrogen (**H**) (**Sc** = 0.22), water

(H_2O) ($\text{Sc} = 0.60$), and acetic acid (CH_3COOH) ($\text{Sc} = 1.16$). It is quite possible because dynamic viscosity improves with the rise in Sc and consequence fluid velocity accelerates. Fig. 2 also illustrates that fluid velocity accelerates with the increase in the chemical reaction (K_R), and this result is suitable for various chemical processes in industries where fluid motion is induced by the change in chemical reaction parameter [36]. In addition, Fig. 2 exhibits the physical significance between fluid velocity profile and Prandtl number (Pr), and it is seen that the velocity profile rises for different species, mercury (Hg) ($\text{Pr} = 0.03$), air ($\text{Pr} = 0.7$), and water (H_2O) ($\text{Pr} = 7.0$) at 20°C . Since, the Prandtl number specifically the ratio of two different diffusivities i.e., momentum diffusivity over thermal diffusivity, and rise in the (Pr) accelerates the velocity profile [10,37]. Fig. 3 explains the effect of thermal radiation (R), buoyance forces (Gr) and (Gc) for the velocity profile. From the velocity profile, it is observed that fluid velocity declines with the growth in the radiation parameter [10]. Though fluid motion accelerates with the rise in thermal radiation, because of internal heat generation [6], but present analysis reflects the opposite effect, which is an important result in thermal industries.



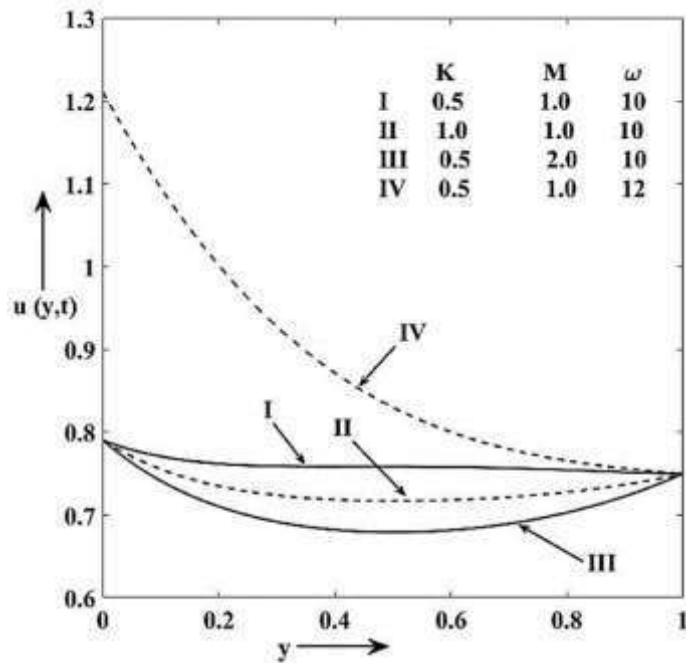
[Download: Download high-res image \(272KB\)](#)

[Download: Download full-size image](#)

Fig. 3. Velocity Profile against y when $\text{K}_R = 2.0$, $\text{Pr} = 0.71$, $\text{K} = 0.5$, $\text{Sc} = 0.22$, $\omega = 10$, $\text{M} = 1.0$.

From Fig. 3, it is also found that velocity profiles accelerate, and it is observed maximum in the middle of the channel with the rise in buoyance forces. It is true because the buoyance force works as a guiding force for fluid motion [10,29]. Further, Fig. 4 shows the effect of the permeability parameter (K), magnetic field (M), and frequency of oscillation (ω) on the velocity profile. It shows that the velocity profile decreases when

the strength of the permeability parameter (**K**) rises, and this result is useful in reservoirs and other fields [29]. Fig. 4 also shows that the velocity detracts due to the high magnetic field. It is a factual result, because flow detracts due to the presence of resistive force, and this resistive force is called Lorentz force [29]. In addition, it is also noted that velocity upsurges with the rise in oscillation frequency [10], and we observe that the engineering discipline (geophysics, and mechanical engineering) has several experimental applications, where such kinds of flows are possible.



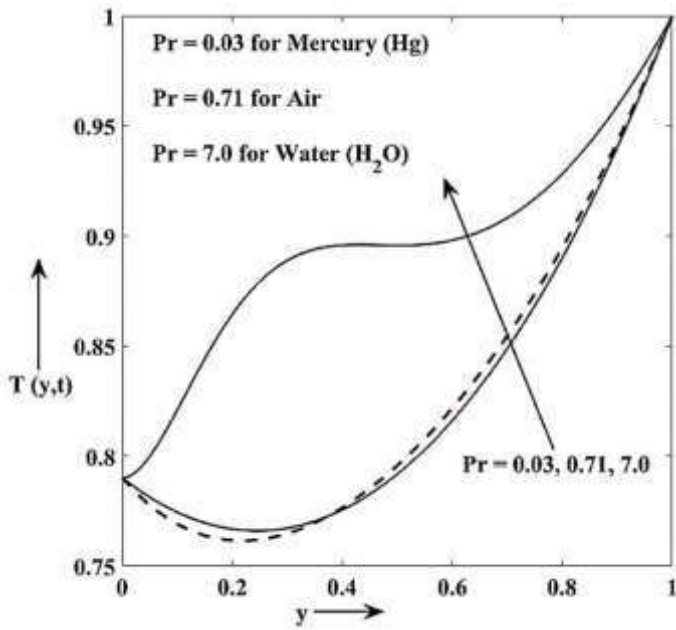
[Download: Download high-res image \(246KB\)](#)

[Download: Download full-size image](#)

Fig. 4. Velocity Profile against y when $K_R = 2.0$, $Gc = 0.5$, $R=1.0$, $Pr = 0.71$, $Gr = 0.5$, $Sc = 0.22$.

4.2. Transient temperature profile

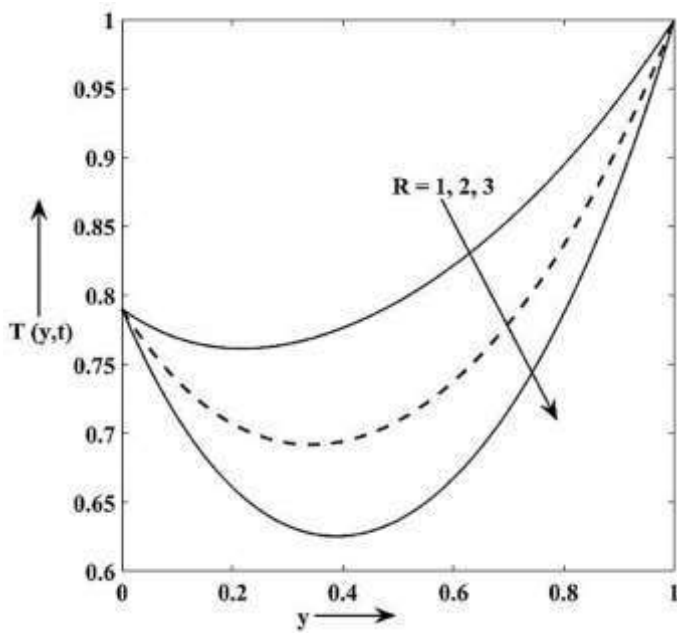
Fig. 5 depicts the effect of Prandtl number (Pr), and it is observed that the temperature profile rises for different species, mercury (Hg) ($Pr = 0.03$), air ($Pr = 0.7$), and water (H_2O) ($Pr = 7.0$) at $20^\circ C$. Since, specific heat increases with the rise in Prandtl number, and therefore temperature profile of water (H_2O) ($Pr = 7.0$) is more with compared to mercury ($Pr = 0.03$) and air ($Pr = 0.7$), and this finding is important in heat transfer systems, like designing of coolants for thermal reactors and other heat transfer devices [10,26]. Further, Fig. 6, Fig. 7 explain the effect of thermal radiation (R) and frequency of oscillation (ω) for the temperature profile and found that the temperature profile declines when both parameters increase.



[Download: Download high-res image \(293KB\)](#)

[Download: Download full-size image](#)

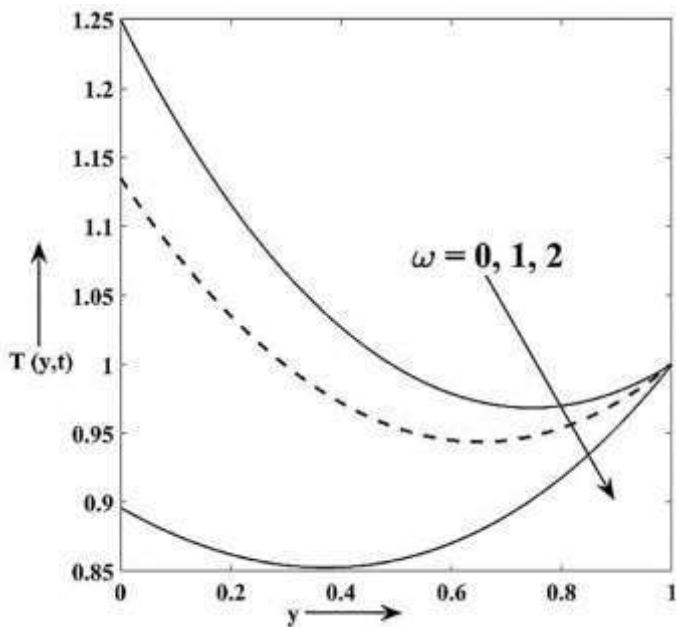
Fig. 5. Temperature Profile against y when $R=1, \omega = 10..$



[Download: Download high-res image \(272KB\)](#)

[Download: Download full-size image](#)

Fig. 6. Temperature Profile against y when $Pr=0.71, \omega = 10.$



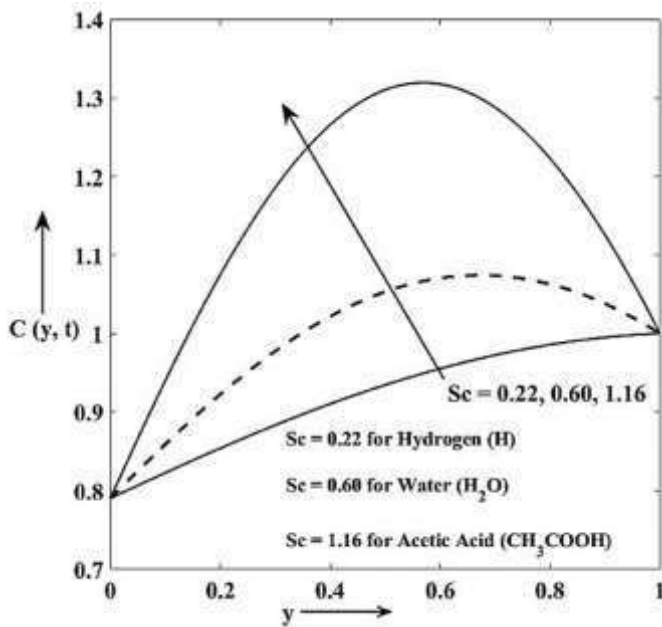
[Download: Download high-res image \(262KB\)](#)

[Download: Download full-size image](#)

Fig. 7. Temperature Profile against y when $Pr=0.71$, $R=1.0$.

4.3. Transient concentration profile

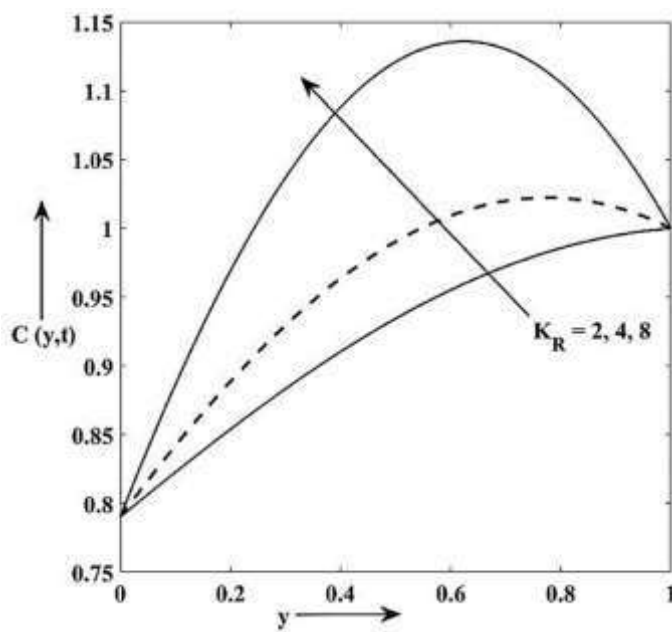
Since, the Schmidt number is the key parameter of mass transfer analysis, which is used when the process of momentum and mass diffusion occurs simultaneously. Fig. 8 explains the nature of the concentration profile with the Schmidt number (Sc). From this figure, it is noticed that the concentration profile rises, and it is observed maximum in the middle part of the channel, for different species, hydrogen (H) ($Sc = 0.22$), water (H_2O) ($Sc = 0.60$), and acetic acid (CH_3COOH) ($Sc = 1.16$). Although, the concentration profile should decline whenever the species of different densities (low to high density) are considered, but the present analysis shows the opposite result, and this result is analogous to Sharma et al. [29]. Fig. 9 explains that the concentration profile props up and, it is achieved maximum in the middle part of the channel due to growth in the chemical reaction parameter (K_R). Further, Fig. 10 depicts that the concentration profile declines due to a change in oscillation frequency (ω).



[Download: Download high-res image \(307KB\)](#)

[Download: Download full-size image](#)

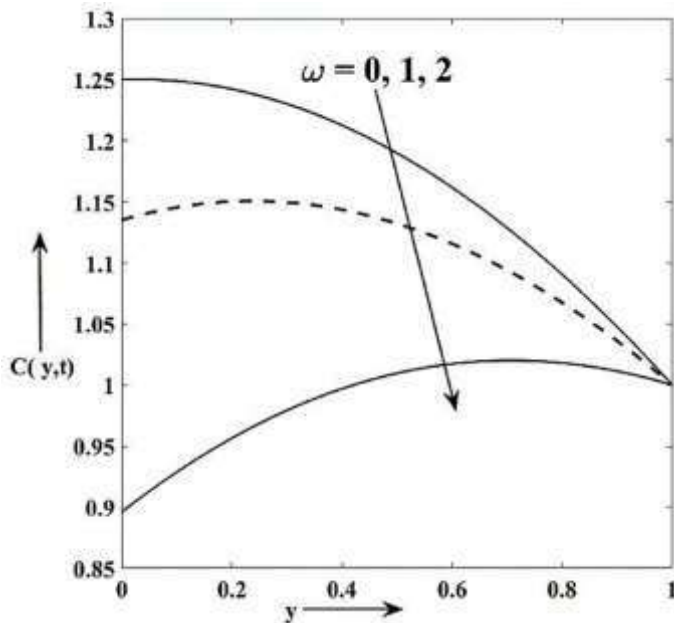
Fig. 8. Concentration Profile against y when $K_R = 2.0, \omega = 10$.



[Download: Download high-res image \(226KB\)](#)

[Download: Download full-size image](#)

Fig. 9. Concentration Profile against y when $Sc = 0.22, \omega = 10$.



[Download: Download high-res image \(250KB\)](#)

[Download: Download full-size image](#)

Fig. 10. Concentration Profile against y when $Sc = 0.22, K_R = 2.0..$

5. Conclusions

Chemical reactive and natural convective MHD oscillatory flow through a porous medium-occupied vertical channel is discussed and momentum, energy and concentration distribution profiles are analysed for the pertained parameters of the flow model (Fig. 1). In this study, the following observations are noticed:

- The fluid velocity is inversely proportionate with the magnetic field because the velocity distribution profile declines for the strong magnetic field. It happens due to the presence of resistive force (Lorentz force). Although, the velocity distribution profile props up with the growth in the chemical reaction. The chemical reaction takes place in a variety of industrial applications, including pulp and paper manufacturing, food preservation, sewage and wastewater treatment facilities, packet bed reactors, chemical and magnetic separation, filtering, etc.
- Since buoyancy force works against gravity, and therefore growth in buoyancy force improves the velocity distribution profile. It happens due to the density difference between fluid layers. In comparison to cold air, hot air is less dense and rises more quickly, and this mechanism is used in thermal industries for cooling/heating devices.

- The rise in oscillation frequency is the cause of the decrease in the temperature, and concentration distribution profile. It is the parameter that declines both temperature and concentration profiles, whereas the change in Schmidt number (for three different species) shows the reverse effect.
- The velocity and temperature profile reduces when the strength of thermal radiation increases.

Future scope

Since, the present flow model and achieved results are relevant to engineering disciplines and find suitable industrial and engineering applications (like; chemical filtration, heat exchangers in thermal industries, cooling in reactors and devices etc.) and therefore, this work can extend in future by taking chemically reactive, magnetized nanofluid flow through an inclined or rotating channel with suction and injection at their boundaries, and the chemical reactive flow inside the tubes/circular cylinder/asymmetric channel under some specific circumstances allied to industrial applications. These kinds of flow models have direct industrial applications, like OFR (Oscillatory Flow Reactor), the design of different types of chemical reactors, and advanced heat exchangers. and transpiration cooling etc.

Credit author statement

Tarun Sharma: Problem solution and methodology; Pooja Sharma: Supervision, drafting, Writing-rewriting and editing; A.H. Seikh: Problem solving, editing, revising; Amjad Iqbal: Methodology, supervising; Navin Kumar: supervision, Editing.

Declaration of competing interest

The authors declare that they have no known competing financial interests or personal relationships that could have appeared to influence the work reported in this paper.

Acknowledgments

The authors extend their appreciation to the Deputyship for Research & Innovation, Ministry of Education in Saudi Arabia for funding this research work through the project no. (IFKSUOR3–318-1).

Data availability

No data was used for the research described in the article.

References

- [1] J.A. Falade, J.C. Ukaegbu, A.C. Egere, S.O. Adesanya
MHD oscillatory flow through a porous channel saturated with porous medium
Alex. Eng. J., 56 (2017), pp. 147-152, [10.1016/j.aej.2016.09.016](https://doi.org/10.1016/j.aej.2016.09.016) ↗
 [View PDF](#) [View article](#) [View in Scopus](#) ↗ [Google Scholar](#) ↗
- [2] G. Ramamurthy, B. Shanker
Magnetohydrodynamic effects on blood flow through a porous channel
Med. Biol. Eng. Comput., 32 (1994), p. 6, [10.1007/BF02524242](https://doi.org/10.1007/BF02524242) ↗
1994;32:655–659
[Google Scholar](#) ↗
- [3] M. Veera Krishna, B.v. Swarnalathamma, J. Prakash
Heat and mass transfer on unsteady MHD oscillatory flow of blood through porous arteriole
Lecture Notes Mech Eng., 207–24 (2018), [10.1007/978-981-10-5329-0_14/COVER](https://doi.org/10.1007/978-981-10-5329-0_14/COVER) ↗
[Google Scholar](#) ↗
- [4] P.C. Ram
Recent developments of heat and mass transfer in hydromagnetic flows
Int. J. Energy Res., 15 (1991), pp. 691-713, [10.1002/ER.4440150902](https://doi.org/10.1002/ER.4440150902) ↗
[View in Scopus](#) ↗ [Google Scholar](#) ↗
- [5] R.N. Barik, G.C. Dash, A. Mohanty
Chemical reaction effect on MHD oscillatory flow through a porous medium bounded by two vertical porous plates with heat source and sores effect
Journal of Applied Analysis and Computation, 3 (2013), pp. 307-321
[Google Scholar](#) ↗
- [6] J.A. Falade, J.C. Ukaegbu, A.C. Egere, S.O. Adesanya
MHD oscillatory flow through a porous channel saturated with porous medium
Alex. Eng. J., 56 (2017), pp. 147-152, [10.1016/j.aej.2016.09.016](https://doi.org/10.1016/j.aej.2016.09.016) ↗
 [View PDF](#) [View article](#) [View in Scopus](#) ↗ [Google Scholar](#) ↗
- [7] S.M. Arifuzzaman, M.S. Khan, M.F.U. Mehedi, B.M.J. Rana, S.F. Ahmmed

Chemically reactive and naturally convective high speed MHD fluid flow through an oscillatory vertical porous plate with heat and radiation absorption effect

Eng. Sci. Technol. Int. J., 21 (2018), pp. 215-228, [10.1016/J.JESTCH.2018.03.004](https://doi.org/10.1016/J.JESTCH.2018.03.004) ↗

 [View PDF](#) [View article](#) [View in Scopus](#) ↗ [Google Scholar](#) ↗

[8] P.v. Satya Narayana, B. Venkateswarlu, B. Devika

Chemical reaction and heat source effects on MHD oscillatory flow in an irregular channel

Ain Shams Eng. J., 7 (2016), pp. 1079-1088, [10.1016/J.ASEJ.2015.07.012](https://doi.org/10.1016/J.ASEJ.2015.07.012) ↗

 [View PDF](#) [View article](#) [View in Scopus](#) ↗ [Google Scholar](#) ↗

[9] Rajan V, Vidhya M, Vijayalakshmi R, Govindarajan A. Chemical Reaction Effects on Radiative MHD Oscillatory Flow in a Porous Channel with Heat and Mass Transfer in an Asymmetric Channel (n.d).

[Google Scholar](#) ↗

[10] T. Sharma, P. Sharma, N. Kumar

Study of dissipative MHD oscillatory unsteady free convective flow in a vertical channel occupied with the porous material in the presence of heat source effect and thermal radiation

J. Phys. Conf. Ser. (2022), Article 012012, [10.1088/1742-6596/2178/1/012012](https://doi.org/10.1088/1742-6596/2178/1/012012) ↗

[View in Scopus](#) ↗ [Google Scholar](#) ↗

[11] N.A.M. Noor, M.A. Admon, S. Shafie

Unsteady MHD squeezing flow of casson fluid over horizontal channel in presence of chemical reaction

J. Adv. Res. Fluid Mech. Therm. Sci., 92 (2022), pp. 49-60, [10.37934/ARFMTS.92.2.4960](https://doi.org/10.37934/ARFMTS.92.2.4960) ↗

[View in Scopus](#) ↗ [Google Scholar](#) ↗

[12] N.A.M. Noor, S. Shafie, M.A. Admon

Impacts of chemical reaction on squeeze flow of MHD Jeffrey fluid in horizontal porous channel with slip condition

Phys. Scripta, 96 (2021), Article 035216, [10.1088/1402-4896/ABD821](https://doi.org/10.1088/1402-4896/ABD821) ↗


[View in Scopus](#) ↗ [Google Scholar](#) ↗

[13] N. Azlina, M. Noor, S. Shafie, M.A. Admon

MHD squeezing flow of casson nanofluid with chemical reaction, thermal radiation and heat generation/absorption

J. Adv. Res. Fluid Mech. Therm. Sci., 68 (2020), pp. 94-111, [10.37934/arfmts.68.2.94111](https://doi.org/10.37934/arfmts.68.2.94111) ↗

[Google Scholar](#) ↗

- [14] N. Azlina, M. Noor, S. Shafie, M.A. Admon
Unsteady MHD flow of cassonnano fluid with chemical reaction, thermal radiation and heat generation/absorption
MATEMATIKA: Malays. J. Ind. Appl. Math., 35 (2019), pp. 33-52,
[10.11113/MATEMATIKA.V35.N4.1262](https://doi.org/10.11113/MATEMATIKA.V35.N4.1262) ↗
[Google Scholar](#) ↗
- [15] N.A.M. Noor, S. Shafie, M.A. Admon
Slip effects on MHD squeezing flow of jeffrey nanofluid in horizontal channel with chemical reaction
Mathematics, 9 (2021), [10.3390/MATH9111215](https://doi.org/10.3390/MATH9111215) ↗
1215 2021;9:1215
[Google Scholar](#) ↗
- [16] J. Sasikumar, A. Govindarjan
Effect of Heat and Mass Transfer on MHD Oscillatory Flow with Chemical Reaction and Slip Conditions in Asymmetric Wavy Channel, 11 (2016)
[Google Scholar](#) ↗
- [17] S.M.R. Ahmed, A.N. Phan, A.P. Harvey
Mass transfer enhancement as a function of oscillatory baffled reactor design
Chem. Eng. Process. Process Intensif., 130 (2018), pp. 229-239, [10.1016/J.CEP.2018.06.016](https://doi.org/10.1016/J.CEP.2018.06.016) ↗
 [View PDF](#) [View article](#) [View in Scopus](#) ↗ [Google Scholar](#) ↗
- [18] J. Sasikumar, D. Bhati, V. Bhaskar
Effect of Heat and Mass Transfer on MHD Oscillatory Flow through Asymmetric Wavy Channel in a Porous Medium with Suction and Injection, 2277 (2020), Article 30009,
[10.1063/5.0025530](https://doi.org/10.1063/5.0025530) ↗
[Google Scholar](#) ↗
- [19] O.D. Makinde, P.Y. Mhone, O.D. Makinde
Heat transfer to MHD oscillatory flow in a channel ölled with porous medium2022) view project mathematical modeling and optimal control analysis of Malaria transmission dynamics with climate variability view project heat transfer to MHD oscillatory flow in A channel filled with porous medium
J. Phys. (2005)
Article in Romanian
[Google Scholar](#) ↗
- [20] O.A. Béq, S.K. Ghosh, M. Narahari

Mathematical modeling of oscillatory MHD Couette flow in a rotating highly permeable medium permeated by an oblique magnetic field
198:235–54

<https://doi.org/10.1080/00986445.2010.500165> ↗ (2010)

[Google Scholar](#) ↗

- [21] K.D. Singh, R. Kumar, R. Kumar
An exact solution of an oscillatory MHD flow through a porous medium bounded by rotating porous channel in the presence of hall current
Int. J. Appl. Math. Mech., 6 (2010), pp. 28-40
[Crossref](#) ↗ [View in Scopus](#) ↗ [Google Scholar](#) ↗
- [22] O. Prakash, O.D. Makinde, D. Kumar
Heat transfer to MHD oscillatory dusty fluid flow in a channel filled with a porous medium
S⁺ Adhan⁺ a, 40 (2015), pp. 1273-1282
[Crossref](#) ↗ [View in Scopus](#) ↗ [Google Scholar](#) ↗
- [23] O. Prakash, O.D. Makinde
MHD oscillatory Couette flow of dusty fluid in a channel filled with a porous medium with radiative heat and buoyancy force
Lat. Am. Appl. Res., 45 (2015), pp. 185-191
[Crossref](#) ↗ [View in Scopus](#) ↗ [Google Scholar](#) ↗
- [24] J. Sasikumar, A. Govindarajan
Free convective MHD oscillatory flow past parallel plates in a porous medium with heat source and chemical reaction
Int. J. Sci. Eng. Res., 6 (2015)
[Google Scholar](#) ↗
- [25] K. Kumari, M. Goyal
Viscous dissipation and mass transfer effects on MHD oscillatory flow in a vertical channel with porous
Medium, 12 (2017), pp. 205-216
[View in Scopus](#) ↗ [Google Scholar](#) ↗
- [26] T. Sharma, P. Sharma, N. Kumar
Entropy generation in thermal radiative oscillatory MHD Couette flow in the influence of heat source
J. Phys. Conf. Ser. (2021), p. 1849, [10.1088/1742-6596/1849/1/012023](https://doi.org/10.1088/1742-6596/1849/1/012023) ↗
[View in Scopus](#) ↗ [Google Scholar](#) ↗
- [27] T. Sharma, P. Sharma, N. Kumar

Chemical reactive magnetized fluid flow through a vertical channel due to heat source and thermal radiation effects

Mater. Today Proc. (2022), [10.1016/J.MATPR.2022.10.298](https://doi.org/10.1016/j.matpr.2022.10.298) ↗

[Google Scholar](#) ↗

- [28] H.R. Deb
Hydromagnetic oscillatory Couette flow of a visco-elastic fluid with dust in a channel with radiative heat
105–15
https://doi.org/10.1007/978-981-15-9927-9_11 ↗ (2021)
[Google Scholar](#) ↗

- [29] B.K. Sharma, P.K. Sharma, S.K. Chauhan
Effect of MHD on unsteady oscillatory Couette flow through porous media
Int. J. Appl. Mech. Eng., 27 (2022), pp. 188-202, [10.2478/IJAME-2022-0012](https://doi.org/10.2478/IJAME-2022-0012) ↗
[View in Scopus](#) ↗ [Google Scholar](#) ↗

- [30] L. Shampine, S. Thompson
Solving ODE's with Matlab
(2003), [10.1017/CBO9780511615542](https://doi.org/10.1017/CBO9780511615542) ↗
[Google Scholar](#) ↗

- [31] F.W. Pietryga
Solving differential equations using MATLAB/simulink. ASEE Annual Conference and Exposition
Conf. Proc. (2005), pp. 12881-12891, [10.18260/1-2--14300](https://doi.org/10.18260/1-2--14300) ↗
[View in Scopus](#) ↗ [Google Scholar](#) ↗

- [32] P. Howard
Solving ODE in MATLAB
(2007)
[Google Scholar](#) ↗

- [33] K. Kumari, M. Goyal
Viscous dissipation and mass transfer effects on MHD oscillatory flow in a vertical channel with porous
Medium, 12 (2017), pp. 205-216
[View in Scopus](#) ↗ [Google Scholar](#) ↗

- [34] A.C. Cogley, W.G. Vincent, S.E. Gilles
Differential approximation for radiative transfer in a nongrey gas near equilibrium

AIAA J., 6 (1968), [10.2514/3.4538](#) ↗

[Google Scholar](#) ↗

[35]

M. Kumari

Optimizing the Problem solving in ordinary differential equations using MATLAB

Int. J. Appl. Eng. Res., 14 (2019), pp. 556-559

[Google Scholar](#) ↗

[36]

M al Zubi, M al Zubi

MHD heat and mass transfer of an oscillatory flow over a vertical permeable plate in a porous medium with chemical reaction

Mod. Mech. Eng., 8 (2018), pp. 179-191, [10.4236/MME.2018.83012](#) ↗

[Google Scholar](#) ↗

[37]

A.O. Ajibade, A.M. Umar, T.M. Kabir

An analytical study on effects of viscous dissipation and suction/injection on a steady mhd natural convection Couette flow of heat generating/absorbing fluid

13:1–12

<https://doi.org/10.1177/16878140211015862> ↗ (2021)

[Google Scholar](#) ↗

Cited by (1)

[Influence of induced magnetic field and chemically reacting on hydromagnetic Couette flow of Jeffrey fluid in an inclined channel with variable viscosity and convective cooling: A Caputo derivative approach](#)

2024, International Journal of Thermofluids

[Show abstract](#) ✓

© 2023 The Authors. Published by Elsevier Ltd.

All content on this site: Copyright © 2024 Elsevier B.V., its licensors, and contributors. All rights are reserved, including those for text and data mining, AI training, and similar technologies. For all open access content, the Creative Commons licensing terms apply.



SOME UNIFIED INTEGRAL FORMULAE ASSOCIATED WITH HURWITZ-LERCH ZETA FUNCTION

Nirmal K. Jangid, Sunil Joshi and Sunil Dutt Purohit

Communicated by Dëshna Loonker

MSC 2010 Classifications: Primary 33C70, 33C99; Secondary 33E20.

Keywords and phrases: Hurwitz-Lerch zeta function, Mac Robert integral, Oberhettinger integral, Lavoie-Trottier integral.

Abstract In the present work, we investigate five new generalised integral formulae by involving the extension form of the Hurwitz-Lerch zeta function and obtain the results in the form of a hypergeometric function in product form by using the properties of the Hadamard product, from which two power series emerge. Furthermore, we also address their special cases by making suitable substitutions. The results obtained here are of a general nature and far more auspicious in the study of applied science, engineering and technology problems.

1 Introduction and Preliminaries

In the field of science and technology, integral formulae are very useful cause of the implementation of the relevant problems. As we know that several integral mechanisms have already been developed but due to time requirements, we are also contributing to the development of new integral formulae associated with Hurwitz-Lerch zeta function.

The Hurwitz-Lerch Zeta function (1.1) and its integral assertion (1.2) are respectively concrete by (see [1] pp. 27, [5] pp. 121 and [6] pp. 194) as below:

$$\phi(z, \varepsilon, \rho) = \sum_{l=0}^{\infty} \frac{z^l}{(n + \rho)^\varepsilon}, \quad (\rho \in C \setminus z_0^-, \varepsilon \in C, \text{ for } |z| < 1; \Re(\varepsilon) > 1, \text{ when } |z| = 1). \quad (1.1)$$

Besides

$$\phi(z, \varepsilon, \rho) = \frac{1}{\Gamma(\varepsilon)} \int_0^\infty \frac{t^{\varepsilon-1} e^{-\rho t}}{1 - z e^{-t}} dt = \frac{1}{\Gamma(\varepsilon)} \int_0^\infty \frac{t^{\varepsilon-1} e^{-(\rho-1)t}}{e^t - z} dt, \quad (1.2)$$

($\Re(\varepsilon) > 0, \Re(\rho) > 0$ for $|z| \leq 1 (z \neq 1)$; $\Re(\varepsilon) > 1$, when $z = 1$).

In this sequel, Goyal and Laddha [4] and Garg et al. [3] defined the new extension formula of Hurwitz-Lerch Zeta function in (1.3) and (1.5) respectively and also defined their integral representation as in (1.4) and (1.6) respectively.

$$\phi_\gamma^*(z, \varepsilon, \rho) = \sum_{l=0}^{\infty} \frac{(\gamma)_n}{l!} \frac{z^l}{(n + \rho)^\varepsilon}, \quad (1.3)$$

($\gamma \in C, \rho \in C \setminus z_0^-, \varepsilon \in C$ when $|z| < 1; \Re(\varepsilon - \gamma) > 1$ when $|z| = 1$),

$$\phi_\gamma^*(z, \varepsilon, \rho) = \frac{1}{\Gamma(\varepsilon)} \int_0^\infty \frac{t^{\varepsilon-1} e^{-\rho t}}{(1 - z e^{-t})^\gamma} dt = \frac{1}{\Gamma(\varepsilon)} \int_0^\infty \frac{t^{\varepsilon-1} e^{-(\rho-\gamma)t}}{(e^t - z)^\gamma} dt, \quad (1.4)$$

($\Re(\varepsilon) > 0, \Re(\rho) > 0$ when $|z| \leq 1 (z \neq 1)$; $\Re(\varepsilon) > 1$ when $z = 1$).

And

$$\phi_{\gamma, u; v}(z, \varepsilon, \rho) = \sum_{l=0}^{\infty} \frac{(\gamma)_l (u)_l}{(v)_l l!} \frac{z^l}{(l + \rho)^\varepsilon}, \quad (1.5)$$

$(\gamma, u, v \in C, \rho \in C \setminus z_0^-, \varepsilon \in C$ when $|z| < 1; \Re(\varepsilon + v - \gamma - u) > 1$ when $|z| = 1)$,

$$\phi_{\gamma,u,v}(z, \varepsilon, \rho) = \frac{1}{\Gamma(\varepsilon)} \int_0^\infty t^{\varepsilon-1} e^{-\rho t} {}_2F_1(\gamma, u; v; ze^{-t}) dt, \tag{1.6}$$

$(\Re(\varepsilon) > 0, \Re(\rho) > 0$ when $|z| \leq 1 (z \neq 1); \Re(\varepsilon) > 1$ when $z = 1)$.

In addition, Parmar [13] introduced and investigated the new extension of the Hurwitz-Lerch Zeta function in the form of beta function as

$$\phi_{\gamma,u,v}(z, \varepsilon, \rho; p) = \sum_{l=0}^\infty \frac{(\gamma)_l B(u+l, v-u; p)}{B(u, v-u) l!} \frac{z^l}{(l+\rho)^\varepsilon}, \tag{1.7}$$

where $p \geq 0, \gamma, u, v \in C, \rho \in C \setminus Z_0^-, \varepsilon \in C$ when $|z| < 1, \Re(\varepsilon + v - \gamma - u) > 1$ when $|z| = 1$.

Where $B(\vartheta, \varphi; p)$ is the extended beta function which is investigated by Chaudhry et al. [1] as follow

$$B(\vartheta, \varphi; p) = B_p(\vartheta, \varphi) = \int_0^1 t^{\vartheta-1} (1-t)^{\varphi-1} e^{-\frac{p}{t(1-t)}} dt, \tag{1.8}$$

where $\Re(p) > 0, \Re(\vartheta) > 0, \Re(\varphi) > 0$.

Shadab et al. [17] recently developed a new and updated version of beta function extension, which goes like this:

$$B_p^\varepsilon(\vartheta, \varphi) = B(\vartheta, \varphi; p, \varepsilon) = \int_0^1 t^{\vartheta-1} (1-t)^{\varphi-1} E_\varepsilon\left(-\frac{p}{t(1-t)}\right) dt, \tag{1.9}$$

where $\Re(r) > 0, \Re(s) > 0$ and $E_\varepsilon(\cdot)$ is the Mittag-Leffler function given as

$$E_\varepsilon(z) = \sum_{l=0}^\infty \frac{z^l}{\Gamma(\varepsilon l + 1)}. \tag{1.10}$$

Recently, Rahman et al. [15] have created a new extension of the Hurwitz-Lerch zeta function in the form of extended beta function (1.9) as

$$\phi_{\gamma,u,v}[z, \varepsilon, \rho; p, \delta] = \phi_{\gamma,u,v}^\delta[z, \varepsilon, \rho; p] = \sum_{l=0}^\infty \frac{(\gamma)_l B_p^\delta(u+l, v-u)}{B(u, v-u) l!} \frac{z^l}{(l+\rho)^\varepsilon}, \tag{1.11}$$

where $[\gamma, u, v \in C, p \geq 0, \delta > 0, \rho \in C \setminus z_0^-, \varepsilon \in C$ when $|z| < 1, \Re(\varepsilon + v - \gamma - u) > 1$ when $|z| = 1]$.

For our present investigation, we need some integral formulae which are given by Mac Robert [6], Oberhettinger [12] and Lavoie-Trottier [5] in equation (1.12), (1.13) and (1.14) respectively are as follows:

$$\int_0^1 y^{\varsigma-1} (1-y)^{\varepsilon-1} [cy + d(1-y)]^{-\varsigma-\varepsilon} dy = \frac{1}{c^\varepsilon d^\varepsilon} \frac{\Gamma(\varsigma)\Gamma(\varepsilon)}{\Gamma(\varsigma+\varepsilon)}, \tag{1.12}$$

provided that $\Re(\varsigma) > 0, \Re(\varepsilon) > 0, c$ and d are nonzero constants so the expression $cy + d(1-y)$, where $0 \leq y \leq 1$.

$$\int_0^\infty \theta^{\varepsilon-1} \left(\theta + c + \sqrt{(\theta^2 + 2c\theta)}\right)^{-\varsigma} d\theta = 2^\varepsilon c^{-\varsigma} \left(\frac{c}{2}\right)^\varepsilon \frac{\Gamma(2\varepsilon)\Gamma(\varsigma-\varepsilon)}{\Gamma(1+\varepsilon+\varsigma)}, \tag{1.13}$$

provided that $0 < \Re(\varepsilon) < \Re(\varsigma)$.

$$\int_0^1 \theta^{\varsigma-1} (1-\theta)^{2\varepsilon-1} \left(1-\frac{\theta}{3}\right)^{2\varsigma-1} \left(1-\frac{\theta}{4}\right)^{\varepsilon-1} d\theta = \left(\frac{2}{3}\right)^{2\varsigma} \frac{\Gamma(\varsigma)\Gamma(\varepsilon)}{\Gamma(\varsigma+\varepsilon)}, \tag{1.14}$$

provided that $\Re(\varsigma) > 0, \Re(\varepsilon) > 0$.

Here we also recall Hadamard product of two analytic functions which are helpful in our current exploration. This will help us to ablate the function which has emerged into the product of two known functions. Let's have 2 power series be

$f(x) = \sum_{n=0}^{\infty} a_n x^n$ ($|x| < R_f$) and $g(x) = \sum_{n=0}^{\infty} b_n x^n$ ($|x| < R_g$), where R_f and R_g are radii of convergence respectively. Then their Hadamard product [6],[14],[16] is describes by the power series as

$$(f * g)(x) = \sum_{n=0}^{\infty} a_n b_n x^n = (g * f)(x) \quad (|x| < R), \tag{1.15}$$

where $R = \lim_{n \rightarrow \infty} \left| \frac{a_n b_n}{a_{n+1} b_{n+1}} \right| = \left(\lim_{n \rightarrow \infty} \left| \frac{a_n}{a_{n+1}} \right| \right) \cdot \left(\lim_{n \rightarrow \infty} \left| \frac{b_n}{b_{n+1}} \right| \right) = R_f \cdot R_g$, in general $R \geq R_f \cdot R_g$.

Several authors contributed in the field of special functions and also associated with Baskakov-Durrmeyer-Stancu type operators see ([7]-[11]). We also recall the generalized hypergeometric function [2] with r and s are numerator and denominator respectively demarcated as

$${}_rF_s \left(\begin{matrix} u_1, u_2, \dots, u_r; \\ v_1, v_2, \dots, v_s; \end{matrix} z \right) = \sum_{l=0}^{\infty} \frac{(u_1)_l (u_2)_l \dots (u_r)_l z^l}{(v_1)_l (v_2)_l \dots (v_s)_l l!}, \tag{1.16}$$

where $z, u_i, v_j \in C, i = 1, 2, \dots, r, j = 1, 2, \dots, s$ and v_j is nonzero, non-negative integer.

2 Main Results

In this section we define five generalized integral formulae by inserting the extension form of Hurwitz-Lerch zeta function (1.11) into the integral formulae (1.12), (1.13) and (1.14) by taking suitable argument into the integrand.

Theorem 1: Let us suppose that $\Re(\varsigma) > 0, \Re(\epsilon) > 0, \gamma, u, v \in C, p \geq 0, \delta > 0, \rho \in C \setminus z_0^-, c$ and d are nonzero constants and $0 \leq y \leq 1$, then

$$\begin{aligned} & \int_0^1 y^{\varsigma-1} (1-y)^{\epsilon-1} [cy + d(1-y)]^{-\varsigma-\epsilon} \phi_{\gamma, u; v}^{\delta} \left(\frac{2cdy(1-y)}{\{cy + d(1-y)\}^2}, \epsilon, \rho; p \right) dy \\ &= \frac{B(\varsigma, \epsilon)}{c^{\varsigma} d^{\epsilon}} \phi_{\gamma, u; v}^{\delta} \left(\frac{1}{2}, \epsilon, \rho; p \right) * {}_3F_2 \left[\varsigma, \epsilon, 1; \frac{\varsigma + \epsilon}{2}, \frac{\varsigma + \epsilon + 1}{2}; \frac{1}{2} \right]. \end{aligned} \tag{2.1}$$

Proof: For our convenience L.H.S. is denoted by I_1 , and by making the use of equation (1.11), then we have

$$I_1 = \int_0^1 y^{\varsigma-1} (1-y)^{\epsilon-1} [cy + d(1-y)]^{-\varsigma-\epsilon} \sum_{l=0}^{\infty} \frac{(\gamma)_l B_p^{\delta}(u+l, v-u)}{B(u, v-u)(l+\rho)^{\epsilon} l!} \left[\frac{2cdy(1-y)}{\{cy + d(1-y)\}^2} \right]^l dy$$

now we are adjusting the order of integration and summation,

$$I_1 = \sum_{l=0}^{\infty} \frac{(\gamma)_l B_p^{\delta}(u+l, v-u)(2cd)^l}{B(u, v-u)(l+\rho)^{\epsilon} l!} \int_0^1 y^{\varsigma+l-1} (1-y)^{\epsilon+l-1} [cy + d(1-y)]^{-\varsigma-\epsilon-2l} dy$$

by making the use of equation (1.12), after some arrangements and simplification, we get

$$I_1 = \sum_{l=0}^{\infty} \frac{(\gamma)_l B_p^{\delta}(u+l, v-u) 2^l}{B(u, v-u)(l+\rho)^{\epsilon} l!} \frac{\Gamma(\varsigma)(\varsigma)_l \Gamma(\epsilon)(\epsilon)_l}{c^{\varsigma} d^{\epsilon} 2^{2l} \left(\frac{\varsigma+\epsilon}{2}\right)_l \left(\frac{\varsigma+\epsilon+1}{2}\right)_l \Gamma(\varsigma+\epsilon)} \tag{2.2}$$

now we are applying the Hadamard product (1.15) in (2.2) and making the use of (1.11) and (1.16), then we get the wanted outcome.

Theorem 2: Let us suppose that $0 < \Re(\epsilon) < \Re(\varsigma), c \in N, \gamma, u, v \in C, p \geq 0, \delta > 0, \rho \in C \setminus z_0^-,$ then

$$\int_0^{\infty} \theta^{\epsilon-1} \left(\theta + c + \sqrt{(\theta^2 + 2c\theta)} \right)^{-\varsigma} \phi_{\gamma, u; v}^{\delta} \left(\frac{y}{\left(\theta + c + \sqrt{(\theta^2 + 2c\theta)} \right)}, \epsilon, \rho; p \right) d\theta$$

$$\begin{aligned}
 &= 2^{1-\epsilon} c^{\epsilon-\varsigma} \Gamma(2\epsilon) \frac{\Gamma(\varsigma-\epsilon)}{\Gamma(\epsilon+\varsigma+1)} \\
 &\times \phi_{\gamma,u;v}^{\delta} \left(\frac{y}{c}, \epsilon, \rho; p \right) * {}_3F_2 \left[\varsigma+1, \varsigma-\epsilon, 1; \varsigma, \varsigma+\epsilon+1; \frac{y}{c} \right]. \tag{2.3}
 \end{aligned}$$

Proof: For our convenience L.H.S. is denoted by I_2 , and by making the use of equation (1.11), then we have

$$\begin{aligned}
 I_2 &= \int_0^{\infty} \theta^{\epsilon-1} \left(\theta + c + \sqrt{(\theta^2 + 2c\theta)} \right)^{-\varsigma} \sum_{l=0}^{\infty} \frac{(\gamma)_l B_p^{\delta}(u+l, v-u)}{B(u, v-u)(l+\rho)^{\epsilon} l!} \\
 &\times \left[\frac{y}{\left(\theta + c + \sqrt{(\theta^2 + 2c\theta)} \right)} \right]^l d\theta
 \end{aligned}$$

now we are adjusting the order of integration and summation,

$$I_2 = \sum_{l=0}^{\infty} \frac{(\gamma)_l B_p^{\delta}(u+l, v-u) y^l}{B(u, v-u)(l+\rho)^{\epsilon} l!} \int_0^{\infty} \theta^{\epsilon-1} \left(\theta + c + \sqrt{(\theta^2 + 2c\theta)} \right)^{-\varsigma-l} d\theta$$

by making the use of equation (1.13), after some simplification and rearranging the terms, we get

$$I_2 = 2^{1-\epsilon} c^{\epsilon-\varsigma} \Gamma(2\epsilon) \frac{\Gamma(\varsigma-\epsilon)}{\Gamma(\epsilon+\varsigma+1)} \sum_{l=0}^{\infty} \frac{(\gamma)_l B_p^{\delta}(u+l, v-u) (\varsigma+1)_l (\varsigma-\epsilon)_l}{B(u, v-u)(l+\rho)^{\epsilon} (\varsigma)_l (\epsilon+\varsigma+1)_l l!} \left(\frac{y}{c} \right)^l \tag{2.4}$$

now we apply the Hadamard product (1.15) in (2.4), and making the use of (1.11) and (1.16), then we get the wanted consequence.

Theorem 3: Let us suppose that $0 < \Re(\epsilon) < \Re(\varsigma)$, $c \in N$, $\gamma, u, v \in C$, $p \geq 0$, $\delta > 0$, $\rho \in C \setminus z_0^-$, then

$$\begin{aligned}
 &\int_0^{\infty} \theta^{\epsilon-1} \left(\theta + c + \sqrt{(\theta^2 + 2c\theta)} \right)^{-\varsigma} \phi_{\gamma,u;v}^{\delta} \left(\frac{y\theta}{\left(\theta + c + \sqrt{(\theta^2 + 2c\theta)} \right)}, \epsilon, \rho; p \right) d\theta \\
 &= 2^{1-\epsilon} c^{\epsilon-\varsigma} \Gamma(2\epsilon) \frac{\Gamma(\varsigma-\epsilon)}{\Gamma(\epsilon+\varsigma+1)} \phi_{\gamma,u;v}^{\delta} \left(\frac{y}{2}, \epsilon, \rho; p \right) \\
 &* {}_4F_3 \left[\varsigma+1, \epsilon, \epsilon + \frac{1}{2}, 1; \varsigma, \frac{\epsilon+\varsigma+1}{2}, \frac{\epsilon+\varsigma+2}{2}; \frac{y}{2} \right]. \tag{2.5}
 \end{aligned}$$

Proof: For our convenience L.H.S. is denoted by I_3 , and by making the use of equation (1.11), then we have

$$\begin{aligned}
 I_3 &= \int_0^{\infty} \theta^{\epsilon-1} \left(\theta + c + \sqrt{(\theta^2 + 2c\theta)} \right)^{-\varsigma} \sum_{l=0}^{\infty} \frac{(\gamma)_l B_p^{\delta}(u+l, v-u)}{B(u, v-u)(l+\rho)^{\epsilon} l!} \\
 &\times \left[\frac{y\theta}{\left(\theta + c + \sqrt{(\theta^2 + 2c\theta)} \right)} \right]^l d\theta
 \end{aligned}$$

now we are adjusting the order of integration and summation,

$$I_3 = \sum_{l=0}^{\infty} \frac{(\gamma)_l B_p^{\delta}(u+l, v-u) y^l}{B(u, v-u)(l+\rho)^{\epsilon} l!} \int_0^{\infty} \theta^{\epsilon+l-1} \left(\theta + c + \sqrt{(\theta^2 + 2c\theta)} \right)^{-\varsigma-l} d\theta$$

by making the use of equation (1.13), after some simplification and rearranging the terms, we get

$$I_3 = 2^{1-\epsilon} e^{\epsilon-\varsigma} \Gamma(2\epsilon) \frac{\Gamma(\varsigma-\epsilon)}{\Gamma(\epsilon+\varsigma+1)} \sum_{l=0}^{\infty} \frac{(\gamma)_l B_p^\delta(u+l, v-u)(\varsigma+1)_l (\epsilon)_l (\epsilon+\frac{1}{2})_l}{B(u, v-u)(l+\rho)^\epsilon (\varsigma)_l (\frac{\epsilon+\varsigma+1}{2})_l (\frac{\epsilon+\varsigma+2}{2})_l l!} \left(\frac{y}{2}\right)^l \tag{2.6}$$

now we put on the Hadamard product (1.15) in (2.6), and making the use of (1.11) and (1.16), then we get the awaited result.

Theorem 4: Let us suppose that $\Re(\varsigma) > 0, \Re(\epsilon) > 0, \gamma, u, v \in C, p \geq 0, \delta > 0, \rho \in C \setminus z_0^-$, then

$$\int_0^1 \theta^{\varsigma-1} (1-\theta)^{2\epsilon-1} \left(1-\frac{\theta}{3}\right)^{2\varsigma-1} \left(1-\frac{\theta}{4}\right)^{\epsilon-1} \phi_{\gamma, u; v}^\delta \left[y \left(1-\frac{\theta}{4}\right) (1-\theta)^2, \epsilon, \rho; p \right] d\theta$$

$$= \left(\frac{2}{3}\right)^{2\varsigma} B(\varsigma, \epsilon) \phi_{\gamma, u; v}^\delta (y, \epsilon, \rho; p) * {}_2F_1[\epsilon, 1; \varsigma + \epsilon; y]. \tag{2.7}$$

Proof: For our convenience L.H.S. is denoted by I_4 , and by making the use of equation (1.11), then we have

$$I_4 = \int_0^1 \theta^{\varsigma-1} (1-\theta)^{2\epsilon-1} \left(1-\frac{\theta}{3}\right)^{2\varsigma-1} \left(1-\frac{\theta}{4}\right)^{\epsilon-1} \sum_{l=0}^{\infty} \frac{(\gamma)_l B_p^\delta(u+l, v-u)}{B(u, v-u)(l+\rho)^\epsilon l!} \times y^l \left(1-\frac{\theta}{4}\right)^l (1-\theta)^{2l} d\theta$$

now we are adjusting the order of integration and summation,

$$I_4 = \sum_{l=0}^{\infty} \frac{(\gamma)_l B_p^\delta(u+l, v-u) y^l}{B(u, v-u)(l+\rho)^\epsilon l!} \int_0^1 \theta^{\varsigma-1} (1-\theta)^{2(\epsilon+l)-1} \left(1-\frac{\theta}{3}\right)^{2\varsigma-1} \left(1-\frac{\theta}{4}\right)^{\epsilon+l-1} d\theta$$

by making the use of equation (1.14), and further simplification and rearranging the terms, we get

$$I_4 = \left(\frac{2}{3}\right)^{2\varsigma} B(\varsigma, \epsilon) \sum_{l=0}^{\infty} \frac{(\gamma)_l B_p^\delta(u+l, v-u)(\epsilon)_l y^l}{B(u, v-u)(l+\rho)^\epsilon (\varsigma+\epsilon)_l l!} \tag{2.8}$$

now we apply the Hadamard product (1.15) in (2.8), and making the use of (1.11) and (1.16), then we get the wanted outcome.

Theorem 5: Let us suppose that $\Re(\varsigma) > 0, \Re(\epsilon) > 0, \gamma, u, v \in C, p \geq 0, \delta > 0, \rho \in C \setminus z_0^-$, then

$$\int_0^1 \theta^{\varsigma-1} (1-\theta)^{2\epsilon-1} \left(1-\frac{\theta}{3}\right)^{2\varsigma-1} \left(1-\frac{\theta}{4}\right)^{\epsilon-1} \phi_{\gamma, u; v}^\delta \left[y\theta \left(1-\frac{\theta}{3}\right)^2, \epsilon, \rho; p \right] d\theta$$

$$= \left(\frac{2}{3}\right)^{2\varsigma} B(\varsigma, \epsilon) \phi_{\gamma, u; v}^\delta \left(\frac{4y}{9}, \epsilon, \rho; p \right) * {}_2F_1 \left[\varsigma, 1; \varsigma + \epsilon; \frac{4y}{9} \right]. \tag{2.9}$$

Proof: For our convenience L.H.S. is denoted by I_5 , and by making the use of equation (1.11), then we have

$$I_5 = \int_0^1 \theta^{\varsigma-1} (1-\theta)^{2\epsilon-1} \left(1-\frac{\theta}{3}\right)^{2\varsigma-1} \left(1-\frac{\theta}{4}\right)^{\epsilon-1} \sum_{l=0}^{\infty} \frac{(\gamma)_l B_p^\delta(u+l, v-u)}{B(u, v-u)(l+\rho)^\epsilon l!} y^l \theta^l \times \left(1-\frac{\theta}{3}\right)^{2l} d\theta$$

now we are adjusting the order of integration and summation,

$$I_5 = \sum_{l=0}^{\infty} \frac{(\gamma)_l B_p^\delta(u+l, v-u)y^l}{B(u, v-u)(l+\rho)^\epsilon l!} \int_0^1 \theta^{s+l-1} (1-\theta)^{2\epsilon-1} \left(1-\frac{\theta}{3}\right)^{2(\varsigma+l)-1} \left(1-\frac{\theta}{4}\right)^{\epsilon-1} d\theta$$

by making the use of equation (1.14), and further simplification and rearranging the terms, we get

$$I_5 = \left(\frac{2}{3}\right)^{2\varsigma} B(\varsigma, \epsilon) \sum_{l=0}^{\infty} \frac{(\gamma)_l B_p^\delta(u+l, v-u)(\varsigma)_l}{B(u, v-u)(l+\rho)^\epsilon (\varsigma+\epsilon)_l l!} \left(\frac{4y}{9}\right)^l \tag{2.10}$$

now we apply the Hadamard product (1.15) in (2.10), and making the use of (1.11) and (1.16), then we get the anticipated consequence.

3 Special cases

In this section we are going to find some integral formulae by substituting particular values, If we put $\delta = p = 1$ in (2.1),(2.3),(2.5),(2.7) and (2.9), then we have our results in the form Hadamard product of Hurwitz-Lerch zeta function investigated by Garg et al. [3] with hypergeometric function, which are defined in the following Corollaries. As if we put $\varsigma = \epsilon = c = d = \delta = p = 1$, in (2.1) then we have Corollary 1 as below:

Corollary 1: Let us suppose that $\Re(\varsigma) > 0, \Re(\epsilon) > 0, \gamma, u, v \in C, \rho \in C \setminus z_0^-, c$ and d are nonzero constants and $0 \leq y \leq 1$. then

$$\int_0^1 \phi_{\gamma, u; v} [2y(1-y), \epsilon, \rho] dy = \phi_{\gamma, u; v} \left(\frac{1}{2}, \epsilon, \rho\right) * {}_2F_1 \left[1, 1; \frac{3}{2}; \frac{1}{2}\right]. \tag{3.1}$$

Similarly, as if we put $\epsilon = \delta = p = 1, \varsigma = 2$, in (2.3) and (2.5), then we have Corollary 2 and Corollary 3 as follows:

Corollary 2: Let us suppose that $0 < \Re(\epsilon) < \Re(\varsigma), c \in N, \gamma, u, v \in C, \rho \in C \setminus z_0^-,$ then

$$\begin{aligned} \int_0^\infty \left(\theta + c + \sqrt{(\theta^2 + 2c\theta)}\right)^{-2} \phi_{\gamma, u; v} \left(\frac{y}{\theta + c + \sqrt{(\theta^2 + 2c\theta)}}, \epsilon, \rho\right) d\theta \\ = \frac{1}{3c} \phi_{\gamma, u; v} \left(\frac{y}{c}, \epsilon, \rho\right) * {}_3F_2 \left[3, 1, 1; 2, 4; \frac{y}{c}\right]. \end{aligned} \tag{3.2}$$

Corollary 3: Let us suppose that $0 < \Re(\epsilon) < \Re(\varsigma), c \in N, \gamma, u, v \in C, \rho \in C \setminus z_0^-,$ then

$$\begin{aligned} \int_0^\infty \left(\theta + c + \sqrt{(\theta^2 + 2c\theta)}\right)^{-2} \phi_{\gamma, u; v} \left(\frac{y\theta}{\theta + c + \sqrt{(\theta^2 + 2c\theta)}}, \epsilon, \rho\right) d\theta \\ = \frac{1}{3c} \phi_{\gamma, u; v} \left(\frac{y}{2}, \epsilon, \rho\right) * {}_4F_3 \left[3, 1, \frac{3}{2}, 1; 2, 2, \frac{5}{2}; \frac{y}{2}\right]. \end{aligned} \tag{3.3}$$

In this manner if we substitute $\varsigma = 1, \epsilon = \delta = p = 1$, in (2.7) and (2.9), then we have Corollary 4 and Corollary 5 as follows:

Corollary 4: Let us suppose that $\Re(\varsigma) > 0, \Re(\epsilon) > 0, \gamma, u, v \in C, \rho \in C \setminus z_0^-,$ then

$$\begin{aligned} \int_0^1 (1-\theta) \left(1-\frac{\theta}{3}\right) \phi_{\gamma, u; v} \left[y \left(1-\frac{\theta}{4}\right) (1-\theta)^2, \epsilon, \rho\right] d\theta \\ = \frac{4}{9} \phi_{\gamma, u; v} (y, \epsilon, \rho) * {}_2F_1 [1, 1; 2; y]. \end{aligned} \tag{3.4}$$

Corollary 5: Let us suppose that $\Re(\varsigma) > 0, \Re(\epsilon) > 0, \gamma, u, v \in C, \rho \in C \setminus z_0^-,$ then

$$\int_0^1 (1-\theta) \left(1 - \frac{\theta}{3}\right) \phi_{\gamma, u; v} \left[y\theta \left(1 - \frac{\theta}{3}\right)^2, \varepsilon, \rho \right] d\theta$$

$$= \frac{4}{9} \phi_{\gamma, u; v} \left(\frac{4y}{9}, \varepsilon, \rho \right) * {}_2F_1 \left[1, 1; 2; \frac{4y}{9} \right]. \quad (3.5)$$

4 Conclusion

In this present investigation, we defined five new generalised integral formulae by involving the extension form of the Hurwitz-Lerch zeta function and deduced the results in the form of hypergeometric functions in product form by using the properties of the Hadamard product of two power series. Furthermore, we also discussed their special cases by making suitable substitutions. The future scope of these integrals is that one can define many other impressive integrals by using different kinds of Hurwitz-Lerch zeta function, trigonometric and hyperbolic functions, after appropriate parametric replacements, special functions product with different kinds of polynomials or multivariable polynomials, which gives remarkable results. The reported findings are general in nature and useful in the study of science and technology.

Acknowledgements

The authors express their sincere thanks to the reviewers for their careful reading and suggestions that helped to improve this paper.

References

- [1] M.A. Chaudhry, A. Qadir, M. Rafique and S.M. Zubair, Extension of Eulers Beta Function, *J. Comput. Appl. Math.* **78**, 19–32 (1997).
- [2] A. Erdelye, W. Magnus, F. Oberhettinger and F.G. Tricomi, Higher Transcendental Functions, Vol.1, *McGraw-Hill, New York, Toronto, London*, (1953).
- [3] M. Garg, K. Jain and S.L. Kalla, A further Study of General Hurwitz-Lerch Zeta Function, *Algebras Groups Geom.* **25**, 311–319 (2008).
- [4] S.P. Goyal and R.K. Laddha, On the Generalized Zeta Function and the Generalized Lambert Function, *Ganita Sandesh* **11**, 99–108 (1997).
- [5] J.L. Lavoie and G. Trottier, On the Sum of Certain Appell's Series, *Ganita* **20**, 43–66 (1969).
- [6] T.M. MacRobert, Beta Functions Formulae and Integrals Involving E-Function, *Math. Annalen* **142**, 450–452 (1961).
- [7] V.N. Mishra, Some Problems on Approximations of Functions in Banach Spaces, *Ph.D. Thesis, Indian Institute of Technology, Roorkee*, 247–667 (2007).
- [8] V.N. Mishra and L.N. Mishra, Trigonometric Approximation of Signals (Functions) in L_p - norm, *Int. J. Contemp. Math. Sci.* **7**, 909–918 (2012).
- [9] V.N. Mishra, K. Khatri, L.N. Mishra and Deepmala, Inverse Result in Simultaneous Approximation by Baskakov-Durrmeyer-Stancu operators, *J. Inequal. Appl.*, (2013), doi:10.1186/1029-242X-2013-586.
- [10] V.N. Mishra, K. Khatri and L.N. Mishra, Statistical Approximation by Kantorovich type Discrete q -Beta operators, *Adv. Diff. Equ.* **2013**, (2013), DOI:10.1186/10.1186/1687-1847-2013-345.
- [11] V.N. Mishra, H.H. Khan, K. Khatri and L.N. Mishra, Hypergeometric Representation for Baskakov-Durrmeyer-Stancu Type Operators, *Bulletin of Mathematical Analysis and Applications* **5**, 18–26 (2013).
- [12] F. Oberhettinger, Tables of Mellin Transform, *Springer-Verlag, New York*, (1974).
- [13] R.K. Parmar, On a certain Extension of Hurwitz-Lerch Zeta Function, *Analele Universitaii de Vest, Timioara, Seria Mathematica-informatica, LII* **2**, 157–170 (2014).
- [14] T. Pohlen, The Hadamard Product and Universal Power Series, Ph.D Thesis, *Universitat Trier, Trier, Germany*, (2009).
- [15] G. Rahman, K.S. Nisar and M. Arshad, A New Extension of Hurwitz-Lerch Zeta Function, *arXiv:1802.07823v1[math.CA]*, (2018).
- [16] R.K. Saxena and R.K. Parmar, Fractional Integration and Differentiation of the Generalized Mathieu Series, *axioms, MDPI*, (2017).

-
- [17] M. Shadab, S. Jabee and J. Choi, An Extension of Beta Function and its Application, *Far East Journal of Mathematical Sciences* **103**, 235–251 (2018).

Author information

Nirmal K. Jangid, Department of Mathematics and Statistics, Manipal University Jaipur, Jaipur, India.
E-mail: nirmaljangid321@gmail.com

Sunil Joshi, Department of Mathematics and Statistics, Manipal University Jaipur, Jaipur, India.
E-mail: sunil.joshi@jaipur.manipal

Sunil Dutt Purohit, Department of HEAS (Mathematics), Rajasthan Technical University, Kota, India.
E-mail: sunil_a_purohit@yahoo.com





Received: October 27, 2021.

Accepted: January 4, 2022.



Research papers

Expanded waste glass/methyl palmitate/carbon nanofibers as effective shape stabilized and thermal enhanced composite phase change material for thermal energy storage

P. Singh^a, R.K. Sharma^a  , Gökhan Hekimoğlu^b  , Ahmet Sarı^{b,c}, Osman Gencel^d, V.V. Tyagi^e

[Show more](#) 

 Share  Cite

<https://doi.org/10.1016/j.est.2023.107205> 

[Get rights and content](#) 

Highlights

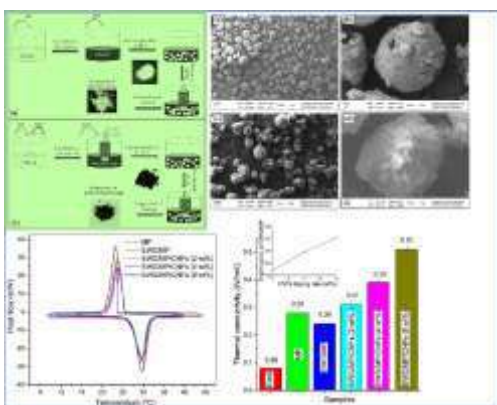
- The performance of shape stabilized PCMs with expanded waste glass and carbon nanofibers was investigated.
- Shape stabilized composites were prepared by impregnation of MP with EWG and CNFs.
- The melting temperature is in the range of 26.61-27.12°C. and melting enthalpies ranges from 96.1-96.7 J/g.
- The TGA outcomes illustrated that FSCPCM and TE-FSCPCMs had well thermal resistance.

- Thermal conductivities of FSCPCM were increased apparently especially with CNF (8 wt.%) incorporation.

Abstract

A prominent choice for phase change materials (PCMs) for passive solar thermoregulation is fatty acids because of their many beneficial characteristics for latent heat thermal energy storage (LHTES). Their low thermal conductivity and additional storage container requirements to prevent leaks during heating time, however, severely restrict their range of applications. In order to address these issues with methyl palmitate (MP) as a phase transition material, it was first doped with carbon nanofibers (CNFs) after being incorporated with expanded waste glass (EWG) using the melting/blending procedure. The SEM, XRD, FTIR, DSC, and TGA techniques were used to investigate the thermal and chemical performance of composite phase change materials (CPCMs). The leak-proof composite phase change materials (LPCPCM) and thermal enhanced shape stabilized composite phase change materials (TE-SSCPCMs) had latent energy between 96.1 and 96.7 J/g and melting temperatures between 26.61 and 27.12 °C. Doping 2, 4, and 8 wt% of CNFs into CPCMs, conductivity got enhanced by 29.2, 62.5, and 112.5% respectively, due to which, the TE-SSCPCM's charging/discharging periods were significantly shortened without changing their LHTES properties much. Further, evidence came from the thermal cycling test, TGA results, and the impressive thermal reliability, LHTES cycle performance, and chemical compatibility of all manufactured composites.

Graphical abstract



[Download: Download high-res image \(299KB\)](#)

[Download: Download full-size image](#)

Introduction

Due to the fact that about one-third of the world's total energy consumption occurs in buildings [1], the upgrade of resource efficiency has emerged as one of the energy technologist's primary concerns. In this context, thermal energy storage (TES) has emerged as a viable alternative methodology for addressing technology and environmental pollution issues within the last three decades [2]. PCMs and LPCPCMs with good thermal durability and performance have been deemed desirable TES components with energy storing and releasing capacity [3], [4]. The focus of several energy studies in recent years has shifted toward the creation of cutting-edge PCMs and LPCPCMs as well as the examination of their temperature control characteristics [5], [6], [7], [8], [9]. It has been found that fatty acids perform well for solar passive LHTES purposes as PCMs due to their desirable and readily available LHTES features [10], [11]. Nevertheless, direct functioning of these organic PCMs permits chemical interlinkage with the surroundings and also results in a leakage issue in solid to liquid state transition. They were enclosed in macro or micro configurations to avoid this complexity [12], [13]. However, PCM encapsulations are significantly more difficult and expensive, resulting in generally poor LHTES capacity. Combining porous, lightweight, and less costly building materials with LPCPCMs that are resistant to leakage is an alternative method. Moreover, fatty acids have a disadvantage of poor thermal conductivity (between 0.15 and 0.25 W/m-K), which significantly affects their rates of phase change (heat charging/discharging) [14]. Furthermore, their incorporation into stabilized clay-based porous building matrices can result in a significant decline in conductivity. Thus, doping this type of LPCPCM with a high thermal conductive material is an effective way for boosting its thermal conductivity. Materials based on carbon such as carbon nanofibers (CNFs) [15], [16], [17], carbon nanotubes (CNTs) [18], [19], expanded graphite [20], graphite nanoplatelets (GNPs) [21], and graphene oxide [22] have primarily been used to increase the thermal conductivity of organic PCMs. CNF is a material that looks and acts like graphite. It is made by carbonating and graphitizing organic fibers. At the atomic level, each CNF is made up of thousands of small fibers that are stacked on top of each other. The carbon atoms in each fiber are organized in a hexagonal pattern. CNF had nearly the same thermal conductivity, resistance to corrosion, durability, and ability to heat energy conversion as carbon nanotubes and graphene, but it was cheaper [23], [24]. So, CNF has gotten a lot of attention as an additive to improve the properties of composite materials [25], [26], [27]. The purpose of this research is to investigate the effect of CNFs on thermal outcomes of LPCPCMs. CNF is an inorganic carbon fiber compound that can have a thermal conductivity up to 900 W/m-K in the same plane. The CNF's percolating configuration worked as a filler with significant thermal conductivity [28]. Huang et al. [16] used the 5 wt% CNF in cetyl alcohol/HDPE composite which increased the thermal conductivity of composite by 1.25 times as compared to original composite thermal conductivity. Liu et al. [17] reported that the thermal conductivity of PEG/SiO₂ composite was increased by 73% due to the incorporation of

3wt% CNFs. Zhang et al. [29] boosted the thermal conductivity of erythritol as about 407.8% by incorporating CNFs by 10wt% mass fraction. As distinct from the aforementioned literature, our aim is to develop a way to both alleviate the leakage issue and the poor thermal conductivity limitation of MP organic PCM without significantly diminishing its LHTES capability. EWG was chosen as an appropriate supporting material to eliminate the PCM's seepage problem due to its numerous positive qualities, such as its high absorption ratio, excellent thermal stability, good interfacial bonding, and long-term economic and ecological friendliness [30]. In the initial stage of the present research, MP, an organic PCM, was integrated into EWG by melting/blending process to create a new LPCPCM. Considering the poor thermal conductivities of the base materials of LPCPCM (0.28 and 0.08 W/m-K for MP and EWG, respectively), the thermal conductivity of LPCPCM was significantly enhanced by loading with CNFs at mass fractions of 2.0, 4.0, and 8.0wt% in the subsequent phase. Using SEM, XRD, and FT-IR, the chemical and morphological features of the produced LPCPCM and TE-SSCPCMs were characterized. The impact of CNFs loading on the thermal conductivities, LHTES characteristics, thermal compatibility, and energy charging and discharging durations of manufactured LPCPCM was studied. A comprehensive study on EWG/MP/CNFs composite has not yet been published, as far as we are aware.

Access through your organization

Check access to the full text by signing in through your organization.

Access through your organization

Section snippets

Materials

Methyl palmitate (MP) was procured by Sigma-Aldrich company. Ethanol used as solvent was provided by Merck Company. Expanded waste glass (EWG) was purchased from Agrekal Company (Antalya-Turkey). Moreover, Carbon nanofibers (CNFs) in this work were purchased from Sigma-Aldrich Company. ...

Preparation of LPCPCM and TE-SSCPCM

By using the melting/blending method, the leak proof composite PCMs (LPCPCMs), EWG/MP and EWG/MP/CNFs were created in shape stabilized form. Following the procedure shown in Fig. 1, EWG/MP was prepared as a shape ...

SEM results of the prepared LPCPCM and TE-SSCPCM

Fig. 3(a-e) depicts SEM images of the EWG, FSCPCM, and TE-FSCPCM-3, which is representative of the other TE-FSCPCMs. As demonstrated in Fig. 3(a, b), the surfaces of EWG are composed of agglomerates of amorphous particles. However, these molecules have an interlinked phase picture, some of them feature holes and fissures that allow PCM molecules to be retained.

The PCM was kept uniformly within the perforations on the surface of the EWG (Fig. 3(c, d)). The CNFs with 8wt% introduced uniformly ...

Conclusions

To concurrently address the leakage problem and low thermal conductivity of MP, it was initially kept in EWG using the melting and blending technique and then loaded with CNFs. The morphology, physicochemical suitability, LHTES characteristics, conductivities, cycle TEST performances, and thermal reliabilities of LPCPCMs and TE-SSCPCMs were analyzed. The following inferences can be taken from the findings:

1. The maximum amount of MP that EWG was able to absorb was 40% by weight. Shape-stabilized ...

...

CRedit authorship contribution statement

P. Singh- Writing - Original draft, Formal analysis

R. K. Sharma- Project administration, Formal analysis

Gökhan Hekimoğlu- Validation

Ahmet Sarı- Visualization

Osman Gencel- Formal analysis

V. V. Tyagi- review & editing ...

Declaration of competing interest

The authors declare that they have no known competing financial interests or personal relationships that could have appeared to influence the work reported in this paper. ...

References (47)

K. Faraj *et al.*

[A review on phase change materials for thermal energy storage in buildings: heating and hybrid applications](#)

J. Energy Storage (2021)

R.A. Lawag *et al.*

[Phase change materials for thermal management and energy storage: a review](#)

J. Energy Storage (2022)

K. Lafdi *et al.*

[Graphite foams infiltrated with phase change materials as alternative materials for space and terrestrial thermal energy storage applications](#)

Carbon (2008)

P. Singh

[Development and characterization a novel leakage-proof form stable composite of graphitic carbon nitride and fatty alcohol for thermal energy storage](#)

J. Energy Storage (2022)

X. Zhang

[Form stable composite phase change materials from palmitic-lauric acid eutectic mixture and carbonized abandoned rice: preparation, characterization, and thermal conductivity enhancement](#)

Energy Build. (2017)

M. Jafaripour *et al.*

[Fabrication and optimization of kaolin/stearic acid composite as a form-stable phase change material for application in the thermal energy storage systems](#)

J. Energy Storage (2021)

Y. Konuklu *et al.*

[Microencapsulation of caprylic acid with different wall materials as phase change material for thermal energy storage](#)

Sol. Energy Mater. Sol. Cells (2014)

T.D. Dao *et al.*

A Pickering emulsion route to a stearic acid/graphene core–shell composite phase change material

Carbon (2016)

A. Elgafy *et al.*

Effect of carbon nanofiber additives on thermal behavior of phase change materials

Carbon (2005)

X. Huang *et al.*

Microstructure and thermal properties of cetyl alcohol/high density polyethylene composite phase change materials with carbon fiber as shape-stabilized thermal storage materials

Appl. Energy (2017)



View more references

Cited by (11)

Carbon-based porous materials for performance-enhanced composite phase change materials in thermal energy storage: Materials, fabrication and applications

2025, Journal of Materials Science and Technology

Show abstract 

Polypyrrole-modified flax fiber sponge impregnated with fatty acids as bio-based form-stable phase change materials for enhanced thermal energy storage and conversion

2024, Journal of Energy Storage

Show abstract 

3D-printed polylactic acid-microencapsulated phase change material composites for building thermal management

2024, Renewable and Sustainable Energy Reviews

Show abstract 

Heat transfer performance enhancement and mechanism analysis of thermal energy storage unit designed by using a modified transient topology optimization model

2024, Journal of Cleaner Production

[Show abstract](#) ✓

Preparation and characterization of lauric acid-stearic acid/fumed silica/expanded graphite thermally conductive enhanced composites

2023, Journal of Energy Storage

[Show abstract](#) ✓

Waste polyvinyl chloride derived latent thermal energy storage composites for waste heat recovery via packed bed system

2023, Journal of Cleaner Production

[Show abstract](#) ✓



[View all citing articles on Scopus](#) ↗

[View full text](#)

© 2023 Elsevier Ltd. All rights reserved.



ELSEVIER

All content on this site: Copyright © 2024 Elsevier B.V., its licensors, and contributors. All rights are reserved, including those for text and data mining, AI training, and similar technologies. For all open access content, the Creative Commons licensing terms apply.

 RELX™

MEMORANDUM OF UNDERSTANDING

BETWEEN



**SEMI-CONDUCTOR LABORATORY
DEPARTMENT OF SPACE, GOVERNMENT OF INDIA
S.A.S. NAGAR**

AND



**MANIPAL UNIVERSITY
JAIPUR**

FOR

**COLLABORATION IN RESEARCH & DEVELOPMENT,
FACULTY AND STUDENT EXCHANGE**



MEMORANDUM OF UNDERSTANDING

In furtherance of their mutual interest in the fields of education and research and as a contribution towards increasing national cooperation, Semi-Conductor Laboratory, Department of Space, Government of India, having its registered address at Sector 72, S.A.S. Nagar – 160071, Punjab, India (hereinafter referred to as "**SCL**", which expression shall mean and include its successors-in-interest, administrators, authorised representatives etc.).

and;

MANIPAL UNIVERSITY JAIPUR, having its Campus at Village - Dehmi Kalan, Off Jaipur-Ajmer Expressway, Jaipur-303007, Rajasthan, India, (hereinafter referred to as "**MUJ**" which expression shall mean and include its successors-in-interest, administrators, authorised representatives etc.), have entered into this Memorandum of Understanding (MoU) on this **27th day of April, 2018** as set forth below:

ARTICLE I

This MoU involves collaboration between SCL and MUJ (both also referred to as institution(s)) in related disciplines.

The two institutions shall seek to promote:

1. Exchange of Staff and Students (Faculty & Research Scholars; Under Graduate, Post Graduate & Doctoral Students and Research Project Employees) regarding Academics and Research for the mutual benefit of both institutions.
2. Exchange of Students for pursuing Courses of Study and Academic Programmes for mutual benefit of both institutions.
3. Collaboration in Teaching, Research & Development and Consultancy Activities.
4. Exchange of Academic and Research Material and Publications/IPRs.
5. Cooperation in Projects and Research Activities of mutual interest.
6. Provision of Cultural and Intellectual enrichment opportunities for the Staff and Students of both institutions.
7. Collaboration in Research & Development in the areas of (i) Advanced VLSI Device Fabrication, (ii) MEMS Fabrication, (iii) VLSI Device / MEMS Characterization, (iv) VLSI/CMOS-RF Circuit Design and (v) VLSI Device Modeling at both MUJ and SCL. This also includes collaboration in setting-up and upkeep of the relevant infrastructure in both the institutions.



8. Publication of Research Papers in International Scientific Journals and in the Conferences.
9. Exchange of Students for Summer/Winter Internships
10. Publication of Intellectual Properties (IPs) developed jointly through Project / Research Collaboration. Such IPs would acknowledge joint inventor-ship of Personnel / Students belonging to both the institutions, as applicable.
11. Writing Books / Booklets jointly in the areas of mutual interest.

ARTICLE II

The activities under this MoU will include:

1. **Staff Exchange:**

Staff exchange activities cover visits to either institution for any of the following purposes:

- (i) Undertaking Joint Research
- (ii) Attachment of Staff for purposes of Curriculum Development & Review, Attendance in Courses and Upgrading of Teaching & Research Skills
- (iii) Participation in Seminars, Colloquia and other types of academic discussions
- (iv) Contributions to Teaching Programmes
- (v) Co-supervision of Post Graduate Students
- (vi) Conduct study tours, joint consultancy and research work.
- (vii) Facilitation for pursuing Academic Courses (Post Graduate & Doctoral) for Department of Space / SCL Employees at MUJ as per eligibility criteria and academic norms of MUJ.

2. **Student Exchange:**

Student exchange activities (for Under Graduate, Post Graduate & Doctoral Students) cover visits to either institution for any of the following purposes:

- (i) Participation in Research
- (ii) Internships for MUJ Students at SCL



25

3. Exchange of Academic Materials:

Exchange of relevant Academic Materials will be carried-out subject to mutual agreement of both institutions.

ARTICLE III

Implementation of cooperation based on this MoU shall be dealt with between the relevant Faculties and Divisions / Departments of both institutions. Wherever necessary, a plan shall be worked-out for each activity setting-forth detailed arrangements for collaboration. Such plans shall be subject to approval of the appropriate authorities of each institution. To facilitate development of such plans, each institution shall nominate a member of its staff to coordinate activities arising under this MoU.

ARTICLE IV

Both institutions agree and undertake to keep confidential at all times information and /or data that may be exchanged, acquired and /or shared in connection with the areas of cooperation, as mentioned above, unless otherwise the same information already exists in the public domain.

ARTICLE V

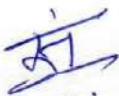
Ownership of findings of any joint research shall be vested equally in both institutions to this MoU and any publications regarding the same shall only be possible after prior written approval from both institutions.

ARTICLE VI

The **MoU** shall remain in force for a period of 10 (TEN) years commencing from the date of signing and may be reviewed by mutual consent by serving 3 (Three) months written notice to the other institution. Upon renewal, both institutions shall select either to proceed with the existing or new terms of understanding.

ARTICLE VII

Both SCL and MUJ reserve the right to terminate this **MoU** by either institution giving 3 (Three) months written notice to the other. Where such termination occurs, the provisions of this **MoU** shall continue to apply to ongoing activities until their completion.





ARTICLE VIII

Participating staff and students involved in any activities under this **MoU** must adhere to the law of the country (India) and the rules & regulations of the host institutions.

ARTICLE IX

If any dispute/difference arises between the institutions in relation to this **MoU**, both the institutions shall resolve the dispute/difference amicably with the help of heads of both the institutions.

ARTICLE X

SCL and MUJ welcome establishment of this MoU for cooperation and jointly agree to provisions as set out above. There are two copies of this MoU equally valid, one for each institution, effective from the date of its signing.

SEMI-CONDUCTOR LABORATORY



ਸੁਰਿੰਦਰ ਸਿੰਘ / Surinder Singh
ਦਿਰੇਕਟਰ / Director
ਸੇਮੀ-ਕੰਡਕਟਰ ਲੈਬੋਰੇਟਰੀ
Semi-Conductor Laboratory
ਅੰਤਰਿਕਸ਼ ਵਿਭਾਗ, ਭਾਰਤ ਸਰਕਾਰ
Department of Space, Govt. of India
ਸੈਕਟਰ-72, ਸਾ.ਅ.ਸਿ. ਨਗਰ-160071, ਪੰਜਾਬ, ਭਾਰਤ
Sector-72, S.A.S. Nagar-160071, Punjab, INDIA


Witness



ਗੁਪ ਪ੍ਰਮੁਖ-ਪਾਇਲੋਟ ਨਿਯੋਜਨ ਗੁਪ
Group Head-Project Planning Group
ਸੇਮੀ-ਕੰਡਕਟਰ ਲੈਬੋਰੇਟਰੀ
Semi-Conductor Laboratory
ਅੰਤਰਿਕਸ਼ ਵਿਭਾਗ, ਭਾਰਤ ਸਰਕਾਰ
Department of Space, Government of India

Date: 27.04.2018

MANIPAL UNIVERSITY JAIPUR



Prof. Vandana Suhag
Registrar

Witness



Dr Amit Jain
Director SHM & Advisor IP

Date: 27.04.2018



MANIPAL UNIVERSITY
JAIPUR



Truechip
The Verification IP Specialist

Memorandum of Understanding

of

"CENTER OF EXCELLENCE"

between

Manipal University Jaipur, India

&

Truechip solutions, Noida, India

This Memorandum of Understanding (MoU) is drawn up and agreed upon to establish the initial framework for cooperation between **Manipal University Jaipur**, Village Dehmi Kalan, Tehsil Sanganer, Off Jaipur-Ajmer Expressway, Near GVK Toll Plaza, Ajmer Road, Jaipur-303007, Rajasthan, India and **Truechip Solutions Pvt. Ltd.** D-67, Sec-2 Noida 201301.

MANIPAL UNIVERSITY JAIPUR, (hereinafter referred to as "MUJ" which expression shall mean and include, unless repugnant to the context or meaning thereof it's successors-in-interest and permitted assigns) a State Private University Constituted vide the Manipal University Jaipur Act 2011 (Act No. 21 of 2011), passed by the State Legislature of Rajasthan, with it's campus at Village Dehmi kalan, Tehsil Sanganer, Off. Jaipur-Ajmer Expressway, Near GVK Toll Plaza, Ajmer Road, Jaipur 303007, Rajasthan has authorized **Prof. (Dr.) Nitu Bhatnagar, Registrar, MUJ** to enter into this MoU on it's behalf as the **FIRST PARTY**.



The permanent campus of the university is set up on 122 acres of land at Village Dehmi Kalan village near Jaipur, and is by far one of the best campuses in the region. MUJ has world class infrastructure, including state-of-the-art research facilities and Modern Library. In line with Manipal University's legacy of providing quality education, the university uses the latest and innovative methods and technology to impart education. The multidisciplinary university offers career-oriented courses at all levels, i.e., UG, PG and Doctoral and across diverse streams, including Engineering, Architecture, Planning, Fashion Design, Hospitality, Humanities, Commerce, Management, Communication, Basic Sciences, Law etc.

AND;

Truechip, the Verification IP specialist, is a leading provider of Design and Verification solutions - which help you, accelerate your design, lowering the cost and the risks associated with the development of your ASIC, FPGA and SOC. Truechip is a privately held company, with a global footprint and sales coverage across North America, Europe and Asia.

Truechip has been serving customers since last 10 years in VLSI with a strong and experienced leadership. Truechip provides industry's first 24x5 support model with specialization in VIP integration, customization and SOC Verification.

"**MUJ**" and "**Truechip**" are hereinafter, wherever the context so admits, collectively referred to as the "**Parties**" and individually as a "**Party**".

AND WHEREAS the purpose of this MoU is to establish an understanding of mutual cooperation between **MUJ** and **Truechip**, providing a common platform for promoting industry-academia collaboration in the field of technology and software which will be beneficial to both the Parties.

Article I: Objectives and Scope

To derive mutual advantages in pursuit of higher learning and improve employability of Manipal University Jaipur's students and providing technical solutions along with enhancement of technical knowledge and expertise for improved products.

The initially proposed activities within the scope of the current MoU are :-

1. Truechip will provide industrial exposure to selected engineering students of Manipal university Jaipur by way of internship opportunities to the extent of feasibility and requirement.



2. Truechip will surely extend its necessary support to deliver guest lectures to the students on technology trends mostly on weekends or mutually agreed date by both the parties.
3. Truechip will give valuable inputs to the first party in teaching /training methodology & to customize suitably the curriculum so that the student/s fit into the industrial scenario meaningfully and also provide suggestions from industry perspective for design / modification of course curriculum to the extent of feasibility.
4. Truechip will guide students of Manipal University Jaipur on the emerging technologies in order to bridge the skill gap & make them industry ready.
5. Truechip believes in sharing knowledge & capability in the concerned areas for mutual benefits & to become trusted partners in the area of knowledge enrichment.
6. Truechip could play a key role in technical upgradation, innovation & competitiveness of the industry. Both parties believe that close co-operation between the two would be of major benefit for the students to enhance their skill & knowledge.
7. Manipal University Jaipur to consider Truechip as preferred employer.
8. Truechip to consider absorption of Manipal University Jaipur's students working on Truechip's projects based on student performance and extent of feasibility.
9. Defining new areas of collaboration that have not been still foreseen but can be beneficial to the Parties.
10. Manipal University Jaipur will cooperate Truechip in promoting its initiative in the form of an open community that will motivate the students to develop a career in VLSI industry. Also, Manipal University Jaipur will allow Truechip in making its students and staff, representatives of this initiative in the university campus and the events organized in this regard.
11. Truechip will help the ECE department of MUJ by providing industrial inputs to B. Tech. Electronics Engineering (VLSI Design and Technology) Course.

Article II: Confidentiality / Secrecy

Each Party and its students, its employees and anyone acting under it for the purpose of this MOU shall maintain strict confidentiality of the information belonging to the other party that may have come into its / their possession of knowledge because of the collaboration activities under this MOU. Such information shall not be divested or



disclosed to any other third party under any circumstances, whatsoever, without obtaining prior written approval from the other party.

"Confidential Information" in this MoU shall mean confidential information and proprietary information concerning MUJ and Truechip including and without limitation: Intellectual Property Rights (IPR), trade secrets, secret information, technical processes, finances, software language codes, any research material, text, dealings, and methods of dealings with the clients or the customers and it's employees together with similar information of confidential or proprietary nature relating to MUJ and Truechip suppliers, employees, agents, distributors, customers and relationship of special trust and confidence with the clients or customers and employees.

Both the parties agree that during and after the term of this MOU, they shall use the confidential information solely for purpose of performing their obligations and/ or exercising their rights under this MOU and shall not disclose to any third party any confidential information without the prior written consent of the other party.

Article III: Non-Exclusivity

The relationship of the Parties under this MoU shall be non-exclusive and both Parties, including their affiliates, subsidiaries and divisions are free to pursue other collaborations of any kind with third parties also.

Article IV: Duration, Termination and Amendment

1. The MoU will be effective from the date of signing by both parties for a period of up to THREE (3) years and may be subject to extension by mutual consent of the Parties, expressed in writing.
2. Either party may terminate this MOU by giving ONE month's advance notice in writing to the other Party.
3. The provisions of the MoU may be amended at any time with the mutual consent of the Parties in writing.
4. The amendment, termination and expiration of this MoU will not affect the terms of activities ongoing at the time of notification of amendment, termination and expiration, unless otherwise agreed upon between the Parties.
5. No action undertaken shall diminish the full autonomy of either institution, nor will either party impose any constraints upon the other in carrying out the agreement.



Article V: Special Provisions

1. During the term of this Memorandum each party may make any press release about the association between the parties.
2. During the term of this memorandum each party agrees to supply information to the other for inclusion in that party's promotional material and agrees to such information being used in each other's promotional material in accordance with such terms as may be specified, but at no cost to the other.
3. Detailed modalities of individual forms of collaboration, activities associated with them and financial aspects of each shall be mutually agreed upon on a case by case basis, and specified, with all necessary details, in separate Agreements.
4. Separate agreement shall be executed with regard to specific project/work initiated in furtherance of this MoU. Financial and other obligations of both the institutions shall be as per that agreement.
5. Both parties agree that either party may use the logo of the other party for promotional documents related to training only subject to the prior approval of both the parties.
6. Truechip shall be entitled to terminate the internships upon consultation with the representatives of Manipal University Jaipur, if the student, to the opinion of Truechip does not sufficiently take the current rules into account or does not follow the instructions given by or on behalf of the organization. And, students shall be entitled to terminate the practical training upon consultation with the MUJ authorities.

Article VI :- Dispute Resolution :-

This MoU shall be governed by the Laws of India. The parties will try in good faith to settle within thirty days any dispute relating to this agreement ("**Dispute**"). If the dispute is not resolved within thirty days after such Dispute arises, the dispute shall be referred to a sole arbitrator appointed mutually by both the parties. In case both the parties do not agree over the name of a sole arbitrator, each party shall appoint an arbitrator for itself and the presiding arbitrator shall be appointed by the arbitrators so appointed by the parties. Arbitration proceedings shall be conducted as per the provisions contained in the Indian Arbitration and Conciliation Act 1996 and rules made thereunder, or any statutory modification thereto or otherwise under any other law prevailing in India at that time for the same. Venue of the arbitration proceedings shall be Jaipur, Rajasthan, India. Award passed by the arbitrator(s) shall be final and binding on both the parties.



The parties shall submit to the exclusive jurisdiction of the courts of Jaipur, Rajasthan.

Article VI :Contact Persons

The nodal officers for the said MOU from both the sides would be as follows:

Manipal University, Jaipur Name: Dr. Tejpal Designation: Associate Professor Email: tej.pal@jaipur.manipal.edu Phone: 9414784217	Truechip Solutions Pvt. Ltd., Noida Name: Mr. Ranveer Designation: Senior Manager Email: Ranveer.singh@truechip.net Phone: (+91) 9999418031
---	--

Hence, both the parties have executed this Agreement / MoU on this ----- day of November, 2022 in covenant to the terms & conditions mentioned hereinabove.

Signature: Ash K. Dhore

Signature RB

Date: 28/11/22

Date: 25/11/2022



Name: Mrs Arti Kishore

Name : Dr. Nitu Bhatnagar

Designation: CEO

Designation: Registrar

Contact Details: (+91) 9999418031

Contact Details: 0141 3999100

Email: ranveer.singh@truechip.net

Email: registrar@jaipur.manipal.edu

**Truechip Solutions Pvt.
Ltd.**

Manipal University Jaipur, India

Witness 1.

Suyash Jain

SUYASH JAIN

Witness 1.

Dr. Kulwant Singh

Witness 2.

Ranveer Singh

Ranveer Singh

Witness 2.

Dr. Tejpal



महाराष्ट्र MAHARASHTRA

2022

09AA 565190

ज्या करणासाठी ज्यांनी मुद्रांक खरेदी केले त्यांनी त्याच कायद्यानुसार
मुद्रांक खरेदी केल्याबाबत 6 महिन्यात वापरणे अनिवार्य आहे.

अनु.क्र. २२५५०६८ JUL 2022 रक्कम - १०००

दस्ताचा प्रकार - एकत्र प्रतिज्ञापत्रासाठी
दस्त नोंदणी करणार आहेत का? होय/नाही -

मिळकतीचे वर्णन -
मुद्रांक विकत घेणाऱ्याचे नांव व पत्ता - Soothe Earth
Nardelcity pune

दुसऱ्या पक्षाकाराचे नांव -
हस्ते व्यक्तीचे नांव व पत्ता - Shrikant Singh



06 JUL 2022

प्रथम मुद्रांक लिपीक
कोषागार पुणे करिण


मुद्रांक विकत घेणाऱ्याची सही

सौ. एन. के. सऊत
परवाना क्र. २२०११५४
भाषिकबाव, पुणे-४११०५१

Memorandum of Understanding

This Memorandum of Understanding Agreement ("Agreement") is entered in to on this the 8th July 2022 by and amongst:

For SootheEarth LLP


Designated Partner



1. **AIC – MUJ Incubation Foundation (U93090RJ2018NPL061558)**, registered under the provisions of the Companies Act 2013 and having its registered office at C/O Manipal University Jaipur, Dehmikalan, Jaipur Ajmer Expressway, Rajasthan - 303007 (herein after referred to as the "**Incubator**" which expression shall, unless it be repugnant to the subject or context thereof, include its successors and permitted assigns)
 2. The persons set out in Schedule I hereto (hereinafter referred to as individually as a "**Founder**" and collectively as the "**Founders**", which expression shall, unless repugnant to the context or meaning thereof, include their respective heirs, executors, administrators and permitted assigns);
- AND**
3. **< SootheEarth LLP > < AAW-4469 >**, a company incorporated under the laws of India and having its registered office at < A7/101, Mangal Bhairav, Nanded City, Sinhgad Road, Pune - 411041 > (hereinafter referred to as the "**Company**", which expression shall unless repugnant to the context or meaning thereof, include its successors and permitted assigns).

Each of the Founders, the Incubator and the Company shall hereinafter be referred to individually as a "**Party**" and collectively as the "**Parties**".

WHEREAS the Company, is seeking professional and infrastructural support and guidance more specifically enumerated in Schedule II (the "**Incubator Facilities**"). The Incubator has hereby committed to support and mentor the Company and the Founders for a period of twelve months from the **Effective Date**.

NOW THEREFORE, in consideration of the foregoing and other good and valuable consideration, the receipt and adequacy of which are hereby expressly acknowledged, the Parties, intending to be legally bound, hereby agree as follows:

1. Definitions & Interpretation:

1.1 Definitions:

Act shall mean the Companies Act, 1956 and the Companies Act, 2013, as may be applicable, together with the rules and regulations hereunder, as may be amended, modified, supplemented or re-enacted from time to time;

Board shall mean the board of directors of the Company;

Business shall mean the <Offering Banana Paper Products, 100% Tree Free and Chemical Free>.

Direct Competitor shall mean any Person engaged in the same or similar business as the Business;

Effective Date shall mean the date on which the Parties mutually agree on the Machine List and Timelines;

Law shall mean any statute, law, regulation, ordinance, rule, judgment, notification, rule of common law, order, decree, bye-law, Governmental Approval, directive, guideline, requirement or other governmental restriction, or any similar form of decision of, or determination by, or any interpretation, policy or administration, having the force of law of any of the foregoing, by any Governmental Authority having jurisdiction over the matter in question, whether in effect as of the date of this Agreement or thereafter;

Success Fee shall mean a claim by Incubator for a success fee or incentive fee calculated at the rate of 5% of total business or funds generated via connections or programs executed or facilitated by incubator. The funds could be generated by Sales, Paid Contracts, Grants received, Investor Capital Raised, etc.

- 1.2 Interpretation:** Any capitalized term used but not defined herein shall have the meaning ascribed thereto in the Investment Agreement.

2. Consideration.

Further for business or funds generated via connections or programs executed or facilitated by AIC a success fees would be charged by the incubator and the same shall be payable within 30 (thirty) days of the contract.

- 3. Relationship:** The Incubator shall be an independent contractor and nothing in this Agreement shall render the Incubator an employee, worker, agent or partner of the Company.



For SootheEarth LLP

Designated Partner

4. Term & Termination:

- 4.1 This Agreement shall come into effect on the Execution Date and shall remain valid and binding on the Parties until such time that it is terminated in accordance with Clause 4.2 below
- 4.2 Termination:
- (i) This Agreement may be terminated at the option of the Incubator if the Success Fee is not transferred in accordance with Clause 2.
- (ii) This Agreement may be terminated at the option of the Incubator in the following circumstances:
- (a) use of the Incubator Facilities by the Company for purposes other than for furtherance of its business;
 - (b) causing damage to the Incubator's property;
 - (c) Breach by the Company of the covenants set out in Schedule III hereto.
- (iii) This Agreement may be terminated at the option of the Company or the Founders if (a) the Effective Date has not occurred within 3 months of the Execution Date or (b) there is a material deviation in the Machine List and Timelines.
- (iv) This Agreement may be terminated at the option of the Company or the Founders in the event the Incubator fails to comply with its responsibilities under this Agreement or materially breaches the terms of this Agreement.
- (v) This Agreement may be terminated at any time by the mutual agreement of the Founders and the Incubator.
- 4.3 In the event of termination by the Incubator for the reasons set out in (ii) above, the Incubator may require the Company to vacate the premises with 7 days' notice, subject to the Dispute Resolution procedure set out herein.
- 4.4 In the event of termination by the Company or the Founders for the reasons set out in (iii)(b) or (iv) above, 50% of the Success Fee must be transferred back to the respective Founders by the Incubator as soon as commercially possible, subject to the Dispute Resolution procedure set out herein.
- 4.5 The termination of this Agreement shall not relieve any Party of any obligation or liability accrued prior to the date of termination.
- 4.6 The clauses of this Agreement which by their nature should survive termination shall survive such termination.

5. Limitation of Liability:

- 5.1 In no event shall the Party be liable to any other Parties for any special, incidental, indirect or consequential damages arising out of or in connection with this Agreement.
- 5.2 In no event shall a Party or any of its partners, officers, employees, representatives or agents be liable for any liability whatsoever for any losses or expenses of any nature suffered by another Party arising directly or indirectly from any act or omission of such Party or its employees, agents or representatives hereunder.

6. Tax Liability: Any and all tax liability that may be incurred by a Party as a consequence of operation of Applicable Law shall be borne by the respective Party.

7. Costs and Expenses: Each Party will bear its own expenses incurred in connection with the preparation, negotiation and execution of this Agreement. In addition, all costs and expenses in relation to payment of any stamp duty, registration duty and service taxes on the Definitive Documents under applicable Law shall be borne equally by the Company and the Incubator.

8. Indemnity: Each Party hereby agree to protect, defend, indemnify and hold harmless the other Parties, their employees, officers, partners, agents or representatives from and against any and all liabilities, damages, fines, penalties and costs (including legal costs and disbursements), arising from or relating to any third party claims, demands, fines, penalties and other sanctions imposed by any authority for non-compliance with any applicable law pursuant to and by virtue of this Agreement; and/ or any losses, liabilities, expenses, damages and / or claims suffered or incurred by the Incubator (including reasonable legal fees) as a result of such Party's negligence, fraud or wilful default in relation to this Agreement.



For SootheEarth LLP

Designated Partner

Each Party shall also indemnify and keep indemnified the other Parties for any breach of the terms and conditions of this Agreement.

9. Intellectual Property:

- 9.1 "Intellectual Property" includes patents, inventions, know how, trade secrets, trademarks, service marks, designs, tools, devices, models, methods, procedures, processes, systems, principles, algorithms, works of authorship, flowcharts, drawings, and other confidential and proprietary information, data, documents, instruction manuals, records, memoranda, notes, user guides, ideas, concepts, information, materials, discoveries, developments, and other copyrightable works, and techniques in either printed or machine-readable form, whether or not copyrightable or patentable
- 9.2 "Intellectual Property Rights" include: (i) all right, title, and interest under any statute or under common law including patent rights; copyrights including moral rights; and any similar rights in respect of Intellectual Property, anywhere in the world, whether negotiable or not; (ii) any licenses, permissions and grants in connection therewith; (iii) applications for any of the foregoing and the right to apply for them in any part of the world; (iv) right to obtain and hold appropriate registrations in Intellectual Property; (v) all extensions and renewals thereof; and (vi) causes of action in the past, present or future, related thereto including the rights to damages and profits, due or accrued, arising out of past, present or future infringements or violations thereof and the right to sue for and recover the same.
- 9.3 Except as set out in this Clause 11, each Party agrees that all Intellectual Property Rights, which are held by the other Party, shall remain in the sole and exclusive ownership of such other Party.
- 9.4 Any Intellectual Property and Intellectual Property Rights developed or conceived by the Company while receiving guidance or support as described in Schedule II shall vest absolutely and irrevocably with the Company.

10. Non-Disclosure:

- 10.1 All information and data belonging to the Company of confidential and proprietary nature be it specifically documented or not, shall be termed as confidential information ("**Confidential Information**"). This includes but is not limited to:
- creative information, including symbols, photographs, animations, videos, models, techniques, experimental methods, designs, concepts, research, insights and other creations;
 - technical information, including research programs and methods, product development plans, functional and technical specifications, technology, inventions, ideas, concepts, drawings, designs, analysis, research, methods, techniques, processes, computer software, data, databases, flowcharts, patent applications, and other technical know-how and materials;
 - business information, including business plans, business strategies and/or data arising thereof, sales and marketing research, materials and plans, accounting and financial information, projections, performance results, cost data, customer information, personnel records and the like;
 - all proprietary information related to the Company; and
 - any other valuable information of the Company designated as confidential by the circumstances in which it is provided.
- 10.2 Confidential Information does not include such information or data that: (a) is or becomes generally known to the public without restriction through no fault of the Incubator, or (b) that the Incubator knew without restriction prior to its disclosure by Company.
- 10.3 The Incubator shall hold in confidence and not disclose or use any Confidential Information, except in connection with this Agreement or with the prior written permission of the Company. This Clause shall survive the termination of this Agreement.
- 10.4 Upon termination of this Agreement or as otherwise requested by the Company, the Incubator will promptly return to the Company all items and copies containing or embodying Confidential Information without retaining any copies (soft or hard copies) with himself

11. Dispute Resolution:

- 11.1 The Parties agree to negotiate in good faith to resolve any dispute between them regarding this Agreement. If the negotiations do not resolve the dispute to the reasonable satisfaction of the Parties, then the dispute shall be submitted to final and binding arbitration at the request of the disputing Parties upon written notice to that effect to the other disputing Parties. In the event of such arbitration:



For SootheEarth LLP
Designated Partner

- 11.1.1 The arbitration shall be conducted in accordance with the Indian Arbitration and Conciliation Act, 1996 (the "**Arbitration Act**") in force at the relevant time (which is deemed to be incorporated into this Agreement by reference);
- 11.1.2 All proceedings of the arbitration shall be in the English language. The venue and seat of arbitration shall be at Jaipur, India;
- 11.1.3 All proceedings shall be conducted before a panel of 3 (three) arbitrators wherein, one arbitrator will be appointed by the claimants, the second arbitrator will be appointed by the respondents and the third arbitrator will be appointed jointly by the other two arbitrators; and
- 11.1.4 Arbitration awards rendered shall be final, binding and shall not be subject to any form of appeal.
- 11.2 Nothing shall preclude a Party from seeking interim equitable or injunctive relief, or both. The pursuit of equitable or injunctive relief shall not be a waiver of the right of the Parties to pursue any other remedy or relief through the arbitration described in this Clause 11.

12. Miscellaneous:

- 12.1 This Agreement may be modified, amended or supplemented only by the mutual written agreement of the Parties. A waiver or any failure or delay by the Incubator to require the enforcement of the obligations, agreements, undertakings or covenants in this Agreement shall not be construed as a waiver by the Incubator of any of its rights, unless made in writing referring specifically to the relevant provisions of this Agreement and signed by a duly authorized representative of the Incubator. Any such waiver shall not affect in any way the validity of this Agreement or the right to enforce such obligation, agreement, undertaking or covenant at any other time. All rights and remedies existing under this Agreement, except as otherwise provided herein are cumulative to, and not exclusive of any rights or remedies otherwise available.
- 12.2 If for any reason whatsoever, any provision of this Agreement is or becomes, or is declared by a court of competent jurisdiction to be, invalid, illegal or unenforceable, then the Parties shall negotiate in good faith to agree on such provision to be substituted, which provisions shall, as nearly as practicable, leave the Parties in the same or nearly similar position to that which prevailed prior to such invalidity, illegality or unenforceability.
- 12.3 Except as may be otherwise provided herein, all notices, requests, waivers and other communications made pursuant to this Agreement shall be in writing and signed by or on behalf of the Party giving it. Such notice shall be served by delivering by hand, registered post, electronic mail or courier to the address set forth below. In each case it shall be marked for the attention of the relevant Party set forth below. Any notice so served shall be deemed to have been duly given (i) in case of delivery by hand, when hand delivered to the other Party; or (ii) when sent by registered post, where 7 (seven) Business Days have elapsed after deposit in the mail with certified mail receipt requested postage prepaid; or (iii) when delivered by courier on the 2nd (second) Business Day after deposit with an overnight delivery service, postage prepaid, with next Business Day delivery guaranteed, provided that the Party issuing the notice receives a confirmation of delivery from the delivery service provider; or (iv) for electronic mail notification, upon confirmation of such notification by any of the means as aforesaid.

To the Founders:

Attention: Shricant Singh Binny
Address: A7/101, Mangal Bhairav, Nanded City, Sinhgad Road, Pune - 411041
Email: ssbinny@sootheearth.com

To the Company:

Attention: Padmavti Shricant Singh
Address: A7/101, Mangal Bhairav, Nanded City, Sinhgad Road, Pune - 411041
Email: padma@sootheearth.com

To the Incubator:

Attention : CEO
Address : C/o Manipal University Jaipur, Dehmikalan, Bagru, Jaipur, Pin- 303007
Email :

- 12.4 No Party shall assign this Agreement or any of its rights or obligations hereunder without the prior written consent of the other Parties.

- 12.6 The Agreement may be executed and delivered in counterparts, each of which shall be deemed an original.
- 12.7 Save and except as otherwise stated in this Agreement, in the event that a Party commits a default of the terms of this Agreement then, the non-defaulting Parties shall, in addition to any other rights and remedies available under this Agreement, be entitled to seek specific performance of this Agreement and such other remedies as may be permitted to it under applicable Law.
- 12.8 Each Party shall act in good faith in the performance of its respective responsibilities under this Agreement and will not unreasonably delay, condition or withhold the giving of any consent, decision or approval that is either requested or reasonably required by any other Party in order to perform its responsibilities.

IN WITNESS, WHEREOF the Parties have put their respective hands on the day and year first herein above written.

Signed and delivered by

For and on behalf of

1. AIC – MUJ Incubation Foundation

Puneet



Chief Executive Officer

2. Founders

Shricant Singh Binny

Founder Name

For SootheEarth LLP
Shricant Singh Binny
Designated Partner

3. Startup Name

SootheEarth LLP

Founder Name: Shricant Singh Binny
Director



For SootheEarth LLP
Shricant Singh Binny
Designated Partner

SCHEDULE I

LIST OF FOUNDERS

1. Founder 1: Shricant Singh Binny
2. Founder 2: Padmavti Shricant Singh



For SootheEarth LLP

Designated Partner

SCHEDULE II

INCUBATOR FACILITIES

1. The Incubator shall provide the Incubator Facilities as listed below for a period of twelve months from the Effective Date ("**Incubation Period**");

A. Physical Infrastructure:

- Developed office space approximately admeasuring <4>. with furniture and air-conditioning machines to occupy and use for Business Incubator activities.
- 24x7 high speed Internet Connectivity
- Access to Maker Space/Fab Lab.

Notwithstanding anything contained in this Agreement, AIC – MUJ Incubation Foundation shall have absolute right and ownership of the office space provided to locate the Company (the company to be promoted by the Promoters). The Estate Officer of the AIC – MUJ Incubation Foundation shall be deemed to be a competent authority under the Public Premises (Eviction of Unauthorised Occupants) Act, 1971 for necessary actions in connection with the office space so occupied by the Company.

B. Common Infrastructure:

The Incubator will provide following facilities to the Company, which will be shared by all Companies located in the Incubator:

- Laser Printer
- Photocopier
- Scanner
- Meeting/Conference room with projection equipment

The ownership of all assets so provided as a part of Incubator supports and services rests with Incubator AIC – MUJ Incubation Foundation as the case may be.

The support and services described in clauses A and B herein above shall be herein after referred to as "Incubator facilities".

C. Network of Mentors and Experts:

Incubator will facilitate liaison with mentors, professionals and experts in technology, legal, financial and related matters on such terms and conditions as may be stipulated by them.

D. Event and Meetings:

Incubator will organise events to facilitate the companies located in the BI in networking and to showcase their technologies. Incubator will also facilitate meetings with visitors of AIC – MUJ Incubation Foundation and its constituent Institutions such as alumni, venture capitalists, industry professionals.

E. Information Pool:

Incubator will maintain access to information and knowledge pool generally useful new enterprises. The Incubator will also facilitate access to departmental laboratories of AIC – MUJ Incubation Foundation Institutions by the Company (Promoters) for their product development purposes with approval of the concerned department.

F. Access to Markets & Talent

Incubator will provide help to incubatee, by providing assistance in marketing, get access to markets and access to desired talent.

2. In the event of a material deviation/delay in the Machine List and Timelines, the Company and the Founders shall have the right to demand that the Incubator extends the incubation period in accordance with such deviation/delay.
3. Further, at the end of the Incubation Period, the Incubator shall, at the Company's request, continue to make the Incubator Facilities listed in A and B above available to the Company upon payment by the Company of a fee to be decided upon by the incubator and the founder.



For SootheEarth LLP

Designated Partner

SCHEDULE III

COVENANTS OF THE COMPANY

1. The Company shall keep Incubator facilities extended for their usage in good condition and shall not cause damage thereto.
2. The Company shall not cause any nuisance or annoyance to other companies or units working in the AIC - MUJ Incubation Foundation.
3. The Company shall not engage in any unlawful activities during its stay in the AIC - MUJ Incubation Foundation. The Company shall comply with provisions of the relevant Rules, Regulations and Acts applicable to it. The Company shall also ensure that its Promoters and its employees do not engage in any unlawful activities during their stay in the AIC - MUJ Incubation Foundation.
4. The Company shall comply with the terms of the AIC - MUJ Incubation Foundation Policy during its stay in the AIC - MUJ Incubation Foundation. Amendments or changes, from time to time, in the Policy shall be binding on the Company unless Incubator decides otherwise. The Company shall be responsible to update itself from time to time on amendments in the Policy. Incubator shall not be held liable for lack of communication and intimation to the Company on specific amendment in the Policy.
5. The Company shall submit information to Incubator about all material changes or development taken place in their companies from time to time such as (but not limited to) change in name of the company, change in project or product profile, change in directors, promoters or shareholders, acquisition of a new office, additional equity or debt investments. Prior concurrence of Incubator shall be obtained for effecting such changes and Incubator shall have a right to stipulate such additional conditions as Incubator in its absolute discretion deem fit for effecting any change as stated herein above.
6. The Company undertakes and agrees that the information to be submitted by it will be correct and Incubator shall not be responsible for verifying the correctness of the information to be submitted by the Company. In the event that any information submitted by the Company is found to be incorrect, Incubator will proceed to take appropriate actions for breach of the provision of this Agreement.
7. The Company shall disclose to Incubator, information on executive involvements of their promoters in other companies or Business Incubator entities. The Company shall also ensure that its promoters, employees or any other person connected to the Company or its promoters shall avoid all conflicting situations and that they shall not use their positions in multiple capacities to the benefit of the other roles. The Company shall disclose to Incubator, information or situation of conflict of interests involving its promoters, employees or any other person connected to the company or its promoters.
8. The performance of the Company shall be subject to the periodical assessment by Incubator. The Company will work with the Incubator to set milestones for the period of incubation. The Company shall submit with Incubator information on quarterly basis in a format as reasonably required by the Incubator. The Company will have to submit their annual reports within a period of 7 days from the date of its approval.



For SootheEarth LLP

Designated Partner



भारतीय गैर न्यायिक
 एक सौ रुपये **Rs. 100**
 Research Methodology Part A Assignment 1 Template

Area of Research:

Name of your Guide:

SL No	Name of Collaborator	Area of Research



AT 404113

Nature of Collaboration:- Choose from the following and Elaborate on it

1. work together on the research project
2. original research proposal development
3. for one or more of the main elements of the research (e.g. the experimental design, construction of research equipment, execution of the experiment, analysis and interpretation of the data)
4. writing up the results in a paper
5. original idea or hypothesis, the theoretical interpretation
6. the original project proposer and/or fund raiser
7. Any other type of collaboration.

FOR UMIDIGI SOLUTIONS LLP
 Dinya Pritwani
 PARTNER

Memorandum of Understanding

This **Memorandum of Understanding Agreement ("Agreement")** is entered into on this the 19th November 2021 by and amongst:

1. **AIC - MUJ Incubation Foundation (U93090RJ2018NPL061558)**, registered under the provisions of the Companies Act 2013 and having its registered office at C/O Manpal University Jaipur, Dehmi kalan, Jaipur Ajmer Expressway, Rajasthan - 303007 (herein after referred to as the "**Incubator**" which expression shall, unless it be repugnant to the subject or context thereof, include its successors and permitted assigns)
 2. The persons set out in Schedule I hereto (hereinafter referred to as individually as a "**Founder**" and collectively as the "**Founders**", which expression shall, unless repugnant to the context or meaning thereof, include their respective heirs, executors, administrators and permitted assigns);
- AND**
3. **UMIDIGI SOLUTIONS LLP (AAP-3631)**, a company incorporated under the laws of India and having its registered office at 175,MODI NAGAR, PURANI CHUNGI, AJMER ROAD, JAIPUR, RAJASTHAN, 302019(hereinafter referred to as the "**Company**", which expression shall unless repugnant to the context or meaning thereof, include its successors and permitted assigns).

Each of the Founders, the Incubator and the Company shall hereinafter be referred to individually as a "**Party**" and collectively as the "**Parties**".

Dinya Pritwani
 PARTNER

FOR UMIDIGI SOLUTIONS LLP
 PARTNER

क्रमांक 2928 दिनांक 19/11/2020

मुद्रांक का मूल्य 1.50/-
क्रेता का नाम Umidigi Infusions LLP

पिता/पति का नाम
पता 175, Modi Nagar, Ajmer Road, Jaipur

मुद्रांक खरीदने का कारण तथा सम्बन्धित
कार्य का मूल्यांकन 549/- 42

बालमुद्रांक परिसरानी
लॉ. स्थान विज्ञापन
ता. नं. 110/2011-12
251, राजनी विहार, हासपुरा
अजमेर रोड, जयपुर

राजस्थान स्टाम्प अधिनियम, 1998 के अन्तर्गत स्टाम्प रशि पर प्रयोजित अधिभार	
1. आधारभूत अथवा परिसर सुविधाओं हेतु (धारा 3-क) -	1.50/-
2. गाय और उसकी नस्ल के संरक्षण और संवर्धन हेतु (धारा 3-ख) -	2.00/-
कुल राशि 3.50/-	
हस्ताक्षर स्टाम्प	

WHEREAS the Company, is seeking professional and infrastructural support and guidance more specifically enumerated in Schedule II (the "**Incubator Facilities**"). The Incubator has hereby committed to support and mentor the Company and the Founders for a period of **twelve months**<Incubation Period> from the **Effective Date**.

NOW THEREFORE, in consideration of the foregoing and other good and valuable consideration, the receipt and adequacy of which are hereby expressly acknowledged, the Parties, intending to be legally bound, hereby agree as follows:

1. Definitions & Interpretation:

1.1 Definitions:

Act shall mean the Companies Act, 1956 and the Companies Act, 2013, as may be applicable, together with the rules and regulations hereunder, as may be amended, modified, supplemented or re-enacted from time to time;

Board shall mean the board of directors of the Company;

Business shall mean the "**Unique solution converting all the waste flowers upcycled into variety of products including incense sticks.**".

Direct Competitor shall mean any Person engaged in the same or similar business as the Business;

Effective Date shall mean the date on which the Parties mutually agree on the Machine List and Timelines;

Law shall mean any statute, law, regulation, ordinance, rule, judgment, notification, rule of common law, order, decree, bye-law, Governmental Approval, directive, guideline, requirement or other governmental restriction, or any similar form of decision of, or determination by, or any interpretation, policy or administration, having the force of law of any of the foregoing, by any Governmental Authority having jurisdiction over the matter in question, whether in effect as of the date of this Agreement or thereafter;

Success Fee shall mean a claim by Incubator for a success fee or incentive fee calculated at the rate of **5% of total business or funds generated** via connections or programs executed or facilitated by incubator. The funds could be generated by Sales, Paid Contracts, Grants received, Investor Capital Raised, etc.

1.2 Interpretation: Any capitalized term used but not defined herein shall have the meaning ascribed thereto in the Investment Agreement.

2. Consideration.

Further for business or funds generated via connections or programs executed or facilitated by AIC a success fees would be charged by the incubator and the same shall be payable within 15 (fifteen) days of receipt of 15% payment from the said contract.

3. Relationship: The Incubator shall be an independent contractor and nothing in this Agreement shall render the Incubator an employee, worker, agent or partner of the Company.

4. Term & Termination:

4.1 This Agreement shall come into effect on the Execution Date and shall remain valid and binding on the Parties until such time that it is terminated in accordance with Clause 4.2 below

4.2 Termination:

(i) This Agreement may be terminated at the option of the Incubator if the Success Fee is not

Divya Prithwani


FOR UMIDIGI INFUSIONS LLP


transferred in accordance with Clause 2.

- (ii) This Agreement may be terminated at the option of the Incubator in the following circumstances:
 - (a) use of the Incubator Facilities by the Company for purposes other than for furtherance of its business;
 - (b) causing damage to the Incubator's property;
 - (c) Breach by the Company of the covenants set out in Schedule III hereto.
- (iii) This Agreement may be terminated at the option of the Company or the Founders if (a) the Effective Date has not occurred within 3 months of the Execution Date or (b) there is a material deviation in the Machine List and Timelines.
- (iv) This Agreement may be terminated at the option of the Company or the Founders in the event the Incubator fails to comply with its responsibilities under this Agreement or materially breaches the terms of this Agreement.
- (v) This Agreement may be terminated at any time by the mutual agreement of the Founders and the Incubator.

4.3 In the event of termination by the Incubator for the reasons set out in (ii) above, the Incubator may require the Company to vacate the premises with 7 days' notice, subject to the Dispute Resolution procedure set out herein.

4.4 In the event of termination by the Company or the Founders for the reasons set out in (iii)(b) or (iv) above, 50% of the Success Fee must be transferred back to the respective Founders by the Incubator as soon as commercially possible, subject to the Dispute Resolution procedure set out herein.

4.5 The termination of this Agreement shall not relieve any Party of any obligation or liability accrued prior to the date of termination.

4.6 The clauses of this Agreement which by their nature should survive termination shall survive such termination.

5. **Limitation of Liability:**

5.1 In no event shall the Party be liable to any other Parties for any special, incidental, indirect or consequential damages arising out of or in connection with this Agreement.

5.2 In no event shall a Party or any of its partners, officers, employees, representatives or agents be liable for any liability whatsoever for any losses or expenses of any nature suffered by another Party arising directly or indirectly from any act or omission of such Party or its employees, agents or representatives hereunder.

6. **Tax Liability:** Any and all tax liability that may be incurred by a Party as a consequence of operation of Applicable Law shall be borne by the respective Party.

7. **Costs and Expenses:** Each Party will bear its own expenses incurred in connection with the preparation, negotiation and execution of this Agreement. In addition, all costs and expenses in relation to payment of any stamp duty, registration duty and service taxes on the Definitive Documents under applicable Law shall be borne equally by the Company and the Incubator.

8. **Indemnity:** Each Party hereby agree to protect, defend, indemnify and hold harmless the other Parties, their employees, officers, partners, agents or representatives from and against any and all liabilities, damages, fines, penalties and costs (including legal costs and disbursements), arising from or relating to any third party claims, demands, fines, penalties and other sanctions imposed by any authority for non-compliance with any applicable law pursuant to and by virtue of this Agreement; and/ or any losses, liabilities, expenses, damages and / or claims suffered or incurred by the Incubator (including reasonable legal fees) as a result of such Party's negligence, fraud or wilful default in relation to this Agreement.




FOR UNIDIGI INFUSIONS LLP

Partner

Each Party shall also indemnify and keep indemnified the other Parties for any breach of the terms and conditions of this Agreement.

9. Intellectual Property:

- 9.1 "Intellectual Property" includes patents, inventions, know how, trade secrets, trademarks, service marks, designs, tools, devices, models, methods, procedures, processes, systems, principles, algorithms, works of authorship, flowcharts, drawings, and other confidential and proprietary information, data, documents, instruction manuals, records, memoranda, notes, user guides, ideas, concepts, information, materials, discoveries, developments, and other copyrightable works, and techniques in either printed or machine-readable form, whether or not copyrightable or patentable
- 9.2 "Intellectual Property Rights" include: (i) all right, title, and interest under any statute or under common law including patent rights; copyrights including moral rights; and any similar rights in respect of Intellectual Property, anywhere in the world, whether negotiable or not; (ii) any licenses, permissions and grants in connection therewith; (iii) applications for any of the foregoing and the right to apply for them in any part of the world; (iv) right to obtain and hold appropriate registrations in Intellectual Property; (v) all extensions and renewals thereof; and (vi) causes of action in the past, present or future, related thereto including the rights to damages and profits, due or accrued, arising out of past, present or future infringements or violations thereof and the right to sue for and recover the same.
- 9.3 Except as set out in this Clause 11, each Party agrees that all Intellectual Property Rights, which are held by the other Party, shall remain in the sole and exclusive ownership of such other Party.
- 9.4 Any Intellectual Property and Intellectual Property Rights developed or conceived by the Company while receiving guidance or support as described in Schedule II shall vest absolutely and irrevocably with the Company.

10. Non-Disclosure:

- 10.1 All information and data belonging to the Company of confidential and proprietary nature be it specifically documented or not, shall be termed as confidential information ("**Confidential Information**"). This includes but is not limited to:
- a. creative information, including symbols, photographs, animations, videos, models, techniques, experimental methods, designs, concepts, research, insights and other creations;
 - b. technical information, including research programs and methods, product development plans, functional and technical specifications, technology, inventions, ideas, concepts, drawings, designs, analysis, research, methods, techniques, processes, computer software, data, databases, flowcharts, patent applications, and other technical know-how and materials;
 - c. business information, including business plans, business strategies and/or data arising thereof, sales and marketing research, materials and plans, accounting and financial information, projections, performance results, cost data, customer information, personnel records and the like;
 - d. all proprietary information related to the Company; and
 - e. any other valuable information of the Company designated as confidential by the circumstances in which it is provided.
- 10.2 Confidential Information does not include such information or data that: (a) is or becomes generally known to the public without restriction through no fault of the Incubator, or (b) that the Incubator knew without restriction prior to its disclosure by Company.
- 10.3 The Incubator shall hold in confidence and not disclose or use any Confidential Information, except in connection with this Agreement or with the prior written permission of the Company. This Clause shall survive the termination of this Agreement.
- 10.4 Upon termination of this Agreement or as otherwise requested by the Company, the

Dinaya Pritywani


Incubator will promptly return to the Company all items and copies containing or embodying Confidential Information without retaining any copies (soft or hard copies) with himself

11. Dispute Resolution:

- 11.1 The Parties agree to negotiate in good faith to resolve any dispute between them regarding this Agreement. If the negotiations do not resolve the dispute to the reasonable satisfaction of the Parties, then the dispute shall be submitted to final and binding arbitration at the request the disputing Parties upon written notice to that effect to the other disputing Parties. In the event of such arbitration:
- 11.1.1 The arbitration shall be conducted in accordance with the Indian Arbitration and Conciliation Act, 1996 (the "**Arbitration Act**") in force at the relevant time (which is deemed to be incorporated into this Agreement by reference);
- 11.1.2 All proceedings of the arbitration shall be in the English language. The venue and seat of arbitration shall be at Jaipur, India;
- 11.1.3 All proceedings shall be conducted before a panel of 3 (three) arbitrators wherein, one arbitrator will be appointed by the claimants, the second arbitrator will be appointed by the respondents and the third arbitrator will be appointed jointly by the other two arbitrators; and
- 11.1.4 Arbitration awards rendered shall be final, binding and shall not be subject to any form of appeal.
- 11.2 Nothing shall preclude a Party from seeking interim equitable or injunctive relief, or both. The pursuit of equitable or injunctive relief shall not be a waiver of the right of the Parties to pursue any other remedy or relief through the arbitration described in this Clause 11.

12. Miscellaneous:

- 12.1 This Agreement may be modified, amended or supplemented only by the mutual written agreement of the Parties. A waiver or any failure or delay by the Incubator to require the enforcement of the obligations, agreements, undertakings or covenants in this Agreement shall not be construed as a waiver by the Incubator of any of its rights, unless made in writing referring specifically to the relevant provisions of this Agreement and signed by a duly authorized representative of the Incubator. Any such waiver shall not affect in any way the validity of this Agreement or the right to enforce such obligation, agreement, undertaking or covenant at any other time. All rights and remedies existing under this Agreement, except as otherwise provided herein are cumulative to, and not exclusive of any rights or remedies otherwise available.
- 12.2 If for any reason whatsoever, any provision of this Agreement is or becomes, or is declared by a court of competent jurisdiction to be, invalid, illegal or unenforceable, then the Parties shall negotiate in good faith to agree on such provision to be substituted, which provisions shall, as nearly as practicable, leave the Parties in the same or nearly similar position to that which prevailed prior to such invalidity, illegality or unenforceability.
- 12.3 Except as may be otherwise provided herein, all notices, requests, waivers and other communications made pursuant to this Agreement shall be in writing and signed by or on behalf of the Party giving it. Such notice shall be served by delivering by hand, registered post, electronic mail or courier to the address set forth below. In each case it shall be marked for the attention of the relevant Party set forth below. Any notice so served shall be deemed to have been duly given (i) in case of delivery by hand, when hand delivered to the other Party; or (ii) when sent by registered post, where 7 (seven) Business Days have elapsed after deposit in the mail with certified mail receipt requested postage prepaid; or (iii) when delivered by courier on the 2nd (second) Business Day after deposit with an overnight delivery service, postage prepaid, with next Business Day delivery guaranteed, provided that the Party issuing the notice receives a confirmation of delivery from the delivery service provider; or (iv) for electronic mail notification, upon confirmation of such notification by any of the means as aforesaid.

Diya Prithvi




To the Founders:

Attention: Prakash Jangid
Address: 175,MODI NAGAR, PURANI CHUNGI, AJMER ROAD, JAIPUR, RAJASTHAN,
302019
Email : malawalas@gmail.com

To the Company:

Attention: Prakash Jangid, Designated Partner
Address: 175,MODI NAGAR, PURANI CHUNGI, AJMER ROAD, JAIPUR, RAJASTHAN,
302019
Email : malawalas@gmail.com

To the Incubator:

Attention: CEO
Address: C/o Manipal University Jaipur, Dehmikalan, Bagru, Jaipur, Pin- 303007
Email : divya.pritwani@jaipur.manipal.edu

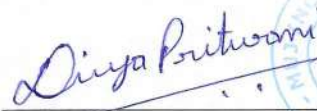
- 12.4 No Party shall assign this Agreement or any of its rights or obligations hereunder without the prior written consent of the other Parties.
- 12.5 This Agreement supersedes all earlier agreements, arrangements, letters, correspondence, understandings etc. with respect to the subject matter of this Agreement. For the avoidance of doubt, it is clarified that this Agreement does not supersede the Investment Agreement.
- 12.6 The Agreement may be executed and delivered in counterparts, each of which shall be deemed an original.
- 12.7 Save and except as otherwise stated in this Agreement, in the event that a Party commits a default of the terms of this Agreement then, the non-defaulting Parties shall, in addition to any other rights and remedies available under this Agreement, be entitled to seek specific performance of this Agreement and such other remedies as may be permitted to it under applicable Law.
- 12.8 Each Party shall act in good faith in the performance of its respective responsibilities under this Agreement and will not unreasonably delay, condition or withhold the giving of any consent, decision or approval that is either requested or reasonably required by any other Party in order to perform its responsibilities.

IN WITNESS, WHEREOF the Parties have put their respective hands on the day and year first herein above written.

Signed and delivered by

For and on behalf of

1. AIC – MUJ Incubation Foundation



Chief Executive Officer

2. Founders



Prakash Jangid


FORUM INFUSIONS LLP
Partner

3. Startup Name

UMIDIGI SOLUTIONS LLP (MALAWALAS)
Prakash Jangid - Designated Partner

SCHEDULE I

LIST OF FOUNDERS

1. Prakash Jangid
2. Rakesh Choudhary

FOR UMIDIGI SOLUTIONS LLP

Partner




SCHEDULE II

INCUBATOR FACILITIES

1. The Incubator shall provide the Incubator Facilities as listed below for a period of twelve months from the Effective Date ("**Incubation Period**"):

A. Physical Infrastructure:

- Developed office space approximately admeasuring <4>. with furniture and air-conditioning machines to occupy and use for Business Incubator activities.
- 24x7 high speed Internet Connectivity
- Access to Maker Space/Fab Lab.

Notwithstanding anything contained in this Agreement, AIC – MUJ Incubation Foundation shall have absolute right and ownership of the office space provided to locate the Company (the company to be promoted by the Promoters). The Estate Officer of the AIC – MUJ Incubation Foundation shall be deemed to be a competent authority under the Public Premises (Eviction of Unauthorised Occupants) Act, 1971 for necessary actions in connection with the office space so occupied by the Company.

B. Common Infrastructure:

The Incubator will provide following facilities to the Company, which will be shared by all Companies located in the Incubator:

- Laser Printer
- Photocopier
- Scanner
- Meeting/Conference room with projection equipment

The ownership of all assets so provided as a part of Incubator supports and services rests with Incubator AIC – MUJ Incubation Foundation as the case may be.

The support and services described in clauses A and B herein above shall be herein after referred to as "Incubator facilities".

C. Network of Mentors and Experts:

Incubator will facilitate liaison with mentors, professionals and experts in technology, legal, financial and related matters on such terms and conditions as may be stipulated by them.

D. Event and Meetings:

Incubator will organise events to facilitate the companies located in the BI in networking and to showcase their technologies. Incubator will also facilitate meetings with visitors of AIC – MUJ Incubation Foundation and its constituent Institutions such as alumni, venture capitalists, industry professionals.

E. Information Pool:

Incubator will maintain access to information and knowledge pool generally useful new enterprises. The Incubator will also facilitate access to departmental laboratories of AIC – MUJ Incubation Foundation Institutions by the Company (Promoters) for their product development purposes with approval of the concerned department.

F. Access to Markets & Talent

Incubator will provide help to incubatee, by providing assistance in marketing, get access to markets and access to desired talent.

G. Access to Investors

Incubator will provide help to incubatee, by providing assistance in Investor connections and investment process.

2. In the event of a material deviation/delay in the Machine List and Timelines, the Company and the Founders shall have the right to demand that the Incubator extends the incubation period in accordance with such deviation/delay.
3. Further, at the end of the Incubation Period, the Incubator shall, at the Company's request, continue to make the Incubator Facilities listed in A and B above available to the Company upon payment by the Company of a fee to be decided upon by the incubator and the founder.

Divya Puthwani



FOR UMEDRA INFUSIONS LLP
[Signature]
Partner


SCHEDULE III

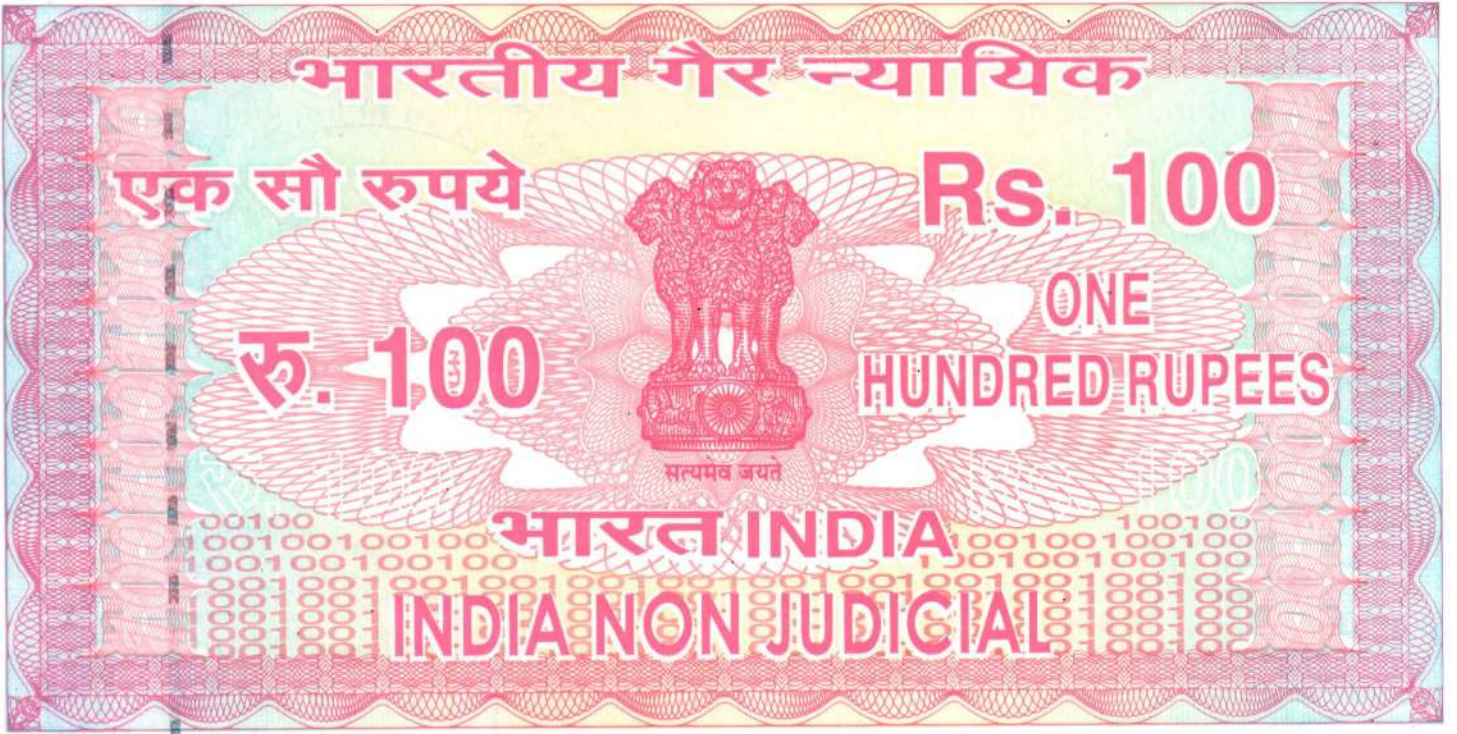
COVENANTS OF THE COMPANY

1. The Company shall keep Incubator facilities extended for their usage in good condition and shall not cause damage thereto.
2. The Company shall not cause any nuisance or annoyance to other companies or units working in the AIC – MUJ Incubation Foundation.
3. The Company shall not engage in any unlawful activities during its stay in the AIC – MUJ Incubation Foundation. The Company shall comply with provisions of the relevant Rules, Regulations and Acts applicable to it. The Company shall also ensure that its Promoters and its employees do not engage in any unlawful activities during their stay in the AIC – MUJ Incubation Foundation.
4. The Company shall comply with the terms of the AIC – MUJ Incubation Foundation Policy during its stay in the AIC – MUJ Incubation Foundation. Amendments or changes, from time to time, in the Policy shall be binding on the Company unless Incubator decides otherwise. The Company shall be responsible to update itself from time to time on amendments in the Policy. Incubator shall not be held liable for lack of communication and intimation to the Company on specific amendment in the Policy.
5. The Company shall submit information to Incubator about all material changes or development taken place in their companies from time to time such as (but not limited to) change in name of the company, change in project or product profile, change in directors, promoters or shareholders, acquisition of a new office, additional equity or debt investments. Prior concurrence of Incubator shall be obtained for effecting such changes and Incubator shall have a right to stipulate such additional conditions as Incubator in its absolute discretion deem fit for effecting any change as stated herein above.
6. The Company undertakes and agrees that the information to be submitted by it will be correct and Incubator shall not be responsible for verifying the correctness of the information to be submitted by the Company. In the event that any information submitted by the Company is found to be incorrect, Incubator will proceed to take appropriate actions for breach of the provision of this Agreement.
7. The Company shall disclose to Incubator, information on executive involvements of their promoters in other companies or Business Incubator entities. The Company shall also ensure that its promoters, employees or any other person connected to the Company or its promoters shall avoid all conflicting situations and that they shall not use their positions in multiple capacities to the benefit of the other roles. The Company shall disclose to Incubator, information or situation of conflict of interests involving its promoters, employees or any other person connected to the company or its promoters.
8. The performance of the Company shall be subject to the periodical assessment by Incubator. The Company will work with the Incubator to set mile stones for the period of incubation. The Company shall submit with Incubator information on quarterly basis in a format as reasonably required by the Incubator. The Company will have to submit their annual reports within a period of 7 days from the date of its approval.

Diya Pritwani



For UMIDIGI INFUSIONS LLP

Partner



తెలంగాణ తెలంగాణ TELANGANA
Sl.No. 49776 Date 17/10/2022 Rs. 100 ✓
Sold to D.A.G. Sai Revanth R.A. Hyd
S/o.W/o.D/r D.Raghavendra Rao
For Whom Weezy Innovations Pvt. Ltd

AV 477518
G. HARAKOTAL
LICENSED STAMP VENDOR
L.No. 15-26-001/1992 RL No. 15-26-009/2022
H.No. EWS-144, Kamala Nagar, Kepra,
ECIL (P) M.M.Dist-600 082 Call: 9440094852

Memorandum of Understanding

This **Memorandum of Understanding** Agreement ("**Agreement**") is entered into on this the 08/09/2022 by and amongst:

- AIC - MUJ Incubation Foundation (U93090RJ2018NPL061558)**, registered under the provisions of the Companies Act 2013 and having its registered office at C/O Manipal University Jaipur, Dehmi kalan, Jaipur Ajmer Expressway, Rajasthan - 303007 (herein after referred to as the "**Incubator**" which expression shall, unless it be repugnant to the subject or context thereof, include its successors and permitted assigns)
 - The persons set out in Schedule I hereto (hereinafter referred to as individually as a "**Founder**" and collectively as the "**Founders**", which expression shall, unless repugnant to the context or meaning thereof, include their respective heirs, executors, administrators and permitted assigns);
- AND**
- Weezy Innovations Pvt. Ltd. (CIN: U74999KA2021PTC146646)**, a company incorporated under the laws of India and having its registered office at #71, 3rd Cross Road, Residency Road Opposite to Samsung Opera House Bangalore - 560025 (hereinafter referred to as the "**Company**", which expression shall unless repugnant to the context or meaning thereof, include its successors and permitted assigns).

Each of the Founders, the Incubator and the Company shall hereinafter be referred to individually as a "**Party**" and collectively as the "**Parties**".

WHEREAS the Company, is seeking professional and infrastructural support and guidance more specifically enumerated in Schedule II (the "**Incubator Facilities**"). The Incubator has hereby committed to support and mentor the Company and the Founders for a period of twelve months from the **Effective Date**.

NOW THEREFORE, in consideration of the foregoing and other good and valuable consideration, the receipt and adequacy of which are hereby expressly acknowledged, the Parties, intending to be legally bound, hereby agree as follows:

For WEEZY INNOVATIONS PVT. LTD.

Punet
AIC - MUI INNOVATION

R.A.H.

DIRECTOR

1. Definitions & Interpretation:

1.1. Definitions:

Act shall mean the Companies Act, 1956 and the Companies Act, 2013, as may be applicable, together with the rules and regulations hereunder, as may be amended, modified, supplemented or re-enacted from time to time;

Board shall mean the board of directors of the Company;

Business shall mean the revolution of urban clothing & fashion all at once, through unique designs that cater to the ever changing style of Z-Generation.

Direct Competitor shall mean any Person engaged in the same or similar business as the Business;

Effective Date shall mean the date on which the Parties mutually agree on the Machine List and Timelines;

Law shall mean any statute, law, regulation, ordinance, rule, judgment, notification, rule of common law, order, decree, bye-law, Governmental Approval, directive, guideline, requirement or other governmental restriction, or any similar form of decision of, or determination by, or any interpretation, policy or administration, having the force of law of any of the foregoing, by any Governmental Authority having jurisdiction over the matter in question, whether in effect as of the date of this Agreement or thereafter;

Success Fee shall mean a claim by Incubator for a success fee or incentive fee calculated at the rate of 5% of total business or funds generated via connections or programs executed or facilitated by incubator. The funds could be generated by Sales, Paid Contracts, Grants received, Investor Capital Raised, etc.

1.2. Interpretation: Any capitalized term used but not defined herein shall have the meaning ascribed thereto in the Investment Agreement.

2. Consideration.

Further for business or funds generated via connections or programs executed or facilitated by AIC a success fees would be charged by the incubator and the same shall be payable within 30 (thirty) days of the contract.

3. Relationship: The Incubator shall be an independent contractor and nothing in this Agreement shall render the Incubator an employee, worker, agent or partner of the Company.

4. Term & Termination:

4.1. This Agreement shall come into effect on the Execution Date and shall remain valid and binding on the Parties until such time that it is terminated in accordance with Clause 4.2 below

4.2. Termination:

(i) This Agreement may be terminated at the option of the Incubator if the Success Fee is not transferred in accordance with Clause 2.

For WEEZY INNOVATIONS PVT. LTD.






DIRECTOR

- (ii) This Agreement may be terminated at the option of the Incubator in the following circumstances:
 - (a) use of the Incubator Facilities by the Company for purposes other than for furtherance of its business;
 - (b) causing damage to the Incubator's property;
 - (c) Breach by the Company of the covenants set out in Schedule III hereto.
- (iii) This Agreement may be terminated at the option of the Company or the Founders if (a) the Effective Date has not occurred within 3 months of the Execution Date or (b) there is a material deviation in the Machine List and Timelines.
- (iv) This Agreement may be terminated at the option of the Company or the Founders in the event the Incubator fails to comply with its responsibilities under this Agreement or materially breaches the terms of this Agreement.
- (v) This Agreement may be terminated at any time by the mutual agreement of the Founders and the Incubator.

4.3 In the event of termination by the Incubator for the reasons set out in (ii) above, the Incubator may require the Company to vacate the premises with 7 days' notice, subject to the Dispute Resolution procedure set out herein.

4.4 In the event of termination by the Company or the Founders for the reasons set out in (iii)(b) or (iv) above, 50% of the Success Fee must be transferred back to the respective Founders by the Incubator as soon as commercially possible, subject to the Dispute Resolution procedure set out herein.

4.5 The termination of this Agreement shall not relieve any Party of any obligation or liability accrued prior to the date of termination.

4.6 The clauses of this Agreement which by their nature should survive termination shall survive such termination.

5. Limitation of Liability:

5.1 In no event shall the Party be liable to any other Parties for any special, incidental, indirect or consequential damages arising out of or in connection with this Agreement.

5.2 In no event shall a Party or any of its partners, officers, employees, representatives or agents be liable for any liability whatsoever for any losses or expenses of any nature suffered by another Party arising directly or indirectly from any act or omission of such Party or its employees, agents or representatives hereunder.

6. Tax Liability: Any and all tax liability that may be incurred by a Party as a consequence of operation of Applicable Law shall be borne by the respective Party.

7. Costs and Expenses: Each Party will bear its own expenses incurred in connection with the preparation, negotiation and execution of this Agreement. In addition, all costs and expenses in relation to payment of any stamp duty, registration duty and service taxes on the Definitive Documents under applicable Law shall be borne equally by the Company and the Incubator.

8. Indemnity: Each Party hereby agree to protect, defend, indemnify and hold harmless the other Parties, their employees, officers, partners, agents or representatives from and against any and all liabilities, damages, fines, penalties and costs (including legal costs and disbursements), arising from or relating to any third party claims, demands, fines, penalties and other sanctions imposed by any authority for non-compliance with any applicable law pursuant to and by virtue of this Agreement; and/ or any losses, liabilities, expenses, damages and / or claims suffered or incurred by the Incubator (including reasonable legal fees) as a result of such Party's negligence, fraud or wilful default in relation to this Agreement.

Each Party shall also indemnify and keep indemnified the other Parties for any breach of the terms and conditions of this Agreement.






For WEEZY INNOVATIONS PVT. LTD.

DIRECTOR

9. **Intellectual Property:**

- 9.1. "Intellectual Property" includes patents, inventions, know how, trade secrets, trade-marks, service marks, designs, tools, devices, models, methods, procedures, processes, systems, principles, algorithms, works of authorship, flowcharts, drawings, and other confidential and proprietary information, data, documents, instruction manuals, records, memoranda, notes, user guides, ideas, concepts, information, materials, discoveries, developments, and other copyrightable works, and techniques in either printed or machine-readable form, whether or not copyrightable or patentable
- 9.2. "Intellectual Property Rights" include: (i) all right, title, and interest under any statute or under common law including patent rights; copyrights including moral rights; and any similar rights in respect of Intellectual Property, anywhere in the world, whether negotiable or not; (ii) any licenses, permissions and grants in connection therewith; (iii) applications for any of the foregoing and the right to apply for them in any part of the world; (iv) right to obtain and hold appropriate registrations in Intellectual Property; (v) all extensions and renewals thereof; and (vi) causes of action in the past, present or future, related thereto including the rights to damages and profits, due or accrued, arising out of past, present or future infringements or violations thereof and the right to sue for and recover the same.
- 9.3. Except as set out in this Clause 11, each Party agrees that all Intellectual Property Rights, which are held by the other Party, shall remain in the sole and exclusive ownership of such other Party.
- 9.4. Any Intellectual Property and Intellectual Property Rights developed or conceived by the Company while receiving guidance or support as described in Schedule II shall vest absolutely and irrevocably with the Company.

10. **Non-Disclosure:**

- 10.1. All information and data belonging to the Company of confidential and proprietary nature be it specifically documented or not, shall be termed as confidential information ("**Confidential Information**"). This includes but is not limited to:
- creative information, including symbols, photographs, animations, videos, models, techniques, experimental methods, designs, concepts, research, insights and other creations;
 - technical information, including research programs and methods, product development plans, functional and technical specifications, technology, inventions, ideas, concepts, drawings, designs, analysis, research, methods, techniques, processes, computer software, data, databases, flowcharts, patent applications, and other technical know-how and materials;
 - business information, including business plans, business strategies and/or data arising thereof, sales and marketing research, materials and plans, accounting and financial information, projections, performance results, cost data, customer information, personnel records and the like;
 - all proprietary information related to the Company; and
 - any other valuable information of the Company designated as confidential by the circumstances in which it is provided.
- 10.2 Confidential Information does not include such information or data that: (a) is or becomes generally known to the public without restriction through no fault of the Incubator, or (b) that the Incubator knew without restriction prior to its disclosure by Company.
- 10.3 The Incubator shall hold in confidence and not disclose or use any Confidential Information, except in connection with this Agreement or with the prior written permission of the Company. This Clause shall survive the termination of this Agreement.
- 10.4 Upon termination of this Agreement or as otherwise requested by the Company, the Incubator will promptly return to the Company all items and copies containing or embodying Confidential Information without retaining any copies (soft or hard copies) with himself

11. **Dispute Resolution:**

- 11.1 The Parties agree to negotiate in good faith to resolve any dispute between them regarding this Agreement. If the negotiations do not resolve the dispute to the reasonable satisfaction of the Parties, then the dispute shall be submitted to final and binding arbitration at the request the disputing Parties upon written notice to that effect to the other disputing Parties. In the event of such arbitration







For WEEZY INNOVATIONS PVT. LTD.

- 11.1.1 The arbitration shall be conducted in accordance with the Indian Arbitration and Conciliation Act, 1996 (the "Arbitration Act") in force at the relevant time (which is deemed to be incorporated into this Agreement by reference);
- 11.1.2 All proceedings of the arbitration shall be in the English language. The venue and seat of arbitration shall be at Jaipur, India;
- 11.1.3 All proceedings shall be conducted before a panel of 3 (three) arbitrators wherein, one arbitrator will be appointed by the claimants, the second arbitrator will be appointed by the respondents and the third arbitrator will be appointed jointly by the other two arbitrators; and
- 11.1.4 Arbitration awards rendered shall be final, binding and shall not be subject to any form of appeal.
- 11.2 Nothing shall preclude a Party from seeking interim equitable or injunctive relief, or both. The pursuit of equitable or injunctive relief shall not be a waiver of the right of the Parties to pursue any other remedy or relief through the arbitration described in this Clause 13.

12 Miscellaneous:

- 12.1 This Agreement may be modified, amended or supplemented only by the mutual written agreement of the Parties. A waiver or any failure or delay by the Incubator to require the enforcement of the obligations, agreements, undertakings or covenants in this Agreement shall not be construed as a waiver by the Incubator of any of its rights, unless made in writing referring specifically to the relevant provisions of this Agreement and signed by a duly authorized representative of the Incubator. Any such waiver shall not affect in any way the validity of this Agreement or the right to enforce such obligation, agreement, undertaking or covenant at any other time. All rights and remedies existing under this Agreement, except as otherwise provided herein are cumulative to, and not exclusive of any rights or remedies otherwise available.
- 12.2 If for any reason whatsoever, any provision of this Agreement is or becomes, or is declared by a court of competent jurisdiction to be, invalid, illegal or unenforceable, then the Parties shall negotiate in good faith to agree on such provision to be substituted, which provisions shall, as nearly as practicable, leave the Parties in the same or nearly similar position to that which prevailed prior to such invalidity, illegality or unenforceability.
- 12.3 Except as may be otherwise provided herein, all notices, requests, waivers and other communications made pursuant to this Agreement shall be in writing and signed by or on behalf of the Party giving it. Such notice shall be served by delivering by hand, registered post, electronic mail or courier to the address set forth below. In each case it shall be marked for the attention of the relevant Party set forth below. Any notice so served shall be deemed to have been duly given (i) in case of delivery by hand, when hand delivered to the other Party; or (ii) when sent by registered post, where 7 (seven) Business Days have elapsed after deposit in the mail with certified mail receipt requested postage prepaid; or (iii) when delivered by courier on the 2nd (second) Business Day after deposit with an overnight delivery service, postage prepaid, with next Business Day delivery guaranteed, provided that the Party issuing the notice receives a confirmation of delivery from the delivery service provider; or (iv) for electronic mail notification, upon confirmation of such notification by any of the means as aforesaid.

To the Founders:

Attention: Gopal Krishna Panda
Address: B/36 Sriramsadhanana Apts, Gokula Mathikeri, Bangalore 54
Email : gopal@weezy.in

To the Company:

Attention: Gopal Krishna Panda
Address: B/36 Sriramsadhanana Apts, Gokula Mathikeri, Bangalore 54
Email: gopal@weezy.in

To the Incubator:

Attention : CEO
Address : C/o Manipal University Jaipur, Dehmikalan, Bagru, Jaipur, Pin- 303007
Email :

- 12.4 No Party shall assign this Agreement or any of its rights or obligations hereunder without the prior written consent of the other Parties.

For WEEZY INNOVATIONS PVT. LTD.

Puneet



Ruth

- 12.5 This Agreement supersedes all earlier agreements, arrangements, letters, correspondence, understandings etc. with respect to the subject matter of this Agreement. For the avoidance of doubt, it is clarified that this Agreement does not supersede the Investment Agreement.
- 12.6 The Agreement may be executed and delivered in counterparts, each of which shall be deemed an original.
- 12.7 Save and except as otherwise stated in this Agreement, in the event that a Party commits a default of the terms of this Agreement then, the non-defaulting Parties shall, in addition to any other rights and remedies available under this Agreement, be entitled to seek specific performance of this Agreement and such other remedies as may be permitted to it under applicable Law.
- 12.8 Each Party shall act in good faith in the performance of its respective responsibilities under this Agreement and will not unreasonably delay, condition or withhold the giving of any consent, decision or approval that is either requested or reasonably required by any other Party in order to perform its responsibilities.

IN WITNESS, WHEREOF the Parties have put their respective hands on the day and year first herein above written.

Signed and delivered by .

For and on behalf of

1. AIC - MUJ Incubation Foundation




Chief Executive Officer



2. Founders


For WEEZY INNOVATIONS PVT. LTD.



Revanth Desai

DIRECTOR

3. Weezy Innovations Private Limited


_____ For WEEZY INNOVATIONS PVT. LTD.

Revanth Desai
Co-Founder

DIRECTOR

SCHEDULE I

LIST OF FOUNDERS

1. Founder - Gopal Krishna Panda
2. Co Founders - Revanth Desai & Thomas Sharon

For WEEZY INNOVATIONS PVT. LTD.

DIRECTOR

SCHEDULE II

INCUBATOR FACILITIES

1. The Incubator shall provide the Incubator Facilities as listed below for a period of twelve months from the Effective Date ("**Incubation Period**"):

A. Physical Infrastructure:

- Developed office space approximately ad measuring <4>. with furniture and air-conditioning machines to occupy and use for Business Incubator activities.
- 24x7 high speed Internet Connectivity
- Access to Maker Space/Fab Lab.

Notwithstanding anything contained in this Agreement, AIC - MUJ Incubation Foundation shall have absolute right and ownership of the office space provided to locate the Company (the company to be promoted by the Promoters). The Estate Officer of the AIC - MUJ Incubation Foundation shall be deemed to be a competent authority under the Public Premises (Eviction of Unauthorised Occupants) Act, 1971 for necessary actions in connection with the office space so occupied by the Company.

B. Common Infrastructure:

The Incubator will provide following facilities to the Company, which will be shared by all Companies located in the Incubator:

- Laser Printer
- Photocopier
- Scanner
- Meeting/Conference room with projection equipment

The ownership of all assets so provided as a part of Incubator supports and services rests with Incubator AIC - MUJ Incubation Foundation as the case may be.

The support and services described in clauses A and B herein above shall be herein after referred to as "Incubator facilities".

C. Network of Mentors and Experts:

Incubator will facilitate liaison with mentors, professionals and experts in technology, legal, financial and related matters on such terms and conditions as may be stipulated by them.

D. Event and Meetings:

Incubator will organise events to facilitate the companies located in the BI in networking and to showcase their technologies. Incubator will also facilitate meetings with visitors of AIC - MUJ Incubation Foundation and its constituent Institutions such as alumni, venture capitalists, industry professionals.

E. Information Pool:

Incubator will maintain access to information and knowledge pool generally useful new enterprises. The Incubator will also facilitate access to departmental laboratories of AIC - MUJ Incubation Foundation Institutions by the Company (Promoters) for their product development purposes with approval of the concerned department.

F. Access to Markets & Talent

Incubator will provide help to incubatee, by providing assistance in marketing, get access to markets and access to desired talent.

2. In the event of a material deviation/delay in the Machine List and Timelines, the Company and the Founders shall have the right to demand that the Incubator extends the incubation period in accordance with such deviation/delay.

3. Further, at the end of the Incubation Period, the Incubator shall, at the Company's request, continue to make the Incubator Facilities listed in A and B above available to the Company upon payment by the Company of a fee to be decided upon by the incubator and the founder.






For WEEZY INNOVATIONS PVT. LTD.

7
DIRECTOR

SCHEDULE III

COVENANTS OF THE COMPANY

1. The Company shall keep Incubator facilities extended for their usage in good condition and shall not cause damage thereto.
2. The Company shall not cause any nuisance or annoyance to other companies or units working in the AIC - MUJ Incubation Foundation.
3. The Company shall not engage in any unlawful activities during its stay in the AIC - MUJ Incubation Foundation. The Company shall comply with provisions of the relevant Rules, Regulations and Acts applicable to it. The Company shall also ensure that its Promoters and its employees do not engage in any unlawful activities during their stay in the AIC - MUJ Incubation Foundation.
4. The Company shall comply with the terms of the AIC - MUJ Incubation Foundation Policy during its stay in the AIC - MUJ Incubation Foundation. Amendments or changes, from time to time, in the Policy shall be binding on the Company unless Incubator decides otherwise. The Company shall be responsible to update itself from time to time on amendments in the Policy. Incubator shall not be held liable for lack of communication and intimation to the Company on specific amendment in the Policy.
5. The Company shall submit information to Incubator about all material changes or development taken place in their companies from time to time such as (but not limited to) change in name of the company, change in project or product profile, change in directors, promoters or shareholders, acquisition of a new office, additional equity or debt investments. Prior concurrence of Incubator shall be obtained for effecting such changes and Incubator shall have a right to stipulate such additional conditions as Incubator in its absolute discretion deem fit for effecting any change as stated herein above.
6. The Company undertakes and agrees that the information to be submitted by it will be correct and Incubator shall not be responsible for verifying the correctness of the information to be submitted by the Company. In the event that any information submitted by the Company is found to be incorrect, Incubator will proceed to take appropriate actions for breach of the provision of this Agreement.
7. The Company shall disclose to Incubator, information on executive involvements of their promoters in other companies or Business Incubator entities. The Company shall also ensure that its promoters, employees or any other person connected to the Company or its promoters shall avoid all conflicting situations and that they shall not use their positions in multiple capacities to the benefit of the other roles. The Company shall disclose to Incubator, information or situation of conflict of interests involving its promoters, employees or any other person connected to the company or its promoters.
8. The performance of the Company shall be subject to the periodical assessment by Incubator. The Company will work with the Incubator to set mile stones for the period of incubation. The Company shall submit with Incubator information on quarterly basis in a format as reasonably required by the Incubator. The Company will have to submit their annual reports within a period of 7 days from the date of its approval.



A handwritten signature in blue ink, consisting of stylized initials, is written over a horizontal line.

For WEEZY INNOVATIONS PVT. LTD.

DIRECTOR



Ref: NITTTR/2023-24

Dated : 18.09.2023

To
Honorable Vice Chancellor / Worthy Registrar
Manipal University, Jaipur

Subject: Short Term Programme on "**Energy efficient and innovative building construction practices**" from 09-13 October, 2023.

Dear Sir/Madam,

We are organizing the above cited STC for the faculty of Engineering Colleges and Polytechnics of all northern states of the country w.e.f. **09-13 October, 2023**. The above mentioned programme is being organized with the prime to acquaint the participants about the energy efficient innovative construction practices.

The importance of energy efficient and green buildings has assumed great urgency today. In light of fast depleting energy resources, energy scarcity and increasing environmental pollution, innovative ways to cut down energy consumption are necessary. The construction industry is one of the largest energy consuming sectors. In modern buildings significant amounts of energy are also consumed to keep the building environment comfortable. Estimates suggest that about 20-25 percent of the total energy demand is due to manufacturing materials required in the building sector, while another 15 percent goes into the running needs of the building like lighting, air-conditioning, room heating and ventilation etc.

In view of the global energy crisis and increasing energy demand is expected to continue and apart from possible end-use restrictions, energy efficiency and energy management is essentially required.

As Manipal University, Jaipur is a renowned university and Department of Architecture is one of the emerging department of the institute so, we want to conduct the above mentioned programme in collaboration of your organisation. We expect the following co-operation from your institution.

- Arrangement of one lecture hall equipped with facilities like LCD Projector, Computer and sound system for Video films show.
- Field study visit to nearby educational places or site. Charges /fuel charges to the institute bus from the institute for the field visit will be paid by NITTTR, Chandigarh
- Arrangement of few lecturers on the topics marked in the time table (send you in few days). Honorarium and TA to the experts will be paid by NITTTR, Chandigarh
- Arrangement of one guest house rooms for NITTTR faculty from **08-13 November, 2023** at your College/ Guest House.
- Stationary to the course participants for the programme will be provided by NITTTR, Chandigarh.
- As per the decision of the Institute, Rs.118/- (Rs. 100/- +18% GST) per participant will be charged from all participants.
- Honorarium of Rs. 2500/- to coordinator and Rs. 1500/- to supporting staff will be provided by NITTTR, Chandigarh
- No working lunch and tea will be provided to the participants by NITTTR, Chandigarh.

As it is a inter-disciplinary programme so we expect a minimum number of participants for the programme may be 30. The details of the programme will be shared on receiving letter of acceptance from your end through the coordinators.

We will highly appreciate your timely communication and approval for the above mentioned course.



(Dr. Amit Goyal)
Course Coordinator
9417569559

CC:
Dr. Sunanda Kapoor, Department of Architecture, Manipal University

Post Event Report



**MANIPAL UNIVERSITY
JAIPUR**

**FACULTY OF DESIGN
SCHOOL OF ARCHITECTURE AND DESIGN**

Short Term Programme

on

Energy Efficient and Innovative Construction Practices

Hybrid Mode

16th to 20th October 2023

Index

1. Introduction	3
2. Objectives of the STP	3
3. Beneficiaries of the Event	3
4. Details of the Guests	3
5. Brief Description of the Event.....	4
6. Brochure of the Event	4
7. Photographs of the Event	5
8. Schedule of the Event	7
9. Attendance of the Event	7
10. Weblink	7
11. Event Coordinators	7



1. Introduction

The importance of energy efficient and green buildings has assumed great urgency today. In light of fast depleting energy resources, energy scarcity and increasing environmental pollution, innovative ways to cut down energy consumption are necessary. The construction industry is one of the largest energy consuming sectors. In modern buildings significant amounts of energy are also consumed to keep the building environment comfortable. Estimates suggest that about 20-25 percent of the total energy demand is due to manufacturing materials required in the building sector, while another 15 percent goes into the running needs of the building like lighting, air-conditioning, room heating and ventilation etc. Increased development of housing and commercial buildings has imposed immense pressure on our dwindling energy sources. The availability of energy is limited and known resources of energy are exhausting fast. Therefore, energy efficiency is assuming importance in different sectors. In view of the global energy crisis and increasing energy demand is expected to continue and apart from possible end-use restrictions, energy efficiency and energy management is essentially required.

2. Objectives of the STP

The objective of STP was to discuss on the below mentioned aspects related to energy efficient and green buildings-

- Basic Knowledge of Energy Efficient Buildings
- Planning and Preparedness
- Solar Passive Architecture
- Vaastu Shastra Myths and Realities
- Innovative Practices/Research in Green Buildings
- Green Buildings-Design and Construction
- Energy efficiency in old traditional buildings
- Solar Devices and their Utilization

3. Beneficiaries of the Event

- Academicians
- Research Scholars
- PG Students (Architecture, Civil, Management and Allied Fields)

4. Details of the Guests

- Dr. Amit Goyal NITTTR, Chandigarh
- Dr. Sanjay Sharma NITTTR, Chandigarh
- Shashwat Singh, Energy Simulation Expert Northumbria University, UK
- Dr. J.M. Mathur, MNIT Jaipur
- Dileep Singh, BoG, ASHRAE





- Ar. Bibhu K. Nayak, Associate Professor, Manipal University Jaipur
- Dr. Madhura Yadav, Professor & Dean, Faculty of Design, Manipal University Jaipur
- Dr. Abhishek Sharma, Professor, Manipal University Jaipur

5. Brief Description of the Event

School of Architecture & Design, Manipal University Jaipur organized a five-day Short-Term Programme titled “Energy Efficient and Innovative Construction Practices” in association with NITTR, Chandigarh. The STP aimed to introduce various Energy Efficient practices adopted in Building Construction. The Short-Term Programme was scheduled from 16th to 20th October 2023 in Hybrid mode. This event also helped to enhance the existing knowledge of various teachers and students to cater the new innovations in the field of architecture and design. The event received good feedback from faculty members and all the participants.

6. Brochure of the Event

	<p>ABOUT NITTR, CHANDIGARH Since its inception in 1967, NITTR (formerly TTTI) Chandigarh has made rapid strides in the areas of engineering and technology and emerging areas like computer, educational technology, entrepreneurship development, rural development, industry-institute interaction and educational management. Presently, the institute conducts more than 400 short-term training programmes annually for polytechnics and engineering colleges teachers, professionals and managers of industries. The institute also conducts a large number of AICTE sponsored Summer and Winter Schools every year. The institute offers six postgraduate programmes in engineering and engineering education through regular and modular modes. In addition to education and training programmes, the institute renders extension services to Polytechnics, undertakes research and development projects and develops print and non-print instructional material.</p>	<p>SHORT TERM PROGRAMME ON ENERGY EFFICIENT AND INNOVATIVE CONSTRUCTION PRACTICES</p> <p>From- 16-20 October, 2023</p> <p>ORGANISED BY</p>  <p>School of Architecture & Design Faculty of Design & MUJ-TEC Manipal University Jaipur [University under Section 2(f) of UGC Act] Dehmi Kalan, Off Jaipur-Ajmer Expressway, Jaipur, Rajasthan</p> <p>In Collaboration with</p>  <p>National Institute of Technical Teachers' Training and Research [Ministry of Human Resource Development, Govt of India] Sector 26, Chandigarh 160 019</p> <p>Venue- Manipal University Jaipur</p>
<p>ABOUT MANIPAL UNIVERSITY Manipal University Jaipur (MUJ) has redefined academic excellence in the region and inspires students of all disciplines to learn and innovate through hands-on practical experience. Manipal University Jaipur (MUJ) was launched in 2011 on an invitation from the Government of Rajasthan, as a self-financed State University. MUJ has redefined academic excellence in the region, with the Manipal way of learning, one that inspires students of all disciplines to learn and innovate through hands on practical experience. Jaipur, being one of the fastest growing cities in India, has increasing demand for quality higher education in the region. Following an allotment of 122 Acres of land at Dehmi Kalan village near Jaipur, the permanent campus of the University has come up at a fast pace and is by far one of the best campuses in the region. The multi-disciplinary university offers career-oriented courses at all levels, i.e., UG, PG and doctoral and across diverse streams, including Engineering, Architecture, Planning, Fashion Design, Interior Design, Fine Arts, Hospitality, Humanities, Journalism and Mass Communication, Basic Sciences, Law, Commerce, Computer Applications, Management, etc. Some PG programmes are also available in the research mode. The university has been granted the ATAL Incubation Centre, funded by Niti Aayog, Government of India.</p>	<p>ABOUT SCHOOL OF ARCHITECTURE AND DESIGN, FACULTY OF DESIGN, MUJ School of Architecture & Design, Jaipur encapsulates the philosophy of creating innovators, empowered with the knowledge for the creation of a dynamic world, pulsating with intellectual acuity and striving for the utopia of a prosperous biosphere for all. The School strives to provide world-class architectural education by coupling state-of-art facilities with a dedicated and experienced faculty team and student-centric academic practices. Also, owing to the location, we have a vantage point in understanding the state of Rajasthan, which is one of the richest states in India in terms of its culture and heritage. The School intends to create an archive of heritage documentation for the state and become forerunners in the conservation of cultural landscape and heritage of the region.</p>	
<p>ORGANISING COMMITTEE Coordinator Prof. (Dr.) Sunanda Kapoor, Head, School of Architecture & Design, Manipal University Jaipur Co-Coordinator Dr. Ashutosh Saini, Assistant Professor, School of Architecture & Design, Manipal University Jaipur Contact: ashutosh.saini@jaipur.manipal.edu</p>	<p>ADDRESS FOR CORRESPONDENCE Dr. Amit Goyal, Assistant Professor Department of Civil Engineering National Institute of Technical Teachers' Training and Research, Sector 26, Chandigarh 160 019 Tel: 0172- 2759656, Mobile No- 09417569559 Fax: (0172) 2793893, 2791366 E-mail: amiteoyalamit23@gmail.com, amiteoyalamit@rediffmail.com.</p>	

<p>INTRODUCTION AND OBJECTIVES</p> <p>The importance of energy efficient and green buildings has assumed great urgency today. In light of fast depleting energy resources, energy scarcity and increasing environmental pollution, innovative ways to cut down energy consumption are necessary. The construction industry is one of the largest energy consuming sectors. In modern buildings significant amounts of energy are also consumed to keep the building environment comfortable. Estimates suggest that about 20-25 percent of the total energy demand is due to manufacturing materials required in the building sector, while another 15 percent goes into the running needs of the building like lighting, air-conditioning, room heating and ventilation etc. Increased development of housing and commercial buildings has imposed immense pressure on our dwindling energy sources. The availability of energy is limited and known resources of energy are exhausting fast. Therefore, energy efficiency is assuming importance in different sectors. In view of the global energy crisis and increasing energy demand is expected to continue and apart from possible end-use restrictions, energy efficiency and energy management is essentially required.</p> <p>COURSE CONTENTS</p> <ul style="list-style-type: none"> ➤ Basic Knowledge of Energy Efficient Buildings ➤ Planning and Preparedness ➤ Solar Passive Architecture ➤ Vastu Shastra Myths and Realities ➤ Innovative Practices/Research in Green Buildings ➤ Green buildings-Design and Construction ➤ Energy efficiency in old traditional buildings ➤ Solar Devices and their Utilization <p>COORDINATORS</p> <p>Programme Coordinator : Dr. Amit Goyal, Assistant Professor, Department of Civil Engineering, NITTR, Chandigarh Dr. Sanjay Sharma, Professor, Department of Civil Engineering, NITTR, Chandigarh</p> <p>Local Coordinators : Coordinator Prof. (Dr.) Sunanda Kapoor, Head, School of Architecture & Design, Manipal University Jaipur Contact: sunanda.kapoor@jaipur.manipal.edu Co-Coordinator Dr. Ashutosh Saini, Assistant Professor, School of Architecture & Design, Manipal University Jaipur Contact: ashutosh.saini@jaipur.manipal.edu</p>	<p>METHODOLOGY</p> <p>The one-weeks programme will be judiciously utilized by integrating theory classes, practicals, field visits, audio-visual presentations and educational video films shows. In order to make the programme participatory, group discussions and project formulations exercises will also be done. Besides the institute faculty, experts will be invited from research and development organizations, science and technology departments, working on green and energy efficient buildings.</p> <p>TARGET GROUP</p> <p>Faculty members of all Engineering Disciplines, Architectural, Management and Humanities streams working in an AICTE approved engineering college/institute can participate in this programme. These faculty members have to get themselves sponsored from the Principal/Head of Institution and register themselves on NITTR Chandigarh Website at www.nittrchd.ac.in [Note: Seats are limited, please get your admission confirmed in advance].</p> <p>LAST DATE</p> <p>Last date of registration for participation in this training programme is 15 October, 2023.</p> <p>REGISTRATION</p> <p>Fee of Rs 118/- is chargeable from the participants engineering college teachers whose names are sponsored by the competent authority (Principal / Director). Click on the following link to register: https://fdp.nittrchd.ac.in/backingup/</p> <p>After successful registration, email the registration form and payment receipt to amitagoyalmit23@gmail.com</p> <p>TADA</p> <p>3 tier AC train travel will be paid to the participants of Govt. Institutes by NITTR, Chandigarh.</p> <p>ACCOMMODATION</p> <p>Accommodation to the participants shall be provided on payment basis.</p> <p>VENUE</p> <p>Room No. 201, Lecture Hall, Second Floor, School of Architecture and Design, Dome Building, Manipal University Jaipur.</p>	<p>SHORT TERM PROGRAMME on Energy Efficient and Innovative Construction Practices at Faculty of Design, Manipal University Jaipur 16-20 October, 2023</p> <p>Name: _____</p> <p>Age: _____ Sex: Male <input type="checkbox"/> Female <input type="checkbox"/></p> <p>Qualification: _____</p> <p>Designation: _____</p> <p>Experience (Teaching/Industrial/Others): _____</p> <p>Institution: _____</p> <p>Address: _____</p> <p>Phone No. with STD Code _____</p> <p>E-Mail : _____</p> <p>Whether Accommodation Needed: Yes <input type="checkbox"/> No <input type="checkbox"/></p> <p>Signature of the Applicant _____</p> <p>Recommendation of the Principal/Head of the Sponsoring Institute (Signature with seal) [Last Date of Submission of Application is 15 October, 2023]</p>
--	--	---

7. Photographs of the Event



Figure 1: Inauguration Ceremony

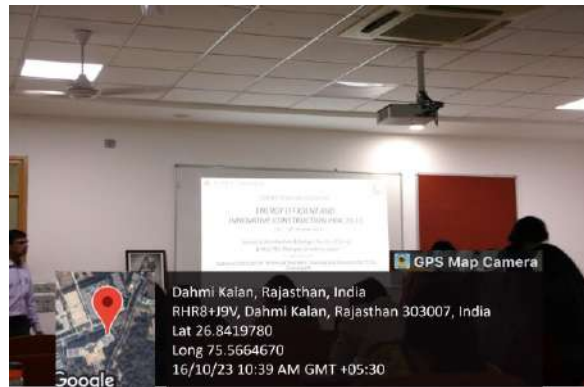


Figure 3: Registrations



Figure 2: Lamp Lighting by Dr. Sunanda Kapoor



Figure 4: Introduction to the STP

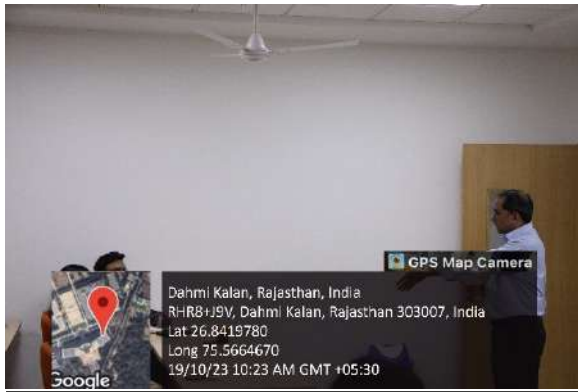


Figure 5: Expert Lecture by Dr. J.M. Mathur

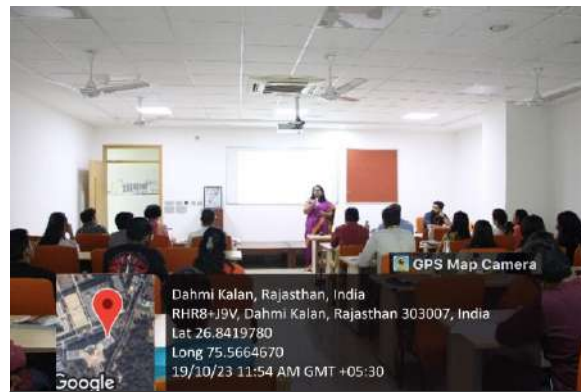


Figure 9: Expert Lecture by Dr. Madhura Yadav



Figure 6: Introduction to STP by Dr. Madhura



Figure 10: Expert Talk by Ar. Sneha Singh



Figure 7: Expert Talk by Dr. Subhash Devrath



Figure 11: Expert Lecture by Dr. Abhishek



Figure 8: Felicitation of Dr. Amit Goyal



Figure 12: Group Photograph post STP

8. Schedule of the Event

**Short Term Programme on 'Energy Efficient and Innovative Construction Practices'
From 16-20 October 2023 at Manipal University Jaipur**

Day/Date	SESSION – I	SESSION – II	1.00 to 2.30 pm	SESSION – III
	10.00 am to 11.30 am	11.30 am to 1.00 pm		2.30 pm to 4.00 pm
Monday 16.10.2023	Registration / Inauguration	Innovation in Clean Construction of Masonry Houses Dr. Amit Goyal NITTTR, Chd	L U N C H B R E A K	Bioinspired building facade design Shashwat Singh Energy Simulation Expert Northumbria University, UK
TUESDAY 17.10.2023	Design in Motion Ar. Bibhu K. Nayak Associate Professor, Manipal University Jaipur	Energy Efficiency HVAC system Expert in efficient HVAC systems Dileep Singh, BoG, The American Society of Heating, Refrigerating and Air-Conditioning Engineers (ASHRAE)		Sustainable Material for Net Zero Arun Jain , Energy expert in Efficient Building techniques BoG The American Society of Heating, Refrigerating and Air-Conditioning Engineers (ASHRAE)
WEDNESDAY 18.10.2023	Building Materials for Green construction Dr. Sanjay Sharma NITTTR, Chd	New Innovation in Earthquake Resistant Clean Construction of Masonry Houses Dr. Amit Goyal NITTTR, Chd		Field Visit to Trinity Aurum C-Scheme Jaipur, first gold rated green building by IGBC in Rajasthan Dr. Amit Goyal NITTTR, Chd
THURSDAY 19.10.2023	Energy consumption in Residential Buildings Dr. J.M. Mathur, MNIT Jaipur	The Energy-Saving Potential of Bamboo-based Materials Dr. Madhura Yadav, Professor & Dean, Faculty of Design, Manipal University Jaipur		Passive Strategies in Architectural Design Dr. Tarush Chandra Expert: Urban Planning MNIT Jaipur
FRIDAY 20.10.2023	Simplified metrics and workflows for microclimate responsive urban buildings design Mr. Naga Vankata Sai Kumar Expert: Energy Simulation Software, Environmental Performance and Design Lab (EPDL), Technion-Israel Institute of Technology	Biochar as construction material for sustainable buildings: From Production to Application Dr. Abhishek Sharma, Professor, Manipal University Jaipur		Group Discussion Valedictory Session

9. Attendance of the Event

*Please see the annexure no. 1

10. Weblink

11. Event Coordinators

- Dr. Amit Goyal, NITTTR Chandigarh
- Prof. Sunanda Kapoor (Professor & Head, SA&D)
- Dr. Ashutosh Saini (Assistant Professor, SA&D)



Prof. (Dr). Sunanda Kapoor
Head, Architecture (SA&D, MUJ)



Dr. Ashutosh Saini
Assistant Professor



Annexure: 1

REGISTRATION & ATTENDANCE SHEET

NITTTR CHANDIGARH
CIVIL ENGINEERING DEPARTMENT
STC ON "ENERGY EFFICIENT AND INNOVATIVE BUILDING CONSTRUCTION PRACTICES"
FROM 16th to 20th OCTOBER, 2023

Course Coordinator: Dr. Amit Goyal
Venue: MANIPAL UNIVERSITY JAIPUR

Sr. No.	Name (In English & Hindi), Designation & Official Address with E-mail and Contact no.	Gender M/F	Category Y/SC/ST/OBC/GEN	Spoken Letter Yes/No	Govt./Aided/Self-Financed	Signature				
						First Day	Second Day	Third Day	Fourth Day	Fifth Day
1.	Dr. Mougeh Sharma Asst. Prof. NSUT, New Delhi Mougeh.sharma@nsut.ac.in 91143-12189.	M	GEN	Yes.	Govt.					
2.	Dr. Sunanda Kapoor Professor Manipal University Jaipur 9872663383	F	GEN	Yes	self financed					
3.	Dr. Ashutosh Saurvi Asst. Professor Manipal University Jaipur, 7012150626	M	OBC	Yes	Self-Financed					
4.	Susmit Sharma Ph.D Scholar MNIT Jaipur 8219124070	F	GEN	Yes	Govt.					
5.	Ar. Siddharth Mishra MUS 9475790100	M	GEN	Yes	Self-Financed					

Head, School of Architecture & Design
Faculty of Design
Manipal University Jaipur





14.	Siddharth Mahila Asst Prof 9549060411	M	GEN.	Yes	Self Finance	Siddharth	Siddharth	Siddharth	Siddharth	Siddharth	Siddharth	Siddharth	Siddharth	Siddharth	Siddharth	Siddharth	Siddharth	Siddharth
15.	AR. SANJEEV PAREEK ASSISTANT PROFESSOR SAKD, MUJ	M	Gen	YES	SELF FINA	---	---	---	---	---	---	---	---	---	---	---	---	---
16.	ANMETHA BUAZI M.EDS STUDENT	F	Gen	Yes	Self Finance	---	---	---	---	---	---	---	---	---	---	---	---	---
17.	Shravya Chauhan M. Des. Student 2524595535	F	Gen	Yes	Self Finance	---	---	---	---	---	---	---	---	---	---	---	---	---
18.	SANA SHAIKH M. DES STUDENT	F	Gen	Yes	---	---	---	---	---	---	---	---	---	---	---	---	---	---
19.	KANIKSHA MALE M. DES (STUDENT)	F	Gen	Y	Self	---	---	---	---	---	---	---	---	---	---	---	---	---
20.	Dr. Subhadra Chandra Devs off	M	Gen	Yes	Self	---	---	---	---	---	---	---	---	---	---	---	---	---
21.	Ramrak Prasad Asst. Professor SAKD MUJ	M	Gen	Yes	Self	---	---	---	---	---	---	---	---	---	---	---	---	---

Head, School of Architecture & Design
Faculty of Design
Manipal University Jaipur




22.	SNIPSA Grosswami Ph.D, MNIT Jaipur	F	ONLINE	₹	P	P	P	P	P	P	P	P	P	P	P	P	P	P	P
23.	Prabhakar Chaturvedi Ph.D. MNIT Jaipur	M	ONLINE		P	P	P	P	P	P	P	P	P	P	P	P	P	P	P
24.	Yogesh Kumar Assistant Professor. PPSUD, Sonat	M	ONLINE		P	P	P	P	P	P	P	P	P	P	P	P	P	P	P
25.	Vijay Lalchandani Assistant Professor LPU	F	ONLINE		P	P	P	P	P	P	P	P	P	P	P	P	P	P	P
26.	Vishalendra Samant Kumar Assistant Professor. SSPA, Maharashtra	F	ONLINE		P	P	P	P	P	P	P	P	P	P	P	P	P	P	P
27.	Rajshankar Saini Ph.D Scholar Shodhi University, H.P.	F	ONLINE		P	P	P	P	P	P	P	P	P	P	P	P	P	P	P
28.	Hemant Kumar Ph.D Scholar IIT Kharagpur.	M	ONLINE		P	P	P	P	P	P	P	P	P	P	P	P	P	P	P
29.	Rajesh Sharma Ph.D. Scholar MNIT Jaipur.	F	ONLINE		P	P	P	P	P	P	P	P	P	P	P	P	P	P	P

Head, School of Architecture & Design
Faculty of Design
Manipal University Jaipur



30.	Satish Kumar Faculty Professor Associate Professor SIIPNA School of Health & Architecture Ph.D. Designer NIT Hanuipur	M	ONLINE		P	P	P	P	P	P	P	P	P	P	P	P	P	P
31.	Priyanka Sharma Ph.D. Designer NIT Hanuipur	F	ONLINE		P	P	P	P	P	P	P	P	P	P	P	P	P	P

Verified by:






Name & Signature of :
Head of School of Architecture & Design
Faculty of Design
Manipal University Jaipur







Research papers

Expanded waste glass/methyl palmitate/carbon nanofibers as effective shape stabilized and thermal enhanced composite phase change material for thermal energy storage

P. Singh^a, R.K. Sharma^a  , Gökhan Hekimoğlu^b  , Ahmet Sarı^{b,c}, Osman Gencel^d, V.V. Tyagi^e

[Show more](#) 

 Share  Cite

<https://doi.org/10.1016/j.est.2023.107205> 

[Get rights and content](#) 

Highlights

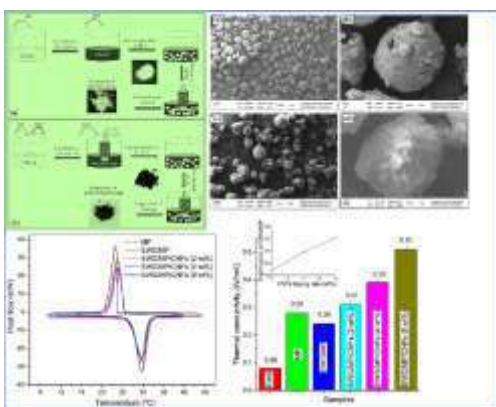
- The performance of shape stabilized PCMs with expanded waste glass and carbon nanofibers was investigated.
- Shape stabilized composites were prepared by impregnation of MP with EWG and CNFs.
- The melting temperature is in the range of 26.61–27.12°C. and melting enthalpies ranges from 96.1–96.7 J/g.
- The TGA outcomes illustrated that FSCPCM and TE-FSCPCMs had well thermal resistance.

- Thermal conductivities of FSCPCM were increased apparently especially with CNF (8 wt.%) incorporation.

Abstract

A prominent choice for phase change materials (PCMs) for passive solar thermoregulation is fatty acids because of their many beneficial characteristics for latent heat thermal energy storage (LHTES). Their low thermal conductivity and additional storage container requirements to prevent leaks during heating time, however, severely restrict their range of applications. In order to address these issues with methyl palmitate (MP) as a phase transition material, it was first doped with carbon nanofibers (CNFs) after being incorporated with expanded waste glass (EWG) using the melting/blending procedure. The SEM, XRD, FTIR, DSC, and TGA techniques were used to investigate the thermal and chemical performance of composite phase change materials (CPCMs). The leak-proof composite phase change materials (LPCPCM) and thermal enhanced shape stabilized composite phase change materials (TE-SSCPCMs) had latent energy between 96.1 and 96.7 J/g and melting temperatures between 26.61 and 27.12 °C. Doping 2, 4, and 8 wt% of CNFs into CPCMs, conductivity got enhanced by 29.2, 62.5, and 112.5% respectively, due to which, the TE-SSCPCM's charging/discharging periods were significantly shortened without changing their LHTES properties much. Further, evidence came from the thermal cycling test, TGA results, and the impressive thermal reliability, LHTES cycle performance, and chemical compatibility of all manufactured composites.

Graphical abstract



[Download: Download high-res image \(299KB\)](#)

[Download: Download full-size image](#)

Introduction

Due to the fact that about one-third of the world's total energy consumption occurs in buildings [1], the upgrade of resource efficiency has emerged as one of the energy technologist's primary concerns. In this context, thermal energy storage (TES) has emerged as a viable alternative methodology for addressing technology and environmental pollution issues within the last three decades [2]. PCMs and LPCPCMs with good thermal durability and performance have been deemed desirable TES components with energy storing and releasing capacity [3], [4]. The focus of several energy studies in recent years has shifted toward the creation of cutting-edge PCMs and LPCPCMs as well as the examination of their temperature control characteristics [5], [6], [7], [8], [9]. It has been found that fatty acids perform well for solar passive LHTES purposes as PCMs due to their desirable and readily available LHTES features [10], [11]. Nevertheless, direct functioning of these organic PCMs permits chemical interlinkage with the surroundings and also results in a leakage issue in solid to liquid state transition. They were enclosed in macro or micro configurations to avoid this complexity [12], [13]. However, PCM encapsulations are significantly more difficult and expensive, resulting in generally poor LHTES capacity. Combining porous, lightweight, and less costly building materials with LPCPCMs that are resistant to leakage is an alternative method. Moreover, fatty acids have a disadvantage of poor thermal conductivity (between 0.15 and 0.25 W/m-K), which significantly affects their rates of phase change (heat charging/discharging) [14]. Furthermore, their incorporation into stabilized clay-based porous building matrices can result in a significant decline in conductivity. Thus, doping this type of LPCPCM with a high thermal conductive material is an effective way for boosting its thermal conductivity. Materials based on carbon such as carbon nanofibers (CNFs) [15], [16], [17], carbon nanotubes (CNTs) [18], [19], expanded graphite [20], graphite nanoplatelets (GNPs) [21], and graphene oxide [22] have primarily been used to increase the thermal conductivity of organic PCMs. CNF is a material that looks and acts like graphite. It is made by carbonating and graphitizing organic fibers. At the atomic level, each CNF is made up of thousands of small fibers that are stacked on top of each other. The carbon atoms in each fiber are organized in a hexagonal pattern. CNF had nearly the same thermal conductivity, resistance to corrosion, durability, and ability to heat energy conversion as carbon nanotubes and graphene, but it was cheaper [23], [24]. So, CNF has gotten a lot of attention as an additive to improve the properties of composite materials [25], [26], [27]. The purpose of this research is to investigate the effect of CNFs on thermal outcomes of LPCPCMs. CNF is an inorganic carbon fiber compound that can have a thermal conductivity up to 900 W/m-K in the same plane. The CNF's percolating configuration worked as a filler with significant thermal conductivity [28]. Huang et al. [16] used the 5wt% CNF in cetyl alcohol/HDPE composite which increased the thermal conductivity of composite by 1.25 times as compared to original composite thermal conductivity. Liu et al. [17] reported that the thermal conductivity of PEG/SiO₂ composite was increased by 73% due to the incorporation of

3wt% CNFs. Zhang et al. [29] boosted the thermal conductivity of erythritol as about 407.8% by incorporating CNFs by 10wt% mass fraction. As distinct from the aforementioned literature, our aim is to develop a way to both alleviate the leakage issue and the poor thermal conductivity limitation of MP organic PCM without significantly diminishing its LHTES capability. EWG was chosen as an appropriate supporting material to eliminate the PCM's seepage problem due to its numerous positive qualities, such as its high absorption ratio, excellent thermal stability, good interfacial bonding, and long-term economic and ecological friendliness [30]. In the initial stage of the present research, MP, an organic PCM, was integrated into EWG by melting/blending process to create a new LPCPCM. Considering the poor thermal conductivities of the base materials of LPCPCM (0.28 and 0.08 W/m-K for MP and EWG, respectively), the thermal conductivity of LPCPCM was significantly enhanced by loading with CNFs at mass fractions of 2.0, 4.0, and 8.0wt% in the subsequent phase. Using SEM, XRD, and FT-IR, the chemical and morphological features of the produced LPCPCM and TE-SSCPCMs were characterized. The impact of CNFs loading on the thermal conductivities, LHTES characteristics, thermal compatibility, and energy charging and discharging durations of manufactured LPCPCM was studied. A comprehensive study on EWG/MP/CNFs composite has not yet been published, as far as we are aware.

Access through your organization

Check access to the full text by signing in through your organization.

Access through [Manipal University Jaipur](#)

Section snippets

Materials

Methyl palmitate (MP) was procured by Sigma-Aldrich company. Ethanol used as solvent was provided by Merck Company. Expanded waste glass (EWG) was purchased from Agrekal Company (Antalya-Turkey). Moreover, Carbon nanofibers (CNFs) in this work were purchased from Sigma-Aldrich Company. ...

Preparation of LPCPCM and TE-SSCPCM

By using the melting/blending method, the leak proof composite PCMs (LPCPCMs), EWG/MP and EWG/MP/CNFs were created in shape stabilized form. Following the procedure shown in Fig. 1, EWG/MP was prepared as a shape ...

SEM results of the prepared LPCPCM and TE-SSCPCM

Fig. 3(a-e) depicts SEM images of the EWG, FSCPCM, and TE-FSCPCM-3, which is representative of the other TE-FSCPCMs. As demonstrated in Fig. 3(a, b), the surfaces of EWG are composed of agglomerates of amorphous particles. However, these molecules have an interlinked phase picture, some of them feature holes and fissures that allow PCM molecules to be retained.

The PCM was kept uniformly within the perforations on the surface of the EWG (Fig. 3(c, d)). The CNFs with 8wt% introduced uniformly ...

Conclusions

To concurrently address the leakage problem and low thermal conductivity of MP, it was initially kept in EWG using the melting and blending technique and then loaded with CNFs. The morphology, physicochemical suitability, LHTES characteristics, conductivities, cycle TEST performances, and thermal reliabilities of LPCPCMs and TE-SSCPCMs were analyzed. The following inferences can be taken from the findings:

1. The maximum amount of MP that EWG was able to absorb was 40% by weight. Shape-stabilized ...

...

CRedit authorship contribution statement

P. Singh- Writing - Original draft, Formal analysis

R. K. Sharma- Project administration, Formal analysis

Gökhan Hekimoğlu- Validation

Ahmet Sarı- Visualization

Osman Gencel- Formal analysis

V. V. Tyagi- review & editing ...

Declaration of competing interest

The authors declare that they have no known competing financial interests or personal relationships that could have appeared to influence the work reported in this paper. ...

References (47)

K. Faraj *et al.*

[A review on phase change materials for thermal energy storage in buildings: heating and hybrid applications](#)

J. Energy Storage (2021)

R.A. Lawag *et al.*

[Phase change materials for thermal management and energy storage: a review](#)

J. Energy Storage (2022)

K. Lafdi *et al.*

[Graphite foams infiltrated with phase change materials as alternative materials for space and terrestrial thermal energy storage applications](#)

Carbon (2008)

P. Singh

[Development and characterization a novel leakage-proof form stable composite of graphitic carbon nitride and fatty alcohol for thermal energy storage](#)

J. Energy Storage (2022)

X. Zhang

[Form stable composite phase change materials from palmitic-lauric acid eutectic mixture and carbonized abandoned rice: preparation, characterization, and thermal conductivity enhancement](#)

Energy Build. (2017)

M. Jafaripour *et al.*

[Fabrication and optimization of kaolin/stearic acid composite as a form-stable phase change material for application in the thermal energy storage systems](#)

J. Energy Storage (2021)

Y. Konuklu *et al.*

[Microencapsulation of caprylic acid with different wall materials as phase change material for thermal energy storage](#)

Sol. Energy Mater. Sol. Cells (2014)

T.D. Dao *et al.*

[A Pickering emulsion route to a stearic acid/graphene core-shell composite phase change material](#)

Carbon (2016)

A. Elgafy *et al.*

[Effect of carbon nanofiber additives on thermal behavior of phase change materials](#)

Carbon (2005)

X. Huang *et al.*

[Microstructure and thermal properties of cetyl alcohol/high density polyethylene composite phase change materials with carbon fiber as shape-stabilized thermal storage materials](#)

Appl. Energy (2017)



[View more references](#)

Cited by (11)

[Carbon-based porous materials for performance-enhanced composite phase change materials in thermal energy storage: Materials, fabrication and applications](#)

2025, Journal of Materials Science and Technology

[Show abstract](#)

[Polypyrrole-modified flax fiber sponge impregnated with fatty acids as bio-based form-stable phase change materials for enhanced thermal energy storage and conversion](#)

2024, Journal of Energy Storage

[Show abstract](#)

[3D-printed polylactic acid-microencapsulated phase change material composites for building thermal management](#)

2024, Renewable and Sustainable Energy Reviews

[Show abstract](#)

Heat transfer performance enhancement and mechanism analysis of thermal energy storage unit designed by using a modified transient topology optimization model

2024, Journal of Cleaner Production

[Show abstract](#) ✓

Preparation and characterization of lauric acid-stearic acid/fumed silica/expanded graphite thermally conductive enhanced composites

2023, Journal of Energy Storage

[Show abstract](#) ✓

Waste polyvinyl chloride derived latent thermal energy storage composites for waste heat recovery via packed bed system

2023, Journal of Cleaner Production

[Show abstract](#) ✓



[View all citing articles on Scopus](#) ↗

[View full text](#)

© 2023 Elsevier Ltd. All rights reserved.





ELSEVIER

All content on this site: Copyright © 2024 Elsevier B.V., its licensors, and contributors. All rights are reserved, including those for text and data mining, AI training, and similar technologies. For all open access content, the Creative Commons licensing terms apply.





5E analysis of a novel designed hot water storage header integrated vacuum tube solar water heater

K. Chopra ^{a d}, V.V. Tyagi ^b  , Sudhir Kumar Pathak ^b, Ravi Kumar Sharma ^c,
Muhamad Mansor ^{d e}, Varun Goel ^f, Ahmet Sari ^{g h}

Show more 

 Share  Cite

<https://doi.org/10.1016/j.tsep.2023.101929> 

[Get rights and content](#) 

Highlights

- 5-E analysis of a novel designed hot water storage header integrated system.
- Thermal and exergy outputs of the system varied by 63–74% and 4–10% respectively.
- Hot water cost by designed & electric heater is 0.15 & 0.47 INR/L respectively.

Abstract

In this study, 5-E analysis of a heat pipe equipped vacuum tube collector system for residential warm water application has been carried out. The issue of overheating in heat pipes and low thermal efficiency is the major key issues associated with heat pipe

vacuum tube collector. This design completely removes the problem of overheating. In addition to this copper fins mounting with condensers of heat pipe enhance the heat transmission rate between the condenser & water stored in a manifold. The results of an experimental investigation reveal that thermal and exergy outputs of the proposed system were obtained almost 63–74% and 4–10% respectively. The average energy gain at the end of the days selected for Run-A, B, and C was calculated to be 7505, 6912, and 6619kJ respectively, whereas the average exergy gain for corresponding runs was found to be 928, 700, and 401 kJ respectively. In addition to this, the proposed system can provide hot water of approximately 125 L, 76 L, and 52 L in temperatures 50°C, 55°C, and 60°C respectively.

Concerning to techno-economic investigation, the per liter cost of warm water generation for the proposed & electric geyser was observed to be 0.15 INR/L & 0.47 INR/L respectively. The levelized energy cost, net present worth, and payback time were found to be 5.48 INR/kWh, 55,819 INR, and 4.12years respectively. The amount of CO₂ mitigation by the developed system was found to be 18.76, 17.28, and 16.54 tCO₂/lifetime for Run-A, B & C respectively.

Introduction

In today's era, non-conventional energy sources utilization has increased rapidly because of the incessant exhaustion of conservative fuels. Among available renewable power sources, solar energy is quite fascinating and promising energy source due to its huge accessibility in maximum parts of the earth free of cost [1]. Solar energy is mainly harnessed in two forms: (i) solar energy is directly changed into electricity using a photovoltaic device (ii) solar energy is transformed into heat energy using thermal collectors [2], [3], [4]. Solar energy can be utilized in several applications like water/air heating, and crop drying. In all solar thermal applications, water heating is consuming a huge amount of conventional energy that will lead to a rise in greenhouse gas (GHG) emissions. Solar heat collectors, which are mostly utilized for water heating, are called solar water heaters. Generally, two types of collectors: vacuum tube collectors & flat plate collectors (FPCs) are utilized for hot water production [5], [6]. The ETCs are dominating the FPCs due to their higher thermal output in cold regions. Also, the convective heat losses are minimum in evacuated tube collectors. Currently, 80–85% of total installed solar collectors are ETCs. Moreover, the ETCs can warm the water to 90°C comparatively at a low cost. Thus, ETC is a promising technology, which can be implemented for hot water applications in fluctuating weather conditions [7], [8].

Nowadays, different designs of vacuum tube collectors are mainly utilized for hot water production. Among these, heat pipe-based vacuum tube collectors are the most efficient and advanced in technology because heat pipe is an efficient heat exchanger unit. Many

researchers have completed various studies on different designs of heat pipe-based vacuum tube collectors for hot water generation. Işka and Yldzba [9] designed a unique hot water collector tank with a novel finned-type cell construction. The performance of the newly developed tank was compared with a PCM-embedded nonfinned tank & a normal insulated tank. The outcomes reveal that the newly constructed tank's thermal energy storage ability is roughly 10% higher than the normal tank and, almost 4–5% more in comparison to a non-finned water tank. Khani et al. [10] evaluated that the integrated system's three-objective optimization decrease reduces environmental impacts, total costs, and monthly environmental emergency rate by 34.31%, 11.4%, and 6.38%, respectively. Nitsas and Koronaki [11] experimentally investigated U-Tube solar vacuum collector in terms of exergy efficiency, energy efficiency, and heat energy output. The results indicate that collector thermal efficiency was 60% and the system gained the highest heat energy output of 5.60kW at approximately noon. The authors observed the highest exergy gain when the temperature of the working fluid was highest. By utilizing a variety of heat-carrying fluids and variable flow rates, the thermal output of a heat pipe-equipped SWH was improved by Shafieian et al. [12]. The different cases, i.e., a flexible flow of nanofluid (Case-I), a fixed flow of nanofluid (Case-II), and a fixed flow of DI water (Case-III), all performed under similar climatic conditions. The exergy output of Cases I and II was found to be higher than Case III by 2.66% and 1.58%, respectively. Al-Joboory [13] performed experiments with two identical ET-SWHs. The first system employs thermosyphon; the second employs twenty wickless heat pipes filled with methanol (50%) as working fluid and serve as heat conductors from the collector to the storage tank. The test results found that the wickless heat pipe system outperforms the thermosyphon one in terms of overall daily efficiency by 22.5% for zero loads, 42.5% for fluctuating loads, and 32.4% for constant loads. The heat pipe based SWH was more suited to local domestic use because it produced higher temperatures and thermal output under all loads and adverse weather situations. Ozsoy and Corumlu [14] analyzed the energy output of a thermosyphon heat pipe (THP) based ETSC using nanofluid (silver-water) used in viable applications. It was discovered that the THP filled with nanofluid upheld its enhanced heat transmission ability. Nanofluid improved the collector efficiency by 20.7% to 40% more than water. The experiment's findings indicate that the THP ETSC can be marginally improved by using silver-water nanofluid. Maraj et al. [15] performed the energy study of a forced flow SWH with an HP-ETC (area of 1.476m^2) in Mediterranean environmental conditions. For a solar collection of 2,212 kWh/year, they determined that the yearly valuable heat gain of the HP-ETC, the valuable energy delivered to the storage tank by the collector, and the delivered energy to the heat consumer were 1,345, 1,311, and 1,009 kWh/year. The forced circulated system had an annual efficiency of 0.516 compared to the HP-ETC's 0.62. Jayanthi et al. [16] performed an experiment to determine the thermal output of a HP-ETSC using DI water and R134a as the heat transfer fluid. The impact of input variables on the thermal output of the

HPSC, such as temperature distribution and time, was looked into, compared, and discussed. The findings revealed that using R134a in place of distilled water increases the HPSC's thermal output. Chopra et al. [17] done the exergy, energy, and financial investigation of the vacuum collector based SWH system for the complex climate of Jammu (India). The system was designed and built for a six-person family. The tests were carried out for six flow rates of a fluid. The highest avg. energy and exergy outputs were 72% and 5.2%, at 20 LPH, while the lowest was 55% and 1.25% at 60 LPH. It was discovered that at 20 and 60 LPH, the max. and min. avg. outlet temperatures were 76.4 and 45 °C, respectively. It was discovered that the cost of producing hot water at the required temperature was 0.12, as opposed to 0.40 and 0.26 INR/L for electric and gas geysers, respectively. The return on investment of the SWH was 4 years, which is a much shorter period. Mehmood et al. [18] created a TRNSYS simulation prototype of an SWH system that uses evacuated tubes fitted with heat pipes and is hybridized with a backup of natural gas to deliver a continuous thermal energy supply. It was discovered that switching from a traditional (gas) water heater to a hybrid solar water heater could save 23% to 56% on backup fuel while also lowering greenhouse gas (GHG) emissions. The results revealed that the hybrid vacuum tubes-based SWH is more effective and eco-friendlier, with a benefit-cost ratio of 1.87, & would result in yearly natural gas savings of 8.79105 kWh, resulting in a reduction of 175.539 tCO₂ emissions. Bhowmik et al. [19] studied the thermal output of serpentine vacuum collector system for different tilt angles. They also validated the experimental results with outcomes obtained from computational fluid dynamics model. The results of CFD depicted that with increasing of diameter of U-Tube from 1/8–3/8" increased the net gain in temperature by 39%. They also concluded that twisted taped with square holes among the various considered geometries observed to be most effective in terms of thermal output in comparison to plain serpentine design. Kuang et al. [20] used convolutional Neural Network technique to forecast the thermal output of vacuum collector system on the basis of collected operational data over many days. Authors concluded that Back Propagation (BP) neural network model having high accuracy than Multiple Linear Regression model. Also Multiple Linear Regression model is not suggested to be used for the evaluation of the performance of vacuum tube collector system because of its inability to handle non-linear problem results in poor accuracy. Modabber and Manesh [21] found that by integrating of solar heating and inlet air cooling system with the existing cogeneration plant (generation of power with hot water), energy performance touch 68% and increase in exergy efficiency was 50%, also reduced the impact of environmental. Haghghi et al. [22] evaluated the thermal performance, environmental and economic aspects of flat plat collector integrated with conventional heating system (run on natural gas). The experimental results revealed that the maximum load of 91.05 and 37.52 kW in cold and warm days respectively can be accomplished by flat plat collector with area of 443.8 and 63.3 m² respectively. In addition to this, they determined that deployment of flat plat

collector reduced the carbon dioxide emission of 84.71 and 84.67kg/MWh in warm and cold seasons respectively.

In the present study, a 5-E analysis of the novel designed hot water storage header integrated vacuum tube solar water heater is carried out. On the basis of the previous research work in the concerned field, the authors find the uniqueness of the present work as:

- 6 In this study, the author has uniquely designed the water storage tank cum header of the heat pipe based vacuum collector. An integrated finned heat exchanger is placed inside the header/water tank to increase the rate of heat transfer due to the welding of copper fins over the condenser of the heat pipe.
- 6 Based on the literature studies related to solar water heaters (summarized in Table 1) the energy efficiency of the proposed system fluctuates in the range of 63–74% which is more efficient than the conventional heat pipe system whose thermal efficiency fluctuates in the range of 42–56% [23]. Also, the increment in the energy gain of the designed system fluctuates in the range of 32–50%, which is higher as compared to the increment in energy gain reported in previous studies (Tabulated in Table 1).
- 6 In most of the existing studies, exergy, energy, and heat transfer investigation of vacuum collector have been done. But these methods do not consider the economic and environmental aspects. The economic and environmental exploration clarifies whether utilization of the proposed system is feasible in terms of the environmental and economic points of view or not. These aspects of the analysis of the system are crucial to be considered during its sustainability analysis. Therefore, in this study along with energy and exergy investigation, enviroeconomic, economic, and exergoeconomic analysis is also carried out for the practical implementation of the proposed solar water heater.
- 6 In the current study, modification in the vacuum collector system reduces the issue of overheating, decreases the overall heat losses and the initial financial investment in the vacuum collector system.

Access through your organization

Check access to the full text by signing in through your organization.

Access through **Manipal University** Jaipur

Section snippets

Experimental setup & methodology

This section is divided into two sub-sections. Firstly, the design and development of the experiment setup were explained comprehensively. Secondly, the research methodology adopted to perform the experiments has been discussed. ...

Thermodynamic, enviro-economic, and exergo-economic analysis

The present section is classified into three subsections namely energy and exergy analysis, enviroeconomic analysis, and exergoeconomic analysis. In the first subsection i.e. in section 3.1, the relations of energy and exergy investigation of designed and fabricated solar collector system has been given which is useful to access the quantitative and qualitative analysis of the designed system. In subsection 3.2, the equations which are useful to access the commercial viability of the designed ...

Experimental error analysis

The uncertainty related to a specific observation is calculated using Holman's Eq. can be given as:
$$\delta U = \left[\left(\frac{\partial U}{\partial x_1} \delta w_1 \right)^2 + \left(\frac{\partial U}{\partial x_2} \delta w_2 \right)^2 + \dots + \left(\frac{\partial U}{\partial x_n} \delta w_n \right)^2 \right]$$

Where $i = 1, 2, \dots, n$ and $U = U(x_1, x_2, \dots, x_n)$ are the independent variables, the dependent variable is x_i , and the independent variable's ambiguity is w_i . For instance, the error in temperature sensors is $\pm 0.6^\circ\text{C}$, whereas the solar power error is $\pm 1.2\%$, and the rotameter error is $\pm 1.5\%$ of the standard deviation.

$$\delta \eta_O = \eta_O \times \sqrt{\left(\frac{\delta EN_{u,O}}{EN_{u,O}} \right)^2 + \left(\frac{\delta EN_{inc,O}}{EN_{inc,O}} \right)^2} \quad \delta \eta_{ex, O} = \eta_{ex, O} \times \sqrt{\left(\frac{\delta EX_{u,O}}{EX_{u,O}} \right)^2 + \left(\frac{\delta E}{E} \right)^2} \dots$$

Result and discussion

The current section provides a compressive discussion of the results of different experiments. In this section, thermal analysis, thermodynamic analysis, financial analysis, enviroeconomic & exergoeconomic analysis of the proposed system for different runs have been presented and discussed. Section 5.1 discuss batch wise hot water temperature, ambient temperature & solar radiation variation with time, Section 5.2 deliberate energy and exergy efficiencies variation, Section 5.3 debate heat ...

Conclusions

The current study provides a compressive discussion of the results of thermal performance analysis, thermodynamic analysis, financial analysis, enviroeconomic & exergoeconomic analysis of the proposed system for different runs. Based on the analysis following observations have been pointed out which are as:

- a) Integration of novel designed manifold with a vacuum tube collector completely removes the problem of overheating. ...
- b) The copper fins mounting with condensers of the heat pipe enhance the ...

...

CRedit authorship contribution statement

K. Chopra: Conceptualization, Methodology, Writing – original draft, Writing – review & editing. **V.V. Tyagi:** Writing – review & editing, Supervision, Project administration.

Sudhir Kumar Pathak: Formal analysis, Writing – review & editing. **Ravi Kumar**

Sharma: Formal analysis. **Muhamad Mansor:** Writing – review & editing. **Varun Goel:**

Formal analysis. **Ahmet Sari:** Visualization, Writing – review & editing. ...

Declaration of Competing Interest

The authors declare that they have no known competing financial interests or personal relationships that could have appeared to influence the work reported in this paper. ...

Acknowledgments

- This work was supported by Tenaga Nasional Berhad (TNB) and UNITEN through the BOLD Refresh Postdoctoral Fellowships under the project code of J510050002-IC-6 BOLDREFRESH2025-Centre of Excellence. ...
- It was also supported by Shri Mata Vaishno Devi University, Katra (J&K) through the research project with unique ID RP-141 (Japan International Cooperation Agency Project for AUN/SEED-NET and the University of Malaya Malaysia). ...

...

References (38)

G. Hekimoğlu *et al.*

Thermal management performance and mechanical properties of a novel cementitious composite containing fly ash/lauric acid-myristic acid as form-stable phase change material

Constr. Build. Mater. (2021)

S. Kumar Pathak *et al.*

Recent development in thermal performance of solar water heating (SWH) systems

Mater. Today Proc. (2022)

M.A. Essa *et al.*

Experimental and Theoretical Analysis for the Performance of Evacuated Tube Collector Integrated with Helical Finned Heat Pipes using PCM Energy Storage

Energy. (2020)

N.B. Ziyadanogullari *et al.*

Thermal performance enhancement of flat-plate solar collectors by means of three different nanofluids

Therm. Sci. Eng. Prog. (2018)

A.K. Pandey *et al.*

Energy, exergy, exergoeconomic and enviroeconomic (4-E) assessment of solar water heater with/without phase change material for building and other applications: A comprehensive review

Sustain. Energy Technol. Assessments. (2021)

S. Faisal Ahmed *et al.*

Recent progress in solar water heaters and solar collectors: A comprehensive review

Therm. Sci. Eng. Prog. (2021)

A. Shafieian *et al.*

Strategies to improve the thermal performance of heat pipe solar collectors in solar systems: A review

Energy Convers. Manag. (2019)

S. Işık *et al.*

Improving thermal energy storage efficiency of solar collector tanks by placing phase change materials in novel finned-type cells

Therm. Sci. Eng. Prog. (2020)

N. Khani *et al.*

Optimal 6E design of an integrated solar energy-driven polygeneration and CO₂ capture system: A machine learning approach

Therm. Sci. Eng. Prog. (2023)

M.T. Nitsas *et al.*

Experimental and theoretical performance evaluation of evacuated tube collectors under mediterranean climate conditions

Therm. Sci. Eng. Prog. (2018)



[View more references](#)

Cited by (6)

Solar thermal potential of phase change material based U-pipe ETSCs for different climatic zones: Evaluating energy matrices and economic viability

2024, Sustainable Materials and Technologies

[Show abstract](#) ✓

Entropy weighted WASPAS and MACBETH approaches for optimizing the performance of solar water heating system

2024, Case Studies in Thermal Engineering

[Show abstract](#) ✓

Solar Water Heating System with Absorption Heat Transformer for Annual Continuous Water Heating ↗

2024, Processes

Design consideration of a filled layer U-pipe evacuated tubular solar collector with flat diffuse reflector: energy and exergy analysis ↗

2024, International Journal of Ambient Energy

Improving the Performance of Unglazed Solar Air Heating Walls Using Mesh Packing and Nano-Enhanced Absorber Coating: An Energy–Exergy and Environmental Assessment ↗

2023, Sustainability (Switzerland)

High Pressure Water Solar Collector as Potential of Mini Steam Power Plant in Iraq ↗

2023, ISAS 2023 - 7th International Symposium on Innovative Approaches in Smart Technologies, Proceedings

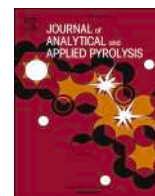
[View full text](#)

© 2023 Published by Elsevier Ltd.



All content on this site: Copyright © 2024 Elsevier B.V., its licensors, and contributors. All rights are reserved, including those for text and data mining, AI training, and similar technologies. For all open access content, the Creative Commons licensing terms apply.





Enhancing the pyrolytic conversion of biosolids to value-added products via mild acid pre-treatment

Ibrahim Gbolahan Hakeem^{a,b}, Pobitra Halder^{b,c}, Savankumar Patel^{a,b}, Abhishek Sharma^{b,d}, Rajender Gupta^e, Aravind Surapaneni^{b,f}, Jorge Paz-Ferreiro^a, Kalpit Shah^{a,b,*}

^a Chemical and Environmental Engineering, School of Engineering, RMIT University, Melbourne, VIC 3000, Australia

^b ARC Training Centre for the Transformation of Australia's Biosolids Resources, RMIT University, Bundoora, VIC 3058, Australia

^c School of Engineering, Deakin University, VIC 3216, Australia

^d Department of Chemical Engineering, Manipal University Jaipur, Rajasthan 303007, India

^e Department of Chemical & Materials Engineering, University of Alberta, Edmonton, Canada

^f South East Water Corporation, Frankston, VIC 3199, Australia

ARTICLE INFO

Keywords:

Demineralisation
Metal passivation
Sewage sludge
Pyrolysis
Heavy metals

ABSTRACT

High concentrations of inorganic matter such as silicates, alkali and alkaline earth metals (AAEMs), and heavy metals (HMs) in biosolids limit their pyrolysis conversion to high-value products. Therefore, the reduction or passivation of the deleterious pyrolytic activities of these native inorganics in biosolids can enhance the yield and quality of products obtained during pyrolysis. The pyrolysis of raw and 3% sulfuric acid pre-treated biosolids was carried out in a fluidised bed reactor at 300–700 °C, and the influence of pre-treatment was examined on biochar properties, gas production, and bio-oil composition. At all temperatures, the selective removal of ash-forming elements (demineralisation) in biosolids by pre-treatment improved organic matter devolatilisation yielding higher bio-oil and lower biochar than untreated biosolids. Demineralisation weakened gas production, particularly at higher pyrolysis temperatures. At 700 °C, the in-situ formation of acidic metal sulfate salts in sulfuric acid-infused biosolids facilitated H⁺ release, thereby increasing H₂ yield to a maximum of 15 mol% compared to 8 mol% from untreated biosolids and 4 mol% from demineralised biosolids. Biochar produced from treated biosolids had considerably lower HMs concentration and higher organic matter retention compared to raw biosolids biochar. The effect of pre-treatment on biochar properties was profound at 700 °C pyrolysis temperature. Pre-treatment increased biochar fixed carbon by 57%, calorific value by 37%, fuel ratio by 44%, doubled the specific surface area from 55 to 107 m²/g, and enhanced porous structure formation. At 300 °C, the major chemical compounds in the bio-oil were amides (20%), N-heterocyclics (25%), and ketones (30%), and higher temperatures favoured phenols and aromatic hydrocarbon production. Pre-treatment enhanced the selectivity of furans by 10-fold, anhydrosugars by 2-fold, and aromatic hydrocarbons by 1.5-fold relative to the raw biosolids bio-oil. Acid pre-treatment is a promising strategy for improving biosolids quality as feedstock for pyrolysis to generate high-value products.

1. Introduction

Biosolids (stabilised sewage sludge) are solid residues of the wastewater treatment process. Biosolids are enriched with plant nutrients (N, P, K), facilitating their widespread application on agricultural land. However, the presence of microbial, organic, and inorganic contaminants is reducing the attractiveness of biosolids for direct land application [1]. Therefore, a substantial volume of biosolids may not be safely applied on land due to increasingly stringent regulations on biosolids

management. Non-combustive thermal techniques such as pyrolysis, gasification, and hydrothermal carbonisation/liquefaction have been widely demonstrated for treating biosolids with the potential for contaminant destruction and resource recovery [2,3]. Pyrolysis is the most promising thermal treatment technique for biosolids processing and has been extensively studied under different conditions. At typical pyrolysis conditions (usually 400–700 °C under an inert atmosphere), pathogens and organic contaminants can be effectively degraded, and the waste volume can be reduced by at least 30% while generating solid

* Corresponding author at: Chemical and Environmental Engineering, School of Engineering, RMIT University, Melbourne, VIC 3000, Australia.

E-mail addresses: ibrahim.hakeem@rmit.edu.au (I.G. Hakeem), kalpit.shah@rmit.edu.au (K. Shah).

<https://doi.org/10.1016/j.jaap.2023.106087>

Received 17 May 2023; Received in revised form 13 July 2023; Accepted 15 July 2023

Available online 18 July 2023

0165-2370/© 2023 Elsevier B.V. All rights reserved.

(biochar), liquid (bio-oil), and gaseous (syngas) products [4]. However, despite these promising outcomes, biosolids pyrolysis can be limited by low conversion, poor selectivity, and product contamination [5]. Unlike lignocellulosic biomass, biosolids can have high amounts of inorganic matter (up to 50 wt%), depending on the source and stabilisation method [6]. The high ash content (and low volatile solids) may limit the suitability of biosolids as a pyrolysis feedstock. The inorganic content such as silicates, aluminates, alkali and alkaline earth minerals (AAEMs), and heavy metals (HMs) can inhibit the conversion of organic matter and interferes with the formation pathway of valuable chemical compounds during pyrolysis [7]. After pyrolysis, the inorganic minerals are largely retained in the biosolids-derived biochar at a higher concentration with deleterious influence on the biochar physicochemical properties and application potential [8]. For example, biosolids biochar with higher HMs concentration may not be attractive for land application. Excessively high amounts of ash content and inorganic minerals in biochar can reduce the oxidation resistance of the biochar carbon, lower the ash fusion temperature, and induce slagging and fouling during combustion for energy recovery [9]. Also, higher concentrations of minerals can lower chars' activation potential, reduce microporous structure development, and decrease the specific surface areas [10].

Three improvement strategies, such as i) feed pre-treatment, ii) use of catalysts, and iii) feed co-processing, have been demonstrated to enhance the pyrolytic conversion of biosolids to high-value products [11]. The extensively studied approaches are co-pyrolysis and in-situ catalytic pyrolysis, which involves the wet or dry mixing of biosolids with other biomass feedstock or catalyst additives [12–14]. Besides the opportunity to manage more than one waste stream, the potential advantages of co-processing biosolids with other feedstock in the presence or absence of catalysts include improved process selectivity, faster conversion kinetics, suppression of pollutant release, and enhanced product properties [15,16]. Co-pyrolysis, catalytic pyrolysis, and their combinations have been demonstrated to improve the pyrolytic conversion of biosolids through beneficial synergistic interactions of co-feedstock and catalysts additive. However, there are still some technical issues that require further attention, such as (i) deconvolution of the complex conversion kinetics and synergistic interactions, (ii) poor product homogeneity arising from feedstock variability and feed particle segregation, and (iii) difficulty in catalyst separation and recovery during in-situ operations.

The chemical pre-treatment of biosolids as an initial process step before pyrolysis has not been fully explored. Previous works suggested that mild acid pre-treatment of biosolids can selectively remove inorganic elements and partially hydrolyse recalcitrant organics to produce organic-rich residue suitable for pyrolysis conversion to bio-oil [8, 17–19]. During acid pre-treatment, protons (H^+) from the acid solution replaced free or loosely bound metal ions in biosolids via an ion exchange mechanism, causing the removal of ash-forming elements [11]. Also, deprotonation of carboxylic O–H and hydroxylic O–H functional groups can produce many H^+ and negatively charged polyions that promote the desorption of metal ions in biosolids [20]. Depending on the severity of the acid pre-treatment conditions, disintegration (hydrolysis) of organic matter in biosolids can occur attributed to the disruption of hydroxyl bonds and cleavage of carbonyl groups, as well as the transformation of crystalline compounds to amorphous form, thereby reducing the structural and thermal recalcitrance of the treated residue [21,22]. For example, mild acid (<5% H_2SO_4 at 25 °C and 1 h) pre-treatment of biosolids was reported to remove about 75–95% of inherent HMs and 80–95% AAEMs, which reduced the ash content by 50% without degradation of organic constituents [17]. Then, the pyrolysis of acid-pre-treated biosolids had higher rates of devolatilisation occurring at lower temperatures to produce lower char residues than untreated biosolids [8,17]. Similarly, Liu et al. [18] reported that acid washing using 0.1 M H_2SO_4 at ambient conditions for 12 h reduced biosolids ash content from 32 wt% to 20 wt% and increased carbon content by 26%. Therefore, acid pre-treatment of biosolids before

pyrolysis may be desired for many reasons, such as (i) reduction of HMs concentration and bioavailability in the resultant biochar, (ii) reduction of ash content and increased organic matter retention in biochar, (iii) enhancement of char textural properties and specific surface area, and (iv) improvement of both energy and chemical value of bio-oil through reduction of water and oxygenates content ordinarily catalysed by native AAEMs. Furthermore, there is an extensive demonstration of acid pre-treatment of biosolids for removing HMs and other limiting contaminants, thereby improving the grade of biosolids for unrestricted beneficial land reuse [20,23,24]. Therefore, biosolids pre-treatment may have a two-fold benefit for improving biosolids quality for land application as well as for pyrolysis upcycling.

Existing studies on integrated acid pre-treatment and pyrolysis were centred on understanding the role of inherent metals on biosolids' thermal decomposition behaviour and pyrolysis kinetics [19,25,26]. The analytical pyrolysis of acid-demineralised biosolids or demineralised biosolids spiked with specific metal additive have been used to elucidate the catalytic role of internal or added metals in fostering or inhibiting the release of gaseous nitrogen and sulfur compounds, degradation characteristics of organic matter, volatiles evolution, and pyrolysis activation energy [19,25–27]. There are limited studies on the bench-scale pyrolysis of acid-treated biosolids [18,28]. The role of acid pre-treatment on the distribution of pyrolysis product fractions (oil, char, and gas) and their properties have not been fully documented in the literature. Also, the observed effect of pre-treatment of biosolids in analytical pyrolysis setup may differ in practical reactor systems such as the fluidised bed reactor where gas-solid interactions are faster due to improved mass and heat transfer. Hence, biosolids pre-treatment before pyrolysis demands an extensive investigation in a typical fluid bed reactor under wide conditions of pre-treatment and pyrolysis.

This work studied the pyrolysis of raw and acid-treated biosolids in a fluidised bed reactor at 300–700 °C to understand the role of pre-treatment on biosolids pyrolysis. It was hypothesised that the removal or passivation of inherent metals in biosolids through acid pre-treatment could enhance the biochar quality, influence the formation path of chemical components in the bio-oil, and affect gas production during pyrolysis. Two pre-treatment scenarios were selected to include (i) biosolids acid treatment followed by water washing as a neutralisation step for selective demineralisation and (ii) biosolids acid treatment having residual acid unwashed for metal passivation. The specific objectives of this work were to study the effect of mild acid pre-treatment on (i) biosolids' physicochemical properties and thermal decomposition behaviour, (ii) pyrolysis product distributions, (iii) biochar quality with respect to carbon retention, calorific value, HMs concentration and bioavailability, and surface morphology, (iv) compositions of chemical compounds in the pyrolysis liquid to assess the chemical value of the bio-oil, and (v) compositions and evolution profile of non-condensable pyrolysis gases.

2. Materials and methods

2.1. Biosolids collection and sample preparation

Biosolids used in this study were collected from Mount Martha Water Recycling Plant, South East Water Corporation, Melbourne, Australia. The plant uses a dissolved air flotation process for sludge activation, then anaerobic followed by aerobic digestion for sludge treatment. The digested sludge is then dosed with polymer additives to coalesce the flocs, followed by mechanical dewatering in a centrifuge and drying in solar dryer shed. The biosolids employed in this study are the final solids from the dryer. The as-obtained biosolids were dried in an oven at 105 °C, ground, and sieved to 100–300 μm particle size before further use.

2.2. Biosolids pre-treatment

The pre-treatment procedure was as described in our previous work [17]. The biosolids were pre-treated using a 3% (v/v) sulfuric solution at a solid-to-liquid ratio of 1:10 (g/mL) at 25 °C under continuous stirring at 600 rpm for 1 h. These conditions were obtained from an earlier optimisation study [17]. At the end of the pre-treatment experiment, the slurry was vacuum filtered to separate into aqueous phase (filtrate) and solid residue (treated biosolids). The residue was divided into two portions. The first portion was washed many times with deionised water until the filtrate pH was near neutral to remove residual acid and other water-soluble inorganics. The second portion was used as obtained with no further water washing to study the effects of residual acid on biosolids pyrolysis performance. The raw (untreated) biosolids were denoted as RB, treated biosolids with water washing were denoted as TB, while treated biosolids with no water washing were denoted as TB_{nw}. The generation of large volumes of aqueous waste is a typical limitation of acid pre-treatment; however, our recent work has developed a closed-loop hydrometallurgical process for managing the generated aqueous acidic leachate stream via recycling and metal recovery [23]. The effect of pre-treatment on the pyrolysis behaviour of biosolids was assessed through Thermogravimetry analysis using a high-temperature TG/DSC Discovery series SDT650 equipment (TA instrument).

2.3. Pyrolysis experiments and products yield

Pyrolysis experiments were carried out in a quartz tubular fluidized bed reactor under atmospheric conditions. The details of the pyrolysis rig and reactor specifications can be found in our previous works [15, 29]. The pyrolysis procedure involves weighing 40 g of dry biosolids feed (RB or TB or TB_{nw}) into a clean, dry pre-weighed reactor. The reactor and its content were inserted vertically into a three-zone electrically controlled furnace with an average heating rate of 35 °C/min. The reactor and its content were continuously flushed with a stream of pure nitrogen to create an inert atmosphere before heating the reactor. The experimental setup is shown in Fig S1. Biosolids pyrolysis was conducted at three temperatures: 300, 500, and 700 °C, which were selected to study the effect of pre-treatment on the product distribution and properties over a wide temperature range. During pyrolysis, a continuous stream of nitrogen flow required to achieve a gas velocity equivalent to 2.5 times the minimum fluidisation velocity was maintained using the Ergun correlation described in our previous work [30]. After reaching the desired temperature, the experiment was continued for 60 min, sufficient to complete the pyrolysis process. At the end of each experiment, biochar was collected from the reactor after cooling down to ambient temperature, and bio-oil was collected from the condensers. Non-condensable pyrolysis gas was continuously analysed on-line using micro-GC equipment connected to the pyrolysis gas cleaning units. Nine primary experiments were conducted, 3 samples by 3 temperatures. The pyrolysis product notations are distinguished by sample name-pyrolysis temperature, e.g., RB300 denoted Raw biosolids pyrolysed at 300 °C. At least a single repeat experiment was conducted for all samples, and average data has been reported with error bars representing the standard deviation. Product yields were calculated using Eqs. (1)–(3).

$$\text{Biochar}(\text{wt}\%) = \frac{\text{Weight of biochar}}{\text{Weight of biosolids feed}} \times 100\% \quad (1)$$

$$\text{Bio-oil}(\text{wt}\%) = \frac{W_{CT, \text{after}} - W_{CT, \text{before}}}{\text{Weight of biosolids feed}} \times 100\% \quad (2)$$

$$\text{Gas}(\text{wt}\%) = 100\% - \text{Biochar}(\text{wt}\%) - \text{Biooil}(\text{wt}\%) \quad (3)$$

Where W_{CT} refers to the weight of the condensers and oil collecting tubes.

2.4. Products characterisation

2.4.1. Biochar

Proximate analysis of biosolids and their biochar were carried out using a TGA 8000 Perkin Elmer equipment, and the ultimate analysis was performed in a CHNS 2400 Series II Perkin Elmer equipment coupled to a thermal conductivity detector. Physicochemical properties such as pH and electrical conductivity (EC) were determined using a pre-calibrated platinum electrode probe. Higher heating value (HHV) was estimated using the correlation of Channiwala and Parikh [31] shown in Eq. (4). Bulk density of the biosolids and biochar samples was determined using the standard measuring cylinder method [30]. FTIR Spectra were captured in absorbance mode over a scanning wavelength of 4000–650 cm^{-1} at 32 scanning times and 4 cm^{-1} resolutions using Frontier FTIR Spectroscopy (Spectrum 100, Perkin Elmer). Scanning electron microscope (SEM) FEI Quanta 200, USA, was used to analyse the surface morphologies of biochar samples after coating with iridium using Leica EM ACE 600 sputter coating instrument. The SEM instrument was operated at 30 kV, and SEM images were captured at the same spot size (5.0) and magnification ($\times 3000$) to compare all samples' surface morphology. Brunauer–Emmett–Teller (BET) Surface Area Analysis was employed to estimate the surface area of the samples using Micromeritics TriStar II instrument.

The concentration of major elements in biosolids and biochar samples was measured using XRF analysis (S4 Pioneer Bruker AXS). Trace elements were measured using ICP-MS analysis following the acid digestion of the biosolids samples in aqua regia following the procedure described in Hakeem et al. [17]. Lastly, the potential soil bioavailable HMs concentration in biochar samples was measured using the diethylenetriamine pentaacetate (DTPA) acid extractable metal procedure [32]. Briefly, the extractant was prepared by weighing 1.97 g of DTPA, 1.47 g of $\text{CaCl}_2 \cdot 2 \text{H}_2\text{O}$, and 14.92 g of triethanolamine and dissolved in deionised water to make up 1 L solution. The pH of the solution was adjusted to 7.3 using concentrated HCl. Then 1 g of biochar sample was added to 10 mL of the pH-adjusted extractant solution, and the mixture was agitated at 250 rpm overnight at room conditions. The metal enrichment factor (MEF_i) and metal retention/recovery (R_i) in the biochar was estimated using Eqs. (5) and (6), respectively [17].

$$\text{HHV} \left(\frac{\text{MJ}}{\text{kg}} \right) = 0.3491C + 1.1783H + 0.1005S - 0.1034O - 0.0151N - 0.0211\text{Ash} \quad (4)$$

$$\text{MEF}_i = \frac{\text{Metal}_i \text{ concentration} \left(\frac{\text{mg}}{\text{kg}} \right) \text{ in biochar}}{\text{Metal}_i \text{ concentration} \left(\frac{\text{mg}}{\text{kg}} \right) \text{ in biosolids}} \quad (5)$$

$$R_i(\%) = \text{MEF}_i \times \text{biochar yield}(\text{wt}\%) \quad (6)$$

2.4.2. Bio-oil compositions

Pure bio-oil oil samples collected from the condenser during pyrolysis were used for the analysis. Bio-oil samples were dissolved in DCM before analysis in a Gas Chromatography-Mass Spectrometry (GC/MS Agilent Technologies, GC/MSD 5977B, 8860 GC system) instrument. HP-5MS (19091S-433UI) capillary column (30 m length, 0.25 mm I.D. and 0.25 μm film thickness) was used in the GC/MS equipment, and the temperature program of the oven was as follows: isothermal hold at 45 °C for 3 min, ramp to 300 °C at 7 °C/min and isothermal hold at 300 °C for 5 min. Other conditions were 300 °C - injection temperature; 280 °C - MS transfer line; 230 °C - MS ion source; 1 μL - splitless injection volume; 23.0 mL/min - total inlet flow, and helium was used as the carrier gas. The relative composition of chemical compounds in each bio-oil sample was determined by peak area normalisation, denoted as peak area percentage [15]. For further analysis, the identified compounds in each bio-oil sample were categorised into different chemical groups such as oxygenated, nitrogenated, hydrocarbons, phenolics,

anhydrosugars, and sulfur-containing compounds. Acids, alcohols, aldehydes, esters, ethers, furans, and ketones were categorised into oxygenated, while pyrazine, pyridine, pyrrole, azole, amines, amides, and nitriles were categorised into nitrogenated. Phenols and their derivatives are phenolics, while saccharides and sugar alcohols are classified as anhydrosugars. Finally, olefin, paraffin, BTXS (benzene, toluene, xylene, and styrene), and PAHs were classified as hydrocarbons. This classification was used to provide insight into the chemical value of the bio-oil based on dominant platform chemical species and study the effect of pre-treatment on the distribution of the chemical compounds.

2.4.3. Pyrolysis gas compositions

The components and relative compositions (mol%) of the gas stream from each pyrolysis experiment were analysed online using a Micro-GC 490 (Agilent Technologies) instrument connected to the gas scrubbing unit from the pyrolysis reactor. The microGC has been calibrated with standard gases such as CO₂, CO, H₂, N₂, O₂ and C1-C4 hydrocarbon. Pyrolysis gasses were sampled every 4 min until the end of the experiment to identify and quantify the gas components. The gas evolution profile during the pyrolysis was obtained by plotting the relative gas compositions as a function of pyrolysis time.

3. Results and discussions

3.1. Effect of pre-treatment on biosolids physicochemical properties

The effect of H₂SO₄ pre-treatment on the physicochemical properties of biosolids is summarised in Table 1. The mild acid pre-treatment (3% H₂SO₄ at 25 °C for 60 min) of biosolids impacted the proximate compositions of the biosolids without substantial change in the ultimate compositions. Hence demineralisation mechanism dominated the pre-treatment process, which selectively removed inorganic matter. The percentage change in carbon contents was far lower than the percentage change in ash content of biosolids after pre-treatment. Specifically, there was a 40% and 20% decrease in ash content for TB and TB_{nw}, respectively and a 10% increase in the volatile matter for the treated samples. In contrast, the carbon, hydrogen, and nitrogen contents of the treated samples differ by less than 10% relative to the raw biosolids, attributed to the loss of acid-soluble light volatiles. The ash content decreased due to the substantial removal (>60%) of ash-forming elements (such as AAEMs, Fe, Al, and HMs) from the biosolids. Devolatilisation was slightly enhanced by pre-treatment due to the hydrolysis of recalcitrant organics, thereby increasing volatile matter from 57% in raw biosolids to over 63% in treated feeds.

There was also a considerable reduction in HMs concentration, particularly Cu and Zn, which are the major limiting HMs in biosolids for land application. Overall, there was about a 75% reduction in HMs concentration in the TB relative to RB. The intensity of demineralisation and HMs reduction, as well as other physicochemical changes, were lesser in TB_{nw} than in TB due to the subsequent water-washing step performed in the latter, which aided the removal of water-soluble inorganics and organic components. The HMs concentration (except Cu) in TB is within the concentration limit prescribed by Victoria EPA for C1-grade (least contaminant grade) biosolids for unrestricted land application [33]. The bioavailability of the residual HMs in TB is considerably low and can be an attractive material for direct land use in its current form [17]. However, other rapidly emerging contaminants in biosolids, such as per- and polyfluoroalkyl substances (PFAS) and microplastics, might still be present in TB. Our earlier work observed that sulfuric acid pre-treatment could not extract PFAS from biosolids; rather, the process concentrated PFAS in the treated solids due to volume reduction [23]. Therefore, the thermal treatment of TB via pyrolysis might be necessary to completely degrade all potential organic and microbial contaminants and produce quality biochar for land beneficiation and other high-value applications.

Table 1
Effect of pre-treatment on biosolids physicochemical properties.

Properties	Compositions/ Elements	Biosolids samples			C1-grade biosolids*
		RB	TB	TB _{nw}	
Proximate analysis (wt% dry basis)	Moisture	1.9	1.8	0.8	
	Volatile matter	57.5	63.4	63.6	
	Fixed carbon	10.6	16.4	11.3	
	Ash	30.0	18.5	24.3	
Ultimate analysis (wt% dry basis) ^a	Carbon	35.4	36.4	32.9	
	Hydrogen	4.4	5.1	4.5	
	Nitrogen	5.6	5.6	5.5	
	Sulfur	0.9	2.3	7.4	
	Oxygen	23.8	32.1	25.5	
pH		6.8	6.0	2.0	
EC (μS/cm)		1885	2400	9385	
HHV (MJ/kg) ^b		14.4	15.1	14.2	
Bulk density (g/cm ³)		0.78	0.73	0.77	
Solids recovery (%)		-	80	95	
Carbon retention (%) ^c		-	82.3	88.3	
Major elements in ash (wt%)	Al	0.74	0.54	0.56	
	Ca	10.18	5.35	8.54	
	Cl	0.35	0.08	0.08	
	Fe	4.23	4.07	2.25	
	Na	0.12	BDL	BDL ^d	
	K	1.07	0.18	0.35	
	Mg	0.53	0.12	0.12	
	P	1.32	0.54	0.51	
	Si	2.69	3.29	2.91	
	Demineralisation efficiency (%) ^e		-	38.6	19.0
AAEMs removal efficiency (%) ^f		-	77.0	65.2	
Heavy metals (mg/kg)	As	2.5	1.3	1.9	20
	Cd	1.3	0.3	0.5	1
	Co	1.3	0.5	0.9	-
	Cu	690	220	500	100
	Cr	20	13	16	400
	Ni	18	7	12	60
	Mn	210	10	53	-
	Pb	20	18	17	300
Zn	850	160	560	200	
HMs removal efficiency (%)		-	76	35	

^a Obtained by difference Oxygen = (100-C-H-N-S-Ash);

^b Estimated using the correlation of Channiwala and Parikh (Eq. 4)

^c $(\text{Carbon content (wt\% in treated feeds)} / (\text{Carbon content (wt\%) in raw biosolids}) \times \text{Solids recovery}(\%))$

^d BDL – Below Detection Limit;

^e Based on ash content reduction;

^f Based on average Na, K, Mg, and Ca content reduction

* Biosolids grade for land application as prescribed by EPA Victoria [33].

Notably, there was an increase in sulfur content in TB_{nw} compared to the other two samples indicating the presence of high residual sulfur from H₂SO₄ pre-treatment without any post-treatment water washing. The sulfur from H₂SO₄ could react with organic matter in biosolids to form organosulfur compounds, which might initiate the release of sulfur-containing volatiles during pyrolysis. The FTIR spectra (Fig S2) of the treated biosolids confirmed the formation of organosulfur compounds such as C-S, C=S, S=O, and SO₂NH₂ groups. The water-washing neutralisation steps neutralised residual sulfuric acid and removed the precipitated metal sulfate salts, raising the treated solids' pH to 6.5 (Table 1). However, the water-washing process caused a loss of total solids with a solids recovery of 85% and carbon retention of 82% in TB compared to 95% solids recovery and 88% carbon retention in TB_{nw}. Pre-treatment had a negligible change on the calorific value of the feed materials due to the contrasting effect of ash and oxygen concentration on the HHV correlation (Eq. (4)); however, pre-treatment reduced the bulk density of the biosolids, which was more profound in TB due to the extra water washing step. The overall observation of the acid pre-

treatment process on the changes in the physicochemical properties of biosolids is comparable with the literature [8,18,19]. For instance, in the study of Liu et al. [18], 0.1 M H₂SO₄ pre-treatment of biosolids at ambient temperature for 12 h reduced the ash content by 12 wt% and increased volatile matter and carbon contents by ~10 wt% relative to the untreated biosolids. Tang et al. [19] using 5% HCl, 25 °C and 6 h for biosolids pre-treatment yielded 8 wt% decrease in ash content and ~5 wt% increase in volatile matter and carbon contents while nitrogen and hydrogen contents remained relatively unchanged compared to the raw biosolids. The current work used 3% H₂SO₄, 25 °C and 1 h to achieve 12 wt% reductions in ash content and 6 wt% increments in volatile matter while ultimate compositions were least impacted.

3.2. Effect of pre-treatment on biosolids thermal decomposition behaviour

The influence of pre-treatment on the pyrolysis behaviour of biosolids is illustrated by the various thermographs shown in Fig. 1. The DTG profile (Fig. 1(A)) occurs in three distinct degradation stages, which are: (I) dehydration (50–165 °C), (II) devolatilisation of organic components (150–600 °C), and (III) decomposition of recalcitrant carbonaceous materials and residual char organics (>600 °C). In stage I, the dehydration peak attributed to the loss of moisture and light volatiles occurred at 100 °C with < 4% mass loss. The major mass loss

(>50%) occurred in stage II over three degradation peaks at 250, 350, and 400 °C, corresponding to the thermal decomposition of carbohydrates, lipids and proteins/biopolymers, respectively [34,35]. The last degradation stage III, with < 10% mass loss, peaked at 750 °C and was attributed to the degradation of recalcitrant organics, such as lignin, and a fraction of inorganics, usually carbonates. There were clear differences in the DTG thermograph of RB, TB, and TB_nw with respect to changes in maximum degradation temperatures and rate of weight loss. The maximum degradation temperature shifted to lower values in treated samples compared to the raw sample. In contrast, the raw sample's degradation rate was higher than the treated biosolids. For example, the maximum degradation temperature was 285 °C for RB, and it shifted to 245 °C for TB_nw and 260 °C for TB, and while the rate of weight loss was 5.5%/°C for RB and it slightly decreased to 5.3%/°C for TB and 4.3%/°C for TB_nw. These differences can be attributed to the partial hydrolysis of organic matter and the removal of inorganics by the pre-treatment step, facilitating the thermal devolatilisation reactions at lower degradation temperatures. However, the pre-treatment process also resulted in the slight dissolution of organic matter, which decreased the overall quantity of volatile matter in the treated samples relative to RB, thereby reducing the rate of volatile degradation. The lower rate of TB_nw degradation compared to the other samples confirmed the formation of thermally stable metal sulfate salts, which inhibited organic

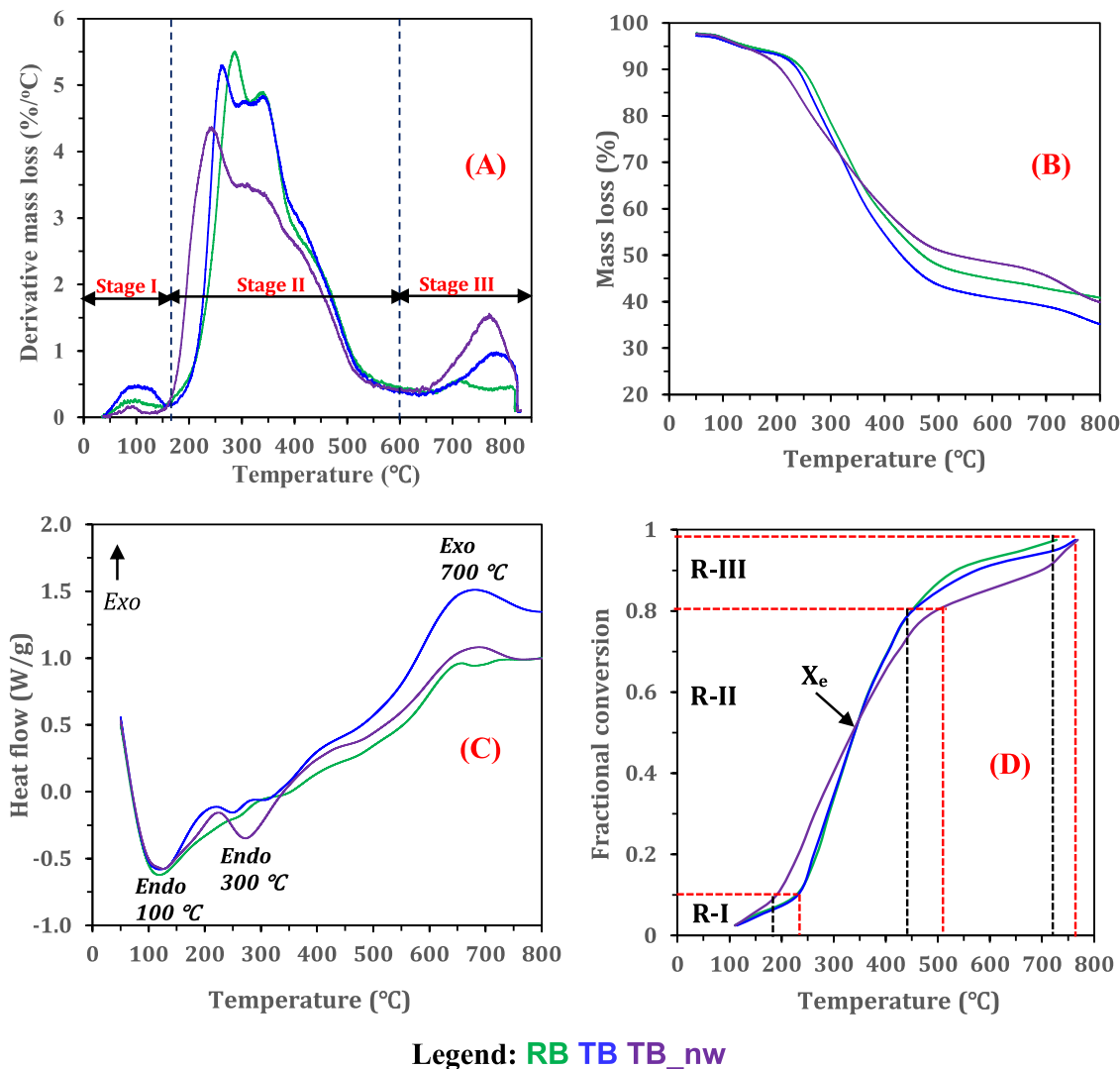


Fig. 1. Effect of pre-treatment on the thermal decomposition behaviour of biosolids (A) DTG thermograph showing decomposition peaks (B) TG mass degradation curve (C) DSC profile showing heat flow (D) plot of fractional conversion as a function of pyrolysis temperature.

matter conversion [36]. The TG curve (Fig. 1(B)) shows that the decomposition profile of TB and RB was closely similar with no overlapping, and at all temperatures, the degradation of TB was always higher than RB. This indicated that both samples have a similar organic matrix, and the lower ash content in TB was largely responsible for the higher mass loss at all temperatures. In contrast, TB_{nw} had a different degradation profile whose mass loss was faster than the other materials up to 320 °C. Beyond this temperature, the mass loss was slower than in the other samples. The residual mass of RB and TB_{nw} was similar (40%), while that of TB was the lowest (35%).

Fig. 1(C) illustrates the DSC curve of the biosolids samples showing the thermal energy flow as a function of pyrolysis temperature. Pyrolysis is an endothermic process where external energy is needed to break chemical bonds and decompose major biochemical components into primary decomposition products. From Fig. 1(C), two distinct endothermic peaks occurred at 100 °C and 300 °C, corresponding to loss of moisture and organic devolatilisation, respectively. After the initial transformation up to 350 °C, the energy needed to heat the feed materials began to decline, and the decrease of heat flow with increasing pyrolysis temperature from 350 to 600 °C was almost linear. During this stage, there are traces of broad endotherms indicating that the decomposition of organic matter at 300–600 °C required minimal thermal energy. However, the non-distinct endotherms made attributing the degradation behaviour to specific organic components difficult. Beyond 600 °C, a small exothermic spike was observed occurring at 650–750 °C attributed to the decomposition of carbon refractories such as aromatic ring, N-alkyl long chain structures, and carbonates with the release of CO₂ [37,38]. The intensity of the endothermic peak at 300 °C in TB_{nw} suggests that the thermal energy required to decompose its organic structure is higher. The infusion of sulfuric acid might have changed the organic structure of TB_{nw} to a thermally recalcitrant matrix through the formation of stable metal sulfate salts, consistent with observations reported in other works [18,39].

The iso-conversional temperature required for the pyrolysis of the three biosolids samples at the same heating rate (20 °C/min) is shown in Fig. 1(D). The figure indicates that the pyrolysis conversion of biosolids occurred over at least three kinetic regimes: i) $\leq 10\%$ conversion occurring at 100–240 °C (R-I), ii) 10–80% conversion occurring at 240–500 °C (R-II), and iii) $\geq 80\%$ conversion at 500–800 °C (R-III). These three kinetic regimes denoted dehydration, primary devolatilisation, and secondary devolatilisation and char cracking stages. However, the temperature required for each conversion stage differs for individual samples. For example, 10% conversion of TB_{nw} occurred at 190 °C and about 230 °C for both RB and TB, suggesting that the dehydration stage occurred faster in TB_{nw} compared to the other two samples. The faster conversion kinetics of TB_{nw} continued into the primary devolatilisation stage up to 50% conversion, after which the rate was slower than RB and TB. Meanwhile, both RB and TB showed similar kinetics, up to 80% conversion, suggesting that the organic structure of both samples is identical. The slightly higher conversion rate of RB beyond 80% can be attributed to the role of native inorganic minerals, which promoted the cracking of recalcitrant organic matter. Notably, the pyrolysis temperature required to achieve 50% conversion was largely similar for all samples (340 °C), as the conversion rate of all samples overlapped at that temperature (indicated by X_c in Fig. 1(D)). Overall, the required pyrolysis temperature was lowest for TB_{nw} at any given conversion $< 50\%$ and was highest at any given conversion $> 50\%$.

3.3. Pyrolysis products distribution: effect of pre-treatment and temperature

The product distribution of raw and treated biosolids at 300–700 °C is shown in Fig. 2. The product yields are expressed in dry feed weight to compare the influence of the temperature and pre-treatment on pyrolysis product distributions (Fig. 2(A)). According to Fig. 2, with

increasing pyrolysis temperature (from 300 to 700 °C), biochar yields decreased while bio-oil and gas products yield increased irrespective of feed material. This trend in product distribution as a function of pyrolysis temperature is consistent with extant literature [29,30,40]. With increasing pyrolysis temperature, mass and heat transfer rates are faster, and several thermolysis decomposition reactions are enhanced with the rapid cleavage of chemical bonds. For all samples, the effect of pyrolysis temperature on biosolids devolatilisation was profound between 300 and 500 °C compared to that between 500 and 700 °C. Nevertheless, bio-oil and gas products yield monotonically increased with temperatures up to 700 °C, indicating that biosolids contain recalcitrant organic fraction requiring higher temperatures to devolatilise. For example, during RB pyrolysis, the conversion was 28.8% at 300 °C; it increased to 49.7% at 500 °C and 58.6% at 700 °C. A similar trend can be observed for TB and TB_{nw}. The DTG profile in Fig. 1(A) showed that most of the organic components in biosolids volatilised at temperatures between 200 and 500 °C. There were only slight improvements in bio-oil and gas yield by raising the temperature to 700 °C.

Pre-treatment had a clear effect on pyrolysis product distribution. From Fig. 2(A), pyrolysis of TB produced lower biochar yield (38.2–65.6 wt%) than that from RB (41.4–71.2 wt%), and the biochar yield from TB_{nw} (43.0–68.7 wt%) was found to be between the yields from RB and TB. In contrast, bio-oil yield from TB (24.7–42.6 wt%) was higher than that from RB (20.6–37.0 wt%) and TB_{nw} (19.6–36.8 wt%). Removal of ash-forming elements from biosolids and partial hydrolysis of the organic matter by H₂SO₄ pre-treatment improved the devolatilisation of TB to produce more bio-oil and less char residues compared to other biosolids samples. It has been indicated that trace levels (< 1 wt%) of certain ash components in biomass have significant catalytic effect during pyrolysis, which can decrease bio-oil yield considerably [41]. From Fig. 1(A), TB_{nw} had the least conversion of all biosolids samples producing the highest biochar yield at 500 and 700 °C. The residual sulfuric acid in TB_{nw} can catalyse crosslinking and polycondensation reactions at higher temperatures to form extra char, thereby increasing biochar yield [42]. The effect of pre-treatment was prominent on the distribution of biochar and bio-oil fractions, suggesting that the removal of inorganics had a remarkable influence on the thermal devolatilisation of organic matter in biosolids. Depending on the metal species and chemical form, mineral components have been shown to play various catalytic roles in releasing pyrolytic volatiles from organic matter [26, 43]. The extent of the interaction of mineral matter on organic matter conversion during biosolids pyrolysis has been elucidated in another work [8]. The gas product yield increased with increasing pyrolysis temperature and was higher for RB and TB_{nw} than for TB. The catalytic effect of the inherent inorganics in RB and residual acid in TB_{nw} facilitated gas production through secondary cracking and dehydration reactions, respectively.

Fig. 2(B) shows the pyrolysis product yield expressed on volatile solids (VS) or dry-ash-free basis to discount the effect of ash matter on product distribution as well as understand the real impact of pre-treatment on the downstream pyrolysis conversion of VS. At all pyrolysis temperatures, RB and TB had a similar yield of bio-oil in the range of 30–53 wt%, and biochar yield (30–59 wt%) was only similar for both samples at 300–500 °C. However, gas and biochar yield varies substantially for RB and TB at 700 °C. This indicates that VS conversion to bio-oil was not negatively impacted by demineralisation as in the case of TB. In contrast, biosolids pre-treatment without the water neutralisation step, as in TB_{nw}, negatively impacted VS conversion to bio-oil during pyrolysis at all temperatures. The higher biochar yield at 500 and 700 °C for treated biosolids compared to the RB clearly indicates the char cracking role of native mineral matter during biosolids pyrolysis. The presence of mineral matter in RB caused a substantial cracking of recalcitrant volatiles at 700 °C to decrease biochar yield and increase gas yield. Consequently, RB conversion was 84% against 75% for treated biosolids. The elevated VS conversion attributed to the internal minerals in RB caused a decrease in fixed carbon and organic matter retention of

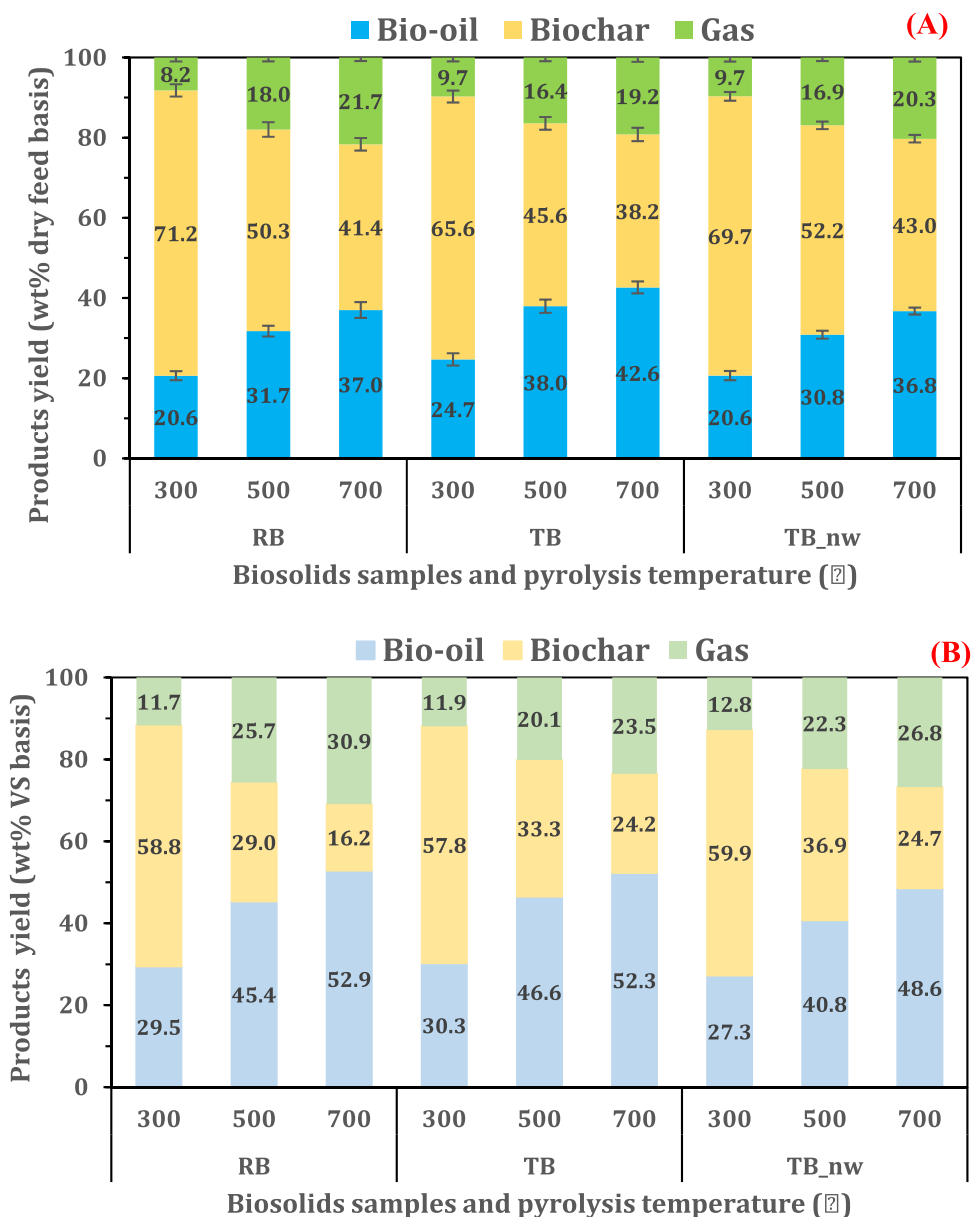


Fig. 2. Effect of pre-treatment and temperature on biosolids pyrolysis product distribution (A) expressed on a dry feed weight basis (B) expressed on volatile solids (dry-ash-free) basis.

the resulting biochar. In contrast, the lower conversion of VS in treated biosolids increased fixed carbon content and organic matter retention in the biochar. The higher biochar yield from the treated samples suggests that the pre-treatment process caused a reduction of thermally labile VS through the dissolution of acid-soluble organics and the loss of total solids during the process. This observation was confirmed by the 80–95% solids recovery and 82–88% carbon retention in treated biosolids relative to RB (Table 1). Besides the loss of total solids and light volatiles during pre-treatment, the residual organic structure might also be impacted by pre-treatment, increasing the stable VS fraction as indicated by the higher fixed carbon contents in treated biosolids. In sum, pre-treatment weakened the pyrolysis conversion of biosolids VS to gas product only at 700 °C.

Under the conditions of this work, there could be more than one mechanism through which acid pre-treatment influenced biosolids organic matter devolatilisation to produce higher bio-oil and lower biochar compared to RB. Perspectives on how biosolids’ devolatilisation could be enhanced by acid pre-treatment with water washing step (as in

TB) have been provided.

- i) The substantial reduction of ash content by pre-treatment increased volatile matter concentration in TB. Since the volatile matter content per solid mass is higher in TB than RB, the pyrolysis of equal amounts of TB and RB implies more volatiles per unit TB mass is available for thermal conversion to bio-oil. The lower biochar yield in TB is due to reduced ash content since ash components are largely retained in the biochar. The proximate compositions of the biosolids changed substantially after pre-treatment, with a major opposite shift in the volatile matter and ash matter contents (Table 1).
- ii) During pre-treatment, complex organic components in biosolids can be hydrolysed into simpler components through the disruption of O-H bonds by H⁺ from acid solution and surface deprotonation reaction causing the cleavage of carbonyl groups in protein and carbohydrate structures [20,22]. The partially hydrolysed organic macromolecules in TB are thermally less stable, and their characteristics decomposition temperature occurs in a lower region than untreated biosolids

Table 2
Effect of pre-treatment on biochar physicochemical properties.

Pyrolysis temperature (°C)	300			500			700		
	RB	TB	TB_nw	RB	TB	TB_nw	RB	TB	TB_nw
Proximate analysis (wt% dry basis)									
Moisture	0.37	0.47	0.45	0.80	0.65	0.84	0.84	0.91	0.89
Volatile matter	46.16	52.11	50.69	29.28	30.67	35.67	20.07	21.70	16.71
Fixed carbon	14.66	18.45	13.28	17.62	27.66	17.15	19.99	31.32	27.26
Ash	38.82	28.97	35.57	52.31	41.02	46.35	59.10	46.06	55.15
Ultimate analysis (wt% dry basis)									
Carbon	39.35	45.08	40.07	32.82	41.67	35.34	30.41	37.27	30.21
Hydrogen	3.18	3.57	2.80	1.01	1.50	1.08	0.29	0.83	0.48
Nitrogen	6.55	7.35	6.39	5.47	5.63	5.21	3.25	4.83	4.01
Sulfur	0.89	2.58	6.13	0.58	3.12	6.06	0.65	3.14	7.32
Oxygen ^a	11.22	12.45	9.04	7.81	7.07	5.97	6.30	7.87	2.84
Other properties									
O/C	0.21	0.21	0.17	0.18	0.13	0.13	0.16	0.16	0.07
H/C	0.97	0.95	0.84	0.37	0.43	0.37	0.11	0.27	0.19
pH	5.8	5.5	4.1	7.8	6.8	6.3	9.8	9.4	9.6
EC ($\mu\text{S}/\text{cm}$)	722	1042	2614	305	1500	1868	2160	3218	2902
Bulk density (g/cm^3)	0.79	0.74	0.69	0.80	0.78	0.67	0.83	0.70	0.65
HHV (MJ/kg) ^b	15.49	18.19	16.13	10.71	14.95	12.54	9.07	12.44	10.33
Fuel ratio (FC/VM) ^c	0.32	0.35	0.26	0.60	0.90	0.48	1.00	1.44	1.63
Organic matter retention (%VS) ^d	58.8	57.8	58.6	29.0	33.3	36.8	16.3	24.2	24.7

^a Obtained by difference, i.e. $\text{O} = 100 - (\text{C} + \text{H} + \text{N} + \text{S} + \text{Ash})$;

^b Estimated by the correlation of Channiwala and Parikh [31] (Eq. 4);

^c Fuel ratio was estimated by dividing the fixed carbon content (wt%) by the volatile matter content (wt%) in each sample;

^d Calculated by dividing the volatile solids (VS) in biochar (Biochar yield (wt%)–ash content (wt%)) by the corresponding VS in the respective feedstock (100 (wt%)–ash content (wt%)).

(The TGA/DTG curve confirmed the shift to lower degradation temperature) (Fig. 1(A)).

The results of this work provide insight into the impact of acid pre-treatment on biosolids pyrolysis product distribution under a wide range of temperatures. However, the findings cannot sufficiently identify the specific organic chemical bonds and components being transformed during pyrolysis, aided or inhibited by pre-treatment. Further studies are needed to comprehensively understand the pre-treatment process and the exact mechanisms through which organic matter devolatilisation occurs to increase bio-oil yield.

3.4. Effect of pre-treatment on biochar quality

3.4.1. Physicochemical properties

The physicochemical properties such as proximate and ultimate analyses, caloric value, pH, carbon retention and bulk densities of the resultant biochar obtained from the three biosolids feed samples at 300–700 °C are summarised in Table 2. Generally, volatile matter (VM) decreased, while fixed carbon (FC) and ash content increased in all biochar samples with increasing pyrolysis temperature. However, the increase in FC was negatively influenced by higher ash contents in biochar as the metal oxides in the ash can further oxidise FC, particularly at higher temperatures. During pyrolysis, thermally labile organic matter in the biosolids is removed, leading to substantial volume reduction. As a result, recalcitrant organic matter and inorganic matter are concentrated in the biochar. Increasing pyrolysis temperature increased the intensity of organic matter degradation and inorganic matter retention. The reduction of VM with increasing temperature had a consequential decrease in the ultimate compositions (C, H, N, O) of the biochar through dehydration, deoxygenation, decarboxylation, and denitrogenation reactions. Pre-treatment had clear effects on the proximate and ultimate compositions of the biochar samples. At all pyrolysis temperatures, biochar obtained from treated feeds had lower ash contents and higher FC than RB-biochar due to the prior removal of the ash-forming elements via the pre-treatment demineralisation process. TB-derived biochar had the highest VM and FC increase, and the lowest ash contents decrease compared to corresponding biochar obtained from

other biosolids feeds, albeit at the cost of biochar yield. Pre-treatment with water neutralisation steps retained higher organic matter in the biochar (24–58%), supported by the higher carbon contents and calorific value in the TB-derived biochar relative to RB and TB_nw biochar (Table 2). Also, the fuel ratio of TB biochar was higher than RB-biochar, particularly at 700 °C; the fuel ratio of treated biosolids biochar was higher by 44–63% than RB-biochar. It is then suggested that removing minerals before pyrolysis can be a promising approach for strengthening biochar carbon-sequestration and energy-recovery potential. Also, the lower ash contents in the TB-derived biochar can enhance the biochar-carbon resistance to thermal and chemical oxidation, thereby increasing the carbon stability, as demonstrated in previous work [8]. However, the increase in sulfur contents in the biochar may be an undesired outcome of the pre-treatment process, particularly when the sulfuric acid pre-treatment is not followed by the water-washing neutralisation step, as in TB_nw. Nevertheless, sulfur is an essential plant micronutrient in biochar for land application, and the pre-treatment can enrich the derived biochar of sulfur contents compared to RB-biochar.

The elemental H/C and O/C ratio is typically used to measure biochar aromaticity and biochemical stability and can be correlated to pyrolysis temperature [44]. The decrease in the H/C ratio indicated higher biochar aromaticity due to the strong degree of carbonisation with increasing pyrolysis temperature [40]. Biochar produced at higher temperatures and from pre-treated biosolids had aromatic and hydrophobic structures through the loss of oxygen-containing functional groups (such as hydroxyl and carboxyl). Nan et al. [8] also observed that removing inherent minerals from sewage sludge via acid pre-treatment facilitated the disappearance of oxygen-containing functional groups such as C=O, O=C–O, and C–O, while promoting C–C/C=C bonds, indicating higher aromatisation of biochar. Pyrolysis temperature plays an important role in shaping biochar's surface chemistry and organic structure. At lower temperatures (<500 °C), the hydrogen-bonding network in the organic compounds is eliminated, and hydroxyl groups are oxidised to carboxyls. At higher temperatures, methylene groups are heavily dehydrogenated to aromatic structures [45]. The bulk (or apparent) densities of the biochar obtained at 300–700 °C from the three biosolids feed samples were found to vary substantially. Generally, there was a monotonic increase in bulk density with increasing pyrolysis

Table 3
Effect of pre-treatment and pyrolysis temperature on metal concentration in biochar.

Temp. (°C)	300			500			700		
	RB	TB	TB_nw	RB	TB	TB_nw	RB	TB	TB_nw
Major metal oxides (wt%)									
Al ₂ O ₃	2.1	1.7	1.7	3.0	2.5	2.0	3.4	2.8	2.7
CaO	14.3	8.7	12.9	17.3	10.8	14.2	18.8	11.7	15.9
Fe ₂ O ₃	6.6	4.6	4.0	8.0	6.0	4.7	8.2	6.4	5.0
K ₂ O	1.5	0.3	0.5	1.8	0.4	0.6	1.9	0.4	0.6
MgO	1.1	0.3	0.3	1.6	0.5	0.4	1.8	0.5	0.5
Na ₂ O	0.5	BDL ^a	BDL	0.7	BDL	BDL	0.7	BDL	BDL
P ₂ O ₅	3.4	1.5	1.3	4.4	1.9	1.4	4.8	2.1	1.7
SiO ₂	7.7	10.6	8.6	10.6	14.9	8.9	11.9	16.0	11.4
Heavy metals (mg/kg)									
As	3.0	2.0	2.5	3.5	2.4	3.0	2.1	1.7	1.9
Cd	1.8	0.5	0.7	2.5	0.7	1	1.8	0.8	0.8
Cr	30	15	23	47	28	32	35	30	22
Cu	890	1100	1600	950	1200	1800	1200	1400	1900
Ni	26	10	17	38	13	24	29	16	16
Pb	29	25	21	37	40	34	40	40	36
Zn	1300	400	770	1500	580	970	1600	530	930

^a BDL – Below detection limit

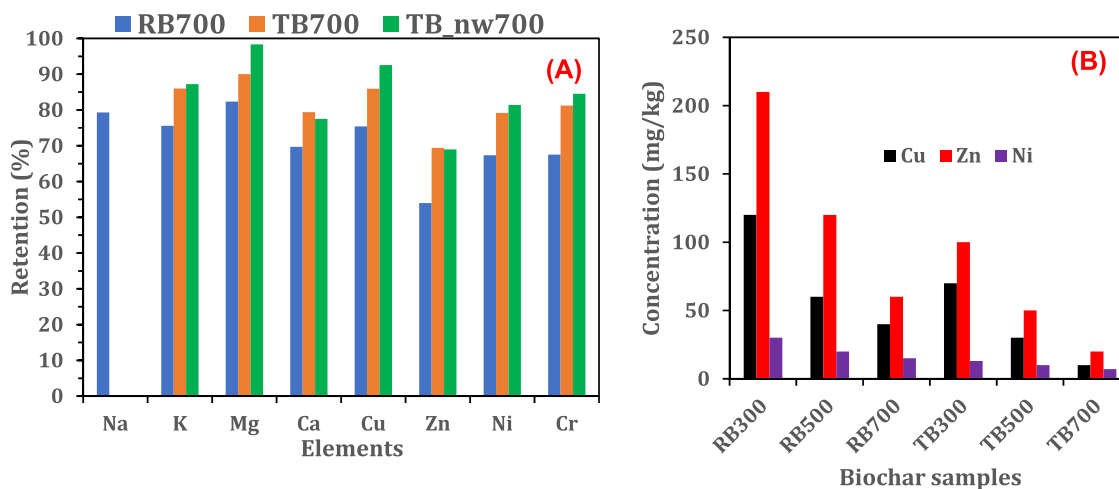


Fig. 3. Effect of pre-treatment on (A) metal retention in biosolids biochar at 700 °C (B) bioavailable HMs concentration in biosolids biochar.

temperature reflected by the extent of volume reduction caused by pyrolysis. The bulk density of the RB-biochar was the highest, followed by TB_nw and TB-biochar, which is reflective of the lower ash content in treated biosolids relative to raw biosolids at a given pyrolysis temperature. Lastly, the pH of the biochar was observed to generally increase with increasing temperature largely due to the destruction of acidic functional groups and the increase in the concentration of basic functional groups such as char-N as well as metal oxides in the ash contents. Biochar produced from TB_nw at 300 °C was more acidic (pH 4) than biochar from other biosolids samples (pH 5.5–5.8) due to residual sulfuric acid in TB_nw. However, the pH of all biochar samples was similar at 700 °C suggesting the inherent acid in TB_nw has no influence on the resultant biochar pH, possibly because acidic metal sulfate salts have been cracked into normal metal sulfate or oxides form.

3.4.2. Metals concentration, retention, and bioavailability

The effect of pre-treatment on the concentration of inorganic elements in biochar was assessed. The compositions and concentration of metal oxides and HMs in the raw and treated biosolids-derived biochar produced at 300–700 °C are summarised in Table 3. The major ash-forming elements enriched in the biochar are oxides of Ca, Si, Fe, P, Al, K, Mg, and Na in decreasing order. Expectedly, the metal concentration increased with increasing pyrolysis temperature (decreasing biochar yield). The metal concentrations were highest for the RB biochar

samples containing the full spectrum of metal components. The prior removal of inorganic elements during pre-treatment substantially reduced the final concentration in the treated biosolids biochar. Notably, Na removal in biosolids via pre-treatment was almost 100%; consequently, Na₂O was only detected in RB biochar and was below the detection limit in all treated biosolids biochar samples. According to Fig. 3(A), the metal contents in the respective biosolids feed were largely retained in their derived biochar with a retention rate of > 90%, confirming the thermal stability of the metal species at the pyrolysis conditions. However, at the highest pyrolysis temperature (700 °C), there appears to be some volatilisation of AAEMs, particularly Ca and K, attributed to the decomposition of Ca-containing minerals such as CaCO₃ in the case of RB and CaSO₄ hydrates in the case of treated biosolids. In addition, the sublimation of KCl at high temperatures may cause K loss from the biochar [29]. Moreover, recalcitrant organics bonded to mineral matter may decompose at high temperatures leading to the release of metal species to the gas phase, lowering their recovery in the biochar [46].

Heavy metals are limiting contaminants in biosolids and their derived char, particularly for land application purposes. The HMs concentration in the biochar obtained from the three biosolids samples at 300–700 °C is shown in Table 3. The concentration generally increases with temperature with an enrichment factor of at least 1.2 times the concentration in the parent biosolids at 300 °C and up to 2.5 times at

700 °C. Up to 500 °C, there was an upward trend in the increase in the HMs concentration. However, at 700 °C, there was a decline in the concentration of the metals attributed to the rise in the thermal volatilities of certain elements. Specifically, at 700 °C, less than 50% of As and Cd were retained in the biochar, and Zn retention was less than 70%. Zhang et al. [47] reported similar observations during sewage sludge pyrolysis, with Hg being completely partitioned in the oil and gas product fractions as low as 300 °C while Cd and As had less than 10% recovery in the biochar at 650 °C. At 700 °C, the thermal volatilities of HMs can be ranked as Cu < Cr < Ni < Pb < Zn < As = Cd, suggesting that Cu, Cr, and Ni were least involved in migration during biosolids pyrolysis. This observation was similar to that reported in previous works [29,47]. Cu had the highest retention in biochar due to the high affinity of Cu to organic matter [17]. The higher organic matter retention in TB/TB_nw biochar also explains the higher Cu concentration in treated biosolids biochar compared to RB biochar. The poor removal of Pb with sulfuric acid resulted in the inconsequential effect of pre-treatment on Pb concentration in the biochar obtained from all samples. The concentration of all other HMs was lower in treated

biosolids biochar compared to RB biochar, with the lowest for TB biochar. However, the enrichment factor for a given HM was higher in TB biochar than in RB biochar. The low ash content in TB weakens the dilution effect resulting in higher MEF. For instance, in biochar obtained at 500 °C, Cd concentration increases by 1.9 times for RB and 2.3 times for TB; similarly, Zn enrichment was 1.8 for TB and 3.6 for TB. Besides the reduction of metal concentration by pre-treatment, there was an increase in the stability of the metal as their recovery in the biochar was higher for treated samples than the RB (Fig. 3(A)). The removal of acid-exchangeable (ionisable) and reducible metal (bound to carbonates and Fe-Mn oxides) fractions during pre-treatment facilitated the transformation and stabilisation of the remaining HMs in the treated samples to oxidisable (bound to organic matter) and residual fractions (bound to silicates) [48]. Therefore, stabilising HMs in the TB and TB_nw biochar compared to RB biochar can reduce the undesired migration of HMs into oil and gas product fraction during biosolids pyrolysis.

The reduction of HMs concentration and the increased metal stability in the biochar facilitated by pre-treatment may not be enough indication of the potential toxicity of the residual HMs. Therefore, DTPA-plant

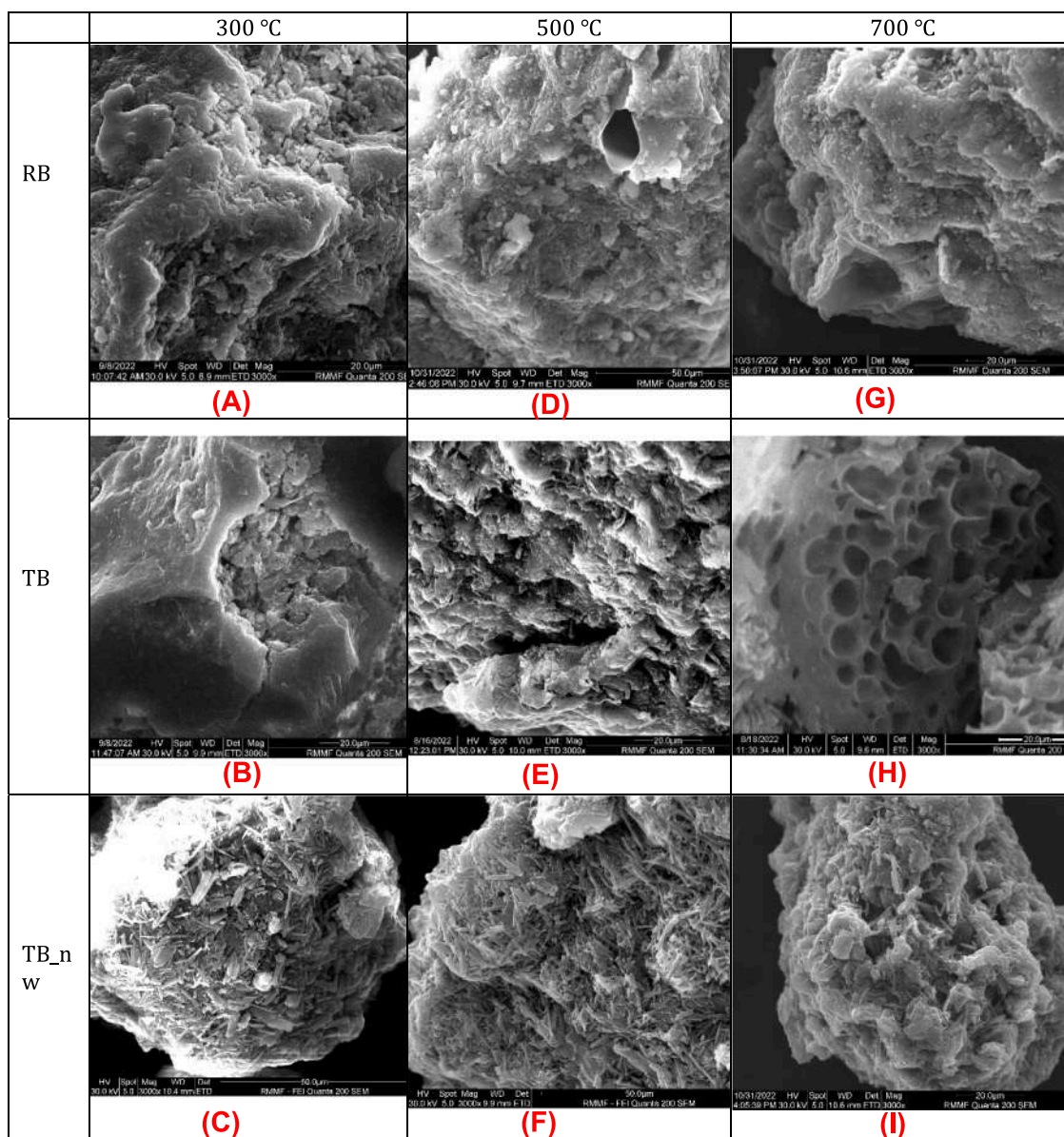


Fig. 4. Effect of pre-treatment and temperature on the surface morphology of biosolids biochar (A) RB300 (B) TB300 (C)TB_nw300 (D) RB500 (E) TB500 (F) TB_nw500 (G) RB700 (H) TB700 (I) TB_nw700.

available HMs concentration was assessed, and the result showed that pre-treatment drastically reduces the bioavailable metal concentration in the biochar (Fig. 3(B)). Specifically, at 500 °C, the DTPA-extractable Cu concentration from RB biochar was 60 mg/kg, while it was 20 mg/kg for TB biochar. Similarly, Zn bioavailable concentration in TB biochar was reduced by at least 50% compared to RB biochar at the same pyrolysis temperature. The effect of pre-treatment follows a similar trend for Ni bioavailable concentration reaching about 7 mg/kg in TB700 compared to 15 mg/kg in RB700. The higher organic matter retention and surface functional groups in TB biochar could promote organometallic complexation reaction, thereby enhancing HMs immobilisation in the char matrix and decreasing the extractable metal concentrations [49].

3.4.3. Morphological properties

The SEM imaging of the biochar obtained from raw and treated biosolids samples at 300–700 °C is shown in Fig. 4. There was a clear distinction in the image of the samples, highlighting the effect of pre-treatment and pyrolysis temperatures on biochar surface morphology. The image of the biochar obtained at 300 °C (Fig. 4(A-C)) showed a bulky structure with particle shrinkage resulting from the dehydration and decarboxylation of organic matter. The char sample from RB and TB appeared similar (Fig. 4(A&B)), and the biochar sample from TB_nw (Fig. 4(C)) had a flaky structure with a surface covering arising from the acidic metal sulfate salts. At 500 °C, the image of the char samples (Fig. 4(D-F)) showed a matured organic conversion with the compact structure becoming disintegrated into small fragments; however, the pore structure is not well developed with traces of pore openings. The char from TB_nw still showed the thermally stable metal sulfate salts coverings, limiting the full development of the pores (Fig. 4(F)). At 700 °C (Fig. 4(G-I)), organic compounds have been completely degraded, and the char cracking reaction removed residual volatiles, opening up pores within the char matrix and exposing the char surface. TB biochar has a strong pore development (Fig. 4(H)) due to enhanced devolatilisation and lower ash residues. The RB700 (Fig. 4(G)), due to its high ash content, had poor pore structure development attributed to the creation of stable organometallic compounds within the aromatic structures, which are recalcitrant to thermal volatilisation at 700 °C [29]. It has been suggested that high levels of ash-forming minerals in biosolids would require higher pyrolysis temperatures for their biochar pore structure to be fully developed compared to low-ash-containing biomass biochar [6]. Hence, reducing the ash minerals in biosolids by mild sulfuric acid pre-treatment was beneficial in producing biochar with a porous structure, albeit the effect was profound only at 700 °C. However, the presence of residual acid and acidic metal sulfate salts inhibited volatile removal and caused pore blockage, as observed in the SEM images of TB_nw.

The BET-specific surface areas and average pore volume of the biochar samples are summarised in Table 4. At 300 °C, the surface area (15–25 m²/g) of the biochar from all feed samples was largely similar;

however, the pore volume of TB (0.024 cm³/g) was almost double of the RB (0.012 cm³/g) supporting the elevated rate of inorganic removal by pre-treatment and organic matter removal from the bulk of TB sample during pyrolysis. Increasing the pyrolysis temperature to 500 °C increased the biochar surface area by at least 40%, reaching 27 m²/g for RB and 40 m²/g for TB, and a further increase in temperature to 700 °C increased the surface area to 55 m²/g for RB and 107 m²/g to TB. The 2-fold higher surface area of TB-biochar compared to RB-biochar was supported by the improved pore structure development of TB biochar, as shown in Fig. 4(H). Higher surface area and pore volume are indicative of the stability of the char structure, which can enhance their application in catalysis and adsorption [6]. The pore size distribution indicates that the biochar materials are largely mesoporous with pore width in the 2–50 nm range. However, the relatively lowest pore width in the case of TB_nw indicates possible pore blockage by the poorly soluble metal sulfate salt, particularly CaSO₄ hydrates that covers the surface as observed under the SEM imaging.

3.5. Effect of pre-treatment on bio-oil compositions

The chemical compositions identified through the GC/MS analysis of the bio-oil obtained from the pyrolysis of raw and treated biosolids are summarised in Table 5. The results showed that the bio-oil is a complex mixture of various chemical compounds grouped into oxygenates, nitrogenated compounds, sulfur-containing, and hydrocarbons. Temperature and pre-treatment considerably affect the evolution of volatile organic compounds in the bio-oil. Generally, for all biosolids samples, the yield of nitrogenated and oxygenated compounds decreased with increasing pyrolysis temperature, while hydrocarbons and phenol yield increased with temperature. The effects of pre-treatment on the distribution of chemical components in the bio-oil varied with pyrolysis temperature. For instance, pre-treatment enhanced hydrocarbon production from 20% in RB to 30–35% in treated biosolids at ≥ 500 °C, whereas anhydrosugars yield was increased from 2.1% in RB to 4.5% in TB only at 300 °C, while phenolics yield was similar for all bio-oils at all temperatures.

The bio-oil obtained at 300 °C consists mainly of high molecular weight nitrogenated and oxygenated compounds, with major chemical species being *N*-heterocyclics and ketones. Nitrogenated compounds in bio-oil originated from the thermal devolatilisation of proteins, while ketonic compounds are from the primary decomposition of carbohydrates. *N*-heterocyclics could be formed by dehydrogenation of the amino group present in proteins and nucleic acids in biosolids and through the addition of HCN and/or NH₃ to benzene/toluene aromatic ring during pyrolysis [50]. Dehydration and decarboxylation of organic matter are prominent thermolysis reactions at lower temperatures resulting in the formation of high-molecular-weight reactive oxygenate fragments such as R-CHO, R-C-O-R, R-CO-OH, and R-O-R [51]. Pyrolysis at 300 °C was selective for producing a few kinds of *N*-heterocyclics, amides/amines, and ketones, irrespective of the biosolids feed

Table 4
Surface properties of biochar samples.

Pyrolysis temperature (°C)	Feed samples	Surface properties		
		BET specific surface area (m ² /g)	BJH average pore volume (cm ³ /g)	BJH average pore width (nm)
300	RB	15.2	0.012	7.94
	TB	25.2	0.024	8.00
	TB_nw	20.5	0.015	7.84
500	RB	26.9	0.021	8.67
	TB	43.7	0.030	8.81
	TB_nw	32.9	0.017	8.22
700	RB	55.3	0.039	7.65
	TB	106.9	0.061	8.54
	TB_nw	72.5	0.043	7.03

Table 5
GC/MS analysis showing the chemical composition of the bio-oil samples.

Bio-oil compositions									
Pyrolysis temperature (°C)	300			500			700		
Biosolids samples	RB	TB	TB_nw	RB	TB	TB_nw	RB	TB	TB_nw
Compounds	Peak Area (%)								
Pyrazine	14.1	2.9	16.3	-	-	2.3	4.5	-	-
Pyridine	8.3	6.4	8.5	3.0	1.5	2.3	1.7	1.0	8.5
Pyrrrole	3.4	0.4	-	8.2	1.4	0.4	1.6	5.7	0.5
Azole	0.3	0.2	-	0.9	6.3	0.9	9.0	8.0	0.5
Amines	5.3	5.8	16.9	3.4	2.0	0.6	1.3	0.4	4.6
Amides	19.3	17.6	8.5	7.4	4.8	2.1	4.2	2.3	1.6
Nitriles	1.8	1.1	3.2	4.5	7.1	7.2	3.8	5.9	6.5
Total Nitrogenated	52.5	34.4	53.4	27.3	23.0	15.8	26.2	23.7	22.2
Esters	1.2	2.9	3.5	8.3	15.0	18.8	14.4	10.9	13.0
Ethers	-	-	-	2.5	-	-	2.5	-	-
Ketones	30.5	37.7	16.7	20.9	11.5	8.8	10.6	8.6	6.1
Aldehydes	-	1.0	-	-	0.8	-	-	0.9	1.0
Acids	2.1	4.5	7.8	4.4	0.9	3.8	3.6	3.3	6.9
Alcohols	2.1	0.5	-	0.8	1.5	9.3	1.5	3.0	6.6
Furans	1.0	10.6	10.4	-	-	-	-	-	0.5
Total Oxygenated	37.0	57.2	38.4	36.9	29.7	40.6	32.6	26.7	34.0
1,4:3,6-Dianhydro- α -D-glucopyranose	1.2	1.9	-	-	-	-	-	-	-
2,3,4-Trimethyllevoglucosan	0.5	0.4	-	-	-	-	-	-	-
Maltol	-	0.7	0.7	-	-	-	-	-	-
Others	0.4	1.5	-	-	-	-	-	-	-
Total Anhydrosugars	2.1	4.5	0.7	-	-	-	-	-	-
Phenols	8.6	1.0	2.7	11.3	9.3	4.7	8.9	10.2	6.0
<i>p</i> -Cresol	-	-	-	4.1	5.3	1.4	4.8	6.2	4.2
Total Phenolics	8.6	1.0	2.7	15.4	14.6	6.1	13.7	16.4	10.2
Olefin	-	0.3	1.0	1.9	2.1	2.1	2.9	2.3	1.8
Paraffin	-	1.2	0.8	6.2	7.7	8.1	11.6	10.4	5.2
BTXS ^a	-	0.6	1.2	12.4	20.6	25.0	13.1	18.6	20.9
Polyaromatic	-	-	-	-	0.4	0.3	-	0.8	2.8
Total Hydrocarbons	-	2.1	3.0	20.5	30.8	35.5	27.6	32.1	30.7
Total S-containing compounds	-	1.0	1.5	-	2.0	2.7	-	0.9	3.0

^a BTXS- Benzene, Toluene, Xylene, and Styrene

samples. However, inherent minerals in RB and residual acid in TB_nw facilitated denitrogenation reactions to generate more volatile-N compounds than TB. For instance, at 300 °C, total N-compounds were 53% for RB and TB_nw and 34% for TB. Significant thermal cracking of heavy N-heterocyclic compounds to simple aromatic/aliphatic N-compounds occurred at higher pyrolysis temperatures (500–700 °C), reducing total nitrogenated compounds in the bio-oil to \approx 23% for all samples. The effect of pre-treatment on the evolution of N-compounds was less intense at 500 and 700 °C. It has been observed that the interaction between mineral matter and N-containing compounds in biosolids was strongly limited by pyrolysis temperature [52].

Notably, anhydrosugars (including sugar alcohols) production was sensitive to pyrolysis temperatures. It was detected only at 300 °C, and the yield was improved by more than 50% following the removal of AAEMs in TB. At 500–700 °C, pre-treatment had no impact on the production of anhydrosugars as they are highly susceptible to secondary degradation facilitated by metal and acid catalysts as well as higher pyrolysis temperatures [53]. However, biosolids pre-treatment favoured the production of sugar dehydration products such as maltol and furans (10%), mainly comprising 3-HMF, furfural, and 5-methyl furfural. The acid catalysis of sugars is a popular route to enhance the formation of furfural compounds [54]. The passivation of AAEMs by acid infusion selectively enhanced sugar dehydration products, such as levoglucosone and furfural, whose yield was observed to be related to the quantity of acid added [55]. Phenols and their derivatives may originate from biosolids pyrolysis through the secondary decomposition of polysaccharides and proteins and are generally enhanced at higher temperatures from aromatisation reactions [56]. At 300 °C, the total phenolics yield was less than 10%, mostly detected in RB bio-oil. At higher temperatures, phenolics yield increased to \approx 15% for both RB and TB, whereas it was no more than 10% for TB_nw. Mineral removal by pre-treatment had no significant effect on phenol production; however,

residual acid in TB_nw suppressed phenol formation relative to RB. Other works [36,57] have also suggested that phenol precursor such as lignin is relatively inert to AAEMs. While AAEMs are largely inert in catalysing the cleavage of the ester group in lignin to produce guaiacols (vinyl-phenols), it has been found effective in promoting the cleavage of β -O-4 aryl ether bonds to produce simple phenolic monomers such as cresols [55]. This could explain the higher yield of *p*-cresol with acid-pre-treated biosolids compared to RB.

Hydrocarbon production increased monotonically with temperature, and it grew from 0% to 3% at 300 °C to 20–35% at 500 °C for all samples, with RB having the lowest yield. Raising the temperature to 700 °C increased hydrocarbon yield to 28% for RB, slightly decreasing the yield to about 32% for treated biosolids. Monoaromatic hydrocarbons, mainly benzene, toluene, xylene, and styrene (BTXS), are the major compounds in the bio-oil at higher temperatures \geq 500 °C. In contrast, aliphatic hydrocarbons, mainly paraffin and olefin, were detected in bio-oil from untreated biosolids at $<$ 500 °C. Acid pre-treatment enhanced aromatisation reactions, which increased the yields of monoaromatic hydrocarbons due to the suppression of AAEMs-catalysed ring opening and fragmentation reactions that would otherwise convert -CH to light oxygenates, COx gases, and char [36,58]. In a previous study [36], acid washing and infusion enhanced the formation of aromatic hydrocarbons by \sim 30%; however, both pre-treatment did not significantly change the yield of olefins, similar to the observation in the current work. The weaker effect of inherent AAEMs caused by acid pre-treatment increased the formation of undesired stable polycyclic aromatic hydrocarbons (PAHs) in bio-oil from TB and TB_nw; however, PAHs were not detected in RB bio-oil at all temperatures. AAEMs and their minerals can enhance the cracking of heavy PAHs into monoaromatics, particularly at higher temperatures [59]. Lastly, aromatic sulfur compounds such as benzisothiazole, thiazolidine, thiophene, and aliphatic S-compounds, mainly methyl sulfides, were detected in the bio-oil obtained from treated

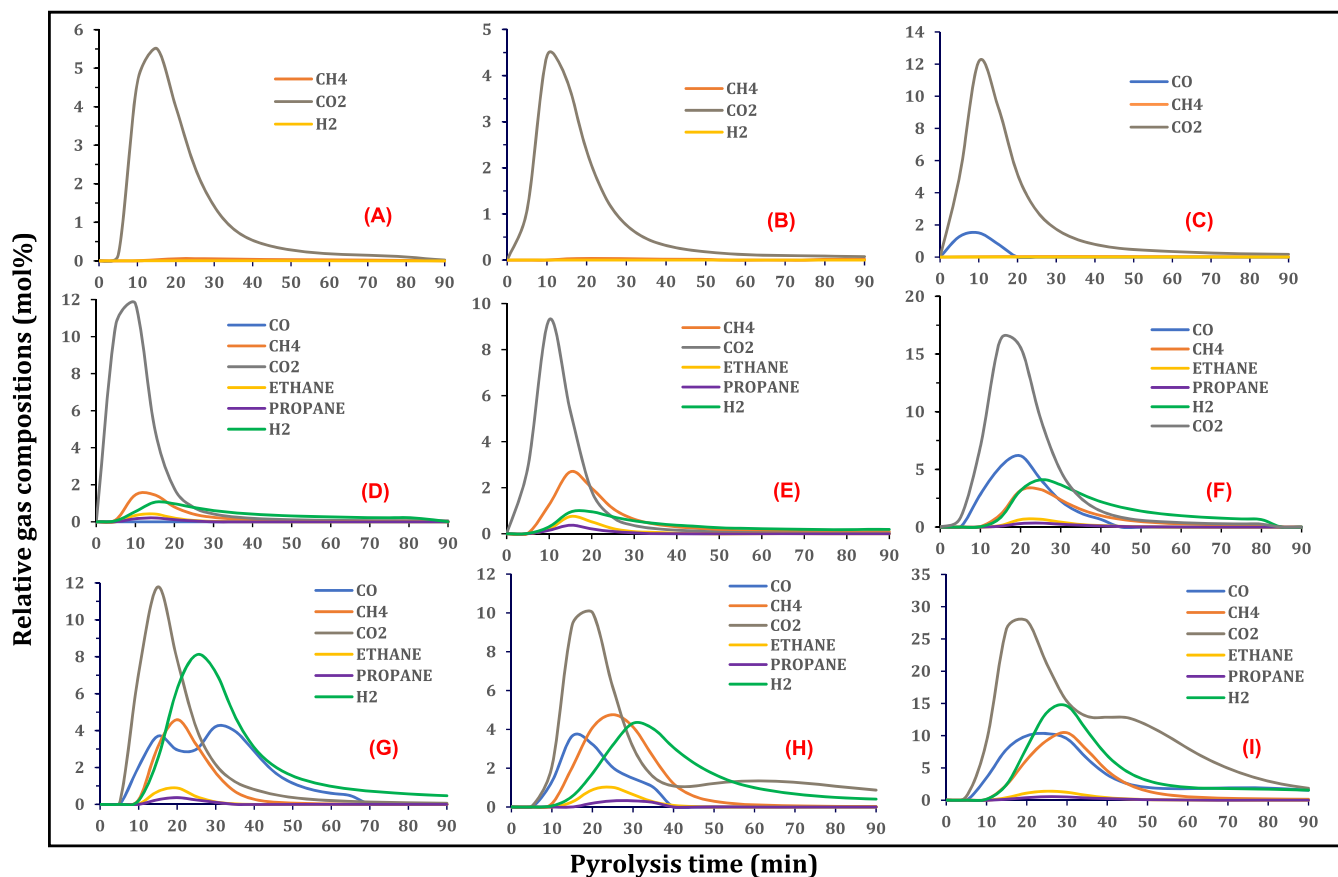


Fig. 5. Effect of pre-treatment and temperature on pyrolysis gas compositions (A) RB300 (B) TB300 (C)TB_nw300 (D) RB500 (E) TB500 (F) TB_nw500 (G) RB700 (H) TB700 (I) TB_nw700.

biosolids. The evolution of these S-compounds was stronger at ≥ 500 °C and for TB_nw (up to 3%). Therefore, the acid treatment should be accompanied by a neutralisation step, as in TB, to mitigate the release of volatile S-compounds.

Due to the generally high nitrogen and oxygen contents, the bio-oil may not be suitable as fuel for energy recovery. However, the chemical value of the bio-oil obtained at 300 °C can be explored for the selective recovery of N-containing compounds, and the ketone-rich fraction can be subjected to catalytic hydrodeoxygenation to produce olefins [60]. Therefore, biosolids pyrolysis at 300 °C may be considered a thermal pre-treatment step for the reduction of nitrogen and oxygen contents and improve hydrocarbon yield during subsequent pyrolysis at higher temperatures [61]. The addition of acid pre-treatment can further enhance the chemical value of the bio-oil by increasing sugars, furans, and aromatic hydrocarbon, as observed in the current work. Fonts et al. [62] reported that ammonia, α -olefins, n-paraffins, aromatic hydrocarbons, nitriles, phenols, fatty acids, short carboxylic acids and indole were the most attractive chemical compounds in biosolids bio-oil.

3.6. Effect of pre-treatment on pyrolysis gas compositions

The evolution profile of non-condensable gases from the pyrolysis of raw and treated biosolids at 300–700 °C is shown in Fig. 5. The identified gas components are carbon oxides (CO and CO₂), H₂, and C₁–C₃ saturated hydrocarbon gases (methane, ethane, and propane). The concentration of the gases was low at the start of pyrolysis as the feed was gradually heated to the desired temperature. The gas concentration steadily increased between 10 and 30 min; after that, the concentration gradually decreased, reaching zero at 60–90 min. The most abundant

gas components were H₂, CO, CO₂ and CH₄, while only traces of ethane and propane were detected at higher pyrolysis temperatures > 500 °C. Generally, gas production increased with increasing pyrolysis temperature due to the profound thermal cracking of primary decomposition products and secondary reactions. At 300 °C (Fig. 5(A–C)), CO₂ was the dominant gas component, with traces of CH₄ and H₂ in the pyrolysis gas stream largely from the decarboxylation of organic matter. At higher pyrolysis temperatures, gasification reactions matured, and more gas components were formed at higher concentrations stemming from the thermal cracking of heavy molecular weight volatiles to lighter ones accompanied by the release of C₁–C₃ hydrocarbons (Fig. 5(D–I)). At 700 °C (Fig. 5(G–I)), the gas evolution was stronger, and the concentrations were highest attributed to the profound secondary cracking reactions heightened by char-volatile interactions [63].

The removal or passivation of inherent metals in biosolids via pre-treatment affected the gas evolution and concentration during pyrolysis, especially at higher pyrolysis temperatures. The pyrolysis of TB produced less CO₂, CO, and H₂ but slightly more C₁–C₃ hydrocarbons than RB, suggesting that pre-treatment inhibited gas production due to the inferior catalytic cracking effect of ash elements. For example, at 700 °C, the highest CO and H₂ concentration was 4.2 mol% and 8 mol%, respectively, for RB (Fig. 5(G)), and it was 3.6 mol% and 4.3 mol%, respectively, for TB (Fig. 5(H)). Secondary cracking was prominent and catalysed by the native metal in RB, leading to higher concentrations of CO and H₂. The second CO peak in RB at 700 °C (Fig. 5(G)) after 30 min pyrolysis time can be attributed to Boudouard char gasification reactions where CO₂ is reacted with carbon to give CO [30]. Notably, the highest gas concentrations were observed during the pyrolysis of TB_nw at all temperatures. The XRD pattern of TB_nw identified Ca(HSO₄)₂ and

Fe(HSO₄)₃ as the major acidic sulfate salts, which facilitated H₂ production via the release of H⁺ through thermal hydrolysis reactions to form normal sulfate salts (CaSO₄ and Fe₂(SO₄)₃) [64]. The presence of residual acid in TB_nw had a remarkable catalytic effect on gas production, with CO₂, CO, CH₄, and H₂ yield reaching a maximum concentration of 28 mol%, 10 mol%, 10.5 mol%, and 15 mol%, respectively (Fig. 5(I)). Whereas, with the full spectrum of metals in RB, the maximum gas concentration at 700 °C was 12 mol% CO₂, 4 mol% CO, 4.5 mol% CH₄, and 8 mol% H₂ (Fig. 5(G)). The improved gas production in TB_nw despite lean mineral matter compared to RB was attributed to the dehydration reactions catalysed by residual H₂SO₄, favouring water-gas reactions [42]. Biosolids acid pre-treatment for demineralisation (as in TB) can be helpful to weaken gas production and CO₂ release, while pre-treatment as in TB_nw strengthened gas production, and CO₂ yield was more than 2-fold higher than that from RB.

4. Conclusions

The quality of biosolids as feedstock for pyrolysis can be improved by acid pre-treatment to selectively remove the ash-forming elements and HMs without degrading the organic matter. Mild acid pre-treatment process (using 3% v/v H₂SO₄ at 25 °C for 60 min) followed by a water washing step achieved about 40% reduction of ash content and a 10% increase in volatile matter with carbon retention of 80%. In contrast, the acid treatment without the water washing step achieved lower demineralisation efficiency (28%) with higher carbon retention (88%). At all operating temperatures, the pyrolysis of neutralised acid-treated biosolids produced higher bio-oil and lower biochar yield due to improved organic matter devolatilisation and inorganic content reduction. The presence of residual acid in treated biosolids inhibited organic matter conversion to bio-oil; however, it enhanced gas production attributed to dehydration reactions and hydrolysis of acidic metal sulfate salts to normal metal sulfate salts. Biochar obtained from treated biosolids had higher organic matter retention, calorific value, fuel ratio, and fixed carbon due to the weakened catalytic cracking of organics, particularly at higher pyrolysis temperatures. Biosolids pre-treatment increased the stability and reduced the concentration and bioavailability of HMs in the derived biochar. The bio-oil composition was impacted by pre-treatment, and at 300 °C, anhydrosugars yield doubled in treated biosolids' bio-oil compared to raw biosolids' bio-oil. While pre-treatment did not have much effect on phenol production, monoaromatic hydrocarbon yield was remarkably improved. However, the evolution of PAHs and sulfur-containing compounds was stronger during the pyrolysis of treated biosolids than raw biosolids. Biosolids acid pre-treatment with the water washing step is preferred to increase bio-oil yield and enhance biochar quality.

CRedit authorship contribution statement

Ibrahim Gbolahan Hakeem: Conceptualization, Methodology, Formal analysis, Investigation, Writing - original draft, Writing - review & editing. **Pobitra Halder:** Validation, Writing - review & editing. **Savankumar Patel:** Writing - review & editing. **Abhishek Sharma:** Writing - review & editing. **Rajender Gupta:** Writing - review & editing. **Aravind Surapaneni:** Resources, Supervision. **Jorge Paz-Ferreiro:** Supervision, Writing - review & editing. **Kalpita Shah:** Conceptualization, Methodology, Validation, Supervision, Project administration.

Declaration of Competing Interest

The authors declare that they have no known competing financial interests or personal relationships that could have appeared to influence the work reported in this paper.

Data availability

Data will be made available on request.

Acknowledgements

This work is supported through Top-Up Scholarships provided by the School of Engineering, RMIT University and the ARC Training Centre for the Transformation of Australia's Biosolids Resource at RMIT University, Australia. The use of the Scanning Electron Microscope instrument in the RMIT Microanalysis and Microscopy Facility is acknowledged. The BET equipment in the Advanced Porous Materials Lab at RMIT University was used in this study. Finally, the first author acknowledged the PhD research stipend scholarship received from RMIT University, Australia.

Appendix A. Supporting information

Supplementary data associated with this article can be found in the online version at [doi:10.1016/j.jaap.2023.106087](https://doi.org/10.1016/j.jaap.2023.106087).

References

- [1] A. Gianico, C.M. Braguglia, A. Gallipoli, D. Montecchio, G. Mininni, Land application of biosolids in Europe: possibilities, con-strains and future perspectives, *Water* 13 (2021) 103, <https://doi.org/10.3390/W13010103>.
- [2] N. Gao, K. Kamran, C. Quan, P.T. Williams, Thermochemical conversion of sewage sludge: A critical review, *Prog. Energy Combust. Sci.* 79 (2020), 100843, <https://doi.org/10.1016/j.pecs.2020.100843>.
- [3] W. Zhang, Y. Liang, Effects of hydrothermal treatments on destruction of per- and polyfluoroalkyl substances in sewage sludge, *Environ. Pollut.* 285 (2021), 117276, <https://doi.org/10.1016/j.envpol.2021.117276>.
- [4] J.J. Ross, D.H. Zitomer, T.R. Miller, C.A. Weirich, P.J. Mcnamara, Emerging investigators series: pyrolysis removes common microconstituents triclocarban, triclosan, and nonylphenol from biosolids, *Environ. Sci. Water Res. Technol.* 2 (2016) 282–289, <https://doi.org/10.1039/C5EW00229J>.
- [5] O.S. Djandja, Z.C. Wang, F. Wang, Y.P. Xu, P.G. Duan, Pyrolysis of municipal sewage sludge for biofuel production: A review, *Ind. Eng. Chem. Res.* 59 (2020) 16939–16956, <https://doi.org/10.1021/acs.iecr.0c01546>.
- [6] S. Patel, S. Kundu, P. Halder, N. Ratnayake, M.H. Marzbali, S. Aktar, E. Selezneva, J. Paz-Ferreiro, A. Surapaneni, C.C. de Figueiredo, A. Sharma, M. Megharaj, K. Shah, A critical literature review on biosolids to biochar: an alternative biosolids management option, *Rev. Environ. Sci. Biotechnol.* 19 (2020) 807–841, <https://doi.org/10.1007/s11157-020-09553-x>.
- [7] P. Giudicianni, V. Gargiulo, C.M. Grottola, M. Alfè, A.I. Ferreiro, M.A.A. Mendes, M. Fagnano, R. Ragucci, Inherent metal elements in biomass pyrolysis: a review, *Energy Fuels* 35 (2021) 5407–5478, <https://doi.org/10.1021/ACS.ENERGYFUELS.0C04046>.
- [8] H. Nan, F. Yang, L. Zhao, O. Mašek, X. Cao, Z. Xiao, Interaction of inherent minerals with carbon during biomass pyrolysis weakens biochar carbon sequestration potential, *ACS Sustain. Chem. Eng.* 7 (2018) 1591–1599, <https://doi.org/10.1021/ACSSUSCHEMENG.8B05364>.
- [9] Y. Niu, H. Tan, S. Hui, Ash-related issues during biomass combustion: Alkali-induced slagging, silicate melt-induced slagging (ash fusion), agglomeration, corrosion, ash utilization, and related countermeasures, *Prog. Energy Combust. Sci.* 52 (2016) 1–61, <https://doi.org/10.1016/j.pecs.2015.09.003>.
- [10] M.J. Bentley, J.P. Kearns, B.M. Murphy, R.S. Summers, Pre-pyrolysis metal and base addition catalyzes pore development and improves organic micropollutant adsorption to pine biochar, *Chemosphere* 286 (2022), 131949, <https://doi.org/10.1016/j.chemosphere.2021.131949>.
- [11] I.G. Hakeem, P. Halder, C.C. Dike, K. Chiang, A. Sharma, J. Paz-Ferreiro, K. Shah, Advances in biosolids pyrolysis: Roles of pre-treatments, catalysts, and co-feeding on products distribution and high-value chemical production, *J. Anal. Appl. Pyrolysis* 166 (2022), 105608, <https://doi.org/10.1016/J.JAAP.2022.105608>.
- [12] R. Patel, P. Zaveri, N.S. Munshi, Microbial fuel cell, the Indian scenario: developments and scopes, *Biofuels* 10 (2019) 101–108, <https://doi.org/10.1080/17597269.2017.1398953>.
- [13] N.A. Haji Morni, C.M. Yeung, H. Tian, Y. Yang, N. Phusunti, M.S. Abu Bakar, A. K. Azad, Catalytic fast Co-Pyrolysis of sewage sludge—sawdust using mixed metal oxides modified with ZSM-5 catalysts on dual-catalysts for product upgrading, *J. Energy Inst.* 94 (2021) 387–397, <https://doi.org/10.1016/J.JOIEI.2020.10.005>.
- [14] Z. Qiu, Y. Zhai, S. Li, X. Liu, X. Liu, B. Wang, Y. Liu, C. Li, Y. Hu, Catalytic co-pyrolysis of sewage sludge and rice husk over biochar catalyst: Bio-oil upgrading and catalytic mechanism, *Waste Manag* 114 (2020) 225–233, <https://doi.org/10.1016/J.WASMAN.2020.07.013>.
- [15] N. Rathnayake, S. Patel, I.G. Hakeem, J. Pazferreiro, A. Sharma, R. Gupta, C. Rees, D. Bergmann, J. Blackbeard, A. Surapaneni, K. Shah, Co-pyrolysis of biosolids with lignocellulosic biomass: Effect of feedstock on product yield and composition, *Process Saf. Environ. Prot.* (2023), <https://doi.org/10.1016/J.PSEP.2023.02.087>.



- [16] X. Wang, S. Deng, H. Tan, A. Adeosun, M. Vujanović, F. Yang, N. Duić, Synergetic effect of sewage sludge and biomass co-pyrolysis: A combined study in thermogravimetric analyzer and a fixed bed reactor, *Energy Convers. Manag* 118 (2016) 399–405, <https://doi.org/10.1016/j.enconman.2016.04.014>.
- [17] I.G. Hakeem, P. Halder, M.H. Marzbali, S. Patel, N. Rathnayake, A. Surapaneni, G. Short, J. Paz-Ferreiro, K. Shah, Mild sulphuric acid pre-treatment for metals removal from biosolids and the fate of metals in the treated biosolids derived biochar, *J. Environ. Chem. Eng.* 10 (2022), 107378, <https://doi.org/10.1016/J.JECE.2022.107378>.
- [18] G. Liu, M.M. Wright, Q. Zhao, R.C. Brown, Hydrocarbon and ammonia production from catalytic pyrolysis of sewage sludge with acid pretreatment, *ACS Sustain. Chem. Eng.* 4 (2016) 1819–1826, <https://doi.org/10.1021/acssuschemeng.6b00016>.
- [19] S. Tang, C. Zheng, Z. Zhang, Effect of inherent minerals on sewage sludge pyrolysis: Product characteristics, kinetics and thermodynamics, *Waste Manag* 80 (2018) 175–185, <https://doi.org/10.1016/j.wasman.2018.09.012>.
- [20] Z. Yang, D. Wang, G. Wang, S. Zhang, Z. Cheng, J. Xian, Y. Pu, T. Li, Y. Jia, Y. Li, W. Zhou, X. Xu, Removal of Pb, Zn, Ni and Cr from industrial sludge by biodegradable washing agents: Caboxyethylthiosuccinic acid and itaconic-acrylic acid, *J. Environ. Chem. Eng.* 9 (2021), 105846, <https://doi.org/10.1016/J.JECE.2021.105846>.
- [21] R. Kumar, V. Strezov, H. Weldekidan, J. He, S. Singh, T. Kan, B. Dastjerdi, Lignocellulose biomass pyrolysis for bio-oil production: A review of biomass pre-treatment methods for production of drop-in fuels, *Renew. Sustain. Energy Rev.* 123 (2020), 109763, <https://doi.org/10.1016/J.RSER.2020.109763>.
- [22] V.T. Pham, C.Y. Guan, P.C. Han, B.M. Matsagar, K.C.W. Wu, T. Ahamad, C. Y. Chang, C.P. Yu, Acid-catalyzed hydrothermal treatment of sewage sludge: effects of reaction temperature and acid concentration on the production of hydrolysis by-products, *Biomass - Convers. Biorefinery.* 13 (2021) 7533–7546, <https://doi.org/10.1007/S13399-021-01495-W/FIGURES/5>.
- [23] I.G. Hakeem, P. Halder, S. Aktar, M.H. Marzbali, A. Sharma, A. Surapaneni, G. Short, J. Paz-Ferreiro, K. Shah, Investigations into the closed-loop hydrometallurgical process for heavy metals removal and recovery from biosolids via mild acid pre-treatment, *Hydrometallurgy* 218 (2023), 106044, <https://doi.org/10.1016/J.HYDROMET.2023.106044>.
- [24] I. Beauchesne, R. Ben Cheikh, G. Mercier, J.F. Blais, T. Ourada, Chemical treatment of sludge: In-depth study on toxic metal removal efficiency, dewatering ability and fertilizing property preservation, *Water Res* 41 (2007) 2028–2038, <https://doi.org/10.1016/J.WATRES.2007.01.051>.
- [25] J. Shao, R. Yan, H. Chen, H. Yang, D.H. Lee, Catalytic effect of metal oxides on pyrolysis of sewage sludge, *Fuel Process. Technol.* 91 (2010) 1113–1118, <https://doi.org/10.1016/j.fuproc.2010.03.023>.
- [26] S. Tang, C. Zheng, F. Yan, N. Shao, Y. Tang, Z. Zhang, Product characteristics and kinetics of sewage sludge pyrolysis driven by alkaline earth metals, *Energy* 153 (2018) 921–932, <https://doi.org/10.1016/j.energy.2018.04.108>.
- [27] S. Tang, S. Tian, C. Zheng, Z. Zhang, Effect of Calcium Hydroxide on the Pyrolysis Behavior of Sewage Sludge: Reaction Characteristics and Kinetics, *Energy Fuels* 31 (2017) 5079–5087, <https://doi.org/10.1021/acs.energyfuels.6b03256>.
- [28] Y. Kim, W. Parker, A technical and economic evaluation of the pyrolysis of sewage sludge for the production of bio-oil, *Bioresour. Technol.* 99 (2008) 1409–1416, <https://doi.org/10.1016/j.biortech.2007.01.056>.
- [29] N. Rathnayake, S. Patel, P. Halder, S. Aktar, J. Pazferreiro, A. Sharma, A. Surapaneni, K. Shah, Co-pyrolysis of biosolids with alum sludge: Effect of temperature and mixing ratio on product properties, *J. Anal. Appl. Pyrolysis* 163 (2022), 105488, <https://doi.org/10.1016/J.JAAP.2022.105488>.
- [30] S. Patel, S. Kundu, P. Halder, G. Velusamy, B. Pramanik, Slow pyrolysis of biosolids in a bubbling fluidised bed reactor using biochar, activated char and lime, *J. Anal. Appl. Pyrolysis* 144 (2019) 1–11, <https://doi.org/10.1016/j.jaap.2019.104697>.
- [31] S.A. Channiwala, P.P. Parikh, A unified correlation for estimating HHV of solid, liquid and gaseous fuels, *Fuel* 81 (2002) 1051–1063, [https://doi.org/10.1016/S0016-2361\(01\)00131-4](https://doi.org/10.1016/S0016-2361(01)00131-4).
- [32] W.L. Lindsay, W.A. Norvell, Development of a DTPA Soil Test for Zinc, Iron, Manganese, and Copper, *Soil Sci. Soc. Am. J.* 42 (1978) 421–428, <https://doi.org/10.2136/SSSAJ1978.03615995004200030009X>.
- [33] E.P.A. Victoria, Guidelines for Environmental Management: Biosolids Land Application, Southbank, Victoria 3006, Australia, 2004.
- [34] X. Wang, L. Sheng, X. Yang, Pyrolysis characteristics and pathways of protein, lipid and carbohydrate isolated from microalgae *Nannochloropsis* sp, *Bioresour. Technol.* 229 (2017) 119–125, <https://doi.org/10.1016/J.BIORTECH.2017.01.018>.
- [35] S.R. Patel, S.K. Kundu, P.K. Halder, A. Setiawan, J. Paz-Ferreiro, A. Surapaneni, K. V. Shah, A Hybrid Kinetic Analysis of the Biosolids Pyrolysis using Thermogravimetric Analyser, *ChemistrySelect* 3 (2018) 13400–13407, <https://doi.org/10.1002/slct.201802957>.
- [36] K. Wang, J. Zhang, B.H. Shanks, R.C. Brown, The deleterious effect of inorganic salts on hydrocarbon yields from catalytic pyrolysis of lignocellulosic biomass and its mitigation, *Appl. Energy* 148 (2015) 115–120, <https://doi.org/10.1016/j.apenergy.2015.03.034>.
- [37] X. Zhu, L. Zhao, F. Fu, Z. Yang, F. Li, W. Yuan, M. Zhou, W. Fang, G. Zhen, X. Lu, X. Zhang, Pyrolysis of pre-dried dewatered sewage sludge under different heating rates: Characteristics and kinetics study, *Fuel* 255 (2019), 115591, <https://doi.org/10.1016/J.FUEL.2019.05.174>.
- [38] N. Gao, J. Li, B. Qi, A. Li, Y. Duan, Z. Wang, Thermal analysis and products distribution of dried sewage sludge pyrolysis, *J. Anal. Appl. Pyrolysis* 105 (2014) 43–48, <https://doi.org/10.1016/J.JAAP.2013.10.002>.
- [39] S. Zhou, Z. Wang, S. Liaw, C. Li, M. Garcia-perez, Effect of sulfuric acid on the pyrolysis of Douglas fir and hybrid poplar wood: Py-GC / MS and TG studies, *J. Anal. Appl. Pyrolysis* 104 (2013) 117–130, <https://doi.org/10.1016/j.jaap.2013.08.013>.
- [40] S. Aktar, M.A. Hossain, N. Rathnayake, S. Patel, G. Gasco, A. Mendez, C. de Figueiredo, A. Surapaneni, K. Shah, J. Paz-Ferreiro, Effects of temperature and carrier gas on physico-chemical properties of biochar derived from biosolids, *J. Anal. Appl. Pyrolysis* 164 (2022), 105542, <https://doi.org/10.1016/J.JAAP.2022.105542>.
- [41] D. Carpenter, T.L. Westover, S. Czernik, W. Jablonski, Biomass feedstocks for renewable fuel production: a review of the impacts of feedstock and pretreatment on the yield and product distribution of fast pyrolysis bio-oils and vapors, *Green. Chem.* 16 (2014) 384–406, <https://doi.org/10.1039/C3GC41631C>.
- [42] S. Zhou, D. Mourant, C. Lievens, Y. Wang, C. Li, M. Garcia-perez, Effect of sulfuric acid concentration on the yield and properties of the bio-oils obtained from the auger and fast pyrolysis of Douglas Fir, *Fuel* 104 (2013) 536–546, <https://doi.org/10.1016/j.fuel.2012.06.010>.
- [43] Y. Zhang, P. Lv, J. Wang, J. Wei, P. Cao, N. Bie, Y. Bai, G. Yu, Product characteristics of rice straw pyrolysis at different temperature: Role of inherent alkali and alkaline earth metals with different occurrence forms, *J. Energy Inst.* 101 (2022) 201–208, <https://doi.org/10.1016/J.JOEI.2022.01.016>.
- [44] X. Sun, R. Shan, X. Li, J. Pan, X. Liu, R. Deng, J. Song, Characterization of 60 types of Chinese biomass waste and resultant biochars in terms of their candidacy for soil application, *GCB Bioenergy* 9 (2017) 1423–1435, <https://doi.org/10.1111/GCBB.12435>.
- [45] X. Xiao, Z. Chen, B. Chen, H/C atomic ratio as a smart linkage between pyrolytic temperatures, aromatic clusters and sorption properties of biochars derived from diverse precursory materials, *Sci. Rep.* 6 (2016), <https://doi.org/10.1038/srep22644>.
- [46] M. Praspaliauskas, N. Pedišius, N. Striugas, Elemental Migration and Transformation from Sewage Sludge to Residual Products during the Pyrolysis Process, *Energy Fuels* 32 (2018) 5199–5208, https://doi.org/10.1021/ACS.ENERGYFUELS.8B00196/ASSET/IMAGES/LARGE/EF-2018-001968_0006.JPEG.
- [47] Z. Zhang, R. Ju, H. Zhou, H. Chen, Migration characteristics of heavy metals during sludge pyrolysis, *Waste Manag* 120 (2021) 25–32, <https://doi.org/10.1016/j.wasman.2020.11.018>.
- [48] D. del Mundo Dacera, S. Babel, Use of citric acid for heavy metals extraction from contaminated sewage sludge for land application, *Water Sci. Technol.* 54 (2006) 129–135, <https://doi.org/10.2166/wst.2006.764>.
- [49] Z. Cui, G. Xu, B. Ormeci, H. Liu, Z. Zhang, Transformation and stabilization of heavy metals during pyrolysis of organic and inorganic-dominated sewage sludges and their mechanisms, *Waste Manag* 150 (2022) 57–65, <https://doi.org/10.1016/J.WASMAN.2022.06.023>.
- [50] A. Fullana, J.A. Conesa, R. Font, I. Martin-Gullon, Pyrolysis of sewage sludge: nitrogenated compounds and pretreatment effects, *J. Anal. Appl. Pyrolysis* 69 (2003) 561–575, [https://doi.org/10.1016/S0165-2370\(03\)00052-4](https://doi.org/10.1016/S0165-2370(03)00052-4).
- [51] X. Yang, B. Wang, Y. Guo, F. Yang, F. Cheng, Co-hydrothermal carbonization of sewage sludge and coal slime for clean solid fuel production: a comprehensive assessment of hydrochar fuel characteristics and combustion behavior, *Biomass - Convers. Biorefinery* (2022), <https://doi.org/10.1007/s13399-022-03601-y>.
- [52] L.H. Wei, L.N. Wen, M.J. Liu, T.H. Yang, Interaction Characteristics of Mineral Matter and Nitrogen during Sewage Sludge Pyrolysis, *Energy Fuels* 30 (2016) 10505–10510, <https://doi.org/10.1021/acs.energyfuels.6b02146>.
- [53] I.G. Hakeem, P. Halder, M.H. Marzbali, S. Patel, S. Kundu, J. Paz-Ferreiro, A. Surapaneni, K. Shah, Research progress on levoglucosan production via pyrolysis of lignocellulosic biomass and its effective recovery from bio-oil, *J. Environ. Chem. Eng.* 9 (2021), 105614, <https://doi.org/10.1016/j.jece.2021.105614>.
- [54] S.R.G. Oudenhoven, R.J.M. Westerhof, N. Aldenkamp, D.W.F. Brilman, S.R.A. Kersten, Demineralization of wood using wood-derived acid: Towards a selective pyrolysis process for fuel and chemicals production, *J. Anal. Appl. Pyrolysis* 103 (2013) 112–118, <https://doi.org/10.1016/j.jaap.2012.10.002>.
- [55] S. Zhou, Y. Xue, J. Cai, C. Cui, Z. Ni, Z. Zhou, An understanding for improved biomass pyrolysis: Toward a systematic comparison of different acid pretreatments, *Chem. Eng. J.* 411 (2021), 128513, <https://doi.org/10.1016/J.CEJ.2021.128513>.
- [56] X. Huang, J.P. Cao, P. Shi, X.Y. Zhao, X.B. Feng, Y.P. Zhao, X. Fan, X.Y. Wei, T. Takarada, Influences of pyrolysis conditions in the production and chemical composition of the bio-oils from fast pyrolysis of sewage sludge, *J. Anal. Appl. Pyrolysis* 110 (2014) 353–362, <https://doi.org/10.1016/J.JAAP.2014.10.003>.
- [57] P.R. Patwardhan, R.C. Brown, B.H. Shanks, Understanding the Fast Pyrolysis of Lignin, *ChemSusChem* 4 (2011) 1629–1636, <https://doi.org/10.1002/CSSC.201100133>.
- [58] D.L. Dalluge, T. Daugaard, P. Johnston, N. Kuzhiyil, M.M. Wright, R.C. Brown, Continuous production of sugars from pyrolysis of acid-infused lignocellulosic biomass, *Green. Chem.* 16 (2014) 4144–4155, <https://doi.org/10.1039/c4gc00602j>.
- [59] S. Hu, L. Jiang, Y. Wang, S. Su, L. Sun, B. Xu, L. He, J. Xiang, Effects of inherent alkali and alkaline earth metallic species on biomass pyrolysis at different temperatures, *Bioresour. Technol.* 192 (2015) 23–30, <https://doi.org/10.1016/j.biortech.2015.05.042>.
- [60] A. Witsuthammakul, T. Sooknoi, Selective hydrodeoxygenation of bio-oil derived products: ketones to olefins, *Catal. Sci. Technol.* 5 (2015) 3639–3648, <https://doi.org/10.1039/C5CY00367A>.
- [61] Y. Liu, Y. Zhai, S. Li, X. Liu, X. Liu, B. Wang, Z. Qiu, C. Li, Production of bio-oil with low oxygen and nitrogen contents by combined hydrothermal pretreatment and

- pyrolysis of sewage sludge, *energy* 203 (2020), 117829, <https://doi.org/10.1016/J.ENERGY.2020.117829>.
- [62] I. Fonts, A. Navarro-Puyuelo, N. Ruiz-Gómez, M. Atienza-Martínez, A. Wisniewski, G. Gea, Assessment of the production of value-added chemical compounds from sewage sludge pyrolysis liquids, *Energy Technol.* 5 (2017) 151–171, <https://doi.org/10.1002/ente.201600183>.
- [63] Q. Guo, Z. Cheng, G. Chen, B. Yan, J. Li, L. Hou, F. Ronsse, Assessment of biomass demineralization on gasification: From experimental investigation, mechanism to potential application, *Sci. Total Environ.* 726 (2020), 138634, <https://doi.org/10.1016/J.SCITOTENV.2020.138634>.
- [64] N. Kuzhiyil, D. Dalluge, X. Bai, H. Kim, Pyrolytic sugars from cellulosic biomass, *ChemSusChem* 0 (2012) 1–10, <https://doi.org/10.1002/cssc.201200341>.



Research papers

Beeswax as a potential replacement of paraffin wax as shape stabilized solar thermal energy storage material: An experimental study

Pushendra Kumar Singh Rathore^a  , Krishna Kumar Gupta^b, Bhaskar Patel^b, R.K. Sharma^c, Naveen Kumar Gupta^d

[Show more](#) 

 Share  Cite

<https://doi.org/10.1016/j.est.2023.107714> 

[Get rights and content](#) 

Highlights

- Beeswax/Bentonite/graphite based SSCPCM for thermal energy storage was prepared.
- SSCPCM shows substantially good thermal energy storage capacity.
- Beeswax based SSCPCM shows excellent heating rate and thermal conductivity.
- SSCPCM was thermally, chemically and physically stable.

Abstract

Thermal Energy Storage (TES) using paraffin wax as Phase Change material (PCM) has been widely used for solar to thermal energy conversion and storage application. Being petroleum by-product, production of paraffin wax have embodied environmental impact and high carbon footprint. Beeswax can replace paraffin's as one of the clean, sustainable, eco-friendly and potential TES PCM. However, TES potential of Beeswax was not investigated thoroughly in previous literatures. Also, limited study has been found which evaluates solar to thermal conversion potential of Beeswax. This study presents a comprehensive analysis of TES performance of Beeswax supported by Bentonite clay and loaded with Graphite was evaluated. Bentonite clay was used as supporting material and Graphite powder is used as additive in varying percentage to form Shape Stabilized Composite Phase Change Material (SSCPCM). SSCPCM was initially investigated for anti-leakage behaviour and was found that Bentonite can hold maximum 40wt% of Beeswax without leakage above phase transition temperature. Thermal energy storage parameters, thermal degradation, solar to thermal conversion performance, chemical stability, surface morphology, and thermal conductivity were evaluated. Bentonite and graphite has shown good morphology to form SSCPCM samples. Also, SSCPCM has proved to be chemically and physically stable thermal energy storage material. Melting enthalpy of 101.79, 100.66, 98.80, 100.43, 96.51, and 105.01 at melting point of 59.43, 58.88, 58.12, 57.98, 57.36, and 57.11 of SSCPCM-0, SSCPCM-1, SSCPCM-3, SSCPCM-5, SSCPCM-7, and SSCPCM-9 was obtained. Adding Graphite has reduced supercooling of SSCPCM samples maximum by 84.13%. Increasing additives in PCM improves heating rate and thermal conductivity of the SSCPCM.

Introduction

Last decade have seen continuous rise in energy demand due to increase in population, globalization, and improvement in living standard. Most of this demand is fulfilled by fossil based fuels such as coal and crude oil. This leads to over-exploitation of limited reserves of fossil fuels causing rapid depletion and excessive greenhouse gas emissions. To mitigate these challenges renewable sources of energy has shown a significant capacity enhancement [1]. Due to abundant availability, low cost, and negligible emissions renewable sources of energy can play a decisive role against climate change. Among various renewable sources, solar energy is one of the major renewable source of energy available to the mankind almost at every location of the planet earth [2]. To harness solar energy various solar technologies such as solar photovoltaic, solar collectors, solar concentrator, solar still, and solar dryers were used for varieties of applications. However, solar energy suffers with serious limitations of limited availability by location, time, and power. These drawbacks leads to poor utilization and low efficiency of solar thermal technologies. To overcome these drawbacks Solar Thermal

Energy Storage (STES) can play a vital role in improving energy efficiency and utilization rate of solar thermal technologies [3].

Thermal Energy Storage (TES) is a technique of storing excessive heat energy in a material and utilizing it as and when it is needed. TES can be classified into two categories (a) Sensible heat storage (b) Latent heat storage [4]. Sensible heat storage is one of the oldest technology of storing thermal energy by rising the temperature of the object whereas in latent heat storage the material undergoes phase transformation to store thermal energy. Phase transformation (solid-liquid and liquid-solid) gives advantage of high energy density at minimum temperature change in comparison to sensible heat storage materials. Latent heat storage using Phase Change Materials (PCM) is the widely used technique for TES for various applications. PCM are the materials which stores thermal energy while undergoing phase transformation (solid-liquid) and releases it by again undergoing phase transformation (liquid-solid) [5]. The storing (charging) and releasing (discharging) of thermal energy in PCM takes place at almost constant temperature or in a narrow temperature range. Additionally, easy availability in large temperature ranges has increased feasibility of latent heat TES technology.

Varieties of PCM are available for TES. However, the most commonly used PCM are paraffin. Paraffin are saturated alkanes having chemical formula as C_nH_{2n+2} . Where n is number of carbon atoms. The melting point of alkanes increases with increase in number of carbon atoms. Paraffin possess various merits such as large melting temperature range, high latent heat, and good storage density with respect to mass [6]. Generally, for building applications the PCM used are having melting temperature range of 20°C to 40°C. However, the melting range of PCM varies depending on climatic temperature of the location [7]. Paraffin suffers with two major drawbacks, first is there low thermal conductivity and second is that they are produced from petroleum products, which is the major producer of harmful emissions. Various attempts were made to overcome the first drawback of low thermal conductivity of paraffin. Loading of Al_2O_3 nanoparticles in paraffin wax was done to improves its thermal conductivity [8]. Result suggest that the thermal conductivity of paraffin wax increases when loaded with Al_2O_3 nanoparticle in liquid state whereas it decreases in liquid state. A study investigates the effect of loading of multi-walled carbon nanotubes, graphene nanoplatelets, and aluminum oxide nanoparticles in PCM [9]. The results shows that after few thermal cycles significant coagulation and deposition of nanoparticles occurs. Also, they suggest that long term stability of paraffin loaded with nanoparticles remains a challenge. Graphene nanoparticles were dispersed in paraffin/water emulsion for enhancing thermal conductivity and photo-thermal performance [10]. Another study shows the effect of loading copper nanoparticles in PCM when subjected to external magnetic field [11]. Some commonly used nanoparticles to improve the thermal energy storage characteristics of the paraffin are graphite [10,12], Al_2O_3 [13], copper nanoparticles [14],

TiO₂ [15], and carbon nanotubes [16]. 1D nanoparticles and 2D nanoparticles are widely used to develop PCM composite with improved thermal, physical, and chemical performance [17]. 1D materials such as Carbon Nanotubes (CNT), Silver nanowires, and Copper nanowires were used as additives in PCM to improve thermal conductivity [18]. Among these 1D materials CNT (SWCNT and MWCNT) is exhaustively analyzed to improve PCM performance. 2D nanomaterials based PCM composites are widely used to improve thermal performance of the PCM [19]. 2D materials have weak van der Waals force and strong covalent bond between in-plane atoms. Widely used 2D materials are Graphene [20], Boron nitride [21], Graphite [22], Nanoclays and MXene [23]. Recently, Mxene based PCM composites are increasingly explored because MXene exhibits high surface area, high thermal conductivity and powerful solar absorption capacity. However, none of these materials were used to evaluate solar to thermal energy storage and conversion of Beeswax. Thus, it can be viewed that there are several methods available which can be considered potential technologies for improving low thermal conductivity of the paraffin. However, none of the articles have discussed the second major drawback i.e. paraffin are the petroleum based products having high carbon footprints. Being petroleum by-product the production and processing of paraffin's is energy intensive and can negatively impact the energy savings measures taken care due to TES using paraffin. A study suggested that the use of PCM based on fossil fuels such as paraffin in buildings is not recommended because of various environmental impact [24]. Environmental risk related to paraffin are also higher especially for the marine environment [25]. Another study suggested to replace traditional fossil based PCM by some ecological friendly PCM in buildings after conducting a life cycle assessment analysis of PCM [26]. A study found that replacing petroleum based paraffin by eco-friendly PCM can reduced 45%–50% greenhouse gas emissions [27]. Thus, it is understood that there is a need to search alternative of petroleum based paraffin wax as thermal energy storage material to reduce the embodied environmental impacts during production and processing [28].

Therefore, the objective of this study is to evaluate the potential of naturally occurring PCM for STES. One of the eco-friendly naturally occurring PCM is Beeswax (BW). Beeswax is produced from bee's hives of honeybees. It is organic non-paraffin PCM. Good thermal energy storage capacity [29,30] has made them a strong contender to replace petroleum based paraffin PCM. This study presents a novel attempt to analyze the solar to thermal energy storage and conversion performance of clean and sustainable PCM called Beeswax. The potential of Beeswax as TES PCM was not evaluated in detail in previous literatures. Also, there is no study available which have analyzed the solar to thermal energy conversion performance of Beeswax. Additionally, in this study chemical and physical stability of Beeswax as Shape Stabilized Composite PCM (SSPCPM) was also investigated.

In this study an eco-friendly and novel Shape Stabilized Composite PCM (SSPCM) was prepared using naturally produced beeswax and naturally occurring Bentonite clay. SSPCM was loaded with graphite at varying wt% to prepare SSCPCM and to investigate its effect on thermo-physical characteristics. Solar to thermal energy conversion performance of the SSCPCM was also investigated.

Access through your organization

Check access to the full text by signing in through your organization.

Access through **Manipal University Jaipur**

Section snippets

Material

Raw Beeswax (BW) was purchased from Madhumakhi Wala located in district Barabanki, India. It has a melting temperature range of 58°C to 62°C, density of 950–961 kg/m³, and have sufficient high latent heat storage capacity as provided by the manufacturer. Bentonite clay was purchased from Sigma-Aldrich in powder form having chemical formula H₂Al₂O₆Si. Graphite powder with average particle size of 44µm and purity of ≥99% was purchased from Aakar Carbons Private Limited, India. Specification ...

Preparation of shape stabilized PCM (SSPCM)

PCM suffers with a major drawback of leakage during phase transition. Therefore, maintaining structural stability during charging and discharging of PCM is important for efficient storage and release of thermal energy. To reduce the chances of leakage of the PCM Shape Stabilized PCM (SSPCM) were prepared. SSPCM was prepared using raw Bentonite clay. Bentonite clay was placed in the furnace at 150°C for 3h to remove water molecules and other unwanted impurities. After 3h, bentonite clay was ...

Characterization

TES parameters such as enthalpy of melting, enthalpy of freezing, melting point, and freezing point are measured using Differential Scanning Calorimetry (DSC). Thermal decomposition of SSCPCM-0, SSCPCM-1, SSCPCM-3, SSCPCM-5, SSCPCM-7, and SSCPCM-9 was measured through Thermogravimetric analysis (TGA). Both DSC and TGA was done using Simultaneous Thermal Analyzer (STA-8000) of Perkin Elmer. STA performs both TGA and DSC analysis in different modes ranging from room temperature to 1600°C. ...

Thermal energy storage characteristics

Thermal energy storage parameters such as melting point, freezing point, melting enthalpy, and freezing enthalpy are the most important characteristic of any PCM to be used as TES material. These characteristics can be investigated through DSC. The DSC curve of pure beeswax and SSCPCM-0, SSCPCM-1, SSCPCM-3, SSCPCM-5, SSCPCM-7, and SSCPCM-9 are shown in Fig. 3(a) and (b) respectively. The heat storage capacity consist of sensible part and latent part. The sensible heating occurs in solid ...

Conclusion

This study investigates the capabilities of Beeswax as potential alternative of paraffin wax for TES as SSCPCM. Various samples of SSCPCM were prepared using Bentonite as supporting material, Beeswax as PCM, and Graphite as additive. Maximum 40wt% of Beeswax was loaded in Bentonite without any leakage during phase transformation. Pure Beeswax shows excellent TES capacity of 206.63J/g (melting) and 203.35J/g (freezing) at melting and freezing temperature of 61.60°C and 54.98°C. Also, about ...

Author statement

We the undersigned declare that this manuscript is original, has not been published before and is not currently being considered for publication elsewhere.

We confirm that the manuscript has been read and approved by all named authors and that there are no other persons who satisfied the criteria for authorship but are not listed. We further confirm that the order of authors listed in the manuscript has been approved by all of us. We understand that the Corresponding Author is the sole contact ...

Declaration of competing interest

The author/authors declare that they have no known competing financial interests or personal relationships that could have appeared to influence the work reported in this paper. ...

[Recommended articles](#)

References (35)

J. Jiang *et al.*

Hybrid generation of renewables increases the energy system's robustness in a changing climate

J. Clean. Prod. (2021)

N. Kannan *et al.*

Solar energy for future world: - a review

Renew. Sust. Energ. Rev. (2016)

J. Xu *et al.*

A review of available technologies for seasonal thermal energy storage

Sol. Energy (2014)

G. Alva *et al.*

An overview of thermal energy storage systems

Energy (2018)

D. Li *et al.*

Incorporation technology of bio-based phase change materials for building envelope: a review

Energy Build. (2022)

A.K. Singh *et al.*

Experimental evaluation of composite concrete incorporated with thermal energy storage material for improved thermal behavior of buildings

Energy (2023)

F. Wang *et al.*

Graphite nanoparticles-dispersed paraffin/water emulsion with enhanced thermal-physical property and photo-thermal performance

Sol. Energy Mater. Sol. Cells (2016)

A. Kumar *et al.*

Study of melting of paraffin dispersed with copper nanoparticles in square cavity subjected to external magnetic field

J. Energy Storage (2022)

A.E. Kabeel *et al.*

Effect of graphite mass concentrations in a mixture of graphite nanoparticles and paraffin wax as hybrid storage materials on performances of solar still

Renew. Energy (2019)

A.N. Keshteli *et al.*

Influence of Al₂O₃ nanoparticle and Y-shaped fins on melting and solidification of paraffin

J. Mol. Liq. (2020)



[View more references](#)

Cited by (34)

[Solar to thermal energy storage performance of composite phase change material supported by copper foam loaded with graphite and boron nitride](#)

2024, Solar Energy

[Show abstract](#)

[Advancements in phase change materials for energy-efficient building construction: A comprehensive review](#)

2024, Journal of Energy Storage

[Show abstract](#)

[A review of lignocellulosic biomass-based shape-stable composite phase change materials](#)

2023, Journal of Energy Storage

[Show abstract](#)

[Location optimization of phase change material for thermal energy storage in concrete block for development of energy efficient buildings](#)

2023, Renewable Energy

[Show abstract](#)

[A comprehensive review on solar to thermal energy conversion and storage using phase change materials](#)

2023, Journal of Energy Storage

[Show abstract](#)

[Microencapsulated phase change materials for enhanced thermal energy storage performance in construction materials: A critical review](#)

2023, Construction and Building Materials

[Show abstract](#) 



[View all citing articles on Scopus](#) 

[View full text](#)

© 2023 Elsevier Ltd. All rights reserved.



All content on this site: Copyright © 2024 Elsevier B.V., its licensors, and contributors. All rights are reserved, including those for text and data mining, AI training, and similar technologies. For all open access content, the Creative Commons licensing terms apply.



Positive temperature coefficient of resistance of Mg-GeO₂ nanowire array film

Cite as: J. Appl. Phys. **133**, 045302 (2023); doi: 10.1063/5.0130729

Submitted: 14 October 2022 · Accepted: 31 December 2022 ·

Published Online: 24 January 2023



Ankita Choudhury,¹ Arka Dey,¹ Chiranjib Ghosh,¹ Avijit Dalal,¹ Rajat Mahapatra,² Saikat Biswas,² Nilanjan Halder,³ and Aniruddha Mondal^{1,a)}

AFFILIATIONS

¹Department of Physics, National Institute of Technology Durgapur, Durgapur 713209, India

²Department of Electronics and Communication Engineering, National Institute of Technology Durgapur, Durgapur 713209, India

³Department of Physics, Manipal University Jaipur, Jaipur 303007, Rajasthan, India

^{a)}Author to whom correspondence should be addressed: aniruddhamo@gmail.com

ABSTRACT

Here, glancing angle deposition is employed to synthesize the undoped GeO₂ and Mg-doped (0.4 and 0.8 at. %) GeO₂ nanowires (NWs) on a Si substrate. The microscopic images show the formation of the NW-like morphology of the grown materials. The gradual decrease in the average ratio of length to diameter depicts the worsening of the formation of NWs with the incorporation of Mg into the GeO₂ host lattice. This also affects the crystallinity characteristics of the materials, which have been demonstrated from the selected area electron diffraction (SAED) pattern of the materials. The polycrystallinity nature of undoped GeO₂ NWs changes to amorphous due to the introduction of Mg, which has been confirmed from both the obtained SAED and x-ray diffraction patterns of the samples. The presence of Mg was confirmed from the obtained broad bands at 473 and 437 cm⁻¹ in the Fourier transmission spectrum of the doped samples. The increasing conductance with the temperature of Au/undoped GeO₂ devices can be explained by the thermionic emission process, whereas the Mg-GeO₂ device shows an overall decrease in conductance with increasing temperature. We have ascribed the origin of this abnormal conductance as the positive temperature coefficient of resistance, which is one of the first reports, due to the generation of random grain boundaries and enormous electron trapping at the Au/Mg-GeO₂ NW junction. Furthermore, the undoped GeO₂ NW device shows good temperature-dependent conductivity as well as stability compared to the doped one.

Published under an exclusive license by AIP Publishing. <https://doi.org/10.1063/5.0130729>

I. INTRODUCTION

Ultra-wide bandgap (UWBG) semiconductors are receiving significant attention from the research community for their usability in the field of scientific and technological applications due to their excellent properties coupled with exceptional thermal and chemical stabilities.^{1–3} These UWBG semiconductors hold promise to meet the emerging needs and demands of current and future technologies.⁴ Germanium dioxide (GeO₂) is one of the widely used UWBG oxide semiconductors. Due to its versatile properties, it achieved unwavering attention in the field of high-power electronics, deep-UV optoelectronics/photronics, and energy storage applications.⁵ GeO₂ is treated as one of the capable materials for optical waveguides and nano-connections in optoelectronic communications due to its attractive optical and electronic properties

and high thermal stability.^{6,7} One-dimensional nanostructures including nanowires, nanotubes, and nanorods have attracted rapidly growing interest due to their fascinating properties and unique applications in areas ranging from physics, chemistry, life sciences, to materials science.⁸ These nanostructures are treated as building blocks in a wide variety of nanoscale electronic and photonic devices. An emerging area of research is the characterization of nanowire networks and their application in macroelectronics and energy harvesting. Metal oxide nanowire networks are an attractive alternative due to the ease of growth of nanowires while still providing appealing electrical properties. Nanowires emerge as one of the most interesting ones as they combine low dimensionality due to their small diameters with high aspect ratios, which makes them a good approximation to one-dimensional structures. Other advantages of these nanowires include access to a large range

[Sign In / Sign Up \(/user/login\)](/user/login)[Submit \(https://susy.mdpi.com/user/manuscripts/upload?journal=symmetry\)](https://susy.mdpi.com/user/manuscripts/upload?journal=symmetry)

Search for Articles:



Advanced Search

[Journals \(/about/journals\)](/about/journals) / [Symmetry \(/journal/symmetry\)](/journal/symmetry) / [Volume 15 \(/2073-8994/15\)](/2073-8994/15) / [Issue 3 \(/2073-8994/15/3\)](/2073-8994/15/3) / [10.3390/sym15030725](https://doi.org/10.3390/sym15030725) /



[\(/journal/symmetry\)](/journal/symmetry)

Submit to this Journal
(https://susy.mdpi.com/user/manuscripts/upload?form%5Bjournal_id%5D%3D44)

Review for this Journal
(<https://susy.mdpi.com/volunteer/journals/review>)

Propose a Special Issue
(</journalproposal/sendproposalspecialissue/symmetry>)

► [Article Menu](#)

Article Menu



[Subscribe SciFeed \(/2073-8994/15/3/725/scifeed_display\)](#)

[Recommended Articles](#)

[Related Info Link](#) ▾

[More by Authors Links](#) ▾

Article Views 1489

Citations 7

[Table of Contents](#) ^

- [Abstract](#)
- [Introduction](#)
- [Flow Analysis](#)
- [Solution Process](#)
- [Correlation Analysis](#)
- [Computational Results and Discussion](#)
- [Conclusions](#)
- [Author Contributions](#)
- [Funding](#)
- [Data Availability Statement](#)
- [Acknowledgments](#)
- [Conflicts of Interest](#)
- [Nomenclature](#)
- [References](#)

⏪

[Order Article Reprints \(/2073-8994/15/3/725/reprints\)](#)


Open Access Article

 [1](#) ([https://v](#)
[domain=www.mc](#)
Altmetric

Heat and Mass Transport in Casson Nanofluid Flow over a 3-D Riga Plate with Cattaneo-Christov Double Flux: A Computational Modeling through Analytical Method

Share



by Karuppusamy Loganathan ¹  (<https://orcid.org/0000-0002-6435-2916>),
S. Eswaramoorthi ²  (<mailto:eswaran.bharathiar@gmail.com>)  (<https://orcid.org/0000-0003-0528-3591>),
P. Chinnasamy ^{3,*}  (<mailto:chinnasamyponnusamy@gmail.com>)  (<https://orcid.org/0000-0002-3202-4299>),
Reema Jain ^{1,*}  (<mailto:reemajain197@gmail.com>)  (<https://orcid.org/0000-0001-9989-247X>),
Ramkumar Sivasakthivel ⁴  (<https://orcid.org/0000-0002-6224-6167>), Rifaqat Ali ⁵ and
N. Nithya Devi ⁶

[Help](#)



[Discuss in groups](#)

[https://s
groups/f
utm_sou](#)



[Endorse](#)



[Comment](#)

¹ Department of Mathematics and Statistics, Manipal University Jaipur, Jaipur 303007, Rajasthan, India

² Department of Mathematics, Dr. N.G.P. Arts and Science College, Coimbatore 641035, Tamil Nadu, India

³ Department of Computer Science and Engineering, MLR Institute of Technology, Hyderabad 500043, Telangana, India

⁴ Department of Computer Science, School of Sciences, CHRIST (Deemed to be University), Bengaluru 560029, Karnataka, India

⁵ Department of Mathematics, College of Science and Arts, King Khalid University, Muhayil 61413, Saudi Arabia

⁶ Department of Science and Humanities, Faculty of Engineering, Karpagam Academy of Higher Education, Coimbatore 641021, Tamil Nadu, India

* Authors to whom correspondence should be addressed.

Symmetry **2023**, *15*(3), 725; <https://doi.org/10.3390/sym15030725>
(<https://doi.org/10.3390/sym15030725>)

Submission received: 2 February 2023 / Revised: 1 March 2023 / Accepted: 7 March 2023 / Published: 14 March 2023

(This article belongs to the Special Issue **Symmetry in System Theory, Control and Computing** (/journal/symmetry/special_issues/I3QT160A8I))

Download 

Browse Figures

(https://pub.mdpi-res.com/symmetry/symmetry-15-00725/article_deploy/html/images/symmetry-15-00725-g001.png?1678790346)

(https://pub.mdpi-res.com/symmetry/symmetry-15-00725/article_deploy/html/images/symmetry-15-00725-g002.png?1678790344)

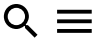
(https://pub.mdpi-res.com/symmetry/symmetry-15-00725/article_deploy/html/images/symmetry-15-00725-g003.png?1678790335)

(https://pub.mdpi-res.com/symmetry/symmetry-15-00725/article_deploy/html/images/symmetry-15-00725-g003.png?1678790335)

(https://pub.mdpi-res.com/symmetry/symmetry-15-00725/article_deploy/html/images/symmetry-15-00725-g003.png?1678790335)

(https://pub.mdpi-res.com/symmetry/symmetry-15-00725/article_deploy/html/images/symmetry-15-00725-g003.png?1678790335)

 (https://pub.mdpi-res.com/symmetry/symmetry-15-00725/article_deploy/html/images/symmetry-15-00725-g004.png?1678790334)
(https://pub.mdpi-res.com/symmetry/symmetry-15-00725/article_deploy/html/images/symmetry-15-00725-g005a.png?1678790343)
(https://pub.mdpi-res.com/symmetry/symmetry-15-00725/article_deploy/html/images/symmetry-15-00725-g005b.png?1678790336)
(https://pub.mdpi-res.com/symmetry/symmetry-15-00725/article_deploy/html/images/symmetry-15-00725-g006.png?1678790340)
(https://pub.mdpi-res.com/symmetry/symmetry-15-00725/article_deploy/html/images/symmetry-15-00725-g007.png?1678790342)
(https://pub.mdpi-res.com/symmetry/symmetry-15-00725/article_deploy/html/images/symmetry-15-00725-g008.png?1678790332)
(https://pub.mdpi-res.com/symmetry/symmetry-15-00725/article_deploy/html/images/symmetry-15-00725-g009.png?1678790338)



[Versions Notes \(/2073-8994/15/3/725/notes\)](/2073-8994/15/3/725/notes)

Abstract

This work examines the non-Newtonian Cassonnanofluid's three-dimensional flow and heat and mass transmission properties over a Riga plate. The Buongiorno nanofluid model, which is included in the present model, includes thermo-migration and random movement of nanoparticles. It also took into account the Cattaneo–Christov double flux processes in the mass and heat equations. The non-Newtonian Casson fluid model and the boundary layer approximation are included in the modeling of nonlinear partial differential systems. The homotopy technique was used to analytically solve the system's governing equations. To examine the impact of dimensionless parameters on velocities, concentrations, temperatures, local Nusselt number, skin friction, and local Sherwood number, a parametric analysis was carried out. The velocity profile is augmented in this study as the size of the modified Hartmann number increases. The greater thermal radiative enhances the heat transport rate. When the mass relaxation parameter is used, the mass flux values start to decrease.

Keywords: 3-D flow (</search?q=3-D+flow>); Casson nanofluid (</search?q=Casson+nanofluid>); Riga plate (</search?q=Riga+plate>); Cattaneo–Christov model (</search?q=Cattaneo%E2%80%93Christov+model>); HAM (</search?q=HAM>)

A new fluid with better performance is valuable for accomplishing in industrial technologies. Choi and Eastman [1] were the first who coined the word nanofluid and showed that the dispersion of nanosized particles increased the thermal physical properties of an ordinary fluid. Recently, various applications have been used in cooling transformers, heat change, food processing, and many others. "In the presence of partial slip, nanofluid past a stretching surface with boundary layer flow was explored by Das [2] and it is realized that the thermophoretic force escalates the heat transfer rate. Kuznetsov and Nield [3] investigated the nanofluid model with Brownian motion and thermophoresis and the heat transfer rate diminished due to these effects. Hamad et al. [4] acquired the results of MHD nanofluid flow on a flat plate. The two nanoparticles namely *Cu* and *Ag* have a greater cooling concert, according to the researchers. The impact of non-Newtonian nanofluid flow on a stretching sheet (SS) was investigated by Nadeem and co-workers [5], who discovered that the nanoparticle volume fraction (NPVF) reinforced the greater amount of the thermophoresis variable. Khan and Pop [6] studied the 2D flow of a nanoliquid owing to an SS using a numerical approach and identified that the presence of the BM parameter controls the heat. Sajid et al. [7] probed the cross non-Newtonian hybrid nanofluid flow with heat sink/source and thermal radiation. They investigated the novel tetra hybrid Tiwari and Das nanofluid model on blood flow arteries. The influence of Reiner–Philippoff hybrid nanofluid flow over a non-linear heat source/sink and mathematical Fourier heat law was delved by Sajid et al. [8]. They solved the problem numerically by employing the Galerkin method of finite elements. Hassan et al. [9] analytically proposed the boundary layer problem due to a SS.

Flows of fluid due to a permeable space are significant in various chemical, manufacturing, biological and industrial systems, such as crude oil purification, water development in reservoirs, grain stockpiling, and blood flow. A relevant analysis of Darcy–Forchheimer fluid flow can be carried out by attempts ([10,11,12,13,14,15]). These analyses incorporate the Darcy law to consider the permeable medium. However, the stability of this law for smaller velocity is inappropriate in plenty of practical conditions where the permeable medium has weak porosity separation near the wall area and a significant flow rate. The viscous and inertial forces have been given by the Darcy–Forchheimer (DF) model. Consequently, this model accurately described the fluid flow and heat transport as the permeable medium. Zubair et al. [16] deliberated the prominent features of Darcy–Forchheimer time flow of nanomaterials using Cattaneo–Christov heat diffusion (CCHD) theory and the speed of liquid increases when elevating the inertia coefficient. The second law analysis with DF model for MHD nanoliquid flow past a SS was conducted by Abbas et al. [17]. Ahmad et al. [18] presented the 3D couple stress MHD flow nanoliquid for DF model due to an exponentially SS. Their outcome explores that the speed of fluid upsurges with enhancing the inertia parameter.

A survey of non-Newtonian fluids in the modern era has paid particular attention to the current engineers and researchers owing various prominent features in the industrial area. The complexity of non-Newtonian fluid has made it difficult to explain all relations in one constitutive expression. So, the non-Newtonian fluid is prominent from viscous material. It is lesser than the order of differential system in the non-Newtonian fluid. A lot of models have been presented with

MDPI (1)

their different properties. One of the non-Newtonian models is known as CF. This model is explained as human blood flow at a low shear rate and explained viscoelastic fluid with prominent features. Thamaraikannan et al. [19] investigated the MHD Casson fluid flow past a porous channel with the effect of body acceleration. Chemically reactive CF induced by exponentially inclined permeability was carried out by Reddy [20]. Hayat et al. [21] explored the chemically reactive flow of CNF over a heated SS with a heat sink/source. They discovered that when mass Biot number is present, the fluid concentration and its associated BL thickness rise. Casson nanofluid was assessed by Aboehashari et al. [22] using heat and mass transport characteristics owing to a stretched surface.

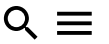
The Riga plate (RP) is a well-known actuator made out of magnets and electrodes that stay there and alternately generate Lorentz's force, which quickly decreases with distance. Zubaidi et al. [23] explored the nanofluid flow over a RP. Chemical reaction and viscosity dissipation in a nanofluid's mixed convective flow on a Riga plate was delved by Vaidya et al. [24]. They noticed that when the modified Hartmann number increased, the velocity profile grew and the temperature profile shrinks. Rafique et al. [25] numerically investigated the micropolar nanofluid flow over a Riga plate. They found that the fluid speed was bolstered as the modified Hartmann number improved. Riga plate with convective boundary conditions on a nanofluid under radial SS was scrutinized by Prasad et al. [26]. They noted that the modified Hartmann number improves the speed profile and slumps the temperature distribution. Darvesh et al. [27] probed the infinite shear rate of the Cross-fluid viscosity model, which is then coupled with the Riga plate and they used the Keller Box method. Recently, the Riga plate model of a nanofluid with a non-Fourier heat flux was numerically inspected by Divya et al. [28]. They found that a rise in the modified Hartmann number leads to weaken the skin friction coefficient.

Influenced by the above-mentioned investigations and applications recently, many researchers are attributing attention to revealing the thermal effect of nanoliquid flow with Cattaneo–Christov flux due to a Darcy–Forchheimer porous medium. However, the investigations over this flow over a Riga plate have not yet begun. To fill this gap the authors examined the Casson nanofluid flow over a 3-D Riga plate with a Cattaneo–Christov flux Darcy–Forchheimer porous medium. The results of this study are helpful in different engineering applications such as glass blowing, the spinning of fibers and the continuous casting of metals.

2. Flow Analysis

We consider the Cattaneo–Christov theory in a 3D Casson nano-liquid flow past a permeable Riga surface. The surface was considered with x and y directions with velocities $u(x) = ax$ and $v(y) = by$, respectively. Let T_W and C_W are represented by the surface of temperature and concentration which are always larger than the ambient temperature and concentration represented by T_∞ and C_∞ . The nanofluid formulation was the physical properties of thermophoresis and Brownian movement parameters. Porous medium was tackled through the Darcy–Forchheimer model. The lower plate was considered as heated with hotter fluid T_f and creates a heat transport coefficient h_c . The known fluid behaves as heat-generating or absorbing. The flow geometry is given in **Figure 1** and the governing equations are taken from [29,30]:

$$\frac{\partial u}{\partial x} + \frac{\partial v}{\partial y} + \frac{\partial w}{\partial z} = 0 \quad (1)$$



$$\left[u \frac{\partial u}{\partial x} + v \frac{\partial u}{\partial y} + w \frac{\partial u}{\partial z} \right] = v \left[\left(\frac{\beta + 1}{\beta} \right) \frac{\partial^2 u}{\partial z^2} \right] - \left[\frac{v}{k_1} u \right] - [Fu^2] + \frac{\pi j_0 M_0 \exp\left(-\frac{\pi}{\epsilon} z\right)}{8\rho} \quad (2)$$

$$\left[u \frac{\partial v}{\partial x} + v \frac{\partial v}{\partial y} + w \frac{\partial v}{\partial z} \right] = v \left[\left(\frac{\beta + 1}{\beta} \right) \frac{\partial^2 v}{\partial z^2} \right] - \left[\frac{v}{k_1} v \right] - [Fv^2] \quad (3)$$

$$\begin{aligned} \rho c_p \left[u \frac{\partial T}{\partial x} + v \frac{\partial T}{\partial y} + w \frac{\partial T}{\partial z} \right] &= K \frac{\partial^2 T}{\partial z^2} + \tau \left[D_B \frac{\partial C}{\partial z} \frac{\partial T}{\partial z} + \frac{D_T}{T_\infty} \left(\frac{\partial T}{\partial z} \right)^2 \right] \\ &- \lambda_E \left[\frac{\partial^2 T}{\partial x^2} u^2 + \frac{\partial^2 T}{\partial y^2} v^2 + \frac{\partial^2 T}{\partial z^2} w^2 + \frac{\partial^2 T}{\partial x \partial y} 2uv + \frac{\partial^2 T}{\partial y \partial z} 2vw + \frac{\partial^2 T}{\partial x \partial z} 2uw + \right. \\ &\left. + \frac{\partial u}{\partial z} \frac{\partial T}{\partial z} w + \frac{\partial v}{\partial x} \frac{\partial T}{\partial x} u + \frac{\partial v}{\partial y} \frac{\partial T}{\partial x} v + \frac{\partial v}{\partial z} \frac{\partial T}{\partial z} w + \frac{\partial w}{\partial x} \frac{\partial T}{\partial x} u + \frac{\partial w}{\partial y} \frac{\partial T}{\partial x} v + \frac{\partial w}{\partial z} \frac{\partial T}{\partial z} w \right] \end{aligned} \quad (4)$$

$$\begin{aligned} u \frac{\partial C}{\partial x} + v \frac{\partial C}{\partial y} + w \frac{\partial C}{\partial z} &= D_B \frac{\partial^2 C}{\partial z^2} + \frac{D_T}{T_\infty} \frac{\partial^2 T}{\partial z^2} - \lambda_c \left[\frac{\partial^2 C}{\partial x^2} u^2 + \frac{\partial^2 C}{\partial y^2} v^2 + \frac{\partial^2 C}{\partial z^2} w^2 + \frac{\partial^2 C}{\partial x \partial y} 2uv + \right. \\ &\left. \frac{\partial u}{\partial x} \frac{\partial C}{\partial x} u + \frac{\partial u}{\partial y} \frac{\partial C}{\partial x} v + \frac{\partial u}{\partial z} \frac{\partial C}{\partial z} w + \frac{\partial v}{\partial x} \frac{\partial C}{\partial x} u + \frac{\partial v}{\partial y} \frac{\partial C}{\partial x} v + \frac{\partial v}{\partial z} \frac{\partial C}{\partial z} w + \frac{\partial w}{\partial x} \frac{\partial C}{\partial x} u + \frac{\partial w}{\partial y} \frac{\partial C}{\partial x} v + \right. \\ &\left. \frac{\partial w}{\partial z} \frac{\partial C}{\partial z} w \right] \end{aligned} \quad (5)$$

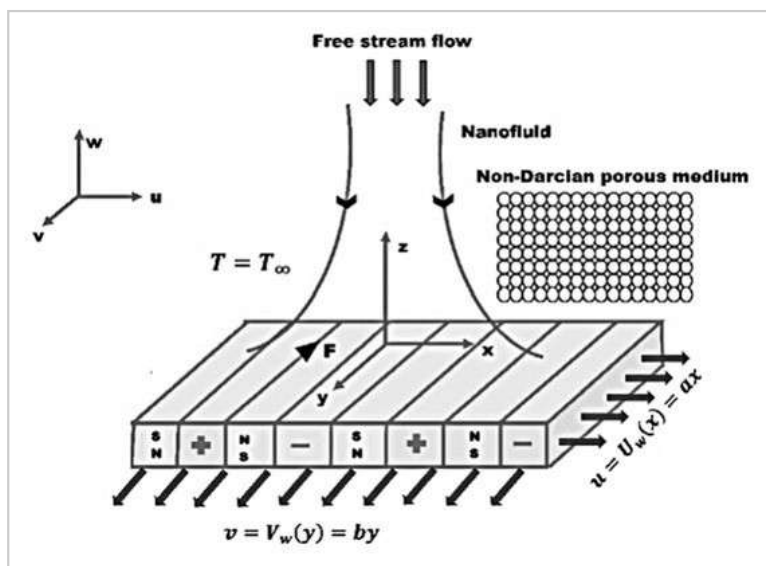
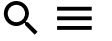


Figure 1. Physical geometry.

The boundary points are

$$\left\{ \begin{aligned} u(x, y, 0) &= ax, v(x, y, 0) = by, w(x, y, 0) = 0, -k \frac{\partial T}{\partial z}(x, y, 0) = h_f [T_f(x, y, 0) - T_\infty] \\ u(x, y, \infty) &\rightarrow 0, v(x, y, \infty) \rightarrow 0, \frac{\partial u}{\partial z}(x, y, \infty) \rightarrow 0, \frac{\partial v}{\partial z}(x, y, \infty) \rightarrow 0, T(x, y, \infty) = T_\infty \end{aligned} \right. \quad (6)$$



Now, we state the symmetry transformations [31]:

$$\begin{aligned} u &= axf'(\eta), \quad \eta = \left(\frac{a}{v}\right)^{0.5}z, \quad v = ayg'(\eta), \quad w = -\sqrt{av}[f(\eta) + g(\eta)], \quad \theta(\eta) = \frac{T - T_\infty}{T_f - T_\infty} \\ \phi(\eta) &= \frac{C - C_\infty}{C_w - C_\infty} \end{aligned} \quad (7)$$

With the help of Equation (7), Equations (2)–(5) will be reduced to the following form

$$\left(1 + \frac{1}{\beta}\right)f'''' - f'^2 + [f + g]f'' - \lambda f' - Frf'^2 + Ha e^{-d_1 \eta} = 0 \quad (8)$$

$$\left(1 + \frac{1}{\beta}\right)g'''' - g'^2 + [f + g]g'' - \lambda g' - Frg'^2 = 0 \quad (9)$$

$$\begin{aligned} \frac{1}{Pr}\theta'' + [f + g]\theta' - \Gamma[f + g]^2\theta'' + [f + g][f' + g']\theta' \\ + Nb\theta'\phi' + Nt\theta'^2 + Hg\theta = 0 \end{aligned} \quad (10)$$

$$\phi'' + Le[f + g]\phi' - Le\Gamma_C[f + g]^2\phi'' + Le[f + g][f' + g']\phi' + \frac{Nt}{Nb}\theta'' = 0 \quad (11)$$

The boundary conditions are,

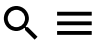
$$\begin{aligned} f(0) = 0, g(0) = 0, \\ f'(0) = 1, g'(0) = \epsilon, f'(\infty) = 0, g'(\infty) = 0, f''(\infty) = 0, g''(\infty) = 0 \\ = -Bi(1 - \theta(0)), \theta(\infty) = 0, \phi(0) = 1, \phi(\infty) = 0 \end{aligned} \quad (12)$$

Here, the non-dimensional variables are defined as

$$\begin{aligned} \lambda = \frac{\nu}{k_1 a}, Fr = \frac{C_b}{\sqrt{k_1}}, Ha = \frac{\pi j_0 M_0}{8a^3 x \rho}, d_1 = -\frac{\pi}{b} \sqrt{\frac{\nu}{a}}, Pr = \frac{\nu}{\alpha_m}, \Gamma = \lambda_E a, Nb = \frac{\tau_{DB}}{\nu}(C_w - C_\infty) \\ Hg = \frac{Q_0}{\rho c_p a}, \Gamma_C = \lambda_C a, \text{ and } Le = \frac{\alpha_m}{D_B} \end{aligned}$$

The engineering concerns “skin friction”, “local Nusselt number (LNN)”, and “local Sherwood number (LSN)” are defined below:

MDPI $Re^{0.5} Cf_x = \left(1 + \frac{1}{\beta}\right) f''(0) = \text{skin friction in } x - \text{direction}$



$$Re^{0.5} Cf_y = \left(1 + \frac{1}{\beta}\right) g''(0) = \text{skin friction in } y - \text{direction}$$

$$Re^{-0.5} Nu_x = -\theta'(0) = \text{local Nusselt number}$$

$$Re^{-0.5} Sh_x = -\phi'(0) = \text{local Sherwood number}$$

3. Solution Process

The transformed nonlinear ODE Equations (8)–(11) with the boundary conditions in Equation (12) are solved using HAM technique. This techniques used solve highly non-linear problems. The advantage of this method is to freely fix initial approximations and linear operators. The flow chart of this method is illustrated in **Figure 2**.

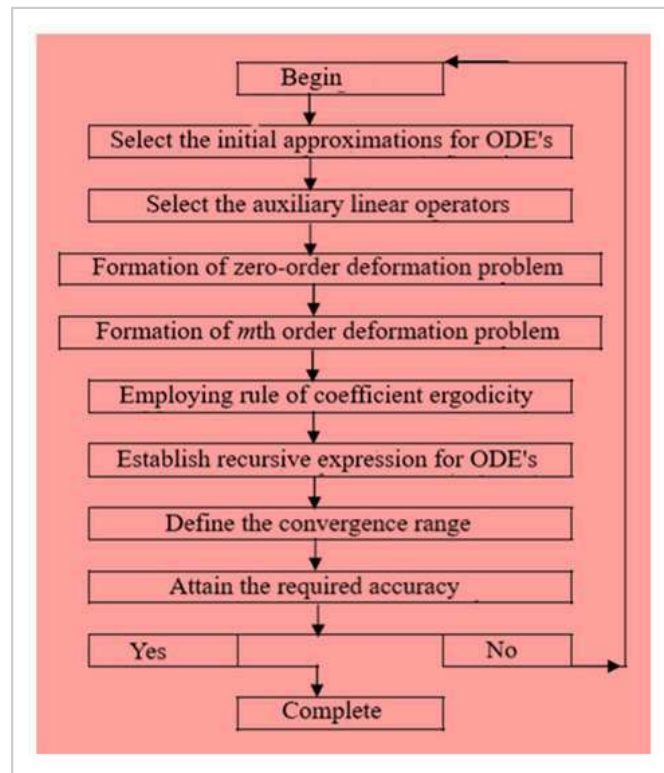


Figure 2. Flow chart of HAM.

The convergences values are of h_f , h_g , h_θ and h_ϕ are plotted in **Figure 3**. The range of convergence is $-1.4 \leq h_f, h_g \leq 0.0$, and $-1.75 \leq h_\theta, h_\phi \leq 0.1$. **Table 1** observes the order of $f''(0)$, $g''(0)$, $\theta'(0)$, and $\phi'(0)$ are 15 th order.

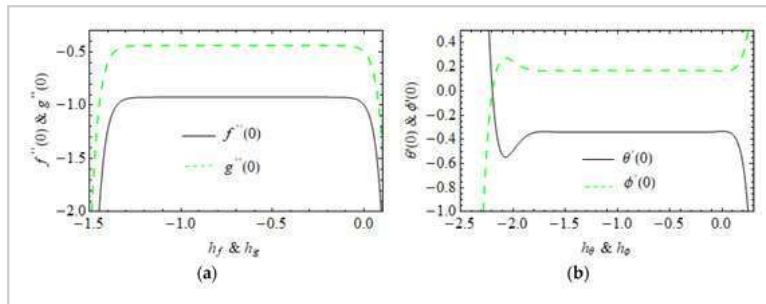


Figure 3. The h - curves of (a) $f''(0)$, $g''(0)$ and (b) $\theta'(0)$, $\phi'(0)$.

Table 1. HAM order.

4. Correlation Analysis

For analyzing the concert of a thermal system design, the system of equations is required. The acquired numerical data are utilized to generate the system of equations using linear regression analysis. The skin friction, heat and mass relationship equations:

$$Re^{0.5}Cf_x = -1.840454 + 0.428572 * Ha - 0.525588 * \lambda + 0.262804 * \beta - 0.340727 * Fr$$

$$Re^{0.5}Cf_y = -0.765295 - 0.014398 * Ha - 0.307248 * \lambda + 0.099039 * \beta - 0.093480 * Fr$$

$$\frac{Nu}{\sqrt{Re}} = 0.343840 + 0.002102 * Ha - 0.004278 * \lambda - 0.001629 * \beta - 0.001564 * Fr$$

$$\frac{Sh}{\sqrt{Re}} = -0.171920 - 0.001051 * Ha + 0.002139 * \lambda + 0.000814 * \beta + 0.000782 * Fr$$

For $Ha = [0.0, 0.3]$, $\lambda = [0.0, 0.2]$, $\beta = [1, 2]$ and $Fr \in [0, 1]$ with maximum error is 0.028.

5. Computational Results and Discussion

In this section, the investigation is taken to scrutinize an essential description of the different dimensional factors on velocity along x and y directions, temperature, and concentration of nanoparticles. **Table 2** elucidates the comparison analysis of Nu_x for numerous parameters from

Muhammad et al. [31]. This table ensures the accuracy of obtained results and the precision of numerical computation utilized in this analysis. It is noted that there is an outstanding achievement with the earlier publication. **Table 3** provides the characteristics of $\Gamma, \Gamma_c, Nb, Nt, Bi$ and Hg on Nu_x and Sh_x for CNF and VNF. It is realized that the HTG grows when mounting the size of Γ, Γ_c and Bi and it decays when improving the size of Nt and Hg for both fluids. Furthermore, the LNN remains fixed when changing the Nb values, see Muhammad et al. [31]. The LSN decays when varying the size of Γ, Γ_c, Nt and Bi and it rise when changing the values of Nb and Hg for both fluids.

Table 2. Comparison of local Nusselt number with Muhammad et al. [31].

Table 3. The LNN and LSN for different combinations of $\Gamma, \Gamma_c, Nb, Nt, Bi$ and Hg for both fluids.

Figure 4a,b display the velocity $f'(\eta)$ and $g'(\eta)$ against the various value of Casson fluid parameter β on $\lambda = 0.2$ and $\lambda = 0$. It is noted that the augmentation of β produces a reduction in velocity profile and boundary layer thickness. The influence of Ha on $f'(\eta)$ and $g'(\eta)$ is employed in **Figure 4c,d** on $\lambda = 0.2$ and $\lambda = 0$. The larger value of Ha increases the velocity profile in both directions. The existence of a modified Hartman number enhanced the motion of Casson fluid. Also, the larger fluid velocity attains when $\lambda = 0.0$ than the $\lambda = 0.2$ when varying β and Ha values in both directions. Moreover, the Riga plate is an electromagnetic device that pushes the movement of the flow in a specific direction. **Figure 5a,b** illustrates the intensification of the temperature with the rising value of Biot number Bi on RP, SP, porous RP and non-porous RP. The Biot number is the leading function of temperature distribution in the case of $Ha = (0.0, 0.3)$ and $\lambda = (0.0, 0.2)$. Physically, enhancing the value of Bi obtained stronger heat convection at the wall of the surface. The impact of Hg on the temperature field on heated RP and SP is exposed in **Figure 5c**. The temperature field enlarges for greater values of Hg . Additionally, heat has been induced due to a greater value of Hg , which is the reason the temperature profile is enlarged in the sense of heating RP and SP. In contrast, an opposite trend is observed in **Figure 5d** for cooling RP and SP. The impact of Nt on $\theta(\eta)$ for fluid heat generating and absorbing on a RP is examined in **Figure 5e** and seen that the $\theta(\eta)$ develops when raising the Nt values. Thermophoresis attained through a temperature difference produces

a faster flow that moves away from the stretching sheet. The temperature inside the surface increases due to faster flow, resulting in an amelioration of the temperature profile. **Figure 5f** elucidates the thermal relaxation time Γ on temperature distribution on heated and cooled RP. It is detected that the temperature field and corresponding thermal layer thickness depreciated by the enhancing value of Γ on heated RP. A larger value of Γ results in particles of materials needing extra time to transport heat near its particles which is responsible for the lessening of the thermal layer. The opposite behavior getting for cooled RP.

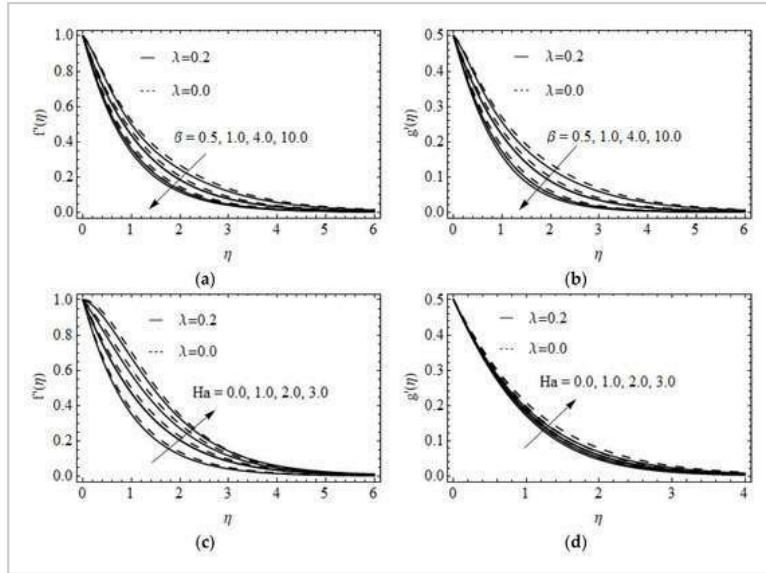
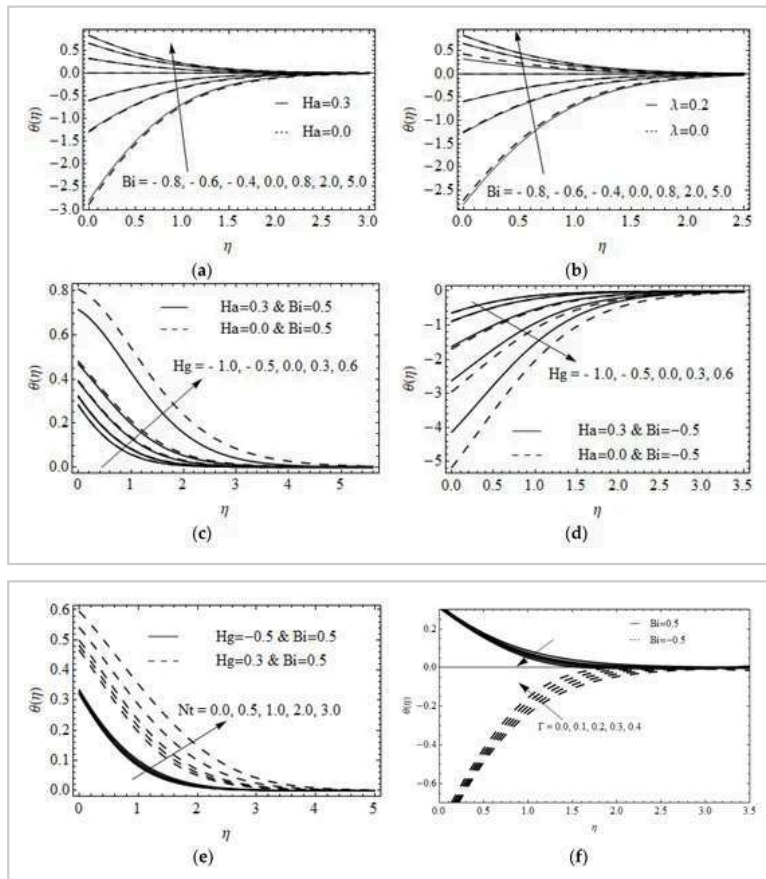


Figure 4. The x -direction (a,c) and y -direction (b,d) velocity for various values of β and Ha for porous and non-porous RP.



The variations of $\theta(\eta)$ for various values of Bi (a,b) over RP and SP (a), porous and non-porous RP (b), Hg (c,d) for convective heating (c) and cooling (d) RP and SP, Nt (e) for heat generating and absorption and Γ (f) for convective heating and cooling RP

Figure 6a,b reveals the influence of Biot number Bi on $\phi(\eta)$ for the case of ($Ha = 0.0, Ha = 0.3$) and ($\lambda = 0.0, \lambda = 0.2$), it is clear from the figure that the concentration of nanoparticles and its corresponding layer thickness are accelerated due to the larger value of Bi for all cases. The variation of Hg on $\phi(\eta)$ for heated and cooled RP and SP was displayed in Figure 6c,d. Increasing the value of Hg leads to accelerate in $\phi(\eta)$ due to heated RP and a reduction cooled RP. The effect of Nb on $\phi(\eta)$ on fluid heat generating and absorbing on heated and cooled RP is shown in Figure 6e,f. It is seen that $\phi(\eta)$ decays when strengthening the Nb in headed RP and the opposite trend attains in cooled RP for both fluid heat generating and absorbing cases. The variation of Ha and λ for CNF and VNF on the drag friction coefficient in the x , and y directions were presented in Figure 7a,b. In Figure 7a shows that the Cf_x climbs with an enhancement in Ha and it is suppresses for a higher size of λ and Cf_y diminishes with an improvement in Ha and λ for both fluids, see Figure 7b. Figure 8a displays the LNN Nu_x for Ha and λ . The growth of Ha escalates the LNN and it decays for larger quantity of λ . On the contrary, Figure 8b presents that the LNN Nu_x and Nu_x is a lessening function of Hg and Nt . The contour plot of LNN for Pr and λ for CNF and VNF was illustrated in Figure 8c,d. The LSN for various values of λ & Ha and Nt & Hg for both fluids were displayed in Figure 9a,b. It is seen that the LSN improves when enhancing the values of λ and Hg . The opposite nature attains for Ha and Nt . The impact of Nb and Nt on LSN for heated and cooled RP was displayed in Figure 9c,d. The quite opposite nature occurs in heating and cooling cases. The contour plot of LSN for various values of Γ_c and Le for both fluids was addressed in Figure 9e,f.

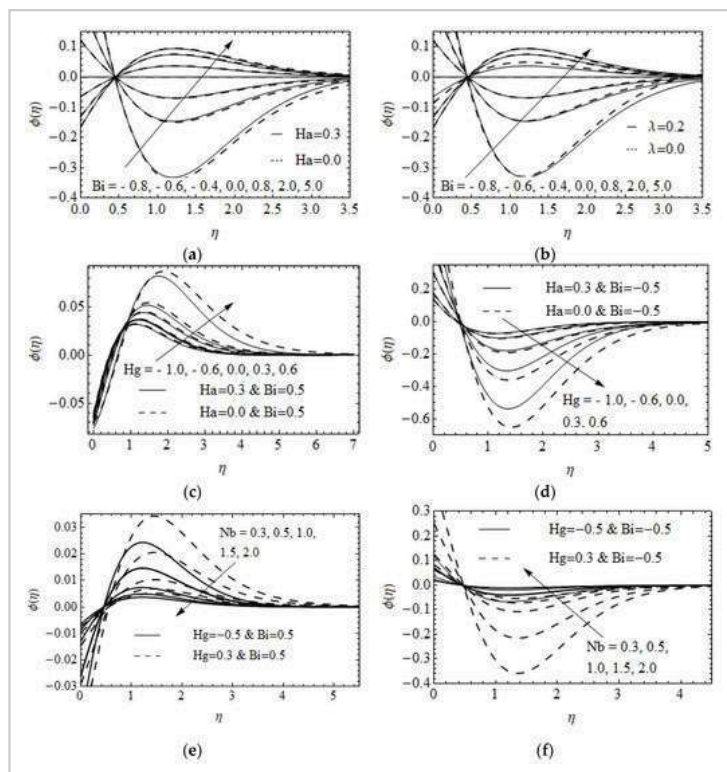


Figure 6. The variations of $\phi(\eta)$ for different values of Bi (a,b) for SP and RP(a), porous and non-porous RP (b), Hg (c,d) for convective heating RP and SP (c) and convective cooling RP and SP (d), Nb (e,f) for convective heating with heat generation and absorption (e) and convective cooling with heat generation and absorption (f).

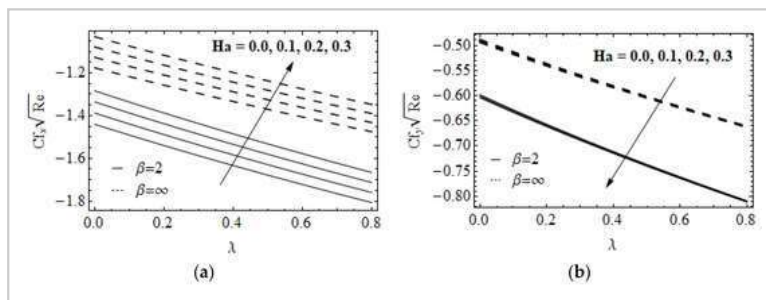


Figure 7. The Skin friction in x -direction (a) and y -direction (b) with different values of Ha and λ for both fluids.

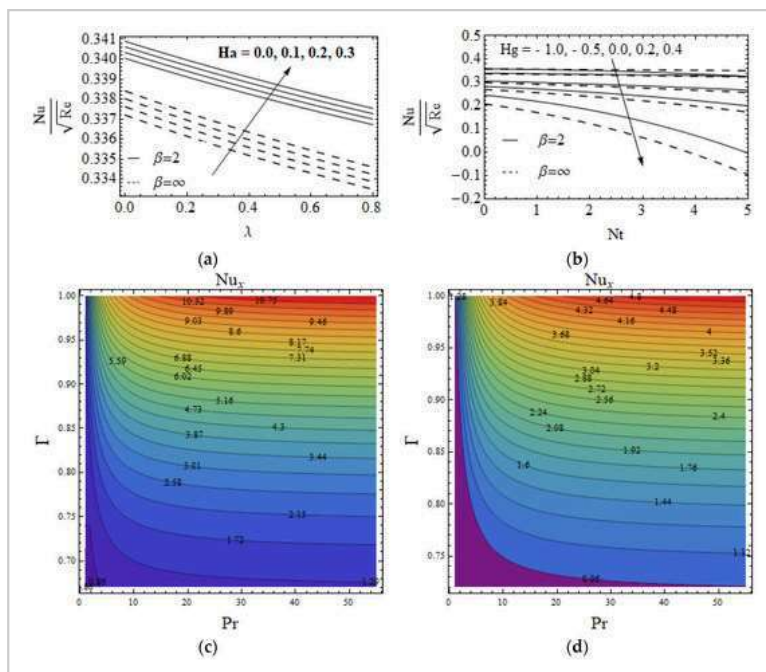


Figure 8. The Nu_x variations Ha & λ (a), Hg & Nt (b) for both fluids and Pr & Γ (c, d) for Casson nanofluid (c) and viscous nanofluid (d).

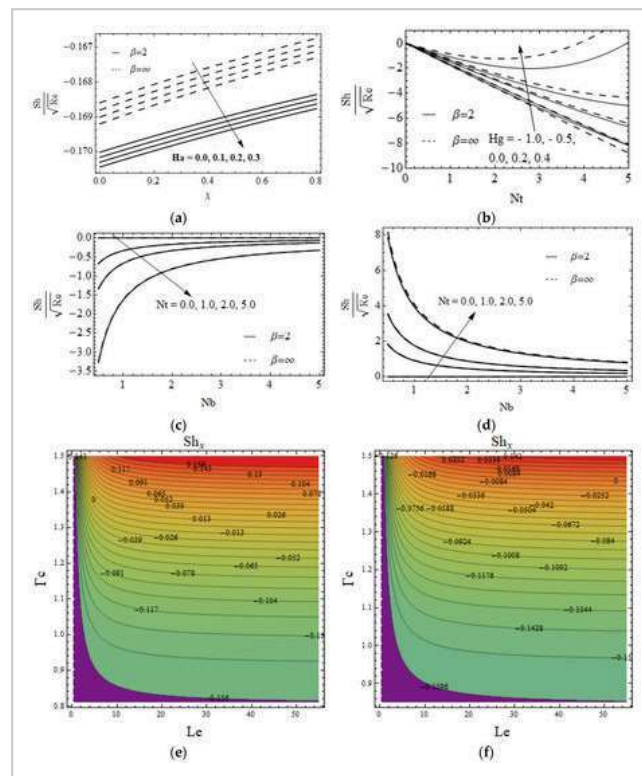


Figure 9. The Sh_x for λ & Ha (a) and Nt & Hg (b) for both fluids and Nb & Nt with $Bi = 0.5$ (c) and $Bi = -0.5$ (d), Le & Γ_C for Casson nanofluid (e) and viscous nanofluid (f).

6. Conclusions

The Darcy–Forchheimer flow of the 3-D Casson nanofluid owing to the Riga plate was investigated using the Cattaneo–Christov dual diffusion theory. In addition, the homotopy technique was used for the solution process. The most important finding is highlighted below.

- The skin friction rate in x – direction enhances and in y – direction decays when enhancing the modified Hartman number.
- The larger skin friction rate occurs in viscous nanofluid than the Casson nanofluid.
- Thermal layer thickness amplifies with an augmented value of Bi .
- A larger value of Hg upsurges in the thermal layer in the case of $Bi = 0.5$ while the thermal layer reduces with a larger value of Hg for $Bi = -0.5$.
- The thermal relaxation parameter improves the local Nusselt number for both fluids.
- In the future, we will extend this work with the Tiwari and Das model with a hybrid nanofluid case.

Author Contributions

Conceptualization, S.E. and K.L.; Methodology, K.L.; Software, K.L.; Validation, P.C. and N.N.D.; Formal analysis, R.S.; Investigation, R.J. and P.C.; Writing—original draft, K.L.; Writing—review & editing, K.L. and R.A.; Project administration, K.L.; Funding acquisition, K.L. All authors have read and agreed to the published version of the manuscript.

Data Availability Statement

Not applicable.

Acknowledgments

The authors extend their appreciation to the Deanship of Scientific Research at King Khalid University for funding the work through a small group project under grant number R.G.P 1/169/43.

Conflicts of Interest

The authors declare no conflict of interest.

Nomenclature

a, b	Constants (–)
Bi	Biot number (–)
C	Concentration (kg m^{-3})
C_∞	Ambient concentration (kg m^{-3})
C_w	Surface concentration of nanoparticles (kg m^{-3})
C_p	Specific heat ($\text{J kg}^{-1}\text{K}^{-1}$)
C_{fx}	Skin friction in x -direction (–)
C_{fy}	Skin friction in y -direction (–)
D_B	Brownian diffusion coefficient ($\text{m}^2 \text{s}^{-1}$)
D_T	Thermophoretic diffusion coefficient ($\text{m}^2 \text{s}^{-1}$)
$f(\eta)$	Velocity similarity function in x – direction (–)
$g(\eta)$	Velocity similarity function in y – direction (–)
Hg	Heat generation/absorption parameter (–)
k	Thermal conductivity ($\text{m kgs}^{-3}\text{K}^{-1}$)
k_1	Permeability of the porous medium
Le	Lewis number (–)
Nb	Brownian motion parameter (–)
Nt	Thermophoresis parameter (–)
Nu_x	Local Nusselt number (–)
Pr	Prandtl number (–)
Re	Reynolds number (–)

Q_0 Heat generation/absorption coefficient (–)

Sh_x Local Sherwood number (–)

T Temperature (K)

T_W Surface temperature of nanoparticles

T_∞ Ambient temperature (K)

u_w Velocity of the sheet (m s^{-1})

u, v, w Velocity components (m s^{-1})

x, y, z Cartesian coordinates (m)

Greeks

β Casson fluid parameter (–)

γ Viscoelastic parameter (–)

$\phi(\eta)$ Concentration similarity function (–)

ϵ Stretching ratio (–)

η Similarity parameter (–)

λ Porous parameter (–)

Γ Heat thermal relaxation time parameter (–)

Γ_c Mass thermal relaxation time parameter (–)

ν Kinematic viscosity ($\text{m}^2 \text{s}^{-1}$)

τ Ratio of the effective heat capacity (–)

$\theta(\eta)$ Temperature similarity function (–)

ρ Density (kg m^{-3})

σ Electrical conductivity ($\text{S}^3 \text{m}^2 \text{kg}^{-1}$)

BM Brownian movement

CNF Casson nanofluid

VNF Viscous nanofluid

RP Riga Plate

LLN Local Nusselt number

LSN Local Sherwood Number

SP Stationary Plate

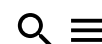
DF Darcy-Forchheimer

CCHF Cattaneo-Christov heat flux

NPVF Nanoparticle volume fraction

SS Stretching sheet

CCHD Cattaneo-Christov heat diffusion



1. Choi, S.U.; Eastman, J.A. Enhancing thermal conductivity of fluids with nanoparticles. *ASME Fluids Eng. Div.* **1995**, *231*, 99–105. [Google Scholar (https://scholar.google.com/scholar_lookup?title=Enhancing+thermal+conductivity+of+fluids+with+nanoparticles&author=Choi,+S.U.&author=Eastman,+J.A.&publication_year=1995&journal=ASME+Fluids+Eng.+Div.&volume=231&pages=99%E2%80%93105)]
2. Das, K. Nanofluid flow over a non-linear permeable stretching sheet with partial slip. *J. Egypt. Math. Soc.* **2015**, *23*, 451–456. [Google Scholar (https://scholar.google.com/scholar_lookup?title=Nanofluid+flow+over+a+non-linear+permeable+stretching+sheet+with+partial+slip&author=Das,+K.&publication_year=2015&journal=J.+Egypt.+Math.+Soc.&volume=23&pages=451%E2%80%93456&doi=10.1016/j.joems.2014.06.014)] [CrossRef (<https://doi.org/10.1016/j.joems.2014.06.014>)] [Green Version (<https://core.ac.uk/download/pdf/82087844.pdf>)]
3. Kuznetsov, A.V.; Nield, D.A. Natural convective boundary layer flow of a nanofluid past a vertical plate. *Int. J. Therm. Sci.* **2010**, *49*, 243–247. [Google Scholar (https://scholar.google.com/scholar_lookup?title=Natural+convective+boundary+layer+flow+of+a+nanofluid+past+a+vertical+plate&author=Kuznetsov,+A.V.&author=Nield,+D.A.&publication_year=2010&journal=Int.+J.+Therm.+Sci.&volume=49&pages=243%E2%80%93247&doi=10.1016/j.ijthermalsci.2009.07.015)] [CrossRef (<https://doi.org/10.1016/j.ijthermalsci.2009.07.015>)]
4. Hamad, M.A.A.; Pop, I.; Ismail, A.M. Magnetic field effects on free convection flow of a nanofluid past a vertical semi-infinite at plate. *Nonlinear Anal. Real World Appl.* **2011**, *12*, 13381346. [Google Scholar (https://scholar.google.com/scholar_lookup?title=Magnetic+field+effects+on+free+convection+flow+of+a+nanofluid+past+a+vertical+semi-infinite+at+plate&author=Hamad,+M.A.A.&author=Pop,+I.&author=Ismail,+A.M.&publication_year=2011&journal=Nonlinear+Anal.+Real+World+Appl.&volume=12&pages=13381346&doi=10.1016/j.nonrwa.2010.09.014)] [CrossRef (<https://doi.org/10.1016/j.nonrwa.2010.09.014>)]
5. Nadeem, S.; Haq, R.U.; Khan, Z.H. Numerical solution of non-Newtonian nanofluid flow over a stretching sheet. *Appl. Nanosci.* **2014**, *4*, 625631. [Google Scholar (https://scholar.google.com/scholar_lookup?title=Numerical+solution+of+non-Newtonian+nanofluid+flow+over+a+stretching+sheet&author=Nadeem,+S.&author=Haq,+R.U.&author=Khan,+Z.H.&publication_year=2014&journal=Appl.+Nanosci.&volume=4&pages=625631&doi=10.1007/s13204-013-0235-8)] [CrossRef (<https://doi.org/10.1007/s13204-013-0235-8>)] [Green Version (<https://core.ac.uk/download/pdf/81846490.pdf>)]

(https://scholar.google.com/scholar_lookup?title=Boundary-layer+flow+of+a+nanofluid+past+a+stretching+sheet&author=Khan,+W.A.&author=Pop,+I.&publication_year=2010&journal=Int.+Heat+Mass+Transf.&volume=53&pages=2477%E2%80%932483&doi=10.1016/j.ijheatmasstransfer.2010.01.032)] [CrossRef (<https://doi.org/10.1016/j.ijheatmasstransfer.2010.01.032>)]

7. Sajid, T.; Jamshed, W.; Eid, M.R.; Altamirano, G.C.; Aslam, F.; Alanzi, A.M.; Abd-Elmonem, A. Magnetized Cross tetra hybrid nanofluid passed a stenosed artery with nonuniform heat source (sink) and thermal radiation: Novel tetra hybrid Tiwari and Das nanofluid model. *J. Magn. Magn. Mater.* **2023**, *569*, 170443. [Google Scholar ([https://scholar.google.com/scholar_lookup?title=Magnetized+Cross+tetra+hybrid+nanofluid+passed+a+stenosed+artery+with+nonuniform+heat+source+\(sink\)+and+thermal+radiation:+Novel+tetra+hybrid+Tiwari+and+Das+nanofluid+model&author=Sajid,+T.&author=Jamshed,+W.&author=Eid,+M.R.&author=Altamirano,+G.C.&author=Aslam,+F.&author=Alanzi,+A.M.&author=Abd-Elmonem,+A.&publication_year=2023&journal=J.+Magn.+Magn.+Mater.&volume=569&pages=170443&doi=10.1016/j.jmmm.2023.170443](https://scholar.google.com/scholar_lookup?title=Magnetized+Cross+tetra+hybrid+nanofluid+passed+a+stenosed+artery+with+nonuniform+heat+source+(sink)+and+thermal+radiation:+Novel+tetra+hybrid+Tiwari+and+Das+nanofluid+model&author=Sajid,+T.&author=Jamshed,+W.&author=Eid,+M.R.&author=Altamirano,+G.C.&author=Aslam,+F.&author=Alanzi,+A.M.&author=Abd-Elmonem,+A.&publication_year=2023&journal=J.+Magn.+Magn.+Mater.&volume=569&pages=170443&doi=10.1016/j.jmmm.2023.170443))] [CrossRef (<https://doi.org/10.1016/j.jmmm.2023.170443>)]
8. Sajid, T.; Jamshed, W.; Ibrahim, R.W.; Eid, M.R.; Abd-Elmonem, A.; Arshad, M. Quadratic regression analysis for nonlinear heat source/sink and mathematical Fourier heat law influences on Reiner-Philippoff hybrid nanofluid flow applying Galerkin finite element method. *J. Magn. Magn. Mater.* **2023**, *568*, 170383. [Google Scholar (https://scholar.google.com/scholar_lookup?title=Quadratic+regression+analysis+for+nonlinear+heat+source/sink+and+mathematical+Fourier+heat+law+influences+on+Reiner-Philippoff+hybrid+nanofluid+flow+applying+Galerkin+finite+element+method&author=Sajid,+T.&author=Jamshed,+W.&author=Ibrahim,+R.W.&author=Eid,+M.R.&author=Abd-Elmonem,+A.&author=Arshad,+M.&publication_year=2023&journal=J.+Magn.+Magn.+Mater.&volume=568&pages=170383&doi=10.1016/j.jmmm.2023.170383)] [CrossRef (<https://doi.org/10.1016/j.jmmm.2023.170383>)]

- Hassani, M.; Tabar, M.M.; Nemati, H.; Domairry, G.; Noori, F. An analytical solution for boundary layer flow of a nanofluid past a stretching sheet. *Int. J. Therm. Sci.* **2011**, *50*, 2256–2263. [Google Scholar (https://scholar.google.com/scholar_lookup?title=An+analytical+solution+for+boundary+layer+flow+of+a+nanofluid+past+a+stretching+sheet&author=Hassani,+M.&author=Tabar,+M.M.&author=Nemati,+H.&author=Domairry,+G.&author=Noori,+F.&publication_year=2011&journal=Int.+J.+Therm.+Sci.&volume=50&pages=2256%E2%80%932263&doi=10.1016/j.ijthermalsci.2011.05.015)] [CrossRef (<https://doi.org/10.1016/j.ijthermalsci.2011.05.015>)]
10. Sriramalu, A.; Kishan, N.; Anand, R.J. Steady Flow and heat transfer of a viscous incompressible fluid flow through porous medium over a stretching sheet. *J. Energy Heat Mass Transf.* **2001**, *23*, 483495. [Google Scholar (https://scholar.google.com/scholar_lookup?title=Steady+Flow+and+heat+transfer+of+a+viscous+incompressible+fluid+flow+through+porous+medium+over+a+stretching+sheet&author=Sriramalu,+A.&author=Kishan,+N.&author=Anand,+R.J.&publication_year=2001&journal=J.+Energy+Heat+Mass+Transf.&volume=23&pages=483495)]
11. Liu, I.C. Flow and heat transfer of viscous fluid saturated in porous media over a permeable non-isothermal stretching sheet. *Transp. Porous Media* **2006**, *64*, 375–392. [Google Scholar (https://scholar.google.com/scholar_lookup?title=Flow+and+heat+transfer+of+viscous+fluid+saturated+in+porous+media+over+a+permeable+non-isothermal+stretching+sheet&author=Liu,+I.C.&publication_year=2006&journal=Transp.+Porous+Media&volume=64&pages=375%E2%80%93392&doi=10.1007/s11242-005-5235-z)] [CrossRef (<https://doi.org/10.1007/s11242-005-5235-z>)]
12. Nadeem, S.; Haq, R.U.; Akbar, N.S.; Khan, Z.H. MHD three-dimensional Casson fluid flow past a porous linearly stretching sheet. *Alex. Eng. J.* **2013**, *52*, 577682. [Google Scholar (https://scholar.google.com/scholar_lookup?title=MHD+three-dimensional+Casson+fluid+flow+past+a+porous+linearly+stretching+sheet&author=Nadeem,+S.&author=Haq,+R.U.&author=Akbar,+N.S.&author=Khan,+Z.H.&publication_year=2013&journal=Alex.+Eng.+J.&volume=52&pages=577682&doi=10.1016/j.aej.2013.08.005)] [CrossRef (<https://doi.org/10.1016/j.aej.2013.08.005>)]
13. Pramanik, S. Casson fluid flow and heat transfer past an exponentially porous stretching surface in presence of thermal radiation. *Ain Shams Eng. J.* **2014**, *5*, 205–212. [Google Scholar (https://scholar.google.com/scholar_lookup?title=Casson+fluid+flow+and+heat+transfer+past+an+exponentially+porous+stretching+surface+in+presence+of+thermal+radiation&author=Pramanik,+S.&publication_year=2014&journal=Ain+Shams+Eng.+J.&volume=5&pages=205%E2%80%93212&doi=10.1016/j.asej.2013.05.003)] [CrossRef (<https://doi.org/10.1016/j.asej.2013.05.003>)] [Green Version (<https://core.ac.uk/download/pdf/82180541.pdf>)]

- Mahanta, G.; Shaw, S. Three-dimensional Casson fluid flow past a porous linearly stretching sheet with convective boundary conditions. *Alex. Eng. J.* **2015**, *54*, 653–6599. [Google Scholar (https://scholar.google.com/scholar_lookup?title=Three-dimensional+Casson+fluid+flow+past+a+porous+linearly+stretching+sheet+with+convective+boundary+conditions&author=Mahanta,+G.&author=Shaw,+S.&publication_year=2015&journal=Alex.+Eng.+J.&volume=54&pages=653%E2%80%936599&doi=10.1016/j.aej.2015.04.014)] [CrossRef (<https://doi.org/10.1016/j.aej.2015.04.014>)]
15. Abbas, T.; Bhatti, M.M.; Ayub, M. Aiding and opposing of mixed convection Casson nanofluid flow with chemical reactions through a porous Riga plate. *Proc. Inst. Mech. Eng. Part E J. Process Mech. Eng.* **2017**, *232*, 519–527. [Google Scholar (https://scholar.google.com/scholar_lookup?title=Aiding+and+opposing+of+mixed+convection+Casson+nano fluid+flow+with+chemical+reactions+through+a+porous+Riga+plate&author=Abbas,+T.&author=Bhatti,+M.M.&author=Ayub,+M.&publication_year=2017&journal=Proc.+Inst.+Mech.+Eng.+Part+E+J.+Process+Mech.+Eng.&volume=232&pages=519%E2%80%93527&doi=10.1177/0954408917719791)] [CrossRef (<https://doi.org/10.1177/0954408917719791>)]
16. Zubair, M.; Shah, Z.; Islam, S.; Khan, W.; Dawar, A. Study of three dimensional Darcy Forchheimer squeezing nanofluid flow with Cattaneo-Christov heat flux based on four different types of nanoparticles through entropy generation analysis. *Adv. Mech. Eng.* **2019**, *11*, 117. [Google Scholar (https://scholar.google.com/scholar_lookup?title=Study+of+three+dimensional+Darcy+Forchheimer+squeezing+nano fluid+flow+with+Cattaneo-Christov+heat+flux+based+on+four+different+types+of+nanoparticles+through+entropy+generation+analysis&author=Zubair,+M.&author=Shah,+Z.&author=Islam,+S.&author=Khan,+W.&author=Dawar,+A.&publication_year=2019&journal=Adv.+Mech.+Eng.&volume=11&pages=117&doi=10.1177/1687814019851308)] [CrossRef (<https://doi.org/10.1177/1687814019851308>)] [Green Version (<https://journals.sagepub.com/doi/pdf/10.1177/1687814019851308>)]
17. Abbas, S.Z.; Khan, W.A.; Kadry, S.; Ijaz, M.; Khan Waqas, M.; Khan, M.I. Entropy optimized Darcy Forchheimernanoid (Silicon dioxide, Molybdenum disulfide) subject to temperature dependent viscosity. *Comput. Methods Programs Biomed.* **2020**, *190*, 105363. [Google Scholar ([https://scholar.google.com/scholar_lookup?title=Entropy+optimized+Darcy+Forchheimernanoid+\(Silicon+dioxide,+Molybdenum+disulfide\)+subject+to+temperature+dependent+viscosity&author=Abbas,+S.Z.&author=Khan,+W.A.&author=Kadry,+S.&author=Ijaz,+M.&author=Khan+Waqas,+M.&author=Khan,+M.I.&publication_year=2020&journal=Comput.+Methods+Programs+Biomed.&volume=190&pages=105363&doi=10.1016/j.cmpb.2020.105363](https://scholar.google.com/scholar_lookup?title=Entropy+optimized+Darcy+Forchheimernanoid+(Silicon+dioxide,+Molybdenum+disulfide)+subject+to+temperature+dependent+viscosity&author=Abbas,+S.Z.&author=Khan,+W.A.&author=Kadry,+S.&author=Ijaz,+M.&author=Khan+Waqas,+M.&author=Khan,+M.I.&publication_year=2020&journal=Comput.+Methods+Programs+Biomed.&volume=190&pages=105363&doi=10.1016/j.cmpb.2020.105363))] [CrossRef (<https://doi.org/10.1016/j.cmpb.2020.105363>)]

Ahmad, M.W.; Kumam, P.; Shah, Z.; Farooq, A.A.; Nawaz, R.; Dawar, A.; Islam, S.; Thounthong, P. Darcy Forchheimer MHD couple stress 3D nanofluid over an exponentially stretching sheet through Cattaneo-Christov convective heat flux with zero nanoparticles mass flux conditions. *Entropy* **2019**, *21*, 867. [Google Scholar (https://scholar.google.com/scholar_lookup?title=Darcy+Forchheimer+MHD+couple+stress+3D+nanofluid+over+an+exponential+y+stretching+sheet+through+Cattaneo-Christov+convective+heat+flux+with+zero+nanoparticles+mass+flux+conditions&author=Ahmad,+M.W.&author=Kumam,+P.&author=Shah,+Z.&author=Farooq,+A.A.&author=Nawaz,+R.&author=Dawar,+A.&author=Islam,+S.&author=Thounthong,+P.&publication_year=2019&journal=Entropy&volume=21&pages=867&doi=10.3390/e21090867)] [CrossRef (<https://doi.org/10.3390/e21090867>)] [Green Version (<https://www.mdpi.com/1099-4300/21/9/867/pdf>)]

19. ThamaraiKannan, N.; Karthikeyan, S.; Chaudhary, D.K.; Kayikci, S. Analytical investigation of magnetohydrodynamic non-Newtonian type Casson nanofluid flow past a porous channel with periodic body acceleration. *Complexity* **2021**, *2021*, 7792422. [Google Scholar (https://scholar.google.com/scholar_lookup?title=Analytical+investigation+of+magnetohydrodynamic+non-Newtonian+type+Casson+nanofluid+flow+past+a+porous+channel+with+periodic+body+acceleration&author=ThamaraiKannan,+N.&author=Karthikeyan,+S.&author=Chaudhary,+D.K.&author=Kayikci,+S.&publication_year=2021&journal=Complexity&volume=2021&pages=7792422&doi=10.1155/2021/7792422)] [CrossRef (<https://doi.org/10.1155/2021/7792422>)]

20. Reddy, P.B.A. Magnetohydrodynamic flow of a Casson fluid over an exponentially inclined permeable stretching surface with thermal radiation and chemical reaction. *Mech. Eng.* **2017**, *232*, 519–527. [Google Scholar (https://scholar.google.com/scholar_lookup?title=Magnetohydrodynamic+flow+of+a+Casson+fluid+over+an+exponentially+inclined+permeable+stretching+surface+with+thermal+radiation+and+chemical+reaction&author=Reddy,+P.B.A.&publication_year=2017&journal=Mech.+Eng.&volume=232&pages=519%E2%80%93527&doi=10.1016/j.asej.2015.12.010)] [CrossRef (<https://doi.org/10.1016/j.asej.2015.12.010>)] [Green Version (<https://core.ac.uk/download/pdf/81164444.pdf>)]

21. Hayat, T.; Bilal Ashraf, M.; Shehzad, S.A.; Alsaedi, A. Mixed convection flow of Casson nanofluid over a stretching sheet with convectively heated chemical reaction and heat source/sink. *J. Appl. Fluid Mech.* **2015**, *8*, 803–813. [Google Scholar (https://scholar.google.com/scholar_lookup?title=Mixed+convection+flow+of+Casson+nanofluid+over+a+stretching+sheet+with+convectively+heated+chemical+reaction+and+heat+source/sink&author=Hayat,+T.&author=Bilal+Ashraf,+M.&author=Shehzad,+S.A.&author=Alsaedi,+A.&publication_year=2015&journal=J.+Appl.+Fluid+Mech.&volume=8&pages=803%E2%80%93813)]

- Abolbashari, M.H.; Freidoonimehr, N.; Nazari, F.; Rashidi, M.M. Analytical modeling of entropy generation for Casson nano-fluid flow induced by a stretching surface. *Adv. Powder Technol.* **2015**, *26*, 542–552. [Google Scholar (https://scholar.google.com/scholar_lookup?title=Analytical+modeling+of+entropy+generation+for+Casson+nano-fluid+flow+induced+by+a+stretching+surface&author=Abolbashari,+M.H.&author=Freidoonimehr,+N.&author=Nazari,+F.&author=Rashidi,+M.M.&publication_year=2015&journal=Adv.+Powder+Technol.&volume=26&pages=542%E2%80%93552&doi=10.1016/j.apt.2015.01.003)] [CrossRef (<https://doi.org/10.1016/j.apt.2015.01.003>)]
23. Al-Zubaidi, A.; Nazeer, M.; Saleem, S.; Hussain, F.; Ahmad, F. Flow of nanofluid towards a Riga surface with heat and mass transfer under the effects of activation energy and thermal radiation. *Int. J. Mod. Phys. B* **2021**, *35*, 2150266. [Google Scholar (https://scholar.google.com/scholar_lookup?title=Flow+of+nanofluid+towards+a+Riga+surface+with+heat+and+mass+transfer+under+the+effects+of+activation+energy+and+thermal+radiation&author=Al-Zubaidi,+A.&author=Nazeer,+M.&author=Saleem,+S.&author=Hussain,+F.&author=Ahmad,+F.&publication_year=2021&journal=Int.+J.+Mod.+Phys.+B&volume=35&pages=2150266&doi=10.1142/S0217979221502660)] [CrossRef (<https://doi.org/10.1142/S0217979221502660>)]
24. Vaidya, H.; Prasad, K.V.; Tlili, I.; Makinde, O.D.; Rajashekhar, C.; Khan, S.U.; Kumar, R.; Mahendra, D.L. Mixed convective nanofluid flow over a non-linearly stretched Riga plate. *Case Stud. Therm. Eng.* **2021**, *24*, 100828. [Google Scholar (https://scholar.google.com/scholar_lookup?title=Mixed+convective+nanofluid+flow+over+a+non-linearly+stretched+Riga+plate&author=Vaidya,+H.&author=Prasad,+K.V.&author=Tlili,+I.&author=Makinde,+O.D.&author=Rajashekhar,+C.&author=Khan,+S.U.&author=Kumar,+R.&author=Mahendra,+D.L.&publication_year=2021&journal=Case+Stud.+Therm.+Eng.&volume=24&pages=100828&doi=10.1016/j.csite.2020.100828)] [CrossRef (<https://doi.org/10.1016/j.csite.2020.100828>)]
25. Rafique, K.; Alotaibi, H.; Ibrar, N.; Khan, I. Stratified flow of micropolar nanofluid over Riga plate: Numerical analysis. *Energies* **2022**, *15*, 316. [Google Scholar (https://scholar.google.com/scholar_lookup?title=Stratified+flow+of+micropolar+nanofluid+over+Riga+plate:+Numerical+analysis&author=Rafique,+K.&author=Alotaibi,+H.&author=Ibrar,+N.&author=Khan,+I.&publication_year=2022&journal=Energies&volume=15&pages=316&doi=10.3390/en15010316)] [CrossRef (<https://doi.org/10.3390/en15010316>)]

- Prasad, K.V.; Vaidya, H.; Mebarek-Oudina, F.; Choudhari, R.; Nisar, K.S.; Jamshed, W. Impact of surface temperature and convective boundary conditions on a nanofluid flow over a radially stretched Riga plate. *Proc. Inst. Mech. Eng. Part E J. Process Mech. Eng.* **2022**, *236*, 942–952. [Google Scholar (https://scholar.google.com/scholar_lookup?title=Impact+of+surface+temperature+and+convective+boundary+conditions+on+a+nanofluid+flow+over+a+radially+stretched+Riga+plate&author=Prasad,+K.V.&author=Vaidya,+H.&author=Mebarek-Oudina,+F.&author=Choudhari,+R.&author=Nisar,+K.S.&author=Jamshed,+W.&publication_year=2022&journal=Proc.+Inst.+Mech.+Eng.+Part+E+J.+Process+Mech.+Eng.&volume=236&pages=942%E2%80%93952&doi=10.1177/09544089211054407)] [CrossRef (<https://doi.org/10.1177/09544089211054407>)]
27. Darvesh, A.; Wahab, H.A.; Sarakorn, W.; Sánchez-Chero, M.; Apaza, O.A.; Villarreyes, S.S.C.; Palacios, A.Z. Infinite shear rate viscosity of cross model over Riga plate with entropy generation and melting process: A numerical Keller box approach. *Results Eng.* **2023**, *17*, 100942. [Google Scholar (https://scholar.google.com/scholar_lookup?title=Infinite+shear+rate+viscosity+of+cross+model+over+Riga+plate+with+entropy+generation+and+melting+process:+A+numerical+Keller+box+approach&author=Darvesh,+A.&author=Wahab,+H.A.&author=Sarakorn,+W.&author=S%C3%A1nchez-Chero,+M.&author=Apaza,+O.A.&author=Villarreyes,+S.S.C.&author=Palacios,+A.Z.&publication_year=2023&journal=Results+Eng.&volume=17&pages=100942&doi=10.1016/j.rineng.2023.100942)] [CrossRef (<https://doi.org/10.1016/j.rineng.2023.100942>)]
28. Divya, S.; Eswaramoorthi, S.; Loganathan, K. Numerical computation of Ag/Al₂O₃ nanofluid over a Riga plate with heat sink/source and non-Fourier heat flux model. *Math. Comput. Appl.* **2023**, *28*, 20. [Google Scholar (https://scholar.google.com/scholar_lookup?title=Numerical+computation+of+Ag/Al2O3+nanofluid+over+a+Riga+plate+with+heat+sink/source+and+non-Fourier+heat+flux+model&author=Divya,+S.&author=Eswaramoorthi,+S.&author=Loganathan,+K.&publication_year=2023&journal=Math.+Comput.+Appl.&volume=28&pages=20&doi=10.3390/mca28010020)] [CrossRef (<https://doi.org/10.3390/mca28010020>)]
29. Ahmad, A.; Asghar, S.; Afzal, S. Flow of nanofluid past a Riga plate. *J. Magn. Magn. Mater.* **2016**, *402*, 44–48. [Google Scholar (https://scholar.google.com/scholar_lookup?title=Flow+of+nanofluid+past+a+Riga+plate&author=Ahmad,+A.&author=Asghar,+S.&author=Afzal,+S.&publication_year=2016&journal=J.+Magn.+Magn.+Mater.&volume=402&pages=44%E2%80%9348&doi=10.1016/j.jmmm.2015.11.043)] [CrossRef (<https://doi.org/10.1016/j.jmmm.2015.11.043>)]

30 Al-Kouz, W.; Owhaib, W. Numerical analysis of Casson nanofluid three-dimensional flow over a rotating frame exposed to a prescribed heat flux with viscous heating. *Sci. Rep.* **2022**, *12*, 4256. [Google Scholar (https://scholar.google.com/scholar_lookup?title=Numerical+analysis+of+Casson+nanofluid+three-dimensional+flow+over+a+rotating+frame+exposed+to+a+prescribed+heat+flux+with+viscous+heating&author=Al-Kouz,+W.&author=Owhaib,+W.&publication_year=2022&journal=Sci.+Rep.&volume=12&pages=4256&doi=10.1038/s41598-022-08211-2)] [CrossRef (<https://doi.org/10.1038/s41598-022-08211-2>)]

31. Muhammad, T.; Alsaedi, A.; Hayat, T.; Shehzad, S.A. A revised model for Darcy-Forchheimer three-dimensional flow of nanofluid subject to convective boundary condition. *Results Phys.* **2017**, *7*, 2791–2797. [Google Scholar (https://scholar.google.com/scholar_lookup?title=A+revised+model+for+Darcy-Forchheimer+three-dimensional+flow+of+nanofluid+subject+to+convective+boundary+condition&author=Muhammad,+T.&author=Alsaedi,+A.&author=Hayat,+T.&author=Shehzad,+S.A.&publication_year=2017&journal=Results+Phys.&volume=7&pages=2791%E2%80%9932797&doi=10.1016/j.rinp.2017.07.052)] [CrossRef (<https://doi.org/10.1016/j.rinp.2017.07.052>)]

Disclaimer/Publisher’s Note: The statements, opinions and data contained in all publications are solely those of the individual author(s) and contributor(s) and not of MDPI and/or the editor(s). MDPI and/or the editor(s) disclaim responsibility for any injury to people or property resulting from any ideas, methods, instructions or products referred to in the content.

© 2023 by the authors. Licensee MDPI, Basel, Switzerland. This article is an open access article distributed under the terms and conditions of the Creative Commons Attribution (CC BY) license (<https://creativecommons.org/licenses/by/4.0/> (<https://creativecommons.org/licenses/by/4.0/>)).

Share and Cite



(mailto:?)

&subject=From%20MDPI%3A%20%22Heat%20and%20Mass%20Transport%20in%20Casson%20Nanofluid%20Flow%20over%20a%203-D%20Riga%20Plate%20with%20Cattaneo-Christov%20Double%20Flux%3A%20A%20Computational%20Modeling%20through%20Analytical%20Method"&body=https://www.mdpi.com/2193842%3A%0A%0AHeat%20and%20Mass%20Transport%20in%20Casson%20Nanofluid%20Flow%20over%20a%203-D%20Riga%20Plate%20with%20Cattaneo-Christov%20Double%20Flux%3A%20A%20Computational%20Modeling%20through%20Analytical%20Method%0A%0AAbstract%3A%20This%20work%20examines%20the%20non-

MDPI (l) **Newtonian%20Cassonnanofluid%26rsquo%3Bs%20three-dimensional%20flow%20and%20heat%20and%20mass%20transmission%20properties%20over%20a%20Riga%20plate.%20The%20Buongiorno%20nanofluid%20model%2C%20which%20is%20included%20in%20the%20present%20model%2C%20includes%20thermo-migration%20and%20random%20movement%20of%20nanoparticles.%20It%20also%20took%20into%20account%20the%20Cattaneo%26ndash%3BChristov%20double%20flux%20processes%20in%20the%20mass%20and%20heat%20equations.%20The%20non-Newtonian%20Casson%20fluid%20model%20and%20the%20boundary%20layer%20approximation%20are%20included%20in%20the%20modeling%20of%20nonlinear%20partial%20differential%20systems.%20The%20homotopy%20technique%20was%20used%20to%20analytically%20solve%20the%20system%26rsquo%3Bs%20governing%20equations.%20To%20examine%20the%20impact%20of%20dimensionless%20parameters%20on%20velocities%2C%20concentrations%2C%20temperatures%2C%20local%20Nusselt%20number%2C%20skin%20friction%2C%20and%20local%20Sherwood%20number%2C%20a%20parametric%20analysis%20was%20carried%20out.%20The%20velocity%20profile%20is%20augmented%20in%20this%20study%20as%20the%20size%20of%20the%20modified%20Hartmann%20number%20increases.%20The%20greater%20thermal%20radiative%20enhances%20the%20heat%20transport%20rate.%20When%20the%20mass%20relaxation%20parameter%20is%20used%2C%20the%20mass%20flux%20values%20start%20to%20decrease.)**

([https://twitter.com/intent/tweet?](https://twitter.com/intent/tweet?text=Heat+and+Mass+Transport+in+Casson+Nanofluid+Flow+over+a+3-D+Riga+Plate+with+Cattaneo-Christov+Double+Flux%3A+A+Computational+Modeling+through+Analytical+Method&hashtags=mdpisymmetry&url=https%3A%2F%2Fwww.mdpi.com%2F2193842&via=Symmetry_M DPI)

[text=Heat+and+Mass+Transport+in+Casson+Nanofluid+Flow+over+a+3-](https://twitter.com/intent/tweet?text=Heat+and+Mass+Transport+in+Casson+Nanofluid+Flow+over+a+3-D+Riga+Plate+with+Cattaneo-Christov+Double+Flux%3A+A+Computational+Modeling+through+Analytical+Method&hashtags=mdpisymmetry&url=https%3A%2F%2Fwww.mdpi.com%2F2193842&via=Symmetry_M DPI)

[D+Riga+Plate+with+Cattaneo-](https://twitter.com/intent/tweet?text=Heat+and+Mass+Transport+in+Casson+Nanofluid+Flow+over+a+3-D+Riga+Plate+with+Cattaneo-Christov+Double+Flux%3A+A+Computational+Modeling+through+Analytical+Method&hashtags=mdpisymmetry&url=https%3A%2F%2Fwww.mdpi.com%2F2193842&via=Symmetry_M DPI)

[Christov+Double+Flux%3A+A+Computational+Modeling+through+Analytical+Method&hashtags=mdpisymmetry&url=https%3A%2F%2Fwww.mdpi.com%2F2193842&via=Symmetry_](https://twitter.com/intent/tweet?text=Heat+and+Mass+Transport+in+Casson+Nanofluid+Flow+over+a+3-D+Riga+Plate+with+Cattaneo-Christov+Double+Flux%3A+A+Computational+Modeling+through+Analytical+Method&hashtags=mdpisymmetry&url=https%3A%2F%2Fwww.mdpi.com%2F2193842&via=Symmetry_M DPI)

[MDPI\) !\[\]\(23d9fc146e83b5c3013cfa32c784f8d5_img.jpg\) \(\[http://www.linkedin.com/shareArticle?\]\(http://www.linkedin.com/shareArticle?mini=true&url=https%3A%2F%2Fwww.mdpi.com%2F2193842&title=Heat%20and%20Mass%20Transport%20in%20Casson%20Nanofluid%20Flow%20over%20a%203-D%20Riga%20Plate%20with%20Cattaneo-Christov%20Double%20Flux%3A%20A%20Computational%20Modeling%20through%20Analytical%20Method%26source%3Dhttps%3A%2F%2Fwww.mdpi.com%26summary%3DThis%20work%20examines%20the%20non-Newtonian%20Cassonnanofluid%E2%80%99s%20three-dimensional%20flow%20and%20heat%20and%20mass%20transmission%20properties%20over%20a%20Riga%20plate.%20The%20Buongiorno%20nanofluid%20model%2C%20which%20is%20included%20in%20the%20present%20model%2C%20includes%20thermo-migration%20and%20random%20movement%20of%20nanoparticles.%20It%20also%20took%20into%20account%20the%20Cattaneo%26ndash%3BChristov%20double%20flux%20processes%20in%20the%20mass%20and%20heat%20equations.%20The%20non-Newtonian%20Casson%20fluid%20model%20and%20the%20boundary%20layer%20approximation%20are%20included%20in%20the%20modeling%20of%20nonlinear%20partial%20differential%20systems.%20The%20homotopy%20technique%20was%20used%20to%20analytically%20solve%20the%20system%26rsquo%3Bs%20governing%20equations.%20To%20examine%20the%20impact%20of%20dimensionless%20parameters%20on%20velocities%2C%20concentrations%2C%20temperatures%2C%20local%20Nusselt%20number%2C%20skin%20friction%2C%20and%20local%20Sherwood%20number%2C%20a%20parametric%20analysis%20was%20carried%20out.%20The%20velocity%20profile%20is%20augmented%20in%20this%20study%20as%20the%20size%20of%20the%20modified%20Hartmann%20number%20increases.%20The%20greater%20thermal%20radiative%20enhances%20the%20heat%20transport%20rate.%20When%20the%20mass%20relaxation%20parameter%20is%20used%2C%20the%20mass%20flux%20values%20start%20to%20decrease.\)\)](https://twitter.com/intent/tweet?text=Heat+and+Mass+Transport+in+Casson+Nanofluid+Flow+over+a+3-D+Riga+Plate+with+Cattaneo-Christov+Double+Flux%3A+A+Computational+Modeling+through+Analytical+Method&hashtags=mdpisymmetry&url=https%3A%2F%2Fwww.mdpi.com%2F2193842&via=Symmetry_M DPI)

[mini=true&url=https%3A%2F%2Fwww.mdpi.com%2F2193842&title=Heat%20and%20Mass%20Transport%20in%20Casson%20Nanofluid%20Flow%20over%20a%203-](https://twitter.com/intent/tweet?text=Heat+and+Mass+Transport+in+Casson+Nanofluid+Flow+over+a+3-D+Riga+Plate+with+Cattaneo-Christov+Double+Flux%3A+A+Computational+Modeling+through+Analytical+Method&hashtags=mdpisymmetry&url=https%3A%2F%2Fwww.mdpi.com%2F2193842&via=Symmetry_M DPI)

[D%20Riga%20Plate%20with%20Cattaneo-](https://twitter.com/intent/tweet?text=Heat+and+Mass+Transport+in+Casson+Nanofluid+Flow+over+a+3-D+Riga+Plate+with+Cattaneo-Christov+Double+Flux%3A+A+Computational+Modeling+through+Analytical+Method&hashtags=mdpisymmetry&url=https%3A%2F%2Fwww.mdpi.com%2F2193842&via=Symmetry_M DPI)

[Christov%20Double%20Flux%3A%20A%20Computational%20Modeling%20through%20Analytical%20Method%26source%3Dhttps%3A%2F%2Fwww.mdpi.com%26summary%3DThis%20work%20examines%20the%20non-](https://twitter.com/intent/tweet?text=Heat+and+Mass+Transport+in+Casson+Nanofluid+Flow+over+a+3-D+Riga+Plate+with+Cattaneo-Christov+Double+Flux%3A+A+Computational+Modeling+through+Analytical+Method&hashtags=mdpisymmetry&url=https%3A%2F%2Fwww.mdpi.com%2F2193842&via=Symmetry_M DPI)

[Newtonian%20Cassonnanofluid%E2%80%99s%20three-](https://twitter.com/intent/tweet?text=Heat+and+Mass+Transport+in+Casson+Nanofluid+Flow+over+a+3-D+Riga+Plate+with+Cattaneo-Christov+Double+Flux%3A+A+Computational+Modeling+through+Analytical+Method&hashtags=mdpisymmetry&url=https%3A%2F%2Fwww.mdpi.com%2F2193842&via=Symmetry_M DPI)

[dimensional%20flow%20and%20heat%20and%20mass%20transmission%20properties%20over%20a%20Riga%20plate.%20The%20Buongiorno%20nanofluid%20model%2C%20which%20is%20included%20in%20the%20present%20model%2C%20includes%20thermo-](https://twitter.com/intent/tweet?text=Heat+and+Mass+Transport+in+Casson+Nanofluid+Flow+over+a+3-D+Riga+Plate+with+Cattaneo-Christov+Double+Flux%3A+A+Computational+Modeling+through+Analytical+Method&hashtags=mdpisymmetry&url=https%3A%2F%2Fwww.mdpi.com%2F2193842&via=Symmetry_M DPI)

[migration%20and%20random%20movement%20of%20nanoparticles.%20It%20also%20took%20into%20account%20the%20Cattaneo%26ndash%3BChristov%20double%20flux%20processes%20in%20the%20mass%20and%20heat%20equations.%20The%20non-Newtonian%20Casson%20fluid%20model%20and%20the%20boundary%20layer%20approximation%20are%20included%20in%20the%20modeling%20of%20nonlinear%20partial%20differential%20systems.%20The%20homotopy%20technique%20was%20used%20to%20analytically%20solve%20the%20system%26rsquo%3Bs%20governing%20equations.%20To%20examine%20the%20impact%20of%20dimensionless%20parameters%20on%20velocities%2C%20concentrations%2C%20temperatures%2C%20local%20Nusselt%20number%2C%20skin%20friction%2C%20and%20local%20Sherwood%20number%2C%20a%20parametric%20analysis%20was%20carried%20out.%20The%20velocity%20profile%20is%20augmented%20in%20this%20study%20as%20the%20size%20of%20the%20modified%20Hartmann%20number%20increases.%20The%20greater%20thermal%20radiative%20enhances%20the%20heat%20transport%20rate.%20When%20the%20mass%20relaxation%20parameter%20is%20used%2C%20the%20mass%20flux%20values%20start%20to%20decrease.\)](https://twitter.com/intent/tweet?text=Heat+and+Mass+Transport+in+Casson+Nanofluid+Flow+over+a+3-D+Riga+Plate+with+Cattaneo-Christov+Double+Flux%3A+A+Computational+Modeling+through+Analytical+Method&hashtags=mdpisymmetry&url=https%3A%2F%2Fwww.mdpi.com%2F2193842&via=Symmetry_M DPI)

[u=https://www.mdpi.com/2193842\)](https://twitter.com/intent/tweet?text=Heat+and+Mass+Transport+in+Casson+Nanofluid+Flow+over+a+3-D+Riga+Plate+with+Cattaneo-Christov+Double+Flux%3A+A+Computational+Modeling+through+Analytical+Method&hashtags=mdpisymmetry&url=https%3A%2F%2Fwww.mdpi.com%2F2193842&via=Symmetry_M DPI)

[!\[\]\(626ce8ac21792b9405bfddfea8e0c96a_img.jpg\) \(\[http://www.reddit.com/submit?\]\(http://www.reddit.com/submit?url=https://www.mdpi.com/2193842\)](https://twitter.com/intent/tweet?text=Heat+and+Mass+Transport+in+Casson+Nanofluid+Flow+over+a+3-D+Riga+Plate+with+Cattaneo-Christov+Double+Flux%3A+A+Computational+Modeling+through+Analytical+Method&hashtags=mdpisymmetry&url=https%3A%2F%2Fwww.mdpi.com%2F2193842&via=Symmetry_M DPI)

[url=https://www.mdpi.com/2193842\)](https://twitter.com/intent/tweet?text=Heat+and+Mass+Transport+in+Casson+Nanofluid+Flow+over+a+3-D+Riga+Plate+with+Cattaneo-Christov+Double+Flux%3A+A+Computational+Modeling+through+Analytical+Method&hashtags=mdpisymmetry&url=https%3A%2F%2Fwww.mdpi.com%2F2193842&via=Symmetry_M DPI)

[\(\[http://www.mendeley.com/import/?\]\(http://www.mendeley.com/import/?url=https://www.mdpi.com/2193842\)](https://twitter.com/intent/tweet?text=Heat+and+Mass+Transport+in+Casson+Nanofluid+Flow+over+a+3-D+Riga+Plate+with+Cattaneo-Christov+Double+Flux%3A+A+Computational+Modeling+through+Analytical+Method&hashtags=mdpisymmetry&url=https%3A%2F%2Fwww.mdpi.com%2F2193842&via=Symmetry_M DPI)

[url=https://www.mdpi.com/2193842\)](https://twitter.com/intent/tweet?text=Heat+and+Mass+Transport+in+Casson+Nanofluid+Flow+over+a+3-D+Riga+Plate+with+Cattaneo-Christov+Double+Flux%3A+A+Computational+Modeling+through+Analytical+Method&hashtags=mdpisymmetry&url=https%3A%2F%2Fwww.mdpi.com%2F2193842&via=Symmetry_M DPI)

MDPI and ACS Style

Loganathan, K.; Eswaramoorthi, S.; Chinnasamy, P.; Jain, R.; Sivasakthivel, R.; Ali, R.; Devi, N.N. Heat and Mass Transport in Casson Nanofluid Flow over a 3-D Riga Plate with Cattaneo-Christov Double Flux: A Computational Modeling through Analytical Method. *Symmetry* **2023**, *15*, 725. <https://doi.org/10.3390/sym15030725>

AMA Style

Loganathan K, Eswaramoorthi S, Chinnasamy P, Jain R, Sivasakthivel R, Ali R, Devi NN. Heat and Mass Transport in Casson Nanofluid Flow over a 3-D Riga Plate with Cattaneo-Christov Double Flux: A Computational Modeling through Analytical Method. *Symmetry*. 2023; 15(3):725. <https://doi.org/10.3390/sym15030725>

Chicago/Turabian Style

Loganathan, Karuppusamy, S. Eswaramoorthi, P. Chinnasamy, Reema Jain, Ramkumar Sivasakthivel, Rifaqat Ali, and N. Nithya Devi. 2023. "Heat and Mass Transport in Casson Nanofluid Flow over a 3-D Riga Plate with Cattaneo-Christov Double Flux: A Computational Modeling through Analytical Method" *Symmetry* 15, no. 3: 725. <https://doi.org/10.3390/sym15030725>

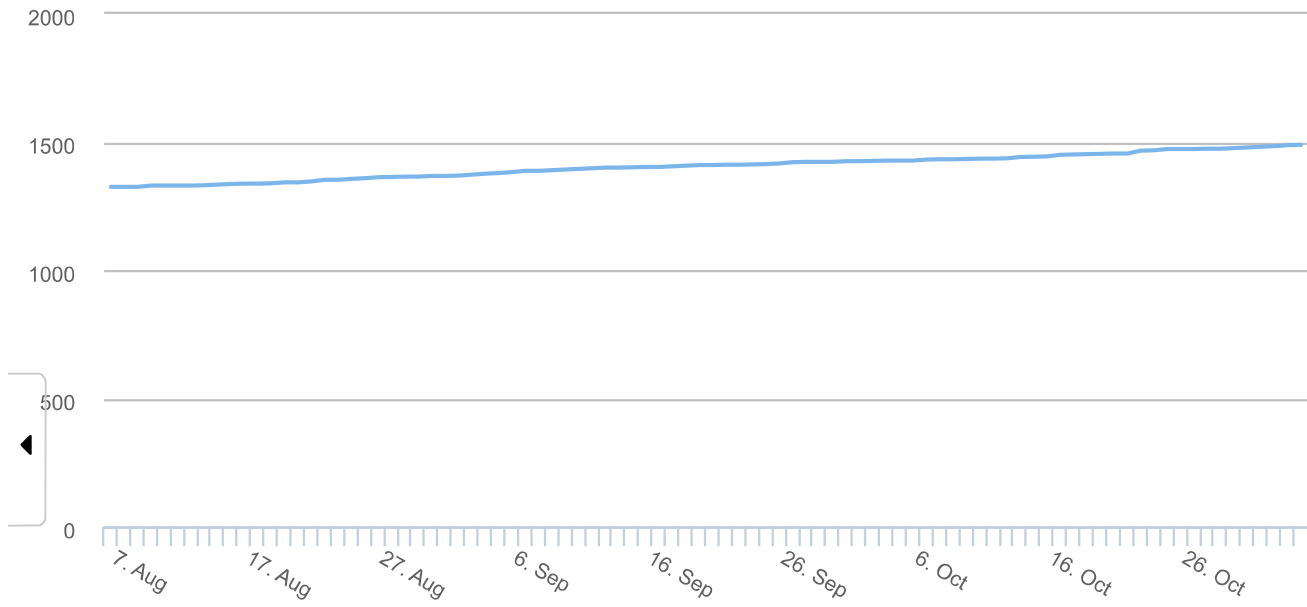
ⓘ Note that from the first issue of 2016, this journal uses article numbers instead of page numbers. See further details [here \(https://www.mdpi.com/about/announcements/784\)](https://www.mdpi.com/about/announcements/784).

Article Metrics

Citations

Web of Science	Scopus	Crossref	ads	Google Scholar
	7 (https://partnerID=HzO:GWVersion=2&	6	(https://ui.adsat	Christov+Doubl

Article access statistics



Article Views

For more information on the journal statistics, click [here \(/journal/symmetry/stats\)](/journal/symmetry/stats).

ⓘ Multiple requests from the same IP address are counted as one view.

[Symmetry \(/journal/symmetry\)](/journal/symmetry), EISSN 2073-8994, Published by MDPI

[RSS \(/rss/journal/symmetry\)](/rss/journal/symmetry) **[Content Alert \(/journal/symmetry/toc-alert\)](/journal/symmetry/toc-alert)**

Further Information

[Article Processing Charges \(/apc\)](/apc)

[Pay an Invoice \(/about/payment\)](/about/payment)

[Open Access Policy \(/openaccess\)](/openaccess)

[Contact MDPI \(/about/contact\)](/about/contact)

[Jobs at MDPI \(https://careers.mdpi.com\)](https://careers.mdpi.com)

Guidelines

[For Authors \(/authors\)](/authors)

[For Reviewers \(/reviewers\)](/reviewers)

[For Editors \(/editors\)](/editors)

[For Librarians \(/librarians\)](/librarians)

[For Publishers \(/publishing_services\)](/publishing_services)

[For Societies \(/societies\)](/societies)

[For Conference Organizers \(/conference_organizers\)](#)
MDPI Initiatives

[Sciforum \(https://sciforum.net\)](https://sciforum.net)

[MDPI Books \(https://www.mdpi.com/books\)](https://www.mdpi.com/books)

[Preprints.org \(https://www.preprints.org\)](https://www.preprints.org)

[Scilit \(https://www.scilit.net\)](https://www.scilit.net)

[SciProfiles \(https://sciprofiles.com?
utm_source=mpdi.com&utm_medium=bottom_menu&utm_campaign=initiative\)](https://sciprofiles.com?utm_source=mpdi.com&utm_medium=bottom_menu&utm_campaign=initiative)

[Encyclopedia \(https://encyclopedia.pub\)](https://encyclopedia.pub)

[JAMS \(https://jams.pub\)](https://jams.pub)

[Proceedings Series \(/about/proceedings\)](#)

Follow MDPI

[LinkedIn \(https://www.linkedin.com/company/mdpi\)](https://www.linkedin.com/company/mdpi)

[Facebook \(https://www.facebook.com/MDPIOpenAccessPublishing\)](https://www.facebook.com/MDPIOpenAccessPublishing)

[Twitter \(https://twitter.com/MDPIOpenAccess\)](https://twitter.com/MDPIOpenAccess)

Subscribe to receive issue release
notifications and newsletters from
MDPI journals

Select options ▼

Enter your email address...

Subscribe

© 1996-2024 MDPI (Basel, Switzerland) unless otherwise stated

[Disclaimer](#) [Terms and Conditions \(/about/terms-and-conditions\)](#)
[Privacy Policy \(/about/privacy\)](#)

अनुसंधान नेशनल रिसर्च फाउंडेशन Anusandhan National Research Foundation

Home

About

Funding

Decision Path

Disclosures

Science For Society

Success Stories

Home > New low-cost technology reduces textile effluent pollution significantly

New low-cost technology reduces textile effluent pollution significantly

A textile and apparel industry, located in the Hanumakonda district, of Telangana has been able to treat its textile wastewater at a very reasonable cost. Thanks to an energy-efficient and eco-friendly technology developed using, biosurfactants and membrane technology.

Textile effluent is heavily contaminated with pollutants such as dyes, dissolved solids, suspended solids and toxic metals and there is a need for robust, efficient technologies to treat such effluent before they are discharged into the environment.

NIT Warangal along with Prime Textiles, Rampur located in Kakatiya Mega Textile Park (KMTP), with support from IMPRINT, a joint effort of MoE and SERB, developed a pilot-scale textile effluent treatment plant using biosurfactants (BS), cavitation (a process in which pressure variations in a liquid can in a short period of time cause countless small cavities to form and then implode--C), and membrane (M) technology.

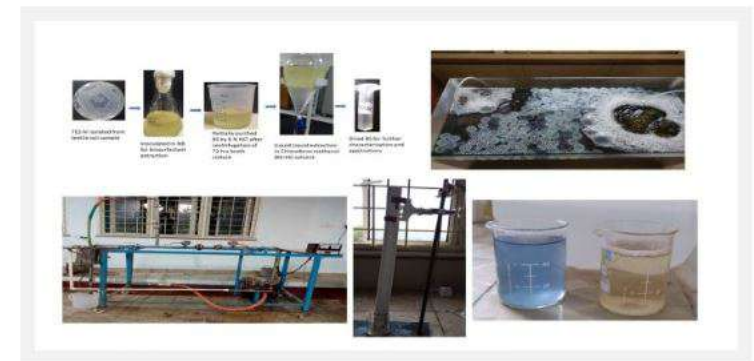


Figure 1 Laboratory developments of the MBBR, HC, and CM systems





Figure 2 Pilot-scale setup installed at Prime Textiles, Rampur

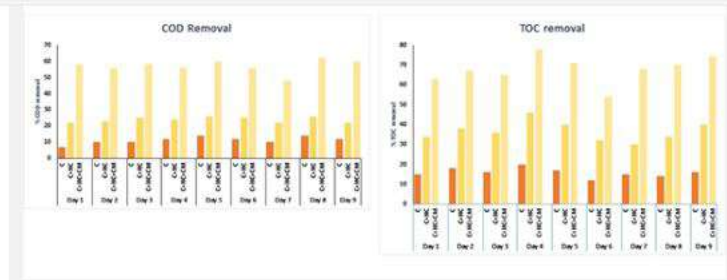


Figure 3 COD and TOC removal using pilot-scale setup



Figure 4 Our team with SERB Scientist Dr. Harish Kumar at the IMPRINT exhibition at IIT Delhi

Initially, the scientists Prof. Shirish H. Sonawane, NIT Warangal, Dr. Murali Mohan Seepana, NIT Warangal, Dr. Ajey Kumar Patel, NIT Warangal and Dr. Mousumi Debnath, Manipal University Jaipur (MUJ) developed individual systems at the laboratories and the process parameters were optimized. The biosurfactant to be used in Moving Bed Biofilm Reactor (MBBR) was extracted from microorganisms isolated from textile effluent and textile effluent contaminated soil by MUJ.

The use of BS in MBBR helped in dye removal and was effective in reducing operational time and cost (with respect to other biological treatment methods). Cavitation (C), an advanced oxidation process (AOP), aided in reducing installation cost as well as reducing carbon footprint.

The ability of the technology to generate oxidizing radicals in-situ, significantly reduced the reliance on external oxidizing agents. On the other hand, modifying the membrane (M) surface using boehmite sol synthesized using sol-gel process, decreased the pore size from micro-scale to nano-scale and led to a significant improvement in its performance. After optimizing individual systems, a pilot-scale setup has been set up at the Prime Textiles premises.

The sequence of events that takes place in the pilot plant plays an important role in the treatment process of the effluent. The coagulation removes turbidity caused by suspended solids by destabilizing the charges of the particles using a chemical coagulant. The biofilm grown on MBBR reduces the heavy metal content, degrades the biodegradable pollutants while the cavitation phenomenon destroys all types of pollutants, resulting in the in situ generation of radicals, and energy which are responsible for the pollutant degradation. Finally, surface modified membrane separates all the pollutants present in the wastewater. With this sequence, the pilot plant of 200 Litres Per Day capacity removes pollutants and the treated water can be utilized for agricultural activities, and cleaning purposes.

This joint effort has led to the transfer of technology and two patents. The technology offers a sustainable solution for the textile effluent from KMTP, converting the toxic wastewater to irrigation source for the nearby agricultural areas and holds immense potential for replacing existing secondary treatment plants due to its lower installation cost and lesser carbon footprint.